TIDAL ELEVATIONS AND TIDAL CURRENTS IN THE NORTHWEST PASSAGE

by

J.A. Stronach, J.A. Helbig and S.S. Salvador
Pacific Ocean Sciences
Burnaby, B.C.

and

H. Melling and R.A. Lake
Institute of Ocean Sciences
Sidney, B.C.

Institute of Ocean Sciences
Department of Fisheries and Oceans
Sidney, B.C.

1987

CANADIAN TECHNICAL REPORT OF HYDROGRAPHY AND OCEAN SCIENCES
NO. 97

Canada

89-00685/

Canadian Technical Report of Hydrography and Ocean Sciences

These reports contain scientific and technical information of a type that represents a contribution to existing knowledge but which is not normally found in the primary literature. The subject matter is generally related to programs and interests of the Ocean Science and Surveys (OSS) sector of the Department of Fisheries and Oceans.

Technical Reports may be cited as full publications. The correct citation appears above the abstract of each report. Each report will be abstracted in Aquatic Sciences and Fisheries Abstracts. Reports are also listed in the Department's annual index to scientific and technical publications.

Technical Reports are produced regionally but are numbered and indexed nationally. Requests for individual reports will be fulfilled by the issuing establishment listed on the front cover and title page. Out of stock reports will be supplied for a fee by commercial agents.

Regional and headquarters establishments of Ocean Science and Surveys ceased publication of their various report series as of December 1981. A complete listing of these publications and the last number issued under each title are published in the *Canadian Journal of Fisheries and Aquatic Sciences*, Volume 38: Index to Publications 1981. The current series began with Report Number 1 in January 1982.

Rapport technique canadien sur l'hydrographie et les sciences océaniques

Ces rapports contiennent des renseignements scientifiques et techniques qui constituent une contribution aux connaissances actuelles mais que l'on ne trouve pas normalement dans les revues scientifiques. Le sujet est généralement rattaché aux programmes et intérêts du service des Sciences et Levés océaniques (SLO) du ministère des Pêches et des Océans.

Les rapports techniques peuvent être considérés comme des publications à part entière. Le titre exact figure au-dessus du résumé du chaque rapport. Les résumés des rapports seront publiés dans la revue Résumés des sciences aquatiques et halieutiques et les titres figureront dans l'index annuel des publications scientifiques et techniques du Ministère.

Les rapports techniques sont produits à l'échelon régional mais sont numérotés et placés dans l'index à l'échelon national. Les demandes de rapports seront satisfaites par l'établissement auteur dont le nom figure sur la couverture et la page de titre. Les rapports épuisés seront fournis contre rétribution par des agents commerciaux.

Les établissements des Sciences et Levés océaniques dans les régions et à l'administration centrale ont cessé de publier leurs diverses séries de rapports depuis décembre 1981. Vous trouverez dans l'index des publications du volume 38 du *Journal canadien des sciences halieutiques et aquatiques*, la liste de ces publications ainsi que le dernier numéro paru dans chaque catégorie. La nouvelle série a commencé avec la publication du Rapport n° 1 en janvier 1982.

Canadian Technical Report of Hydrography and Ocean Sciences No. 97

1987

TIDAL ELEVATIONS AND TIDAL CURRENTS IN THE NORTHWEST PASSAGE

by

J.A. Stronach, J.A. Helbig and S.S. Salvador
Pacific Ocean Sciences
Burnaby, B.C.

and

H. Melling and R.A. Lake
Institute of Ocean Sciences
Sidney, B.C.

Institute of Ocean Sciences
Department of Fisheries and Oceans
Sidney, B.C.

PREFACE

This report is one of eleven pertaining to an investigation of the physical oceanography of the Canadian Arctic Archipelago. Three reports appear as volumes of the Canadian Data Report of Hydrography and Ocean Sciences No. 39, and document and present CTD measurements acquired during the three years of the project. A further three reports appear as volumes of Report No. 51 in the same series, and document and present current and tide measurements. Two contractor reports document and discuss wide-ranging CTD surveys within the Archipelago and adjacent waters in the late winters of 1982 and 1983 (Canadian Technical Report of Hydrography and Ocean Sciences Nos. 15 and 16). The present report is an overview of tidal measurements and phenomena in the Northwest Passage and is one of three attempting to synthesize present and past measurements within this vast and complex system of channels into an up-to-date description of its physical oceanography. The two companion reports discuss water masses and baroclinic structure and non-tidal residual flows respectively.

Copyright Minister of Supply and Services Canada - 1988
Cat. No. Fs 97-18/97 ISSN 0711-6764

Correct Citation for this publication:
Stronach, J.A., J.A. Helbig, S.S. Salvador, H. Melling and R.A. Lake. 1987. Tidal Elevations and Tidal Currents in the Northwest Passage. Can. Tech. Rep. Hydrogr. Ocean Sci. No. 97:346 pp.

TABLE OF CONTENTS

PREFACE . . . ii
TABLE OF CONTENTS . . . iii
LIST OF FIGURES . . . vi
ABSTRACT . . . xiv
ACKNOWLEDGEMENTS . . . xvi
PROCESSING ERRORS . . . xvii

1 INTRODUCTION . . . 1
- 1.1 GEOGRAPHY . . . 1
- 1.2 OCEANOGRAPHY, METEOROLOGY AND ICE . . . 3
- 1.3 REPORT ORGANIZATION . . . 4

2 DATA SOURCES . . . 6
- 2.1 TIDE GAUGE DATA . . . 6
- 2.2 CURRENT STATIONS . . . 7
- 2.3 THE FIELD PROGRAMMES . . . 7
- 2.4 UNITS . . . 9

3 STABILITY OF TIDAL CONSTITUENTS . . . 10
- 3.1 INFERENCE . . . 11
- 3.2 STABILITY OF TIDAL ELEVATION HARMONIC CONSTANTS . . . 20
  - 3.2.1 DIURNAL AND SEMI-DIURNAL TIDES . . . 20
  - 3.2.2 LONG PERIOD AND SHORT PERIOD TIDES . . . 22
- 3.3 STABILITY OF HARMONIC CONSTANTS FOR CURRENTS . . . 23
  - 3.3.1 BARROW STRAIT STATION 42 . . . 24
  - 3.3.2 BARROW STRAIT STATION 46 . . . 28
  - 3.3.3 PENNY STRAIT . . . 31
  - 3.3.4 AUSTIN CHANNEL . . . 36

4 SPATIAL DISTRIBUTIONS . . . 39
- 4.1 CO-RANGE AND CO-PHASE DIAGRAMS . . . 40
  - 4.1.1 PARRY CHANNEL–THE NORTHWEST PASSAGE . . . 40
  - 4.1.2 PRINCE REGENT INLET AND GULF OF BOOTHIA . . . 42
  - 4.1.3 M'CLINTOCK CHANNEL . . . 43
  - 4.1.4 PRINCE OF WALES STRAIT . . . 43
  - 4.1.5 THE QUEEN ELIZABETH ISLANDS REGION . . . 43
- 4.2 ELLIPSE PLOTS . . . 45
  - 4.2.1 PARRY CHANNEL–THE NORTHWEST PASSAGE . . . 46
    - 4.2.1.1 LANCASTER SOUND . . . 46
    - 4.2.1.2 BARROW STRAIT . . . 47
    - 4.2.1.3 VISCOUNT MELVILLE SOUND . . . 47

        4.2.1.4 M'CLURE STRAIT 48
    4.2.2 WATERWAYS ADJOINING PARRY CHANNEL 48
        4.2.2.1 WELLINGTON CHANNEL 48
        4.2.2.2 PEEL SOUND 49
        4.2.2.3 M'CLINTOCK CHANNEL 49
        4.2.2.4 AUSTIN AND BYAM MARTIN CHANNELS 50
        4.2.2.5 PRINCE OF WALES STRAIT 51
    4.2.3 THE QUEEN ELIZABETH ISLANDS REGION 51
        4.2.3.1 PENNY STRAIT 51
        4.2.3.2 MACLEAN, DESBARATS AND DANISH STRAITS 51
    4.2.4 REGIONS OF EXTREME CURRENTS 52
        4.2.4.1 PIONEER CHANNEL 53

5 VERTICAL STRUCTURE OF TIDAL CURRENTS 54
    5.1 DATA AVAILABILITY 54
    5.2 LANCASTER SOUND 55
    5.3 WELLINGTON CHANNEL 56
    5.4 BARROW STRAIT 57
        5.4.1 BARROW STRAIT STATION 46B 57
        5.4.2 BARROW STRAIT STATION 46 59
        5.4.3 BARROW STRAIT STATION 46A 60
        5.4.4 BARROW STRAIT STATION 44 61
        5.4.5 BARROW STRAIT STATION 42 62
        5.4.6 BARROW STRAIT STATION 42A 64
        5.4.7 BARROW STRAIT STATION 42B 66
    5.5 PEEL SOUND 67
        5.5.1 PEEL SOUND STATION 84 67
        5.5.2 PEEL SOUND STATION 82 68
    5.6 BARROW STRAIT WESTERN STATIONS 70
    5.7 PENNY STRAIT 73
        5.7.1 PENNY STRAIT EAST 73
        5.7.2 PENNY STRAIT WEST 74
    5.8 DANISH STRAIT 75
    5.9 AUSTIN CHANNEL 76

6 DATA INTERPRETATION 78
    6.1 A KELVIN WAVE MODEL 78
        6.1.1 PARRY CHANNEL 79
        6.1.2 GULF OF BOOTHIA 80
        6.1.3 PRINCE OF WALES STRAIT 80
        6.1.4 SUMMARY OF KELVIN WAVE MODELS 81
    6.2 VELOCITY PROFILES 81
        6.2.1 FITS TO A BAROCLINIC MODEL 82
        6.2.2 A FRICTIONALLY DETERMINED PROFILE 83

7 INERTIAL CURRENTS 84

8 REFERENCES 88

APPENDIX A : TIDAL PROPAGATION 92
  A.1 THE EXTERNAL FORCINGS 93
  A.2 TIDAL WAVES IN COASTAL SEAS 98
  A.3 POINCARE WAVES 100
  A.4 THE KELVIN WAVE 102
  A.5 BAROTROPIC WAVES IN BASINS 103

APPENDIX B : GLOBAL TIDAL MODELS 107
  B.1 COMPLICATIONS TO THE EXTERNAL FORCING TERMS 107
  B.2 THE SCHWIDERSKII MODEL 108
  B.3 DIURNAL TIDES 109
  B.4 SEMI-DIURNAL TIDES 111
  B.5 OTHER MODELS 111

APPENDIX C : TIDAL CURRENTS AND THEIR VERTICAL STRUCTURE 112
  C.1 BAROCLINIC TIDAL CURRENTS 112
  C.2 THE FRICTIONAL BOUNDARY LAYER 114

APPENDIX D : A MODIFIED POLLARD-MILLARD MODEL 119

APPENDIX E : STATION LOCATIONS 127

FIGURES 141

LIST OF FIGURES

Figure 1.1.1 The study area, comprising the major waterways of the Northwest Passage.

Figure 1.1.2 Bathymetry of the study area.

Figure 1.2.1 Vertical profile of salinity temperature and density in Barrrow Strait, from Buckingham *et al.*, (1987).

Figure 1.2.2 Cross-section of salinity values in Barrow Strait, from Buckingham *et al.* (1987)

Figure 2.1.1 Tide gauge locations.

Figure 2.2.1. Location of short and long term current meter stations.

Figure 3.1.1 Time series of the amplitude of the major semi-diurnal constituents at four stations in Prince of Wales Strait. Inference has not been used.

Figure 3.1.2. Time series of the amplitude of the major diurnal tidal constituents at four stations in Prince of Wales Strait. Inference has not been used.

Figure 3.1.3. A synthetic time series of S_2 and K_2 tides over a six month period.

Figure 3.2.1 Time series of the amplitude of the major semi-diurnal constituents at four stations in Prince of Wales Strait.

Figure 3.2.2 Time series of the phase of the major semi-diurnal constituents at four stations in Prince of Wales Strait.

Figure 3.2.3 Time series of the amplitude of the major diurnal constituents at four stations in Prince of Wales Strait.

Figure 3.2.4 Time series of the phase of the major diurnal constituents at four stations in Prince of Wales Strait.

Figure 3.2.5 Time series of the amplitude of the major diurnal and semi-diurnal constituents at stations in Barrow Strait and Penny Strait.

Figure 3.2.6 Time series of the phase of the major diurnal and semi-diurnal constituents at stations in Barrow Strait and Penny Strait.

Figure 3.2.7 Low-pass filtered sea level data for station 42 in Barrow Strait for 1984-85.

Figure 3.2.8 Time series of the amplitude of the Z_0 and MSf constituents at four stations in Prince of Wales Strait.

Figure 3.2.9 Time series of the amplitude of the M_4, MS_4 and MK_3 constituents at four stations in Prince of Wales Strait.

Figure 3.2.10 Time series of the amplitude of the MSf, M_4, MS_4 and MK_3 constituent at stations in Barrow Strait and Penny Strait.

Figure 3.3.1. Time series of the M_2 ellipse parameters (major and minor amplitudes, inclination and phase), and the rotary spectral parameters (amplitudes and phase of clockwise and counter-clockwise components) at Station 42, Barrow Strait at 51 m.

Figure 3.3.2. Time series of the M_2 ellipse parameters (major and minor amplitudes, inclination and phase), and the rotary spectral parameters (amplitudes and phase of clockwise and counter-clockwise components) at Station 42, Barrow Strait at 100 m.

Figure 3.3.3. Time series of the K_1 ellipse parameters (major and minor amplitudes, inclination and phase), and the rotary spectral parameters (amplitudes and phase of clockwise and counter-clockwise components) at Station 42, Barrow Strait at 51 m.

Figure 3.3.4. Time series of the K_1 ellipse parameters (major and minor amplitudes, inclination and phase), and the rotary spectral parameters (amplitudes and phase of clockwise and counter-clockwise components) at Station 42, Barrow Strait at 100 m.

Figure 3.3.5. Time series of the M_2 ellipse parameters (major and minor amplitudes, inclination and phase), and the rotary spectral parameters (amplitudes and phase of clockwise and counter-clockwise components) at Station 46, Barrow Strait at 25 m.

Figure 3.3.6. Time series of the M_2 ellipse parameters (major and minor amplitudes, inclination and phase), and the rotary spectral parameters (amplitudes and phase of clockwise and counter-clockwise components) at Station 46, Barrow Strait at 60 m.

Figure 3.3.7. Time series of the M_2 ellipse parameters (major and minor amplitudes, inclination and phase), and the rotary spectral parameters (amplitudes and phase of clockwise and counter-clockwise components) at Station 46, Barrow Strait at 150 m.

Figure 3.3.8. Time series of the K_1 ellipse parameters (major and minor amplitudes, inclination and phase), and the rotary spectral parameters (amplitudes and phase of clockwise and counter-clockwise components) at Station 46, Barrow Strait at 25 m.

Figure 3.3.9. Time series of the K_1 ellipse parameters (major and minor amplitudes, inclination and phase), and the rotary spectral parameters (amplitudes and phase of clockwise and counter-clockwise components) at Station 46, Barrow Strait at 60 m.

Figure 3.3.10. Time series of the K_1 ellipse parameters (major and minor amplitudes, inclination and phase), and the rotary spectral parameters (amplitudes and phase of clockwise and counter-clockwise components) at Station 46, Barrow Strait at 150 m.

Figure 3.3.11. Time series of the M_2 ellipse parameters (major and minor amplitudes, inclination and phase), and the rotary spectral parameters (amplitudes and phase of clockwise and counter-clockwise components) at Station PSE-S, Penny Strait, at 43 m.

Figure 3.3.12. Time series of the M_2 ellipse parameters (major and minor amplitudes, inclination and phase), and the rotary spectral parameters (amplitudes and phase of clockwise and counter-clockwise components) at Station PSE-D, Penny Strait, at 131 m.

Figure 3.3.13. Time series of the K_1 ellipse parameters (major and minor amplitudes, inclination and phase), and the rotary spectral parameters (amplitudes and phase of clockwise and counter-clockwise components) at Station PSE-S, Penny Strait, at 43 m.

Figure 3.3.14. Time series of the K_1 ellipse parameters (major and minor amplitudes, inclination and phase), and the rotary spectral parameters (amplitudes and phase of clockwise and counter-clockwise components) at Station PSE-D, Penny Strait, at 131 m.

Figure 3.3.15. Time series of the M_2 ellipse parameters (major and minor amplitudes, inclination and phase), and the rotary spectral parameters (amplitudes and phase of clockwise and counter-clockwise components) at Station PSW-S, Penny Strait, at 49 m.

Figure 3.3.16. Time series of the M_2 ellipse parameters (major and minor amplitudes, inclination and phase), and the rotary spectral parameters (amplitudes and phase of clockwise and counter-clockwise components) at Station PSW-D, Penny Strait, at 138 m.

Figure 3.3.17. Time series of the K_1 ellipse parameters (major and minor amplitudes, inclination and phase), and the rotary spectral parameters (amplitudes and phase of clockwise and counter-clockwise components) at Station PSW-S, Penny Strait, at 49 m.

Figure 3.3.18. Time series of the K_1 ellipse parameters (major and minor amplitudes, inclination and phase), and the rotary spectral parameters (amplitudes and phase of clockwise and counter-clockwise components) at Station PSW-D, Penny Strait, at 138 m.

Figure 3.3.19. Time series of the M_2 ellipse parameters (major and minor amplitudes, inclination and phase), and the rotary spectral parameters (amplitudes and phase of clockwise and counter-clockwise components) at Station 71, Austin Channel, at 73m

Figure 3.3.20. Time series of the M_2 ellipse parameters (major and minor amplitudes, inclination and phase), and the rotary spectral parameters (amplitudes and phase of clockwise and counter-clockwise components) at Station 71, Austin Channel, at 123 m.

Figure 3.3.21. Time series of the K_1 ellipse parameters (major and minor amplitudes, inclination and phase), and the rotary spectral parameters (amplitudes and phase of clockwise and counter-clockwise components) at Station 71, Austin Channel, at 73m

Figure 3.3.22. Time series of the K_1 ellipse parameters (major and minor amplitudes, inclination and phase), and the rotary spectral parameters (amplitudes and phase of clockwise and counter-clockwise components) at Station 71, Austin Channel, at 123 m.

Figure 4.1.1 Chart of the Arctic showing subregions used in the description of the horizontal distribution of tidal elevations.

Figure 4.1.2 Parry Channel M_2 co-phase and co-range diagram.

Figure 4.1.3 Parry Channel S_2 co-phase and co-range diagram.

Figure 4.1.4 Parry Channel K_1 co-phase and co-range diagram.

Figure 4.1.5 Parry Channel O_1 co-phase and co-range diagram.

Figure 4.1.6 Parry Channel MSf co-phase and co-range diagram.

Figure 4.1.7 Parry Channel MK_3 co-phase and co-range diagram.

Figure 4.1.8 Parry Channel phase age.

Figure 4.1.9 Parry Channel tidal character.

Figure 4.1.10 Prince Regent Inlet / Gulf of Boothia M_2 co-phase and co-range diagram.

Figure 4.1.11 Prince Regent Inlet / Gulf of Boothia N_2 co-phase and co-range diagram.

Figure 4.1.12 Prince Regent Inlet / Gulf of Boothia K_1 co-phase and co-range diagram.

Figure 4.1.13 Prince Regent Inlet / Gulf of Boothia phase age.

Figure 4.1.14 Prince Regent Inlet / Gulf of Boothia tidal character.
Figure 4.1.15 M'Clintock Channel M_2 co-phase and co-range diagram.
Figure 4.1.16 M'Clintock Channel K_1 co-phase and co-range diagram.
Figure 4.1.17 M'Clintock Channel phase age.
Figure 4.1.18 M'Clintock Channel tidal character.
Figure 4.1.19 Prince of Wales Strait M_2 co-phase and co-range diagram.
Figure 4.1.20 Prince of Wales Strait K_1 co-phase and co-range diagram.
Figure 4.1.21 Prince of Wales Strait O_1 co-phase and co-range diagram.
Figure 4.1.22 Prince of Wales Strait phase age.
Figure 4.1.23 Prince of Wales Strait tidal character.
Figure 4.1.24 Queen Elizabeth Island Region M_2 co-phase and co-range diagram.
Figure 4.1.25 Queen Elizabeth Island Region K_1 co-phase and co-range diagram.
Figure 4.1.26 Queen Elizabeth Island Region phase age.
Figure 4.1.27 Queen Elizabeth Island Region tidal character.
Figure 4.2.1 Definition of ellipse parameters.
Figure 4.2.2 Chart of the Arctic showing subregions used in the description of the horizontal distribution of tidal currents.
Figure 4.2.3. Lancaster Sound current meter stations.
Figure 4.2.4. Lancaster Sound M_2 current ellipses.
Figure 4.2.5. Lancaster Sound S_2 current ellipses.
Figure 4.2.6. Lancaster Sound K_1 current ellipses.
Figure 4.2.7. Lancaster Sound O_1 current ellipses.
Figure 4.2.8. Lancaster Sound Mf current ellipses.
Figure 4.2.9. Barrow Strait current meter stations.
Figure 4.2.10. Barrow Strait M_2 current ellipses.
Figure 4.2.11. Barrow Strait S_2 current ellipses.
Figure 4.2.12. Barrow Strait K_1 current ellipses.
Figure 4.2.13. Barrow Strait O_1 current ellipses.
Figure 4.2.14. Eastern Viscount Melville Sound current meter stations.
Figure 4.2.15. Western Viscount Melville Sound current meter stations.
Figure 4.2.16. Eastern Viscount Melville Sound M_2 current ellipses.
Figure 4.2.17. Eastern Viscount Melville Sound S_2 current ellipses.
Figure 4.2.18. Western Viscount Melville Sound M_2 current ellipses.
Figure 4.2.19. Western Viscount Melville Sound S_2 current ellipses.
Figure 4.2.20. Eastern Viscount Melville Sound K_1 current ellipses.
Figure 4.2.21. Eastern Viscount Melville Sound O_1 current ellipses.

Figure 4.2.22. Western Viscount Melville Sound K_1 current ellipses.
Figure 4.2.23. Western Viscount Melville Sound O_1 current ellipses.
Figure 4.2.24. Western Viscount Melville Sound Mf current ellipses.
Figure 4.2.25. M'Clure Strait current meter stations.
Figure 4.2.26. M'Clure Strait M_2 current ellipses.
Figure 4.2.27. M'Clure Strait S_2 current ellipses.
Figure 4.2.28. M'Clure Strait K_1 current ellipses.
Figure 4.2.29. M'Clure Strait O_1 current ellipses.
Figure 4.2.30. Wellington Channel current meter stations.
Figure 4.2.31. Wellington Channel M_2 current ellipses.
Figure 4.2.32. Wellington Channel S_2 current ellipses.
Figure 4.2.33. Wellington Channel K_1 current ellipses.
Figure 4.2.34. Wellington Channel O_1 current ellipses.
Figure 4.2.35. (Unused)
Figure 4.2.36. Peel Sound current meter stations.
Figure 4.2.37. Peel Sound M_2 current ellipses.
Figure 4.2.38. Peel Sound S_2 current ellipses.
Figure 4.2.39. Peel Sound K_1 current ellipses.
Figure 4.2.40. Peel Sound O_1 current ellipses.
Figure 4.2.41. M'Clintock Channel current meter stations.
Figure 4.2.42. M'Clintock Channel M_2 current ellipses.
Figure 4.2.43. M'Clintock Channel S_2 current ellipses.
Figure 4.2.44. M'Clintock Channel K_1 current ellipses.
Figure 4.2.45. M'Clintock Channel O_1 current ellipses.
Figure 4.2.46. Austin Channel current meter stations.
Figure 4.2.47. Byam Martin Channel current meter stations.
Figure 4.2.48. Austin Channel M_2 current ellipses.
Figure 4.2.49. Austin Channel S_2 current ellipses.
Figure 4.2.50. Byam Martin Channel M_2 current ellipses.
Figure 4.2.51. Byam Martin Channel S_2 current ellipses.
Figure 4.2.52. Austin Channel K_1 current ellipses.
Figure 4.2.53. Austin Channel O_1 current ellipses.
Figure 4.2.54. Byam Martin Channel K_1 current ellipses.
Figure 4.2.55. Byam Martin Channel O_1 current ellipses.
Figure 4.2.56. Prince of Wales Strait current meter stations.
Figure 4.2.57. Prince of Wales Strait M_2 current ellipses.

Figure 4.2.58. Prince of Wales Strait S_2 current ellipses.

Figure 4.2.59. Prince of Wales Strait K_1 current ellipses.

Figure 4.2.60. Prince of Wales Strait O_1 current ellipses.

Figure 4.2.61. Penny Strait current meter stations.

Figure 4.2.62. Penny Strait M_2 current ellipses.

Figure 4.2.63. Penny Strait S_2 current ellipses.

Figure 4.2.64. Penny Strait K_1 current ellipses.

Figure 4.2.65. Penny Strait O_1 current ellipses.

Figure 4.2.66. Maclean / Desbarats / Danish Channel current meter stations.

Figure 4.2.67. Maclean / Desbarats / Danish Channel M_2 current ellipses.

Figure 4.2.68. Maclean / Desbarats / Danish Channel S_2 current ellipses.

Figure 4.2.69. Maclean / Desbarats / Danish Channel K_1 current ellipses.

Figure 4.2.70. Maclean / Desbarats / Danish Channel O_1 current ellipses.

Figure 4.2.71. Pioneer Channel current meter stations.

Figure 4.2.72. Pioneer Channel M_2 current ellipses.

Figure 4.2.73. Pioneer Channel S_2 current ellipses.

Figure 4.2.74. Pioneer Channel K_1 current ellipses.

Figure 4.2.75. Pioneer Channel O_1 current ellipses.

Figure 5.4.1 Vertical profile of the Amplitude of the M2 Counterclockwise component in Barrow Strait.

Figure 5.4.2 Vertical profile of the Amplitude of the M2 Clockwise component in Barrow Strait.

Figure 5.4.3 Vertical profile of the Amplitude of the K1 Counterclockwise component in Barrow Strait.

Figure 5.4.4 Vertical profile of the Amplitude of the K1 Clockwise component in Barrow Strait.

Figure 5.5.1 Vertical profile of the Amplitude of the M2 Counterclockwise component in Peel Sound.

Figure 5.5.2 Vertical profile of the Amplitude of the M2 Clockwise component in Peel Sound.

Figure 5.5.3 Vertical profile of the Amplitude of the K1 Counterclockwise component in Peel Sound.

Figure 5.5.4 Vertical profile of the Amplitude of the K1 Clockwise component in Peel Sound.

Figure 6.1.1 The Kelvin wave model for the M2 tide in Parry Channel.

Figure 6.1.2 The Kelvin wave model for the K1 tide in Parry Channel.

Figure 6.1.3. The Kelvin wave model for the M2 tide in the Gulf of Boothia system.

Figure 6.1.4. The Kelvin wave model for the K1 tide in the Gulf of Boothia system.

Figure 6.1.5. The Kelvin wave model for the M2 tide in Prince of Wales Strait.

Figure 6.2.1. The vertical profile of density and Brunt-Väisälä frequency at a station in Barrow Strait.

Figure 6.2.2. The barotropic and first two baroclinic modes corresponding to the density profile of Figure 6.2.1.

Figure 6.2.3. The fitted profile of clockwise amplitudes of the M2 currents at station 46B, and the observed data for Barrow Strait. Barotropic and second baroclinic modes were used.

Figure 6.2.4. The fitted profile of clockwise amplitudes of the M2 currents at station 46B, and the observed data for Barrow Strait. Barotropic and first and second baroclinic modes were used.

Figure 6.2.5. The fitted profile of clockwise amplitudes of the M2 currents at station 46B, and the observed data for Barrow Strait. An Ekman boundary layer model was used, eddy viscosity of 10 cm^2/s in the top layer, 50 cm^2/s in the bottom.

Figure 6.2.6. The fitted profile of counterclockwise amplitudes of the M2 currents at station 46B, and the observed data for Barrow Strait. An Ekman boundary layer model was used, eddy viscosity of 10 cm^2/s in the top layer, 50 cm^2/s in the bottom.

Figure 7.1. Inertial current model response to forcing by Resolute Bay winds for the 1000 hour period beginning 20 Sept. 1984. The mixed layer depth is 20 m and the frictional decay time is 5 days. The lowest panel shows the east-west velocity component; the heavy line denotes the low-passed signal. The uppermost panel depicts the windstress magnitude in the inertial band (positive and negative frequencies).

Figure 7.2 Resolute Bay windstress magnitude (in Pascals) during 1983-84.

Figure 7.3 Resolute Bay windstress magnitude (in Pascals) during 1984-85.

Figure 7.4 East-west component of the observed clockwise inertial band currents at PSW-S.

Figure 7.5 East-west component of the clockwise residual inertial band currents at PSW-S.

Figure 7.6 Clockwise and anticlockwise residual inertial band current magnitudes at PSW-S.

Figure A.1. The lunar part of the astronomical tidal potential.

Figure A.2. The wave numbers for an incident and reflected Poincaré wave.

Figure A.3. A schematic diagram of tidal waves in a channel open at one end.

Figure A.4. The envelope of tidal amplitudes for a model of the Irish Sea (From Taylor, 1920).

Figure A.5. Tidal current ellipse patterns for a model of the Irish Sea (From Taylor, 1920).

Figure A.6. Taylor's ellipse diagram for the Irish Sea, decomposed into separate Kelvin and Poincaré wave parts.

Figure A.7. The change in the amphidromic pattern as the reflected wave is successively reduced in amplitude (From Hendershott and Speranza, 1971).

Figure B.1. Base map of the Arctic Ocean.

Figure B.2. Amplitude contours of the K1 tide in the Arctic Ocean, as calculated by Schwiderski.

Figure B.3. Phase contours of the K1 tide in the Arctic Ocean, as calculated by Schwiderski.

Figure B.4. Amplitude contours of the O1 tide in the Arctic Ocean, as calculated by Schwiderski.

Figure B.5. Phase contours of the O1 tide in the Arctic Ocean, as calculated by Schwiderski.

Figure B.6. Amplitude contours of the P1 tide in the Arctic Ocean, as calculated by Schwiderski.

Figure B.7. Phase contours of the P1 tide in the Arctic Ocean, as calculated by Schwiderski.

Figure B.8. Amplitude contours of the M2 tide in the Arctic Ocean, as calculated by Schwiderski.

Figure B.9. Phase contours of the M2 tide in the Arctic Ocean, as calculated by Schwiderski.

Figure B.10. Amplitude contours of the S2 tide in the Arctic Ocean, as calculated by Schwiderski.

Figure B.11. Phase contours of the S2 tide in the Arctic Ocean, as calculated by Schwiderski.

Figure B.12. Amplitude contours of the N2 tide in the Arctic Ocean, as calculated by Schwiderski.

Figure B.13. Phase contours of the N2 tide in the Arctic Ocean, as calculated by Schwiderski.

Figure D.1. Schematic illustration of the modified Pollard-Millard model.

Figure D.2 Real part of (1) the upper layer impulse response function (light curve) and (2) the lower layer impulse response function (heavy line), both normalized by $r_1 h_1$.

Figure D.3 The 1984 windstress spectrum for Resolute Bay, the baroclinic gain (heavy line), and the predicted upper layer current spectrum (dotted line) normalized to one.

ABSTRACT

Stronach, J.A., J.A. Helbig, S.S. Salvador, H. Melling and R.A. Lake. 1987.
Tidal Elevations and Tidal Currents in the Northwest Passage. Can. Tech. Rep. Hydrogr. Ocean Sci. No. 97:346 pp.

All the existing data on tidal heights and tidal currents within the Northwest Passage and adjacent waterways to the north and south are presented as a summary of tidal phenomena in the Canadian Arctic Archipelago. The temporal stability of tidal constituents is investigated through examination of available year-long tide and current records, and the vertical consistency is documented for those few sites where currents have been measured simultaneously at several depths. Tidal height variations are summarized on regional maps of co-range and co-phase, and tidal current variations on maps displaying tidal ellipses. These maps are discussed in terms of Kelvin-wave theory, and the observed propagation patterns are modelled for the principal constituents channels using simplified channel geometries. Variations in tidal currents with both depth and time are strongest in the semi-diurnal band and for the clockwise rotary component. Explanations for the vertical structure are presented based on internal tide and frictional models., The presence of the inertial frequency in the semi-diurnal band plays an important role in both explanations. Temporal variations are discussed with reference to contamination by internal tides or by inertial waves. Tidal phenomena in the Northwest Passage are placed in a north polar context through review of tidal variations in the Arctic Ocean.

Key Words: tide, Northwest Passage, Arctic, inertial.

SOMMAIRE

Stronach, J.A., J.A. Helbig, S.S. Salvador, H. Melling and R.A. Lake. 1987.
Tidal Elevations and Tidal Currents in the Northwest Passage. Can. Tech. Rep. Hydrogr. Ocean Sci. No. 97:346 pp.

Les auteurs présentent, sous la forme d'un résumé des phénomènes cotidaux dans l'archipel arctique canadien, l'ensemble des données actuelles sur la hauteur des marées et les courants de marée dans le passage du Nord-Ouest et les voies d'eau voisines situees au nord et au sud. La stabilité temporelle des constituants cotidaux est traitée par un examen des enrigestrements, d'une durée d'une année, des marées et courants disponibles. Ils présentent aussi des données sur la constance verticale des courants de marée dans les rares endroits oû ils ont été déterminés simultanément en plusiers profondeurs. Les variations de hauteur des marées sont résumées sur

des cartes régionales d'isoamplitudes et d'isophases, et les variations de courants cotidaux sur des cartes d'ellipses de marée. Les auteurs traitent de ces cartes dans le contexte de la théorie des ondes de Kelvin et modélisent les régimes de propagation observés dans le cas des principaux chenaux dont la géométrie a été simplifiée. Les varitations en fonction de la profonduer et du temps des courants de marée sont les plus élevées dans la bande semi-diurne et pour la composante de rotation vers la droite. Les auteurs expliquet leur structure verticale a l'aide de modèles de marée interne et de frottement. Les deux explications donneés reposent en grande partie sur l'existence d'une fréquence d'inertie au sein de la bande semi-diurne. Les auteurs traitent des variations temporelles en faisant référence à la contamination par des marées internes ou des ondes d'inertie. Les phénomènes cotidaux du passage du Nord-Ouest sont placés dans le contexte général de la zone polaire nord de par un examen des variations des marées dans l'océan Arctique.

Mots clés: marée, passage diiu Nord-Ouest, Arctique, inertie.

ACKNOWLEDGMENTS

The effort expended on the Northwest Passage Oceanography Program since its inception 5 years ago is considerable, and the number of people and organizations who have contributed to its success is correspondingly large. Without detailing their specific contributions, our appreciation is extended to the following: Syd Moorhouse, Denny Richards, John MacNeill, Gary Moonie, Bob Sudar, Ron Cooke, Paul Johnson, Al Koppel, Andrew Wharton, Bill Green, Jeff Richards, Lyn Lewis and Ron Perkin, all of the Arctic Group within the Physics Division at the Institute of Ocean Sciences; David Fissel, David Lemon, Rick Birch and Doug Knight of Arctic Sciences Ltd.; Simon Prinsenberg and Bert Bennett, formerly of the Bayfield Laboratory for Marine Science and Surveys, Burlington, Ontario; George Hobson and the staff of the Polar Continental Shelf Project, Energy, Mines and Resources, Canada; Dick MacDougall of the Canadian Hydrographic Service; Pan Arctic Oils Ltd.; Bradley Air Services Ltd.; Quasar Helicopters Ltd.

In respect of particular contributions to this report the authors wish to thank Bill Buckingham of the Institute of Ocean Sciences for his painstaking and careful work in processing and documenting the current meter and tide gauge data. We thank S. Prinsenberg, F.S. Stephenson and D.A. St. Jacques for freely providing their data. We thank F.E. Stephenson also for reviewing the manuscript, and L.S.C. Thomson for technical editing.

Funding was provided by the Marine Transportation Research and Development Programme (Transport Canada), and support in kind by the Department of Fisheries and Oceans and by the Polar Continental Shelf Project of the Department of Energy, Mines and Resources.

PROCESSING ERRORS

The versions of the calibrated current records used to produce the time series plots appearing in the three volumes of the Canadian Data Report of Hydrography and Ocean Sciences No. 51, and used in the preparation of this overview report contain some errors. These were discovered subsequent to the use of these files. The records involved, and the corrections to the 'old' calibrated files (and derived parameters) necessary to convert them to the new versions of the calibrated data are as follows:

YEAR	S/N	SITE:DEPTH	NECESSARY CORRECTION
NWP83	1936	CM58:18.5m	Add 60 degrees to 'old directions'
NWP83	1939	CM57:18.5m	Add 15 degrees to 'old directions'
NWP83	3387	CM65:18.5m	Add 67 degrees to 'old directions'
NWP83	5456	CM83:18.5m	Add -45 degrees to 'old directions'
NWP84	0217	WC13:18.5m	Add -78 degrees to 'old directions'
NWP84	0218	WC12:18.5m	Add -116 degrees to 'old directions'
NWP84	5471	PS02:138.m	Add -80 degrees to 'old directions'

1 INTRODUCTION

The "Northwest Passage" has figured in maritime activity and politics since the days of Queen Elizabeth I, when it was thought that not only did such a route to the riches of the Orient exist, but that it would be commercially viable, in competition with the activities of Spain to the south. Over the succeeding centuries, vast amounts of time, money and lives have been expended in the search for this route, as well as for the economic and military benefits perceived to accrue to the nation controlling the Northwest Passage. Much of this history is recorded in the geographic names attached to the region - Hudson, Frobisher, Parry, Beaufort and Larsen. (Sailing Directions - Arctic Canada, 1982 provides a concise summary of the history of exploration in the region). Even today, the region is one of considerable interest from both a political and an economic point of view, constituting an ice-covered connection between the Atlantic, Pacific and Arctic Oceans.

This report concerns itself with tidal propagation in the Northwest Passage and adjacent waterways. The impetus for the report is two-fold. First, the Northwest Passage is a region of potentially increasing marine traffic, and, in support of that activity, various agencies have, in the past five years, increased their current and water level measurement programs in the region. Notable are the Northwest Passage field programs carried out by the Institute of Ocean Sciences (NWP82, NWP83, NWP84 and NWP85) which have added an immense amount of information to the existing data base of tidal and current measurements in the Northwest Passage. As well, the Bayfield Marine Laboratory (Burlington, Ontario) has carried out intensive measurements in Barrow Strait region, and some of the waterways leading off of the Northwest Passage. It is thus appropriate to assemble these various measurements (as well as other relevant measurements) into a compact report summarizing what is known about tides in the region.

1.1 GEOGRAPHY

Figure 1.1.1 is a base map of the region, showing major place names used in this report. The major waterway of the Northwest Passage is Parry Channel, which in turn consists of four bodies of water: M'Clure Strait, Viscount Melville Sound, Barrow Strait and Lancaster Sound. Each segment is about 300 km long, and varies between 80 and 160 km in width.

The geometry of the Northwest Passage is quite complicated; the bounding walls can be viewed as a collection of islands, separating the assortment of channels and water bodies which lead off Parry Channel. The regional bathymetry is illustrated in Figure 1.1.2 (Figure 1.1.1 is to be used for location names). The eastern entrance to the Northwest Passage is through Baffin Bay, a deep oceanic basin with depths extending to 2400 metres. At the entrance to Lancaster Sound, water depths have shoaled to about 800 m. Along Lancaster Sound, depths shoal to the west, until, as Lancaster Sound joins Barrow Strait, they attain values of less than 200 m. Barrow

Strait has a sill depth (minimum depth) of 125 m. Proceeding further west, depths in Viscount Melville Sound are between 500 and 200 m, and M'Clure Strait is typically 400 m to 440 m deep.

Along the southern shore, and proceeding from east to west, the major channels and embayments abutting on Parry Channel are as follows. Admiralty Inlet is a major indentation in Baffin Island - 20 km wide, 200 km long and with depths varying from 200 to 700 m. Next is the combination of Prince Regent Inlet, the Gulf of Boothia and Committee Bay. Each component is between 250 and 300 km long; Prince Regent Inlet is about 80 km wide while Boothia and Committee Bay are somewhat wider (120-200 km), although the overall system is considerably longer than it is wide. Depths vary between 400 and 200 m in Prince Regent Inlet which shoals to the south as it merges into the Gulf of Boothia; depths continue to decrease in Boothia until they are less than 100 m in Committee Bay. (Note however that Committee Bay has yet to be surveyed adequately).

The next major waterway to the west is M'Clintock Channel which is about 120 km wide and extends south from Viscount Melville Sound for 800 km. Peel Sound is a narrow channel connecting the middle of M'CLintock Channel back to Barrow Strait. At its southern end, M'Clintock Channel connects around the south of Victoria Island to Amundsen Gulf and the Beaufort Sea. The most western waterway leading off to the south is Prince of Wales Strait, which separates Banks Island from Victoria Island. It is only 20 km wide, and about 250 km long. Depths are quite variable, typically over 100 m, but shoaling to 35 m.

The above channels connect the Northwest Passage southward to the mainland of Arctic Canada. The channels leading off the north connect the Northwest Passage to the islands to the north: the Queen Elizabeth Islands, the Parry Islands and the Sverdrup Islands, and eventually to the Arctic Ocean. Some of these passages are of navigational importance, because of the mineral wealth on some of the northern islands. The major waterways are as follows.

Wellington Channel passes between Devon Island and Cornwall Island. Depths range from 100 to 200 m. At its northern end, the depth field becomes very irregular, as it merges into Penny Strait. The geometry and bathymetry in this region are quite complex, and likely lead to less systematic tidal propagation. The next major channel to the north is Austin Channel, with Bathurst Island on the east and the pair Byam Island and Melville Island on the west. This channel merges into Byam Martin Channel. Penny Strait and Byam Martin Channel lead into a complex of waterways separating the various islands to the north, of which Norwegian Bay is the easternmost.

As is clear from the above description of the geography and bathymetry of the Northern Passage, the region is characterized by the large number of islands and channels. The bottom bathymetry is seen to be equally complicated, so one can anticipate a similar complexity in the tides.

1.2 OCEANOGRAPHY, METEOROLOGY AND ICE

Tidal phenomena are driven by the extremely predictable motion of the sun and moon. One thus expects a high degree of predictability in tidal water levels and currents, after non-tidal phenomena are filtered out mathematically. However, even if the forcing of a physical system is periodic and regular, the response may vary due to changes in the intrinsic properties of the system. As well, there may be other non-tidal phenomena which occur at tidal frequencies, and standard analysis procedures may not be able to differentiate between the two. Processes which can change the intrinsic properties of the system are such things as changes in water density or ice cover. Processes which can mask tidal phenomena are such things as diurnally-varying wind patterns. Thus, we must examine the physical oceanography and meteorology of the region.

The first and foremost meteorological fact is that the region is very cold. Not only is the amount of incident sunlight small, but the whiteness of snow and ice lead to a high reflection of incident energy. Thus, there is very little seasonal warming of the water due to direct solar influence. Not only is the sunlight very weak, but the length of day is variable, ranging from almost continuous daylight to almost continuous darkness throughout a yearly period. As well, there is a major seasonal effect due to the annual cycle of ice formation and melting. During these freezing and melting processes, the water remains in near-equilibrium with ice, so that the temperature remains reasonably uniform in the upper 25 - 50 m. However, as the ice grows, it excludes salt, and as it melts, it dilutes the saline underlying water. Thus, there is a large seasonal cycle in salinity, as well as a substantial vertical gradient of salinity and density at some times.

The dominant wind direction is from the west, but this is not a region of persistent strong winds. The resulting mean drift is to the east, with mean water currents of order 10 cm/s. Since the Beaufort Sea and Arctic Ocean act as a source of ice, the mean drift results in a situation where ice may be carried out of the eastern part of the Northwest Passage, but not the western part. Thus, there is considerable interest in the bypass provided by such routes as M'Clintock Channel and Prince of Wales Strait. The ice is generally solid from about December to late July in the western portion. Only during the summer months is the ice cover sufficiently loose that navigation is possible.

Although this report is primarily concerned with tidal phenomena rather than physical oceanography, it is worthwhile to examine a vertical hydrographic profile in Barrow Strait, as well as a salinity section across the Strait. Figure 1.2.1 is a vertical profile of temperature, salinity and density taken in the middle of Barrow Strait in April 1985 (Buckingham, Lake and Melling, 1987a). It is apparent that the major factor controlling the vertical density structure is the vertical salinity structure, with temperature playing a minor role. We also note the occurrence of considerably fresher water immediately under the ice pack. A cross-section of temperature, salinity, density and geostrophic currents is informative. Figure 1.2.2 is taken from Brooks (1982,unpublished manuscript), and is a section across Barrow Strait, for a similar time of year as Figure 1.2.2. The striking feature is the organization of the density field so that lighter water favors the southern shore. Recall that the mean drift here is eastward, so the usual geostrophic rule of "lighter water on the right" applies. Along channel currents, calculated based on the measured density distribution vary between 2.5 and 12.5 cm/s, and are typically between 5 and 7.5 cm/s.

1.3 REPORT ORGANIZATION

This report must examine a number of factors related to tidal effects, and is aimed at a fairly wide audience. Thus, some of the more technical parts are relegated to Appendices, while the body of the report contains the more descriptive features. Appendix A discusses barotropic tidal wave propagation, particularly Kelvin and Poincaré waves. Appendix B illustrates the nature of global tidal propagation in waters north of 65 degrees latitude, to provide the appropriate framework in which to view the Northwest Passage as a minor shunt between the two major bodies of water, Baffin Bay and the Arctic Ocean. Appendix C provides the theoretical framework with which to examine the complexities of tidal currents: vertical modes, as determined by frictional effects and internal tide (baroclinic) effects. Appendix D discusses the non-tidal phenomena of inertial currents, which are of potential significance in the semi-diurnal tidal band. Appendix E provides a list of the stations used in this report.

We begin in Chapter 2 to examine the various field programs which provided data for the report.

Next, in Chapter 3, we examine the time-series nature of the tide, primarily by examining the harmonic constants from a number of one-year installations, analyzed as a sequence of 12 one-month data sets. That is, at a particular water level station, we examine the seasonal aspects of the tide, with a view to establishing how representative is the remainder of the data, which is based on 1 to 3-month records. As well, there will emerge some speculation concerning how the dynamics of the system is inferred to change through the course of the season. At the conclusion of Chapter 3, we try to establish the reliability of using harmonic constants from a one-month record to predict tidal elevations.

Chapter 4 examines the spatial patterns of the tide. The classical approaches are to plot co-range and co-phase diagrams for tidal elevations, and to plot ellipses for the tidal streams. These are the two most informative plots, and so we present them for the various sub-regions of the Northwest Passage.

Chapter 5 focuses on the vertical variability of tidal currents. There are a number of stations where more than one current meter was moored on a vertical line, so the vertical variation of currents can be examined, and links to internal waves and frictional effects can be inferred.

Chapter 6 combines various pieces of the theory presented in the Appendices with the data presented in Chapters 3, 4 and 5 to arrive at a conceptual model of tidal propagation in the Northwest Passage. Such things as amplitude and phase of the incident and reflected Kelvin waves in the system, energy flux, and Stokes drift are examined. As well, we attempt to understand the nature of the horizontal, vertical and temporal variations in the tidal streams.

Chapter 7 summarizes the analysis of year-long current meter records for inertial currents. The results are primarily negative as the inertial energy was always small. However, this does not preclude the potential importance of inertial currents in the upper mixed layers, as the current meters were all moored well below the pycnocline.

Chapter 8 provides a brief summary of the report, and points to the aspects of the tide which need further clarification.

2 DATA SOURCES

The data used in this report are obtained from various Canadian government agencies which have installed tide gauges and current meters over the period from 1977 to 1985 - the Ocean Physics Division at the Institute of Ocean Sciences, Sidney, B.C., the Canadian Hydrographic Service (Sidney, B.C.) the Arctic Oceanographic Group at the Bayfield Laboratory, Burlington, Ontario, and the Canadian Hydrographic Service (Burlington, Ontario). The major intensive measurements, in terms of year-long mooring of current meters and tide gauges, was carried out by the Institute of Ocean Sciences under projects known as Northwest Passage 82, Northwest Passage 83 and Northwest Passage 84 (NWP82, NWP83, and NWP84). As well, the Burlington Group maintained and recovered a few year-long moorings from Barrow Strait. The Canadian Hydrographic Service has maintained a few year-long tide gauges in the Arctic, as well as several shorter term stations. Attention was concentrated on the Northwest Passage, so some data from the very northern extremities of the Canadian Arctic, as well as data in the regions immediately adjacent to the Northwest Territories have not been incorporated in this report.

2.1 TIDE GAUGE DATA

Figure 2.1.1 illustrates the locations of tide gauge data used in the preparation of this report. Station names in general correspond to the various cited data reports, although there may be some discrepancies as only provisional names were available in some cases for this report. Table E.1 in Appendix E supplies a list of the station locations, and the date range over which the gauge provided the data used in this report.

At all of the sites a minimum one month record was available for analysis. In addition, longer term records were available from certain sites. These data were essential in carrying out the inference calculations, described later in the report. The long-term gauges are listed in Table 2.1.1.

TABLE 2.1.1

LONG-TERM WATER LEVEL STATIONS

STATION	SOURCE
87,89,92,93	NWP 82
42, FSRG	NWP 84
3757,3920,4140 4205,5275,5560 6150,6210,6240 6290,6360,6424 6485,6955	Standard stations previously or presently maintained by the Canadian Hydrographic Service

2.2 CURRENT STATIONS

Current meters were generally situated to define currents across a cross-section of a channel, particularly in the NWP82, NWP83 and NWP84 programs, and in the Bayfield studies of Barrow Strait. The data used in this study are summarized in Table E.2, and in Figure 2.2.1. There is considerable duplication of station names, so that references to a particular station will often have to include the water body in which the station is located.

Certain of the above stations involved moorings which were in place for as long as a year. These long term stations are listed in Table 2.2.2.

TABLE 2.2.2

LONG TERM TIDAL CURRENT STATIONS

STATION	SOURCE
42	Frozen Sea Research Group NWP84
PSE	Penny Strait East NWP84
PSW	Penny Strait West NWP84
71	Frozen Sea Research Group NWP84

2.3 THE FIELD PROGRAMS

The bulk of the data comes from two ongoing studies of tides in the Arctic - the Institute of Ocean Sciences Northwest Passage studies, extending from 1982 to 1985, and the programs carried out by staff of the Bayfield Marine Laboratory from 1976 to 1983. The NWP series of measurements covered much of the region with a series of 3-month moorings, as well as 5 year-long moorings in the Barrow Strait-Wellington Channel region. We will describe these programs separately but briefly.

NWP82

This program involved mooring 10 current meters in Prince of Wales Strait for 3 months (covering approximately the period from April to June), 7 meters across Viscount Melville Sound (unfortunately, the meter in the centre of the channel did not produce data) and 7 meters across M'Clure Strait. In general, from the tidal point of view, one would say that these sections were quite densely covered with stations. As well, at the two ends of each section, water level recorders were installed. Not only do these water level recorders add to the knowledge of the spatial distribution of the tide, but in conjunction with the current meter data, they allow one to infer a considerable amount about the propagation properties of the tide: the energy flux across each section, and the relative strengths of the standing wave to propagating wave.

The current meters were all moored at about 20 m depth below the ice, thus they are likely out of the region of direct boundary effects associated with the ice cover.

In addition, 4 water level recorders were maintained for a one year period, all in Prince of Wales Strait. Instruments 89 and 93 were located in the same place (Banks Island, opposite current meter 1), station 87 was located on the opposite shore of Prince of Wales Strait on Victoria Island, and station 92 was located in Jesse Harbour on Banks Island. Details of this field program are contained in Buckingham, Lake and Melling (1987b).

NWP83

This field program was similar to NWP82, except that the region of interest shifted further east. Now the interest lay in the channels leading away from the Northwest Passage: M'Clintock Channel to the south and the combination of Austin Channel and Byam Martin Channel to the north. Thus, a line of 5 meters (of which 4 produced data) was laid across M'Clintock Channel, 5 across Byam Martin Channel, one meter in Austin Channel, and six in Viscount Melville Sound (57, 58, 74, 72 and 78, 81). Fewer water level recorders were available, and no long-term stations for water level were successful. However, the mooring in Austin Channel, station 71, was maintained for a one year period. Details are contained in Buckingham, Lake and Melling(1987c).

NWP84

Interest shifted further east again, to Barrow Strait (stations 42 and 46), Wellington Channel (stations 1 - 14) and to Penny Strait. Year long water levels in Barrow Strait and Penny Strait were obtained, as well as year long subsurface current measurements in Barrow Strait and Penny Strait. These year long records are very important in establishing the seasonal variability of the tidal constituents, as well as the seasonal changes in low frequency motions and water levels. Details of the field program are described in Buckingham, Lake and Melling (1987d).

The Bayfield Studies

The Bayfield Laboratory for Marine Science and Surveys (Canadian Hydrographic Service and the Arctic Oceanographic Group) carried out similar studies, extending from 1976 to the present. Each of these is reported in a separate manuscript report. See Sandilands, Solvason and St. Jacques (1985a,1985b,1985c, 1985d) and St. Jacques,Sandilands and Solvason (1985) for details, plus further Barrow Strait reports yet to appear in final form.

Other studies contributed to this report. The most important is probably the three current meters moored at the eastern end of Lancaster Sound by Arctic Sciences Ltd. as these meters provide essential information on the eastern boundary of the tidal propagation.

2.4 UNITS

It is appropriate to mention the unit conventions used in this report. Tidal elevations are expressed in centimetres, currents in centimetres per second, and water depths in metres. Horizontal distances are expressed in kilometres. Tidal phases are expressed in degrees, as Greenwich phases. Thus, phases are expressed relative to a single time zone, allowing one to view contoured phase diagrams, for instance, as a snapshot of the instantaneous phase of the tide over the entire region.

As well, tidal measurements used in this report were exclusively obtained using bottom-located pressure sensors. Consequently, the water levels reported are contaminated to a certain extent by atmospheric-pressure fluctuations, and steric effects. These effects are not large, the annual cycle of sea level pressure at Resolute corresponding to a range of 10 cm of water. Daily fluctuations are much smaller. Thus, longer period sea level oscillations (*e.g.* annual) would be somewhat contaminated by atmospheric effects, but semi-diurnal and diurnal tides negligibly contaminated.

3 STABILITY OF TIDAL CONSTITUENTS

Water levels and associated currents are driven by a number of forces, of which tidal forcing is usually the most important, and is certainly the most predictable, depending solely on the highly predictable motions of the sun and moon with respect to the earth. A key assumption in tidal analysis and prediction is that tidal water levels and associated streams may be mathematically separated from other effects, because they occur at a fixed set of frequencies. Thus, a time series of water levels or streams may be harmonically analyzed, producing a set of amplitudes and phases corresponding to the known forcing frequencies. Further, it is assumed that the parameters describing the physical response of the system are constant in time. Thus, the physical system's response is stationary, so that the harmonic constants remain the same from one month to the next, and from year to year. Non-linear interactions are recognized as being present, and are dealt with by adding to the set of standard astronomical frequencies the sum and difference frequencies corresponding to all reasonable interactions.

If the physical system is not stationary, *e.g.* if ice cover changes the inertial or frictional properties of the system, then the prediction of water levels and currents is considerably more complicated. For instance, the harmonic constants appropriate for summer and winter may differ.

The assumption that there are no other forcing mechanisms at or near the selected tidal frequencies is not exactly true. The amplitudes and phases produced by a tidal analysis are a mixture of tide and possibly other things, and we may not be sure what is really predictable from these constants, and what is likely to be different and unpredictable from one month to the next. It is an interesting fact that harmonic analysis is not energy conserving, and that it fairly effectively selects out only those motions corresponding to the tidal frequencies. Thus, one can usually separately analyze the tidal and non-tidal parts of a signal, by using harmonic analysis to "de-tide" the signal. However, there are some circumstances when the separation into tidal and non-tidal is not so easy. There are three likely sources of this additional non-tidal energy in the tidal band:

1. Inertial oscillations: These motions arise because the physical system in effect does a temporal Fourier transform of the wind field, and for certain types of storm conditions, finds significant forcing at the local inertial frequency. As shown in Appendix A, motions occurring at this frequency are characterized by a high degree of kinetic energy, or large currents. For the latitudes of the Northwest Passage, this frequency is in the middle of the semi-diurnal band, and will likely cause considerable contamination of the semi-diurnal tidal signal. The inertial response is typically characterized by patches of a few days at a time in which currents at the inertial period are excited, followed by quiescent periods. The initiation of each patch of increased

inertial activity is usually the passage of a major storm system. The nature of inertial oscillations in the presence of ice cover is not necessarily as straightforward as in the above description, which was based on open ocean data at lower latitudes.

2. Passing meteorological disturbances may give rise to low frequency oscillations, which tidal analysis cannot readily distinguish as a non-tidal signal. Thus, the long period tidal constituents may be contaminated through mechanisms such as the inverted barometer effect.

3. The physical system may change. For instance, there are reported to be differences in tidal amplitudes depending on the degree of ice cover. (Godin and Barber, 1977). The ice has the effect of introducing an additional friction, reducing the water depth, as well as isolating the system from additional wind forcing.

We will explore in this chapter the stability of the tidal constituents available to this study. There are six water level stations of use, four in Prince of Wales Strait (NWP82), one in Barrow Strait (NWP84) and one in Penny Strait (NWP84). As well, there are six current meter records which extend over about one year - 2 in Barrow Strait, and 4 in Penny Strait. At each current meter site, the meters are paired, one at about 50 m.and the other at about 100 m. The usual procedure is to analyze the year-long record as a group of 1-month long records, allowing a time series of harmonic constants to be formed. As well, the year long record was analyzed in its entirety.

Most, if not all, of the tidal data was obtained using seafloor-mounted bottom pressure gauges. Thus, the tide heights discussed in this report contain as well the effects of atmospheric pressure fluctuations. These fluctuations will not contaminate the diurnal and semi-diurnal constituents to a significant degree, but there is a seasonal variation of atmoshperic pressure equivalent to about 10 cm of water which will contaminate primarily the longer period tides. Whenever reference to tide height or sea level is made in this report, then, we are in fact referring to the variations in pressure felt by a bottom-mounted pressure recorder.

Because of the likely contamination of the current records by inertial oscillations and baroclinic effects, we will discuss elevations and currents separately. Before we discuss these analyses, we must first examine the use of inference to improve the harmonic analysis of relatively short (*e.g.* 1-month) records. This procedure is used to separate constituents close in frequency which cannot be distinguished by harmonic analysis because of the shortness of the record involved.

3.1 INFERENCE

Figures 3.1.1 and 3.1.2 are plots of the monthly values of the major diurnal and semi-diurnal constituents for the four Prince of Wales stations, prior to using inference in the harmonic analysis. It is apparent that, based on one-month long records, there is a considerable variation in the amplitude of the K_1 tide, but not the O_1, this modulation having about a 6 month period. The S_2 tide is similarly affected, and to a certain extent the N_2 as well, although it is so small it is hard to tell. The modulation of amplitude (as well as phase) may be partially due to inherent variability of the tidal response, but most is due to contamination by constituents of nearly identical periods. As is the case in Fourier analysis, harmonic analysis cannot separate constituents which are close in frequency if the record length is too short. In many cases, this difficulty may be alleviated by the use of a procedure known as inference. Except for the above analyses, all other harmonic analyses include inferred constituents.

We are confronted with two aspects to the inference question - the question of how the frequencies of the tidal forcing are distributed, and the statistical analysis question of how one can separate two (or more) close constituents.

We discuss the first point, the source of the problem. As described in Appendix A, tides are driven by the motion of the sun and moon around the earth. These motions, to a crude approximation, are relatively straightforward, and should lead to a relatively simple tide, keyed to such repeatable events as the rising and setting of the sun and moon. However, a more detailed examination of these phenomena reveals considerable complexity. For instance, the length of day changes throughout the year - this will affect the amplitude of the solar tidal potential. The lunar potential is affected by such things as the periodic variation in the height of the moon above the horizon. As for the lunar and solar interaction, sometimes the moon is a full moon, sometimes a half moon and sometimes a new moon, in a repeating sequence. As well, although the period of the sun's motion around the earth (taking a "classical" frame of reference, with the earth at the centre) is 24 hours, the period of the moon's motion is 24.84 hours. There are thus two major fundamental periodicities involved, that of the sun and the moon respectively. The tidal potential associated with each of these frequencies undergoes several long-term modulations, such as the change in length of daylight hours, corresponding to an annual cycle in the relative orientations of sun and earth.

We can illustrate the way in which these effects give rise to the dense set of frequencies in the tidal potential by considering the solar semi-diurnal tidal potential. The major part of the solar contribution to the semi-diurnal tidal potential may be written as: (Dronkers Formula 12.3):

$$V = V_0 \cos^2\phi\{0.919\cos(2\theta - 2h) + 0.079\cos(2\theta) + 0.002\cos(2\theta + 2h)\} \qquad (3.1)$$

where θ is local "sidereal time" (*i.e.* the longitude of the sun relative to the astronomically significant vernal equinox) and has a periodicity of 23 hours 56 minutes and 4 seconds and h is the mean (daily) longitude of the sun. Since the earth rotates once about the sun in one year, h repeats itself every year. The use of sidereal time is associated with the derivation of the tidal potential in the centre of mass coordinate system, which must take into account both the rotation of the earth about its polar axis as well as the rotation of the earth about the sun. The $\cos^2\phi$ term represents the latitudinal spatial variability of the tidal potential, ϕ being the latitude. The remaining trigonometric terms represent both time and space periodicity, since the angle to the sun, $\theta + h$ changes with time for a stationary observer, as well as varying with location over the globe at any particular time.

The above formula shows the typical contribution to the tidal potential: a high frequency oscillation, at frequency 2θ, (or period of about 12 hours) modulated by longer period oscillations. Making use of trigonometric identities, and the fact that $\theta = t + h$, where t is solar time (*i.e.* repeats every 24 hours) the above contribution may be written as:

$$V = V_0\cos^2\phi\{0.919\cos(2t) + 0.079\cos(2t+2h) + 0.002\cos(2t+4h)\} \tag{3.2}$$

where the first term in the parentheses represents the S_2, the major semi-diurnal solar constituent, the second represents the K_2, or "declinational" constituent, and the third term is so small it has no name.

One slightly confusing aspect is the factor of two for each of the angular arguments. As discussed in Appendix A, the tidal potential is "double-humped" - there is a maximum value of the side of the earth facing the sun as well as one on the side facing away from the sun.

The above discussion was concerned with the solar contribution to the tidal potential. Similar considerations arise when considering the lunar contribution, except that the fundamental period is not 24 hours but rather 24.84 hours. There are thus two sources for the complexity of tidal constituent frequencies: the fact that the motions of the sun and moon have similar but not identical periodicities, and the fact that both of these forcing mechanisms undergo a variety of longer term modulations, which may be expressed algebraically as a sum of close frequencies.

Table 3.1.1 lists the major tidal constituents which are available from a one month analysis, as well as those which are also relatively important and which must be inferred after a one month analysis. The amplitudes of tides at Dundas Station, the largest tides in this study, are also listed, along with the astronomical forcing amplitudes.

TABLE 3.1.1
COMPARISON OF OBSERVED AMPLITUDES AT DUNDAS STATION AND ASTRONOMICAL AMPLITUDES AT THE EQUATOR

Frequency (deg/hr)	Name	Inferred from	Dundas (cm)	Astronomical at Equator (cm)	Dundas (relative to M_2)	Astronomical at Equator (relative to M_2)
0.5	MM		2.09	2.2	0.031	0.091
1.02	MSf		0.79	0.2	0.012	0.008
1.10	Mf	MSf	1.06	4.2	0.006	0.174
12.38	ALP1		0.39		0.006	
12.85	2Q1		0.18	0.3	0.000	0.012
13.40	Q1		1.18	1.9	0.003	0.079
13.94	O1		12.70	10.0	0.190	0.413
14.03	TAU1	O1	0.16		0.002	
14.50	NO1		1.41		0.021	
14.96	P1	K1	9.20	4.7	0.138	0.194
15.00	S1	K1	1.19		0.018	
15.04	K1		28.20	14.1	0.423	0.583
15.59	J1		1.30	0.8	0.019	0.033
16.06	SO1	OO1	0.13		0.002	
16.14	OO1		0.69		0.010	
16.68	UPS1		0.15		0.002	
27.42	EPS2		0.53		0.008	
27.90	2N2	MU2	1.84	6.3	0.028	0.260
27.97	MU2		2.21	5.8	0.038	0.240
28.44	N2		13.64	4.2	0.204	0.174
28.51	NU2	N2	2.61	0.9	0.039	0.037
28.98	M2		66.70	24.2	1.000	1.000
29.53	L2		1.69	0.7	0.025	0.029
30.00	S2		24.56	11.3	0.368	0.467
30.08	K2	S2	7.19	3.1	0.108	0.128
30.63	ETA2		0.58		0.009	

TABLE 3.1.1 (cont.)
COMPARISON OF OBSERVED AMPLITUDES AT DUNDAS STATION AND ASTRONOMICAL AMPLITUDES AT THE EQUATOR

Frequency (deg/hr)	Name	Inferred from	Dundas (cm)	Astronomical at Equator (cm)	Dundas (relative to M_2)	Astronomical at Equator (relative to M_2)
42.93	MO3		0.22		0.003	
43.48	M3		0.42		0.006	
44.03	MK3		0.33		0.005	
45.04	SK3		0.24		0.004	
57.42	MN4		0.13		0.002	
57.97	M4		0.29		0.004	
58.44	SN4		0.03		0.000	
58.98	MS4		0.20		0.003	
60.00	S4		0.06		0.001	
73.01	2MK5		0.28		0.004	
75.04	2SK5		0.01		0.000	
86.41	2MN6		0.02		0.000	
86.95	M6		0.07		0.001	
87.97	2MS6		0.08		0.001	
88.98	2SM6		0.03		0.000	
101.99	3MK7		0.01		0.000	
115.94	M8		0.01		0.000	

We note that there are more constituents observed at Dundas than listed in the Astronomical column. This is due to the fact that the response to tidal forcing is a non-linear phenomenon, and the non-linear terms in the governing equations (both acceleration and friction) generate an expanded set of constituents, whose frequencies are sum and difference frequencies of the forcing frequencies. These new frequencies are often referred to as the shallow water constituents, because they are more strongly generated in shallow water. Note that the "sum" frequencies appear as such combinations as M_4, $2SK_5$, *etc.*, whereas the "difference" frequencies contribute to MM and MSf, for example.

We return now to the original problem: there is significant tidal energy represented by constituents which cannot be separated by a 1-month analysis. How can this problem be dealt with?

Figure 3.1.3 plots the sum of the above two semi-diurnal forcings (S_2 and K_2) for a 3 month period. This time period is one half of the synodic period, the time interval between two consecutive conjunctions of phase. At the start of the synodic period, the two constituents are in phase, and thus combine positively. Half a synodic period later, they are entirely out of phase, and interfere destructively, and at the end of the synodic period they are back in phase again. Also evident is that over a one month period, little information about the long-term modulation is available: one is merely confronted with an amplitude which changes somewhat over the analysis period. Thus, there is not sufficient information in a short record to separate pairs of such constituents, and the result of analysis will be a single contaminated constituent, both in terms of phase and amplitude. For instance, for a one month record, one will obtain only a poor representation for the S_2 tide, and no information about the K_2. However, we are not entirely helpless. The outcome of the original analysis will be an S_2 constituent, with a contaminated phase and amplitude, A^*_{S2}, and phase, g^*_{S2}. For a particular tidal record, we may not have sufficient length of record to describe the long-term modulations, but we are likely to have that information from nearby gauges. In particular, we will know, for instance, the ratio of the K_2 amplitude to the S_2 and their phase difference:

$$\mathrm{Amp}(K_2) \,/\, \mathrm{Amp}(S_2) = R$$

$$\mathrm{phase}(K_2) - \mathrm{phase}(S_2) = e, \text{ say.}$$

After some algebraic manipulations, one can extract values of phase and amplitude for both of the inferred constituents, S_2 and K_2 from the original contaminated values, A^*_{S2}, and g^*_{S2}, as described in Foreman (1977) for instance. The major point is: how well does one know the amplitude ratio and phase difference? Lacking any other information, one can use the astronomical values, but one can improve upon these values of a reliable nearby long-term tide gauge exists. Table 3.1.2 tabulates the major amplitude ratios and phase differences of the standard long-term tidal stations in the Arctic. It is apparent that in general the diurnal and semi-diurnal constituents are fairly stable as far as the spatial variability of the inference parameters is concerned. However, the fortnightly inference relations are very disparate. In view of this, we chose to use inference to tidy up the diurnal and semi-diurnal bands only.

In general, the ratios and phase differences for all but the fortnightly tides are reasonably uniform over the region. Certain stations, *e.g.* 6290 and 6485, are at considerable variance with the rest as far as phase is concerned, but on the whole, one has reasonable confidence in the ratios and differences in the above table for the diurnal and semi-diurnal constituents. A further complication arises: we have illustrated the values for the elevation tide only. What about the tidal streams? It turns out that the harmonic constants for currents are considerably more variable over a long term (6 month) period that the constants for elevations, and one cannot rely on the seasonal variations being purely a tidal phenomenon. For inferring currents, we assumed that the major and minor amplitudes are inferred in the same way as tidal elevations, that the g for current was inferred in the same manner as the g for tides and that the inclination of the parent and child are the same.

The effect of inference can be seen in Figures 3.2.1 and 3.2.3 where Figures 3.1.1 and 3.1.2 are repeated, using inferred constituent time series. It is apparent that inference has removed much of the modulation in the K_1 signal, and additionally provided a P_1 constituent. As well, the S_2 is more nearly constant, as is the N_2, and there are now K_2 and NU_2 constituents, although they are not plotted. Thus, much of the apparent variability in the tidal constituents was removed by inferring contaminating constituents.

The benefits of this approach would be seen if one were to use the harmonic constants to predict tidal heights at some time other than the measurement period. Consider the K_1-P_1 part of the tidal signal. As is apparent from Table 3.1.2 and Figures 3.1.2 and 3.2.3, the amplitude of that part of the tide due to the K_1-P_1 pair undergoes a ±30% modulation with a period of about 6 months, a time period known as the synodic period. The phase modulation is not apparent from Table 3.1.2, but in Table 3.1.3 the phases of the contaminated K_1 and S_2 constituents at Station 87 are tabulated. (The contaminated signal represents the combination of K_1 and P_1 effects). For K_1, the phase changes from 46° to 82° over a half the synodic period - a change in timing of high water of about 2.4 hours. The regular change in phase and amplitude over a synodic period is an important aspect of the observed tide, and cannot be obtained from K_1 alone: one needs a P_1 signal as well to reproduce this change in timing of the K_1-P_1 part of the diurnal tide. Similar cosiderations apply to the S_2-K_2 pair, as well as the other interfereing constituent pairs. The small errors inherent in the inference method, due to an inadequate definition of "nearby gauge", are much smaller than the large errors incurred by ignoring inference.

TABLE 3.1.2
AMPLITUDE RATIOS AND GREENWICH PHASE DIFFERENCES OF THE MAJOR INTERFERING CONSTITUENTS

STA-TION	$A_{Mf}:A_{MSf}$	$g_{MSf}-g_{Mf}$	$A_{P1}:A_{K1}$	$g_{K1}-g_{P1}$	$A_{NU2}:A_{N2}$	$g_{N2}-g_{NU2}$	$A_{K2}:A_{S2}$	$g_{S2}-g_{K2}$
87	4.5	-256	.266	8.9	.235	3.7	.289	.6
89	4.0	-180	.298	7.0	.224	8.4	.295	3.3
92	5.0	-82	.287	3.2	.161	-10.1	.279	8.6
93	4.0	-173	.298	7.1	.227	8.2	.296	3.1
3756	12.0	-149	.298	1.0	.206	-1.6	.297	3.4
3920	4.1	53	.321	2.2	.200	-4.5	.284	2.9
4140	3.0	-72	.321	1.4	.205	-6.5	.279	0.9
4205	0.9	105	.336	2.8	.189	3.4	.277	-0.3
5275	1.1	-86	.306	3.1	.140	-3.0	.377	-19.6
5560			.318	4.9	.176	-2.4	.251	7.6
6150	1.1	-38	.285	24.3	.276	-6.4	.344	4.3
6210	1.4	-33	.304	10.9	.216	-16.2	.334	-4.8
6240	1.3	-15	.268	14.1	.294	-9.3	.398	2.4
6290	0.9	-5	.286	4.5	.417	-61.0	.473	-36.6
6360	1.7	-87	.307	-0.1	.172	-10.7	.291	4.5
6424	2.7	-104	.319	2.2	.163	10.1	.336	11.1
6485	1.3	-170	.311	12.9	.187	-36.4	.220	1.9
6955	1.9	-103	.305	6.1	.221	5.6	.308	2.4
8442	1.8	-2	.311	6.3	.185	-6.6	.286	2.6
FSRG	1.1	-31	.347	13.7	.180	-5.3	.285	-13.3
MEAN	2.8	-107	.305	6.6	.213	-7.0	.310	-0.8
S.D.	2.7	91	.020	6.0	.060	16.4	.056	10.9
Astro-nomical ratio	21.0		0.333		.214		.274	

TABLE 3.1.3
AMPLITUDES AND PHASES OF K_1 AND S_2 AT STATION 87 WITHOUT THE USE OF INFERENCE

Start - End Dates	K_1 Amp	K_1 Phase	S_2 Amp	S_2 Phase
April 10 '82 - May 12 '82	1.9	46	11.6	291
May 12 '82 - June 13 '82	2.4	54	8.5	283
June 13 '82 - July 15 '82	2.5	67	6.8	296
July 15 '82 - Aug. 16 '82	2.3	83	7.8	305
Aug. 16 '82 - Sep. 16 '82	2.0	74	9.8	303
Sep. 17 '82 - Oct. 18 '82	1.9	70	11.3	286
Oct. 18 '82 - Nov. 19 '82	2.4	51	10.7	277
Nov. 19 '82 - Dec. 21 '82	2.9	51	8.3	284
Dec. 21 '82 - Jan. 22 '83 .	3.1	62	7.2	306
Jan. 22 '83 - Feb. 23 '83	2.6	80	10.2	316
Feb. 23 '83 - Mar. 26 '83	2.0	84	12.4	309
Mar. 26 '83 - Apr. 27 '83	1.7	55	12.7	296

3.2 STABILITY OF TIDAL ELEVATION HARMONIC CONSTANTS

There were 6 tide gauges which were moored for approximately one year - 4 during the NWP 82 experiment in Prince of Wales Strait, and 2 during the NWP 84 experiment, one in Barrow Strait and the other in Penny Strait. Each record was broken up into successive rcords of length approximately 29 days (non-overlapping) and subjected to the standard analysis package. The Rayleigh criterion was set to 1.00, so the allowed list of constituent in Table 3.1.1 was found. Stations 89 and 93 in Prince of Wales Strait were actually at identical locations, and one of them is thus redundant. However, both are retained in this discussion, to reinforce the fact that the small variations noted below are not due to instrumental problems.

3.2.1 DIURNAL AND SEMI-DIURNAL TIDES

PRINCE OF WALES STRAIT

We consider first Prince of Wales Strait. Figures 3.2.1 and 3.2.2 illustrate the time series of amplitude and phase for the principal semi-diurnal constituents M_2, S_2 and N_2, and Figures 3.2.3 and 3.2.4 illustrate the amplitude and phase time series for the principal diurnal constituents K_1, O_1 and P_1. The spatial variations are discussed in Chapter 4, we will here merely concern ourselves with the temporal variation of amplitudes. We do note, for later discussion, that Jesse Harbour is in an entirely different tidal regime from the other three stations.

Considering the semi-diurnal band, the M_2 is the least stable constituent - at Stations 87, 89 and 93 its amplitude ranges from 18 to 21 cm, although the variation in phase is reasonably small, 5 degrees. The variations at these stations are identical: a rise in June, diminishing until Oct-Nov, and then rising again. The spatial coherence of these variations is quite remarkable, although its origin is unclear at the moment. Jesse Harbour, station 92, behaved entirely differently - the M_2 amplitude rose in the summer months, rather than falling. Interestingly, this behaviour did not appear in the other semi-diurnal constituents at Jesse Harbour.

The phases of the semi-diurnal constituents at the three stations, 87, 89 and 93 don't display particularly strong seasonal variations, but there is an amazing spatial correlation again, with Jesse Harbour again differing from the other three. With only one gauge, for instance, one would be tempted to say that the N_2 variation was primarily due to errors in analyzing for a small constituent. However, when the three tide gauges at stations 87, 89 and 93 produce the same annual variation of values, one suspects an underlying common physical forcing. Once again, the seasonal variations at Jesse Harbour are entirely different from the other gauges in the Prince of Wales Strait, and the numerical value of the phases are also different - by about 180 degrees. The amplitude of the phase variations is about three times as large as well. These interesting differences between Jesse Harbour and the stations to the north fit into a consistent spatial pattern, described in Section 4.1.4.

The most notable feature of the diurnal tides is that they are about one sixth of the size of the semi-diurnal tides. Nevertheless, certain features again repeat themselves at the three similar stations. For instance, the K_1 amplitude undergoes a slight seasonal modulation, with maximum October and minimum in June and March. This slight seasonal effect may in fact be a remnant of inference, although we were careful to infer both the P_1 and S_1 constituents. The O_1 constituent is on average somewhat larger than K_1 at station 87, for no obvious reason. The phases are reasonably constant. The close relationship between K_1 and P_1 phases is not a geophysical phenomenon, but merely the result of the constant phase difference used in inference.

BARROW STRAIT AND PENNY STRAIT

Two other long-term tide gauges are available, one in Barrow Strait, off the south coast of Cornwallis Island (Station 42), and one in Penny Strait, off John Barrow Island (Station FSRG). The amplitude time series are plotted in Figure 3.2.5 and the phases in Figure 3.2.6.

Considering first the Barrow Strait station, #42, the diurnal and semi-diurnal amplitudes do not indicate significant variations over the course of the year. There is a hint that the M_2 undergoes a small seasonal modulation, but it would be difficult to be convinced of this, since the record is only one year long. Similarly, the K_1 appears to vary slightly on a seasonal basis. The phases of the diurnal and semi-diurnal constituents are reasonably constant, although the O_1 constituent undergoes a 13 degree change throughout the year, corresponding to about a one hour difference in the elevation associated with it.

The situation at John Barrow is quite different. Here, most of the major constituents indicate larger variabilities in amplitude, as well as much larger variations in phase. In fact, the O_1 phase varies by 45 degrees over the course of the year. This is quite remarkable, although the associated tide, about 3 cm in amplitude, is not very significant. To put this "error" into perspective, Figure 3.2.7 plots the low pass filtered sea-level data (bottom pressure in fact) for station #42. The seasonal variations in water level are about 40 cm, swamping any "errors" in O_1 for instance.

In Table 3.2.1 the means and standard deviations of the 6 major constituents are tabulated for these two stations and the 4 stations in Prince of Wales Strait.

TABLE 3.2.1

MEANS AND STANDARD DEVIATIONS OF THE SIX PRINCIPAL TIDAL CONSTITUENTS

(Amplitudes in cm, Greenwich phases referenced to Greewich Mean Time)

STATION	M2				S2				N2			
	Amp	S.D.	Phase	S.D.	Amp	S.D.	Phase	S.D.	Amp	S.D.	Phase	S.D.
87	17.6	1.1	236	2	9.5	0.6	296	5	2.9	0.3	203	4
89	19.1	0.9	248	2	10.3	0.6	305	4	3.2	0.3	216	4
92	11.3	1.5	73	6	2.3	0.4	105	5	2.5	0.2	50	8
93	19.1	1.0	247	8	10.3	0.7	303	8	3.2	0.3	215	9
42	45.7	1.4	173	2	18.3	1.1	223	4	9.2	0.4	144	3
FSRG	30.7	2.6	188	2	11.7	0.9	230	6	6.4	0.6	155	7

STATION	K1				O1				P1			
	Amp	S.D.	Phase	S.D.	Amp	S.D.	Phase	S.D.	Amp	S.D.	Phase	S.D.
87	2.3	0.1	65	6	2.5	0.3	185	3	0.6	0.0	56	6
89	3.1	0.2	55	5	2.3	0.2	189	3	0.9	0.0	48	5
92	4.6	0.3	118	4	2.9	0.2	163	4	1.3	0.1	115	4
93	3.1	0.2	54	8	2.3	0.2	189	4	0.9	0.0	47	8
42	17.9	0.8	336	2	10.2	0.5	274	5	5.6	0.3	329	4
FSRG	8.6	1.2	350	6	5.3	0.9	283	15	3.0	0.4	336	7

3.2.2 LONG PERIOD AND SHORT PERIOD TIDES

PRINCE OF WALES STRAIT

The time series of the MSf and Z_0 tides in Prince of Wales Strait are plotted in Figure 3.2.8. The Z_0 field reveals a consistent pattern of reaching a maximum in September, and a seasonal range of about 10 cm. The pattern is similar to Figure 3.2.7, although the amplitude is reduced. Note that the seasonal range is greater than the variations in the diurnal and semi-diurnal constituents. As well, the modulation of the Z_0 tide is about the same size as the annual variation in atmospheric pressure (Sailing Directions, Arctic Canada), so is likely related to a response to large-scale atmospheric forcing. The MSf signal is highly variable - ranging between 1 and 10 cm amplitude. There appears to be little pattern to these variations, indicating the presence of considerable non-tidal energy in the long period bands. In fact, when inference was used in an attempt to separate MSf and Mf, the result was noisier than the original contaminated signal, indicating that the variations in amplitude of MSf are of a non-tidal nature.

The high frequency bands in Prince of Wales Strait are particularly interesting, Figure 3.2.9. All 4 stations indicate similar long-term behaviour of the M_4 and MS_4 constituents - a minimum at the end of August, and a maximum in December. Generally, these higher amplitudes correlate with the onset of the larger long-period amplitudes, which occur in the September to January period. The MK_3 constituent is, if anything, 180° out of phase with this pattern. The interest in these short-period tides is mainly sparked by the interesting way in which they are generated - by the non-linear aspects of the propagation of the tide through shallow or constricted waterways. Since tidal streams are quite small in Prince of Wales Strait, the non-linear effects are quite small, as are the shallow water tides. We make no attempt in this report to explain the interesting correlation between the various stations in the seasonal modulation of the amplitudes of these constituents.

BARROW STRAIT AND PENNY STRAIT

These constituents are plotted in Figure 3.2.10. Considering first the long period MSf, one would be tempted to say that inference might remove some of the annual variations in amplitude. However, when this was tried, the inferred conditions varied more than the originals, in the same manner as for Prince of Wales Strait. This is understandable if one considers the Station 42 data - there are three maxima and two or three minima in the cycle, whereas the Mf and MSf interference produces exactly two maxima and two minima a year. Thus, the long term modulation was not tidal, and trying to correct it as if it were, makes the situation even more variable. Similarly, the John Barrow data illustrates one maximum per year, unlike the MSF-Mf interference, which has two.

Considering the high frequency bands, one would have to say that the M_4 and MS_4 are in the noise region. However, the MK_3 illustrates significant annual modulation. Most interesting at John Barrow Island, the MK_3 amplitude attains a maximum at about the same time as the MSf and the O_1, all three of which are both astronomical as well as shallow water constituents driven by non-linear interactions. Interestingly as well, the seasonal variation in MK_3 at Station 42 is 180° out of phase with the Penny Strait station.

3.3 STABILITY OF HARMONIC CONSTANTS FOR CURRENTS

A large number of short-term stations were occupied, which enabled the spatial distribution of tidal currents to be determined. However, these moorings were in general installed in March and taken out in May, thus covering only part of the season. At four locations however, long-term moorings were installed, and the results are discussed here. The long-term stations were:

Station 42 on the north side of Barrow Strait, meters at 52m and 100m, 1984-85
Station 46 on the south side of Barrow Strait, meters at 25, 60 and 150m, 1982
Station 71 in Austin Channel, meters at 73 and 123 meters, 1983-84
Station PSE in Penny Strait, meters at 43 and 131 m, 1984-85
Station PSW in Penny Strait, meter at 49 and 138 m, 1984-85.

These time series produce some very interesting results. The accompanying diagrams convey a considerable amount of information, but must be read with care. The data for a single current meter occupies one page. Time series of the major and minor amplitudes are plotted in one panel, and phase and inclination in the panel below. Then, time series of the rotary spectral parameters are plotted: the amplitude of the clockwise and counterclockwise vectors, and their phases. In particular, note that there are two scales on each graph, corresponding to the two different time series plotted on each panel. This may introduce some confusion, but was essential to present the data in an orderly manner. Note that the scale size remains the same for both parameters plotted on the same graph - the origin is merely shifted.

Some general remarks are in order. These time series exhibited considerable variation over the year, all four standard parameters (major semi-axis, minor semi-axis, inclination and phase) illustrating significant variation. However, many of the series became more regular when plotted in terms of rotary spectral values. In general, the counter-clockwise component became almost constant over the year, while the clockwise underwent considerable fluctuation. This is in accord with the notion that inertial oscillations will contaminate the tidal signal. We will not discuss that effect to any great extent in this section, being content to point it out now, and discuss it in more detail in Chapter 5, dealing with inertial oscillations in particular.

3.3.1 BARROW STRAIT STATION 42

Two meters were deployed, at 51 m and 100m, in water of depth 130 m. The M_2 data are plotted in Figures 3.3.1 and 3.3.2, and the K_1 data in Figures 3.3.3 and 3.3.4.

M2
At both metered depths, the currents are reasonably rectilinear: the minor axis is less than 1/6 the major. The inclination is approximately along the direction of the channel, 176° at 51 m and 192° at 100m. The local phase of tidal elevations is about 175°, and the phase of the currents is approximately 225°, so that the flood is maximal about 1.5 hours after local high water. Aside from the fact that the counter-clockwise component is the most stable, it is very interesting to note how the relative roles of the two rotary components change in the water column. The counter clockwise component remains constant at about 7 cm/s at both meters,

slightly faster at 50 m than at 100. However,the clockwise component changes from about 10 cm/s at 50 m to 5 cm/s at 100 m. If one were to decompose the clockwise component farther, it would be as a barotropic 7.5 cm/s signal, with a first baroclinic mode of 2.5 cm/s amplitude, with a positive value at 50 m and negative at 100m. This speculation will be expanded in Chapter 5. The two barotropic values would constitute a barotropic Kelvin wave, and the remaining baroclinic signal would constitute a first mode internal Poincaré wave, a not unreasonable model.

K1

The diurnal currents do not exhibit the same simplification when plotted as rotary spectra. There are two reasons for this, which must be explained in light of the theorteical notions presented in the Appendices. It is possible that the semi-diurnal tides can more readily excite Poincaré waves, which are purely clockwise polarized. As well, the semi-diurnal tides "feel" the effect of the Earth's rotation in more interesting ways, exciting additional modes, particularly in the clockwise polarized currents. We will discuss these features in more detail in Chapters 5 and 6. Returning to the time series of K_1 amplitudes, we note that the currents are quite rectilinear, and aligned with the channel. The 25° migration in phase over the year at 51 m would produce almost a 2 hour error in timing. Currents appear to be quite barotropic, there is only a small change of amplitude or phase with depth.

The following table summarizes the means and standard deviations of the M_2, S_2, K_1, and O_1 harmonic constants for Station 42, including data from a 2 month long mooring at 18 m.

BARROW STRAIT STATION 42 HARMONIC CONSTANTS

(Inclination is measured in a Cartesian sense, phase is Greenwich phase, time zone is Greenwich Mean Time)

M2

Depth (m)	Major (cm/s)	S.D. (cm/s)	Minor (cm/s)	S.D. (cm/s)	Incl. (deg)	S.D. (deg)	Phase (deg)	S.D. (deg)
18	10.9	0.5	5.7	0.1	208	8	241	6
51	17.8	1.6	-2.5	1.5	176	3	220	3
100	12.1	0.8	1.6	0.8	192	4	235	4

Depth (m)	CW Amp (cm/s)	S.D. (cm/s)	CCW Amp (cm/s)	S.D. (cm/s)	CW phase (deg)	S.D. (deg)	CCW Phase (deg)	S.D. (deg)
18	2.6	0.3	8.3	0.2	89	14	326	1
51	10.1	1.5	7.6	0.3	36	6	316	2
100	5.3	0.8	6.8	0.3	67	7	317	2

S2

Depth (m)	Major (cm/s)	S.D. (cm/s)	Minor (cm/s)	S.D. (cm/s)	Incl. (deg)	S.D. (deg)	Phase (deg)	S.D. (deg)
18	3.3	0.0	2.2	0.7	237	15	316	17
51	7.3	0.7	-1.3	0.7	179	5	266	7
100	4.3	0.5	0.5	0.5	191	11	276	13

Depth (m)	CW Amp (cm/s)	S.D. (cm/s)	CCW Amp (cm/s)	S.D. (cm/s)	CW phase (deg)	S.D. (deg)	CCW Phase (deg)	S.D. (deg)
18	0.6	0.3	2.8	0.3	192	32	281	1
51	4.3	0.6	3.0	0.3	86	11	273	4
100	1.9	0.5	2.4	0.2	106	24	275	4

BARROW STRAIT STATION 42 HARMONIC CONSTANTS

(Inclination is measured in a Cartesian sense, phase is Greenwich phase, time zone is Greenwich Mean Time)

K1

Depth (m)	Major (cm/s)	S.D. (cm/s)	Minor (cm/s)	S.D. (cm/s)	Incl. (deg)	S.D. (deg)	Phase (deg)	S.D. (deg)
18	11.9	0.2	0.5	0.0	196	1	346	2
51	12.2	0.4	-0.4	0.5	176	5	346	5
100	11.5	0.4	0.2	0.9	184	2	352	4

Depth (m)	CW Amp (cm/s)	S.D. (cm/s)	CCW Amp (cm/s)	S.D. (cm/s)	CW phase (deg)	S.D. (deg)	CCW Phase (deg)	S.D. (deg)
18	5.7	0.1	6.2	0.1	183	3	210	1
51	6.3	0.4	5.9	0.3	161	9	190	5
100	5.7	0.5	5.8	0.5	176	3	192	5

O1

Depth (m)	Major (cm/s)	S.D. (cm/s)	Minor (cm/s)	S.D. (cm/s)	Incl. (deg)	S.D. (deg)	Phase (deg)	S.D. (deg)
18	5.5	0.1	0.2	0.2	197	4	285	1
51	5.2	0.4	-0.9	0.4	183	8	290	6
100	4.7	0.5	-0.4	0.5	196	6	303	6

Depth (m)	CW Amp (cm/s)	S.D. (cm/s)	CCW Amp (cm/s)	S.D. (cm/s)	CW phase (deg)	S.D. (deg)	CCW Phase (deg)	S.D. (deg)
18	2.7	0.0	2.8	0.2	123	5	275	3
51	3.0	0.3	2.2	0.2	113	9	252	10
100	2.6	0.4	2.1	0.4	138	8	253	9

3.3.2 BARROW STRAIT STATION 46

Data from three depths are available- 25m, 60m, and 150m, in water of depth 170m. The M2 data are plotted in Figure 3.3.5-3.3.7, and the K1 data in Figures 3.3.8-3.3.10.

M2

These time series (Figures 3.3.5-3.3.7) illustrate a similar tidal regime to that at station 42: the currents are rectilinear with the exception of the 150 m currents, the phase is between 230 and 240 degrees, and the inclination is along the channel. It is perhaps of some interest that at 150 m, the semi-minor axis is as large as 1/2 the semi-major. As at station 42, plotting the rotary spectra reduced considerably the amount of variability over the year in the clockwise component. The clockwise amplitude remained at about 8 cm/s throughout the water column. the counterclockwise varied from 8 cm/s at 25 m to 10 cm/s at 60 m and 3 cm/s at 150 m, or from 0 to 2 to -5 if one first subtracts a value of 8 to correspond to the counterclockwise signal. As at station 42, the clockwise signal undergoes a considerable modulation throughout the year, suggestive of a seasonal cycle of forcings for the baroclinic mode, or a seasonal change in the water column properties which support it. For this reason, the Station 46 M_2 data, Figures 3.3.5 -3.3.7 illustrate a large change in the phase and inclination of the signal, which could raise some questions about the directional accuracy. At 150 m depth, the inclination undergoes an 80 degree change over the year, which seems somewhat high, given that the semi-major amplitude was 11 cm/s. However, the pattern of the seasonal modulation is similar at all depths, indicating that some organized variation was afoot, presumably the internal Poincaré mechanism alluded to.

K1

The K1 constituent is not quite as interesting as M2. It is almost purely a rectilinear current, with negligible minor amplitude. Nevertheless, there is some improvement in the stability of the amplitudes when rotary components are plotted. The phase of the counterclockwise components is considerably more stable that the phase of the clockwise, implying that the change in inclination over the year is not due to instrumental problems, but rather seasonal response of the current regime. The phase is about 355° and the phase of elevations is about 335° in this region, indicating that maximal flood occurs about 1.5 hours after local high water.

The following tables summarize the time series data, presenting mean and standard deviations of harmonic constants for the principal constituents M_2, S_2, K_1 and O_1.

BARROW STRAIT STATION 46B HARMONIC CONSTANTS

(Inclination is measured in a Cartesian sense, phase is Greenwich phase, time zone is Greenwich Mean Time)

M2

Depth (m)	Major (cm/s)	S.D. (cm/s)	Minor (cm/s)	S.D. (cm/s)	Incl. (deg)	S.D. (deg)	Phase (deg)	S.D. (deg)
25	16.4	2.2	-0.0	2.1	199	4	236	5
60	18.1	0.9	-2.0	1.3	180	6	229	2
150	10.9	1.6	5.2	1.8	184	27	247	16

Depth (m)	CW Amp (cm/s)	S.D. (cm/s)	CCW Amp (cm/s)	S.D. (cm/s)	CW phase (deg)	S.D. (deg)	CCW Phase (deg)	S.D. (deg)
25	8.2	2.1	8.2	0.5	75	9	324	3
60	10.1	1.1	8.0	0.3	49	6	311	6
150	2.8	1.7	8.0	0.3	72	40	297	20

S2

Depth (m)	Major (cm/s)	S.D. (cm/s)	Minor (cm/s)	S.D. (cm/s)	Incl. (deg)	S.D. (deg)	Phase (deg)	S.D. (deg)
25	5.7	0.8	0.5	1.1	203	7	281	5
60	6.9	1.4	-1.2	1.0	181	4	271	5
150	5.4	1.6	1.7	0.6	161	51	215	46

Depth (m)	CW Amp (cm/s)	S.D. (cm/s)	CCW Amp (cm/s)	S.D. (cm/s)	CW phase (deg)	S.D. (deg)	CCW Phase (deg)	S.D. (deg)
25	2.6	0.8	3.1	0.4	125	12	282	4
60	4.0	0.8	2.8	0.9	92	7	271	6
150	1.8	0.9	3.6	0.8	331	55	263	12

BARROW STRAIT STATION 46B HARMONIC CONSTANTS

(Inclination is measured in a Cartesian sense, phase is Greenwich phase, time zone is Greenwich Mean Time)

K1

Depth (m)	Major (cm/s)	S.D. (cm/s)	Minor (cm/s)	S.D. (cm/s)	Incl. (deg)	S.D. (deg)	Phase (deg)	S.D. (deg)
25	15.1	1.4	-0.6	0.5	198	3	357	2
60	14.5	0.6	-1.5	0.5	181	3	356	2
150	12.6	1.0	-2.4	0.2	172	8	360	4

Depth (m)	CW Amp (cm/s)	S.D. (cm/s)	CCW Amp (cm/s)	S.D. (cm/s)	CW phase (deg)	S.D. (deg)	CCW Phase (deg)	S.D. (deg)
25	7.9	0.8	7.2	0.6	195	5	201	2
60	8.0	0.4	6.5	0.4	177	4	185	4
150	7.5	0.5	5.1	0.5	172	8	172	9

O1

Depth (m)	Major (cm/s)	S.D. (cm/s)	Minor (cm/s)	S.D. (cm/s)	Incl. (deg)	S.D. (deg)	Phase (deg)	S.D. (deg)
25	6.9	0.8	0.8	0.3	198	5	303	7
60	6.8	0.3	-1.8	0.8	188	9	299	3
150	6.8	1.0	-3.4	1.2	207	23	274	16

Depth (m)	CW Amp (cm/s)	S.D. (cm/s)	CCW Amp (cm/s)	S.D. (cm/s)	CW phase (deg)	S.D. (deg)	CCW Phase (deg)	S.D. (deg)
25	3.0	0.3	3.8	0.5	141	10	255	7
60	4.3	0.5	2.5	0.4	127	8	249	10
150	5.1	0.5	1.7	1.0	121	12	293	37

3.3.3 PENNY STRAIT

Four current meters are of interest - Penny Strait East at 43 and 131 m, (PSE-S and PSE-D), and Penny Strait West at 49 and 138 m (PSW-S and PSW-D). The Penny Strait East data are plotted in Figures 3.3.11-3.3.14, and the Penny Strait West data are plotted in Figures 3.3.15-3.3.18. Both stations were in water of depth 190m.

M2

This region is expected to be the most confusing, because of complex bottom topography, and the changing orientation of the channel. Indeed, the shallower meters, being farther from the bottom, both display the more stable rotary amplitudes, although there is a sizeable migration of phases, of about 40 degrees in 4 months. The characteristic phase of the currents is about 260 to 300 degrees, and the phase of the elevation is about 190 degrees; the two are almost in quadrature, implying a limited flow of energy north from Barrow Strait. The inclinations are not aligned with the channel, and are best presented in the ellipse plots of Chapter 4.

For the two shallower meters, plotting the rotary spectral values again produces a stable counterclockwise amplitude, but the phase is not particular constant with time for either the clockwise or counterclockwise component. The deeper moorings do not even produce stable amplitude for the counterclockwise component. However, we note that at both depths at Penny Strait East the seasonal cycle of the phase time series is about the same. At Penny Strait West, the correspondence between top and bottom is not nearly as good, and in fact, probably nonexistent. It would seem that topography causes currents to have low spatial coherence, and seasonal changes cause them to be unpredictable, from a tidal point of view. In particular, there appears to be a strong seasonal effect in the harmonic constants, but with only one year of data, there is really insufficient information to state what the seasonal effects would be.

K1

For K1, the shallower meters show a stronger counterclockwise component, while the two components are of similar magnitude at the deeper meters. There is a 45 degree change of inclination from November to January, quite a large effect.

The following tables summarize the time series data, presenting mean and standard deviations of harmonic constants for the principal constituents M_2, S_2, K_1 and O_1.

PENNY STRAIT EASTERN STATION

(Inclination is measured in a Cartesian sense, phase is Greenwich phase, time zone is Greenwich Mean Time)

M2

Depth (m)	Major (cm/s)	S.D. (cm/s)	Minor (cm/s)	S.D. (cm/s)	Incl. (deg)	S.D. (deg)	Phase (deg)	S.D. (deg)
43	26.0	1.3	-6.8	1.1	31	15	260	4
131	14.6	1.8	-1.2	0.9	33	17	306	4

Depth (m)	CW Amp (cm/s)	S.D. (cm/s)	CCW Amp (cm/s)	S.D. (cm/s)	CW phase (deg)	S.D. (deg)	CCW Phase (deg)	S.D. (deg)
43	16.3	1.0	9.6	0.4	291	17	131	13
131	7.9	1.2	6.7	0.8	338	18	87	16

S2

Depth (m)	Major (cm/s)	S.D. (cm/s)	Minor (cm/s)	S.D. (cm/s)	Incl. (deg)	S.D. (deg)	Phase (deg)	S.D. (deg)
45	10.3	0.8	-2.4	1.0	32	16	316	8
131	5.5	1.2	0.0	1.6	43	20	350	15

Depth (m)	CW Amp (cm/s)	S.D. (cm/s)	CCW Amp (cm/s)	S.D. (cm/s)	CW phase (deg)	S.D. (deg)	CCW Phase (deg)	S.D. (deg)
45	6.3	0.7	3.9	0.6	348	22	76	13
131	2.7	1.1	2.8	0.8	34	26	53	23

PENNY STRAIT EASTERN STATION

(Inclination is measured in a Cartesian sense, phase is Greenwich phase, time zone is Greenwich Mean Time)

K1

Depth (m)	Major (cm/s)	S.D. (cm/s)	Minor (cm/s)	S.D. (cm/s)	Incl. (deg)	S.D. (deg)	Phase (deg)	S.D. (deg)
43	14.6	0.7	-1.5	0.8	24	14	17	3
131	12.8	1.7	-0.4	0.8	18	16	31	7

Depth (m)	CW Amp (cm/s)	S.D. (cm/s)	CCW Amp (cm/s)	S.D. (cm/s)	CW phase (deg)	S.D. (deg)	CCW Phase (deg)	S.D. (deg)
43	8.1	0.6	6.6	0.4	41	14	7	14
131	6.6	0.9	6.2	1.0	49	15	348	20

O1

Depth (m)	Major (cm/s)	S.D. (cm/s)	Minor (cm/s)	S.D. (cm/s)	Incl. (deg)	S.D. (deg)	Phase (deg)	S.D. (deg)
43	8.8	0.9	-0.6	0.9	19	12	316	6
131	8.1	1.6	-0.3	1.0	15	14	317	13

Depth (m)	CW Amp (cm/s)	S.D. (cm/s)	CCW Amp (cm/s)	S.D. (cm/s)	CW phase (deg)	S.D. (deg)	CCW Phase (deg)	S.D. (deg)
43	4.7	0.7	4.1	0.6	336	14	63	13
131	4.2	0.9	3.9	1.0	332	19	59	19

PENNY STRAIT WESTERN STATION

(Inclination is measured in a Cartesian sense, phase is Greenwich phase, time zone is Greenwich Mean Time)

M2

Depth (m)	Major (cm/s)	S.D. (cm/s)	Minor (cm/s)	S.D. (cm/s)	Incl. (deg)	S.D. (deg)	Phase (deg)	S.D. (deg)
49	18.3	2.8	-2.6	2.7	132	10	283	5
138	14.4	1.0	-1.1	1.3	17	7	282	10

Depth (m)	CW Amp (cm/s)	S.D. (cm/s)	CCW Amp (cm/s)	S.D. (cm/s)	CW phase (deg)	S.D. (deg)	CCW Phase (deg)	S.D. (deg)
49	10.4	2.7	7.9	0.5	54	10	209	11
138	7.7	1.0	6.6	0.6	299	14	95	10

S2

Depth (m)	Major (cm/s)	S.D. (cm/s)	Minor (cm/s)	S.D. (cm/s)	Incl. (deg)	S.D. (deg)	Phase (deg)	S.D. (deg)
49	8.1	2.6	-1.2	2.0	123	20	333	19
138	5.9	1.4	-0.7	1.4	19	18	350	20

Depth (m)	CW Amp (cm/s)	S.D. (cm/s)	CCW Amp (cm/s)	S.D. (cm/s)	CW phase (deg)	S.D. (deg)	CCW Phase (deg)	S.D. (deg)
49	4.7	2.0	3.4	1.1	96	35	150	17
138	3.3	1.3	2.6	0.5	7	35	29	14

PENNY STRAIT WESTERN STATION

(Inclination is measured in a Cartesian sense, phase is Greenwich phase, time zone is Greenwich Mean Time)

K1

Depth (m)	Major (cm/s)	S.D. (cm/s)	Minor (cm/s)	S.D. (cm/s)	Incl. (deg)	S.D. (deg)	Phase (deg)	S.D. (deg)
49	12.4	2.2	-5.8	1.8	103	9	23	15
138	4.1	1.1	-0.3	0.5	90	29	45	10

Depth (m)	CW Amp (cm/s)	S.D. (cm/s)	CCW Amp (cm/s)	S.D. (cm/s)	CW phase (deg)	S.D. (deg)	CCW Phase (deg)	S.D. (deg)
49	9.1	1.6	3.3	1.3	126	10	79	23
138	2.2	0.7	1.9	0.6	134	31	45	31

O1

Depth (m)	Major (cm/s)	S.D. (cm/s)	Minor (cm/s)	S.D. (cm/s)	Incl. (deg)	S.D. (deg)	Phase (deg)	S.D. (deg)
49	7.5	1.1	-3.9	1.0	108	24	324	29
138	3.3	0.7	-0.8	0.7	68	19	355	10

Depth (m)	CW Amp (cm/s)	S.D. (cm/s)	CCW Amp (cm/s)	S.D. (cm/s)	CW phase (deg)	S.D. (deg)	CCW Phase (deg)	S.D. (deg)
49	5.7	0.9	1.8	0.6	72	12	140	50
138	2.0	0.4	1.2	0.6	63	23	73	20

3.3.4 AUSTIN CHANNEL

Two time series are available, at 73m and 123 m, in water of depth 173 m. The M_2 data are plotted in Figures 3.3.19 and 3.3.20, and the K_1 data are plotted in Figures 3.3.21 and 3.3.22.

M2

Tidal currents may be expected to behave somewhat differently at this station. First, its geographic location is not so straightforward, being in the bend of a channel, which partially accounts for the smaller amplitudes, and the fact that the major and minor axes are similar in magnitude. the inclination is to the west, about 195° at 73 m and 160° at 123 m, and the phase is about 310 degrees, in a region where the elevation phase is 245° so that the phase relationship is similar to Barrow Strait - currents reach their flood maximum about 2.0 hours after high water. Once again, the composition into rotary spectra results in enhanced stability of the counter clockwise component. Interestingly, the clockwise component is the larger at both depths, so the rather simple model presented for Barrow Strait is not as applicable. Phases are again the more variable, with typical ranges of 30 degrees over a year, corresponding to about a 1 hour variability in the phase of any tidal phenomena.

K1

For the K1 constituent, the counterclockwise component is smaller at the shallower meter and larger at the deeper meter. Although currents are small, the general tendency is for quite stable harmonic constants. The inclinations are similar to that for the M_2.

The following tables summarize the time series data, presenting mean and standard deviations of harmonic constants for the principal constituents M_2, S_2, K_1 and O_1.

AUSTIN CHANNEL HARMONIC CONSTANTS

(Inclination is measured in a Cartesian sense, phase is Greenwich phase, time zone is Greenwich Mean Time)

M2

Depth (m)	Major (cm/s)	S.D. (cm/s)	Minor (cm/s)	S.D. (cm/s)	Incl. (deg)	S.D. (deg)	Phase (deg)	S.D. (deg)
73	5.9	0.5	-3.0	0.4	18	5	128	6
123	4.5	0.6	-1.2	0.4	40	5	159	6

Depth (m)	CW Amp (cm/s)	S.D. (cm/s)	CCW Amp (cm/s)	S.D. (cm/s)	CW phase (deg)	S.D. (deg)	CCW Phase (deg)	S.D. (deg)
73	4.5	0.4	1.5	0.2	145	9	251	5
123	2.8	0.5	1.6	0.2	200	10	241	3

S2

Depth (m)	Major (cm/s)	S.D. (cm/s)	Minor (cm/s)	S.D. (cm/s)	Incl. (deg)	S.D. (deg)	Phase (deg)	S.D. (deg)
73	3.0	0.6	-1.2	0.5	24	5	191	8
123	2.1	0.4	-0.2	0.3	45	12	219	13

Depth (m)	CW Amp (cm/s)	S.D. (cm/s)	CCW Amp (cm/s)	S.D. (cm/s)	CW phase (deg)	S.D. (deg)	CCW Phase (deg)	S.D. (deg)
73	2.1	0.6	0.9	0.1	215	11	193	7
123	1.1	0.3	0.9	0.1	264	24	186	9

AUSTIN CHANNEL HARMONIC CONSTANTS

(Inclination is measured in a Cartesian sense, phase is Greenwich phase, time zone is Greenwich Mean Time)

K1

Depth (m)	Major (cm/s)	S.D. (cm/s)	Minor (cm/s)	S.D. (cm/s)	Incl. (deg)	S.D. (deg)	Phase (deg)	S.D. (deg)
73	5.3	0.3	-1.0	0.4	12	3	231	4
123	4.8	0.3	0.7	0.3	23	3	247	4

Depth (m)	CW Amp (cm/s)	S.D. (cm/s)	CCW Amp (cm/s)	S.D. (cm/s)	CW phase (deg)	S.D. (deg)	CCW Phase (deg)	S.D. (deg)
73	3.2	0.3	2.2	0.1	243	6	140	5
123	2.0	0.2	2.8	0.2	270	5	137	5

O1

Depth (m)	Major (cm/s)	S.D. (cm/s)	Minor (cm/s)	S.D. (cm/s)	Incl. (deg)	S.D. (deg)	Phase (deg)	S.D. (deg)
73	3.8	0.3	-0.6	0.4	10	4	164	8
123	3.5	0.4	0.7	0.3	22	6	181	9

Depth (m)	CW Amp (cm/s)	S.D. (cm/s)	CCW Amp (cm/s)	S.D. (cm/s)	CW phase (deg)	S.D. (deg)	CCW Phase (deg)	S.D. (deg)
73	2.2	0.3	1.6	0.1	173	11	206	6
123	1.4	0.2	2.1	0.2	204	13	201	8

4 SPATIAL DISTRIBUTIONS

Tides are a very large scale phenomenon and the tide at any given location depends on the geometry and bathymetry of the larger basin of which it is a part. Consequently, tides display coherent spatial patterns. This chapter is devoted to a presentation of the horizontal observed in sea-level elevations and currents; the next chapter discusses observed vertical current profiles at a selected set of locations. The following extensive compendium of figures include co-range and co-phase diagrams, contour plots of phase age and the ratio of diurnal to semi-diurnal character for tidal elevations, and ellipse plots for currents. In interpreting these figures, frequent reference will be made to the wave-like character of the tide although the emphasis here is descriptive; a detailed discussion of the theoretical implications of the observed patterns is deferred to Chapter 6. The reader unfamiliar with tidal or physical oceanographic phenomena should simply skip over these references.

Co-range / co-phase plots are useful in two respects. First, they present the amplitude and phase of the tide in a readily assimilable form. In a practical sense, they are used to judge data quality and density. For example, one may use them to decide if a given station fits into the overall pattern revealed by its neighbors or if the observed data is sufficiently dense in regions of rapid change to resolve tidal features of interest. These diagrams thus assist in the design of further field programs and, ultimately, in tidal prediction. From a theoretical point of view, they illustrate several aspects of tidal propagation which aid in the analysis of the dynamic character of the system.

The phase age is defined as the time in hours between new moon and the observed spring tide. If the tides behaved according to an idealized equilibrium theory (Appendix B), the conjunction of the moon, earth, and sun would coincide with the spring tide. Since the appearance of a full or new moon is readily observed, this parameter is one on practical significance. The ratio, $R = (K1 + O1) / (M2 + S2)$, of the sum of the two largest diurnal amplitudes to the sum of the of the largest semi-diurnal amplitudes is a commonly used measure of the character of the tide. For $R < 0.25$, the tide is considered primarily semi-diurnal, for $0.25 < R < 1.25$ it is called mixed, and for $R > 1.25$ the tide is primarily diurnal.

Ellipse plots also convey information of a both a practical and theoretical nature for currents. For example, they provide an indication of the magnitude of the tidal streams, and the degree of circular polarization. From a theoretical viewpoint, they contain information concerning the degree of standing or progressive wave character, the types of waves present (Kelvin and/or Poincaré), and the direction of the net energy flux, All the results presented in this chapter are based ultimately on the calculated harmonic constants; averages of individual non-overlapping one month analyses were used for the figures. Since almost all of the observed current data is limited to one-month or three-month duration in the spring prior to ice-breakup, it is clear that the ellipse plots are biased towards spring conditions. Thus it would be prudent to anticipate significant deviations over the remainder of the year. Indeed, this was indicated in the time series plots of harmonic constants given in Chapter 3. On the other hand, the harmonic constants for elevation are more stable, although actual water levels are subject to strong, non-tidal seasonal variations.

4.1 CO-RANGE / CO-PHASE DIAGRAMS

For presentation, the study area was divided into five subregions: Parry Channel, the Prince Regent Inlet - Gulf of Boothia system, M'Clintock Channel, Prince of Wales Strait and the Queen Elizabeth Islands region (Figure 4.1.1). Each is discussed separately. The figures consist of two panels per constituent, one listing the observed values at each tidal station and the other showing a contoured (and hence a smoothed and interpolated) representation. Plots of phase age and diurnal/semi-diurnal character complete each discussion.

Four representative tidal constituents are considered: the two major semi-diurnal components, M_2 and S_2; and the two largest diurnal constituents, K_1 and O_1. For Parry Channel, additional plots are included for one long period tide, MSf (period: 14.7 days) and one high frequency, shallow water component, MK_3 (period: 8 hours and 11 minutes). Strictly speaking, both these two components are shallow water constituents that are not driven directly by astronomical forces but rather arise from the non-linear interaction among the major tidal components, and they should be largest where bottom friction and the tidal streams are large. Specifically, MK_3 is forced by the interaction between M_2 and K_1, while MSf results from an interaction among M_2, S_2 and N_2. In fact, however, MSf is the tidal parent for the larger Mf and minor Mm constituents in the harmonic analysis scheme, neither of which which were inferred. Thus the MSf constants also embody these signals. Even more importantly, the MSf amplitude and phase are contaminated by non-tidal, fortnightly band currents and sea-level fluctuations. Indeed, the non-tidal contribution to the harmonic constants often exceeds the purely tidal contribution. The stability of the amplitudes and phases and the pattern of co-phase and co-range lines will indicate the importance of non-tidal effects: if the constants do not vary significantly with time, and if the spatial plots suggest a coherent pattern, then one may infer that the MSf signal is largely tidal. In summary, the MSf constituent represents the typical fortnightly tide, contaminated by non-tidal effects.

4.1.1 PARRY CHANNEL - THE NORTHWEST PASSAGE (Figures 4.1.2 - 4.1.9)

Parry Channel is the largest region considered here, but on a global scale it is still a relatively minor waterway between the much larger Arctic Ocean and Baffin Bay. Consequently, the tides there should have an intermediate character moderated by local geometric and bathymetric features. That is they should gradually evolve from the large tides of Baffin Bay to the almost insignificant tides observed at the western intersection with the Arctic Ocean. (Appendix A, Tides in the Arctic Ocean). This is indeed the case, and an attempt is made in this chapter and the next to show how the observed data fits into this overall pattern. Unfortunately, there is insufficient data to extend the plots into M'Clure Strait. Data from the Schwiderski model could be used, except that it's accuracy in the Arctic is questionable, compared to the observed data which was used to construct the remainder of the plot. It's inclusion led to very large and unrealistic phase and amplitude changes through M'Clure Strait. Mould Bay data was considered, but the location of that station did not significantly extend the interpolation polygon into M'Clure Strait, and in fact that station is outside the boundaries of the Parry Channel base map selected for this report. Data from the Northwest coast of Banks Island is required to complete the description of tides in Parry Channel.

As the M_2 tidal wave propagates from east to west, its amplitude diminishes. Much of the drop occurs in Barrow Strait, suggesting increased frictional dissipation in its relatively shallow waters. South of Melville Island in Viscount Melville Sound, there exists both a local minimum and maximum in amplitudes. The minimum is due to what appear to be anomalously low values observed at the easternmost Melville Island stations. These values were retained for the computer-generated plots since there were no apparent reason to reject it, but they should be accepted with caution. Moreover, this station is not demonstrably anomalous in the diurnal tidal band (see below). The S_2 tide is similar to M_2 (Figure 4.1.2.) and is not discussed separately.

The K_1 amplitude also drops dramatically during the east to west transit of the K_1 tidal wave, and again much of this decrease is concentrated in Barrow Strait. However, the phase changes more uniformly along the channel, compared with the semi-diurnal band. The eastern Melville Island station amplitudes do not appear to be low, lending support to their retention in the semi-diurnal plots.

The O_1 tide is very interesting because it departs from this pattern. While its amplitude attenuates along the channel similar to K_1, its phase is much more complex and exhibits a minimum in Viscount Melville Strait. Moreover, this minimum is much stronger along the southern shore with a cross-channel phase difference of about 30°(or two hours at diurnal frequencies). A picture more consistent with K_1 could be obtained by discarding the two southern values from Banks Island and Victoria Island, but they represent recent and presumably accurate measurements. Alternatively, one might argue that the dissimilarity is due to the shallow water tide of identical frequency that is driven by the non-linear interaction between the M_2 and K_1 tides. However if this explanation is true, then other shallow water constituents should also be significant, and they are not, as is shown in the next section. In particular, the MK_3 tide, which also arises from a M_2 - K_1 interaction, is uniformly small, as will be seen. It is clear that a consistent explanation will require further investigation.

The amplitude of the MSf component is everywhere small, nowhere exceeding 6 cm, and the co-phase lines do not suggest a coherent propagation pattern. Rather it is more likely that a large fraction of the observed sea-level variance (in fact, bottom pressure variance) at this frequency is due to non-tidal effects.

The MK_3 amplitude is extremely small, exhibiting a maximum of only 0.5 cm. Its phase plot shows that it is not a simple propagating wave tide; if it were, its phase would change 3 times more rapidly than the diurnal tides. The most active area is to the east of Barrow Strait.

The phase difference between new or full moon and the subsequent spring tide lies between 48 and 72 hours. That is, spring tides are expected 2 - 3 days following conjunction, a relatively large value compared with most other bodies of water. R is everywhere smaller than 0.4: the tides range from purely semi-diurnal to mixed, predominately semi-diurnal.

4.1.2 PRINCE REGENT INLET AND GULF OF BOOTHIA (Figures 4.1.10 - 4.1.14)

A long narrow channel closed at one end is likely to respond in a predictable manner to tidal forcing at the open boundary with Parry Channel and partial reflection of the incident wave from the closed end. As discussed in Chapter 6, this proves to be the case for the Prince Regent Inlet - Gulf of Boothia system.

As the M_2 tide propagates into Prince Regent Inlet, it observes the standard rule of "larger tidal range on the right", and rotates about the degenerate amphidrome located near Van Koenig Point on the Baffin Island shore. Amplitudes are largest near the opening, decrease to a minimum at Van Koenig Point, and then increase again towards the south.

S_2 is very similar to M_2 and is not plotted; N_2, however, deviates considerably from the general pattern and thus is plotted here. Whereas, the M_2 and S_2 phases increase southward uniformly along the Baffin Island coast and the M_2 and S_2 tidal waves peak approximately 1.25 hours later at Van Koenig Point than at the northern entrance, the N_2 phase initially increases, but then falls so that high water at Van Koenig Point leads that at the entrance by about one half hour.

K_1 and O_1 increase in amplitude monotonically towards the head of the Gulf. The phase progression is not as uniform, but suggests propagation inward from the entrance. At a given latitude, the phase along the western shore leads the eastern shore by about 20° (approximately 1.4 hours).

Phase age decreases from about 60 hours at the entrance to less than 48 hours in sections of the Gulf of Boothia. *R* increases from 0.4 at the mouth to about 1.0; that is, the diurnal character becomes more important as one proceeds up-channel, consistent with the increasing amplitude of K_1.

4.1.3 M'CLINTOCK CHANNEL (Figures 4.1.16 - 4.1.18)

M'Clintock Channel is similar in shape and size to the Prince Regent Inlet - Gulf of Boothia system, and one should expect a similar tidal regime. This is indeed the case. The propagation of the M_2 wave downchannel from Parry Channel is obvious. A characteristic feature of this system is the continuation of the wave around Prince of Wales Island and out Peel Sound. A similar pattern, but more slowly varying is seen in the diurnal tide.

The phase age exceeds three days, somewhat greater than that observed in Parry Channel. Although the M_2 amplitude is approximately twice that of K_1, the ratio *R* is everywhere near unity, significantly greater than the value of 0.4 at the open boundary.

4.1.4 PRINCE OF WALES STRAIT (Figures 4.1.19 - 4.1.23)

The tides within Prince of Wales Strait are determined by those at the two open boundaries and consequently prove to be somewhat more complex than those observed in the other basins. M_2 appears to propagate northward along the channel: its amplitude is generally larger on the Victoria Island side, and its phase increases uniformly towards the north to a maximum near the northern entrance. S_2 displays a similar pattern and is not shown. Diurnal amplitudes are very small, never exceeding 5 cm. The K_1 tide propagates from north to south, whereas O_1 propagates from the southern entrance to the north like the semi-diurnal constituents.

The phase age is almost uniform within Prince of Wales Strait except near Station 92 (Jesse Harbour) where it decreases from about 72 hours to less than 48 hours. The tide is semi-diurnal, but becomes more mixed in character towards the southern open boundary with Amundsen Gulf.

4.1.5 THE QUEEN ELIZABETH ISLANDS REGION (Figures 4.1.24 - 4.1.27)

The remainder of the tide gauges available to this study were those installed in the waters surrounding the Queen Elizabeth Islands. Unlike the other regions, this area is not channel-like and its connections with Baffin Bay and the Arctic Ocean are more diffuse. Thus one should expect different tidal patterns to emerge, and indeed this is the case.

M_2 generally decreases in amplitude and increases in phase towards the west, consistent with westward phase propagation. The general alignment of phase and elevation contours implies considerable frictional damping of the wave on its westward progression. M_2 amplitudes drop from approximately 80 cm in the east to about 10 cm in the west, whereas S_2 drops from about 30 cm in Baffin Bay to less than 5 cm at the western edge (not shown). Much the same pattern prevails for the diurnal tides. The K_1 amplitude falls from about 20 cm in the east to less than 5 cm along the western edge of the basin. Similarly O_1 is everywhere small as it decreases from approximately 8 cm to less than 1 cm (not shown).

Phase age varies slowly from less than 48 hours in the east to more than 60 hours in the west, somewhat less than the values directly south in Parry Channel. Tidal character is predominantly semi-diurnal.

4.2 ELLIPSE PLOTS

Distillation of the large amount of available current meter data into a readily assimilable set was a formidable challenge. To reduce data quantity, the calculated monthly harmonic constants at each station were simply averaged. For some stations however, data was obtained from separate moorings deployed over a period of years, and a simple averaging procedure was not justified statistically as the individual estimates differed dramatically from the mean. In these cases the harmonic constants were chosen subjectively; supporting information is contained in the tables. In any event, the reader is cautioned to remember in making comparisons that data from different areas may have been collected in different years, and that no estimate is available of the interannual variability of currents.

A few comments are required regarding the interpretation of the ellipse plots. Each ellipse represents the path traced out by the velocity vector in one tidal period. The length of the vector at any time is proportional to the speed and may be estimated from the scale; note, however, that the scale differs from plot to plot. The indicated vector for each ellipse also defines the phase. Several choices of phase are available, but probably the most useful is that with respect to local high water, because this choice defines the direction of mean energy flux. That is, the direction of the current at local high water points in the direction of net energy flow for each constituent. In addition to its obvious meaning, this choice makes analysis of the wavelike nature of the tide more direct. For example, a phase difference of zero indicates a purely progressive wave, whereas a phase shift of 90° implies a standing. Intermediate values represent waves with intermediate character. Finally, the sense of rotation of the velocity vector is indicated by the curved arrow. This is of particular relevance since the possibility exists that the semi-diurnal constituents are contaminated by inertial oscillations, which are purely clockwise polarized. As the ellipticity of the ellipse decreases - that is as the currents become more nearly rectilinear - the significance of the rotational sense diminishes. Relatively little comment will be made regarding the direction of polarization since variations with either depth or distance are difficult to explain and are probably of little value to the non-technical observer. The ellipse plotting scheme is summarized in Figure 4.2.1.

Three geographic sub-regions are used for presentation and differ somewhat from the areas used for the co-range/co-phase plots (Figure 4.2.2). The first consists of various sections of Parry Channel; the second is made up of waterways that adjoining Parry Channel and includes M'Clintock Channel and Prince of Wales Strait, both of which are treated distinctly in the discussion of the elevation fields; and the third includes the waters surrounding the Queen Elizabeth Islands. Each region is discussed separately. Where meters have been moored at more than one depth, their ellipses have been grouped into four depth ranges: (1) *near surface* (0 - 25 m); (2) *upper layer* (35 - 75 m); (3) *intermediate* (100 - 225 m); and *deep* (> 500 m). In most cases, the ellipse plots are self-explanatory, and the accompanying descriptions are therefore relatively terse.

4.2.1 PARRY CHANNEL - THE NORTHWEST PASSAGE

Several features in Parry Channel can be anticipated based on the co-range/co-phase diagrams. First, the energy flux should be generally westward coincident with the direction of propagation. Second, current amplitudes should diminish towards the west coincident with tidal range. Third, the ellipses in Barrow Strait should reflect the enhanced dissipation there and probably should be more circular due to the likely importance of Poincaré waves.

For discussion, Parry Channel is broken into in seven distinct geographic blocks, three within the main channel and four representing the three southern and one northern side-channels.

4.2.1.1 LANCASTER SOUND (Figures 4.2.3 - 4.2.8)

Although the data here are sparse (3 moorings in 1979), they represent three of the four vertical layers: the upper, intermediate, and deep zones. Moreover, these data are crucial to understanding the tidal dynamics of the Northwest Passage since they are the only data observed near the open boundary with Baffin Bay.

The M_2 ellipses are consistent with expectation and portray near-rectilinear flow, westward energy transport, and a barotropic character (at least below 40 m). The S_2 ellipses paint a similar picture with the exception of the upper layer meter at Station 01-L where the currents are nearly circular. The clockwise polarization suggest contamination by inertial currents, but the investigation discussed in Chapter 6 suggests that the inertial energy was relatively small below the near-surface waters. Moreover, N_2 behaves similarly at all three upper layer stations (not shown), and since M_2 lies between S_2 and N_2 in frequency, it is not sensible to ascribe the decreased eccentricity to inertial currents. The question requires further study. In any case, the semi-diurnal currents are quite weak (< 10 cm/s).

Despite their modest contribution to sea surface elevation, the diurnal currents are stronger than the semi-diurnal flows, with amplitudes of about 15 cm/s for K_1 and 10 cm/s for O_1. The relative constancy of the K_1 and O_1 ellipses implies the tide is barotropic below 40 m.

The moorings were in place long enough to deduce the fortnightly tide. However, commensurate sea level data was not available, so the direction of energy transport for this constituent cannot be estimated; the indicated phase is simply the Greenwich phase. The currents are nearly rectilinear and are strong at about 30 cm/s. Indeed, the fortnightly tidal variance is greater than that observed for either the semi-diurnal or diurnal constituents. It is not possible to estimate what percentage of this variance is non-tidal.

4.2.1.2 **BARROW STRAIT** (Figures 4.2.9 - 4.2.13)

The semi-diurnal ellipses display certain expected properties: currents are more circular in mid-channel, indicative of Poincaré waves that are no doubt generated by the shoaling, narrowing topography of Barrow Strait; and all meters indicate a westward component to the energy flux, although there exist interesting variations about the mean. There are also interesting changes in polarization with depth, with the near-surface currents tending to be more circular (note the exception of Station 46B). Speeds generally peak at mid-depth, although the near-surface meters may lie within the ice boundary layer and thus may be slowed by the effective drag exerted by the ice. If this is the case, the near-surface ellipse orientation should lie 10 - 40° to the left of the deeper currents due to the influence of the earth's rotation. This appears to be true except for S_2 at Station 44-BSW. this hypothesis and others are explored more fully in Chapter 6.

The diurnal currents are much more rectilinear, and are of similar magnitude to the semi-diurnal currents, a major change from Lancaster Sound. Again energy flows to the west, but with much less variability in direction.

4.2.1.3 **VISCOUNT MELVILLE SOUND** (Figures 4.2.14 - 4.2.24)

Results from Viscount Melville Sound are presented in two sets of figures, one representing a set of scattered stations occupied at different times by different groups in the eastern section and the other a line of stations further west stretching between Melville and Stefansson Islands that were occupied during NWP-82. One might expect the currents to begin to display properties more characteristic of the Beaufort Sea, namely smaller magnitudes.

M_2 and S_2 are similar in most respects and are not weaker than their Barrow Strait counterparts. Again an energy flux with a westward component is found at most stations but not all. Some of these anomalies may be explained by the the obvious geometric or bathymetric influence on the flow (for example to the east of Byam Martin Island), but the others merit further investigation. Currents near Barrow Strait tend to be more circularly polarized than those further west. One may speculate that this is due to Poincaré waves generated in Barrow Strait, but there is no way of easily testing this hypothesis. Little consistency in the rotational direction (clockwise or counterclockwise) is observed.

The diurnal currents are similar in magnitude to the semi-diurnal streams, although the K_1 velocities are now noticeably slower than M_2. Magnitudes tend to decrease to the west, and with a few notable exceptions, the currents are consistent with a general westward flow of energy. The implied energy flux at Station 21 north of Steffansson Island is difficult to understand, but it may be due to the local bathymetry and the adjacent small island. Similar remarks apply to the weak onshore flux at Station 25 and eastward flux at Station 24. The large diurnal current observed at Station 72 is presumably a shallow water effect, as the station lies in only 40 metres of water. Most of the ellipses are clockwise polarized.

The meters along the cross-section were moored long enough to estimate the MSf constituent, but the results are difficult to accept because they indicate a cross-channel flow. Again, the percentage of non-tidal variance present cannot be estimated. In any case, the fortnightly signal is quite small.

4.2.1.4 M'CLURE STRAIT (Figures 4.2.25 - 4.2.29)

The co-range/co-phase diagrams identified M'Clure Strait as an interesting region because much of the transition to the Beaufort Sea regime likely occurs there. The data include a single line of near-surface current meters moored across the strait.

Both the semi-diurnal and diurnal currents are noticeably weaker than those observed elsewhere in Parry Channel. M_2 is the most energetic constituent with typical speeds of 7 cm/s. It is nearly rectilinear on the northern side and becomes more circular in mid-channel and on the southern shore. The same pattern is not observed for S_2, however, which displays cross-channel, nearly rectilinear flow in the south. The semi-diurnal energy flux is complex with a westward flow at the northernmost two stations and a confused pattern elsewhere.

By contrast, the diurnal streams are more coherent, albeit significantly weaker. Both the K_1 and O_1 currents are almost rectilinear, and there is a general pattern of outward (to the Beaufort Sea) energy transport with the exception of K_1 at Station 14 and O_1 at Stations 12 and 13.

4.2.2 WATERWAYS ADJOINING PARRY CHANNEL

4.2.2.1 WELLINGTON CHANNEL (Figures 4.2.30 - 4.2.34)

Current meters were moored across both ends of Wellington Channel during NWP84 and were maintained long enough to permit the extraction of the fortnightly signal.

As expected, the current at most meters is directed along-strait, and the energy flux is everywhere to the north. The currents are almost strictly rectilinear along the northern line but less so in the south. Along the southern line, the semi-diurnal currents are uniformly counterclockwise polarized in contrast to the diurnal flows which are strictly clockwise polarized.

The Mf currents are less than 10 cm/s in magnitude, and the ellipses do not portray a coherent picture, probably due to contamination by non-tidal phenomena.

4.2.2.2 **PEEL SOUND** (Figures 4.2.36 - 4.2.40) (Figure number 4.2.35 is not used)

A line of five moorings near the open boundary with Barrow Strait was occupied during 1981; meters on two of the moorings sampled the near-surface, upper layer, and deep sectors.

M_2 is again the most intense constituent with typical speeds of 10 cm/s, roughly twice the strength of S_2 and about four times stronger than the diurnal flows. Energy is transported out of Peel Sound into Barrow Strait in the semi-diurnal band and into Peel Sound in the diurnal band.

The semi-diurnal currents display a very interesting vertical structure. In particular, the M_2 ellipses are almost circular in the near surface layer, become more eccentric with depth (50 m and 100 m), and become circular again as the bottom is approached. In addition, both the shallow and deep ellipses are anticlockwise polarized whereas both ellipses at 50 m are clockwise polarized. The S_2 pattern is similar but more complex. For example, at 10 and 200 m, the currents rotate in opposite directions. Moreover, the energy flux at 200 m is southward in contrast to the other observed semi-diurnal flows. Two possible explanations for this interesting behaviour are offered in Chapter 6.

By comparison, the diurnal currents are straightforward. They are nearly rectilinear, and all transport energy southwards. Variations with depth are minor implying a predominately barotropic tide.

4.2.2.3 **M'CLINTOCK CHANNEL** (Figures 4.2.41 - 4.2.45)

A string of near surface meters was laid across M'Clintock Channel near the opening to Viscount Melville Sound during NWP84. Unfortunately, the mid-channel moorings did not return usable information.

The semi-diurnal currents display varying degrees of ellipticity but are more circular away from the channel walls. In all cases, the M_2 and S_2 streams rotate anti-clockwise and transport energy southward. The currents are weak, however, with a typical magnitudes below 10 cm/s. These observations are consistent with the co-range/co-phase plots and imply that most of the energy incident from Parry Channel is absorbed within the system.

With the exception of K_1 at Station 87, the diurnal streams are very weak. The flows are nearly rectilinear and are generally aligned along-channel.

4.2.2.4 AUSTIN AND BYAM MARTIN CHANNEL (Figures 4.2.46 - 4.2.55)

Together, Austin and Byam Martin Channels form a passage between Parry Channel and the waters of the Queen Elizabeth Islands. Austin Channel is relatively short (100 km) and is split by a large shoal at the opening to Viscount Melville Sound into two subchannels. The principal passageway to the west is the most direct route to Byam Martin Channel and typically 200 m deep. The eastern sector is longer and shallower, but is nowhere less than 100 m in depth. Byam Martin Channel is about the same length but is slightly deeper on average with depths everywhere exceeding 150 m.

Data in Austin Channel are of varying quality and were obtained during several separate efforts made over a period of a few years. For example, Stations 882 and 895 were occupied in 1978; 895 returned a month's data, but only 9 days data were obtained at 882. By contrast, meters were maintained at 73 and 123 m for a full year during 1983-84 at Station 71. Finally, the near surface meter at Station 71 produced data for 2 months in 1983, simultaneous with the other 2 meters at that station. Geographically, Stations 895 and 892 were positioned within the main western channel while the remaining stations were located in the eastern channel. In addition, Station 71 was just to the north of a NW-SE oriented ridge that shoals to about 7 m. The Byam Martin Channel line was in place for two months (Apr - May) in 1983.

The semi-diurnal currents in Austin Channel are all clockwise polarized and only slightly elliptic. With the exception of the deep flux at Station 71, energy flows approximately parallel to the entrance to Austin Channel, in a southwestward direction across the shoal - presumably a continuation of the general westward flow of energy in Parry Channel. The deep Station 71 energy flux is difficult to explain, because it is directed nearly perpendicular to the ridge. In Byam Martin Channel, the currents are much more rectilinear and slightly stronger. The S_2 ellipses all imply a southward flow of energy, but the M_2 pattern is confused and is difficult to explain.

The diurnal currents are weaker, but exhibit a similar pattern. The Austin Channel currents are less elliptical and display a non-uniform rotational sense. Energy flow is directed into the western section of Austin Channel at the open boundary, and to the southwest at the inner stations. In Byam Martin Strait, the currents are again more rectilinear, and with the exception of Station 65 imply a northward transport of energy. Since only 20 days of data were obtained at 65, this result may not be general. The rotational sense is uniformly clockwise.

4.2.2.5 PRINCE OF WALES STRAIT (Figures 4.2.56 - 4.2.60)

A string of near-surface moorings was occupied for three months in 1982 (Apr-Jun) across Prince of Wales Strait near the northern boundary with Melville Sound.

Tidal currents within Prince of Wales Strait are strong in comparison with other Northwest Passage locations. M_2 streams exceed 15 cm/s in places, about twice the speed of the other major constituents. Diurnal flows are slower, but still significant. Ellipses are highly rectilinear and directed along channel. In the semi-diurnal band, the S_2 energy flux is strictly down-channel from Viscount Melville Sound toward the Beaufort Sea, generally opposing the M_2 flux which also displays a tendency for cross-channel transport. In the diurnal band, the K_1 tidal wave carries energy downchannel whereas the O_1 wave transports energy into Viscount Melville Sound.

4.2.3 THE QUEEN ELIZABETH ISLANDS REGION

4.2.3.1 PENNY STRAIT (Figures 4.2.61 - 4.2.65)

Penny Strait is a short and narrow (60 by 40 km) channel separating Bathurst and Devon Islands; it connects the waters surrounding the Queen Elizabeth Islands with Queens Channel which in turn ultimately communicates with Parry Channel through Wellington Channel. Penny Strait is split in turn by a string of islands including John Barrow and Hyde Parker. Depths to the east are typically 150 m or more, while those to the west are somewhat shallower.

Stations PS-E and PS-W lie on opposite sides of this chain, and PS-E was positioned near several shoals with depths of about 90 m. Both moorings were maintained for a full year during 1984-85. On the other hand, Stations 12-E and 14-W represent only a month's data collected in 1976 and are thus less reliable.

The tidal currents are relatively strong in both bands; M_2 amplitudes, for example, exceed 20 cm/s in the upper layer at both PS-E and PS-W. The shallow flow is directed along channel, but the deeper currents are all cross-channel except for the along-channel upper layer streams at PS-W. The uniformity of the deep currents implies bathymetric control, but further study is required to explain these unusual results. A similar pattern is seen in the diurnal band at PS-E, except that the flow at PS-W is aligned with the channel.

4.2.3.2 MACLEAN / DESBARATS / DANISH STRAITS (Figures 4.2.66 - 4.2.70)

Maclean, Desbarats, and Danish Straits make up part of the inner waters of the Queen Elizabeth Island archipelago. All are deep, with soundings in excess of 300 m. Five currents meters were moored in these waters for about a month (April) in 1979.

Currents in Danish Strait are the strongest and most rectilinear, as they are undoubtedly controlled by the relatively narrow channel width; currents in Desbarats Channel are nearly circular, and those in MacLean Strait are intermediate in character. All the streams in Maclean and Desbarats Straits are circularly polarized, opposite to that observed in Danish Channel. In general, the energy flux in both tidal bands is westward at all stations.

4.2.4 REGIONS OF EXTREME CURRENTS

It is always of considerable interest to note regions of extremely rapid currents. Pioneer Channel, at the northern end of Wellington Channel, is a region noted for high currents, and data from that are will be presented in the following section. Other regions of strong currents are summarized in the following table. The Fury and Hecla Strait information is from Sadler *et al*. (1979), the remainder from "Sailing Directions - Arctic Canada, Vol II." With the exception of Pioneer Channel, the data is quite qualitative.

TABLE 4.2.1
SUMMARY OF LOCAL STRONG TIDAL FLOWS

REGION	LOCATION	Current Description
Pioneer Channel	North end of Wellington Channel	M2 amplitudes of 54 cm/s; total tidal signal maximum is about 1 m/s
Labrador Narrows - Fury and Hecla Strait	Connects Foxe Basin to the Gulf of Boothia	A steady current of 1 to 2.5 m/s flows to the east. Sadler *et al*. note tidal currents of up to 3 m/s.
Hell Gate /Cardigan Strait	Connects Jones Sound to Norwegian Bay	a permanent south-going current of 0.75 - 1.75 m/s exists in conjunction with tidal streams of about 0.5 m/s.
Bellot Strait	Separates Somerset Island from Boothia Peninsula	Tidal streams up to 8 knots have been observed.

4.2.4.1 **PIONEER CHANNEL** (Figures 4.2.71 - 4.2.75)

Pioneer Channel is a connection between the north end of Wellington Channel and Penny Strait. It separates Sheills Peninsula, on the southwest tip of Devon Island from Dundas Island. The bottom bathymetry is quite complicated, depths varying from 20m to 50m, and the *thalweg* of the channel is aligned almost north-south, rather than the east-west direction indicated by the relevant coastlines. One of the stations (#5) was situated in a polynya, the remainder under the ice at nearby locations. Station 4 was situated somewhat to the west of Pioneer Channel, out of the complex current field within the Channel itself. With the exception of Station 4, currents are strong, and tend to be organized into and eddy-like structure.

Considering the semi-diurnal band first, we note that the M_2 amplitude at Station 2 is 51 cm/s, the largest of any station in this study. As well, Stations 1 and 3 are counter-flowing, suggesting an eddy situated in the middle of the channel. The polynya station does not differ significantly from its neighbour, Station 1. The S_2 currents display similar behaviour, but with slightly reduced amplitudes.

The overall pattern of the diurnal band is similar to the semi-diurnal, with Stations 1 and 3 being counter-flowing, and Station 1 tending to a north-south flow. Interestingly, the O_1 amplitudes are larger than the K_1, no doubt in response to the large velocities in the the channel, and hence enhanced non-linear interactions (Recall that O_1 is both an astronomical tide and one of the products of M_2 and K_1). The diurnal currents at the polynya station are similar to the neighboring Station 1, although significantly reduced in amplitude.

5 VERTICAL STRUCTURE OF TIDAL CURRENTS

5.1 DATA AVAILABILITY

In Chapters 3 and 4, it was noted that there was considerable vertical variation of tidal current parameters. In this section, this vertical variation will be presented in more detail. Attention is concentrated on those stations where there were two or more meters moored on a line. The relevant stations are tabulated in Table 5.1.

TABLE 5.1

STATIONS USED TO DESCRIBE VERTICAL STRUCTURE OF CURRENTS

STATION	LOCATION	LAT	LONG	METER DEPTH	WATER DEPTH
1	Lancaster Sound	74° 5.5	81° 10.0	39,203	772
3	Lancaster Sound	74° 7.4	82° 13.0	51,216	741
2W12,2W100	Wellington Channel	75° 15.9'	93° 0.5'	12,100	133
3W12,3W100	Wellington Channel	75° 15.8	92° 51.0	12,100	160
46B	Barrow Strait	74° 13.3	93° 38.3	25,60,150	170
46	Barrow Strait	74° 13.4	93° 41.2	10,50,150	170
46A	Barrow Strait	74° 13.1	93° 45.5	10,40,60,80,150	170
44-BSW	Barrow Strait	74° 24.1	93° 54.7	10,50,142	162
42	Barrow Strait	74° 34.0	94° 1.1	18,51,100	129
42A	Barrow Strait	74° 34.0	94° 1.1	10,40,60,80,120	139
42B	Barrow Strait	74° 34.0	94° 1.1	10,50,115	139
84	Peel Sound	73° 41.6	96° 0.0	10,50,100,225	230
82	Peel Sound	73° 41.6	96° 37.0	10,50,100,200	230
828	Barrow Strait	74° 40.3	96° 43.8	4,50	210
838	Barrow Strait	74° 38.2	97° 58.2	4,50	88
842	Barrow Strait	74° 26.7	97° 6.4	4,50	137
835	Barrow Strait	74° 52.8	98° 17.0	4,50	92
845	Barrow Strait	74° 40.3	96° 43.8	4,50	126
838	Barrow Strait	74° 10.0	98° 34.0	4,50	210
PSE-S, PSE-D	Penny Strait	76° 38.0	96° 54.0	43,131	186
PSW-S, PSW-D	Penny Strait	76° 36.0	97° 25.0	49,138	190
932	Danish Strait	77° 50.0	100° 46.0	5,50	210
71	Austin Channel	75° 23.0	102° 38.0	18,73,123	173

The data from each station will be examined according to the ordering in Table 5.1. In each case, the ellipse parameters are tabulated for the four largest constituents, M_2, S_2, K_1 and O_1. In addition, in most cases the rotary spectral parameters are also tabulated.

The reader is reminded of a few conventions used in the following tables. Depths are in metres. Current amplitudes are in cm/s, and phases are Greenwich phases, using as time zone Greenwich Mean Time. Inclination of the current ellipses is with respect to a Cartesian co-ordinate system, with an inclination of 0 degrees corresponding to flow to the east, 90 degrees to flow to the north.

5.2 Lancaster Sound, Stations 1 and 3

The vertical structure at these two stations is adequately represented in the relevant ellipse plots, Figures 4.2.4 - 4.2.7. The following table lists the harmonic constants for the major constituents M_2, S_2, K_1 and O_1.

		M_2 constituent				S_2 constituent			
Stn.	Depth (m)	Major (cm/s)	Minor (cm/s)	Incli- nation (deg)	Phase (deg)	Major (cm/s)	Minor (cm/s)	Incli- nation (deg)	Phase (deg)
1	39	3.6	-0.3	197	120	3.4	-2.1	145	135
1	203	4.0	-0.2	185	100	1.5	-0.2	185	147
3	51	4.3	0.6	190	104	2.2	0.4	187	142
3	326	4.7	-0.3	193	106	1.8	-0.0	177	143

		K_1 constituent				O_1 constituent			
Stn.	Depth (m)	Major (cm/s)	Minor (cm/s)	Incli- nation (deg)	Phase (deg)	Major (cm/s)	Minor (cm/s)	Incli- nation (deg)	Phase (deg)
1	39	6.1	-0.7	169	297	3.7	-0.6	181	228
1	203	5.9	0.2	181	298	2.9	0.1	183	235
3	51	8.2	1.9	165	104	4.0	0.6	332	35
3	216	8.2	1.8	172	295	3.6	0.2	170	231

Considering first the semi-diurnal constituents, the M_2 currents are almost uniform in the vertical. However, the S_2 currents at station 1 are not, the deeper currents being considerably smaller. The N_2 exhibited similar behaviour to S_2 at both stations 1 and 3. Similarly, for the diurnal constituents, the K_1 is quite uniform in the vertical, the O_1 less so.

5.3 Wellington Channel Stations

These two stations are part of a line extending across Wellington Channel, about midway along its length. The meters were in place for 3 months in 1978.

		M_2 constituent				S_2 constituent			
Stn.	Depth (m)	Major (cm/s)	Minor (cm/s)	Incli-nation (deg)	Phase (deg)	Major (cm/s)	Minor (cm/s)	Incli-nation (deg)	Phase (deg)
2	12	4.9	2.8	287	8	2.4	0.6	242	11
2	100	6.8	-0.7	278	1	2.8	-0.8	285	54
3	12	6.0	1.8	287	358	2.7	0.0	273	39
3	100	7.6	-1.4	293	8	2.7	-0.4	301	63

		K_1 constituent				O_1 constituent			
Stn.	Depth (m)	Major (cm/s)	Minor (cm/s)	Incli nation (deg)	Phase (deg)	Major (cm/s)	Minor (cm/s)	Incli nation (deg)	Phase (deg)
2	12	9.9	-0.8	297	177	5.9	-0.6	296	129
2	100	8.3	-0.8	280	168	4.8	-0.6	280	113
3	12	10.8	-0.3	295	173	6.5	-0.4	296	124
3	100	8.5	-0.4	285	171	4.8	-0.3	284	119

There is some variation in the vertical at these stations - the S_2 phase differs by about 43 degrees (1.3 hours) between 12 m and 100 m at station 2, and the semi-diurnal amplitudes tend to be larger at 100 m than at 12 m. For the diurnal constituents, however, the current at 12 m is larger than at 100 m.

5.4 Barrow Strait Station 42-46

The available data for Barrow Strait extends from 1981 to 1985, and is based on stations 41, 42, 44, 46 and 47. Only stations 42, 44 and 46 (A & B) had simultaneous measurement of currents at more than one depth, so consideration is restricted to these stations. Currents differ somewhat between these stations, so a separate tabulation is presented for each station. Figures 5.4.1, 5.4.2, 5.4.3, and 5.4.4 present composite plots of the profiles of tidal current amplitudes for the M_2 and K_1 constituents at all stations, plotting clockwise and counterclockwise amplitudes respectively for each. We note in advance, in the four figures, a number of important features. K_1 is almost vertically uniform, and the clockwise and counterclockwise components are of about equal magnitude. For M_2 however, only the counterclockwise constituent is vertically uniform, the clockwise being extremely variable, but in a systematic manner. The "average" of the clockwise usually is about of the same magnitude as the counterclockwise constituent.

5.4.1 Barrow Strait Station 46B

Barrow Strait Station 46B M_2 Constituent

Depth (m)	Major (cm/s)	Minor (cm/s)	Incli-nation (deg)	Phase (deg)	CW Amp (cm/s)	CCW Amp (cm/s)	CW phase (deg)	CCW Phase (deg)
25	16.4	-0.0	199	236	8.2	8.2	75	324
60	18.1	-2.0	180	229	10.1	8.0	49	311
150	10.9	5.2	184	247	2.8	8.0	72	297

First, we note that the M_2 currents are primarily rectilinear at 25 m., and become increasingly circularly polarized as one descends the water column. The counterclockwise component remains relatively constant at 8 cm/s, whereas the clockwise amplitude varies between 10 cm/s and 2 cm/s over the three depths.

Barrow Strait Station 46B S_2 Constituent

Depth (m)	Major (cm/s)	Minor (cm/s)	Incli-nation (deg)	Phase (deg)	CW Amp (cm/s)	CCW Amp (cm/s)	CW phase (deg)	CCW Phase (deg)
25	5.7	0.5	203	281	2.6	3.1	125	282
60	6.9	-1.2	181	271	4.0	2.8	92	271
150	5.4	1.7	116	215	1.8	3.6	330	263

A similar pattern applies to the S_2 constituent, although the currents are considerably smaller, so likely to be noise-contaminated. Still, the 25 m currents are the most rectilinear, and the counterclockwise component is the most uniform in the vertical.

Barrow Strait Station 46B K_1 Constituent

Depth (m)	Major (cm/s)	Minor (cm/s)	Incli-nation (deg)	Phase (deg)	CW Amp (cm/s)	CCW Amp (cm/s)	CW phase (deg)	CCW Phase (deg)
25	15.1	-0.6	198	357	7.9	7.2	195	201
60	14.5	-1.5	181	356	8.0	6.5	177	185
150	12.6	-2.4	172	360	7.5	5.1	172	172

For the K_1 constituent, the 25 m current is still the most rectilinear, but the clockwise component is more uniform in the vertical.

Barrow Strait Station 46B O_1 Constituent

Depth (m)	Major (cm/s)	Minor (cm/s)	Incli-nation (deg)	Phase (deg)	CW Amp (cm/s)	CCW Amp (cm/s)	CW phase (deg)	CCW Phase (deg)
25	6.9	0.8	198	303	3.0	3.8	141	255
60	6.8	-1.8	188	299	4.3	2.5	127	249
150	6.8	-3.4	207	274	5.1	1.7	121	294

The O_1 exhibits considerable vertical variability, although again the 25 m current is the most rectilinear. Interestingly, for this constituent, the major amplitude is the most vertically uniform of the current parameters.

5.4.2 Barrow Strait Station 46

At this station, 3 meters in the vertical were installed, approximately 3 nautical miles west of station 46. The values are tabulated below.

Barrow Strait Station 46 M_2 Constituent

Depth (m)	Major (cm/s)	Minor (cm/s)	Inclination (deg)	Phase (deg)	CW Amp (cm/s)	CCW Amp (cm/s)	CW Phase (deg)	CCW Phase (deg)
10	12.5	4.6	207	249	3.9	8.6	96	318
50	15.9	1.5	194	239	7.2	8.7	73	315
150	12.2	2.8	176	221	4.7	7.5	37	315

Barrow Strait Station 46 S_2 constituent

Depth (m)	Major (cm/s)	Minor (cm/s)	Inclination (deg)	Phase (deg)	CW Amp (cm/s)	CCW Amp (cm/s)	CW Phase (deg)	CCW Phase (deg)
10	4.6	1.8	199	290	1.5	3.2	130	269
50	5.9	0.7	196	289	2.6	3.3	125	266
150	4.7	0.7	160	250	2.0	2.7	50	270

Barrow Strait Station 46 K_1 constituent

Depth (m)	Major (cm/s)	Minor (cm/s)	Inclination (deg)	Phase (deg)	CW Amp (cm/s)	CCW Amp (cm/s)	CW Phase (deg)	CCW Phase (deg)
10	14.9	-0.5	199	001	7.7	7.2	200	199
50	15.5	0.7	190	353	7.4	8.1	184	197
150	14.5	-0.4	162	343	7.4	7.0	145	179

Barrow Strait Station 46 O_1 constituent

Depth (m)	Major (cm/s)	Minor (cm/s)	Inclination (deg)	Phase (deg)	CW Amp (cm/s)	CCW Amp (cm/s)	CW Phase (deg)	CCW Phase (deg)
10	14.9	-0.5	199	001	3.2	3.0	149	248
50	15.5	0.7	190	353	2.6	3.3	110	234
150	14.5	-0.4	162	343	5.0	2.1	106	265

5.4.3 Barrow Strait Station 46A

This station is located 4 nautical miles west of station 46, and again only one month of data is available. The relevant data is listed in the following tables.

Barrow Strait Station 46A M_2 constituent

Depth (m)	Major (cm/s)	Minor (cm/s)	Inclination (deg)	Phase (deg)	CW Amp (cm/s)	CCW Amp (cm/s)	CW Phase (deg)	CCW Phase (deg)
10	10.9	6.4	194	236	2.3	8.7	70	319
80	20.1	-2.6	196	229	11.3	8.8	65	327
150	13.8	5.7	212	250	4.0	9.7	102	321

Barrow Strait Station 46A S_2 constituent

Depth (m)	Major (cm/s)	Minor (cm/s)	Inclination. (deg)	Phase (deg)	CW Amp (cm/s)	CCW Amp (cm/s)	CW Phase (deg)	CCW Phase (deg)
10	4.5	1.9	168	255	1.3	3.2	63	274
80	8.0	-1.6	198	277	4.8	3.2	115	281
150	5.6	1.3	203	285	2.1	3.5	128	278

Barrow Strait Station 46A K_1 constituent

Depth (m)	Major (cm/s)	Minor (cm/s)	Inclination (deg)	Phase (deg)	CW Amp (cm/s)	CCW MP (cm/s)	CW Phase (deg)	CCW Phase (deg)
10	13.5	0.3	195	352	6.6	6.9	187	203
80	15.5	-0.3	200	349	7.9	7.6	189	211
150	16.4	0.6	207	358	7.9	8.5	205	209

Barrow Strait Station 46A O_1 constituent

Depth (m)	Major (cm/s)	Minor (cm/s)	Inclination (deg)	Phase (deg)	CW Amp (cm/s)	CCW MP (cm/s)	CW Phase (deg)	CCW Phase (deg)
10	5.6	0.1	195	298	2.8	2.9	133	256
80	6.6	-0.0	194	298	3.3	3.3	132	256
150	7.2	0.7	203	307	3.2	3.9	150	256

5.4.4 Barrow Strait Station 44

Station 44 is in the middle of Barrow Strait. Data from meters at 10,50, and 142 metres are available, and are listed in the following table.

Barrow Strait Station 44 M_2 constituent

Depth (m)	Major (cm/s)	Minor (cm/s)	Incli- nation (deg)	Phase (deg)	CW Amp (cm/s)	CCW Amp (cm/s)	CW Phase (deg)	CCW Phase (deg)
10	7.5	6.7	217	247	0.4	7.1	105	329
50	18.7	-3.0	196	211	10.9	7.8	47	346
142	10.3	5.1	192	216	2.6	7.7	47	336

Barrow Strait Station 44 S_2 constituent

Depth (m)	Major (cm/s)	Minor (cm/s)	Incli- nation (deg)	Phase (deg)	CW Amp (cm/s)	CCW Amp (cm/s)	CW Phase (deg)	CCW Phase (deg)
10	3.8	1.7	323	41	1.0	2.7	3.4	289
50	7.2	-1.1	198	260	4.2	3.1	98	298
142	4.4	1.5	175	250	1.4	2.9	65	286

Barrow Strait Station 44 K_1 constituent

Depth (m)	Major (cm/s)	Minor (cm/s)	Incli- nation (deg)	Phase (deg)	CW Amp (cm/s)	CCW Amp (cm/s)	CW Phase (deg)	CCW Phase (deg)
10	11.5	-1.0	193	354	6.3	5.2	187	199
50	13.6	-2.2	185	337	7.9	5.7	162	208
142	13.5	-1.9	189	342	7.7	5.8	171	207

Barrow Strait Station 44 O_1 constituent

Depth (m)	Major (cm/s)	Minor (cm/s)	Incli- nation (deg)	Phase (deg)	CW Amp (cm/s)	CCW Amp (cm/s)	CW Phase (deg)	CCW Phase (deg)
10	4.8	-0.2	189	294	2.5	2.3	123	254
50	5.6	-1.3	184	283	3.5	2.1	107	261
142	5.7	-1.4	193	287	3.5	2.2	119	266

5.4.5 Barrow Strait Station 42

Barrow Strait in the vicinity of Station 42 was occupied by three moorings, on different years. Stations 42 was a 12 month series of measurements at the three depths 18, 51, and 100m in 1984-85. Station 42A was a one-month series at 10, 40, 60, 80, and Station 42B was a one-month station with depths at 10, 50, and 115 m.

Barrow Strait Station 42 M_2 constituent								
Depth (m)	Major (cm/s)	Minor (cm/s)	Incli-nation (deg)	Phase (deg)	CW Amp (cm/s)	CCW Amp (cm/s)	CW phase (deg)	CCW Phase (deg)
18	10.9	5.7	208	241	2.6	8.3	89	326
51	17.8	-2.5	176	220	10.1	7.6	36	316
100	12.1	1.6	192	235	5.3	6.8	67	317

Barrow Strait Station 42 S_2 constituent								
Depth (m)	Major (cm/s)	Minor (cm/s)	Incli-nation (deg)	Phase (deg)	CW Amp (cm/s)	CCW Amp (cm/s)	CW phase (deg)	CCW Phase (deg)
18	3.3	2.2	237	316	0.6	2.8	192	281
51	7.3	-1.3	179	266	4.3	3.0	86	273
100	4.3	0.5	191	276	1.9	2.4	107	275

Barrow Strait Station 42 K_1 constituent								
Depth (m)	Major (cm/s)	Minor (cm/s)	Inclination (deg)	Phase (deg)	CW Amp (cm/s)	CCW Amp (cm/s)	CW phase (deg)	CCW Phase (deg)
18	11.9	0.5	196	346	5.7	6.2	183	210
51	12.2	-0.4	176	346	6.3	5.9	161	190
100	11.5	0.2	184	352	5.7	5.8	176	192

Barrow Strait Station 42 O_1 constituent								
Depth (m)	Major (cm/s)	Minor (cm/s)	Inclination (deg)	Phase (deg)	CW Amp (cm/s)	CCW Amp (cm/s)	CW phase (deg)	CCW Phase (deg)
18	5.5	0.2	197	285	2.7	2.8	123	275
51	5.2	-0.9	183	290	3.0	2.2	113	252
100	4.7	-0.4	196	303	2.6	2.1	138	253

5.4.6 Barrow Strait Station 42A

Station 42A has 5 meters in the vertical:

Barrow Strait Station 42A M_2 constituent

Depth (m)	Major (cm/s)	Minor (cm/s)	Incli- nation (deg)	Phase (deg)	CW Amp (cm/s)	CCW Amp (cm/s)	CW Phase (deg)	CCW Phase (deg)
10	12.8	2.9	179	227	4.9	7.9	46	312
40	21.6	-4.6	195	236	13.1	8.5	71	319
60	20.2	-3.6	198	239	11.9	8.3	77	319
80	17.2	-0.9	200	235	9.1	8.1	75	325
120	10.3	4.7	195	225	2.8	7.5	61	330

Barrow Strait Station 42A S_2 constituent

Depth (m)	Major (cm/s)	Minor (cm/s)	Incli- nation (deg)	Phase (deg)	CW Amp (cm/s)	CCW Amp (cm/s)	CW Phase (deg)	CCW Phase (deg)
10	5.6	1.0	176	272	2.3	3.3	88	264
40	8.6	-1.6	197	284	5.1	3.5	122	273
60	7.6	-1.0	202	287	4.3	3.3	129	275
80	6.6	-0.4	202	278	3.5	3.1	120	284
120	5.3	2.2	197	276	1.5	3.8	113	281

Barrow Strait Station 42A K_1 Constituent

Depth (m)	Major (cm/s)	Minor (cm/s)	Incli- nation (deg)	Phase (deg)	CW Amp (cm/s)	CCW Amp (cm/s)	CW Phase (deg)	CCW Phase (deg)
10	13.0	-0.5	184	352	6.7	6.2	177	193
40	13.7	-1.7	192	350	7.7	6.0	181	202
60	13.3	-1.4	88	10	7.3	5.9	198	178
80	13.7	-1.8	196	348	7.8	6.0	184	208
120	11.5	-0.9	206	2	6.2	5.3	208	204

Barrow Strait Station 42A O_1 constituent

Depth (m)	Major (cm/s)	Minor (cm/s)	Incli- nation (deg)	Phase (deg)	CW Amp (cm/s)	CCW Amp (cm/s)	CW Phase (deg)	CCW Phase (deg)
10	5.0	0.8	171	303	2.1	2.9	114	228
40	6.3	-0.4	178	289	3.3	2.9	107	250
60	6.2	-0.5	177	292	3.4	2.9	110	245
80	5.9	-0.5	187	293	3.2	2.7	120	254
120	5.9	0.2	196	305	2.9	3.0	142	251

5.4.7 Barrow Strait Station 42B

Station 42B has three meters in the vertical.

Barrow Strait Station 42B M_2 constituent

Depth (m)	Major (cm/s)	Minor (cm/s)	Inclination (deg)	Phase (deg)	CW Amp (cm/s)	CCW Amp (cm/s)	CW Phase (deg)	CCW Phase (deg)
10	9.6	5.7	204	229	2.0	7.6	73	336
50	22.3	-4.3	176	215	13.3	9.0	31	321
115	11.7	5.0	198	228	3.3	8.3	66	331

Barrow Strait Station 42B S_2 constituent

Depth (m)	Major (cm/s)	Minor (cm/s)	Inclination (deg)	Phase (deg)	CW Amp (cm/s)	CCW Amp (cm/s)	CW Phase (deg)	CCW Phase (deg)
10	4.4	1.7	191	256	1.3	3.0	88	293
50	8.3	-1.7	176	268	5.0	3.3	84	268
115	4.7	1.4	175	257	1.6	3.1	73	278

Barrow Strait Station 42B K_1 constituent

Depth (m)	Major (cm/s)	Minor (cm/s)	Inclination (deg)	Phase (deg)	CW Amp (cm/s)	CCW Amp (cm/s)	CW Phase (deg)	CCW Phase (deg)
10	13.4	-0.4	193	348	6.9	6.5	181	205
50	14.6	-1.3	175	342	8.0	6.6	157	193
115	12.9	-0.5	189	346	6.7	6.2	175	203

Barrow Strait Station 42B O_1 constituent

Depth (m)	Major (cm/s)	Minor (cm/s)	Inclination (deg)	Phase (deg)	CW Amp (cm/s)	CCW Amp (cm/s)	CW Phase (deg)	CCW Phase (deg)
10	5.2	0.1	191	296	2.5	2.6	127	255
50	5.6	-0.9	182	218	3.2	2.4	103	260
115	4.9	-1.4	199	279	3.2	1.8	119	280

5.5 Peel Sound Station 84 and 82

Currents across the northern entrance to Peel Sound were measured at 5 stations extending from one side of the channel to the other in 1981. At two of these stations, 82 and 84, three additional meters were installed (total of 4 at each station), to provide information on the vertical structure. Figures 5.5.1, 5.5.2, 5.5.3, and 5.5.4 present composite plots of the profiles of tidal current amplitudes for the M_2 and K_1 constituents at both stations, plotting clockwise and counterclockwise amplitudes respectively for each. We note in advance, in the four figures, a number of important features. K_1 is almost vertically uniform, and the clockwise and counterclockwise components are of about equal magnitude. For M_2 however, only the counterclockwise constituent is vertically uniform, the clockwise being extremely variable, but in a systematic manner. The "average" of the clockwise usually is about of the same magnitude as the counterclockwise constituent.

5.5.1 Station 84

Station 84 has 4 meters in the vertical.

Peel Sound Station 84 M_2 constituent

Depth (m)	Major (cm/s)	Minor (cm/s)	Incli- nation (deg)	Phase (deg)	CW Amp (cm/s)	CCW Amp (cm/s)	CW Phase (deg)	CCW Phase (deg)
10	5.9	4.5	255	279	0.7	5.2	175	336
50	14.1	-3.0	256	274	8.5	5.6	171	342
100	10.6	0.3	277	289	5.2	5.5	206	348
225	8.3	4.2	260	268	2.0	6.3	168	352

Peel Sound Station 84 S_2 constituent

Depth (m)	Major (cm/s)	Minor (cm/s)	Incli- nation (deg)	Phase (deg)	CW Amp (cm/s)	CCW Amp (cm/s)	CW Phase (deg)	CCW Phase (deg)
10	3.0	1.1	235	331	1.0	2.0	207	264
50	5.8	-1.7	268	352	3.7	2.0	260	276
100	4.0	0.1	268	347	1.9	2.0	255	281
225	2.8	1.3	251	338	0.8	2.1	229	274

Peel Sound Station 84 K_1 constituent								
Depth (m)	Major (cm/s)	Minor (cm/s)	Incli- nation (deg)	Phase (deg)	CW Amp (cm/s)	CCW Amp (cm/s)	CW Phase (deg)	CCW Phase (deg)
10	2.9	-0.2	272	323	1.5	1.3	235	309
50	3.2	0.0	259	316	1.6	1.6	215	303
100	3.2	-0.1	269	319	1.7	1.6	228	310
225	3.1	0.2	274	327	1.5	1.7	241	307

Peel Sound Station 84 O_1 constituent								
Depth (m)	Major (cm/s)	Minor (cm/s)	Incli- nation (deg)	Phase (deg)	CW Amp (cm/s)	CCW Amp (cm/s)	CW Phase (deg)	CCW Phase (deg)
10	0.8	-0.4	268	222	0.6	0.2	130	47
50	1.1	-0.2	266	206	0.7	0.4	112	60
100	0.7	-0.4	270	219	0.5	0.2	129	50
225	1.4	0.0	276	194	0.7	0.7	110	82

5.5.2 Station 82

Station 82 similarly has 4 meters in the vertical.

Peel Sound Station 82 M_2 constituent								
Depth (m)	Major (cm/s)	Minor (cm/s)	Incli- nation (deg)	Phase (deg)	CW Amp (cm/s)	CCW Amp (cm/s)	CW Phase (deg)	CCW Phase (deg)
10	5.2	3.7	249	285	0.8	4.5	173	324
50	13.3	-3.4	270	283	8.4	5.0	193	348
100	10.4	-0.3	287	300	5.3	5.1	227	347
200	6.1	4.9	139	143	0.6	5.5	282	356

Peel Sound Station 82 S_2 constituent

Depth (m)	Major (cm/s)	Minor (cm/s)	Incli- nation (deg)	Phase (deg)	CW Amp (cm/s)	CCW Amp (cm/s)	CW Phase (deg)	CCW Phase (deg)
10	3.6	-0.7	249	351	2.2	1.5	240	258
50	5.0	-1.0	287	360	3.0	2.0	287	287
100	4.0	-0.3	284	3	2.1	1.8	287	282
200	2.5	1.7	295	221	0.4	2.1	155	74

Peel Sound Station 82 K_1 constituent

Depth (m)	Major (cm/s)	Minor (cm/s)	Incli- nation (deg)	Phase (deg)	CW Amp (cm/s)	CCW Amp (cm/s)	CW Phase (deg)	CCW Phase (deg)
10	2.7	-0.5	275	337	1.6	1.1	253	298
50	2.8	0.2	267	320	1.3	1.5	227	308
100	2.5	0.0	288	320	1.3	1.3	248	328
200	2.4	0.1	300	332	1.1	1.2	272	328

Peel Sound Station 82 O_1 constituent

Depth (m)	Major (cm/s)	Minor (cm/s)	Incli- nation (deg)	Phase (deg)	CW Amp (cm/s)	CCW Amp (cm/s)	CW Phase (deg)	CCW Phase (deg)
10	1.1	-0.4	284	217	0.7	0.4	141	67
50	1.2	0.0	304	213	0.6	0.6	157	91
100	0.9	0.1	298	194	0.4	0.5	132	105
200	1.2	-0.1	328	208	0.6	0.6	176	119

5.6 Barrow Strait Western Stations

A group of stations was occupied throughout the western region of Barrow Strait. Meters were installed at 4 m and at 50 m. The 4 m measurements are within the boundary layer under the ice, where currents are smaller than at mid-depth.

Western Barrow Strait Stations M_2 constituent

Station	Depth (m)	Major (cm/s)	Minor (cm/s)	Inclination (deg)	Phase (deg)	CW Amp (cm/s)	CCW Amp (cm/s)	CW Phase (deg)	CCW Phase (deg)
828	4	5.3	3.6	312	8.1	0.8	4.5	320	304
828	50	7.2	0.4	167	204	3.4	3.8	11	323
838	4	9.9	-0.2	201	217	5.1	4.8	59	344
838	50	15.9	-5.2	196	214	10.6	5.3	51	342
842	4	7.5	4.5	166	227	1.5	6.0	33	300
842	50	8.9	-6.5	178	284	6.6	3.4	102	255
835	4	8.2	5.1	290	355	1.5	6.6	265	314
835	50	25.2	-7.2	184	217	16.2	9.0	41	326
845	4	8.0	6.1	203	215	0.9	7.0	58	348
845	50	19.3	-5.0	182	231	12.2	7.1	56	314

Western Barrow Strait Stations S_2 constituent

Station	Depth (m)	Major (cm/s)	Minor (cm/s)	Incli-nation (deg)	Phase (deg)	CW Amp (cm/s)	CCW Amp (cm/s)	CW Phase (deg)	CCW Phase (deg)
828	4	2.9	1.2	313	64	0.9	2.0	17	249
828	50	2.7	-0.1	167	262	1.4	1.3	69	265
838	4	4.9	-0.1	202	268	2.5	2.4	110	295
838	50	7.5	-2.9	196	262	5.2	2.3	98	294
842	4	8.0	2.4	126	238	1.0	3.1	8.4	244
842	50	10.0	-3.2	178	284	0.3	0.4	338	238
835	4	3.2	2.1	311	49	0.5	2.7	0	262
835	50	11.0	-2.5	182	271	6.8	4.2	93	272
845	4	4.5	2.0	175	238	1.2	3.2	52	297
845	50	10.6	-4.2	200	278	7.4	3.2	118	282

Western Barrow Strait Station K_1 constituent

Station	Depth (m)	Major (cm/s)	Minor (cm/s)	Incli-nation (deg)	Phase (deg)	CW Amp (cm/s)	CCW Amp (cm/s)	CW Phase (deg)	CCW Phase (deg)
828	4	5.9	-1.4	328	190	3.7	2.3	158	139
828	50	4.7	-0.4	165	3.3	2.6	2.2	169	162
838	4	5.7	-3.2	204	3	4.5	1.3	207	202
838	50	9.1	-4.6	185	333	6.9	2.2	158	212
842	4	8.5	-2.0	158	16	5.2	3.2	182	135
842	50	9.2	-0.2	163	29	0.7	1.4	133	182
835	4	5.0	-1.0	177	356	3.0	2.0	174	180
835	50	7.3	-2.3	168	341	4.8	2.5	149	187
845	4	6.1	0.7	221	10	2.7	3.4	231	210
845	50	7.8	-0.3	203	11	4.1	3.8	214	191

Western Barrow Strait Stations O_1 constituent

Station	Depth (m)	Major (cm/s)	Minor (cm/s)	Incli-nation (deg)	Phase (deg)	CW Amp (cm/s)	CCW Amp (cm/s)	CW Phase (deg)	CCW Phase (deg)
828	4	2.5	-0.2	320	154	1.4	1.1	113	166
828	50	2.3	-0.6	162	314	1.5	0.8	115	208
838	4	3.7	-1.6	214	294	2.6	1.0	148	281
838	50	3.6	-2.0	214	266	2.8	0.8	120	309
842	4	4.0	-0.6	160	335	2.3	1.7	135	185
842	50	4.1	0.8	161	324	0.6	1.0	53	224
835	4	2.3	-0.4	169	332	1.4	1.0	141	196
835	50	3.1	-0.7	334	125	1.9	1.2	99	209
845	4	3.3	0.5	215	329	1.4	1.9	184	247
845	50	3.5	-0.7	196	0	2.1	1.4	194	196

5.7 Penny Strait

Two stations, PSE and PSW were occupied as part of NWP84. At each station, two meters in the vertical were installed, and data collected for a one-year period. The current patterns are not nearly as straightforward as in Barrow Strait, a consequence of the more complicated bathymetry.

5.7.1 Penny Strait East

Penny Strait East M_2 Constituent

Depth (m)	Major (cm/s)	Minor (cm/s)	Incli-nation (deg)	Phase (deg)	CW Amp (cm/s)	CCW Amp (cm/s)	CW phase (deg)	CCW Phase (deg)
43	26	-6.8	31	260	16.3	9.6	291	131
131	14.6	-1.2	33	306	7.9	6.7	338	87

Penny Strait East S_2 Constituent

Depth (m)	Major (cm/s)	Minor (cm/s)	Incli-nation (deg)	Phase (deg)	CW Amp (cm/s)	CCW Amp (cm/s)	CW phase (deg)	CCW Phase (deg)
45	10.3	-2.4	32	316	6.3	3.9	348	76
131	5.5	0.0	43	350	2.7	2.8	34	53

Penny Strait East K_1 Constituent

Depth (m)	Major (cm/s)	Minor (cm/s)	Incli-nation (deg)	Phase (deg)	CW Amp (cm/s)	CCW Amp (cm/s)	CW phase (deg)	CCW Phase (deg)
43	14.6	-1.5	24	17	8.1	6.6	41	7
131	12.8	-0.4	18	31	6.6	6.2	49	348

Penny Strait East O_1 Constituent

Depth (m)	Major (cm/s)	Minor (cm/s)	Incli-nation (deg)	Phase (deg)	CW Amp (cm/s)	CCW Amp (cm/s)	CW phase (deg)	CCW Phase (deg)
43	8.8	-0.6	19	316	4.7	4.1	336	63
131	8.1	-0.3	15	316	4.2	3.9	332	59

5.7.2 Penny Strait West

Penny Strait West M_2 Constituent								
Depth (m)	Major (cm/s)	Minor (cm/s)	Inclination (deg)	Phase (deg)	CW Amp (cm/s)	CCW Amp (cm/s)	CW phase (deg)	CCW Phase (deg)
43	18.3	-2.6	131.8	283	10.4	7.9	54	209
131	14.4	-1.1	17	282	7.7	6.6	299	95

Penny Strait West S_2 Constituent								
Depth (m)	Major (cm/s)	Minor (cm/s)	Inclination (deg)	Phase (deg)	CW Amp (cm/s)	CCW Amp (cm/s)	CW phase (deg)	CCW Phase (deg)
43	8.1	-1.2	123	333	4.7	3.4	96	150
131	5.9	-0.7	19	350	3.3	2.6	7	29

Penny Strait West K_1 Constituent								
Depth (m)	Major (cm/s)	Minor (cm/s)	Inclination (deg)	Phase (deg)	CW Amp (cm/s)	CCW Amp (cm/s)	CW phase (deg)	CCW Phase (deg)
43	12.4	-5.8	103	23	9.1	3.3	126	79
131	4.1	-0.3	90	45	2.2	1.9	135	46

Penny Strait West O_1 Constituent								
Depth (m)	Major (cm/s)	Minor (cm/s)	Inclination (deg)	Phase (deg)	CW Amp (cm/s)	CCW Amp (cm/s)	CW phase (deg)	CCW Phase (deg)
43	7.5	-3.9	108	324	5.7	1.8	72	140
131	3.3	-0.8	68	355	2.0	1.2	63	73

5.8 Danish Strait

This station was occupied for one month in 1979. It is the only station in the Queen Elizabeth Island region for which there is more than one meter in the vertical. The shallower meter is in the boundary layer of the under-ice flow, as for the stations in western Barrow Strait.

Danish Strait M_2 Constituent

Depth (m)	Major (cm/s)	Minor (cm/s)	Incli-nation (deg)	Phase (deg)	CW Amp (cm/s)	CCW Amp (cm/s)	CW phase (deg)	CCW Phase (deg)
4	8.4	2.6	311	75	2.9	5.5	26	235
50	10.5	-0.2	159	279	5.3	5.1	77	240

Danish Strait S_2 Constituent

Depth (m)	Major (cm/s)	Minor (cm/s)	Incli-nation (deg)	Phase (deg)	CW Amp (cm/s)	CCW Amp (cm/s)	CW phase (deg)	CCW Phase (deg)
4	3.8	0.8	300	92	1.5	2.3	33	208
50	4.1	0.1	164	300	2.0	2.1	104	224

Danish Strait K_1 Constituent

Depth (m)	Major (cm/s)	Minor (cm/s)	Incli-nation (deg)	Phase (deg)	CW Amp (cm/s)	CCW Amp (cm/s)	CW phase (deg)	CCW Phase (deg)
4	4.5	0.7	159	22	1.9	2.6	180	137
50	4.3	0.2	160	14	2.0	2.3	171	147

Danish Strait O_1 Constituent

Depth (m)	Major (cm/s)	Minor (cm/s)	Incli-nation (deg)	Phase (deg)	CW Amp (cm/s)	CCW Amp (cm/s)	CW phase (deg)	CCW Phase (deg)
4	2.9	0.5	332	165	1.2	1.7	137	167
50	3.1	0.4	329	153	1.4	1.8	122	176

5.9 Austin Channel

One location in Austin Channel was occupied for a year, part of NWP83. Data from year-long moorings at 73 and 123 m is available, as well as 2 months of data from a mooring at 18 m. Except for M_2, the constituents at 18 m are quite dissimilar to the constituents at the lower depths.

Austin Channel Station 71 M_2 Constituent

Depth (m)	Major (cm/s)	Minor (cm/s)	Incli-nation (deg)	Phase (deg)	CW Amp (cm/s)	CCW Amp (cm/s)	CW phase (deg)	CCW Phase (deg)
18	5.7	-2.2	339	135	4.0	1.8	111	200
73	5.9	-3.0	18	128	4.5	1.5	145	251
123	4.5	-1.2	40	159	2.8	1.6	200	241

Austin Channel Station 71 S_2 Constituent

Depth (m)	Major (cm/s)	Minor (cm/s)	Incli-nation (deg)	Phase (deg)	CW Amp (cm/s)	CCW Amp (cm/s)	CW phase (deg)	CCW Phase (deg)
18	3.8	-1.9	59	349	2.9	0.9	48	69
73	3.0	-1.2	24	191	2.1	0.9	215	193
123	2.1	-0.2	45	219	1.1	0.9	264	186

Austin Channel Station 71 K_1 Constituent								
Depth (m)	Major (cm/s)	Minor (cm/s)	Incli-nation (deg)	Phase (deg)	CW Amp (cm/s)	CCW Amp (cm/s)	CW phase (deg)	CCW Phase (deg)
18	5.1	-1.0	343	307	3.0	2.0	290	37
73	5.3	-1.0	12	232	3.2	2.2	243	140
123	4.8	0.7	23	247	2.0	2.8	270	137

Austin Channel Station 71 O_1 Constituent								
Depth (m)	Major (cm/s)	Minor (cm/s)	Incli-nation (deg)	Phase (deg)	CW Amp (cm/s)	CCW Amp (cm/s)	CW phase (deg)	CCW Phase (deg)
18	3.8	-0.7	338	275	2.2	1.5	252	63
73	3.8	-0.6	10	164	2.2	1.6	173	206
123	3.5	0.7	23	181	1.4	2.1	204	201

6 DATA INTERPRETATION

The previous chapters have been concerned with presenting the available data, primarily by means of spatial plots, time series plots and tables. In this final chapter, we wish to examine the data from the point of view of various models of tidal propagation in the Arctic. In Section 1, a comparison will be made between the observed co-range and co-phase diagrams and those produced by simple Kelvin wave models for Parry Strait, the Gulf of Boothia and Prince of Wales Strait. Many simplifications enter into these models, but the agreement is quite impressive nevertheless. As well, the Kelvin wave model predicts the current harmonic parameters, and these will be compared with observations for a few selected mooring locations.

In Section 2, we address the question of the vertical variability of currents, within the framework of models discussed in Appendix C: can the vertical structure be attributed purely to a baroclinic model or to a frictional model?

6.1 A KELVIN WAVE MODEL

As illustrated in Figure A.3, the Kelvin wave model consists of an incident and a reflected Kelvin wave. Poincaré waves are neglected in this model. The incident and reflected waves have differing amplitudes, a consequence of energy loss in the system. Thus, there are four free parameters in such a model: the amplitude and phase of both the incident and reflected waves. Two tide gauges, one on each side of the channel, provide the four items of independent data (amplitude and phase on each side) which allow one to solve for the incident and reflected waves. One can then assume, (Hendershott and Speranza, 1971) that the amplitude of the incident and reflected waves are constant along the channel, but the reflected wave is smaller, having lost energy at the inner end of the model region. The major simplification in this model is that we assume the same channel cross-section (width and depth) throughout the length of the channel. Channels are in general not uniform, having either or both depth and width changes along their length. With this qualification, we will examine then the results of the model for M_2 and K_1 tides.

6.1.1 Parry Strait

Values of the elevation harmonic constants at the Lancaster Sound end of Parry Channel were used to determine the incident and reflected waves. The channel was assumed to be 1000 km long, 80 km wide, and 400 m deep. The following table summarizes the wave properties.

Cons.	Incident Wave		Reflected Wave		Velocity at Entrance		Observed Velocity		Energy Flux
	Amp	Phase	Amp	Phase	Amp	Phase	Amp	Phase	10^{15} erg/sec
M_2	45.3	137°	19.2	150°	4.0	127°	4.2	108°	41.6
K_1	37.2	294°	18.7	148°	8.0	305°	7.1	297°	25.5

Figure 6.1.1 plots the co-amplitude and co-phase contours for the M_2 constituent, and Figure 6.1.2 plots the contours for the K_1 constituent. The M_2 displays a considerable similarity to the observed contours, Figure 4.1.2. However, it does not indicate the same large gradient in amplitude across Barrow Strait, primarily because the horizontal scale size is proportional to the wave speed, which is in turn proportional to the square root of the depth. Since Barrow Strait is quite shallow, one expects the spatial rate of change of amplitude to be larger along it. The Kelvin wave model assumes a uniform depth, so does not "see" the shoaling in Barrow Strait. The model predicts an amphidrome in Viscount Melville Sound, and increasing amplitudes farther west. There may be a slight amphidromic tendency in the observed data, but there is quite definitely a decrease in amplitude to the west of Viscount Melville Sound - the simple model becomes less and less accurate the farther one proceeds from its initiation region, Lancaster Sound.

For the K_1 tide, the distribution of phase between Lancaster Sound and Viscount Melville Sound is approximately correct, but the distribution of amplitude is quite wrong - the observed data indicate a steady decrease in amplitude from East to West, whereas the Kelvin model indicates a growth west of Barrow Strait.

6.1.2 Gulf of Boothia

The Gulf of Boothia model assumed a channel 700 km long, 60 km wide and 80 m deep. the following table summarizes the Kelvin wave model. The co-amplitude and co-phase diagrams for M_2 and K_1 are drawn in Figure 6.1.3 and 6.1.4.

Cons.	Incident Wave		Reflected Wave		Velocity at entrance		Observed Velocity		Energy Flux
	Amp	Phase	Amp	Phase	Amp	Phase	Amp	Phase	10^{15} erg/sec
M_2	42.5	173°	24.3	121°	10.0	216°	5.2	180°	15.2
K_1	41.9	297°	24.8	111°	16.0	296°	9.9	284°	14.1

Because the Gulf of Boothia system is considerably simpler than Parry Channel, this simpler model appears to work much better. Both of the constituent co-amplitude and co-phase diagrams have a great deal of similarity with their observationally-based counterparts, Figures 4.1.10 and 4.1.12. The location of the amphidrome in the case of M_2, and the steady increase in amplitude along the channel in the case of K_1 are both duplicated by the Kelvin wave model. The magnitude of velocities at the entrance is not well reproduced, partly because a shallow depth for the model was used, representative of wave propagation over the entire channel, rather than the depth at the entrance.

6.1.3 Prince of Wales Strait

The Kelvin wave model for this channel assumed a length of 350 km, a width of 40 km, and a depth of 120 m. Only the M_2 co-amplitude and co-range diagram is plotted, (Figure 6.1.5) as the K_1 model was not very successful. (The amplitude and phase of K_1 according to the model were uniform throughout the system). The observed velocities are based on the NWP 82 section.

Cons.	Incident Wave		Reflected Wave		Velocity at NWP82		Observed Velocity		Energy Flux
	Amp	Phase	Amp	Phase	Amp	Phase	Amp	Phase	10^{15} erg/sec
M_2	14.6	131°	11.4	11°	6.1	166°	13	156°	0.56°
K_1	2.7	88°	2.7	145°	0.2	26°	3.5	45°	0.0

* This value is the flux in from the south: there is also a flux of $0.50 \cdot 10^{15}$ erg/sec from the north - Prince of Wales Strait draws energy from both its northern and southern openings.

The M_2 model works quite well, providing a similar distribution of amplitude and phase to that observed. Applied in reverse, using data from the northern end, the model predicted an inflow of energy from the northern opening. However, it failed when applied to the K_1 tide - it predicted essentially no change of wave properties from their values at the opening to Amundsen Gulf, clearly in contrast to the observations. The velocity amplitude for K_1 also appears to be at variance with the observations.

6.1.4 Summary of Kelvin Models

The above three examples illustrated the performance of a very simple model for three different channels. The Gulf of Boothia model was the most successful, mainly because it was the only system with a single opening. A major conclusion to be drawn, however, is that there are in fact two Kelvin waves in each of the systems. As well, the energy flux was estimated by the models. If the Gulf of Boothia is typical, we see a major aspect of tidal propagation in Parry Channel - much of the energy flux into Parry Channel is lost due to propagation of energy out of the system into side channels : the Gulf of Boothia withdrew 37% of the M_2 energy, and 55% of the K_1 energy. Assuming an rms velocity of 10 cm/s, (a high estimate) and a bottom friction constant of 0.003, the dissipation over the Parry Channel model region is given by:

$$\rho \cdot l \cdot w \cdot u_{rms}^3 \qquad (6.1.1)$$

The above estimate is $2.4 \cdot 10^{15}$ erg/sec, considerably smaller than the flux into the Boothia region. The other channels undoubtedly contribute to the energy losses for Parry Channel, and probably account for the extreme attenuation of the K_1 tide along the channel, considerably in excess of the Kelvin wave model.

6.2 VELOCITY PROFILES

In Chapter 5, it was shown that there is considerable vertical structure in the current profiles, but that most of this variability was confined to the clockwise-rotating component. This is similar to the results of Chapter 3, where it was shown that much of the temporal variability in harmonic constants was confined to the clockwise component. These results are particularly striking in Barrow Strait, where the topography and bathymetry are somewhat simpler that at the other stations where suitable data were available. We wish to explore in this section the nature of the vertical variability of tidal currents. We recall from Chapter 5 that only the semi-diurnal tides were subject to the variation of currents with depth, and suspect that the closeness of the Coriolis frequency to the tidal frequency may be important.

6.2.1 Fits to a Baroclinic Model

Figure 6.2.1 plots the vertical profile of density and Brunt-Väisälä frequency at a station near the south side of Barrow Strait - the salinity and temperature profile was plotted in Figure 1.2.1. Next, the three lowest modes corresponding to the solution of equation (C.13) are plotted in Figure 6.2.2. Next, the data from one mooring, station 46B, is fitted to the modal structure, using a least squares algorithm. Two fits were done, using all three modes (of which one is barotropic) and using only modes 0 and 2. Figures 6.2.3 and 6.2.4 respectively plot these fitted curves, as well as data from all of the Barrow Strait stations. These plots are purely exploratory - much of the data has been temporally averaged, and only the amplitude of the clockwise component has been fitted, whereas one should really fit separately Amp· cos(g) and Amp· sin(g), in order to deal with the vertical variation of phase as well. However, these plots are suggestive of the fit possible using observed density structures.

The magnitudes of the various modes used in the fit are given in the following table, where each mode has been normalized to 1.0 at its maximum:

Figure	Mode 0	Mode 1	Mode 2
6.2.3	6.47	-3.73	-2.58
6.2.4	6.34	0.0	-6.26

Once the vertical problem has been solved, the scale size of the horizontal problem can be determined. Using the three values of H_n, the M_2 tidal frequency, and a value of f appropriate to Barrow Strait, we obtain the following table, indicating the horizontal solutions of (C.12) which are possible, further assuming a Poincaré wave cross-channel nature.

Mode	along-channel character
0	trapped, $1/e$ distance of 25 km, 12 km, 8 km etc.
1	trapped, $1/e$ distance of 31 km, 15 km, 10 km, etc.
2	one propagating mode, λ = 195 km, and trapped modes of $1/e$ distance of 16 km, 10 km, *etc.*

The trapped barotropic mode does not occur to any significant extent, indicated by the fact that the barotropic parts of both the clockwise and counterclockwise waves occur with about equal magnitude, as required for the Kelvin wave, the principal wave in the system. It is interesting to note that the 2nd mode is the earliest (in the sequence of internal modes) to allow a propagating wave, with scale size about the length of Barrow Strait. The second mode and the barotropic mode together, Figure 6.2.4, provide an adequate fit to the observed profiles.

In conclusion, it appears that there is good evidence of an internal Poincaré wave in Barrow Strait, and that further, more careful analysis could probably clarify the exploratory arguments presented here.

6.2.2 A Frictionally-determined Profile

Having presented above the possibility of an internal Poincaré wave as the source of the vertical structure of currents, we now examine whether frictional effects could also be responsible. The model must be strongly dependent on the closeness of the Coriolis parameter and the tidal frequency, because we only observe these vertical effects in semi-diurnal tides. As shown in Appendix C, these effects can arise when one decomposes the traditional Ekman solution into clockwise and counterclockwise currents. We present, in Figure 6.2.5, a plot of the Ekman solution for the Barrow Strait region for the clockwise component, and in Figure 6.2.6, the counterclockwise fit. In both cases, a value of eddy viscosity of 10 cm^2/s for the upper boundary layer and 50 cm^2/s for the lower boundary layer was used. In both cases, the model reproduces the vertical structure: uniform for the counterclockwise component, and a strong mid-depth maximum for the clockwise.

Now there is a real conundrum. Which of the two models is correct, or where in the continuum between them does reality lie? This report is intended to summarize and present the available data, rather than to solve the question of the vertical structure of the semi-diurnal currents. It is remarkable that the vertical variability is explainable by either of two acceptable models : only 1 or 2 vertical baroclinic modes were required to obtain a quite reasonable fit, or alternatively, the eddy viscosity parameters used were within the realm of believability. The vertical variability has now been isolated to the clockwise components for the semi-diurnal tides. A combination of more detailed analyses, and numerical modelling, will undoubtedly unravel this mystery.

7 INERTIAL CURRENTS

Inertial oscillations are episodic transient phenomena of the ocean that are most often observed after the passage of a storm. They are characterized by strictly circular polarized currents that rotate clockwise (in the Northern Hemisphere) with a frequency that lies within a few percent of the local inertial frequency $f = 2\Omega \sin(\text{latitude})$. Viewed from above, their velocity vector at any given point traces out a circle in the horizontal plane in one inertial period $T_I = 2\pi/f$. In a uniform, quiescent ocean, inertial currents are truly "inertial": their frequency coincides exactly with f. In the real ocean, however, inertial oscillations are probably better thought of as very low frequency internal waves, whose structure and frequency depends on the density stratification and ambient mean currents. These long internal waves may be observed in two distinct forms: as normal modes or as freely propagating wave packets. In the later case inertial waves are generated in the near-surface waters by the wind and then propagate downwards through the water column.

In the Arctic, the inertial frequency lies within the semi-diurnal tidal band. For example, f coincides with the M_2 at 74.48°N and with S_2 at 85.78°N. Thus inertial currents can contaminate the tidal signal and confound the analysis of short current meter records. Conversely, the investigator interested in inertial currents must separate them from the tides. Moreover, Fissel(1982) found significant inertial current energy in the near-surface waters of western Baffin Bay and Lancaster Sound. During the ice-free season, observed semi-diurnal currents had typical amplitudes of 10- 20 cm/s and maxima of approximately 35 cm/s, about twice the values found under solid ice cover. These is no reason to expect that inertial currents are not important in the remainder of the Northwest Passage. This chapter is addressed towards determining that importance.

Before examining the available data however, it is useful to consider the character of inertial motion in greater detail. This is accomplished by examining a simple model of the oceanic response to forcing by storms. As discussed in detail in Appendix C, the ocean is idealized as a two layer system with an upper layer of thickness h_1 and density ρ_1 overlying a deeper layer of thickness h_2 and density ρ_2. The two layers are assumed to be immiscible but are dynamically linked through sea surface and interfacial displacements and through an interfacial stress which is assumed to be proportional to the velocity difference across the interface. The model is not meant to faithfully reproduce all the features of the ocean's response to winds, rather it contains enough physics through simple parameterizations to reproduce the essential features of the response and to elucidate the respective roles played by winds, density stratification, and dissipation. Specifically, the model implies the following general characteristics of inertial motions in the ocean: (1) Inertial currents span a range of frequencies near the inertial frequency. (2) The response is primarily trapped in the mixed layer which is preferentially excited in the ratio $(h_1 + h2)/h_1$. (3) Upper layer currents tend to achieve maximum values quickly and then decay slowly over a period of a few days. (4) Lower layer currents grow more slowly but never reach values more than about 10% of those observed in the upper layer. (5) The precise response depends in a complicated manner on the wind history over a several day period as the wind may either enhance or attenuate inertial motions depending on the phasing of winds and currents. (6) Specifically, storms characterized by winds that vary rapidly in speed or direction are most effective in generating inertial currents; more precisely, it is the degree of windstress variance at near-inertial frequencies that governs a storms potential for inertial current generation. We note in conclusion that Fissel's results concur with points (2) - (4); in particular he observed significant inertial motions at 35 m but not in deep water (> 200 m).

An example of the model response illustrates these points and provides a framework for the examination of the observed data (Figure 7.1). The model was forced for a 1000 hour (41 day) period in late summer using observed winds from Resolute Bay during late summer in 1984; wind stress was computed using the Large-Pond formulation (Large and Pond,1980), and a 20 m mixed layer was assumed, consistent with the density profile of Figure 6.2.1. Model response in terms of the east-west mixed layer velocity component is shown in the lowest panel; and reveals several events with peak speeds up to 40 cm /s. Clearly, the primary response is inertial: the low-frequency part (denoted by the heavy line) is relatively small. Moreover, currents below the mixed layer (not shown) are very weak, a few cm/s at most. A comparison of events makes it clear that the nature of the inertial response depends in a complicated manner on the precise wind history. For example, the relatively weak storm at hour 200 drives much stronger currents than does the more intense system at hour 600, which is richer in inertial band wind energy (upper panel). Similarly, the next storm (hour 800) is of similar magnitude, yet it forces significantly stronger currents. To summarize the implications of this simple example, one should expect near surface inertial currents to be significant in the Northwest passage and consequently to contaminate and, indeed, at times to dominate the semi-diurnal tidal flow. Below the mixed layer, the importance of inertial effects should diminish drastically, with maximum currents of a few cm/s.

Of the current records available in the Northwest Passage through 1985, only four moorings were of sufficient duration to merit investigation, namely Station 71 in Austin Channel in 1983-84, and Stations 42 in Barrow Strait and PSE and PSW in Penny Strait during 1984-85 (Figures 4.2.9, 4.2.46, and 4.2.61). Each mooring held two meters, one at approximately 50 m (73 m at 71) and one 100 m or deeper. Now the mixed layer depth in the Northwest Passage is of the order of 20 m (recall Figure 6.2.1) implying that all the meters were moored below the mixed layer. Consequently the results obtained in the appendix suggest any observed inertial effects will be small. On the other hand, the time series plots of semi-diurnal harmonic amplitudes revealed systematic differences between the clockwise and anticlockwise components at these stations; the anticlockwise component was generally stable while the clockwise component fluctuated significantly about its mean value. It is thus of considerable interest to investigate inertial effects at these stations; however it turns out that the observed inertial currents are indeed small and that the seasonal variation cannot be explained by them. Rather other mechanisms must be found. We note emphatically though, that these results do not preclude the potential importance of inertial currents at shallower depths. Indeed given the results of Fissel and the ubiquity of inertial motions in the upper ocean, it would be most surprising if they were not. The available data are simply not adequate to successfully address this problem.

Finally, we turn to the analysis of the long-term current meter records. Tides and inertial currents can be separated in several ways, but all methods improve as the quantity of data increases. In particular, a time series should be several months in duration to ensure the statistically reliability of the results. We have chosen to "detide" the records by subtracting predicted tidal currents from the full signal. First, a one month period (May) was selected shortly after spring deployment during which solid ice cover should have been present. This data section was harmonically analyzed for tidal currents, and the resulting harmonic constants were then used to construct the predicted signal for the remainder of the year. This technique suffers several obvious defects. First it depends on the generality of the data selected for harmonic analysis. If, for example, the system exhibits seasonally varying internal tides, the harmonic constants and in particular the phases will also vary. Moreover, the technique is vulnerable to instrumental timing errors including long term drift. Perhaps more importantly though, large-scale atmospheric forcing can temporarily alter the propagation speed of the tidal wave resulting in a slight delay or advance of the tide. The subtraction of the predicted tide would then yield a large residual. This is especially confounding because such periods are also times one would anticipate significant inertial activity. A technique that circumvents this problem is available and is based on the fact that inertial currents force extremely small variations in sea surface elevation. That is the pressure record from a tide gauge is almost immune to inertial effects. Thus one can calculate a relationship between currents and sea surface elevation during an inertial free period (the admittance function- a linear regression in frequency space) and use that relationship to infer currents from elevations at later times. However, this approach was not employed because the preliminary results were primarily negative and did not warrant further investigation.

The windstress magnitude computed from winds observed at Resolute Bay for 1983-84 and 1984-85 is shown in Figures 7.2 and 7.3, and should provide a general description of the windfield at each station since all four stations lie within 250 km of Resolute Bay, a distance considerably smaller than a typical storm diameter. Although a one-to-one relationship between large overall stress and large inertial band stress values does not exist, significant inertial band variance generally does not occur in the absence of strong winds (recall Figure 7.1). Hence it would be surprising to find significant inertial activity in the ocean during indicated periods of calm. It is immediately evident that the most intense storms occur during periods of ice cover, although several significant wind events did occur during the summer of 1983, and should have been capable of generating inertial currents. The apparent quiescence during the Jan-Mar period of both years is puzzling and warrants investigation.

The results are shown in several formats in Figures 7.4-7.6. Station PSW-S (49 m) is considered in greater detail than the others, but only for illustrative purposes. First Figure 7.4 displays the east-west component of the observed clockwise polarized inertial (semi-diurnal) band currents including tides. No obvious inertial events are obvious, at least of sufficient magnitude to dominate the tidal signal. The meager spring - neap cycle in June - August is notable however. It might be ascribed to destructive interference between tides and inertial currents, but that would demand a long term and very improbable constancy of relative phase. A more likely explanation would invoke internal tidal effects.

The inertial band clockwise rotating residual currents obtained by detiding the observed signal are shown in Figure 7.5. Most of the periods of significant residuals lack the characteristic signature of inertial currents: a rapid increase in magnitude followed by a more gradual decay over a period of a few days. Moreover, most of these periods tend to be separated by a fortnight, and indeed, occur during spring tides suggesting incomplete detiding due to time shifts. The most promising event occurs in late November and coincides with strong wind forcing, albeit under ice. Figure 7.6 shows the residual currents in a different format and permits comparison of the clockwise and anticlockwise signals. This is particularly useful in detecting timing shifts because they affect both components proportional to their harmonic amplitudes. By contrast an inertial event should be characterized by a large increase in clockwise energy with a relatively minor change in the anticlockwise component. Thus the summer period of anomalous spring - neap tides is indicated as a prolonged interval of enhanced clockwise currents, as are several shorter-lived sequences, the most prominent of which is the late November event identified earlier. Comparison with the deeper residuals demonstrates that these periods are limited to depths less than 140 m, although a slight enhancement is noted in late November. Moreover no unusual activity is found at the neighbouring PSE-E.

Similar results are found at the other stations and thus are not shown. Even if the intervals of large clockwise activity are accepted as purely inertial in character, they imply rather meager currents: amplitudes of 10 cm/s or less and extreme values below 20 cm/s. In summary then, this analysis has demonstrated that inertial currents do not appear to be significant at depths below 40 m in the areas surveyed (Barrow Strait, Austin Channel, and Penny Strait). By implication they are unimportant elsewhere since a similar density structure (mixed layer depth) prevails throughout the Northwest Passage.

8 REFERENCES

Birch, J.R., D.B. Fissel, D.D. Lemon, A.B. Cornford, R.A. Lake, B.D. Smiley, R.W. MacDonald and R.H. Herlinveaux. Arctic Data Compilation and Appraisal. Volume 3. Northwest Passage: Physical Oceanography - Temprature, Salinity, Currents and Water Levels. Can. Data Rep. Hydrogr. Ocean Sci. No 5(3): 262 pp.

Bolduc, P-A, J.D. Taylor and F.G. Barber. 1986. Sea-level at Port Leopold NWT in 1848. Arctic 39, 264-266.

Fissel, D.B., L. Cuypers, D.D. Lemon, J.R. Birch, A.B. Cornford, R.A. Lake, B.D. Smiley, R.W. MacDonald and R.H. Herlinveaux. Arctic Data Compilation and Appraisal. Volume 6. Queen Elizabeth Islands: Physical Oceanography - Temprature, Salinity, Currents and Water Levels. Can. Data Rep. Hydrogr. Ocean Sci. No 5(6): 214 pp.

Buckingham, W.R., R. Lake and H. Melling. 1987a. Temperature and Salinity Measurements in the Northwest Passage. Vol.3, March-April 1984. Can. Data Rep. Hydrogr. Ocean Sci. No. 39: 604 pp.

Buckingham, W.R., R. Lake and H. Melling. 1987b. Current and Sea-Level Measurements in the Northwest Passage. Vol.1, March 1982 - April 1983. Can. Data Rep. Hydrogr. Ocean Sci. No. 51: 128 pp.

Buckingham, W.R., R. Lake and H. Melling. 1987c. Current and Sea-Level Measurements in the Northwest Passage. Vol.2, March 1983 - April 1984. Can. Data Rep. Hydrogr. Ocean Sci. No. 51: 84 pp.

Buckingham, W.R., R. Lake and H. Melling. 1987d. Current and Sea-Level Measurements in the Northwest Passage. Vol.3, March 1984 - April 1985. Can. Data Rep. Hydrogr. Ocean Sci. No. 51: 139 pp.

Brooks, D.J. 1982. Arctic Oceanographic Survey, Barrow Strait 1982 Field Report. Unpublished Manuscript.

Cogley, A.C., 1976. Circularly polarized inertial wave vectors in rotating fluids. J. Atm. Sc., 33:1223-1233.

Ekman, V. Walfrid. 1932. Studien zur Dynamik der Meeresströmungen. Gerlands Beitr. z. Geophysik, Bd. 36, p 385-438. Leipzig.

Fissel, D.B. 1982. Tidal currents and inertial oscillations in Northwestern Baffin Bay. Arctic, 35:201-210.

Fissel, D.B. and G.R. Wilton. 1977. Subsurface current measurements in eastern Lancaster Sound, N.W.T. - Summer 1977. Fisheries and Environment Canada, Contractor Report Series 78-3.

Fissel, D.B., L. Cuypers, D.D. Lemon, J.R. Birch, A.B. Cornford, R.A. Lake, B.D. Smiley, R.W. MacDonald and R.H. Herlinveaux. Arctic Data Compilation and Appraisal. Volume 6. Queen Elizabeth Islands: Physical Oceanography - Temprature, Salinity, Currents and Water Levels. Can. Data Rep. Hydrogr. Ocean Sci. No 5(6): 214 pp.

Godin, G. 1980. Cotidal Charts for Canada. MEDS/DFO Manuscript Report Series 55. 93 pp.

Godin, G. 1980. Modification of the Tide in the Canadian Arctic by an Ice Cover. MEDS/DFO Manuscript Report Series 56. 29 pp.

Godin, G. and F. G. Barber. 1980. Variability of the tide at some sites in the Canadian Arctic. Arctic, vol. 33, no. 1. pp 30-37.

Greisman, P. 1984. Tidal Propagation Measurements in Foxe Basin. Can. Contr. Rep. Hydrogr. Ocean Sci. No. 18.

Greisman, P., S. Grant, A. Blaskovitch and B. Van Hardenberg. 1985. Tidal Propagation Measurements in Baffin Bay, Lancaster Sound and Nares Strait. Can. Contr. Rep. Hydrogr. Ocean Sci. No. 25. 548 pp.

Greisman, P., and R.A. Lake. 1978. Current Observations in the Channels of the Canadian Arctic Archipelago adjacent to Bathurst Island. IOS/DFO Pacific Marine Science Report 78-23. 127 pp.

Hendershott, M.C. and A. Speranza, 1971. Co-oscillating tides in long, narrow bays; the Taylor problem revisited. Deep Sea Res. 18:959-980.

Henry, R.F. and M.G.G. Foreman. 1977. Numerical Model Studies of the Semi-Diurnal Tides in the Southern Beaufort Sea. Pacific Marine Science Report 77-1. 71 pp.

Kowalik, Zygmunt. 1981. A study of the M_2 tide in the ice-covered Arctic Ocean. Modeling, Identification and Control. 2, pp 201-223.

Large, W.R. and S. Pond. 1980. Open ocean momentum flux in moderate to strong winds. J. Phys. Oceanogr. 11:324-336.

LeBlond, P.H. and L.A. Mysak, 1978. Waves in the Ocean. Elsevier. Amsterdam. 602 pp.

Murty, T.S. 1985. Modification of hydrographic characte5istics, tides and normal modes by ice cover. Mar. Geod. 9, 451-468.

Peck, G.S. 1977. Arctic Oceanographic Data Report 1976 - Penny Strait. CCIW/DFO Data Report Series No. 77-2. 154 pp.

Peck, G.S. 1978. Arctic Oceanographic Data Report 1977 - Western Viscount Melville Sound. CCIW/DFO Data Report Series No. 78-3. 150 pp.

Peck, G.S. 1980. Arctic Oceanographic Data Report 1978 - Volume 2. CCIW/DFO Data Report Series No. 80-1. 163 pp.

Platzman, G.W., 1971. Ocean tides and related waves. In: W.H. Reid (Editor), Mathematical Problems in the Geophysical Sciences. Am. Math. Soc., Providence, Rhode Island, 14:239-291.

Pollard, R.T. and R.C. Millard. 1970. Comparisons between observed and simulated inertial oscillations. Deep-Sea Research, 17: 813-821.

Sadler, H.E. H.V. Serson and R.K. Chow. The Oceanography of Fury and Hecla Strait. Tec. Mem. 79-11. Defense Research Establishment Pacific. Victoria, B.C.

Sailing Directions - Arctic Canada Vol I. Published by Government of Canada, Fisheries and Oceans, Scientific Information and Publications Branch. Ottawa. 284 pp.

St. Jacques, D.A., R.G. Sandilands, and R. R Solvason. 1985. 1983 Tidal Survey of Prince Regent Inlet, N.W.T. Data Report. Canadian Hydrographic Service. Bayfield Laboratory for Marine Sciences and Surveys. Burlington, Ontario.

Sandilands, R.G., R. R Solvason and D. A. St. Jacques. 1986. 1985 Tidal Survey in the Vicinity of Cameron Island N.W.T. Data Report. Canadian Hydrographic Service. Bayfield Laboratory for Marine Sciences and Surveys. Burlington, Ontario.

Sandilands, R.G., R. R Solvason and D. A. St. Jacques. 1985a. 1981 Tidal Survey of Norwegian Bay, N.W.T. Data Report. Canadian Hydrographic Service. Bayfield Laboratory for Marine Sciences and Surveys. Burlington, Ontario.

Sandilands, R.G., R. R Solvason and D. A. St. Jacques. 1985b. 1984 Tidal Survey of the Gulf of Boothia, N.W.T. Data Report. Canadian Hydrographic Service. Bayfield Laboratory for Marine Sciences and Surveys. Burlington, Ontario.

Sandilands, R.G., R. R Solvason and D. A. St. Jacques. 1985c. 1980 Tidal Survey of M'Clintock Channel, N.W.T. Data Report. Canadian Hydrographic Service. Bayfield Laboratory for Marine Sciences and Surveys. Burlington, Ontario.

Sandilands, R.G., R. R Solvason and D. A. St. Jacques. 1985d. 1979 Arctic Tidal Survey. Data Report. Canadian Hydrographic Service. Bayfield Laboratory for Marine Sciences and Surveys. Burlington, Ontario.

Schwiderski, E.W. 1980. On Charting Global Ocean Tides. Rev. Geophys. Space Phys. 18:243-268.

Sverdrup, H.U. 1926. Dynamics of tides on the Northern Siberian shelf. Geophys. publ., 4, No. 5, Oslo.

Taylor, G.I., 1920. Tidal oscillations in gulfs and rectangular channels. Proc. Lond. Math. Soc., 20:148-181.

Thomson, R.E. and W.S. Huggett. 1980. M_2 Baroclinic Tides in Johnstone Strait, British Columbia. J. Phys. Oceanogr. 10, 1509-1539.

APPENDIX A - TIDAL PROPAGATION

In this Appendix we will present a brief theoretical description of tidal propagation. Tidal elevations and streams are caused by the relative motions of the sun, the moon and the earth. The net effect of the gravitational attraction and the rotation of the system results in a tidal potential which tends to modify the sea surface height over the entire surface of the globe: were it not for the complicated hydrodynamics of water movements over the surface of the earth, this potential would cause water levels to be higher directly underneath the sun or moon, as well as on the opposite side of the earth. To an observer on the earth, this tidal potential is not stationary, rotating around the earth in a similar manner to the motion of the sun and moon themselves. The moving potential sets up currents in the ocean basin, as the oceans respond to this forcing. These currents propagate as waves through the ocean, and reflect off the continental coastlines, setting up a complex pattern of elevations and currents. Viewed in more detail, the continental coastlines are not continuous, but are broken by various gulfs and bays. As the tidal waves propagate along the coast they also enter these coastal seas, and frequently are amplified as they propagate therein. Thus, tidal elevations and currents within a particular body of water are determined by two things - the direct astronomical forcing, as well as the effect of the tide in contiguous bodies of water.

A simplified but adequate set of equations describing tidal motions is:

$$\partial u/\partial t = -g\partial\zeta/\partial x + fv + F_x \tag{A1}$$

$$\partial v/\partial t = -g\partial\zeta/\partial y - fu + F_y \tag{A2}$$

$$\partial\zeta/\partial t = -\partial(uh)/\partial x - \partial(vh)/\partial y \tag{A3}$$

where:
u = x-component of velocity
v = y-component of velocity
g = acceleration of gravity
ζ = tidal surface elevation
f = Coriolis parameter, 2 Ω sin (*latitude*), where Ω is the rate of rotation of the earth
h = water depth
F_x, F_y = astronomical forcings and terrestrial tide response

The above equations are derived from the full equations of motion by assuming no vertical dependence in u or v. Certain other simplifications have been made in the above equations, which are generally acceptable for most tidal situations. Frictional effects have been ignored, as well as the non-linear convective acceleration terms. In the deeper ocean basins these terms are generally quite small, although they are important in shallower coastal seas. As well, effects of stratification are ignored, although we will see in Appendix C that they are not necessarily trivial. Our major concern at the moment is the deepwater tidal propagation.

The solution to the above equations, (u, v, ζ) depends on the external forcings, F_x and F_y, and on the boundary conditions applied to the model region. The usual boundary conditions are the requirement for no flow through a coastline, and a prescribed motion of the water surface along any open boundary, where the body of water of interest is connected to other water bodies. These latter elevation data are in general available from tide gauges or from a larger-area numerical model, if one is thinking in terms of a numerical model.

We are interested in a number of solutions to the above equations, corresponding to different sizes of water bodies. First, we will examine the nature of the external forcings. Next, we will examine the types of tidal phenomena in bodies of water whose dimensions are typical of those in the Northwest Passage. This latter examination will form the basis for the discussion of Chapter 6, Analytical Models of Tides in the Northwest Passage. The description of tides in the entire world ocean is discussed in Appendix B, using for illustrative purposes the tides as calculated by Schwiderski (1978). This latter examination will allow us to appreciate the large scale tidal regime in which the Northwest Passage plays the role of a minor connector between the Arctic and Atlantic Oceans.

A.1 THE EXTERNAL FORCINGS

Ultimately, tides are caused by the attractions of the sun and moon in conjunction with the centripetal accelerations that the earth's oceans experience as the earth-moon and earth-sun systems rotate. The algebraic discussion of this gravitational attraction appears in numerous textbooks, and is not repeated here. The fundamental result is that the tidal forcing can be written as the gradient of a tidal potential and hence written as the slope of an equivalent height of water multiplied by the acceleration of gravity. This hypothetical equivalent height of water is referred to as the equilibrium tide. Figure A1 illustrates the earth-moon part of the equilibrium tide. A similar effect occurs for the earth-sun system. In terms of the equilibrium tide, the astronomical forcing may be written as

$$F_{x,astronomical} = g\partial\eta/\partial x \tag{A4}$$

$$F_{y,astronomical} = g\partial\eta/\partial y \tag{A5}$$

where η is the equilibrium tide.

The astronomical forcings are periodic, but modulated over longer time scales, and can be written as:

$$\eta = \sum \eta_\nu \tag{A6}$$

The subscript ν labels the species of the tide. There is a semi-diurnal tide ($\nu = 2$) associated with a bulge in the equilibrium tide when the moon is overhead, as well as when the moon is overhead on the other side of the world about twelve hours later, giving rise to two high waters per day. Similarly, there is another species, ($\nu = 1$) associated solely with the sun or moon being overhead, which gives rise to the diurnal tide. However, the elevation of the moon above the equator, and its distance from the earth, and hence the strength of the tidal potential, changes on an approximately monthly basis. This effect can be mathematically described by writing each tidal species as a sum of a number of periodic terms, each of about the same period. At certain times in the month, these constituents are more or less in phase, giving rise to large tidal forcings, while at other times they are out of phase, so the tidal forcing is reduced. Thus, a particular species may be decomposed as:

$$\eta_\nu = \sum_i K_i A_\nu(\theta)\cos\left(\sigma_i t + x_i + \nu\lambda\right) \tag{A7}$$

where:
t = time
σ_i = frequency
x_i = phase of tide with respect to Greenwich Midnight (a convenient way to define the phase at a zero of relative time t)
λ = east longitude (illustrating that the tide propagates towards the west)
K_i = amplitude given in the following table
A = a function of latitude, ϑ.

The amplitudes K_i for the major semi-diurnal constituents are listed in Table A1, as well as the period of their motion.

TABLE A1
THE EQUILIBRIUM AMPLITUDES OF THE MAJOR TIDAL CONSTITUENTS

Constituent	Tidal Mode	Amplitude (cm)	Period (hr)
M_2	principal lunar	24.2	12.42
S_2	principal solar	11.3	12.00
N_2	elliptical lunar	4.6	12.66
K_2	declinational luni-solar	3.1	11.97
K_1	declinational luni-solar	14.2	23.94
O_1	principal lunar	10.1	25.82
P_1	principal solar	4.7	24.07
Q_1	elliptical lunar	1.9	26.88

Including the latitudinal dependence, each constituent of the semi-diurnal tidal potential is completely described by

$$z = K\cos^2\theta\cos(\sigma t + x + 2\lambda) \tag{A8}$$

and each of the diurnal constituents by

$$z = 2K\sin\theta\cos\theta\cos(\sigma t + x + \lambda) \tag{A9}$$

Interestingly, for the Arctic regions, the tidal forcing is quite small, decreasing to zero at the North Pole. The amplitude at various latitudes is tabulated in Table A2.

TABLE A2
THE DEPENDENCE OF THE EQUILIBRIUM TIDE ON LATITUDE
(AMPLITUDES IN cm)

	0°	70°	75°	80°	85°	90°
M_2	24.2	2.8	1.6	0.7	0.2	0.0
S_2	11.3	1.3	0.8	0.3	0.1	0.0
N_2	4.6	0.5	0.3	0.1	0.0	0.0
K_2	3.1	0.4	0.2	0.1	0.0	0.0
K_1	14.2	9.1	7.1	4.8	2.5	0.0
O_1	10.1	6.5	5.0	3.4	1.7	0.0
P_1	4.7	3.0	2.3	1.6	0.0	0.0
Q_1	1.9	1.2	0.9	0.7	0.0	0.0

Since the tidal forcing occurs at the fixed periods tabulated in Table A1 (as well as other similar but smaller constituents, also at fixed periods) then the observed response of the complex ocean basins will also be at these frequencies, augmented by frequencies due to non-linear interactions. Thus, at any location in the ocean the time dependent nature of the tide can be written in a similar form to the forcing. Thus,

$$z = \sum A_i \cos\left(\sigma_i t + V_{o.i} - g_i\right) \tag{A10}$$

where

Ai = the amplitude of the observed elevation constituent

$Vo.i$ = the phase which the equilibrium tide would assume at Greenwich at the time corresponding to the origin of time, $t = 0$

g_i = the phase between the equilibrium tide at Greenwich and the observed tide at the observation site.

i runs over all constituents, e.g. M_2, K_1, MK_3, etc.

Although the temporal dependence is readily summarized by equation (A10), the spatial dependence can be quite complicated. The speed at which ocean waves (the response) propagate over the ocean differs from the speed at which the above forcings propagate over the ocean. This difference means that the forcing cannot be in phase with the response, which is partly the cause of the complicated tidal patterns over the world ocean. In fact, the propagation speed of the tidal forcing differs at different latitudes, according to Table A3.

TABLE A3
PROPAGATION SPEED OF EQUILIBRIUM TIDE

Latitude	0°	70°	75°	80°	85°
M2 speed (m/s)	318	240	162	81	0
K1 speed (m/s)	159	120	81	40	0

The speed of tidal waves (to be derived later) is given in the following table:

TABLE A4
SPEED OF KELVIN (TIDAL) WAVES

Depth(m)	100	500	1000	2000	4000
Speed (m/s)	31	70	99	140	198

Interestingly, as one travels toward the higher latitudes, the speed at which the tidal forcing propagates decreases, until it is slower than the speed at which tidal waves can propagate in the water. Thus, near the North Pole, the forced response of the basin can be very close to an assumption of the equilibrium surface. Elsewhere, the tidal amplitude cannot assume the simple forms given in equations (A8) and (A9), but must depend on the propagation and reflection properties of waves which are excited by the moving source, the equilibrium tide. Thus, since the tidal wave in the Atlantic Ocean cannot keep up with the rapidly propagating tidal forcing, its spatial response pattern is quite complicated. This complicated tidal regime then will propagate into the Arctic. Thus, there are two fundamental sources of tides in the Arctic: the direct forcing by the sun and moon, as well as the propagation of tidal waves into the Arctic Ocean from the Atlantic (and to a lesser extent, from the Pacific).

A.2 TIDAL WAVES IN COASTAL SEAS

We now return to equations (A1), (A2) and (A3), to be solved in smaller bodies of water, such as Parry Channel. In these cases, a rectangular coordinate system is adequate, and it is suitable to ignore the astronomical forcing because the major tidal effects are due to tidal waves propagating in from other bodies of water. Thus, the only source of tidal energy is that which propagates in from contiguous bodies of water. In the absence of local forcing, the resulting waves are known as "free" waves. It will also be fruitful to schematize the water body into a rectangular channel or gulf. The gain in understanding by being able to develop explicit analytic solutions outweighs the loss of exact agreement with coastal geometry and bathymetry.

Recalling that we can separate the tidal response into a number of discrete frequencies, we will write

$$(\zeta, u, v) = \Re\left\{(Z, U, V)e^{i\sigma t}\right\} \tag{A11}$$

and solving (A1), (A2), (A3) for Z, U, and V, we have:

$$U = \frac{g}{\left(\sigma^2 - f^2\right)} \cdot \left(-i\sigma\frac{\partial Z}{\partial x} + f\frac{\partial Z}{\partial y}\right) \tag{A12}$$

$$V = \frac{g}{\left(\sigma^2 - f^2\right)} \cdot (-i\sigma \partial Z/\partial y - f \partial Z/\partial x) \tag{A13}$$

The equation for Z becomes:

$$\nabla^2 Z + \frac{\left(\sigma^2 - f^2\right)}{gh} Z = 0 \tag{A14}$$

assuming f and h are uniform. We are thus eliminating Rossby waves (waves generated by variable f) and topographic waves (waves generated by variable h).

Any solution of equation (A21) can be shown to be built of a sum of the primary waves:

$$Z = \sum_j Z_{o,j} \cdot e^{i(k_j x + l_j y)} \tag{A15}$$

where $Z_{o,j}$ is a constant.

Substituting (A22) into equation (A21), and suppressing the *j* subscript, we obtain the dispersion relation, which must be satisfied for any valid (*k*, *l*) combination.

$$\sigma = \pm [f^2 + (k^2 + 1^2) gh]^{1/2} \tag{A16}$$

and the equations for *U* and *V*:

$$(U, V) = \frac{Z_o}{h} \cdot (A, B) \exp(i(kx + ly)) \tag{A17}$$

where

$$A = (\sigma k + ifl)/(k^2 + l^2) \tag{A18}$$

$$B = (\sigma l - ifk)/(k^2 + l^2) \tag{A19}$$

The above wave is usually referred to as a Sverdrup wave, after its originator, H.U. Sverdrup, who first applied it to a description of tides on the continental shelf off Siberia, (Sverdrup, 1926). By a proper choice of a collection of Z_j and k_j and l_j one should, in principle, be able to match any water body geometry, in such a way that velocities normal to the coast are zero, and elevations along open boundaries equal the observed values.

The phase speed of the Sverdrup wave is given by:

$$c_p = \pm (f^2/(k^2 + 1^2) + gh)^{1/2} \tag{A20}$$

This speed is faster than for a non-rotating system in which $f = 0$. As well, for a given value of *k* and *l*, two waves are possible, as specified by the ± sign. Also, it can be shown that in the horizontal plane, the current vector traces out a clockwise ellipse over a time $1 / (2\pi\sigma)$.

From equation (A16) σ must be greater than or equal to f, if both k and l are real, as for a propagating wave. The Coriolis parameter, f, increases from zero at the equator to a frequency corresponding to the K_2 tide at the North Pole. Thus, Sverdrup waves at tidal frequencies cannot propagate north of latitudes given in the following table:

TABLE A5
LIMITING LATITUDES FOR SVERDRUP WAVE PROPAGATION

Constituent	Latitude
Q1	26.45°
O1	27.61°
P1	29.82°
K1	30.00°
N2	70.98°
M2	74.47°
S2	85.76°
K2	90.00°

Thus, no diurnal Sverdrup waves can be found in the Arctic, and the semi-diurnal tides can only propagate as Sverdrup waves for a limited distance into the Arctic Ocean.

How then does the tide propagate into the Arctic? We will examine various special cases of the Sverdrup wave: the Poincaré wave, the Kelvin wave and the Proudman wave.

A.3 POINCARE WAVES

We first examine the Poincaré wave, by asking "What happens when a Sverdrup wave is incident at a coastline and is reflected?" Consider the situation shown in Figure A2. An incident wave arrives with wavenumber $(k, -l)$ and the reflected wave leaves with wavenumber (k,l). We have required that the x-component wave-number remain the same for both waves, and the y-component wavenumber be reversed. From equations (A15) to (A19) we identify the incident wave as:

$$1/2(Z_o, A^*, B^*)\exp(i(kx - ly - \sigma t)) \qquad \text{(A21)}$$

and the reflected wave as

$$1/2R\left(Z_o, A, B\right)\exp(i(kx+ly-\sigma t)) \tag{A22}$$

where R is the reflection coefficient and the factor 1/2 is inserted for later convenience. Since the coastline is a solid wall, there must be zero mass flux through it, (v=0), thus

$$-1/2B^{*}+1/2RB=0$$

Thus, $R = B^{*}/B = exp(-2i\ argB)$. Note that $|R| = 1$, the effect of reflection being solely a phase change. Adding the two waves, and taking real parts, we obtain the following wave:

$$\zeta = Z_o\cos(ly - argB)\cos(kx-\sigma t) \tag{A23}$$

$$u = |A|\cos(ly - argB + argA)\cos(kx-\sigma t) \tag{A24}$$

$$v = -|B|\sin(ly)\sin(kx-\sigma t) \tag{A25}$$

(Note that a slight change in time origin simplified the $\cos(kx\text{-}\sigma t)$ terms above.)

This new wave is called a Poincaré wave, characterized by propagation along the coast, ($\cos(kx-\sigma t)$) and by an offshore nodal structure, ($\sin(ly)$). Note that not only is v identically zero along the coastline, but also at locations given by ($\sin(ly) = 0$), or at $y = n\pi/l$. Alternatively, given a channel of width L, only those Poincaré waves with l-wavenumber equal to $n\pi/L$ are allowed. Recall however that these waves will still not propagate into the Arctic Ocean, because the tidal frequencies are too low compared to f. The dispersion relation remains unaltered. Thus, these types of Poincaré waves cannot explain the propagating tides in the Arctic.

However, it is not essential that the x-component wavenumber be purely real. If it is made purely imaginary (replacing k with $-ik$) we can still retain the cross-channel nodal structure in the y-direction, but the terms involving kx will become exponential terms, so that the wave is written:

$$\zeta = Z_o\cos(ly - argB)e^{kx}\cos\sigma t \tag{A26}$$

$$u = |A|\cos(ly - \arg B + \arg A)e^{kx}\cos\sigma t \tag{A27}$$

$$v = |B|\sin(ly)e^{kx}\sin\sigma t \tag{A28}$$

This is the more usual form of a Poincaré wave: a cross channel nodal structure, $(\cos(ly))$, and a "trapped" component, $(\exp(kx))$, replacing the propagating component. Although this wave can now exist at the high latitudes of the Arctic Ocean (because σ may be less than f), it is not a very good candidate for a tidal wave, because it has no propagating component.

A.4 THE KELVIN WAVE

We still have not found a wave which can freely propagate into the Arctic Ocean. The answer again lies in examining the dispersion relation, equation (A16). The problem is that we need to find conditions under which σ is less than f. This can only occur if $(k^2 + l^2)$ is less than zero. For the Poincaré wave case, where there were in effect two reflecting Sverdrup waves, it was profitable to let k be purely imaginary. Now, we will instead let l be purely imaginary, and consider only one Sverdrup wave. Making this explicit identification, we can write the wave solution as:

$$(\zeta, u, v) = \left(Z_o, Z_o A/h, Z_o B/h\right)\exp(ly)\cos(kx - \sigma t) \tag{A29}$$

where

$$A = (\sigma k + fl)/\left(k^2 - l^2\right) \tag{A30}$$

$$B = (\sigma l + fk)/\left(k^2 - l^2\right) \tag{A31}$$

$$\sigma = \pm\left(f^2 + \left(k^2 - 1^2\right)/gh\right)^{1/2} \tag{A32}$$

This is a boundary wave: it propagates along a boundary, in the x-direction, $\cos(kx - \sigma t)$, and decays away from that boundary, $(\exp(ly))$. We also note that σ may be less than f, essential for tidal propagation. An interesting and important result is that for a given (σ, k) two values of l are possible:

$$l = \pm\left(k^2 + \left(f^2 - \sigma^2\right)/gh\right)^{1/2} \tag{A33}$$

The sign of l determines if the wave decreases to the left ($l<0$) or decreases to the right ($l>0$), for the particular case of $k>0$. The naming of these waves is problematic. If $l<0$, the waves decay to the left, and they are known as Kelvin waves. If the waves decay to the right, they are known as Proudman waves.

The special case of a Kelvin wave for which $l = -kf/\sigma$ is usually known as "the Kelvin wave". Platzmann refers to it as the prototype Kelvin wave. In the prototype Kelvin wave, $k^2 = \sigma^2 / gh$ is independent of wavelength. The formulae for (ζ, u, v) are:

$$(\zeta, u, v) = \left(Z_o, Z_o\sqrt{(gh)}/h, 0\right)\exp(-fy/gh)\cos(kx-\sigma t) \tag{A34}$$

Note that $v \equiv 0$. This will make it very easy to apply Kelvin waves to the solution of tides in channels and rectangular seas. Also, note that the current ellipses are rectilinear -- there is only a u-component of motion.

The more general Kelvin/Proudman wave has form

$$(\zeta, u, v) = \left(Z_o, Z_o(k+fl)/\left(k^2+1^2\right), Z_o/h(\sigma 1+fk)\right)\exp(ly)\cos(kx-\sigma t) \tag{A35}$$

This expression is quite complex, and has almost passed the point where algebra clarifies the situation.

A.5 BAROTROPIC TIDES IN BASINS

The simplest way to model a tidal basin is to assume that it is a rectangle, and that a Kelvin wave propagates into the basin, reflects off the far end, and exits, Figure A3. For most of the basin this is a plausible solution, because the cross-channel velocity in a Kelvin wave is identically zero, so that the wave can satisfy the boundary condition of no flow through the side wall for any width of channel. However, at the head of the gulf, u, the velocity normal to the wall at the end, is not zero. Along this channel end, it is usual to postulate a collection of Poincaré waves, which satisfy the cross-channel boundary condition $l = n\pi/L$ and which decay away from the end of the wall - k is chosen purely imaginary. These waves are thus trapped to the head of the gulf, and will not be detected at points distant from the head. In this case, it is possible for a complete reflection of the Kelvin wave. The Poincaré wave amplitudes are chosen so that the velocities normal to the head of the bay due to the Poincaré waves exactly balance the velocities due to the incident and reflected Kelvin waves. Thus, if the head of the gulf is at $x = 0$, the incident Kelvin wave u-velocity is given by:

$$u = U_1\exp(-fy/gh)\cos(\sigma t)$$

the reflected wave u-velocity is given by:

$$u = U_r \exp(f(y-l)/gh)\cos(\sigma t)$$

and the Poincaré waves are given by:

$$u = \sum U_{P_j}$$

where each component Poincaré wave is in turn given by:

$$U_{P_j} = \big(U_j \cos(ly)\cos(argB - argA) + \sin(ly)\sin(argB - argA)\big)\cos\sigma t$$

The problem has been reduced to a determination of the Fourier coefficients of the sum of two exponential functions. Taylor (1920) was the first to work out this solution in detail. His original diagrams are presented in Figures A4 and A5.

First, consider the elevation pattern. Neglecting the moment the Poincaré waves at the head of the gulf, the two Kelvin waves are:

$$Z = Z_i \exp(-fy/gh)\cos(kx - \sigma t) + Z_r \exp(f(y-L)/gh)\cos(-kx - \sigma t) \tag{A42}$$

If f, the Coriolis parameter, were zero, this would be the equation of a standing wave. The presence of the y-dependence adds considerably to the complexity of this rotating, standing wave. Figure A4, from Taylor (1920) shows contours of equal amplitude (dashed lines), and lines of constant phase (solid lines). The amplitude contours are known as co-range lines, and are really the contour of amplitude A_i in equation (A10). Similarly, the lines of equal phase are known as co-tidal lines, and the phase selected for contouring is local high water, or contours of equal Greenwich phase, g_i from equation (A10). The regions of zero amplitude are known as amphidromes. The amphidrome spacing is governed by $\cos(kx)$, so the amphidromes are one half wavelength apart, corresponding to maxima in the absolute value of $\cos(kx)$. The sense of rotation of the co-tide lines are counterclockwise, which could be expected from the following argument. Along the wall labelled I, the incident wave is considerably stronger than the reflected, the latter having been modulated by the term $\exp(-fL/gh)$. Thus, we measure primarily the incident wave's phase, which increase as x increases towards the head. Conversely, along the shoreline labelled R, we primarily sense the phase of the reflected wave, which propagates outward.

Next we consider the ellipse plots, the curves traced by the vector *(u,v)* at a particular point, Figure A5. This diagram, too, is from Taylor(1920). We note that along the shoreline, the velocity is rectilinear - it merely reverses direction as the tide changes. However, near the head of the gulf, the velocity vectors trace out ellipses - indicating the presence of Poincaré waves.

The velocity field is composed of a rectilinear Kelvin wave and elliptical Poincaré waves. Figure A6 plots the separate Kelvin and Poincaré waves, indicating the polarization (sense of rotation) for each location. It is seen that while the Poincaré currents rotate clockwise, the overall current vectors rotate counterclockwise. Because of the phase relationship between the Kelvin and Poincaré modes the intrinsic sense of rotation of the Poincaré mode has been changed from clockwise to a counterclockwise sense in the combined wave. This points to the problem of trying to separate Kelvin and Poincaré waves in observed data.

In summary then:

1.Currents are generally rectilinear, except near the head, (where Poincaré waves are required to satisfy the condition of no flow through a solid boundary);

2. Amphidromes, points of minimal tidal elevation, are found in the system. These are the counterpart of nodes in the vibrating string problem.

3. The tidal phase rotates counter-clockwise around the amphidrome;

4. Current vectors trace out a clockwise ellipse, for a barotropic flow;

5. The propagation of high water phase is not uniform along the coast - the cotidal lines bunch together near cell boundaries.

Note that we have so far assumed equal amplitudes for the incident and reflected Kelvin waves. In general, these two waves are not equal, because the incident wave loses energy as it propagates into the system, and the reflected wave similarly loses energy as it propagates from the head to the mouth. This energy loss can be modelled by an attenuation of each wave along its path, but this would lead to a rather complex solution. It is more expedient to assume that most of the energy is lost at the head of the gulf, and thus assume that the amplitude of each wave is constant as it moves through the system, but the reflection coefficient is less than 1.0. This particular modelling approach was first described by Hendershott and Speranza (1971) and Figure (A7) reproduced from their paper, illustrates the effect that changing the reflected amplitude has on the co-range and co-phase pattern: as the reflected wave is damped more heavily, the amphidrome moves to the left shore, looking toward the head of the bay, *i.e.*, the incident wave becomes more dominant.

The Kelvin wave solution is certainly the easiest to apply analytically to a semi-enclosed gulf. As we will see in Appendix B, in the Arctic, some of the tidal patterns deviate from the barotropic Kelvin wave pattern, and we are required to postulate a more complicated Proudman wave field. For example, the K_1 tide (Figures B2 and B3) sets up what appears to be a standard amphidrome off the Queen Elizabeth Islands. However, the phase goes the wrong way around the amphidrome! We speculate that the wave field here is not a Kelvin wave, but a pair of Proudman waves.

APPENDIX B - GLOBAL TIDAL MODELS

Although the dimensions of the Northwest Passage are large by most standards, the Northwest Passage represents only a minor set of channels connecting Baffin Bay and the Arctic Ocean. It is appropriate then to consider tides in the Northwest Passage as the response to tides in the larger basins, Baffin Bay and the Arctic Ocean. Schwiderski has developed a procedure to calculate the tidal amplitudes and phases over the entire globe, using observed elevation data and applying dynamical constraints to an interpolation scheme. Schwiderski claims a high degree of accuracy in the method, so we will use his data as our description of tides in the waters surrounding the Northwest Passage. We note that Schwiderski did not provide an estimate of tides in the Northwest Passage, due to the insignificance of the Northwest Passage on a global tidal scale. We first examine the changes in wave propagation theory which must be incorporated in a global tidal model.

B.1 SOME COMPLICATIONS TO THE EXTERNAL FORCING TERMS

There are two types of external forcings: the direct forcing due to the gravitational attraction of the sun and moon, and the response of the solid (as opposed to oceanic) earth to the tidal forcing (the terrestrial tide), and to the oceanic tide (the oceanic tidal loading). We first examine the astronomical forcings.

There are a number of complications to the simple picture of the equilibrium tide presented so far. Principally they are due to the fact that the solid earth is not rigid, and so will sustain tidal oscillations as well. These oscillations then affect the height of the water column, affecting the continuity equation (A3). Both oceanic and terrestrial tides alter the distribution of mass on the earth, and thus alter the gravitational attraction which defined the equilibrium tide. This latter alteration to the equilibrium tide is quite difficult to calculate, but not insignificant for oceanic tides.

Elastic waves in the earth can propagate faster than the equilibrium tide, so it is possible for the terrestrial tide to remain in phase with the equilibrium tide. Thus, the sea floor tide will be approximately the same shape as the equilibrium tide. Since the sea floor is moving up and down in response to tidal forcing, its effect had to be included in the continuity equation (A3).

After accounting for all of the above, and invoking a somewhat simplified model of the tidal response of the solid earth, the following set of equations is obtained:

$$\partial u/\partial t=-g\partial/\partial x(0.9\zeta-0.7\eta)+fv \tag{B1}$$

$$\partial v/\partial t=-g\partial/\partial y(0.9\zeta-0.7\eta)-fu \tag{B2}$$

$$\partial\zeta/\partial t = -(\partial/\partial\lambda)(uh) - \partial/\partial y(vh) \qquad \text{(B3)}$$

The algebraic effect of the complete specification of tidal dynamics including the effects of tides on the sea floor is to reduce the surface slope by 10% in the momentum equations, and to reduce the equilibrium tide by 30%. It is important to point out that the 10% reduction in surface slope only applies to large bodies of water such as the Atlantic Ocean, for which the simple elastic earth models apply. In smaller bodies, the spatial variation of the water surface tide is usually much larger than the other effects, so we can ignore the explicit equilibrium tide, and restore the coefficient of surface slope to 1.0 in the momentum equations.

B.2 THE SCHWIDERSKI MODEL

Schwiderski (1980 and references therein) has prepared maps of the major tidal constituents for the entire globe. His study was motivated by a desire to provide sea level predictions for various military and civilian purposes, particularly related to satellite measurement of the earth's shape. For such measurements it is essential to be able to accurately remove tidal signals from the global pattern of sea level. Schwiderski's solution technique was to solve equations (B1) - (B3), including complicated bottom friction and eddy viscosity terms, using a finite difference method in space and time. The resulting time series at each grid point were harmonically analyzed to produce maps of Greenwich amplitude and phase. the equations were solved on the spherical geometry of the earth, so (B1) - (B3) had to be modified to spherical coordinates. The most interesting aspect of Schwiderski's work was that he was able to incorporate a number of observed tidal values from tidal stations around the world. Essentially, at selected locations where there was a reliable tidal measurement of elevation, that value was inserted into the finite difference model in place of the calculated value as the model was running. In general, this would lead to "noisy" solutions in the vicinity of each of these artificial points, the "continuity gap" in Schwiderski's terminology, but an elevated frictional coefficient was used to smooth the velocity field around each empirical tidal point. As well, most of the points were near a coastline, and Schwiderski allowed water to cross the coastal boundary, monitoring the degree to which this additional flow improved the continuity gap at the empirical tidal stations.

In summary, Schwiderski was able to incorporate the known astronomical forcing, a reasonable model of the terrestrial tidal influence, and a number of empirical data into a model which allowed 10 cm accuracy of tidal prediction over the global ocean. One might criticize the model on the basis that Schwiderski had to use very complicated bottom friction and eddy diffusion formulations, whereas in fact most of it occurs over the continental shelves and in adjacent coastal seas, which were not resolved by Schwiderski's 1° x 1° model. However, for purposes of visualizing the propagation of the tide over the globe, the maps produced by Schwiderski are excellent. We note, however, that Schwiderski's calculatios appear to be particularly poor along the Queen Elizabeth Islands, where he underestimates the M_2 tide by as much as 10 cm.

Figure B.1 provides a base map for the region, as well as contouring the 200 m and 3000 m depths. The depth field is well characterized by these contours. The Arctic Ocean is characterized by an extensive shallow region adjacent to Russia, much of which is less than 200 m deep, and a deep basin in the middle, most of which exceeds 3000 m in depth. Closer examination reveals more structure to the Arctic Ocean than is contained in the preceding summary. The shallow region north of Russia is composed of a number of different water bodies, the East Siberian Sea, Laptev Sea, Kara Sea and Barents Sea. The Barents Sea is somewhat deeper than the others, a typical depth being 500 m. The two major basins are in fact part of a more complex system: the Canada Basin and the Amundsen Basin are predominant, separated by the Lomonosov Ridge, in which depths shoal to 1000 m. Between the Canada Basin and the Lomonosov Ridge there is another basin, the smaller Makarov Basin, separated from the Canada Basin by the Alpha and Mendeleev Ridges. Similarly, between the Amundsen Basin and the shallow coastal seas of Russia is located the Nansen Basin, separated from the Amundsen Basin by the Arctic Midocean Ridge. The deep basins are covered by a permanent ice pack, which maintains a regular clockwise rotation, driven by the average wind field over the area.

Figure B.2 - B.13 are the contours of amplitude and phase for the constituents M_2, S_2, N_2, K_1, O_1 and P_1. The increment of phase is chosen to be 30 degrees (1 hour for semi-diurnal constituents and 2 hours for diurnals). The contoured levels of amplitude varied according to the size of the constituent. They are tabulated below.

Constituent	Contour Levels(cm)
M_2	1 2 5 10 15 20 30 40 60 80
N_2	1 2 3 4 5 10 15 20
S_2	1 2 3 4 5 10 15 20 30 40
K_1	1 2 3 4 5 10
O_1	1 2 3 4 5 10
P_1	1 2 3 4 5

Reference is made to Appendix A for a more complete discussion of the significance of co-range and co-phase plots.

B.3 DIURNAL TIDES

We consider first the propagation of the K_1 tide, representing the "typical" diurnal tide in this basin. There are two main amphidromes in the system, suggesting that the tide propagates in from the Atlantic, and is reflected off the opposite end of the basin, the Alaska coast. The separation between amphidromes is one-half a wavelength. For water of 3000 m depth, the phase speed is 170 m/s, and the diurnal wave half-wavelength is 7,400 km. For scaling purposes, the distance from Spitsbergen to Alaska is 3,200 km, or one-quarter wavelength. The first amphidrome is located approximately one-quarter wavelength from the end, which explains the presence of the amphidrome off Spitsbergen. At this amphidrome, the lines of constant phase rotate counterclockwise, as in the standard case shown in Figure A4. The amphidrome system off the Queen Elizabeth Islands is a bit of a puzzle. The first feature of interest is that the lines of constant phase rotate clockwise. This sense of rotation precludes the presence of Kelvin waves in determining the amphidrome system, and allows us to speculate that this amphidrome is formed by the more esoteric Proudman wave, in which amplitudes grow rather than decay to the left. Thus, as we move around the amphidrome, the phase is more determined by the wave attached to the opposite shore, and has the appearance of rotating backwards. Recall that the Proudman wave the water level increases to the left when viewed in the direction of propagation. Thus, along the right hand shore, looking toward the head, we are not primarily sampling the phase of the incident wave, but the phase of the wave travelling back out, because its amplitude increases to the left when looking in the direction of propagation. The other characteristic of the Proudman wave is that the lateral velocity is not identically zero, as is the case for a Kelvin wave. This feature fits into the geometry, because although one can, to a certain extent, ignore the Siberian Shelf in describing the progression of a Kelvin wave into the system and its reflection, there must be a lateral flow to provide the large tides observed on the shelf. This lateral flow can come from the Proudman wave. The Proudman wave does not satisfy a condition of zero velocity transverse to the direction of propagation. This is in fact fortunate, because the lateral flow will be required to form the tidal complement on the shallow East Siberian Sea -- it is connected to the Proudman wave in the Canada Basin by a "leaky" lateral boundary condition.

The K_1 amplitudes over most of the sea vary between 1 and 5 cm, except for a region in the Barents Sea where they reach 10 cm. These amplitudes are considerably less than the equilibrium tide over much of the region, even allowing for the 30% reduction discussed on Appendix A. This is an interesting situation, which does not arise over much of the world oceans.

The P1 tide is not the next most significant diurnal tide, but it is closest in frequency to the K_1 tide. Not surprisingly, the P_1 amplitude-phase relationship is identical to K_1, to the extent one can determine from an inspection of the corresponding plots. This identical behaviour is of particular relevance to the inference process, as it means that the inference assumption of identical propagation properties for K_1 and P_1 is valid.

The O_1 tide is the second strongest diurnal tide. Its propagation properties are however completely different from those of K_1 and P_1. There are a few amphidrome systems in the Barents Sea and Kara Sea regions, a result of reflections on the shelf, but the deep-ocean propagation appears to be a unidirectional propagation out of the region and toward the Atlantic as indicated by the direction of increasing phase. The O_1 frequency is the difference between the M_2 and K_1, so it would be tempting to identify the O_1 propagation as determined by non-linear interactions between the stronger M_2 and K_1 tides. However, the deep basins, and consequent small currents really preclude this explanation.

B.4 SEMI-DIURNAL TIDES

The M_2 is the largest semi-diurnal constituent. Its amplitude pattern reveals a major amphidrome located in the Canada basin, and another east of Greenland. These two amphidromes fit into the standard description of two counter-propagating Kelvin waves, with amphidromes separated by a half wavelength. The half wavelength for a semi-diurnal constituent in this basin is about 3,700 km, and the separation between the two amphidromes is also about 3,700 km, so the Kelvin wave theory has some credibility here. The most striking feature is perhaps the minimum in amplitude centred over the North Pole, and the associated corkscrew distribution of phase. This feature must in some way be related to the equilibrium tidal forcing. The other features of note are the well-defined amphidrome in Baffin Bay and the various smaller amphidromes on the Siberian shelf, indicating multiple reflections occurring in that region.

The N_2 and S_2 constituents have similar propagation properties to the M_2, except they don't indicate the anomalous behaviour at the North Pole.

B.5 OTHER MODELS

Various authors have modelled the Arctic Ocean as a regional model. A particularly applicable approach is that of Kowalik (1981) who considered as well the effect of ice cover on the tide in the Arctic Ocean. Kowalik ignored the astronomical forcing, a remarkable omission considering the size of the basin. In addition to identifying a change in phase and amplitude in the M_2 tide as a consequence of ice cover, Kowalik also found that the M_2 tide generated, through non-linear interactions, a residual pack ice drift. The effect of ice cover on the M_2 tide will reduce amplitudes by 1 to 2 cm, and produce some phase lag, typically not more than 2°.

A numerical model of barotropic tidal propagation, based on an irregular triangular grid, has been developed at the Institute of Ocean Sciences, Patricia Bay (R.F. Henry, pers. comm.). This model provides good agreement with the observed tidal elevation constants, and somewhat poorer reproduction of the observed currents.

Tidal propagation in the eastern approaches to the Northwest Passage has been described by Greisman (1984) and by Greismann *et al.* (1985). Both of these reports provide more detail on the very large tides which exist in Baffin Bay and Foxe Basin, and which provide the energy for all of the tidal phenomena presented in this report.

APPENDIX C - TIDAL CURRENTS AND THEIR VERTICAL STRUCTURE

In general, there is a fairly strong similiarity between the co-range and co-phase plots based on observed data and the simplified analytical model of tides in coastal seas presented in Appendix A. However, upon examining the currents fields, one finds that there is considerable complexity - Appendix A assumed that currents were uniform in the vertical, whereas in reality they frequently are not, and both phase and amplitude change considerably over the water column. We wish now to examine two possible ways for currents to be non-uniform in the vertical - frictional interaction , and baroclinic responses. In Appendix D, we examine a further complication to the current field, but one which has a more complicated time dependence - inertial oscillations.

C.1 BAROCLINIC TIDAL CURRENTS

We return to equations 1, 2, and 3 of Appendix A, but in a somewhat more primitive form: this time, it is not assumed that the water column and currents are vertically homogeneous, and the vertical integration implied in Equations A1, A2 and A3 has not yet been performed. We then have the set of equations:

$$u_t = fv + \frac{1}{\rho_o} p_x = 0 \tag{C1}$$

$$v_t + fu + \frac{1}{\rho_o} p_y = 0 \tag{C2}$$

$$p_z + \rho g = 0 \tag{C3}$$

$$u_x + v_y + w_z = 0 \tag{C4}$$

$$\rho_t + \rho_{oz} w = 0 \tag{C5}$$

where all variables u, v, w, p and ρ depend not only on x, y, and t but also on z. The last equation above states that density fluctuations result from small vertical advection of water parcels which retain their original ambient density - there is no mixing in this model. After considerable algebra, and ignoring the β effect, the above equations may be combined into one equation for the pressure (see Leblond and Mysak, 1978, sec. 15 for details):

$$\nabla_h^2 p + \Psi \rho_o \left(p_z / \rho_o N^2 \right)_z = 0 \tag{C6}$$

where the operator

$$\Psi = \partial_{tt} + f^2 \tag{C7}$$

and

$$N^2 = -g\rho_{0z}/\rho \tag{C8}$$

The boundary condition, $w = 0$ at $z = -H$ becomes

$$p_{zt} = 0 \text{ at } z = -H \tag{C9}$$

and at the surface the boundary condition equating w to the time derivative of the surface elevation becomes

$$\left(N^2/g\right)p_t + p_{zt} = 0 \text{ at } z = 0 \tag{C10}$$

A key step is to assume that the pressure p may be written as:

$$p = \Pi_n(z)\,p_n(x,y,t) \tag{C11}$$

We then obtain two equations:

$$\rho_0 \frac{d}{dz}\left(\frac{1}{\rho_0 N^2}\frac{d\Pi_n}{dz}\right) + \frac{1}{gh_n}\Pi_n(z) = 0 \tag{C12}$$

$$\nabla_h^2 p_n - \frac{1}{gh_n}\Psi p_n = 0 \tag{C13}$$

The bottom boundary condition becomes

$$\frac{d\Pi_n}{dz} = 0 \text{ at } z = -H \tag{C14}$$

and the surface boundary condition becomes

$$\frac{d\Pi_n}{dz} + \frac{N^2}{g}\Pi_n = 0 \text{ at } z = 0 \tag{C15}$$

Equation (C13) is solved using the observed density profiles, and the boundary conditions (C14) and (C15). The resulting solution is both the vertical profile Π_n and also the eigenvalue gh_n. Note that the vertical equation (C13) and its associated boundary conditions have no dependence on either the tidal frequency or the Coriolis parameter. These two factors enter only into the horizontal equation (C12).

Equation (C13) is strikingly similar to the equation (A14) for the barotropic case. In fact, the largest h_n turns out to be, when Equation (C13) is solved, almost exactly the depth of the water column, in which case (C13) for that mode is identical to (A14). Thus, it was acceptable to ignore baroclinic effects while determining the barotropic response in Appendix A.

Now when one has a profile of velocities (which have the same vertical form as the pressures) one can in principle use the eigenvectors (which are a complete set) to match the observed profile and determine the degree to which each mode contributes to the overall motion. For instance, one often finds that estuarine flow is two layered. The first baroclinic mode is one which has two layers - the number of layers is (n + 1) - and this mode is frequently found to be the strongest in estuarine-dominated flows (Thomson and Hugget, 1980). With a set of eigenvalues and amplitudes of the eigenvalues, one could then in principle determine the acceptable values of k and l entering into the solution of Equation (C12). In this way, the vertical profile will determine the horizontal solution.

In Chapter 6, we presented examples of the computation of modal profiles from density profiles, and the way in which these modes can be used to fit the observed data. We point out here that the method has one fundamental limitation: it tells us which modes are present, but not the forcing responsible for them.

C.2 THE FRICTION BOUNDARY LAYER

The previous section concerned the baroclinic response of the system, depending on the interaction of the internal density and pressure surfaces. In this section, a barotropic mechanism will be discussed. For purposes of this section, it will be assumed that the fluid density is uniform, although in practice it is not, and the density gradients undoubtedly affect the nature of the turbulence. We will also make a very bold assumption that the spatial pressure gradients do not change: thus u and v do not change in the horizontal plane. However, the results with even these omissions are so striking that they are of considerable interest.

We begin by decomposing the flow into two components:

$$u = u^{EKMAN} + u^{TIDAL} \tag{C16}$$

where the first term is the Ekman current, associated with frictional boundary layers, and the second is the vertically uniform tidal current, which would appear in a barotropic tidal model for instance. Adding a vertical eddy viscosity term to equations (C1), and (C2), and assuming a vertically uniform pressure gradient, we obtain:

$$\left(u_t^E - f v^E\right) + \left(u_t^T - f v^T\right) = -\frac{1}{\rho} P_x + A_v u_{zz}^E + A_v u_{zz}^T \tag{C17}$$

$$\left(v_t^E + f u^E\right) + \left(v_t^T + f u^T\right) = -\frac{1}{\rho} P_y + A_v v_{zz}^E + A_v v_{zz}^T \tag{C18}$$

The tidal components are a solution away from the boundaries, where presumably there is no vertical variability. In addition, the tidal components are not required to satisfy boundary conditions at the top or bottom surfaces - the Ekman components will be required to complete the solution in these regions. Thus, the tidal equations are:

$$\left(u_t^T - f v^T\right) = -\frac{1}{\rho} P_x \tag{C19}$$

$$\left(v_t^T + f u^T\right) = -\frac{1}{\rho} P_y \tag{C20}$$

The remaining terms, the Ekman equations, are then:

$$\left(u_t^E - f v^E\right) = A_v u_{zz}^E \tag{C21}$$

$$\left(v_t^E + f u^E\right) = A_v v_{zz}^E \tag{C22}$$

The sum of the two solutions is assumed to satisify a no slip boundary condition at the top and bottom surfaces, in recognition of the ice covered nature in the Northwest Passage. The latter is a considerable simplification, in view of the complex nature of the ice-water interaction in winter, and the open conditions in summer. However, it is our purpose mainly to suggest possible explanations for the interesting current variability in the Arctic, not provide a complete solution at this point. The boundary condition is then:

$$u^E + u^T = 0 \text{ at } z = 0 \tag{C23}$$

$$u^E \to 0 \text{ as } z \to -\infty \tag{C24}$$

Note in the above that we are making the usual boundary layer approximation: the Ekman term is required to die out at infinity.

All variables are assumed to have a sinusoidal time dependence:

$$e^{i\sigma t} \text{ or } e^{-i\sigma t} \tag{C25}$$

The equations are much simpler to solve if written in complex notation

$$w = u + iv \tag{C26}$$

We note an important point here. In general a current can be either clockwise of counterclockwise polarized. Thus, the real and imaginary parts of w have an implied dependence on σ and the sign of σ. If the sign of the σ is > 0, then the current vector rotates counterclockwise, while for the sign of the σ term < 0, the vector rotates clockwise with time.

The tidal component satisfies: (C27)

$$w_t^T + ifw^T = -\frac{1}{\rho}\left(P_x + iP_y\right)$$

with solution

$$w^T = \frac{iP_x - P_y}{\rho(\sigma + f)} \tag{C28}$$

or

$$u^T = -\frac{P_y}{\rho(\sigma + f)} \tag{C29}$$

$$v^T = \frac{P_x}{\rho(\sigma + f)}$$

The form of these solutions is quite similar to those in Appendix A, in the limit of k and l becoming zero - very long waves.

The solution of the Ekman equation is much more interesting. The equation is:

$$w_t^E + ifw_t^E = A_v \frac{\partial^2 w^E}{\partial z^2} \tag{C30}$$

with boundary conditions

$$w^E(0) = -w^T \ ; \ w^E(-\infty) = 0 \tag{C31}$$

The general solution is:

$$w^E = B\exp\left[\left(\frac{(f+\sigma)}{A_v}\right)^{1/2}\frac{(1+i)}{\sqrt{2}}z\right]e^{i\sigma t} \tag{C32}$$

In the above, a positive sign for σ was assumed, so this solution can match a counterclockwise tidal solution, w_{T+}:

$$w(z) = w_*^T\left(1 - \exp\left[\left(\frac{(f+\sigma)}{A_v}\right)^{1/2}\frac{(1+i)}{\sqrt{2}}z\right]\right)e^{i\sigma t} \tag{C33}$$

Correspondingly, if a negative sign for the sigma term is assumed, the total solution is:

$$w(z) = w_*^T\left(1 - \exp\left[\left(\frac{(f-\sigma)}{A_v}\right)^{1/2}\frac{(1+i)}{\sqrt{2}}z\right]\right)e^{i\sigma t} \tag{C34}$$

The most striking feature of these two solutions is the difference in the vertical scale. The 1 over e distance for the counterclockwise case is given by:

$$\sqrt{\frac{A_v}{f+\sigma}}$$

while for the clockwise case it is given by

$$\sqrt{\frac{A_v}{f-\sigma}}$$

Now we see the potential coplexity due to the closeness of σ and f for semi diurnal tides in the Arctic: the vertical scale distance approaches infinity, and the boundary layer occupies the entire water column.

We need to do a bit more work to get the above solutions into a form suitable for comparisons with data. First, we note that the solutions remain the same, considering the bottom boundary layer, if one replaces the z dependence with a dependence on (-H - z) near the bottom of the water column. As well, we note that although the above solutions were constructed for z approaching $-\infty$, they are valid within a bounded region, as long as the two bounding solutions are sufficiently far apart for the exponentials in the above solutions to decay sufficiently. Thus, a profile can be constructed, using the two solutions.

APPENDIX D A MODIFIED POLLARD-MILLARD MODEL

In this appendix, a simple model for inertial motions is developed that explains most of the observed features of inertial currents in a very straightforward way. The model is an extension of the pioneering work of Pollard and Millard (1970) in which the ocean is idealized as a two layer system with with an upper layer of thickness h_1 and density ρ_1 overlying a deeper layer of thickness h_2 and density ρ_2 (Figure D1). The two layers are assumed to be immiscible but are dynamically linked through an interfacial stress. This model is not designed to faithfully represent the real ocean, rather it is designed to reveal the essential characteristics of inertial oscillations in a stratified ocean.

The vertically integrated two layer equations of motion are (e.g. LeBlond and Mysak, 1978):

Upper Layer

$$u_{1t} - fv_1 = -g\eta_{1x} + \left(\tau_S^x - \tau_I^x\right)/\rho_1 h_1 \tag{D1}$$

$$v_{1t} + fu_1 = -g\eta_{1y} + \left(\tau_S^y - \tau_I^y\right)/\rho_1 h_1 \tag{D2}$$

$$h_1\left(u_{1x} + v_{1y}\right) = \left(\eta_2 - \eta_1\right)_t \tag{D3}$$

Lower Layer

$$u_{2t} - fv_2 = -g\left[\eta_2 - \delta\left(\eta_2 - \eta_1\right)\right]_x + \left(\tau_I^x - \tau_B^x\right)/\rho_2 h_2 \tag{D4}$$

$$v_{2t} + fu_2 = -g\left[\eta_2 - \delta\left(\eta_2 - \eta_1\right)\right]_y + \left(\tau_I^y - \tau_B^y\right)/\rho_2 h_2 \tag{D5}$$

$$h_2\left(u_{2x} + v_{2y}\right) = \eta_{2t} \tag{D6}$$

Here $\underline{u}_i = (u_i, v_i)$ is the velocity in the ith layer; η_1 and η_2 are the respective displacements of the sea surface and the interface; $\underline{\tau}_S$, $\underline{\tau}_I$, $\underline{\tau}_B$ are the surface wind stress, the interfacial stress, and the bottom stress respectively; the superscripts x and y refer to the components of the vector stresses, while the subscripts x and y on the other variables denote their partial derivatives; finally $\delta = (\rho_2 - \rho_1)/\rho_2$ gives the fractional jump in density across the interface. This is a crude representation of the true density structure (recall Figure 6.2.1), but it contains the essential elements necessary for this discussion. Typically, δ is the order of 10^{-3}.

Now (D1) - (D6) describe dynamics in addition to those that occur on inertial time and space scales. In order to concentrate solely on inertial scale motions driven by the wind, we will assume that the currents may be decomposed into inertial scale motions $\underline{u}_E$ and a residual flow $\underline{u}_G$. Specifically, we assume that that $\underline{u}_G$ is geostrophically balanced by the pressure gradients due to the sloping sea surface and interface. This is a traditional approximation that dates back at least to Ekman (1932) (hence the subscript *E)* and is valid provided the dynamics are linear. With this assumption all pressure effects cancel and (D1) - (D6) reduce to:

Upper Layer

$$u_{E_{1t}} - f v_{E_1} = \left(\tau_S^x - \tau_I^x\right)/\rho_1 h_1 \tag{D7}$$

$$v_{E_{1t}} + f u_{E_1} = \left(\tau_S^y - \tau_I^y\right)/\rho_1 h_1 \tag{D8}$$

Lower Layer

$$u_{E_{2t}} - f v_{E_2} = \left(\tau_I^x - \tau_B^x\right)/\rho_2 h_2 \tag{D9}$$

$$v_{E_{2t}} + f u_{E_2} = \left(\tau_I^y - \tau_B^y\right)/\rho_2 h_2 \tag{D10}$$

(Henceforth the subscript *E* will be dropped.)

The analysis is greatly simplified at this stage by exploiting the two dimensionality of the problem with a transformation to the complex plane. We define

$$w_i = u_i + i \cdot v_i \tag{D11}$$

and

$$\tau_i = \tau^x + i \cdot \tau^y \tag{D12}$$

to obtain the reduced set of equations

$$w_{1t} + i f w_1 = \left(\tau_S - \tau_I\right)/\rho_1 h_1 \tag{D13}$$

$$w_{2t} + i f w_2 = \left(\tau_I - \tau_B\right)/\rho_2 h_2 \tag{D14}$$

To close the problem, we must express the stress terms in terms of the layer velocities. Of course, the windstress τ_S is assumed to be given. For simplicity, we will ignore bottom friction and set $\tau_B = 0$; the real physics in this problem lies in the specification of τ_I. Probably the most realistic choice would be to express τ_I as a quadratic function of the velocity difference ($w_1 - w_2$). However, this would destroy the linearity of (D13) - (D14), and we thus adopt the analytically convenient form

$$\tau_I = c\bar{\rho}\left(w_1 - w_2\right) \tag{D15}$$

where c is a drag coefficient with units of speed and $\rho = (\rho_1 + \rho_2)/2$ is the mean density. The problem thus assumes the form:

$$w_{1t} + ifw_1 = \tau_s/\rho_1 h_1 - r_1(w_1 - w_2) \tag{D16}$$

$$w_{2t} + ifw_2 = r_2(w_1 - w_2) \tag{D17}$$

where

$$r_1 = \bar{\rho}c/\rho_1 h_1 \tag{D18}$$

$$r_2 = \bar{\rho}c/\rho_2 h_2 = \frac{\Delta}{1+\delta} r_1 \tag{D19}$$

and $\Delta = h_1/h_2$ is the ratio of layer depths.

These may be solved for w_1 and w_2 separately, but it more instructive to recast the problem in terms of a barotropic mode W^{bt} and a baroclinic mode W^{bc}, which are defined by:

$$W^{bt} = (r_2 w_1 + r_1 w_2)/r \approx (h_1 w_1 + h_2 w_2)/H \tag{D20}$$

and

$$W^{bc} = w_1 - w_2 \tag{D21}$$

Here $H = h_1 + h_2$ is the total water depth, and $r = r_1 + r_2$ is the baroclinic friction constant. Finally then, the model equations become:

$$W^{bt}_t + ifW^{bt} = (r_1/r)\tau/\rho_1 h_1 \tag{D22}$$

$$W^{bc}_t + ifW^{bc} + rW^{bc} = \tau/\rho_1 h_1 \tag{D23}$$

where the subscript s has been dropped from the windstress. Solution is straightforward, and we find:

$$W^{bt} = \frac{r_2}{r\rho_1 h_1}\int_{-\infty}^{t} e^{-if(t-s)}\tau(s)ds \tag{D24}$$

$$W^{bc} = \frac{1}{\rho_1 h_1}\int_{-\infty}^{t} e^{-r(t-s)}e^{-if(t-s)}\tau(s)ds \tag{D25}$$

The solution for each mode is given by a convolution integral of the form

$$W = \int_{-\infty}^{t} h(t-s)\tau(s)ds = h(t) * \tau(t) \tag{D26}$$

The function *h(t)* clearly represents the response to δ-function like forcing, and is consequently called the *impulse response function*. It embodies all the dynamics of the system. Specifically, we have

$$h^{bt} = (r_2/r)(\rho_1 h_1)^{-1} e^{-ift} = (\rho_2 H)^{-1} e^{-ift} + O(\Delta\delta) \tag{D27}$$

$$h^{bc} = (\rho_1 h_1)^{-1} e^{-rt} e^{-ift} \tag{D28}$$

Several features of these solutions are immediately evident. First, the currents depend linearly on the forcing surface wind stress. However, the response depends not only on the present value of the wind but also on its full time history. Since the impulse response function defines the importance of past forcing, it is often referred to as the "system memory". Second, h^{bc} is inversely proportional to the mixed layer depth h_1: the shallower the upper layer, the more intense the baroclinic response. In like manner, the relative magnitude of the barotropic response is inversely proportional to the total water depth H; the ratio of the barotropic to the baroclinic response is this proportional to $h_1/H = \Delta/(1+\Delta)$ which is typically about 10^{-1}. Third, both h^{bt} and h^{bc} oscillate at the inertial frequency, characteristic of inertial currents. In addition, the magnitude of the impulse response for the baroclinic response decays with a time constant

$$T^{bc}_{damp} = 1/r = c^{-1}(\rho_1/\bar{\rho})(h_1 h_2/H) \approx h_1/c \tag{D29}$$

which is inversely proportional to the drag coefficient c and directly proportional to the reduced depth $h_1 h_2/H = h_1/(1+\Delta) \approx h_1$. The damping time decreases with increasing interfacial friction and decreases with a decreasing mixed layer depth. It is typically a few days. By contrast, $|h^{bt}|$ is time invariant because no bottom friction was included in the model. If it had, a form similar to h^{bc} would have been found, but with a smaller friction coefficient.

We are now ready to examine the currents in each layer. Inversion of (D22) - (D23) gives

$$w_1 = W^{bt} + (r_1/r)W^{bc} \approx W^{bt} + (h_2/H)W^{bc} \tag{D30}$$

$$w_2 = W^{bt} - (r_2/r)W^{bc} \approx W^{bt} - (h_1/H)W^{bc} \tag{D31}$$

The corresponding impulse response functions are

$$h_1(t) = (1/\rho_1 h_1)(\Delta + e^{-rt})e^{-ift}/(1+\Delta) \tag{D32}$$

$$h_2(t) = (1/\rho_1 H)(1 - e^{-rt})e^{-ift} \tag{D33}$$

(The time dependence of $h_i(t)$ will always be explicitly expressed to prevent confusion with the layer depths). The real parts of $h_1(t)$ and $h_2(t)$ are plotted in Figure D.2 for the characteristic parameter choices: $\Delta = h_1/h_2 = 10^{-1}$, $\delta = (\rho_2 - \rho_1)/\rho_2 \approx 10^{-3}$, $r = 1/125$ hours^{-1}, and $f = 2\pi/T_I = 2\pi/12.45$ hours^{-1} (appropriate to 74° latitude).

The response ratio is given by

$$h_2(t)/h_1(t) = \Delta\left(\frac{1-e^{-rt}}{\Delta+e^{-rt}}\right). \tag{D34}$$

which clearly shows that the upper layer currents dominate those below. For short times they are roughly a factor of Δ^{-1} larger than their lower layer counterparts. For long times the currents in each layer asymptotically converge, but are weak compared with the initial upper layer response. In particular, we find the ratio of maximum responses is given by

$$\left|h_{2\max}(t)/h_{1\max}(t)\right| = \left|h_2(\infty)/h_1(0)\right| = h_1/H = \Delta/(1+\Delta) \approx 10^{-1} \tag{D35}$$

It is useful to rewrite the general solution (D26) as

$$W(t) = W(t_o) + \int_{t_o}^{t} h(t-s)\tau(s)ds. \tag{D36}$$

The solution at time t depends on the initial state $W(t_o)$ and the windstress following time t_o. If t is large compared with t_o the solution will be essentially independent of the initial state; if however, $(t - t_o)$ is of the same order or smaller than $1/r$, then the initial state will be very important. In particular for small times, the solution becomes

$$W(t_o+\Delta t) \approx W(t_o) + h(t_o)\tau(t_o)\Delta t. \tag{D37}$$

The wind may either enhance or attenuate the existing inertial flow depending on the relative phasing of the wind and current. Maximum inertial response is achieved by winds that rotate clockwise at or near the inertial frequency.

In general, the response is a complicated function of the wind, and although the impulse response functions contain all the system dynamics, they do not readily reveal all features of the response to real wind forcing. For example, it is difficult to evaluate wind systems *a priori* for their efficiency in exciting inertial motions; after all, no real wind systems are truly spike-like. Also, the presence of friction in the system implies a broadening of the response around the inertial frequency and begs the question of whether other types of motion can be generated in addition to purely inertial currents. Finally, we have no way of knowing if certain storm types can preferentially excite one mode or the other.

All these questions can be answered by a simple transformation from the time domain to the frequency domain. First however, a few more definitions and mathematical manipulations are necessary. The Fourier transform (indicated by a tilde) of the basic convolution equation (D26) defines the system response in frequency space

$$\tilde{W}(\omega) = \tilde{H}(\omega)\cdot\tilde{\tau}(\omega). \tag{D38}$$

where the *frequency response function* $H(\omega)$ is defined by

$$\tilde{H}(\omega) = \frac{1}{2\pi}\int_{-\infty}^{\infty} h(t)e^{-i\omega t}dt. \tag{D39}$$

The rather complicated convolution becomes a simple product in frequency space. Now the complex valued function H(ω) may be rewritten in polar form in terms of the purely real gain and phase functions, G(ω) and Φ(ω):

$$\tilde{H}(\omega) = |H(\omega)|e^{-i\Phi(\omega)} = G(\omega)e^{-i\Phi(\omega)} \tag{D40}$$

It is important to appreciate the difference between positive and negative frequencies in this representation. The velocity w in either layer is given by a superposition of frequency components

$$w(t) = \int_{-\infty}^{\infty} \tilde{W}(\omega)e^{i\omega t}d\omega \tag{D41}$$

so that the contribution from the frequency band centred on ω with width Δω is just

$$w_{\omega}(t) = \tilde{W}(\omega)\Delta\omega e^{i\omega_{o}t} = |\tilde{W}(\omega)|\Delta\omega e^{i\omega t}e^{-i\phi_{V}(\omega)}. \tag{D42}$$

If ω is positive (negative), the velocity vector rotates anticlockwise (clockwise) uniformly with time, tracing out a circle of radius $W(\omega)$ Δω every 2π/ω time units. The phase angle defines the current direction at time t = 0. Substitution of (D38) into (D42) gives

$$w_{\omega}(t) = \tilde{H}(\omega)\tilde{\tau}(\omega)\Delta\omega e^{i\omega t} = [G(\omega)|\tau(\omega)|\Delta\omega]e^{-i[\phi_{\tau}(\omega)+\Phi(\omega)]} \tag{D43}$$

where ϕ_τ is the windstress phase (*i.e.*, the direction of the ωth component of the windstress vector at $t = 0$.) Thus the phase function Φ indicates the angle by which the response lags or leads the windstress vector. If ω is positive (negative) a positive value of Φ implies that the response lags (leads) the windstress at frequency ω.

To conclude these introductory remarks, it is easy to show that the power spectrum $S(\omega)$ of the measured response in each layer is given by

$$S(\omega) = G^{2}(\omega)S_{\tau}(\omega) \tag{D44}$$

and is directly proportional to the forcing windstress spectrum. The system cannot respond at any frequency unless it is directly forced at that frequency.

For the two modes we find:

Barotropic Mode

$$\tilde{H}^{bt}(\omega) = \left(1/\rho_{2}H\right)\delta(\omega + f) \tag{D45}$$

$$G^{bt}(\omega)=\left(1/\rho_2 H\right)\delta(\omega+f); \qquad \Phi^{bt}(\omega)=0 \qquad \text{(D46)}$$

$$S^{bt}(\omega)=\left(1/\rho_2 H\right)^2 S_\tau(\omega)\delta(\omega+f) \qquad \text{(D47)}$$

Baroclinic Mode

$$H^{bc}(\omega)=\left(1/\rho_1 h_1\right)[r+i(\omega+f)]^{-1} \qquad \text{(D48)}$$

$$G^{bc}(\omega)=\left(1/\rho_1 h_1\right)\left[r^2+(\omega+f)^2\right]^{-1/2}; \qquad \Phi^{bc}(\omega)=arctan\left(\frac{\omega+f}{r}\right) \qquad \text{(D49)}$$

$$S^{bc}(\omega)=\left(1/\rho_1 h_1\right)^2\left[r^2+(\omega+f)^2\right]^{-1}S_\tau(\omega) \qquad \text{(D50)}$$

The role of friction is clearly revealed in (D48) - (D50). As r decreases, the baroclinic response becomes more highly concentrated around $\omega = -f$ and the system becomes resonant, as it is for the barotropic mode. Note again however, that if bottom friction had been included in the model the barotropic frequency response would also have a finite spread like the baroclinic response.

The baroclinic gain is plotted in Figure D.3 for the parameters of Figure D.1. Superimposed are the estimated Resolute Bay windstress spectrum for 1984 and the product $G_{bc}^2(\omega)\cdot S_\tau(\omega)$ representing the theoretical baroclinic power spectrum. (Note the logarithmic scales). The major conclusion to be drawn is that only those storms with a relatively large proportion of near-inertial variance are effective in forcing inertial currents. The response at lower frequencies is due to the large windstress variance on the synoptic timescale of a few days. To revert to the time domain, a time series plot of inertial current energy would typically reveal a sequence of inertial events modulated by the passage of storms every few days. The intensity of the event would depend directly on the fraction of windstress variance near the inertial frequency.

We note in passing that the ratio of the baroclinic gain at the inertial frequency $\omega=-f$ to its value at $\omega=+f$ is given by

$$G^{bc}(-f)/G^{bc}(+f)\approx r/2f<1\%$$

This expression is useful in deducing whether or not an observed inertial band signal is indeed generated by inertial currents. That is, if inertial band variance is due to leakage from the tidal signal, one would expect a ratio considerably larger.

Finally, we note that no wind system can preferentially excite the barotropic mode and hence the lower layer. Ignoring the δ-functions, the ratio of barotropic to baroclinic spectra at the inertial frequency is

$$S^{bt}(-f)/S^{bc}(-f)=\left(\frac{\rho_1 h_1}{\rho_2 H}\right)^2\frac{T_I}{2\pi T^{bc}_{damp}} \ll \left(h_1/H\right)^2 \ll 1. \qquad \text{(D51)}$$

In summary, the principal conclusions to be drawn from this simple model include: (1) Inertial currents span a range of frequencies near the inertial frequency. (2) The response is primarily trapped in the mixed layer which is preferentially excited in the ratio $(h_1+h2)/h_1$. (3) Upper layer currents tend to achieve maximum values quickly and then decay slowly over a period of a few days. (4) Lower layer currents grow more slowly but never reach values more than about 10% of those observed in the upper layer. (5) The precise response depends in a complicated manner on the wind history over a several day period as the wind may either enhance or attenuate inertial motions depending on the phasing of winds and currents. (6) Specifically, storms characterized by winds that vary rapidly in speed or direction are most effective in generating inertial currents; more precisely, it is the degree of windstress variance at near-inertial frequencies that governs a storm's potential for inertial current generation.

APPENDIX E STATION LOCATIONS

TABLE E.1 TIDAL ELEVATION STATIONS

STATION	LOCATION	LAT	LONG	START	END
BST	BORDEN STATION	73 44.0	82 0.0	15/11/84	17/ 5/85
DUNH	DUNDAS HARBOUR	74 31.0	82 25.0	22/ 8/78	12/ 5/79
5865	ARCTIC BAY	73 2.0	85 10.0	1/ 2/77	1/ 3/77
5970	CROWN PRINCE FREDERICK	70 2.0	86 50.0	1/ 5/76	27/ 5/76
65908	PEAK VALLEY, BAFFIN ISLAND	73 42.0	87 52.0	18/ 3/83	1/ 5/83
66605	HYPERITE POINT	78 8.0	88 53.0	4/ 3/81	19/ 4/81
5530	MAXWELL BAY	74 41.0	88 54.0	1/ 9/73	1/10/73
66595	WEST BJORNE PENINSULA	77 42.0	88 57.0	18/ 1/81	12/ 6/81
66580	BAY OF WOE, JONES SOUND	76 25.0	89 1.0	4/ 3/81	19/ 4/81
65912	PORT BOWEN, BAFFIN ISLAND	73 17.0	89 3.0	18/ 3/83	1/ 5/83
65975	CAPE CHAPMAN	69 18.0	89 15.0	9/ 3/84	19/ 4/84
66584	LANDS END, ELLSMERE I.	76 54.0	89 25.0	4/ 3/81	19/ 4/81
65950	EASTER CAPE	70 55.0	89 27.0	8/ 3/84	19/ 4/84
5920	MCBEAN ISLAND	72 38.0	89 38.0	19/ 4/79	11/ 6/79
65935	CAPE KATER	71 58.0	90 4.0	8/ 3/84	19/ 4/84
65906	WHALER PT., SOMERSET I.	73 49.0	90 18.0	18/ 3/83	1/ 5/83
5905	PORT LEOPOLD	73 50.0	90 20.0	1/ 1/77	29/ 1/77
65960	MARTIN ISLANDS	70 19.0	91 40.0	9/ 3/84	19/ 4/84
65918	FURY PT., SOMERSET ISLAND	72 54.0	91 48.0	15/ 3/83	27/ 4/83
66598	CAPE SOUTHWEST	78 13.0	91 50.0	4/ 3/81	19/ 4/81
5510	BEECHY I.	74 43.0	91 54.0	1/ 1/77	1/ 1/77
66755	GRIFFIN INLET, DEVON I.	75 7.0	92 10.0	4/ 3/79	20/ 4/79
65940	CAPE AUGHERSTON	71 29.0	93 17.0	9/ 3/84	20/ 4/84
WEL	WELLINGTON CHANNEL (WEST)	75 12.6	93 29.6	6/ 4/84	7/ 6/84
6150	SPENCE BAY	69 32.2	93 31.3	15/ 8/79	15/ 8/80
40604	GIFFORD POINT, SOMERSET I.	74 10.0	93 37.0	1/ 4/82	9/ 5/82
46	BARROW STRAIT	74 13.0	93 46.0	1/ 4/83	28/ 4/83
5910	CUNNINGHAM INLET	74 8.0	93 53.0	1/ 8/76	7/ 9/76
44	BARROW STRAIT	74 24.0	93 54.0	1/ 4/83	27/ 4/83
66588	BERE BAY, BELCHER CHAN.	76 57.0	94 10.0	5/ 3/81	20/ 4/81
41503	ASSISTANCE BAY	74 37.0	94 14.0	1/ 4/81	31/ 3/82
65917	BELLOT STRAIT, EAST END	72 1.0	94 20.0	20/ 3/83	29/ 4/83
42	SOUTH CORNWALLIS ISLAND	74 34.2	94 31.2	20/ 5/84	21/ 6/84
42	SOUTH CORNWALLIS ISLAND	74 34.2	94 31.2	13/ 6/84	14/ 7/84
42	SOUTH CORNWALLIS ISLAND	74 34.2	94 31.2	7/ 7/84	7/ 8/84
42	SOUTH CORNWALLIS ISLAND	74 34.2	94 31.2	30/ 7/84	31/ 8/84
42	SOUTH CORNWALLIS ISLAND	74 34.2	94 31.2	23/ 8/84	24/ 9/84
42	SOUTH CORNWALLIS ISLAND	74 34.2	94 31.2	16/ 9/84	17/10/84
42	SOUTH CORNWALLIS ISLAND	74 34.2	94 31.2	10/10/84	10/11/84

TABLE E.1 TIDAL ELEVATION STATIONS (cont.)

STATION	LOCATION	LAT	LONG	START	END
42	SOUTH CORNWALLIS ISLAND	74 34.2	94 31.2	2/11/84	4/12/84
42	SOUTH CORNWALLIS ISLAND	74 34.2	94 31.2	26/11/84	28/12/84
42	SOUTH CORNWALLIS ISLAND	74 34.2	94 31.2	20/12/84	20/ 1/85
42	SOUTH CORNWALLIS ISLAND	74 34.2	94 31.2	13/ 1/85	13/ 2/85
42	SOUTH CORNWALLIS ISLAND	74 34.2	94 31.2	5/ 2/85	9/ 3/85
42	SOUTH CORNWALLIS ISLAND	74 34.2	94 31.2	1/ 3/85	2/ 4/85
42	SOUTH CORNWALLIS ISLAND	74 34.2	94 31.2	26/ 4/84	28/ 5/84
66760	STUART BAY	75 38.0	94 35.0	24/ 3/80	26/ 4/80
5560	RESOLUTE	74 41.0	94 54.0	1/ 2/75	31/ 1/76
66102	BELLOT STRAIT, WEST END	71 58.0	95 8.0	20/ 3/83	29/ 4/83
6090	OTRICK ISLAND	72 36.0	95 33.0	15/ 4/79	15/ 6/79
6080	WADSWORTH I.	73 26.0	95 41.0	15/ 4/79	15/ 6/79
41502	CAPE GRANITE	73 42.0	95 45.0	1/ 4/81	8/ 5/81
6110	TASMANIA ISLAND	71 12.0	96 25.0	1/ 5/79	21/ 6/79
66781	NORAH ISLAND	77 1.0	96 37.0	8/ 3/79	20/ 4/79
6757	LITTLE CORNWALLIS I.	75 21.0	96 48.0	1/ 9/73	27/ 9/73
PELB	PELHAM BAY	76 45.0	96 54.0	16/ 3/76	22/ 4/76
30601	CAPE BRIGGS	73 38.0	96 54.0	1/ 4/81	14/ 5/81
FSRG	JOHN BARROW ISLAND	76 39.7	96 54.6	16/ 5/84	17/ 6/84
FSRG	JOHN BARROW ISLAND	76 39.7	96 54.6	3/ 7/84	3/ 8/84
FSRG	JOHN BARROW ISLAND	76 39.7	96 54.6	26/ 7/84	27/ 8/84
FSRG	JOHN BARROW ISLAND	76 39.7	96 54.6	19/ 8/84	20/ 9/84
FSRG	JOHN BARROW ISLAND	76 39.7	96 54.6	12/ 9/84	13/10/84
FSRG	JOHN BARROW ISLAND	76 39.7	96 54.6	6/10/84	6/11/84
FSRG	JOHN BARROW ISLAND	76 39.7	96 54.6	29/10/84	30/11/84
FSRG	JOHN BARROW ISLAND	76 39.7	96 54.6	22/11/84	24/12/84
FSRG	JOHN BARROW ISLAND	76 39.7	96 54.6	16/12/84	16/ 1/85
FSRG	JOHN BARROW ISLAND	76 39.7	96 54.6	9/ 1/85	9/ 2/85
FSRG	JOHN BARROW ISLAND	76 39.7	96 54.6	1/ 2/85	5/ 3/85
FSRG	JOHN BARROW ISLAND	76 39.7	96 54.6	25/ 2/85	29/ 3/85
FSRG	JOHN BARROW ISLAND	76 39.7	96 54.6	22/ 4/84	24/ 5/84
66770	HYDE PARKER ISLAND	76 29.0	97 6.0	1/ 3/79	13/ 4/79
McD	McDOUGALL SOUND (W)	75 30.8	97 12.8	25/ 3/77	15/ 6/77
65590	LOWTHER ISLAND	74 39.0	97 25.0	22/ 3/81	8/ 5/81
6765	AIRSTRIP POINT	76 5.0	97 44.0	1/ 7/62	29/ 7/62
6210	GLADMAN POINT	68 39.3	97 44.4	15/ 8/79	11/ 8/80
66140	CAPE FELIX	69 56.0	97 58.0	19/ 3/80	22/ 4/80
5600	CAPE CAPEL	75 2.0	98 2.2	1/ 8/71	31/ 8/71
40803	ALLISON BAY	74 58.0	99 22.0	23/ 3/81	8/ 5/81
66130	THACKERAY POINT	71 40.0	99 42.0	23/ 3/80	23/ 4/80
366	BATHURST ISLAND (CAPE COCKBURN)	74 57.1	100 26.9	6/ 4/83	23/ 4/83
66138	JOHN HALKETT ISLAND	70 1.0	100 48.0	19/ 3/80	22/ 4/80
66785	SEYMOUR ISLAND	76 48.0	101 14.0	3/ 3/79	14/ 4/79
66124	MINTO HEAD	73 6.0	102 15.0	17/ 3/80	23/ 4/80

TABLE E.1 TIDAL ELEVATION STATIONS (cont.)

STATION	LOCATION	LAT	LONG	START	END
66789	MASSEY ISLAND	76 4.0	102 17.0	14/ 3/85	23/ 4/85
66786	CAMERON ISLAND	76 25.0	103 0.0	15/ 3/85	24/ 4/85
66791	ALEXANDER ISLAND	75 45.0	103 17.0	15/ 3/85	24/ 4/85
66787	CAMERON ISLAND	76 19.0	104 2.0	15/ 3/85	24/ 4/85
66833	BYAM ISLAND	75 1.0	104 13.0	1/ 3/77	2/ 4/77
66128	CAPE STANG	71 29.0	104 16.0	17/ 3/80	22/ 4/80
80	CAPE ALDRIDGE	76 5.5	104 25.5	2/ 4/83	22/ 5/83
66120	STEPHANSSON I. EAST	73 23.0	104 28.0	17/ 3/80	23/ 4/80
66788	CAMERON ISLAND	76 30.0	104 35.0	15/ 3/85	24/ 4/85
66793	LOUGHEED ISLAND	77 27.0	104 53.0	3/ 3/79	23/ 4/79
6240	CAMBRIDGE BAY	69 6.7	105 3.7	4/ 8/79	8/ 8/80
BM_W	BYAM MARTIN CHANNEL (WEST)	75 54.9	105 36.2	11/ 4/84	11/ 6/84
6835	RAE POINT	75 22.0	105 42.0	1/ 9/75	30/ 8/76
6834	BYAM CHANNEL	75 8.0	105 50.0	1/ 7/73	7/ 8/73
12	STEFANSSON ISLAND	73 44.6	106 20.8	18/ 4/82	18/ 6/82
11	VISCOUNT MELVILLE, ROSS POINT	74 56.5	107 29.0	17/ 4/82	8/ 6/82
366	BRIDPORT INLET	75 3.8	108 45.8	17/ 3/79	2/ 7/79
301	BRIDPORT INLET	75 0.0	108 54.0	21/ 8/78	25/10/78
66795	VESSEY HAMILTON ISLAND	76 53.0	109 0.0	6/ 3/79	23/ 4/79
CBTY	CAPE BOUNTY	74 51.0	109 32.0	9/ 3/77	16/ 4/77
66797	MACKENZIE KING ISLAND	77 29.0	110 14.0	2/ 3/79	23/ 4/79
65643	NATKUSIAK PENINSULA	73 1.0	110 28.0	1/ 3/77	31/ 3/77
5645	WINTER HARBOUR	74 47.0	110 48.0	1/ 1/77	31/ 1/77
08	M'CLURE STRAIT, C.DUNDAS	74 28.2	113 46.0	7/ 3/82	19/ 6/82
6290	COPPERMINE	67 49.0	115 5.0	1/ 1/73	1/10/73
PPNT	PEEL POINT	73 16.0	115 11.0	20/ 4/77	11/ 5/77
09	M'CLURE STRAIT, NW PARKER PT.	73 51.8	116 15.0	5/ 3/82	19/ 6/82
87	VICTORIA ISLAND	73 5.0	116 22.5	12/ 5/82	13/ 6/82
87	VICTORIA ISLAND	73 5.0	116 22.5	13/ 6/82	15/ 7/82
87	VICTORIA ISLAND	73 5.0	116 22.5	15/ 7/82	16/ 8/82
87	VICTORIA ISLAND	73 5.0	116 22.5	16/ 8/82	16/ 9/82
87	VICTORIA ISLAND	73 5.0	116 22.5	17/ 9/82	18/10/82
87	VICTORIA ISLAND	73 5.0	116 22.5	18/10/82	19/11/82
87	VICTORIA ISLAND	73 5.0	116 22.5	19/11/82	21/12/82
87	VICTORIA ISLAND	73 5.0	116 22.5	21/12/82	22/ 1/83
87	VICTORIA ISLAND	73 5.0	116 22.5	22/ 1/83	23/ 2/83
87	VICTORIA ISLAND	73 5.0	116 22.5	23/ 2/83	26/ 3/83
87	VICTORIA ISLAND	73 5.0	116 22.5	26/ 3/83	27/ 4/83
87	VICTORIA ISLAND	73 5.0	116 22.5	10/ 4/82	12/ 5/82
87	VICTORIA ISLAND	73 5.0	116 22.5	10/ 4/82	12/ 5/82

TABLE E.1 TIDAL ELEVATION STATIONS (cont.)

STATION	LOCATION	LAT	LONG	START	END
89	BANKS ISLAND	73 15.1	116 28.0	11/ 4/82	12/ 5/82
89	BANKS ISLAND	73 15.1	116 28.0	12/ 5/82	13/ 6/82
89	BANKS ISLAND	73 15.1	116 28.0	13/ 6/82	15/ 7/82
89	BANKS ISLAND	73 15.1	116 28.0	15/ 7/82	16/ 8/82
89	BANKS ISLAND	73 15.1	116 28.0	16/ 8/82	17/ 9/82
89	BANKS ISLAND	73 15.1	116 28.0	17/ 9/82	19/10/82
89	BANKS ISLAND	73 15.1	116 28.0	19/10/82	19/11/82
89	BANKS ISLAND	73 15.1	116 28.0	19/11/82	21/12/82
89	BANKS ISLAND	73 15.1	116 28.0	21/12/82	22/ 1/83
89	BANKS ISLAND	73 15.1	116 28.0	22/ 1/83	23/ 2/83
89	BANKS ISLAND	73 15.1	116 28.0	23/ 2/83	27/ 3/83
89	BANKS ISLAND	73 15.1	116 28.0	27/ 3/83	28/ 4/83
89	BANKS ISLAND	73 15.1	116 28.0	3/ 4/83	5/ 5/83
93	BANKS ISLAND	73 15.1	116 28.0	11/ 4/82	12/ 5/82
93	BANKS ISLAND	73 15.1	116 28.0	12/ 5/82	13/ 6/82
93	BANKS ISLAND	73 15.1	116 28.0	13/ 6/82	15/ 7/82
93	BANKS ISLAND	73 15.1	116 28.0	15/ 7/82	16/ 8/82
93	BANKS ISLAND	73 15.1	116 28.0	16/ 8/82	17/ 9/82
93	BANKS ISLAND	73 15.1	116 28.0	17/ 9/82	19/10/82
93	BANKS ISLAND	73 15.1	116 28.0	19/10/82	19/11/82
93	BANKS ISLAND	73 15.1	116 28.0	19/11/82	21/12/82
93	BANKS ISLAND	73 15.1	116 28.0	21/12/82	22/ 1/83
93	BANKS ISLAND	73 15.1	116 28.0	22/ 1/83	23/ 2/83
93	BANKS ISLAND	73 15.1	116 28.0	23/ 2/83	27/ 3/83
93	BANKS ISLAND	73 15.1	116 28.0	27/ 3/83	28/ 4/83
6395	WALKER BAY, VICTORIA I.	71 37.0	117 52.0	30/ 3/82	0/ 5/82
66359	VICTORIA I. , WEST SIDE	72 41.0	118 0.0	5/ 3/82	16/ 4/82
66405	JOHNSON PT., BANKS I.	72 45.0	118 27.0	5/ 3/82	16/ 4/82
20101	JOHNSON PT, BANKS I.	72 45.0	118 27.0	1/ 3/82	10/ 4/82
6955	MOULD BAY	76 17.0	119 28.0	1/ 6/83	29/ 5/84

TABLE E.1 TIDAL ELEVATION STATIONS (cont.)

STATION	LOCATION	LAT	LONG	START	END
92	JESSE HARBOUR	72 14.1	120 12.8	9/ 4/82	11/ 5/82
92	JESSE HARBOUR	72 14.1	120 12.8	11/ 5/82	12/ 6/82
92	JESSE HARBOUR	72 14.1	120 12.8	12/ 6/82	14/ 7/82
92	JESSE HARBOUR	72 14.1	120 12.8	14/ 7/82	15/ 8/82
92	JESSE HARBOUR	72 14.1	120 12.8	15/ 8/82	15/ 9/82
92	JESSE HARBOUR	72 14.1	120 12.8	15/ 9/82	17/10/82
92	JESSE HARBOUR	72 14.1	120 12.8	17/10/82	18/11/82
92	JESSE HARBOUR	72 14.1	120 12.8	18/11/82	20/12/82
92	JESSE HARBOUR	72 14.1	120 12.8	20/12/82	21/ 1/83
92	JESSE HARBOUR	72 14.1	120 12.8	21/ 1/83	22/ 2/83
92	JESSE HARBOUR	72 14.1	120 12.8	22/ 2/83	25/ 3/83
92	JESSE HARBOUR	72 14.1	120 12.8	25/ 3/83	26/ 4/83
6410	DE SALIS BAY, BANKS I.	71 26.0	121 32.0	29/ 3/82	0/ 5/82
6360	CAPE PARRY	70 9.0	124 40.5	5/ 3/83	6/ 8/84
6424	SACHS HARBOUR	71 58.0	125 15.0	1/12/82	4/ 8/83
6485	TUKTOYAKTUK	69 27.2	133 0.0	21/10/83	21/ 7/84

TABLE E.2 CURRENT METER LOCATIONS

STATION	METER	LOCATION	WATER DEPTH	METER DEPTH	LAT	LONG	START	END
01-L	01-L	LANCASTER SOUND	772	39	74 5.5	81 10.0	29/ 7/77	25/ 9/77
01-L	01-L	LANCASTER SOUND	772	203	74 5.5	81 10.0	29/ 7/77	29/ 9/77
03-L	03-L	LANCASTER SOUND	741	51	74 7.4	82 13.0	29/ 7/77	29/ 9/77
03-L	03-L	LANCASTER SOUND	741	216	74 7.4	82 13.0	29/ 7/77	29/ 9/77
04-L	04-L	LANCASTER SOUND	724	549	73 51.0	82 13.0	29/ 7/77	29/ 9/77
PRB	PRB	PRINCE REGENT INLET	200	10	73 14.0	89 5.0	18/ 3/83	1/ 5/83
PRC	PRC	PRINCE REGENT INLET	200	10	73 49.0	90 17.5	18/ 3/83	1/ 5/83
PRA	PRA	PRINCE REGENT INLET	200	10	72 53.5	91 44.0	15/ 3/83	2/ 5/83
08	3223-WE	WELLINGTON CHANNEL	110	18	74 48.0	92 9.0	13/ 5/84	9/ 6/84
08	3223-WE	WELLINGTON CHANNEL SOUTH	110	18	74 48.0	92 9.0	19/ 4/84	21/ 5/84
09	1305	WELLINGTON CHANNEL SOUTH	110	18	74 48.0	92 13.0	19/ 4/84	4/ 5/84
10	1932-WE	WELLINGTON CHANNEL SOUTH	110	18	74 48.0	92 22.0	19/ 4/84	19/ 5/84
11	1939-WE	WELLINGTON CHANNEL SOUTH	110	18	74 48.0	92 28.0	13/ 5/84	1/ 6/84
11	1939-WE	WELLINGTON CHANNEL SOUTH	110	18	74 48.0	92 28.0	19/ 4/84	21/ 5/84
01-WE	801	WELLINGTON CHANNEL NORTH	133	18	75 13.0	92 32.0	1/ 5/84	7/ 6/84
01-WE	801	WELLINGTON CHANNEL NORTH	133	18	75 13.0	92 32.0	7/ 4/84	9/ 5/84
03	1930-WE	WELLINGTON CHANNEL NORTH	133	18	75 14.0	92 35.0	1/ 5/84	7/ 6/84
03	1930-WE	WELLINGTON CHANNEL NORTH	133	18	75 14.0	92 35.0	7/ 4/84	9/ 5/84
4W12	4W12	WELLINGTON CHANNEL	188	12	75 16.3	92 37.2	6/ 4/78	8/ 7/78
04	1931-WE	WELLINGTON CHANNEL NORTH	133	18	75 14.0	92 40.0	1/ 5/84	7/ 6/84
04	1931-WE	WELLINGTON CHANNEL NORTH	133	18	75 14.0	92 40.0	8/ 4/84	9/ 5/84
05	2687	WELLINGTON CHANNEL	133	18	75 14.0	92 44.0	1/ 5/84	7/ 6/84
05	2687	WELLINGTON CHANNEL	133	18	75 14.0	92 44.0	8/ 4/84	9/ 5/84
13	218	WELLINGTON CHANNEL SOUTH	110	18	74 48.0	92 48.0	1/ 5/84	1/ 6/84
13	218	WELLINGTON CHANNEL SOUTH	110	18	74 48.0	92 48.0	24/ 5/84	9/ 6/84
3W20	3W20	WELLINGTON CHANNEL	160	12	75 15.8	92 51.0	4/ 4/78	9/ 7/78
3W99	3W99	WELLINGTON CHANNEL	160	100	75 15.8	92 51.0	3/ 4/78	8/ 7/78
06	2686	WELLINGTON CHANNEL	133	18	75 14.0	93 0.0	13/ 5/84	9/ 6/84
06	2686	WELLINGTON CHANNEL	133	18	75 14.0	93 0.0	19/ 4/84	21/ 5/84
2W99	2W99	WELLINGTON CHANNEL	133	100	75 15.9	93 0.5	19/ 4/78	7/ 7/78
2W12	2W12	WELLINGTON CHANNEL	146	12	75 19.9	93 0.5	20/ 4/78	10/ 7/78
1W12	1W12	WELLINGTON CHANNEL	232	12	75 15.5	93 17.5	25/ 4/78	9/ 7/78
12	217	WELLINGTON CHANNEL SOUTH	110	18	74 48.0	93 18.0	1/ 5/84	1/ 6/84
12	217	WELLINGTON CHANNEL SOUTH	110	18	74 48.0	93 18.0	24/ 5/84	9/ 6/84
14	2695	WELLINGTON CHANNEL	110	18	74 48.0	93 18.0	13/ 5/84	9/ 6/84
14	2695	WELLINGTON CHANNEL	110	18	74 48.0	93 18.0	19/ 4/84	21/ 5/84
07	3228	WELLINGTON CHANNEL	133	18	75 15.0	93 23.0	13/ 5/84	9/ 6/84
07	3228	WELLINGTON CHANNEL	133	18	75 15.0	93 23.0	19/ 4/84	21/ 5/84
47	47	BARROW STRAIT	55	10	74 11.3	93 33.9	20/ 3/82	14/ 4/82

TABLE E.2 CURRENT METER LOCATIONS (cont.)

STATION	METER	LOCATION	WATER DEPTH	METER DEPTH	LAT	LONG	START	END
46B	46B	BARROW STRAIT	170	25	74 13.3	93 38.3	15/ 4/81	31/ 5/81
46B	46B	BARROW STRAIT	170	25	74 13.3	93 38.3	15/ 5/81	30/ 6/81
46B	46B	BARROW STRAIT	170	25	74 13.3	93 38.3	15/ 6/81	31/ 7/81
46B	46B	BARROW STRAIT	170	25	74 13.3	93 38.3	15/ 7/81	31/ 8/81
46B	46B	BARROW STRAIT	170	25	74 13.3	93 38.3	15/ 9/81	31/10/81
46B	46B	BARROW STRAIT	170	25	74 13.3	93 38.3	15/10/81	30/10/81
46B	46B	BARROW STRAIT	170	25	74 13.3	93 38.3	15/11/81	29/12/81
46B	46B	BARROW STRAIT	170	60	74 13.3	93 38.3	15/ 4/81	31/ 5/81
46B	46B	BARROW STRAIT	170	60	74 13.3	93 38.3	15/ 5/81	30/ 6/81
46B	46B	BARROW STRAIT	170	60	74 13.3	93 38.3	15/ 6/81	31/ 7/81
46B	46B	BARROW STRAIT	170	60	74 13.3	93 38.3	15/ 7/81	31/ 8/81
46B	46B	BARROW STRAIT	170	60	74 13.3	93 38.3	15/ 8/81	30/ 9/81
46B	46B	BARROW STRAIT	170	60	74 13.3	93 38.3	15/ 9/81	31/10/81
46B	46B	BARROW STRAIT	170	60	74 13.3	93 38.3	15/10/81	30/11/81
46B	46B	BARROW STRAIT	170	60	74 13.3	93 38.3	15/11/81	29/12/81
46B	46B	BARROW STRAIT	170	150	74 13.3	93 38.3	15/ 4/81	31/ 5/81
46B	46B	BARROW STRAIT	170	150	74 13.3	93 38.3	15/ 5/81	30/ 6/81
46B	46B	BARROW STRAIT	170	150	74 13.3	93 38.3	15/ 6/81	31/ 7/81
46B	46B	BARROW STRAIT	170	150	74 13.3	93 38.3	15/ 8/81	30/ 9/81
46B	46B	BARROW STRAIT	170	150	74 13.3	93 38.3	15/ 9/81	31/10/81
46B	46B	BARROW STRAIT	170	150	74 13.3	93 38.3	15/10/81	30/11/81
46B	46B	BARROW STRAIT	170	150	74 13.3	93 38.3	15/11/81	29/12/81
46B	46B	BARROW STRAIT	170	150	74 13.3	93 38.3	17/ 7/81	31/ 8/81
46	46	BARROW STRAIT	170	10	74 13.4	93 41.2	19/ 3/82	19/ 4/82
46	46	BARROW STRAIT	170	50	74 13.4	93 41.2	20/ 3/82	19/ 4/82
46	46	BARROW STRAIT	170	150	74 13.4	93 41.2	20/ 3/82	19/ 4/82
47	47	BARROW STRAIT	55	10	74 11.3	93 43.0	29/ 3/83	27/ 4/83
46A	46A	BARROW STRAIT	170	10	74 13.1	93 45.5	29/ 3/83	27/ 4/83
46A	46A	BARROW STRAIT	170	40	74 13.1	93 45.5	25/ 3/83	31/ 3/83
46A	46A	BARROW STRAIT	170	60	74 13.1	93 45.5	25/ 3/83	3/ 4/83
46A	46A	BARROW STRAIT	170	80	74 13.1	93 45.5	25/ 3/83	23/ 4/83
46A	46A	BARROW STRAIT	170	150	74 13.1	93 45.5	25/ 3/83	23/ 4/83
46	1936-BS	BARROW STRAIT SOUTH	170	18	74 13.0	93 47.0	19/ 5/84	8/ 6/84
46	1936-BS	BARROW STRAIT SOUTH	170	18	74 13.0	93 47.0	25/ 4/84	27/ 5/84
44-BSE	44-BSE	BARROW STRAIT	162	10	74 24.1	93 54.1	29/ 3/83	27/ 4/83
44-BSW	44-BSW	BARROW STRAIT	162	10	74 24.1	93 54.7	20/ 3/82	20/ 4/82
44-BSW	44-BSW	BARROW STRAIT	162	50	74 24.1	93 54.7	23/ 3/82	20/ 4/82
44-BSW	44-BSW	BARROW STRAIT	162	142	74 24.1	93 54.7	23/ 3/82	20/ 4/82
42	138	BARROW STRAIT	129	18	74 34.0	94 1.1	20/ 5/84	8/ 6/84
42	1386	BARROW STRAIT	129	18	74 34.0	94 1.1	27/ 4/84	28/ 5/84

TABLE E.2 CURRENT METER LOCATIONS (cont.)

STATION	METER	LOCATION	WATER DEPTH	METER DEPTH	LAT	LONG	START	END
42	1935	BARROW STRAIT	129	100	74 34.0	94 1.1	2/11/84	4/12/84
42	1935	BARROW STRAIT	139	100	74 34.0	94 1.1	7/ 7/84	7/ 8/84
42	1935	BARROW STRAIT	139	100	74 34.0	94 1.1	10/10/84	10/11/84
42	1935	BARROW STRAIT	139	100	74 34.0	94 1.1	13/ 6/84	14/ 7/84
42	1935	BARROW STRAIT	139	100	74 34.0	94 1.1	16/ 9/84	17/10/84
42	1935	BARROW STRAIT	139	100	74 34.0	94 1.1	20/ 5/84	21/ 6/84
42	1935	BARROW STRAIT	139	100	74 34.0	94 1.1	20/12/84	20/ 1/85
42	1935	BARROW STRAIT	139	100	74 34.0	94 1.1	23/ 8/84	24/ 9/84
42	1935	BARROW STRAIT	129	100	74 34.0	94 1.1	26/ 4/84	28/ 5/84
42	1935	BARROW STRAIT	139	100	74 34.0	94 1.1	26/11/84	28/12/84
42	1935	BARROW STRAIT	139	100	74 34.0	94 1.1	30/ 7/84	31/ 8/84
42	3388-BS	BARROW STRAIT	129	51	74 34.0	94 1.1	1/ 3/85	2/ 4/85
42	3388-BS	BARROW STRAIT	129	51	74 34.0	94 1.1	2/11/84	4/12/84
42	3388-BS	BARROW STRAIT	129	51	74 34.0	94 1.1	5/ 2/85	9/ 3/85
42	3388-BS	BARROW STRAIT	129	51	74 34.0	94 1.1	7/ 7/84	7/ 8/84
42	3388-BS	BARROW STRAIT	129	51	74 34.0	94 1.1	10/10/84	10/11/84
42	3388-BS	BARROW STRAIT	129	51	74 34.0	94 1.1	13/ 1/85	13/ 2/85
42	3388-BS	BARROW STRAIT	129	51	74 34.0	94 1.1	13/ 6/84	14/ 7/84
42	3388-BS	BARROW STRAIT	129	51	74 34.0	94 1.1	16/ 9/84	17/10/84
42	3388-BS	BARROW STRAIT	129	51	74 34.0	94 1.1	20/ 5/84	21/ 6/84
42	3388-	BARROW STRAIT	129	51	74 34.0	94 1.1	20/12/84	20/ 1/85
42	3388-	BARROW STRAIT	129	51	74 34.0	94 1.1	23/ 8/84	24/ 9/84
42	3388-	BARROW STRAIT	129	51	74 34.0	94 1.1	25/ 3/85	12/ 4/85
42	3388-BS	BARROW STRAIT	129	51	74 34.0	94 1.1	26/ 4/84	28/ 5/84
42	3388-BS	BARROW STRAIT	129	51	74 34.0	94 1.1	26/11/84	28/12/84
42	3388-BS	BARROW STRAIT	129	51	74 34.0	94 1.1	30/ 7/84	31/ 8/84
42A	42A	BARROW STRAIT	139	10	74 34.0	94 1.1	29/ 3/83	27/ 4/83
42A	42A	BARROW STRAIT	139	120	74 34.0	94 1.1	28/ 3/83	25/ 4/83
42A	42A	BARROW STRAIT	139	40	74 34.0	94 1.1	28/ 3/83	25/ 4/83
42A	42A	BARROW STRAIT	139	60	74 34.0	94 1.1	28/ 3/83	25/ 4/83
42A	42A	BARROW STRAIT	139	80	74 34.0	94 1.1	28/ 3/83	25/ 4/83
42B	42	BARROW STRAIT	139	10	74 34.0	94 1.1	19/ 3/82	22/ 4/82
42B	42	BARROW STRAIT	139	50	74 34.0	94 1.1	24/ 3/82	22/ 4/82
42B	42	BARROW STRAIT	139	115	74 34.0	94 1.1	24/ 3/82	22/ 4/82
41-10	41-10	BARROW STRAIT	98	10	74 36.2	94 2.8	29/ 3/83	27/ 4/83
41	41	BARROW STRAIT	98	10	74 36.2	94 2.8	19/ 3/82	22/ 4/82
05-D	3278-DI	DUNDAS ISLAND	200	2	76 9.0	94 54.0	12/ 3/80	31/ 3/80
01-D	3395-DI	DUNDAS ISLAND	200	12	76 10.0	94 55.0	8/ 3/80	10/ 4/80
02-D	3388-DI	DUNDAS ISLAND	200	12	76 11.0	94 58.0	8/ 3/80	10/ 4/80
03-D	3386	DUNDAS ISLAND	200	12	76 12.0	95 0.0	8/ 3/80	10/ 4/80

TABLE E.2 CURRENT METER LOCATIONS (cont.)

STATION	METER	LOCATION	WATER DEPTH	METER DEPTH	LAT	LONG	START	END
04-D	3385	DUNDAS ISLAND	200	12	76 11.0	95 33.0	9/ 3/80	10/ 4/80
85	85	PEEL SOUND	200	10	73 41.6	95 48.2	29/ 3/81	27/ 4/81
84	84	PEEL SOUND	200	10	73 41.6	96 0.0	23/ 3/81	24/ 4/81
84	84	PEEL SOUND	200	50	73 41.6	96 0.0	23/ 3/81	24/ 4/81
84	84	PEEL SOUND	200	100	73 41.6	96 0.0	23/ 3/81	24/ 4/81
84	84	PEEL SOUND	200	225	73 41.6	96 0.0	23/ 3/81	24/ 4/81
83	83	PEEL SOUND	230	10	73 41.6	96 18.5	29/ 3/81	27/ 4/81
82	82	PEEL SOUND	230	10	73 41.6	96 37.0	28/ 3/81	26/ 4/81
82	82	PEEL SOUND	230	50	73 41.6	96 37.0	28/ 3/81	26/ 4/81
82	82	PEEL SOUND	230	100	73 41.6	96 37.0	28/ 3/81	26/ 4/81
82	82	PEEL SOUND	230	200	73 41.6	96 37.0	28/ 3/81	26/ 4/81
828	828	BARROW STRAIT	210	4	74 40.3	96 43.8	10/ 3/78	12/ 4/78
828	828	BARROW STRAIT	210	50	74 40.3	96 43.8	10/ 3/78	2/ 4/78
81	81	PEEL SOUND	200	10	73 41.6	96 49.0	29/ 3/81	27/ 4/81
PSE-S	5361-PS	PENNY STRAIT	186	43	76 38.0	96 54.0	1/ 2/85	5/ 3/85
PSE-S	5361-PS	PENNY STRAIT	186	43	76 38.0	96 54.0	3/ 7/84	3/ 8/84
PSE-S	5361-PS	PENNY STRAIT	186	43	76 38.0	96 54.0	6/10/84	6/11/84
PSE-S	5361-PS	PENNY STRAIT	186	43	76 38.0	96 54.0	9/ 1/85	9/ 2/85
PSE-S	5361-PS	PENNY STRAIT	186	43	76 38.0	96 54.0	9/ 6/84	11/ 7/84
PSE-S	5361-PS	PENNY STRAIT	186	43	76 38.0	96 54.0	12/ 9/84	14/10/84
PSE-S	5361-PS	PENNY STRAIT	186	43	76 38.0	96 54.0	16/ 5/84	17/ 6/84
PSE-S	5361-PS	PENNY STRAIT	186	43	76 38.0	96 54.0	16/12/84	17/ 1/85
PSE-S	5361-PS	PENNY STRAIT	186	43	76 38.0	96 54.0	19/ 8/84	20/ 9/84
PSE-S	5361-PS	PENNY STRAIT	186	43	76 38.0	96 54.0	21/ 3/85	16/ 4/85
PSE-S	5361-PS	PENNY STRAIT	186	43	76 38.0	96 54.0	22/11/84	24/12/84
PSE-S	5361-PS	PENNY STRAIT	186	43	76 38.0	96 54.0	23/ 4/84	24/ 5/84
PSE-S	5361-PS	PENNY STRAIT	186	43	76 38.0	96 54.0	25/ 2/85	29/ 3/85
PSE-S	5361-PS	PENNY STRAIT	186	43	76 38.0	96 54.0	26/ 7/84	27/ 8/84
PSE-S	5361-PS	PENNY STRAIT	186	43	76 38.0	96 54.0	29/10/84	30/11/84
PSE-D	5456-PS	PENNY STRAIT	186	131	76 38.0	96 54.0	1/ 2/85	5/ 3/85
PSE-D	5456-PS	PENNY STRAIT	186	131	76 38.0	96 54.0	3/ 7/84	3/ 8/84
PSE-D	5456-PS	PENNY STRAIT	186	131	76 38.0	96 54.0	6/10/84	6/11/84
PSE-D	5456-PS	PENNY STRAIT	186	131	76 38.0	96 54.0	9/ 1/85	9/ 2/85
PSE-D	5456-PS	PENNY STRAIT	186	131	76 38.0	96 54.0	9/ 6/84	11/ 7/84
PSE-D	5456-PS	PENNY STRAIT	186	131	76 38.0	96 54.0	12/ 9/84	14/10/84
PSE-D	5456-PS	PENNY STRAIT	186	131	76 38.0	96 54.0	16/ 5/84	17/ 6/84
PSE-D	5456-PS	PENNY STRAIT	186	131	76 38.0	96 54.0	16/12/84	17/ 1/85
PSE-D	5456-PS	PENNY STRAIT	186	131	76 38.0	96 54.0	19/ 8/84	20/ 9/84
PSE-D	5456-PS	PENNY STRAIT	186	131	76 38.0	96 54.0	21/ 3/85	16/ 4/85
PSE-D	5456-PS	PENNY STRAIT	186	131	76 38.0	96 54.0	22/11/84	24/12/84

TABLE E.2 CURRENT METER LOCATIONS (cont.)

STATION	METER	LOCATION	WATER DEPTH	METER DEPTH	LAT	LONG	START	END
PSE-D	5456-PS	PENNY STRAIT	186	131	76 38.0	96 54.0	23/ 4/84	24/ 5/84
PSE-D	5456-PS	PENNY STRAIT	186	131	76 38.0	96 54.0	25/ 2/85	29/ 3/85
PSE-D	5456-PS	PENNY STRAIT	186	131	76 38.0	96 54.0	26/ 7/84	27/ 8/84
PSE-D	5456-PS	PENNY STRAIT	186	131	76 38.0	96 54.0	29/10/84	30/11/84
12E	12E	PENNY STRAIT	187	18	76 41.5	97 7.0	13/ 4/76	7/ 5/76
14E	14E	PENNY STRAIT	260	18	76 38.5	97 23.8	17/ 4/76	7/ 5/76
14M	14M	PENNY STRAIT	260	18	76 38.5	97 23.8	17/ 4/76	7/ 5/76
PSW-S	5391-PS	PENNY STRAIT	190	49	76 36.0	97 25.0	2/ 2/85	6/ 3/85
PSW-S	5391-PS	PENNY STRAIT	190	49	76 36.0	97 25.0	4/ 7/84	4/ 8/84
PSW-S	5391-PS	PENNY STRAIT	190	49	76 36.0	97 25.0	7/10/84	7/11/84
PSW-S	5391-PS	PENNY STRAIT	190	49	76 36.0	97 25.0	10/ 1/85	10/ 2/85
PSW-S	5391-PS	PENNY STRAIT	190	49	76 36.0	97 25.0	10/ 6/84	11/ 7/84
PSW-S	5391-PS	PENNY STRAIT	190	49	76 36.0	97 25.0	13/ 9/84	14/10/84
PSW-S	5391-PS	PENNY STRAIT	190	49	76 36.0	97 25.0	17/ 5/84	18/ 6/84
PSW-S	5391-PS	PENNY STRAIT	190	49	76 36.0	97 25.0	17/12/84	17/ 1/85
PSW-S	5391-PS	PENNY STRAIT	190	49	76 36.0	97 25.0	20/ 8/84	21/ 9/84
PSW-S	5391-PS	PENNY STRAIT	190	49	76 36.0	97 25.0	22/ 3/85	12/ 4/85
PSW-S	5391-PS	PENNY STRAIT	190	49	76 36.0	97 25.0	23/ 4/84	25/ 5/84
PSW-S	5391-PS	PENNY STRAIT	190	49	76 36.0	97 25.0	23/11/84	25/12/84
PSW-S	5391-PS	PENNY STRAIT	190	49	76 36.0	97 25.0	26/ 2/85	30/ 3/85
PSW-S	5391-PS	PENNY STRAIT	190	49	76 36.0	97 25.0	27/ 7/84	28/ 8/84
PSW-S	5391-PS	PENNY STRAIT	190	49	76 36.0	97 25.0	30/10/84	1/12/84
PSW-D	5471-PS	PENNY STRAIT	190	138	76 36.0	97 25.0	2/ 2/85	6/ 3/85
PSW-D	5471-PS	PENNY STRAIT	190	138	76 36.0	97 25.0	4/ 7/84	4/ 8/84
PSW-D	5471-PS	PENNY STRAIT	190	138	76 36.0	97 25.0	7/10/84	7/11/84
PSW-D	5471-PS	PENNY STRAIT	190	138	76 36.0	97 25.0	10/ 1/85	10/ 2/85
PSW-D	5471-PS	PENNY STRAIT	190	138	76 36.0	97 25.0	10/ 6/84	11/ 7/84
PSW-D	5471-PS	PENNY STRAIT	190	138	76 36.0	97 25.0	13/ 9/84	14/10/84
PSW-D	5471-PS	PENNY STRAIT	190	138	76 36.0	97 25.0	17/ 5/84	18/ 6/84
PSW-D	5471-PS	PENNY STRAIT	190	138	76 36.0	97 25.0	17/12/84	17/ 1/85
PSW-D	5471-PS	PENNY STRAIT	190	138	76 36.0	97 25.0	20/ 8/84	21/ 9/84
PSW-D	5471-PS	PENNY STRAIT	190	138	76 36.0	97 25.0	22/ 3/85	18/ 4/85
PSW-D	5471-PS	PENNY STRAIT	190	138	76 36.0	97 25.0	23/ 4/84	25/ 5/84
PSW-D	5471-PS	PENNY STRAIT	190	138	76 36.0	97 25.0	23/11/84	25/12/84
PSW-D	5471-PS	PENNY STRAIT	190	138	76 36.0	97 25.0	26/ 2/85	30/ 3/85
PSW-D	5471-PS	PENNY STRAIT	190	138	76 36.0	97 25.0	27/ 7/84	28/ 8/84
PSW-D	5471-PS	PENNY STRAIT	190	138	76 36.0	97 25.0	30/10/84	1/12/84
838	838	BARROW STRAIT	88	4	74 38.3	97 58.2	13/ 3/78	29/ 4/78
838	838	BARROW STRAIT	88	50	74 38.3	97 58.2	13/ 3/78	22/ 4/78
842	842	BARROW STRAIT	137	50	74 26.7	98 6.4	11/ 3/78	23/ 4/78

TABLE E.2 CURRENT METER LOCATIONS (cont.)

STATION	METER	LOCATION	WATER DEPTH	METER DEPTH	LAT	LONG	START	END
842	842	BARROW STRAIT	137	50	74 26.7	98 6.4	11/ 3/78	12/ 4/78
835	835	BARROW STRAIT	92	4	74 52.8	98 17.0	11/ 3/78	22/ 4/78
835	835	BARROW STRAIT	92	50	74 52.8	98 17.0	11/ 3/78	22/ 4/78
845	845	BARROW STRAIT	126	4	74 10.0	98 34.0	11/ 3/78	23/ 4/78
845	845	BARROW STRAIT	126	50	74 10.0	98 34.0	11/ 3/78	23/ 4/78
72	2467	CAPE COCKBURN	40	18	74 57.0	100 27.0	6/ 4/83	8/ 5/83
72	2467	CAPE COCKBURN	40	18	74 57.0	100 27.0	30/ 4/83	22/ 5/83
932-50	932-50	DANISH STRAIT	210	50	77 50.0	100 46.0	8/ 4/79	8/ 5/79
932-05	932-05	DANISH STRAIT	210	5	77 50.0	100 46.0	8/ 4/79	8/ 5/79
74	1932-CC	CAPE COCKBURN	150	18	74 51.0	100 50.0	6/ 4/83	8/ 5/83
74	1932-CC	CAPE COCKBURN	150	18	74 51.0	100 50.0	30/ 4/83	22/ 5/83
81	5361-CB	CAPE BERKELEY	50	18	73 53.0	101 0.0	6/ 4/83	8/ 5/83
81	5361-CB	CAPE BERKELEY	50	18	73 53.0	101 0.0	24/ 5/83	11/ 6/83
81	5361-CB	CAPE BERKELEY	50	18	73 53.0	101 0.0	30/ 4/83	1/ 6/83
79	1931-CB	CAPE BERKELEY	127	18	74 0.0	101 40.0	6/ 4/83	2/ 5/83
71	3395-AC	AUSTIN CHANNEL	173	18	75 23.0	102 38.0	1/ 4/83	2/ 5/83
71	3395-AC	AUSTIN CHANNEL	173	18	75 23.0	102 38.0	24/ 4/83	23/ 5/83
71	3395-AC	AUSTIN CHANNEL	173	18	75 23.0	102 38.0	30/ 3/83	22/ 5/83
71	2466-AC	AUSTIN CHANNEL	173	73	75 23.0	102 38.0	1/ 4/83	2/ 5/83
71	2466-AC	AUSTIN CHANNEL	139	73	75 23.0	102 38.0	3/ 2/84	6/ 3/84
71	2466-AC	AUSTIN CHANNEL	173	73	75 23.0	102 38.0	4/ 7/83	5/ 8/83
71	2466-AC	AUSTIN CHANNEL	173	73	75 23.0	102 38.0	7/10/83	8/11/83
71	2466-AC	AUSTIN CHANNEL	173	73	75 23.0	102 38.0	10/ 1/84	11/ 2/84
71	2466-AC	AUSTIN CHANNEL	173	73	75 23.0	102 38.0	11/ 6/83	12/ 7/83
71	2466-AC	AUSTIN CHANNEL	173	73	75 23.0	102 38.0	14/ 9/83	15/10/83
71	2466-AC	AUSTIN CHANNEL	173	73	75 23.0	102 38.0	18/ 5/83	19/ 6/83
71	2466-AC	AUSTIN CHANNEL	173	73	75 23.0	102 38.0	18/12/83	18/ 1/84
71	2466-AC	AUSTIN CHANNEL	173	73	75 23.0	102 38.0	21/ 8/83	22/ 9/83
71	2466-AC	AUSTIN CHANNEL	173	73	75 23.0	102 38.0	22/ 3/84	29/ 4/84
71	2466-AC	AUSTIN CHANNEL	173	73	75 23.0	102 38.0	24/ 4/83	26/ 5/83
71	2466-AC	AUSTIN CHANNEL	173	73	75 23.0	102 38.0	24/11/83	26/12/83
71	2466-AC	AUSTIN CHANNEL	173	73	75 23.0	102 38.0	27/ 2/84	30/ 3/84
71	2466-AC	AUSTIN CHANNEL	173	73	75 23.0	102 38.0	28/ 7/83	29/ 8/83
71	2466-AC	AUSTIN CHANNEL	173	73	75 23.0	102 38.0	31/10/83	2/12/83
71	2470	AUSTIN CHANNEL	173	123	75 23.0	102 38.0	3/ 2/84	6/ 3/84
71	2470	AUSTIN CHANNEL	173	123	75 23.0	102 38.0	4/ 7/83	5/ 8/83
71	2470	AUSTIN CHANNEL	173	123	75 23.0	102 38.0	7/10/83	8/11/83
71	2470	AUSTIN CHANNEL	173	123	75 23.0	102 38.0	10/ 1/84	11/ 2/84
71	2470	AUSTIN CHANNEL	173	123	75 23.0	102 38.0	11/ 6/83	12/ 7/83
71	2470	AUSTIN CHANNEL	173	123	75 23.0	102 38.0	14/ 9/83	15/10/83

TABLE E.2 CURRENT METER LOCATIONS (cont.)

STATION	METER	LOCATION	WATER DEPTH	METER DEPTH	LAT	LONG	START	END
71	2470	AUSTIN CHANNEL	173	123	75 23.0	102 38.0	18/ 5/83	19/ 6/83
71	2470	AUSTIN CHANNEL	173	123	75 23.0	102 38.0	18/12/83	18/ 1/84
71	2470	AUSTIN CHANNEL	173	123	75 23.0	102 38.0	21/ 8/83	22/ 9/83
71	2470	AUSTIN CHANNEL	173	123	75 23.0	102 38.0	22/ 3/84	29/ 4/84
71	2470	AUSTIN CHANNEL	173	123	75 23.0	102 38.0	24/ 4/83	26/ 5/83
71	2470	AUSTIN CHANNEL	173	123	75 23.0	102 38.0	24/11/83	26/12/83
71	2470	AUSTIN CHANNEL	173	123	75 23.0	102 38.0	27/ 2/84	30/ 3/84
71	2470	AUSTIN CHANNEL	173	123	75 23.0	102 38.0	28/ 7/83	29/ 8/83
71	2470	AUSTIN CHANNEL	173	123	75 23.0	102 38.0	31/10/83	2/12/83
87	972	M'CLINTOCK CHANNEL	200	18	72 51.0	102 54.0	7/ 4/83	8/ 5/83
87	972	M'CLINTOCK CHANNEL	200	18	72 51.0	102 54.0	7/ 4/84	23/ 4/84
935-50	935-50	MACLEAN STRAIT	350	50	77 37.0	102 55.0	8/ 4/79	24/ 4/79
895	895	BARROW STRAIT	147	5	75 7.4	102 59.6	15/ 3/78	19/ 4/78
882	882	AUSTIN CHANNEL	180	50	75 27.3	103 5.4	15/ 3/78	26/ 3/78
86	5474	M'CLINTOCK CHANNEL	305	18	72 52.0	103 9.0	1/ 5/83	2/ 6/83
86	5474	M'CLINTOCK CHANNEL	305	18	72 52.0	103 9.0	7/ 4/83	9/ 5/83
86	5474	M'CLINTOCK CHANNEL	305	18	72 52.0	103 9.0	25/ 5/83	10/ 6/83
912-50	912-50	DESBARATS STRAIT	195	50	76 55.0	103 49.0	3/ 4/79	1/ 5/79
914-50	914-50	DESBARATS STRAIT	325	50	76 47.0	103 52.0	4/ 4/79	3/ 5/79
937-50	937-50	MACLEAN STRAIT	290	50	77 30.0	103 58.0	8/ 4/79	7/ 5/79
58	1936-BM	BYAM MARTIN ISLAND	65	18	74 59.0	104 13.0	3/ 4/83	5/ 5/83
58	1936-BM	BYAM MARTIN ISLAND	65	18	74 59.0	104 13.0	27/ 4/83	23/ 5/83
57	1939-BM	BYAM MARTIN ISLAND	65	18	74 52.0	104 13.0	3/ 4/83	4/ 5/83
66	3388-BM	BYAM MARTIN CHANNEL	166	18	76 5.0	104 28.0	2/ 4/83	4/ 5/83
66	3388-BM	BYAM MARTIN CHANNEL	166	18	76 5.0	104 28.0	26/ 4/83	22/ 5/83
66	3388-BM	BYAM MARTIN CHANNEL	173	18	76 5.0	104 28.0	30/ 3/83	19/ 5/83
83	5456-MC	M'CLINTOCK CHANNEL	200	18	72 55.0	104 29.0	1/ 5/83	2/ 6/83
83	5456-MC	M'CLINTOCK CHANNEL	200	18	72 55.0	104 29.0	7/ 4/83	9/ 5/83
83	5456-MC	M'CLINTOCK CHANNEL	200	18	72 55.0	104 29.0	25/ 5/83	10/ 6/83
65	3387-BM	BYAM MARTIN CHANNEL	166	18	76 3.0	104 39.0	2/ 4/83	19/ 4/83
65	3387-BM	BYAM MARTIN CHANNEL	166	18	76 3.0	104 39.0	30/ 3/83	16/ 4/83
82	1930-MC	M'CLINTOCK CHANNEL	60	18	72 56.0	104 52.0	1/ 5/83	2/ 6/83
82	1930-MC	M'CLINTOCK CHANNEL	60	18	72 56.0	104 52.0	7/ 4/83	9/ 5/83
82	1930-MC	M'CLINTOCK CHANNEL	60	18	72 56.0	104 52.0	25/ 5/83	10/ 6/83
63	3278-BM	BYAM MARTIN CHANNEL	166	18	75 58.0	105 11.0	2/ 4/83	4/ 5/83
63	3278-BM	BYAM MARTIN CHANNEL	166	18	75 58.0	105 11.0	26/ 4/83	22/ 5/83
63	3278-BM	BYAM MARTIN CHANNEL	166	18	75 58.0	105 11.0	30/ 3/83	19/ 5/83
62	3223-BM	BYAM MARTIN CHANNEL	166	18	75 56.0	105 23.0	2/ 4/83	4/ 5/83
62	3223-BM	BYAM MARTIN CHANNEL	166	18	75 56.0	105 23.0	26/ 4/83	23/ 5/83
62	3223-BM	BYAM MARTIN CHANNEL	166	18	75 56.0	105 23.0	30/ 3/83	20/ 5/83

TABLE E.2 CURRENT METER LOCATIONS (cont.)

STATION	METER	LOCATION	WATER DEPTH	METER DEPTH	LAT	LONG	START	END
20	1931-VM	VISCOUNT MELVILLE SOUND	200	18	73 49.0	106 26.0	12/ 5/82	19/ 6/82
20	1931-VM	VISCOUNT MELVILLE SOUND	200	18	73 49.0	106 26.0	18/ 4/82	20/ 5/82
21	3387-VM	VISCOUNT MELVILLE SOUND	200	18	73 54.0	106 30.0	12/ 5/82	30/ 5/82
21	3387-VM	VISCOUNT MELVILLE SOUND	200	18	73 54.0	106 30.0	19/ 4/82	20/ 5/82
22	1930-VM	VISCOUNT MELVILLE SOUND	300	18	74 1.0	106 36.0	12/ 5/82	19/ 6/82
22	1930-VM	VISCOUNT MELVILLE SOUND	300	18	74 1.0	106 36.0	19/ 4/82	20/ 5/82
24	1932-VM	VISCOUNT MELVILLE SOUND	200	18	74 41.0	107 6.0	11/ 5/82	19/ 6/82
24	1932-VM	VISCOUNT MELVILLE SOUND	200	18	74 41.0	107 6.0	18/ 4/82	19/ 5/82
25	5361-VM	VISCOUNT MELVILLE SOUND	200	18	74 48.0	107 11.0	11/ 5/82	20/ 6/82
25	5361-VM	VISCOUNT MELVILLE SOUND	200	18	74 48.0	107 11.0	18/ 4/82	19/ 5/82
26	5389	VISCOUNT MELVILLE SOUND	16	18	74 51.0	107 14.0	12/ 5/82	20/ 6/82
26	5389	VISCOUNT MELVILLE SOUND	16	18	74 51.0	107 14.0	18/ 4/82	20/ 5/82
924-05	924-05	N BYAM MARTIN- DESBARATS STRAIT	439	5	76 52.0	107 52.0	3/ 4/79	2/ 5/79
02-BR	02-BR	BRIDPORT INLET	16	20	74 59.8	108 51.0	26/ 3/79	30/ 7/79
01-BR	01-BR	BRIDPORT INLET	16	20	74 57.8	108 55.0	25/ 3/79	30/ 7/79
01-BR	01-BR	BRIDPORT INLET	145	50	74 57.8	108 55.0	25/ 3/79	5/ 7/79
19	1939-VM	VISCOUNT MELVILLE SOUND	200	18	73 30.0	113 19.0	3/ 5/82	4/ 6/82
19	1939-VM	VISCOUNT MELVILLE SOUND	200	18	73 30.0	113 19.0	9/ 4/82	11/ 5/82
19	1939-VM	VISCOUNT MELVILLE SOUND	200	18	73 30.0	113 19.0	27/ 5/82	22/ 6/82
31A06	31A06	M'CLURE STRAIT	200	6	74 20.3	113 21.8	6/ 4/77	7/ 5/77
17	5390	M'CLURE STRAIT	400	18	74 27.0	113 51.0	1/ 5/82	2/ 6/82
17	5390	M'CLURE STRAIT	400	18	74 27.0	113 51.0	7/ 4/82	9/ 5/82
17	5390	M'CLURE STRAIT	400	18	74 27.0	113 51.0	25/ 5/82	21/ 6/82
18	5391-VM	VISCOUNT MELVILLE SOUND	200	18	73 20.0	113 58.0	3/ 5/82	4/ 6/82
18	5391-VM	VISCOUNT MELVILLE SOUND	200	18	73 20.0	113 58.0	9/ 4/82	11/ 5/82
18	5391-VM	VISCOUNT MELVILLE SOUND	200	18	73 20.0	113 58.0	27/ 5/82	22/ 6/82
16	5473	M'CLURE STRAIT	400	18	74 25.0	114 0.0	7/ 4/82	8/ 5/82
16	5473	M`CLURE STRAIT	400	18	74 25.0	114 0.0	24/ 5/82	21/ 6/82
16	5473	M'CLURE STRAIT	400	18	74 25.0	114 0.0	30/ 4/82	1/ 6/82
15	2466-MS	M'CLURE STRAIT	488	18	74 18.0	114 30.0	1/ 5/82	2/ 6/82
15	2466-MS	M'CLURE STRAIT	488	18	74 18.0	114 30.0	7/ 4/82	9/ 5/82
15	2466-MS	M'CLURE STRAIT	488	18	74 18.0	114 30.0	25/ 5/82	21/ 6/82
34A06	34A06	M'CLURE STRAIT	200	6	73 43.0	114 46.0	4/ 4/77	5/ 5/77
14	5472	M'CLURE STRAIT	488	18	74 10.0	115 2.0	1/ 5/82	2/ 6/82
14	5472	M'CLURE STRAIT	488	18	74 10.0	115 2.0	7/ 4/82	9/ 5/82
14	5472	M'CLURE STRAIT	488	18	74 10.0	115 2.0	25/ 5/82	21/ 6/82
13	5471-MS	M'CLURE STRAIT	488	18	74 0.0	115 28.0	7/ 4/82	8/ 5/82
13	5471-MS	M'CLURE STRAIT	488	18	74 0.0	115 28.0	24/ 5/82	21/ 6/82
13	5471-MS	M'CLURE STRAIT	488	18	74 0.0	115 28.0	30/ 4/82	1/ 6/82

TABLE E.2 CURRENT METER LOCATIONS (cont.)

STATION	METER	LOCATION	WATER DEPTH	METER DEPTH	LAT	LONG	START	END
42A06	42A06	PRINCE OF WALES STRAIT	60	6	73 21.0	115 36.1	2/ 4/77	11/ 5/77
42A34	42A34	PRINCE OF WALES STRAIT	60	34	73 21.0	115 36.1	2/ 4/77	11/ 5/77
12	5456-MS	M'CLURE STRAIT	488	18	73 56.0	115 52.0	7/ 4/82	8/ 5/82
12	5456-MS	M'CLURE STRAIT	488	18	73 56.0	115 52.0	24/ 5/82	21/ 6/82
12	5456-MS	M'CLURE STRAIT	488	18	73 56.0	115 52.0	30/ 4/82	1/ 6/82
10	10	PRINCE OF WALES STRAIT	210	18	73 12.0	115 58.1	23/ 5/82	24/ 6/82
10	10	PRINCE OF WALES STRAIT	210	18	73 12.0	115 58.1	24/ 4/82	26/ 5/82
10	10	PRINCE OF WALES STRAIT	210	18	73 12.0	115 58.1	25/ 3/82	26/ 4/82
08	08	PRINCE OF WALES STRAIT	46	20	73 9.0	116 8.0	25/ 3/82	25/ 4/82
11	1936-MS	M'CLURE STRAIT	300	18	73 56.0	116 9.0	31/ 3/82	5/ 5/82
07	07	PRINCE OF WALES STRAIT (NORTH)	46	20	73 9.0	116 10.0	21/ 4/82	22/ 5/82
07	07	PRINCE OF WALES STRAIT (NORTH)	46	20	73 9.0	116 10.0	25/ 3/82	25/ 4/82
06	06	PRINCE OF WALES STRAIT	90	20	73 11.0	116 13.0	23/ 4/82	25/ 5/82
06	06	PRINCE OF WALES STRAIT	90	20	73 11.0	116 13.0	23/ 5/82	24/ 6/82
06	06	PRINCE OF WALES STRAIT	90	20	73 11.0	116 13.0	25/ 3/82	25/ 4/82
04	04-PWSN	PRINCE OF WALES STRAIT (NORTH)	46	20	73 12.0	116 14.0	26/ 3/82	7/ 4/82
05	05	PRINCE OF WALES STRAIT (NORTH)	68	20	73 12.0	116 15.0	23/ 4/82	25/ 5/82
05	05	PRINCE OF WALES STRAIT (NORTH)	68	20	73 12.0	116 15.0	23/ 5/82	24/ 6/82
05	05	PRINCE OF WALES STRAIT (NORTH)	68	20	73 12.0	116 15.0	25/ 3/82	25/ 4/82
01	01-PWSN	PRINCE OF WALES STRAIT (NORTH)	68	20	73 16.0	116 17.0	23/ 5/82	24/ 6/82
01	01-PWSN	PRINCE OF WALES STRAIT (NORTH)	68	20	73 16.0	116 17.0	24/ 4/82	25/ 5/82
01	01-PWSN	PRINCE OF WALES STRAIT (NORTH)	68	20	73 16.0	116 17.0	25/ 3/82	26/ 4/82
02	02-PWSN	PRINCE OF WALES STRAIT (NORTH)	46	18	73 15.0	116 17.0	23/ 4/82	25/ 5/82
02	02-PWSN	PRINCE OF WALES STRAIT (NORTH)	46	18	73 15.0	116 17.0	23/ 5/82	23/ 6/82
02	02-PWSN	PRINCE OF WALES STRAIT (NORTH)	46	20	73 15.0	116 17.0	25/ 3/82	26/ 4/82
03	03-PWSN	PRINCE OF WALES STRAIT (NORTH)	68	20	73 16.0	116 17.0	24/ 3/82	19/ 4/82
09	09	PRINCE OF WALES STRAIT (NORTH)	90	20	73 5.0	116 35.0	12/ 5/82	13/ 6/82
09	09	PRINCE OF WALES STRAIT (NORTH)	90	20	73 5.0	116 35.0	18/ 4/82	20/ 5/82
09	09	PRINCE OF WALES STRAIT (NORTH)	90	20	73 5.0	116 35.0	25/ 3/82	26/ 4/82
01	01-PWSW	PRINCE OF WALES STRAIT	40	10	72 47.0	117 50.0	30/ 3/82	28/ 4/82

FIGURES

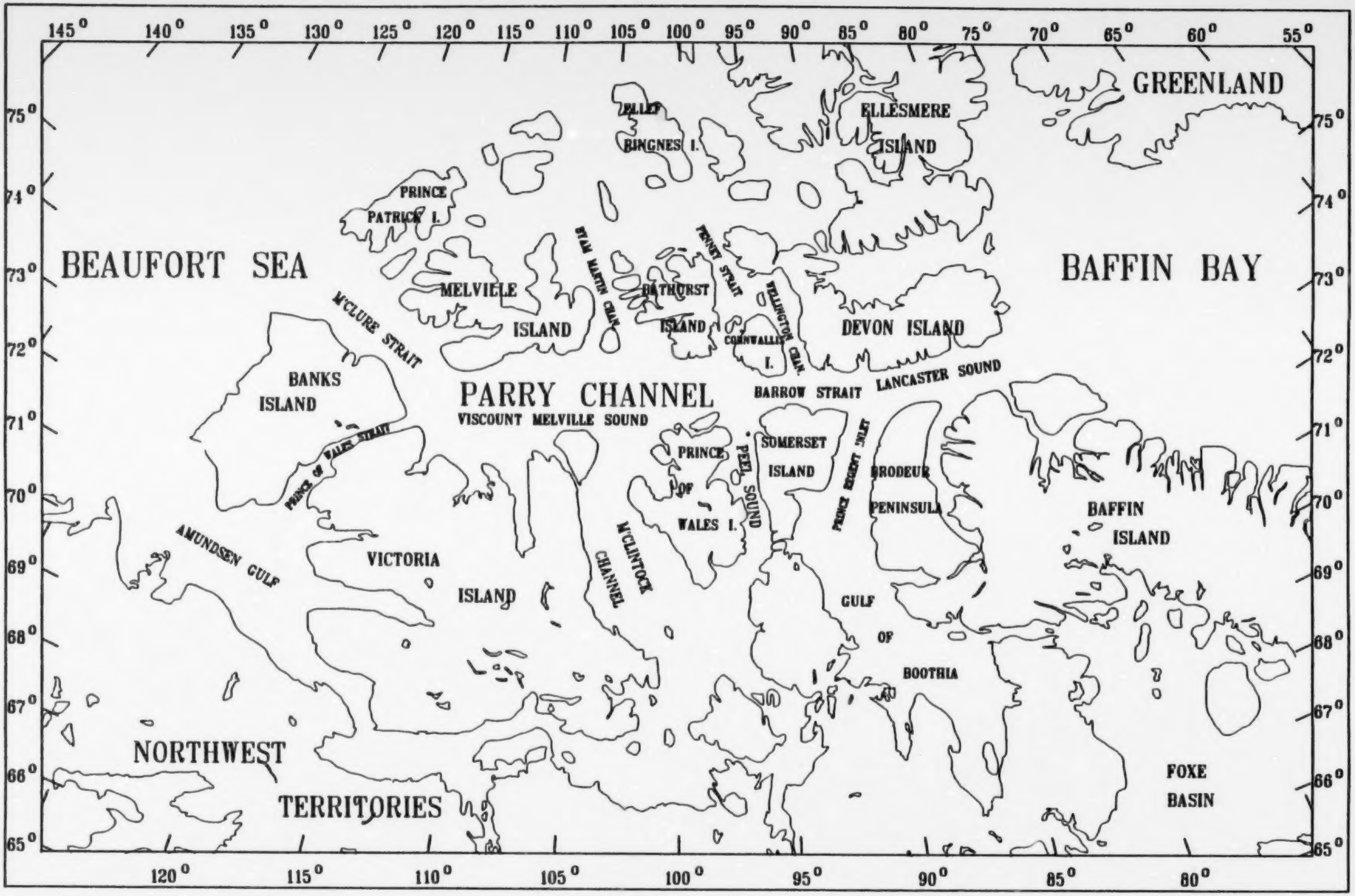
145°
140°
135°
130°
125°
120°
115°
110°
105°
100°
95°
90°
85°
80°
75°
70°
65°
60°
55°
75°
74°
73°
72°
71°
70°
69°
68°
67°
66°
65°
120°
115°
110°
105°
100°
95°
90°
85°
80°
GREENLAND
ELLESMERE ISLAND
ELLEF RINGNES I.
BAFFIN BAY
BEAUFORT SEA
PRINCE PATRICK I.
MELVILLE ISLAND
BYAM MARTIN CHAN.
BATHURST ISLAND
PENNY STRAIT
WELLINGTON CHAN.
CORNWALLIS I.
DEVON ISLAND
LANCASTER SOUND
BARROW STRAIT
M'CLURE STRAIT
BANKS ISLAND
PARRY CHANNEL
VISCOUNT MELVILLE SOUND
PRINCE OF WALES STRAIT
PRINCE OF WALES I.
PEEL SOUND
SOMERSET ISLAND
PRINCE REGENT INLET
BRODEUR PENINSULA
BAFFIN ISLAND
AMUNDSEN GULF
VICTORIA ISLAND
M'CLINTOCK CHANNEL
GULF OF BOOTHIA
NORTHWEST TERRITORIES
FOXE BASIN

Figure 1.1.1 The study area, comprising the major waterways of the Northwest Passage.

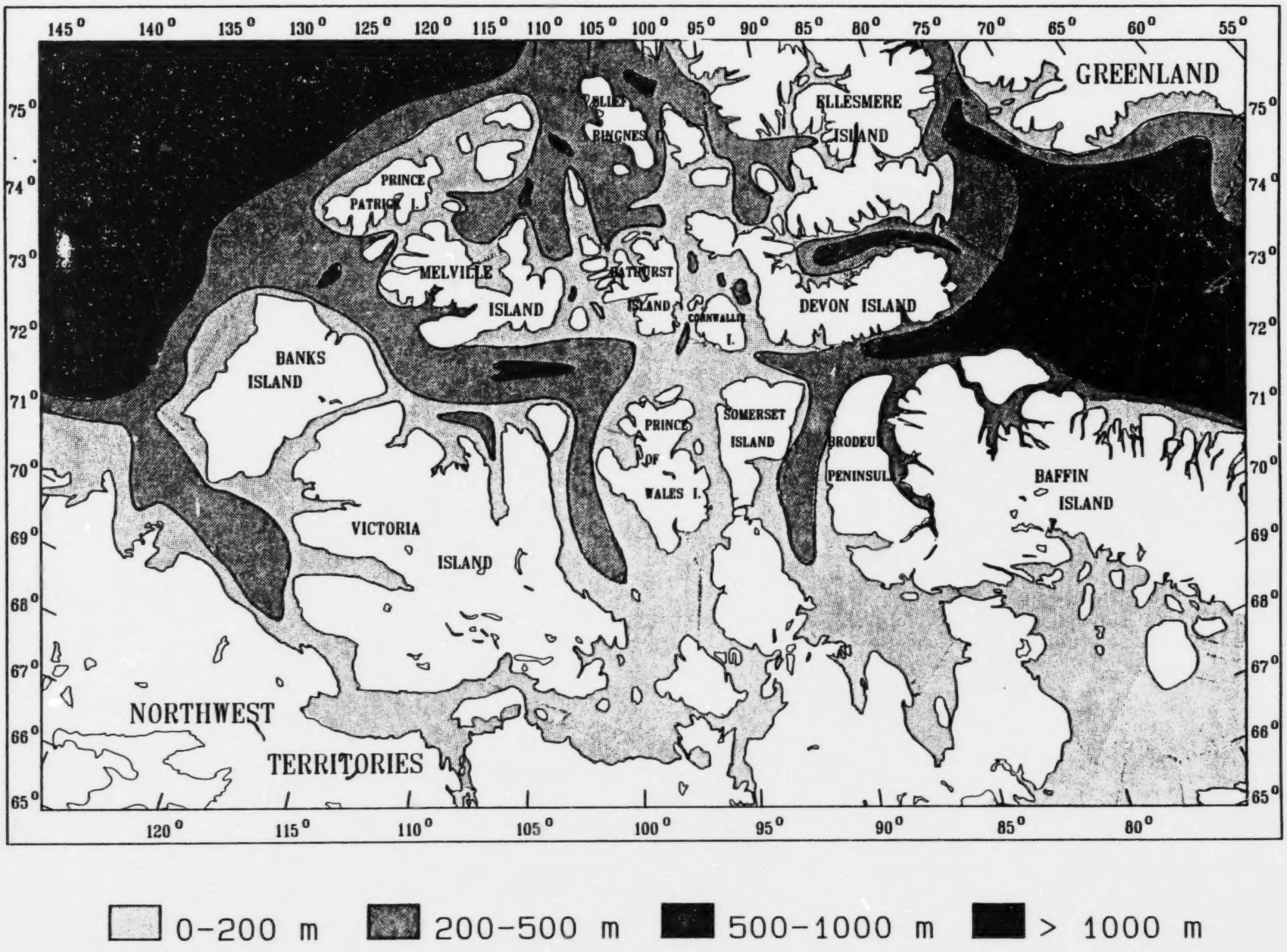
145°
140°
135°
130°
125°
120°
115°
110°
105°
100°
95°
90°
85°
80°
75°
70°
65°
60°
55°
75°
74°
73°
72°
71°
70°
69°
68°
67°
66°
65°
120°
115°
110°
105°
100°
95°
90°
85°
80°
GREENLAND
ELLESMERE ISLAND
ELLEF RINGNES I.
PRINCE PATRICK I.
MELVILLE ISLAND
BATHURST ISLAND
CORNWALLIS I.
DEVON ISLAND
BANKS ISLAND
PRINCE OF WALES I.
SOMERSET ISLAND
BRODEUR PENINSULA
BAFFIN ISLAND
VICTORIA ISLAND
NORTHWEST TERRITORIES
0-200 m
200-500 m
500-1000 m
> 1000 m

Figure 1.1.2 Bathymetry of the study area.

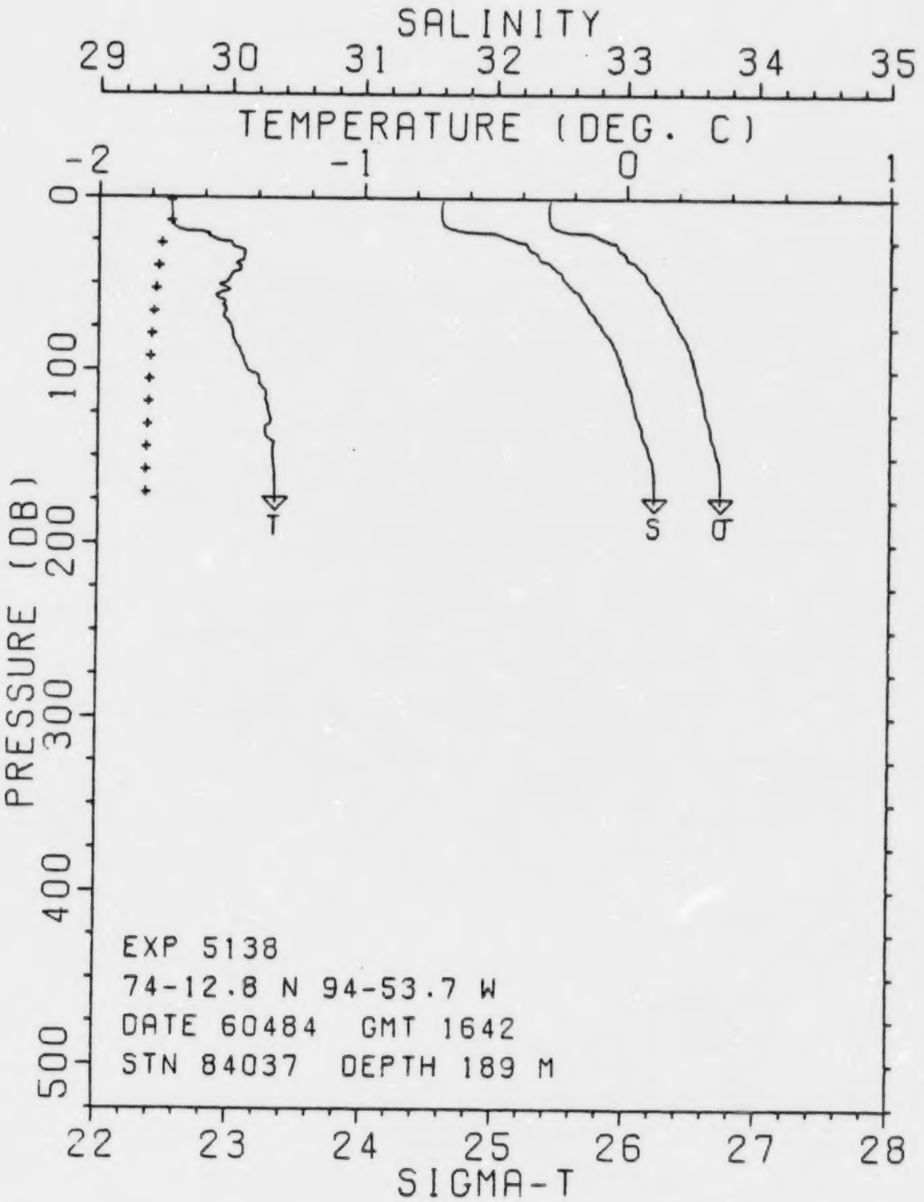

Figure 1.2.1 Vertical profile of salinity temperature and density in Barrrow Strait, from Buckingham et al., (1987).

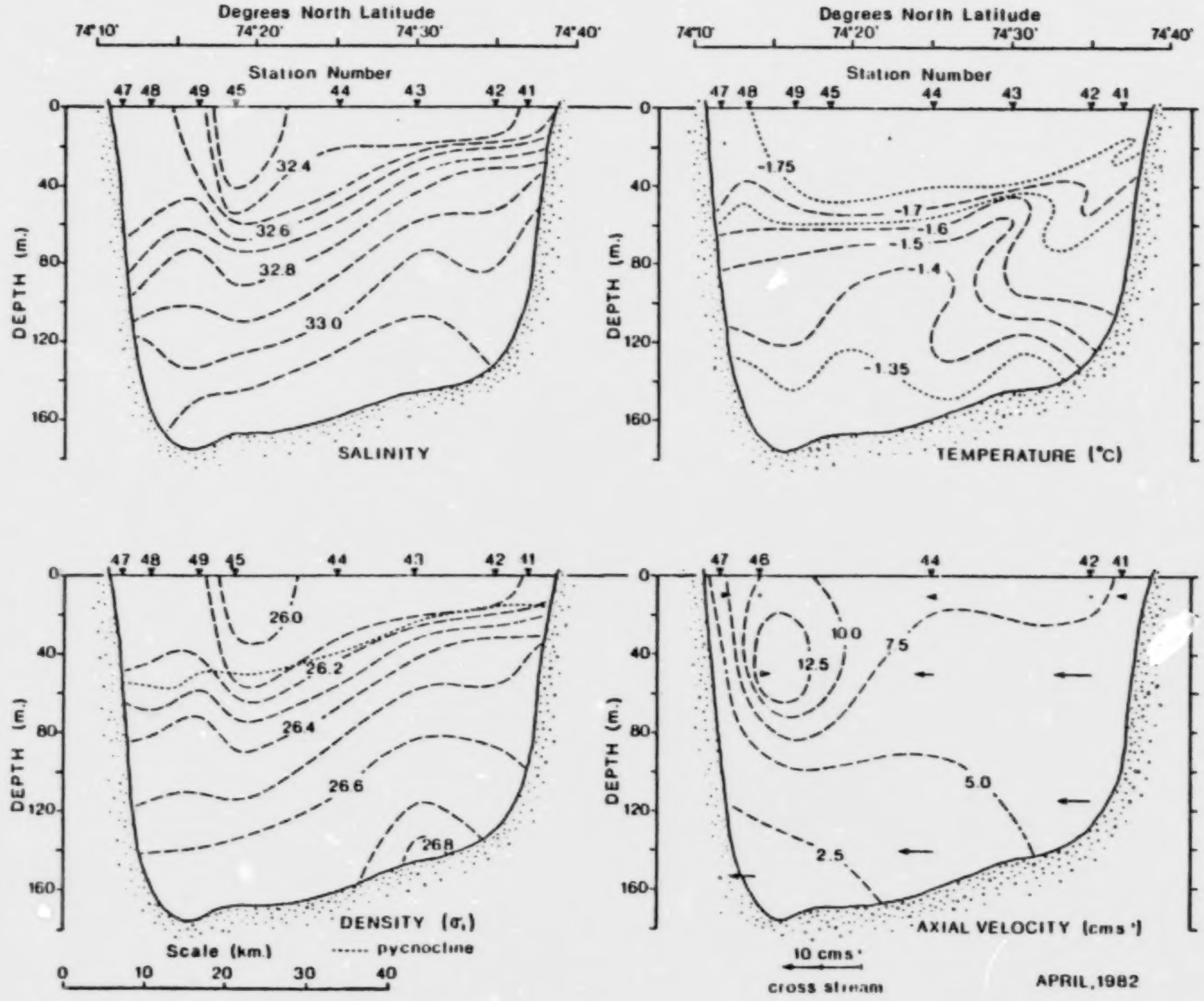

Figure 1.2.2 Cross-section of salinity values in Barrow Strait, from Brooks (1982).

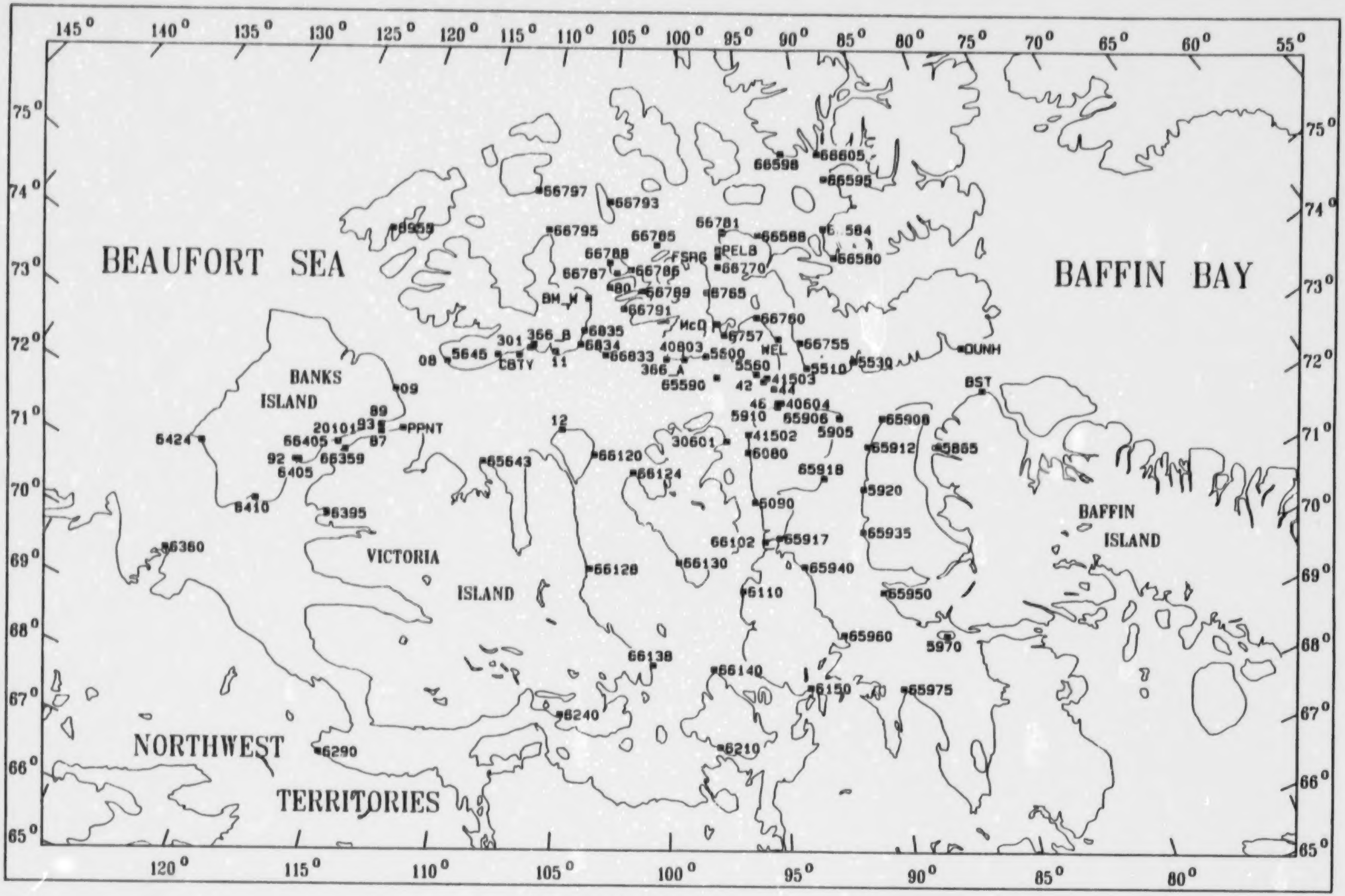
145°
140°
135°
130°
125°
120°
115°
110°
105°
100°
95°
90°
85°
80°
75°
70°
65°
60°
55°
75°
74°
73°
72°
71°
70°
69°
68°
67°
66°
65°
BEAUFORT SEA
BAFFIN BAY
BANKS ISLAND
VICTORIA ISLAND
BAFFIN ISLAND
NORTHWEST TERRITORIES
66598
66605
66595
66797
66793
6959
66795
66785
66781
66588
6_584
66580
66788
FSAG
PELB
66787
66786
66770
80
66789
6765
BM_W
66791
66760
McQ
6757
6835
66755
301
366_B
6834
WEL
5645
66833
40803
5600
08
CBTY
11
366_A
5560
5510
5530
DUNH
65590
42
41503
44
BST
09
46
40604
89
5910
65906
65908
20101
93
PPNT
12
30601
41502
5905
6424
66405
87
65643
66120
6080
65912
5865
92
66359
6405
66124
65918
6410
5920
6395
6090
66102
65917
65935
6360
66128
66130
65940
6110
65950
65960
5970
66138
66140
6150
65975
6240
6290
6210
120°
115°
110°
105°
100°
95°
90°
85°
80°

Figure 2.1.1 Tide gauge locations.

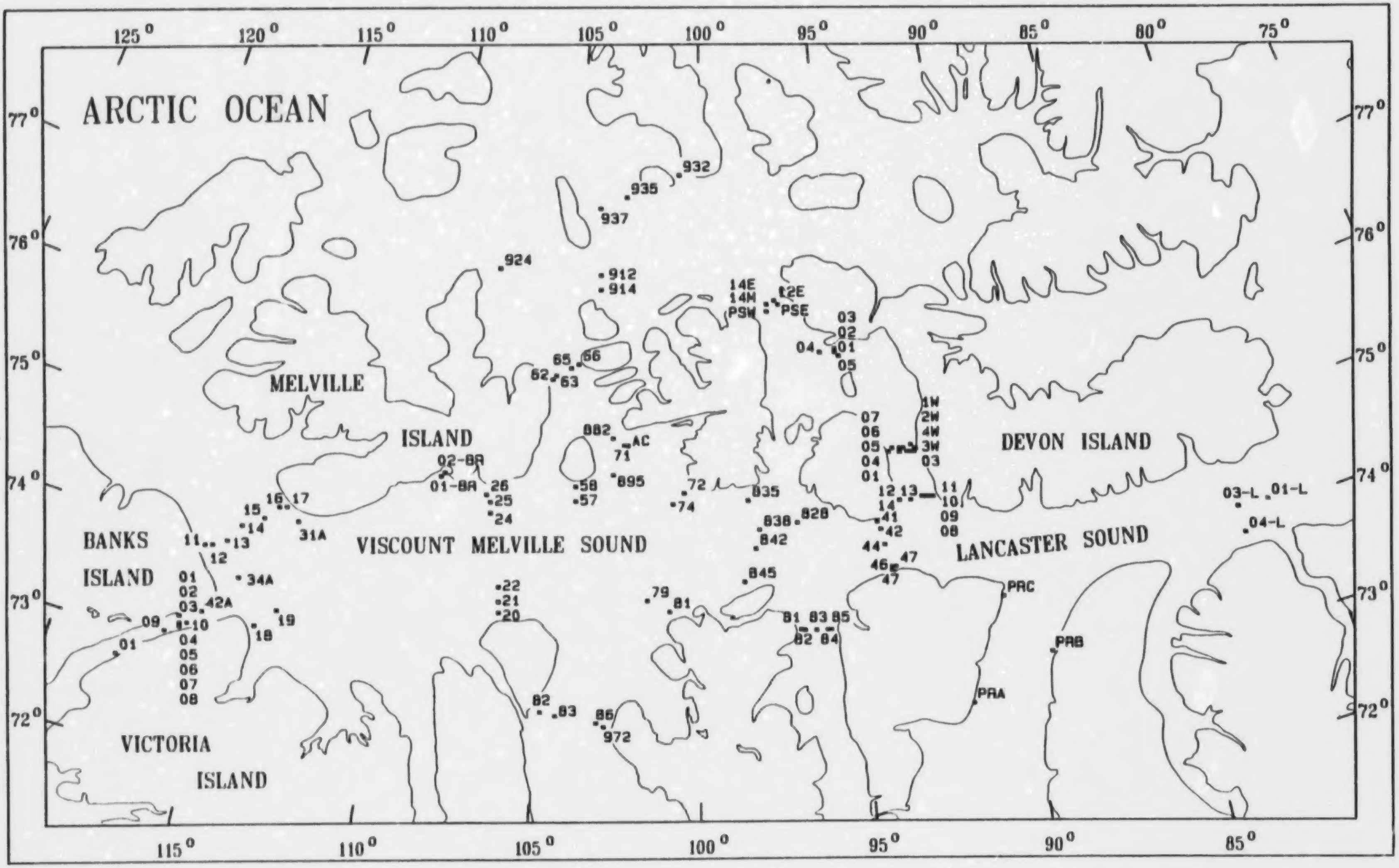
125°
120°
115°
110°
105°
100°
95°
90°
85°
80°
75°
77°
76°
75°
74°
73°
72°
ARCTIC OCEAN
MELVILLE
ISLAND
BANKS
ISLAND
VICTORIA
ISLAND
VISCOUNT MELVILLE SOUND
DEVON ISLAND
LANCASTER SOUND
932
935
937
924
912
914
14E
14W
PSW
12E
PSE
03
02
01
04
05
65
66
62
63
882
AC
71
895
58
57
02-BA
01-BA
26
25
24
72
74
835
838
828
842
845
07
06
05
04
01
1W
2W
4W
3W
03
12
13
14
11
10
09
08
41
42
44
46
47
47
03-L
01-L
04-L
16
17
15
14
31A
11
13
12
34A
01
02
03
42A
10
04
05
06
07
08
09
01
19
18
22
21
20
79
81
81
83
85
82
84
PRC
PRB
PRA
82
83
86
972
115°
110°
105°
100°
95°
90°
85°

Figure 2.2.1. Current meter locations.

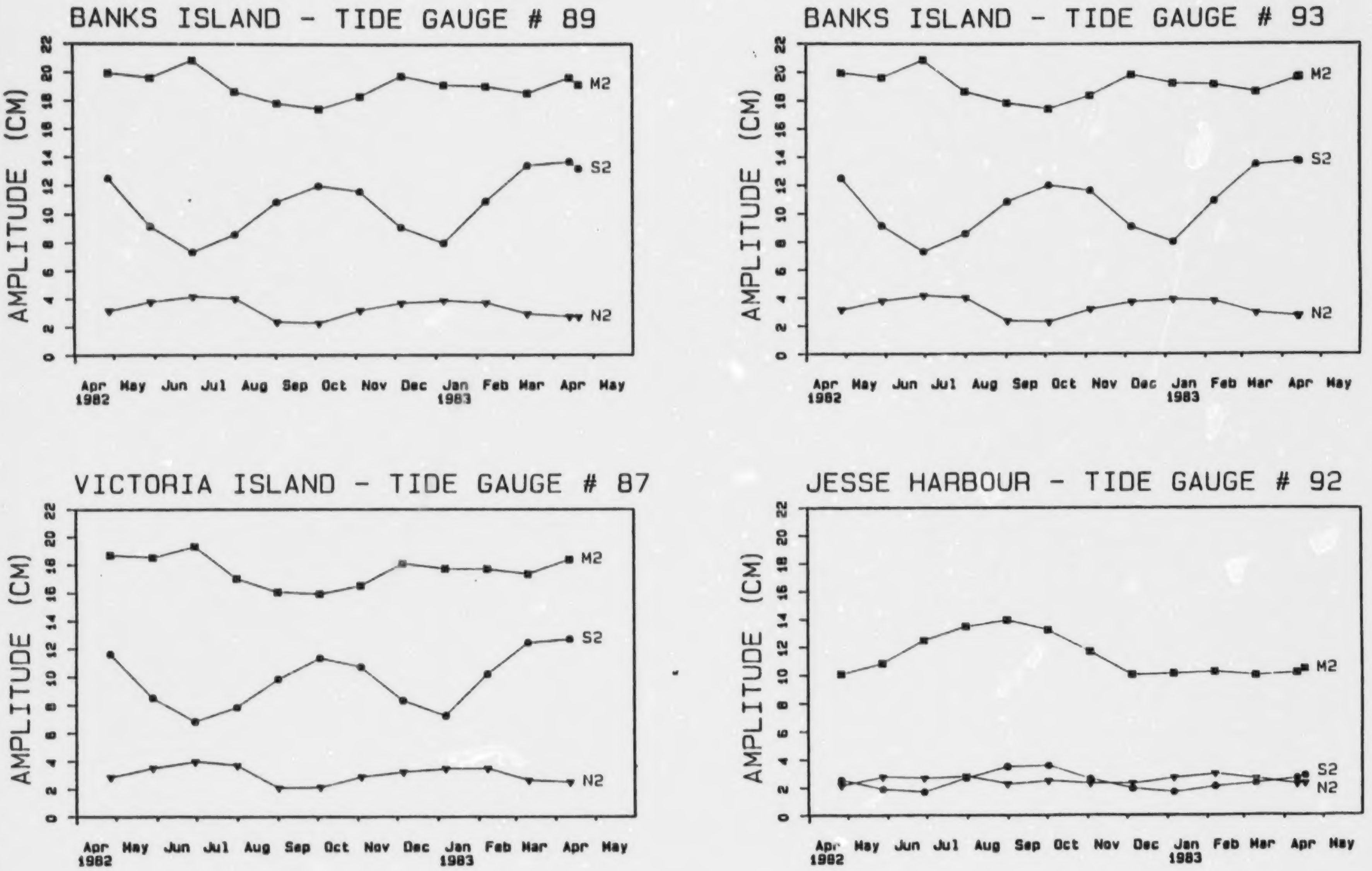
BANKS ISLAND - TIDE GAUGE # 89

BANKS ISLAND - TIDE GAUGE # 93

VICTORIA ISLAND - TIDE GAUGE # 87

JESSE HARBOUR - TIDE GAUGE # 92

Figure 3.1.1 Time series of the amplitude of the major semi-diurnal constituents at four stations in Prince of Wales Strait. Inference has not been used.

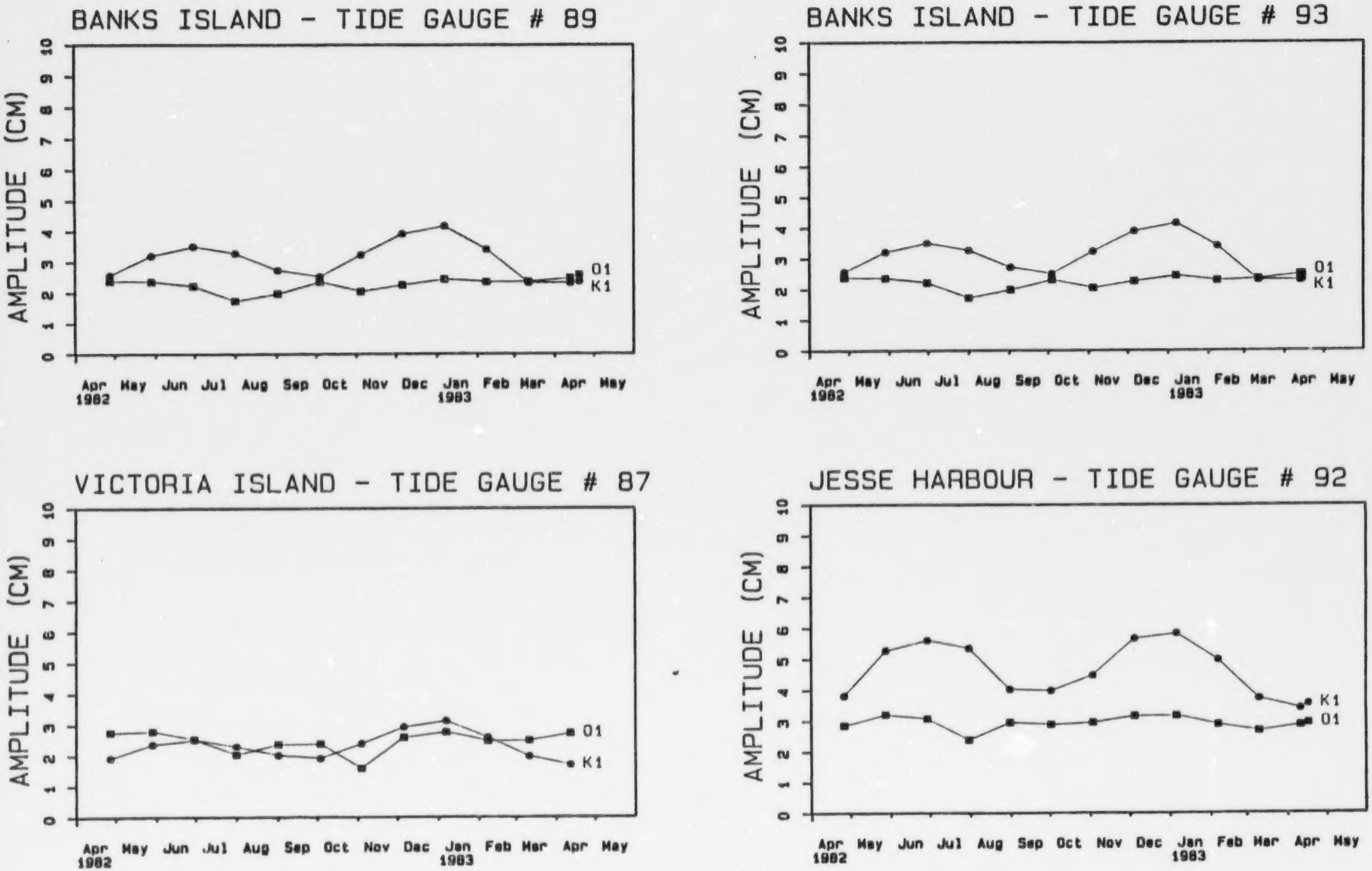

Figure 3.1.2. Time series of the amplitude of the major diurnal tidal constituents at four stations in Prince of Wales Strait. Inference has not been used.

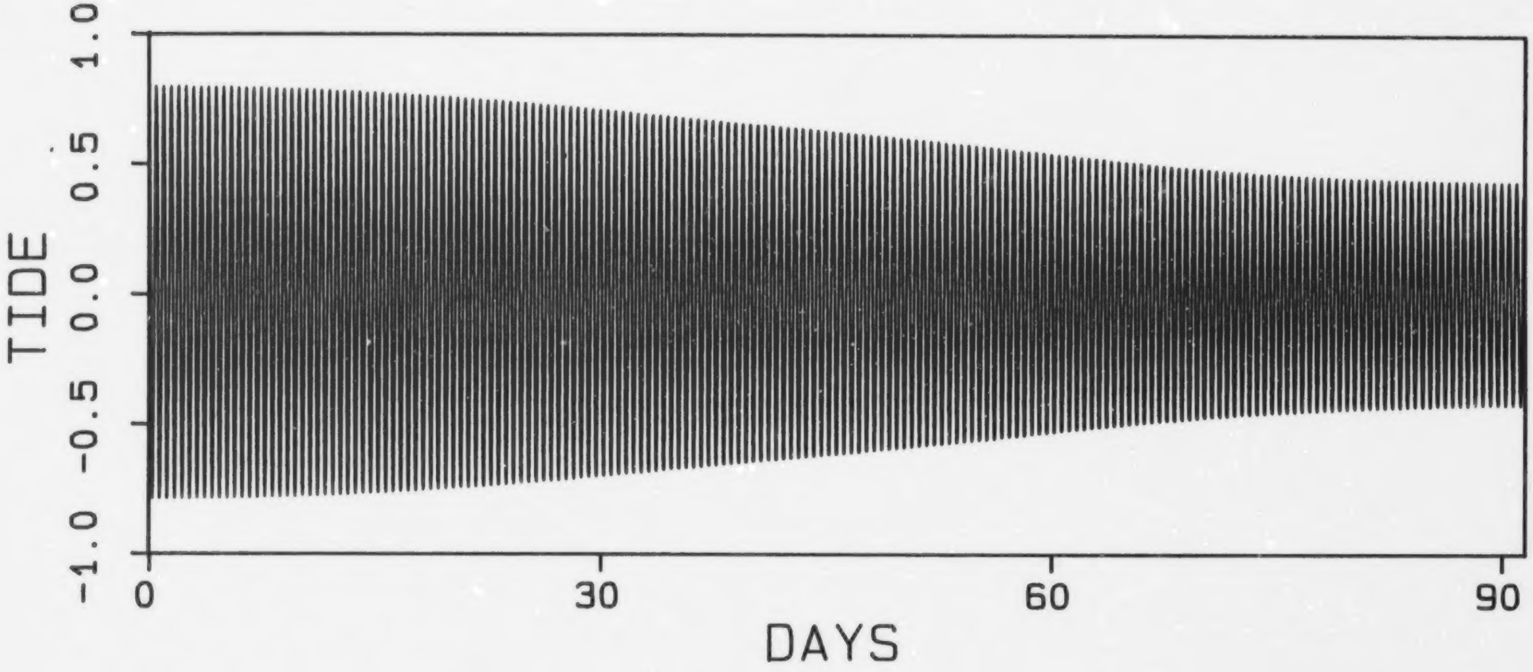

Figure 3.1.3. A synthetic time series of S_2 and K_2 tides over a three month period.

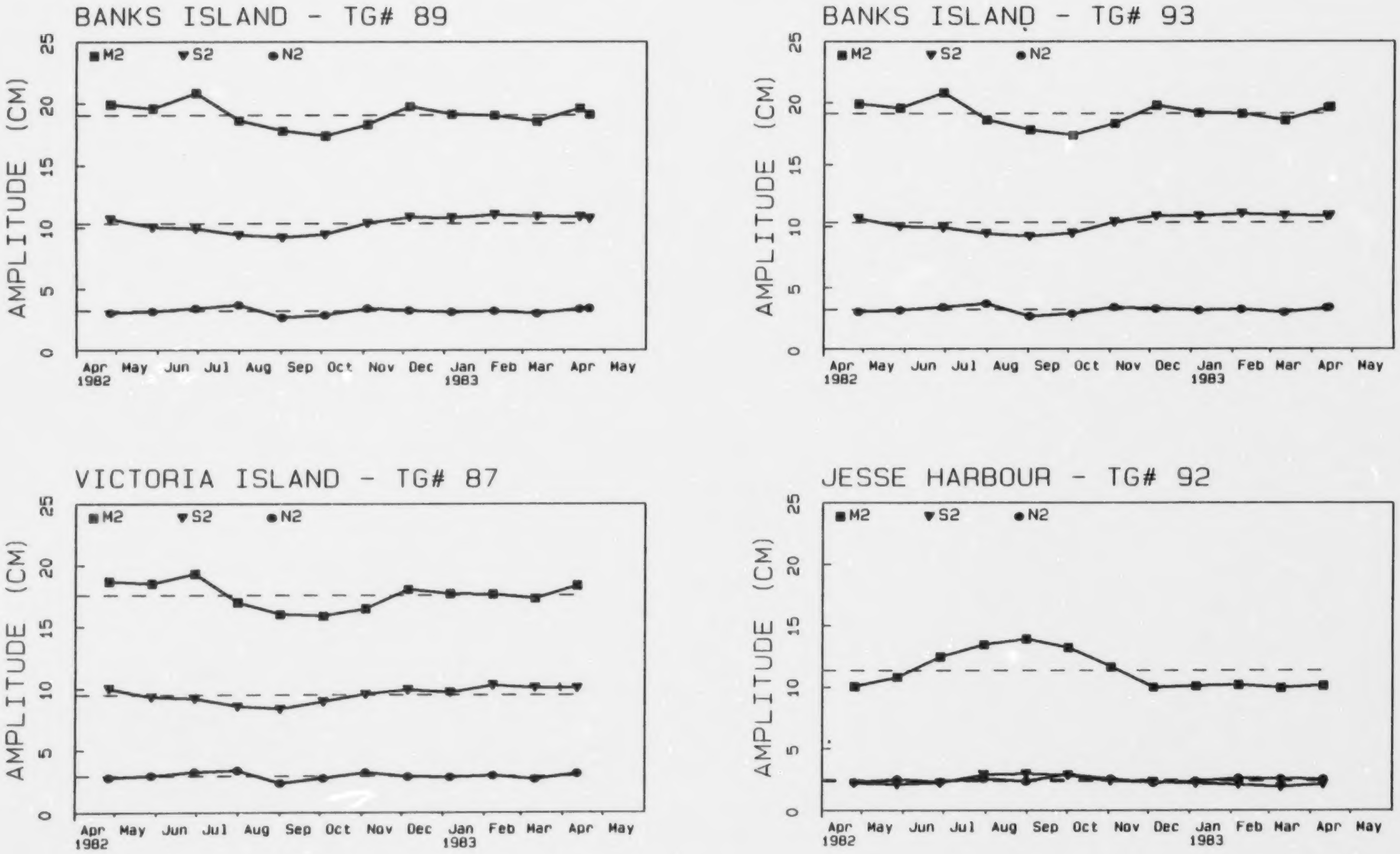

Figure 3.2.1 Time series of the amplitude of the major semi-diurnal constituents at four stations in Prince of Wales Strait.

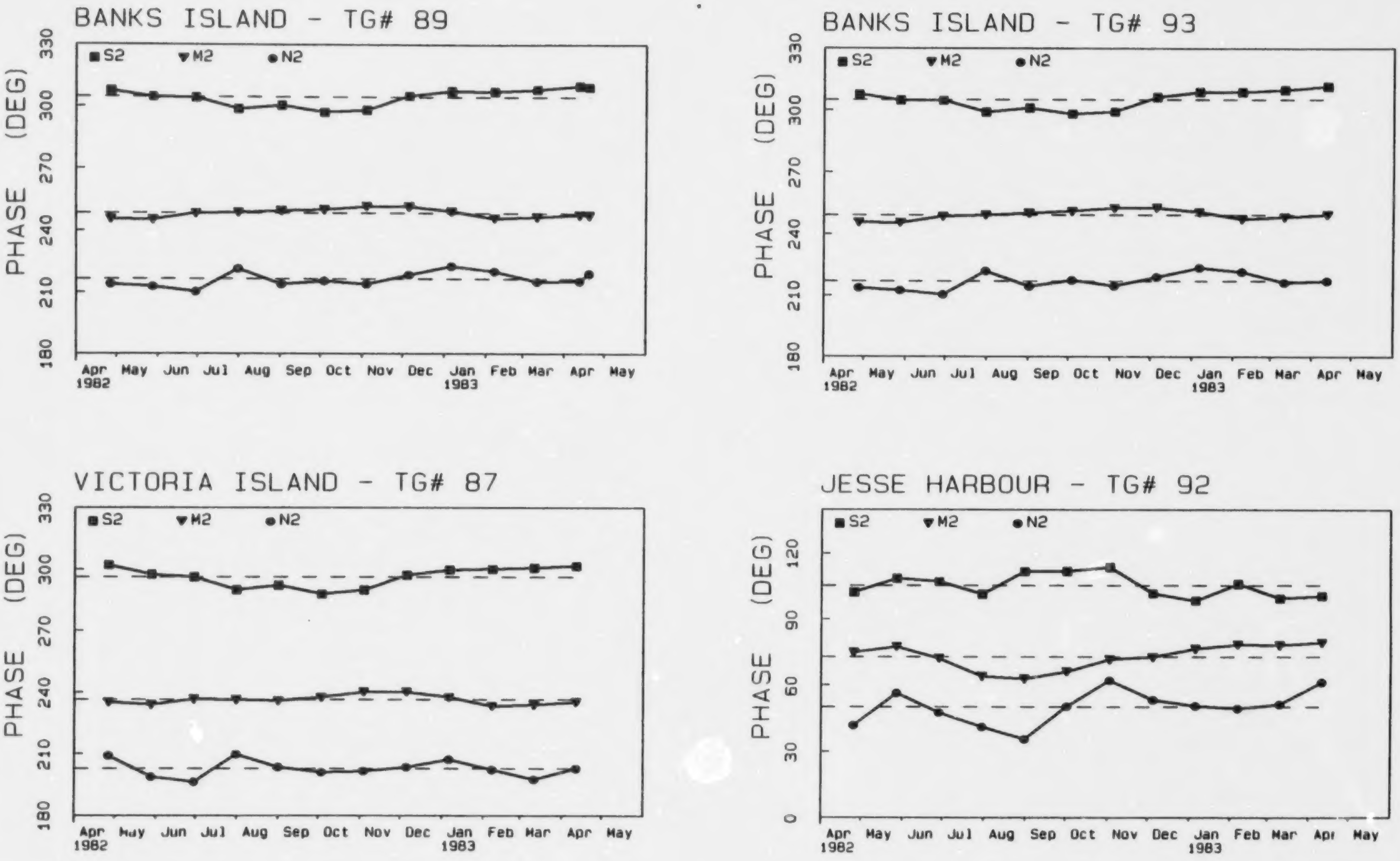

Figure 3.2.2 Time series of the phase of the major semi-diurnal constituents at four stations in Prince of Wales Strait.

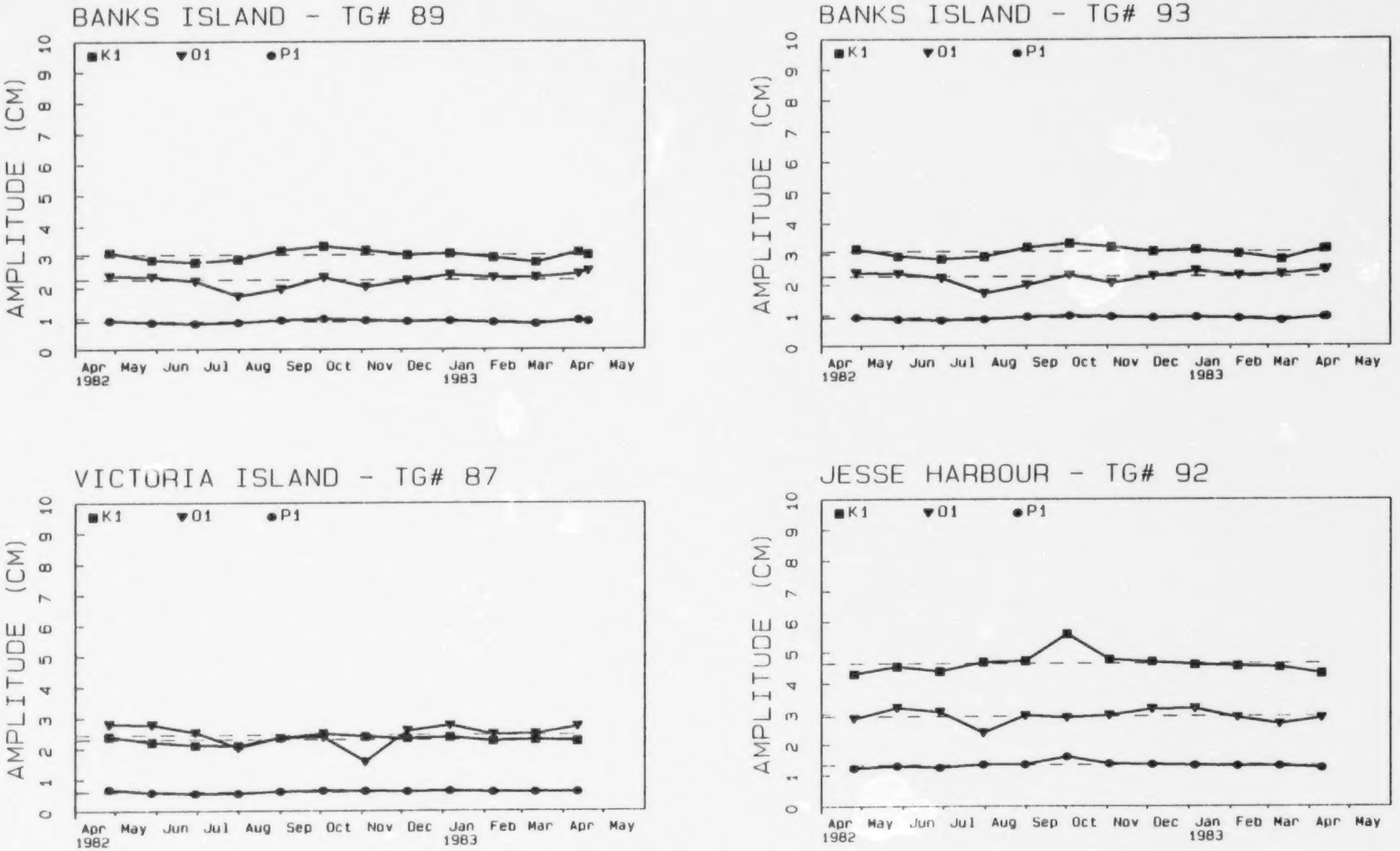

BANKS ISLAND - TG# 89

BANKS ISLAND - TG# 93

VICTORIA ISLAND - TG# 87

JESSE HARBOUR - TG# 92

Figure 3.2.3 Time series of the amplitude of the major diurnal constituents at four stations in Prince of Wales Strait.

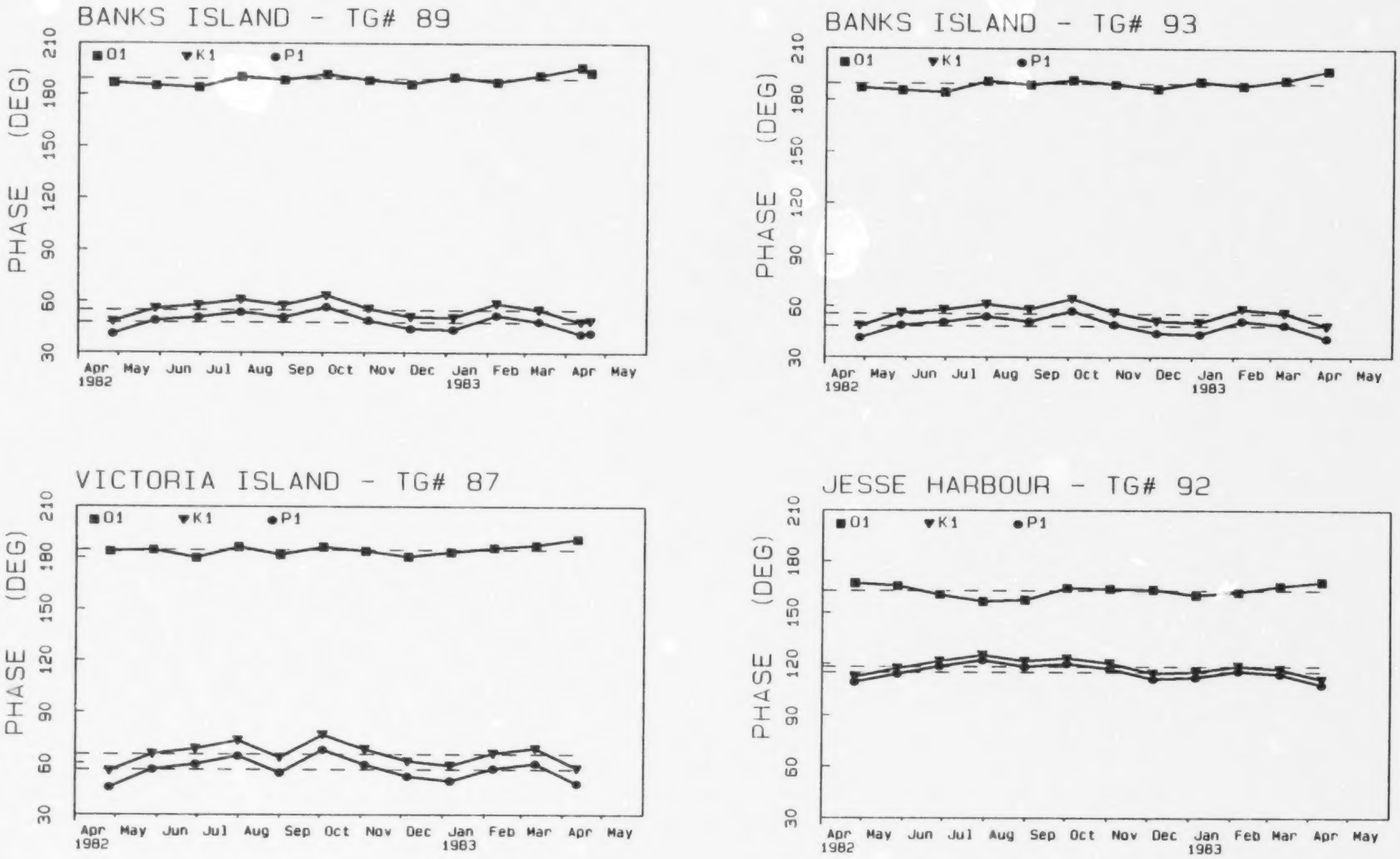

Figure 3.2.4 Time series of the phase of the major diurnal constituents at four stations in Prince of Wales Strait.

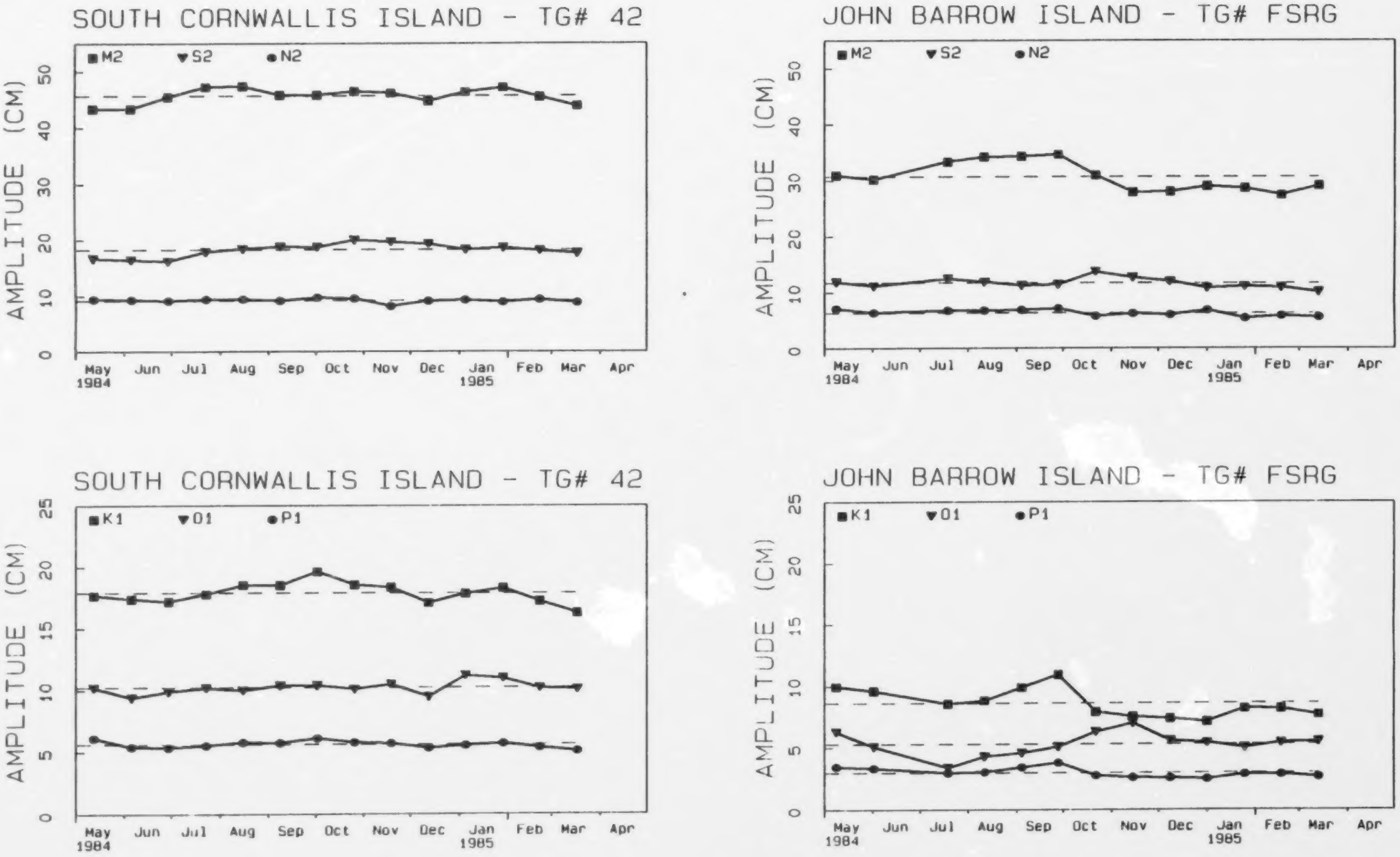

Figure 3.2.5 Time series of the amplitude of the major diurnal and semi-diurnal constituents at stations in Barrow Strait and Penny Strait.

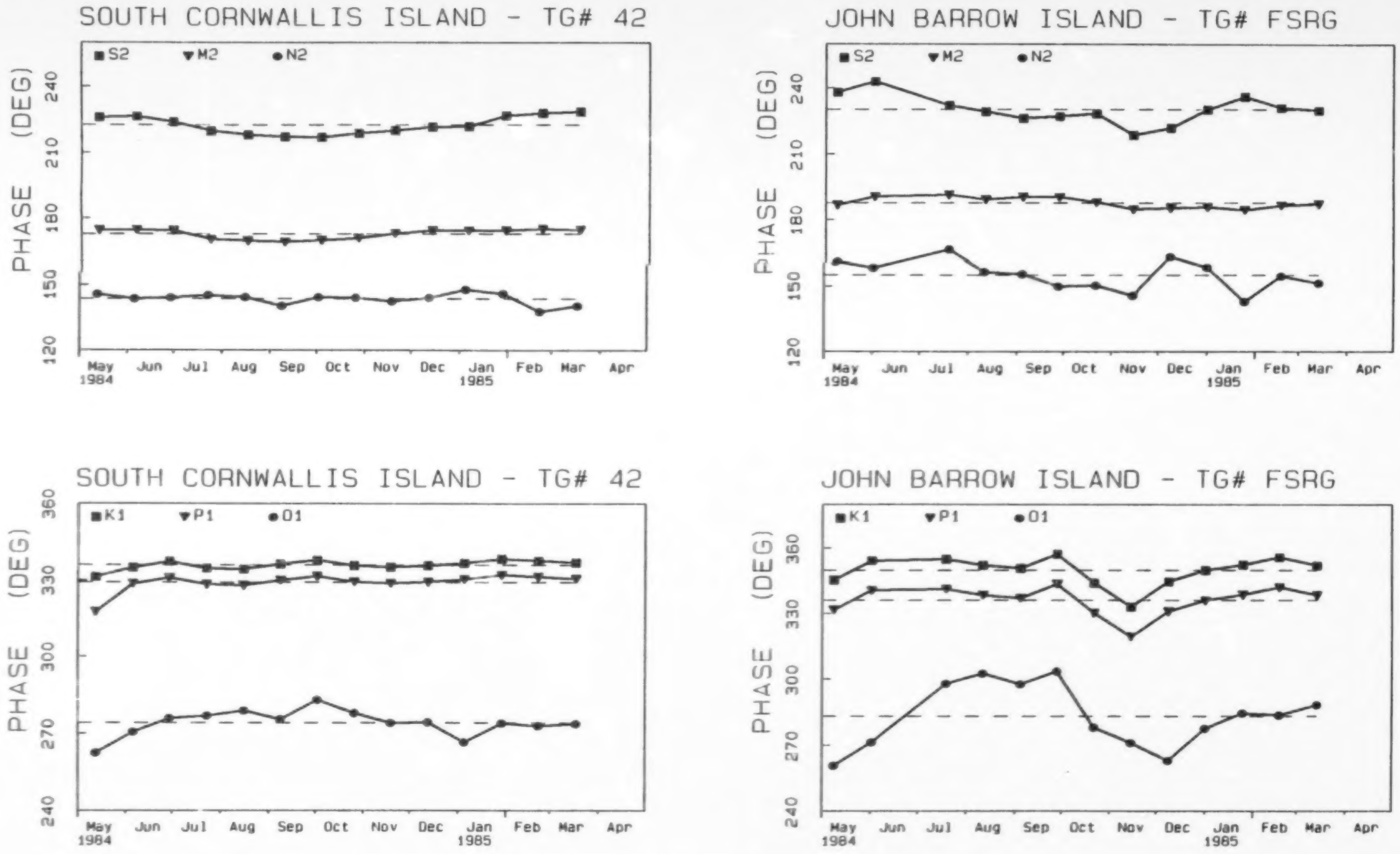

Figure 3.2.6 Time series of the phase of the major diurnal and semi-diurnal constituents at stations in Barrow Strait and Penny Strait.

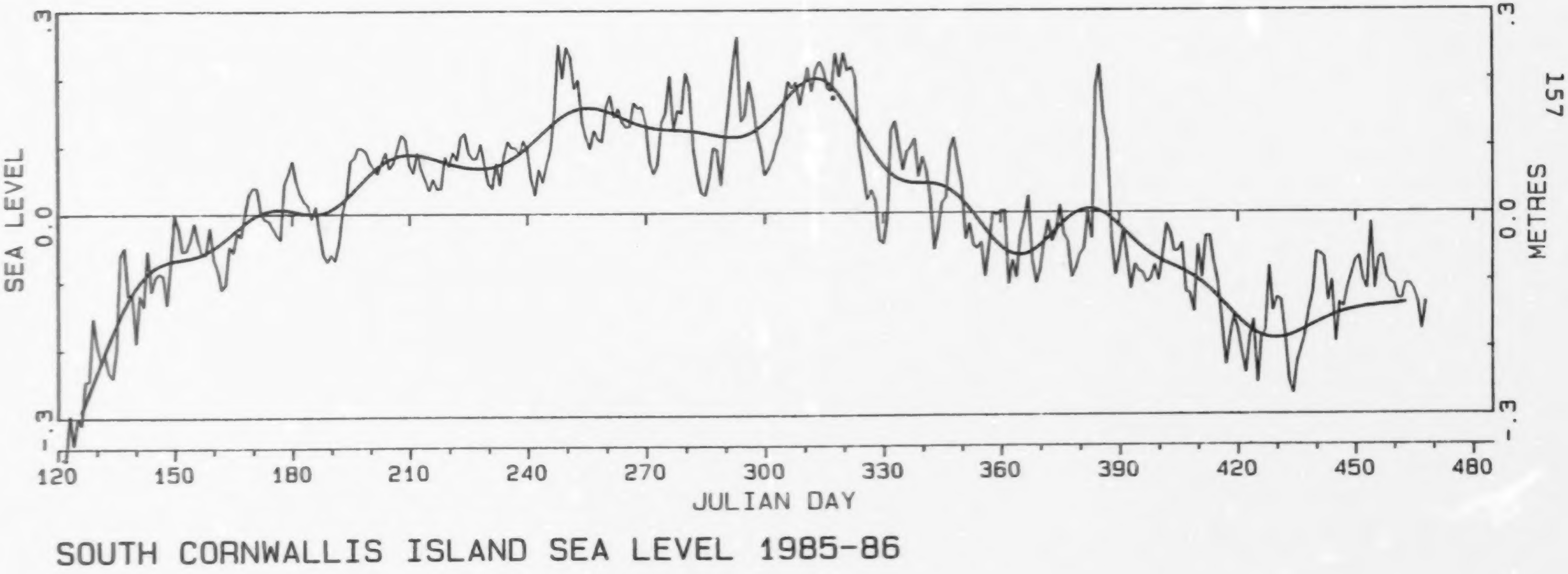

Figure 3.2.7 Low-pass filtered sea level data for station 42 in Barrow Strait for 1984-85.

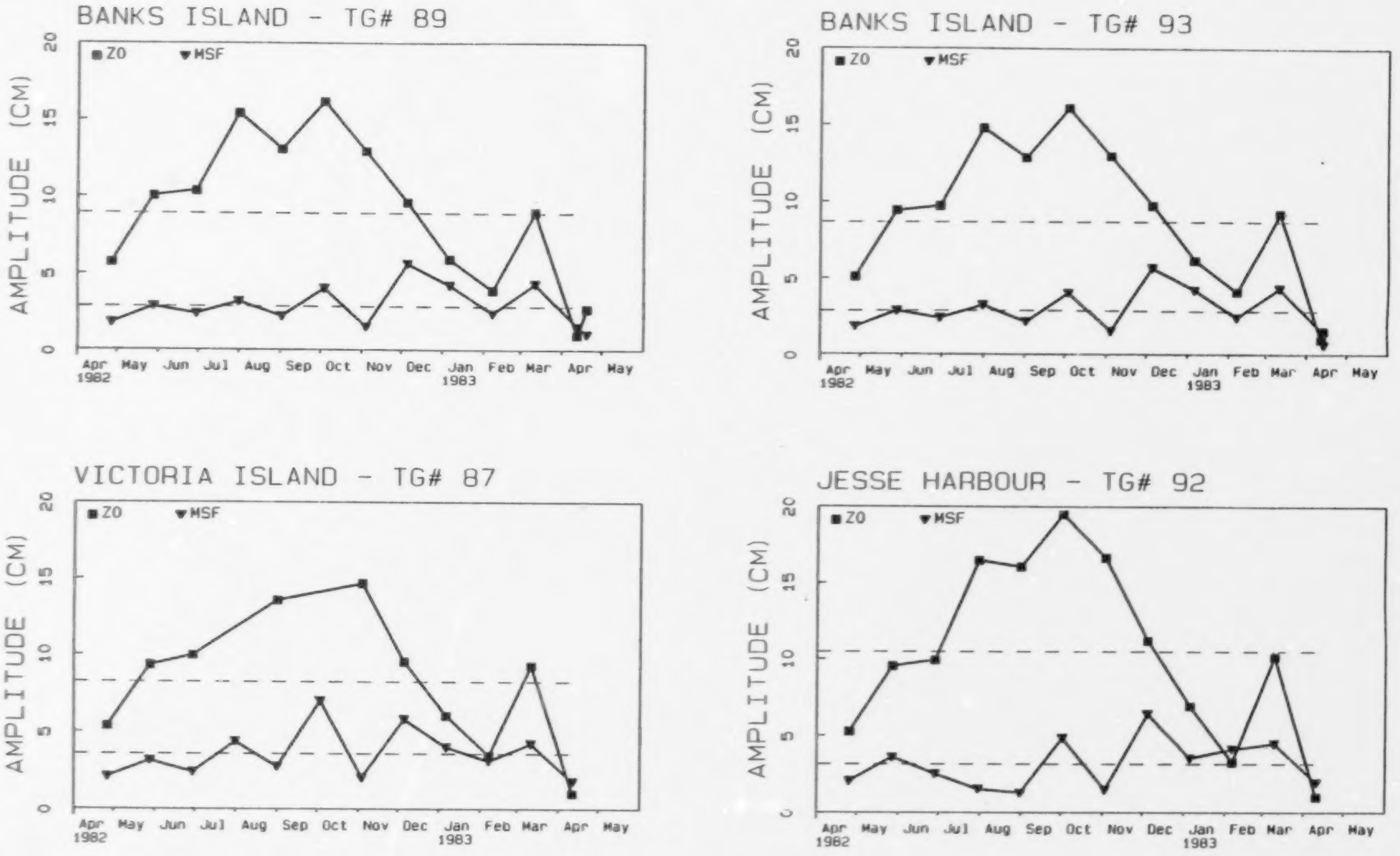

Figure 3.2.8 Time series of the amplitude of the Z_0 and MSf constituents at four stations in Prince of Wales Strait.

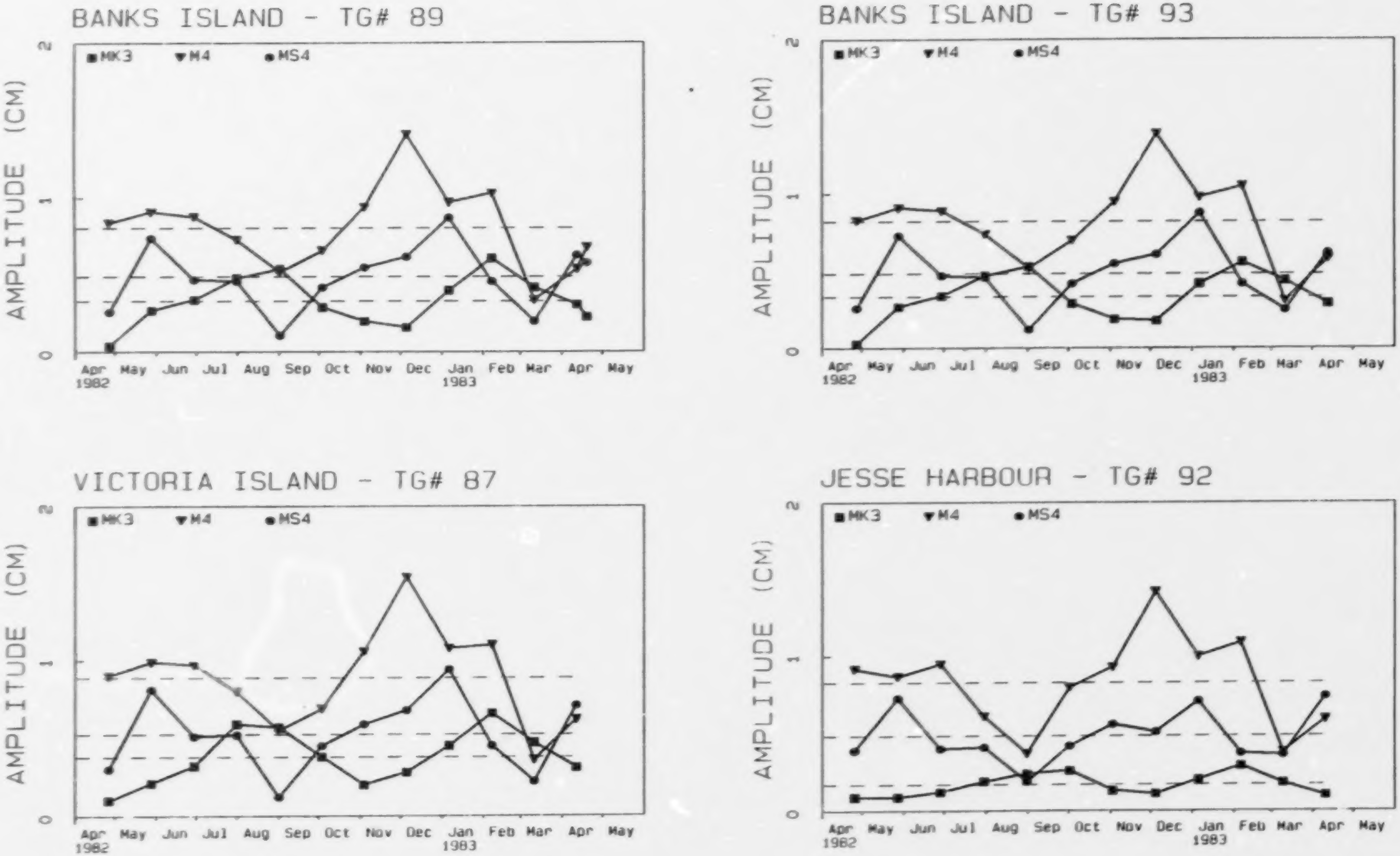

Figure 3.2.9 Time series of the amplitude of the M_4, MS_4 and MK_3 constituents at four stations in Prince of Wales Strait.

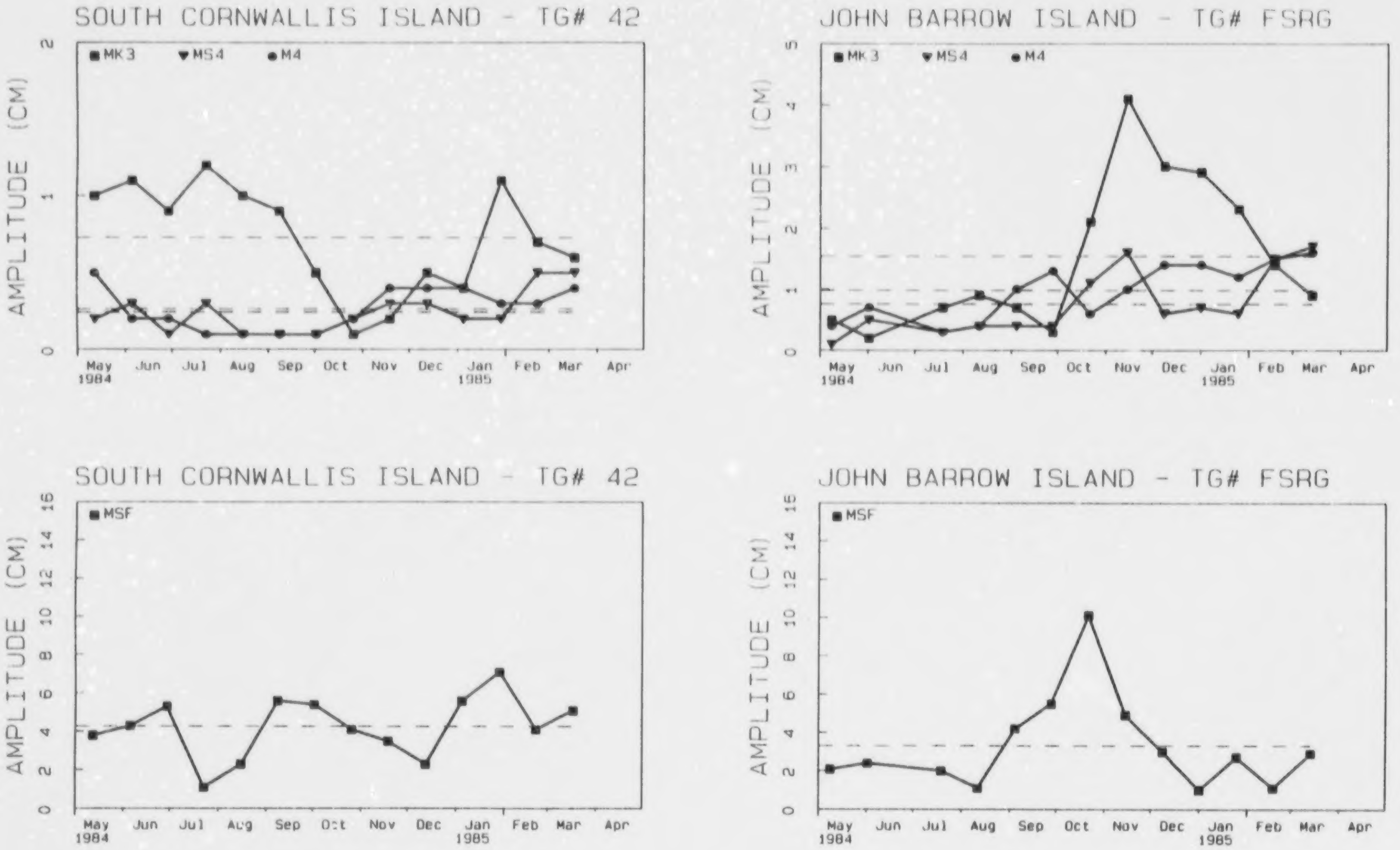

Figure 3.2.10 Time series of the amplitude of the MSf, M_4, MS_4 and MK_3 constituents at stations in Barrow Strait and Penny Strait.

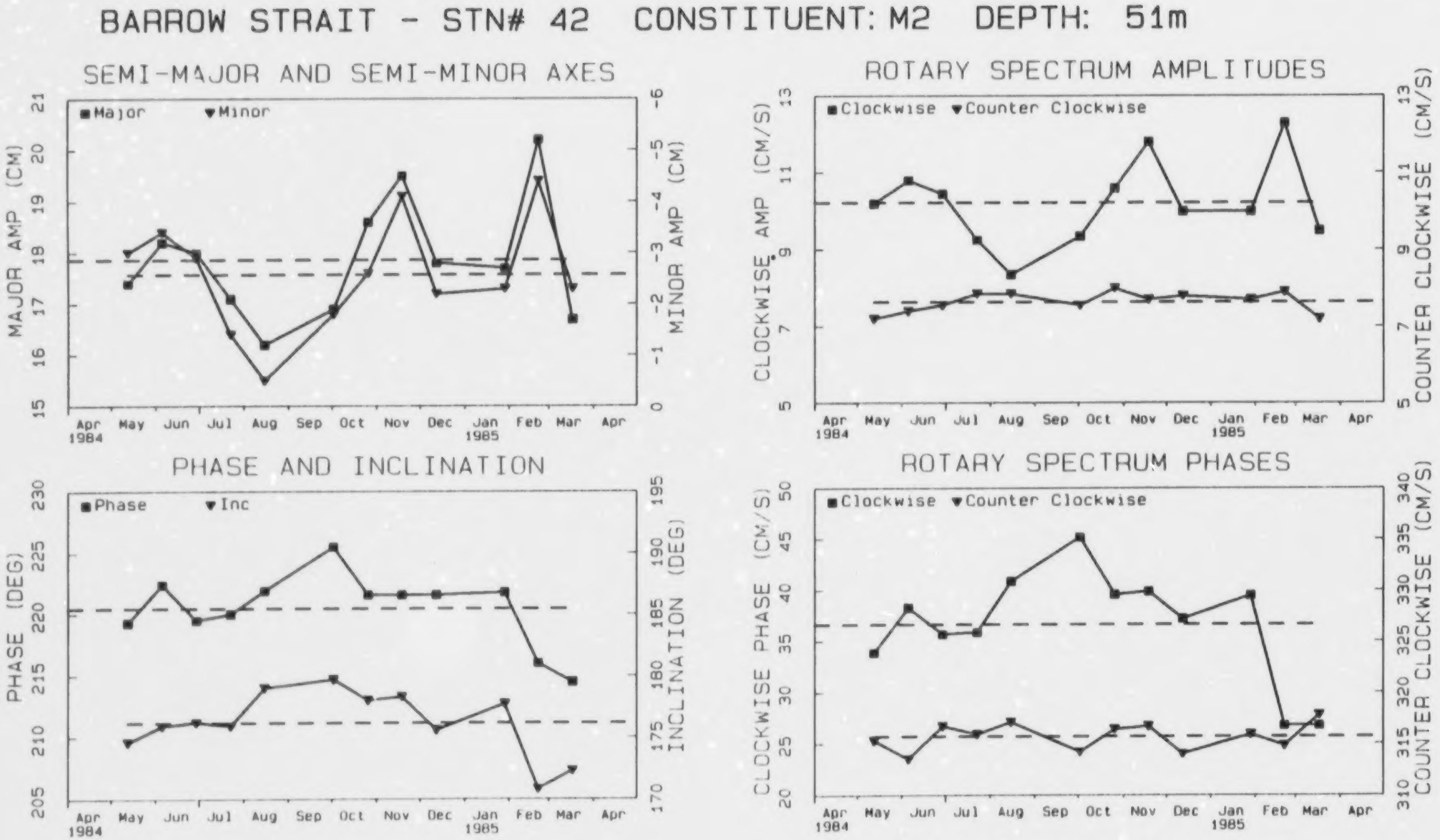

Figure 3.3.1. Time series of the M_2 ellipse parameters (major and minor amplitudes, inclination and phase), and the rotary spectral parameters (amplitudes and phase of clockwise and counter-clockwise components) at Station 42, Barrow Strait at 51 m.

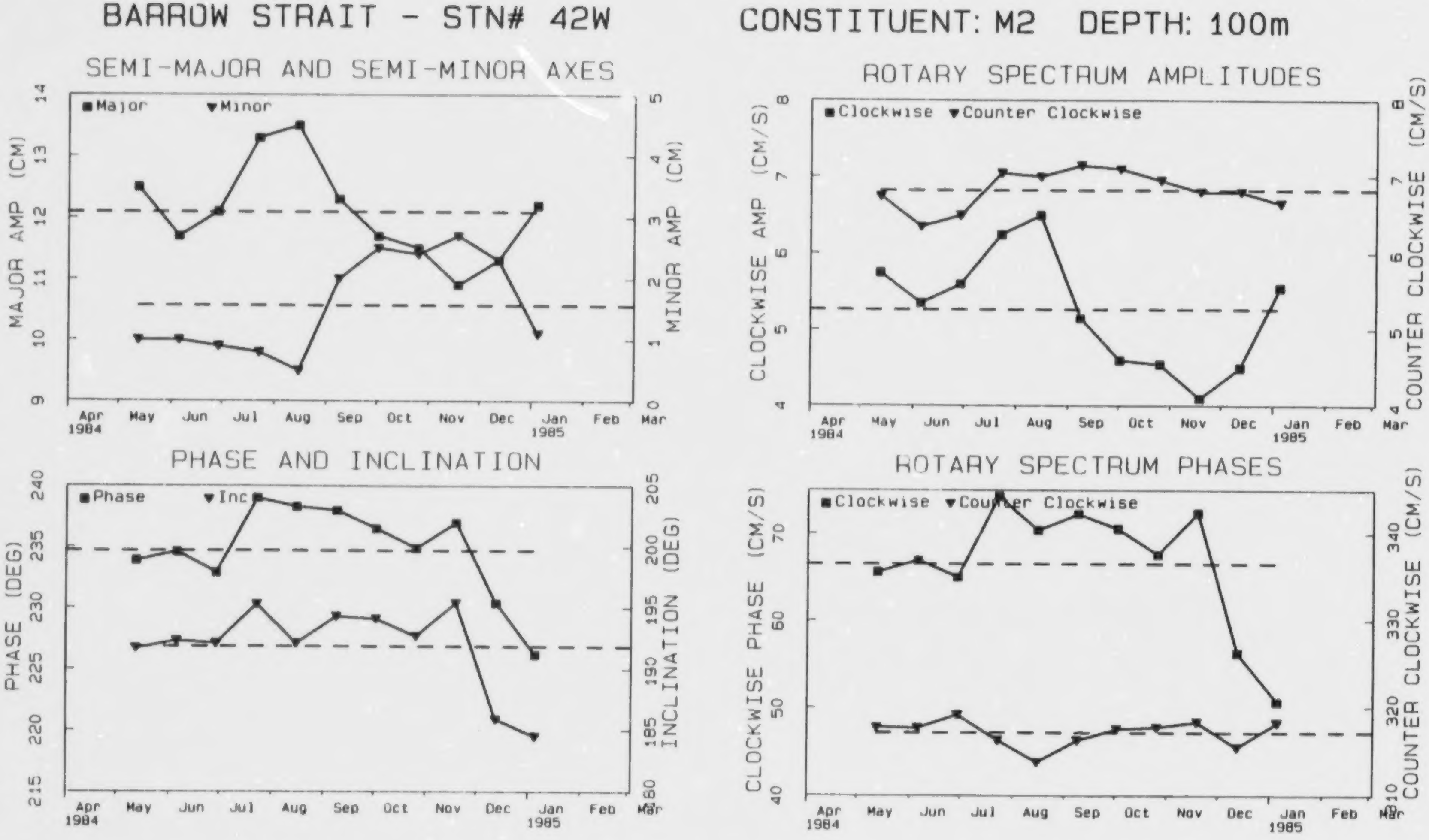

Figure 3.3.2. Time series of the M_2 ellipse parameters (major and minor amplitudes, inclination and phase), and the rotary spectral parameters (amplitudes and phase of clockwise and counter-clockwise components) at Station 42, Barrow Strait at 100 m.

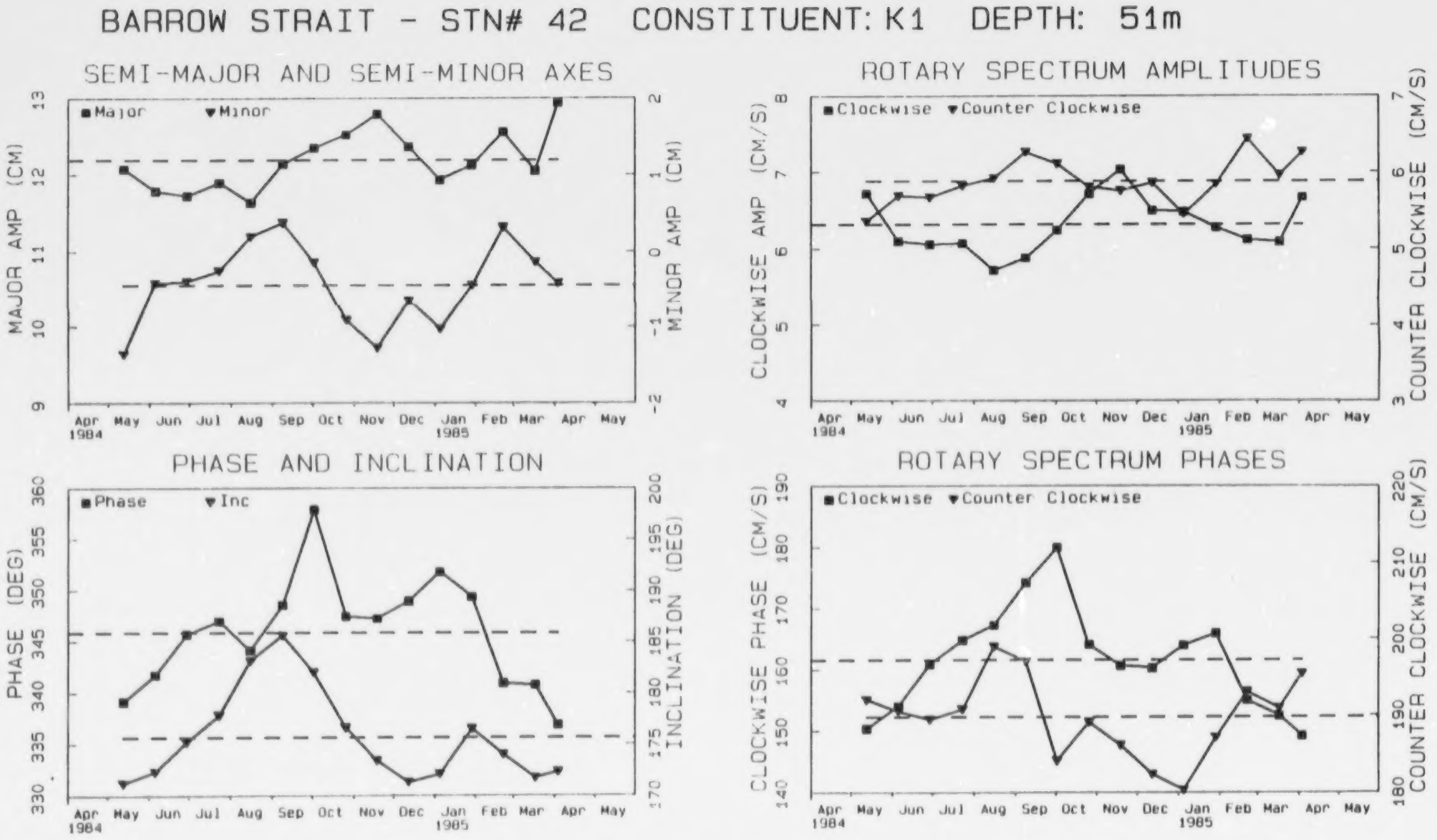

Figure 3.3.3. Time series of the K_1 ellipse parameters (major and minor amplitudes, inclination and phase), and the rotary spectral parameters (amplitudes and phase of clockwise and counter-clockwise components) at Station 42, Barrow Strait at 51 m.

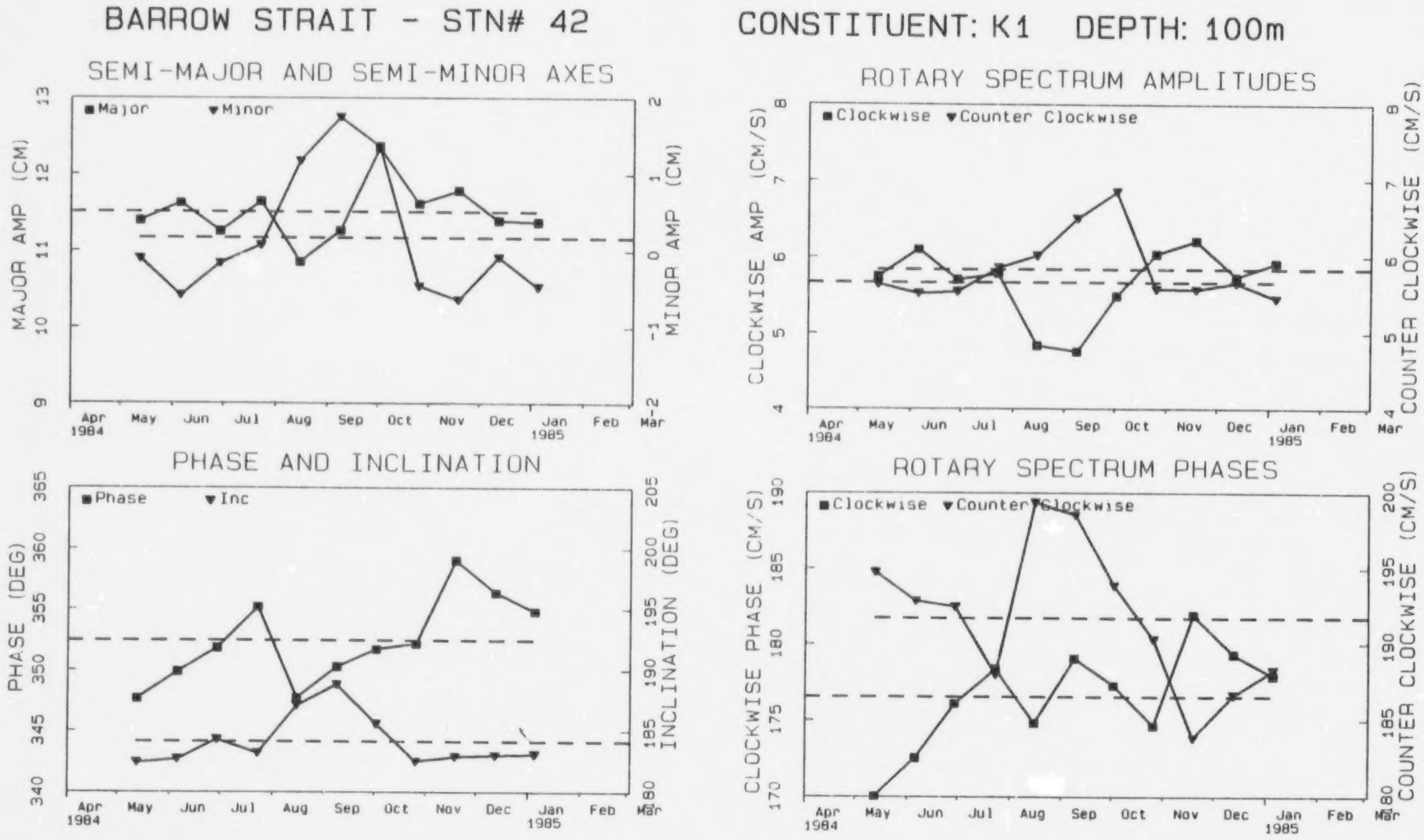

Figure 3.3.4. Time series of the K_1 ellipse parameters (major and minor amplitudes, inclination and phase), and the rotary spectral parameters (amplitudes and phase of clockwise and counter-clockwise components) at Station 42, Barrow Strait at 100 m.

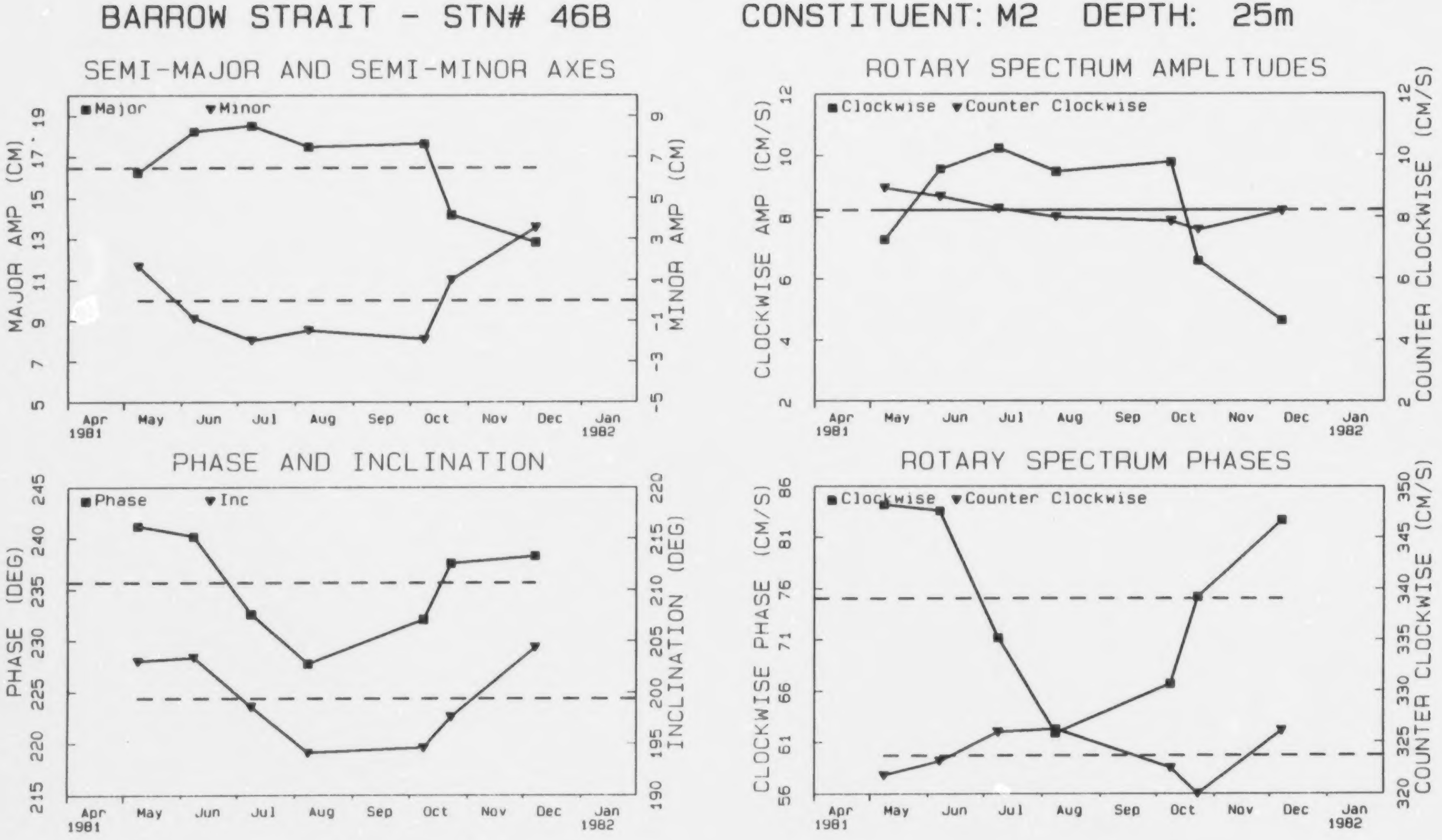

Figure 3.3.5. Time series of the M_2 ellipse parameters (major and minor amplitudes, inclination and phase), and the rotary spectral parameters (amplitudes and phase of clockwise and counter-clockwise components) at Station 46, Barrow Strait at 25 m.

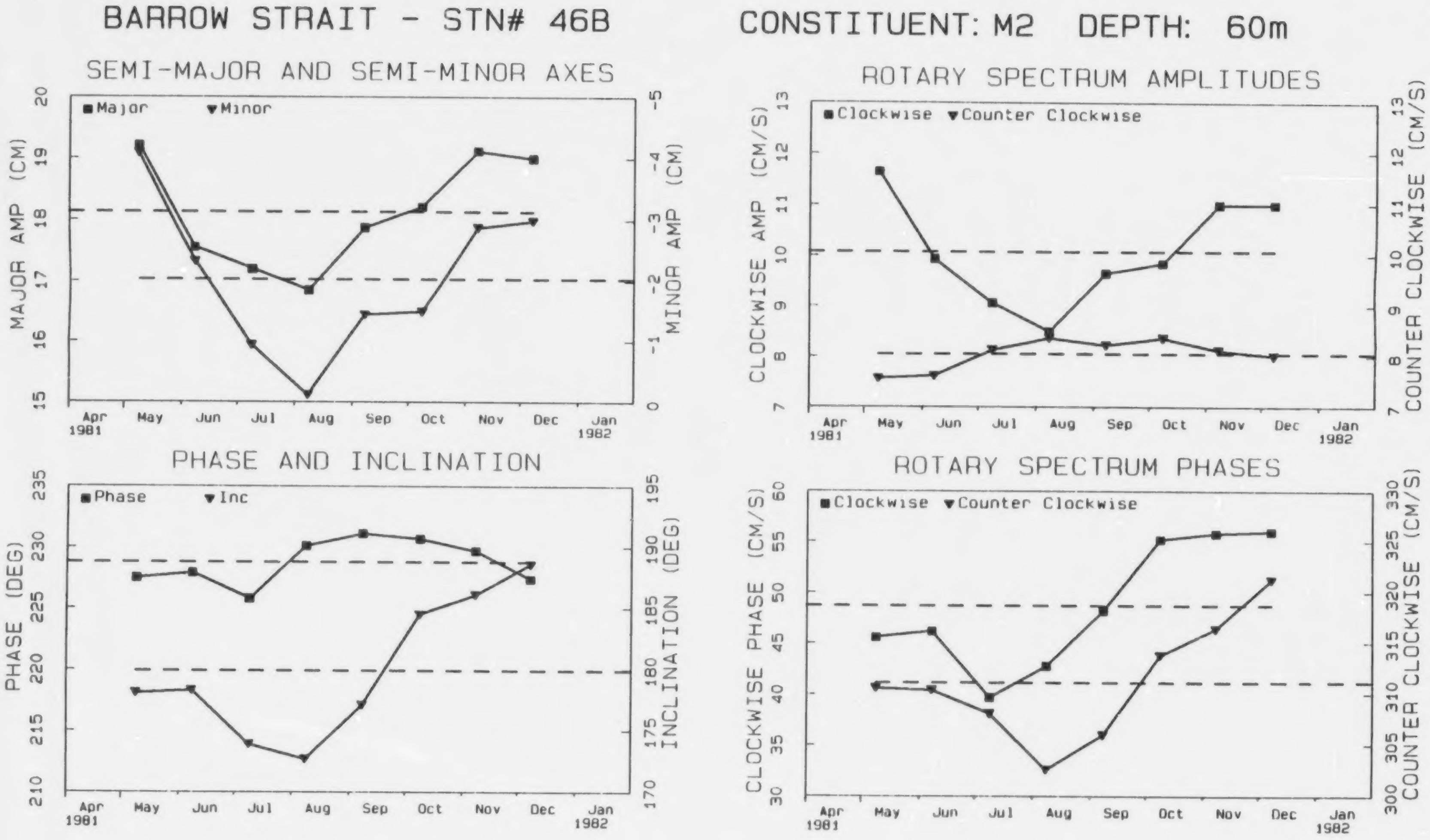

Figure 3.3.6. Time series of the M_2 ellipse parameters (major and minor amplitudes, inclination and phase), and the rotary spectral parameters (amplitudes and phase of clockwise and counter-clockwise components) at Station 46, Barrow Strait at 60 m.

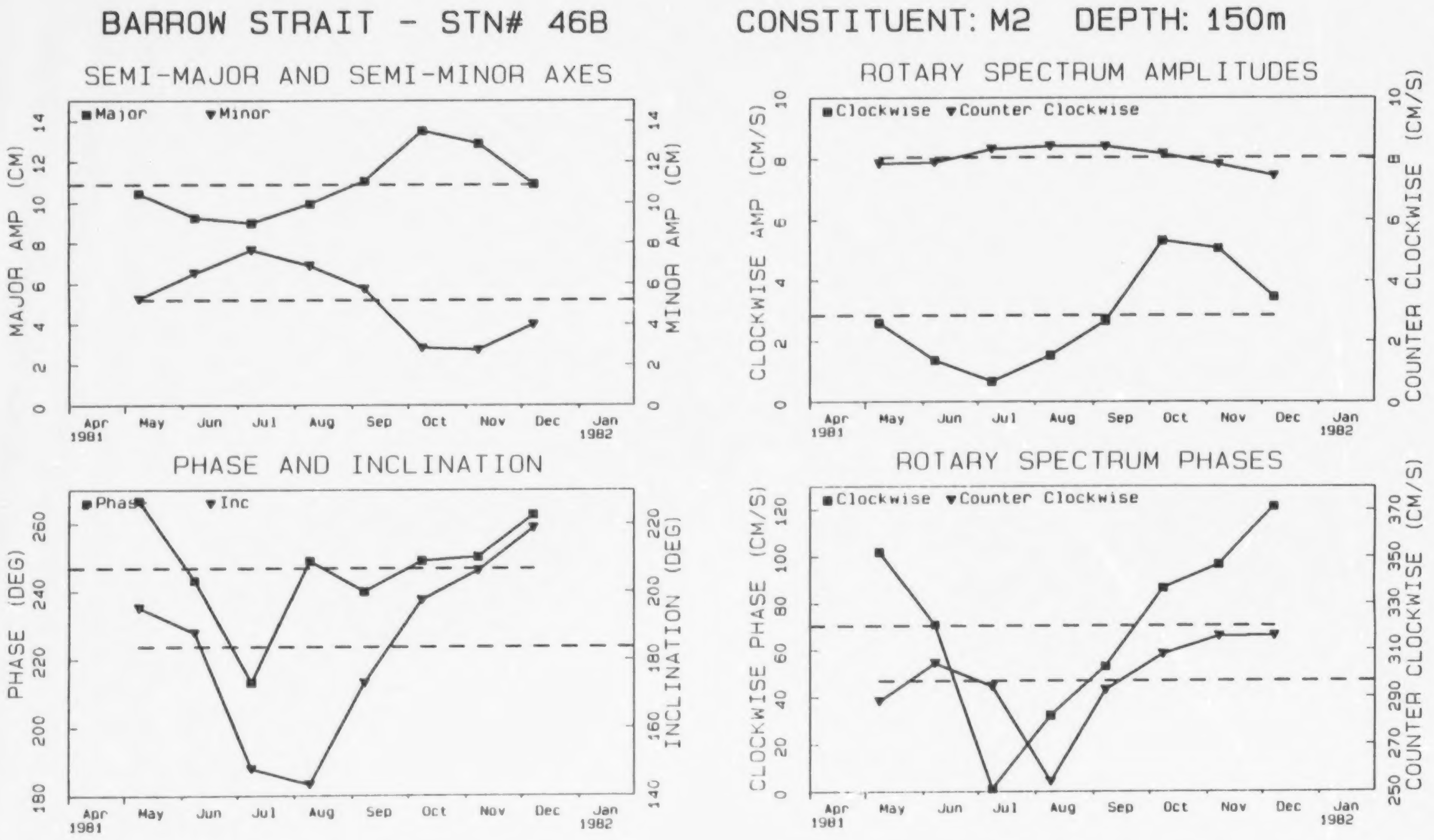

Figure 3.3.7. Time series of the M_2 ellipse parameters (major and minor amplitudes, inclination and phase), and the rotary spectral parameters (amplitudes and phase of clockwise and counter-clockwise components) at Station 46, Barrow Strait at 150 m.

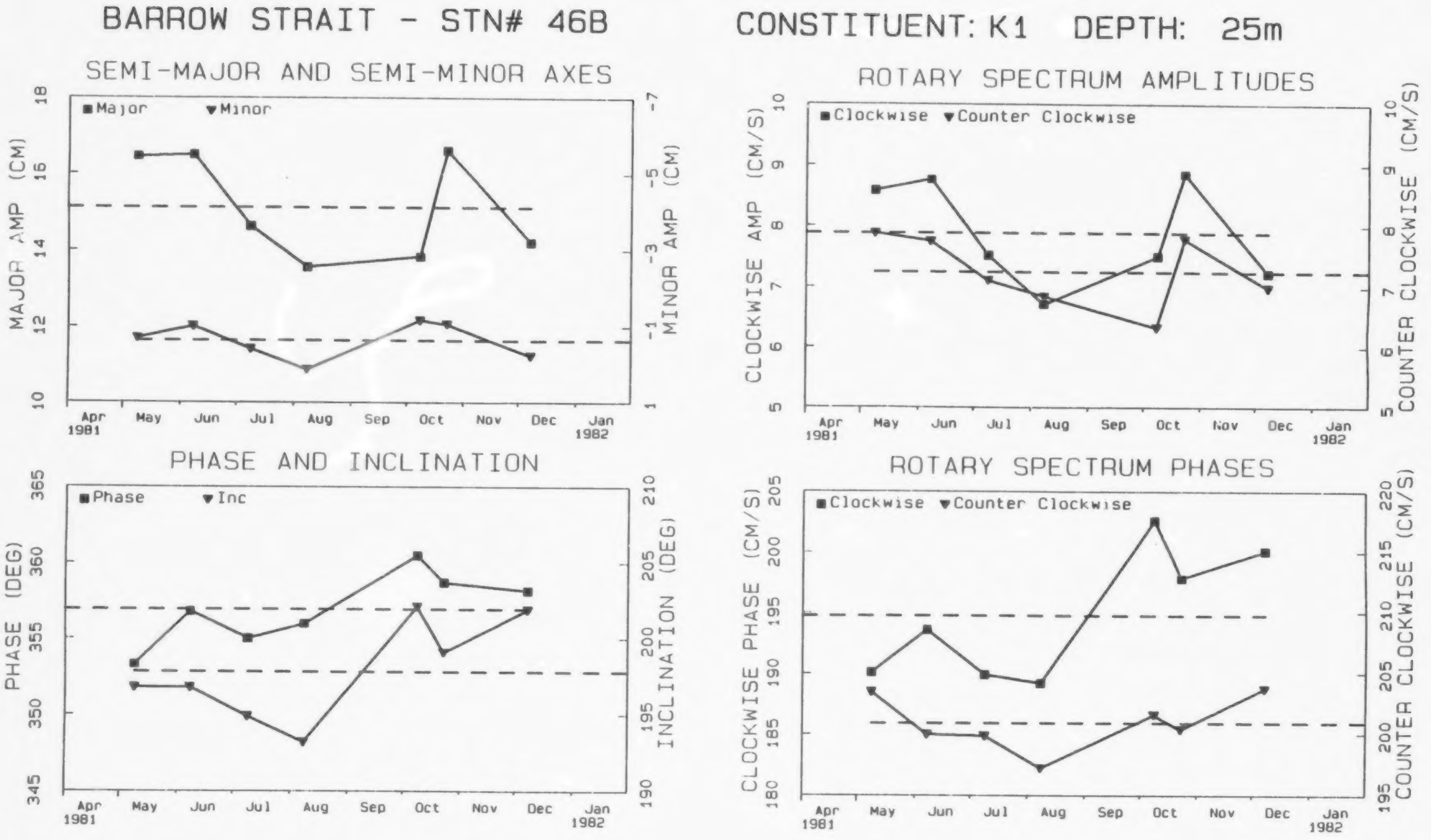

Figure 3.3.8. Time series of the K_1 ellipse parameters (major and minor amplitudes, inclination and phase), and the rotary spectral parameters (amplitudes and phase of clockwise and counter-clockwise components) at Station 46, Barrow Strait at 25 m.

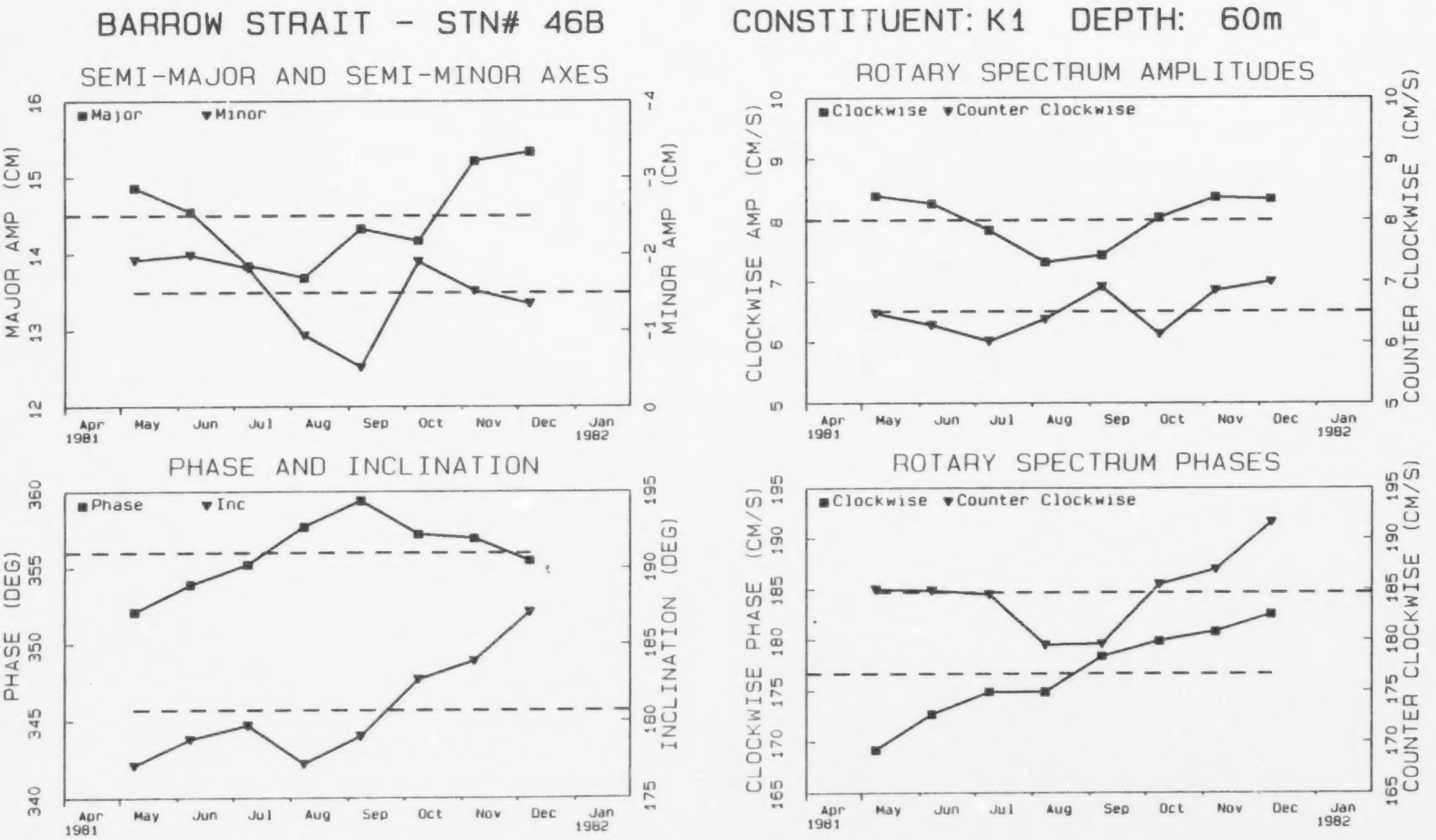

Figure 3.3.9. Time series of the K_1 ellipse parameters (major and minor amplitudes, inclination and phase), and the rotary spectral parameters (amplitudes and phase of clockwise and counter-clockwise components) at Station 46, Barrow Strait at 60 m.

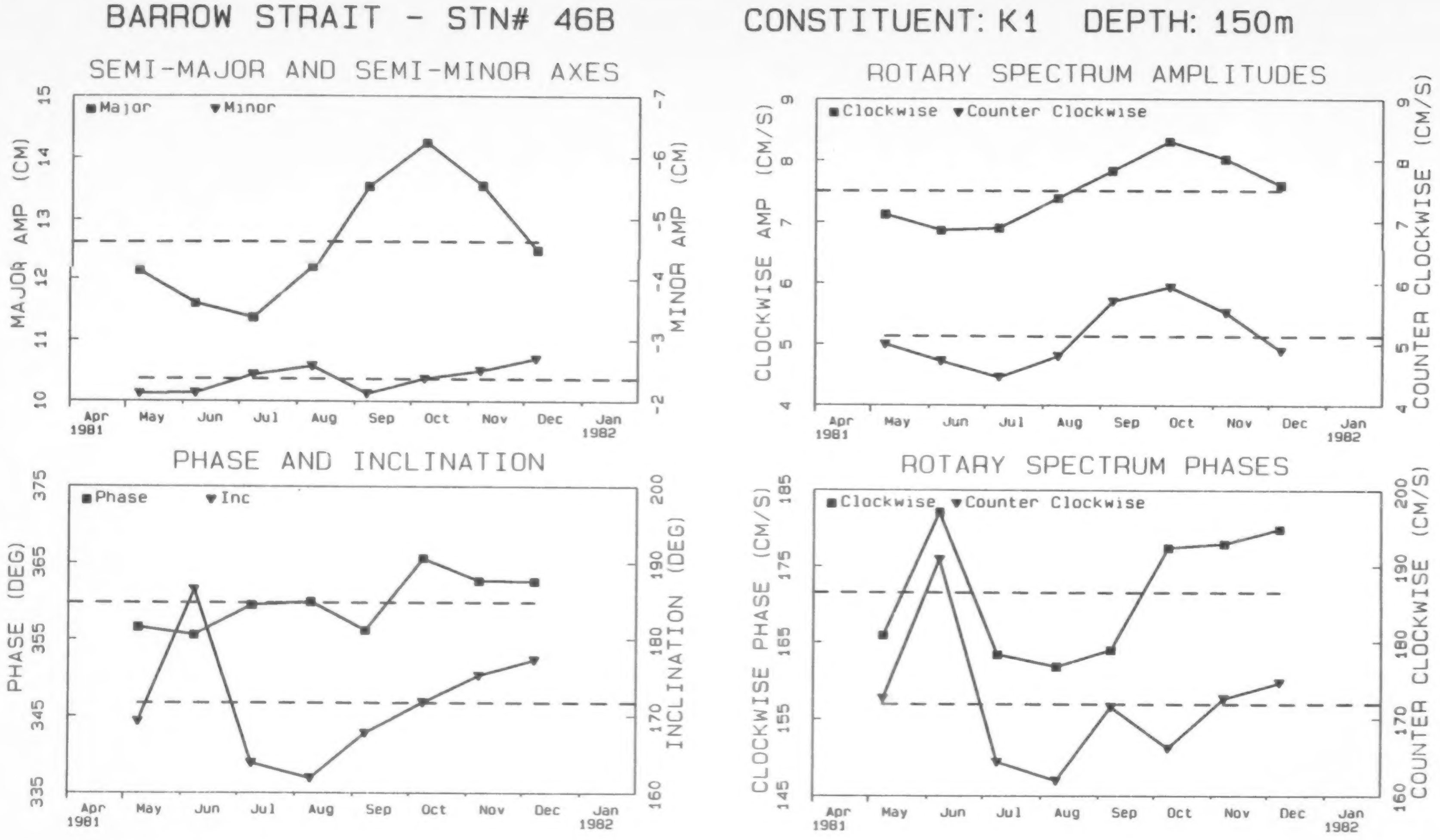

Figure 3.3.10. Time series of the K_1 ellipse parameters (major and minor amplitudes, inclination and phase), and the rotary spectral parameters (amplitudes and phase of clockwise and counter-clockwise components) at Station 46, Barrow Strait at 150 m.

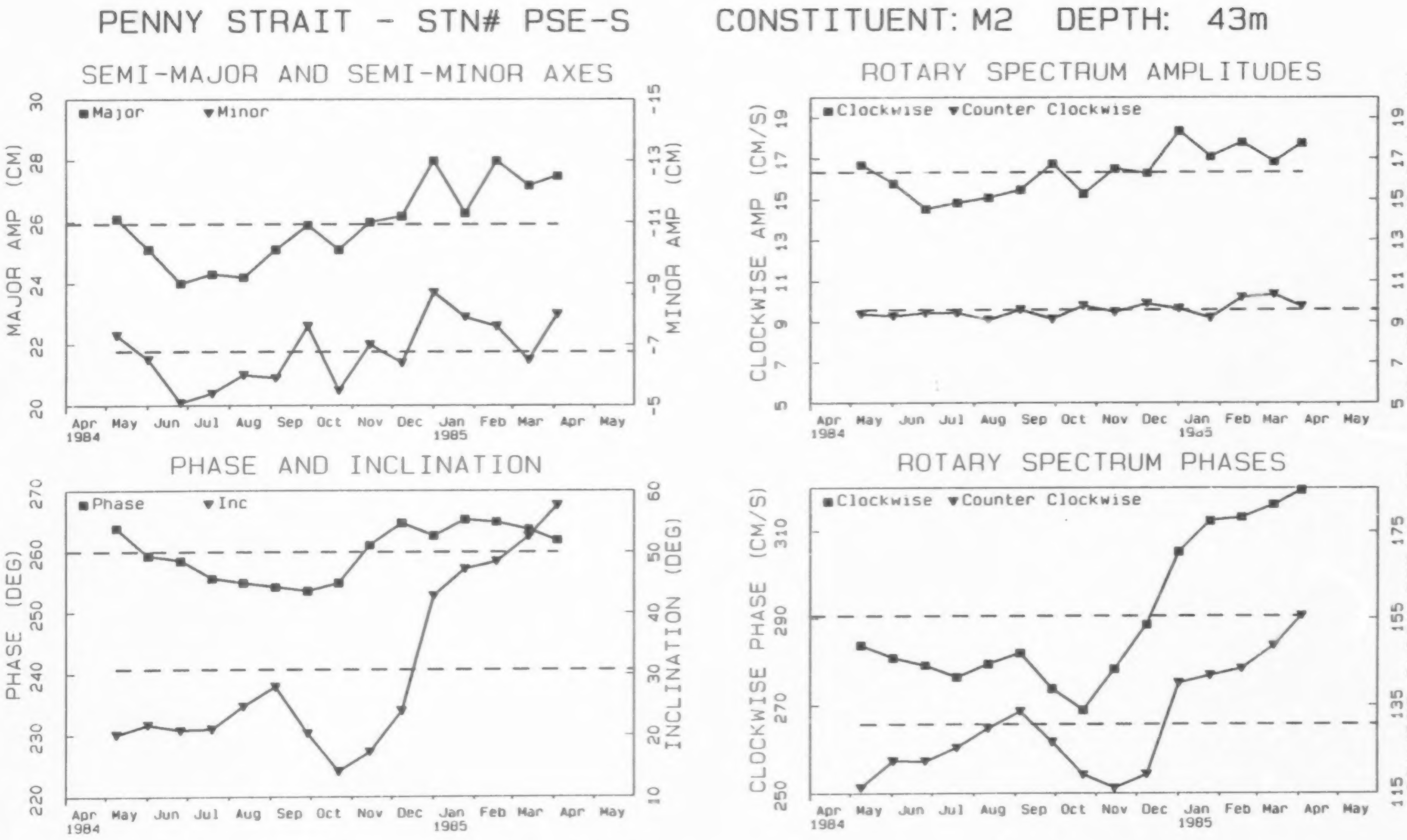

Figure 3.3.11. Time series of the M_2 ellipse parameters (major and minor amplitudes, inclination and phase), and the rotary spectral parameters (amplitudes and phase of clockwise and counter-clockwise components) at Station PSE-S, Penny Strait, at 43 m.

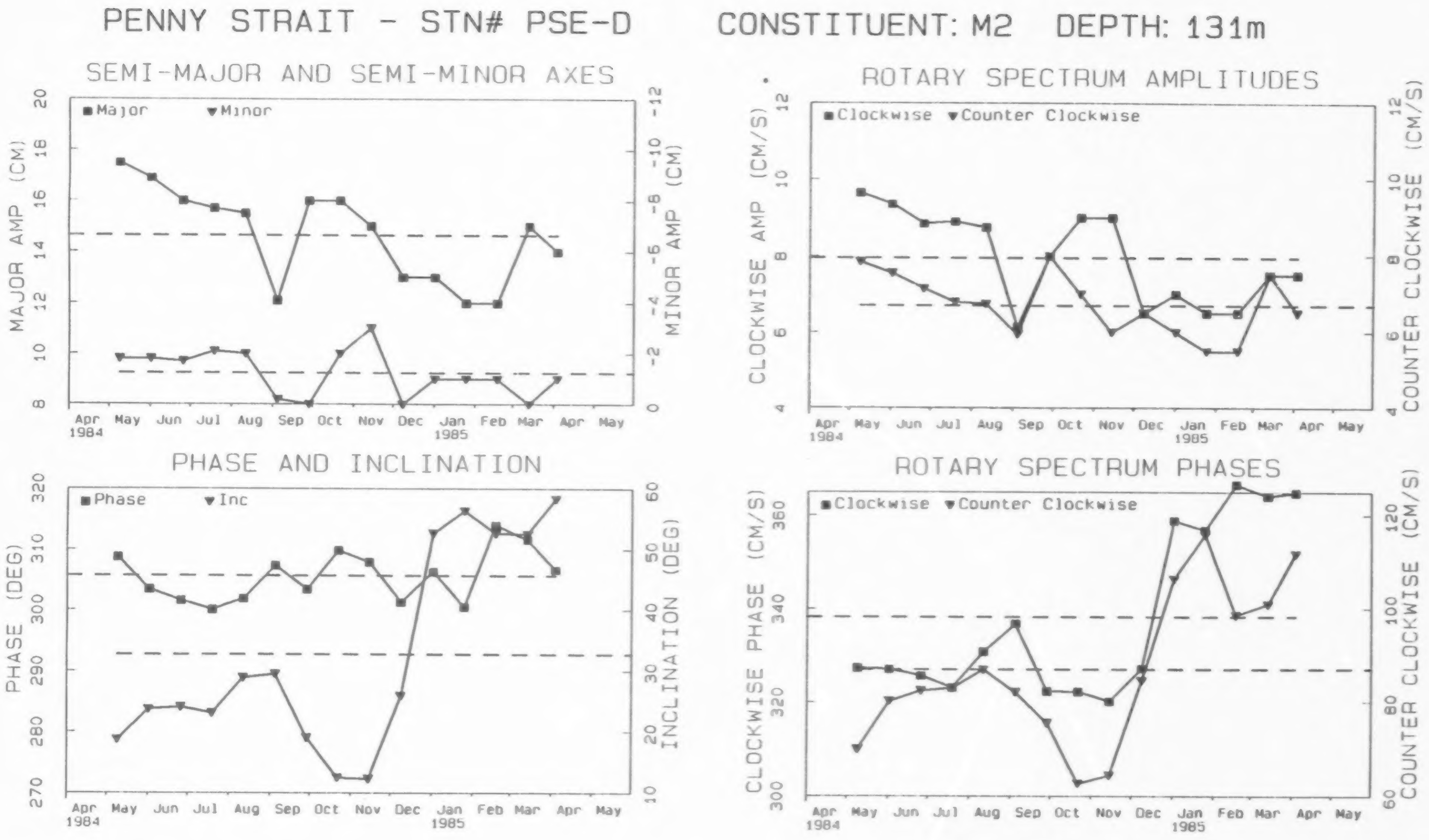

Figure 3.3.12. Time series of the M_2 ellipse parameters (major and minor amplitudes, inclination and phase), and the rotary spectral parameters (amplitudes and phase of clockwise and counter-clockwise components) at Station PSE-D, Penny Strait, at 131 m.

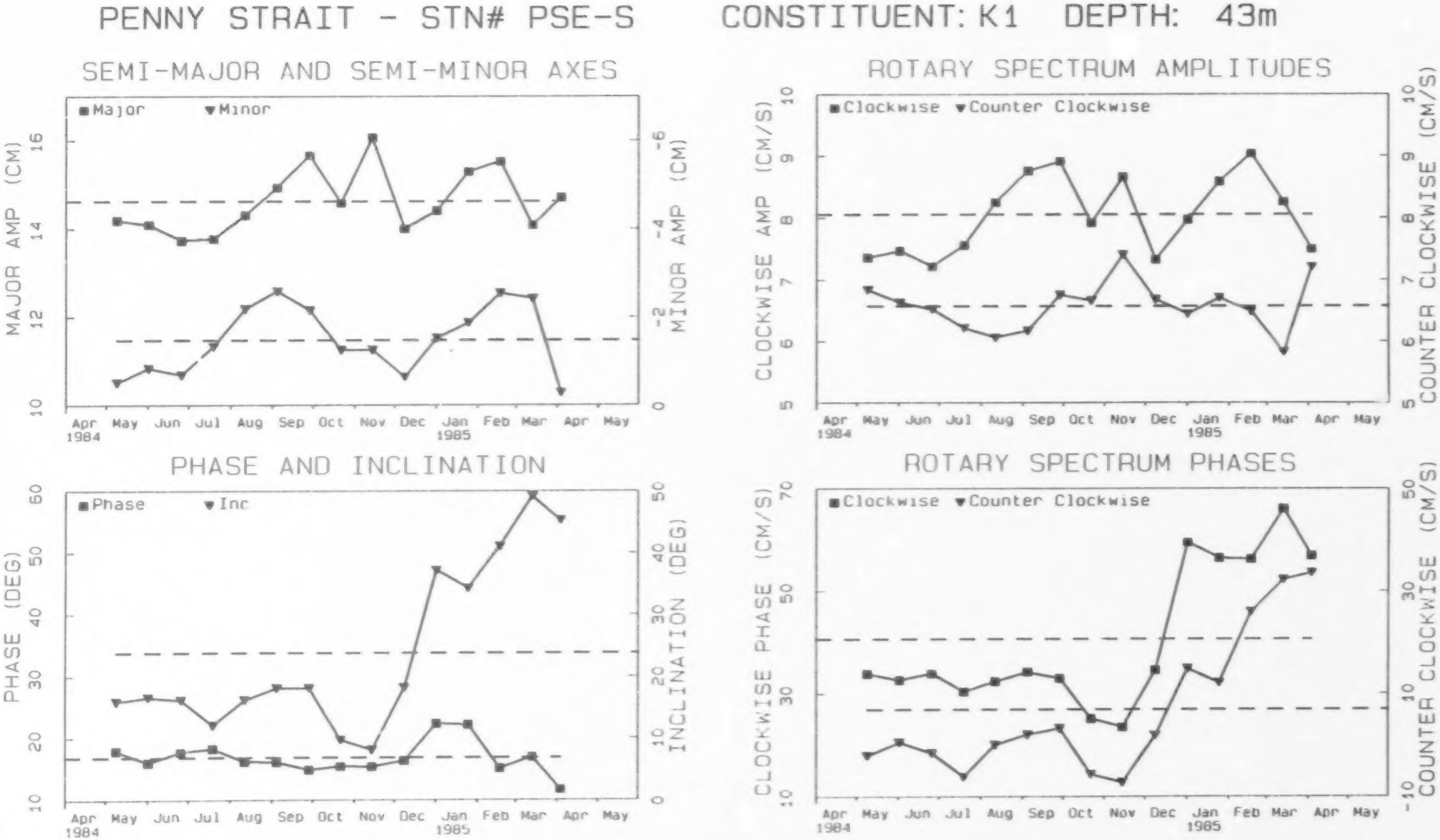

Figure 3.3.13. Time series of the K_1 ellipse parameters (major and minor amplitudes, inclination and phase), and the rotary spectral parameters (amplitudes and phase of clockwise and counter-clockwise components) at Station PSE-S, Penny Strait, at 43 m.

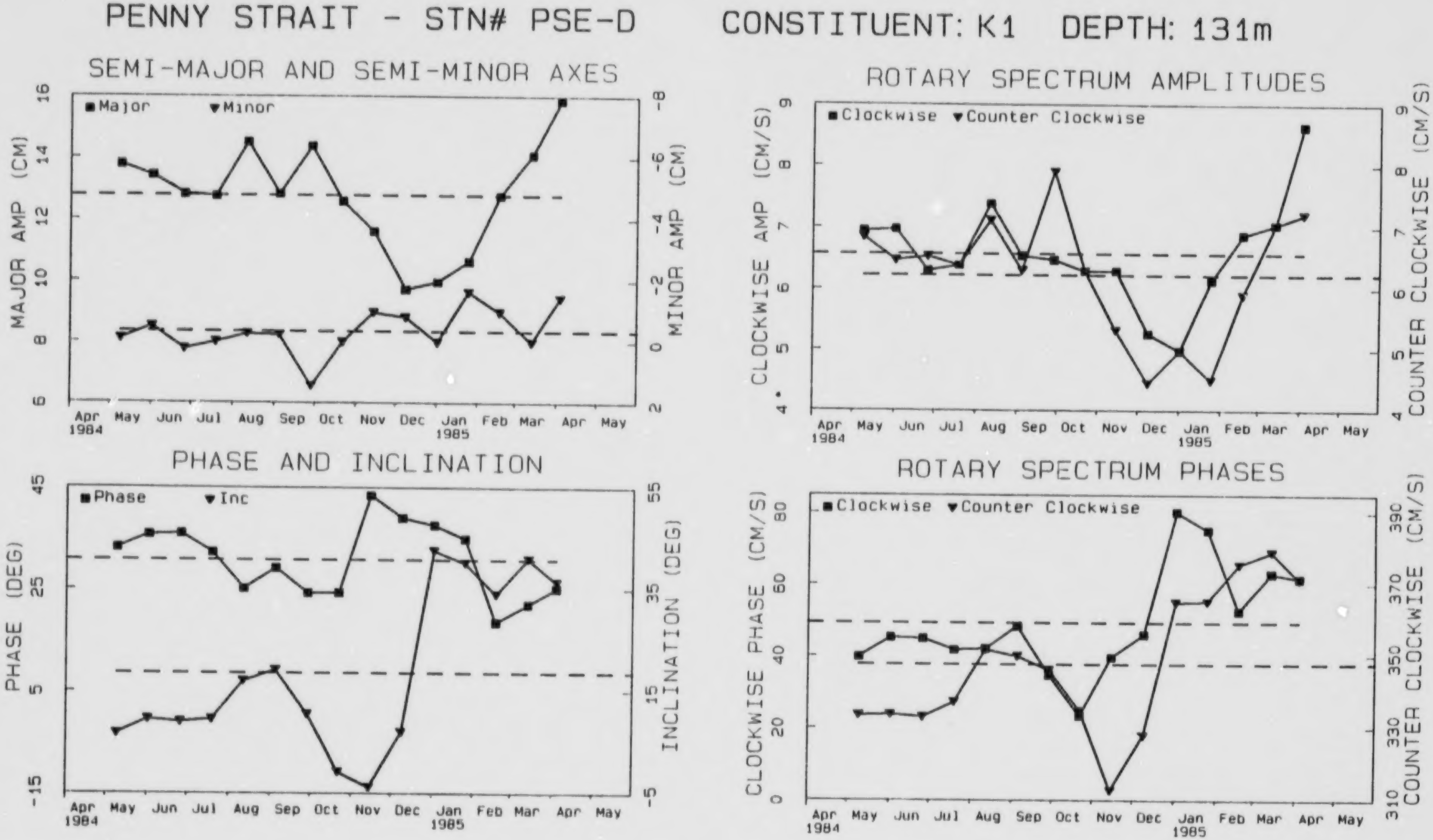

Figure 3.3.14. Time series of the K_1 ellipse parameters (major and minor amplitudes, inclination and phase), and the rotary spectral parameters (amplitudes and phase of clockwise and counter-clockwise components) at Station PSE-D, Penny Strait, at 131 m.

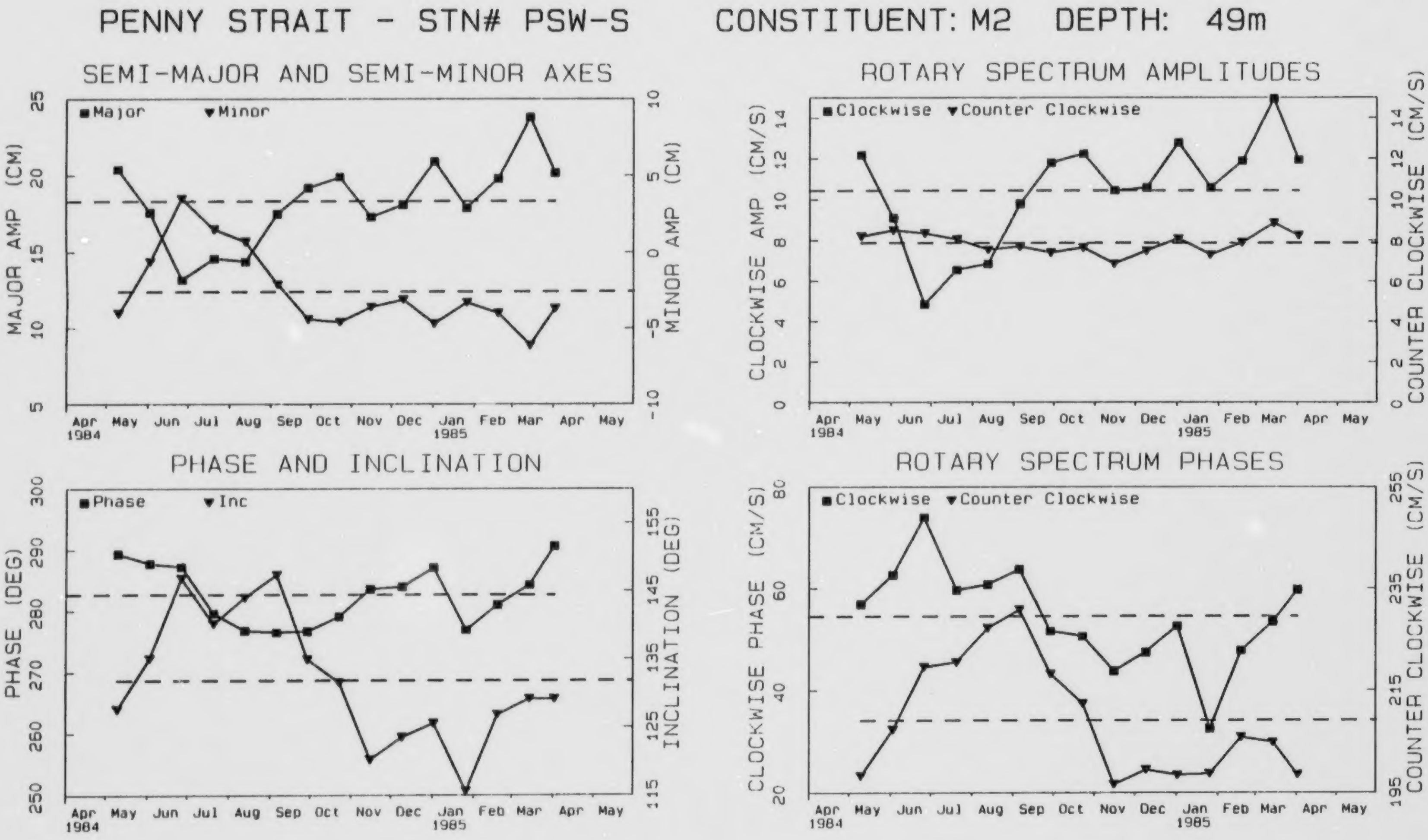

Figure 3.3.15. Time series of the M_2 ellipse parameters (major and minor amplitudes, inclination and phase), and the rotary spectral parameters (amplitudes and phase of clockwise and counter-clockwise components) at Station PSW-S, Penny Strait, at 49 m.

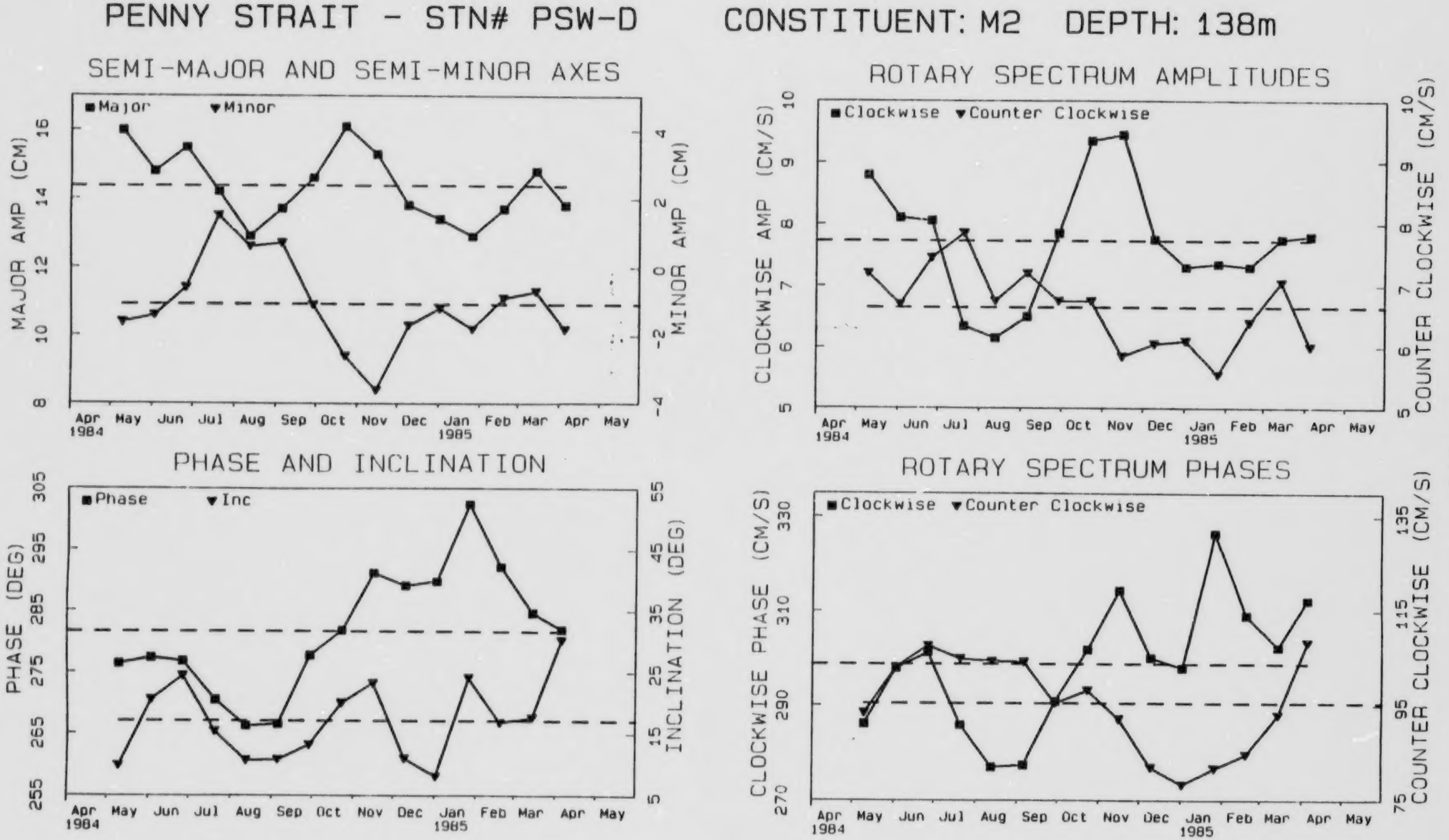

Figure 3.3.16. Time series of the M_2 ellipse parameters (major and minor amplitudes, inclination and phase), and the rotary spectral parameters (amplitudes and phase of clockwise and counter-clockwise components) at Station PSW-D, Penny Strait, at 138 m.

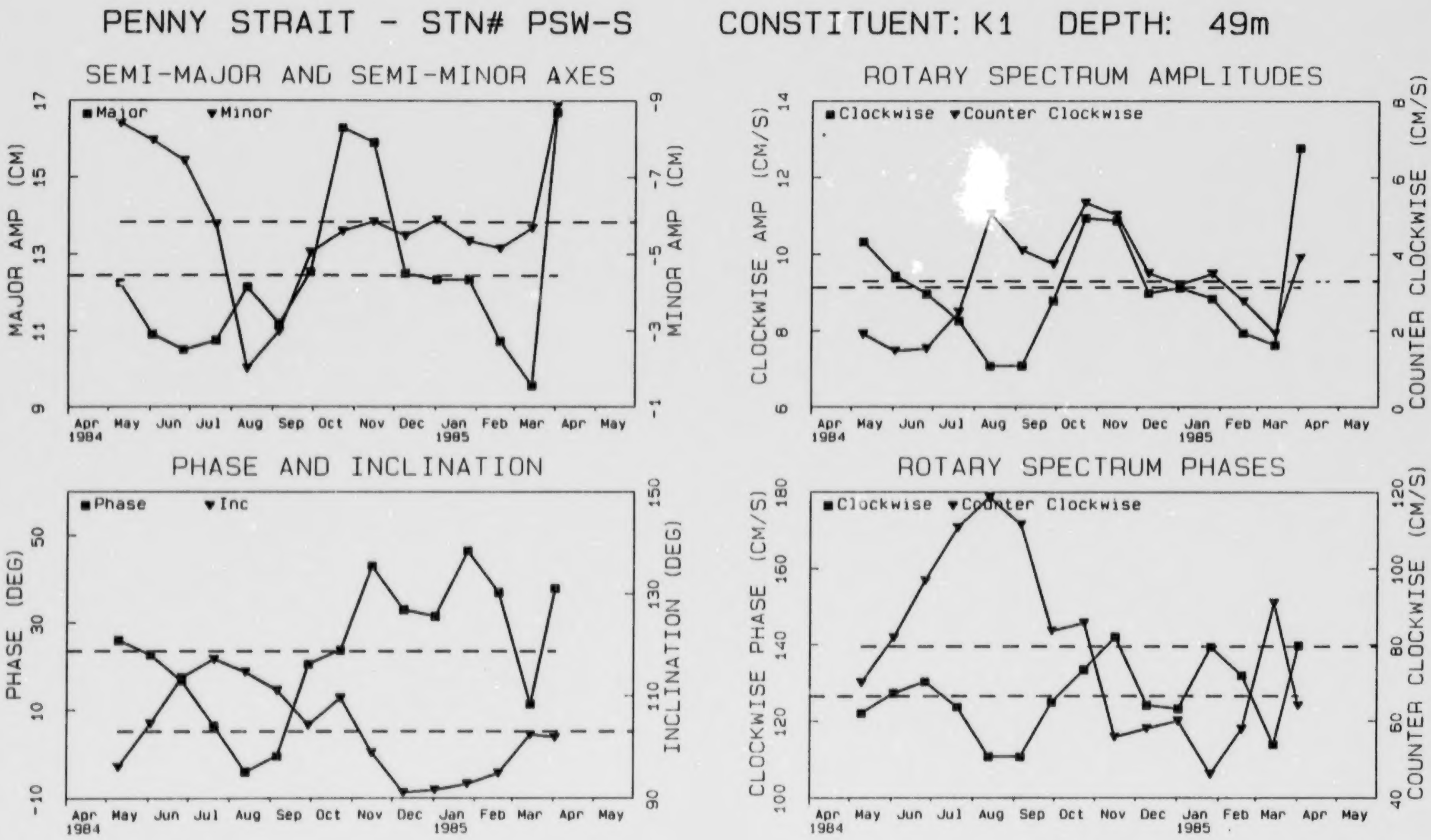

Figure 3.3.17. Time series of the K_1 ellipse parameters (major and minor amplitudes, inclination and phase), and the rotary spectral parameters (amplitudes and phase of clockwise and counter-clockwise components) at Station PSW-S, Penny Strait, at 49 m.

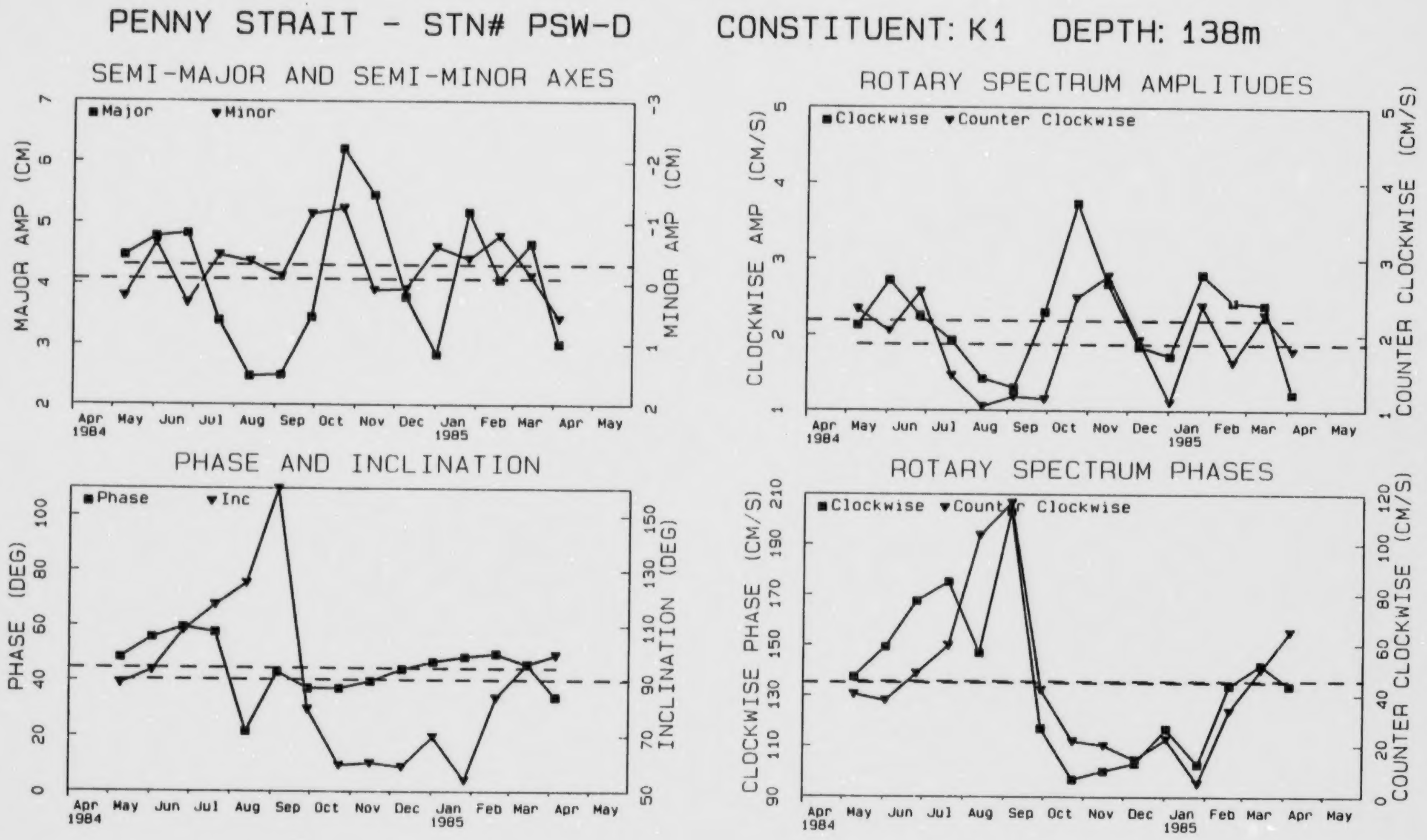

Figure 3.3.18. Time series of the K_1 ellipse parameters (major and minor amplitudes, inclination and phase), and the rotary spectral parameters (amplitudes and phase of clockwise and counter-clockwise components) at Station PSW-D, Penny Strait, at 138 m.

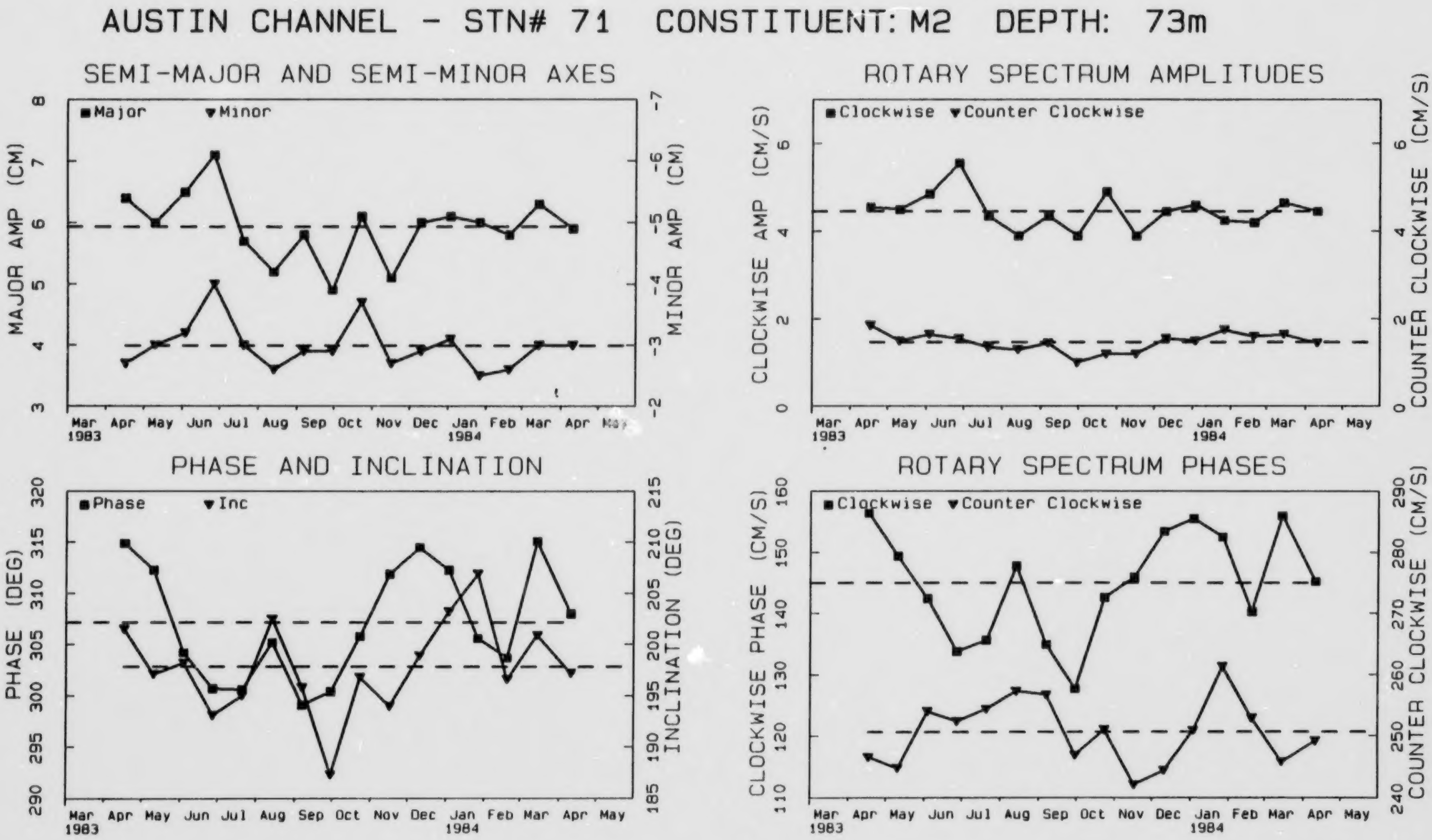

Figure 3.3.19. Time series of the M_2 ellipse parameters (major and minor amplitudes, inclination and phase), and the rotary spectral parameters (amplitudes and phase of clockwise and counter-clockwise components) at Station 71, Austin Channel, at 73 m.

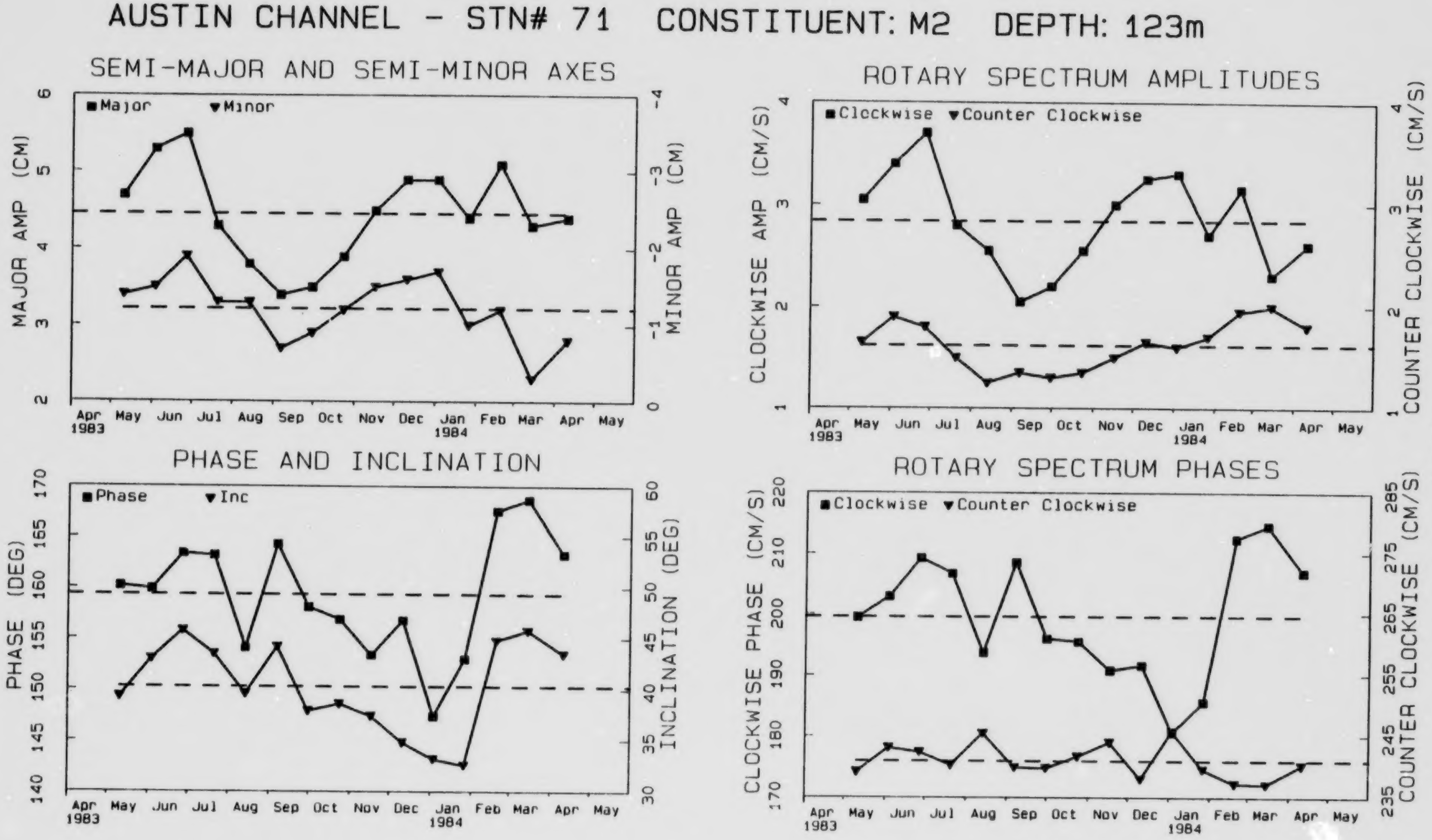

Figure 3.3.20. Time series of the M_2 ellipse parameters (major and minor amplitudes, inclination and phase), and the rotary spectral parameters (amplitudes and phase of clockwise and counter-clockwise components) at Station 71, Austin Channel, at 123 m.

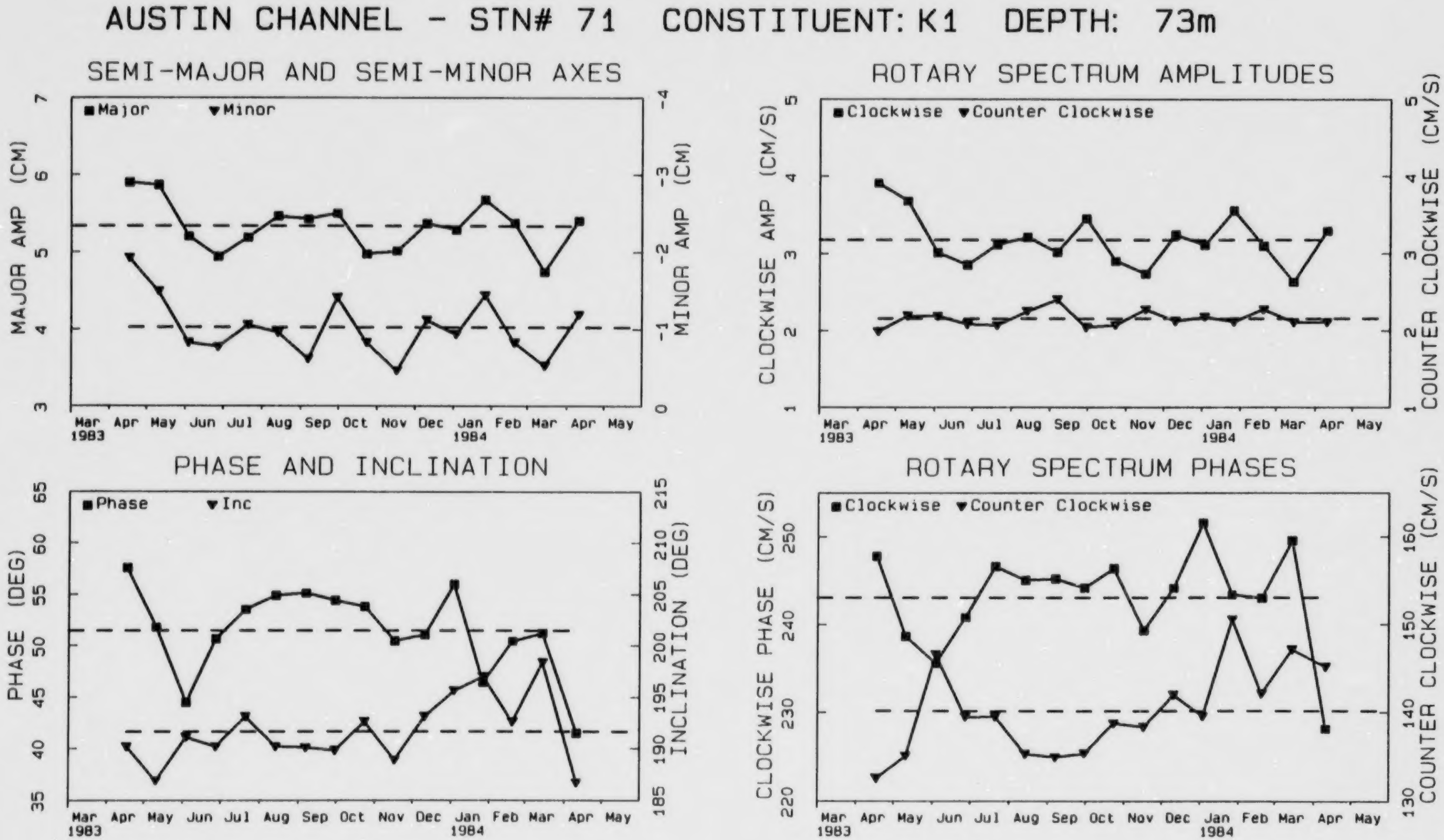

Figure 3.3.21. Time series of the K_1 ellipse parameters (major and minor amplitudes, inclination and phase), and the rotary spectral parameters (amplitudes and phase of clockwise and counter-clockwise components) at Station 71, Austin Channel, at 73 m.

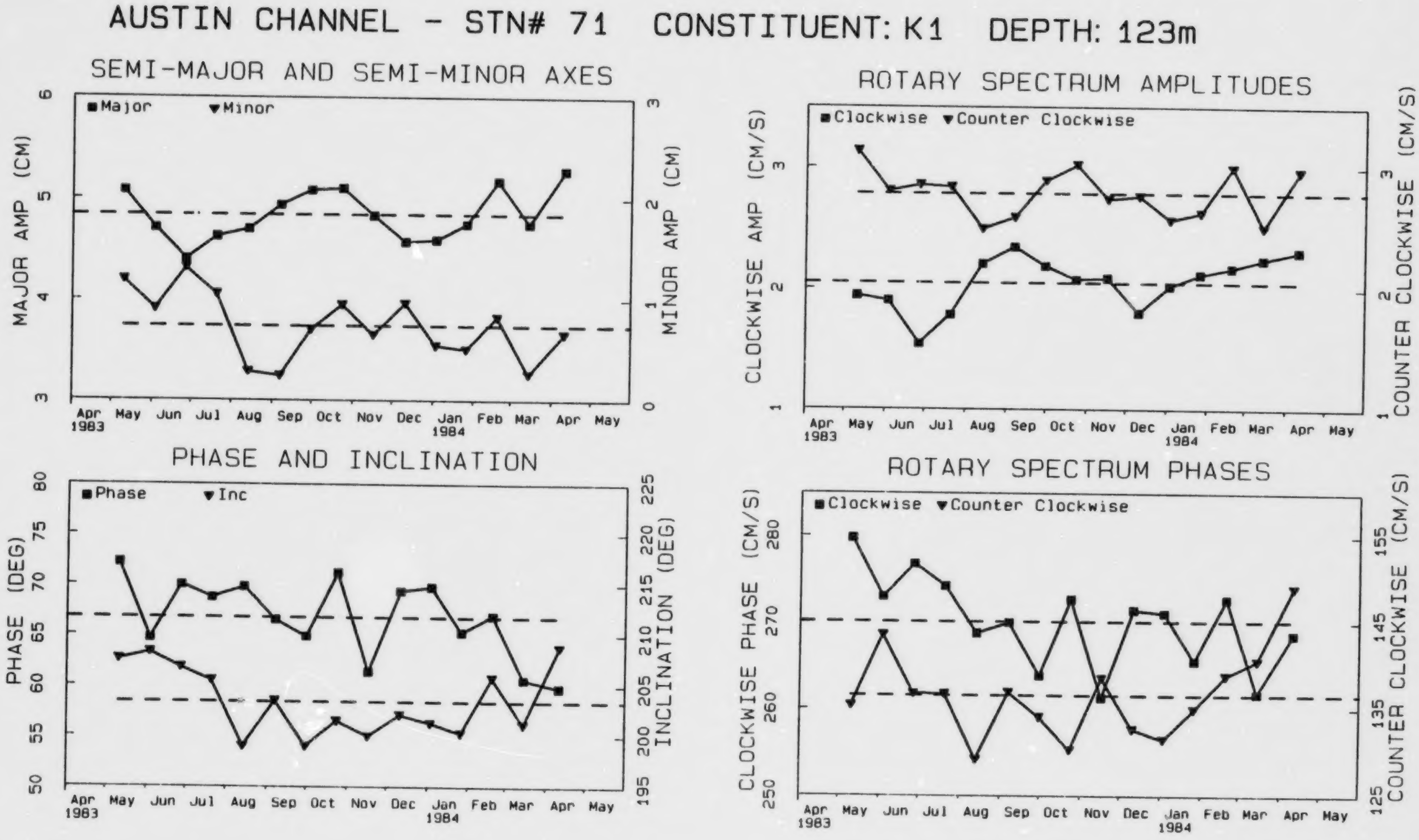

Figure 3.3.22. Time series of the K_1 ellipse parameters (major and minor amplitudes, inclination and phase), and the rotary spectral parameters (amplitudes and phase of clockwise and counter-clockwise components) At Station 71, Austin Channel, at 123 m.

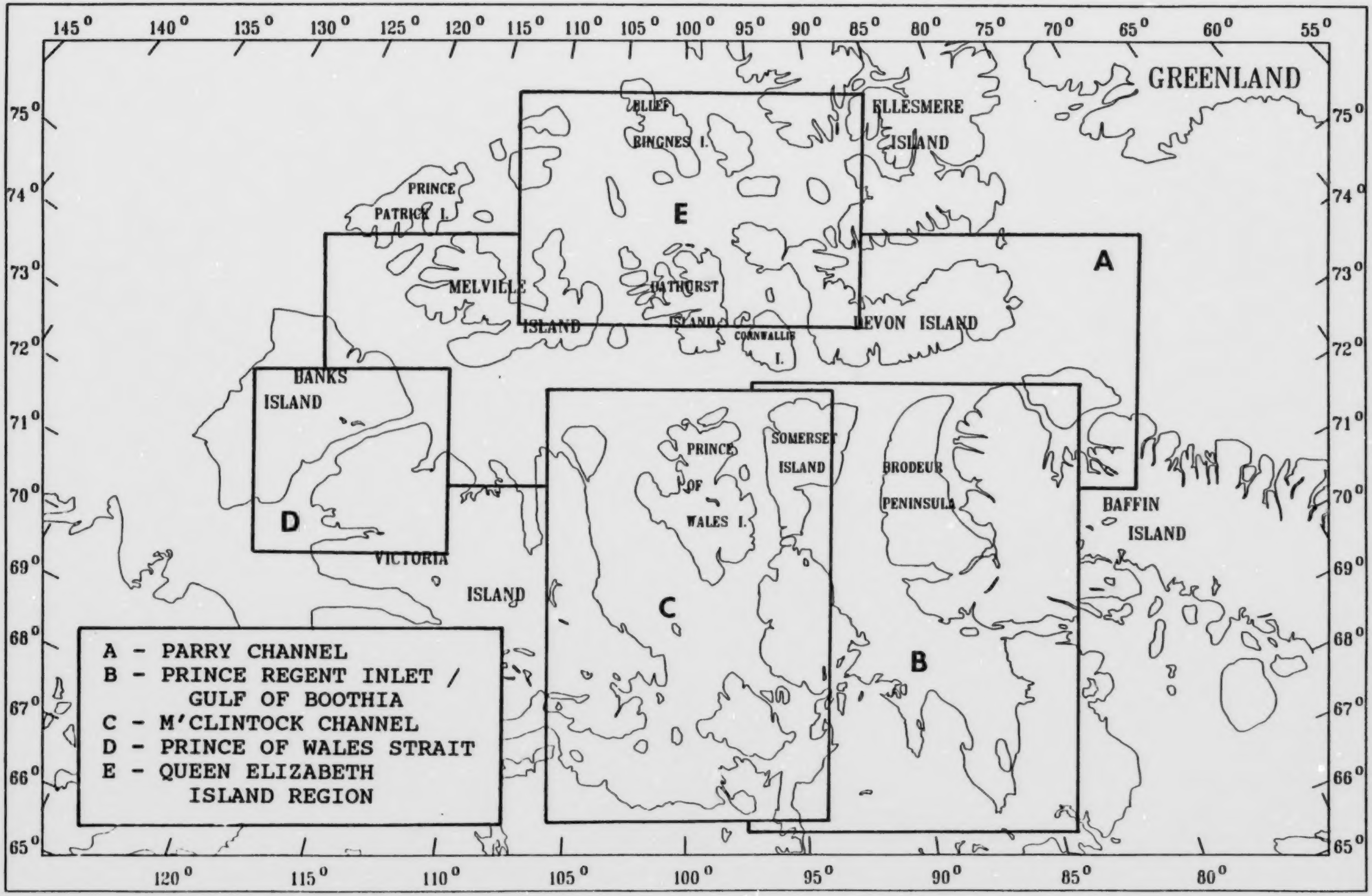
145°
140°
135°
130°
125°
120°
115°
110°
105°
100°
95°
90°
85°
80°
75°
70°
65°
60°
55°
75°
74°
73°
72°
71°
70°
69°
68°
67°
66°
65°
120°
115°
110°
105°
100°
95°
90°
85°
80°
GREENLAND
ELLESMERE
ISLAND
ELLEF
RINGNES I.
E
PRINCE
PATRICK I.
MELVILLE
ISLAND
BATHURST
ISLAND
CORNWALLIS
I.
DEVON ISLAND
A
BANKS
ISLAND
D
VICTORIA
ISLAND
PRINCE
OF
WALES I.
SOMERSET
ISLAND
BRODEUR
PENINSULA
BAFFIN
ISLAND
C
B
A - PARRY CHANNEL
B - PRINCE REGENT INLET / GULF OF BOOTHIA
C - M'CLINTOCK CHANNEL
D - PRINCE OF WALES STRAIT
E - QUEEN ELIZABETH ISLAND REGION

Figure 4.1.1 Chart of the Arctic showing subregions used in the description of the horizontal distribution of tidal elevations.

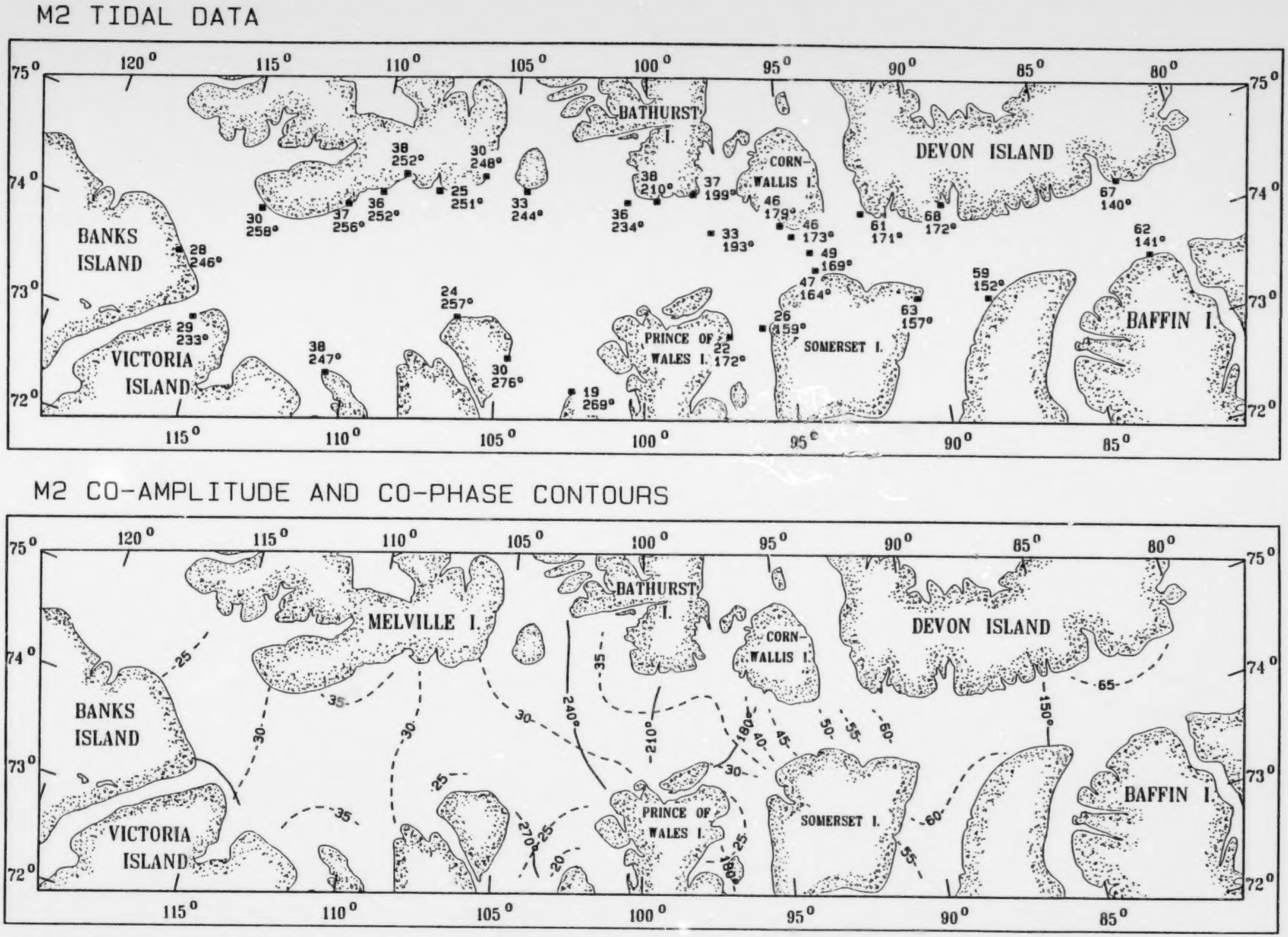
M2 TIDAL DATA
M2 CO-AMPLITUDE AND CO-PHASE CONTOURS
BANKS ISLAND
VICTORIA ISLAND
MELVILLE I.
BATHURST I.
CORN-WALLIS I.
DEVON ISLAND
PRINCE OF WALES I.
SOMERSET I.
BAFFIN I.
75°
74°
73°
72°
120°
115°
110°
105°
100°
95°
90°
85°
80°
28 246°
29 233°
30 258°
37 256°
36 252°
38 252°
25 251°
30 248°
33 244°
38 247°
24 257°
30 276°
19 269°
36 234°
38 210°
37 199°
33 193°
46 179°
46 173°
49 169°
47 164°
26 159°
22 172°
61 171°
68 172°
63 157°
59 152°
67 140°
62 141°
25
30
35
240°
210°
180°
270°
20
40
45
50
55
60
65
150°

Figure 4.1.2 Parry Channel M_2 co-phase and co-range diagram.

S2 DATA VALUES

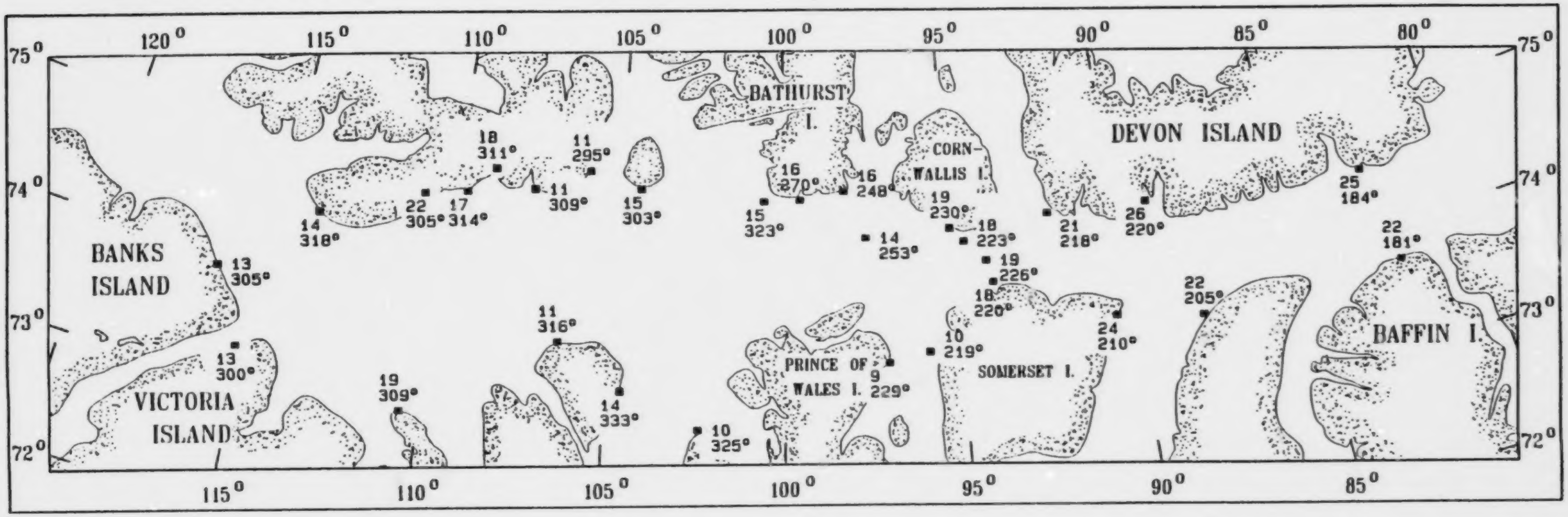
120°
115°
110°
105°
100°
95°
90°
85°
80°
75°
74°
73°
72°
BANKS ISLAND
VICTORIA ISLAND
BATHURST I.
CORN-WALLIS I.
DEVON ISLAND
PRINCE OF WALES I.
SOMERSET I.
BAFFIN I.
13 305°
13 300°
14 318°
22 305°
17 314°
18 311°
11 309°
11 295°
15 303°
19 309°
11 316°
14 333°
10 325°
15 323°
16 270°
16 248°
14 253°
19 230°
18 223°
19 226°
18 220°
10 219°
9 229°
21 218°
24 210°
26 220°
22 205°
25 184°
22 181°

S2 CO-AMPLITUDE AND CO-PHASE CONTOURS

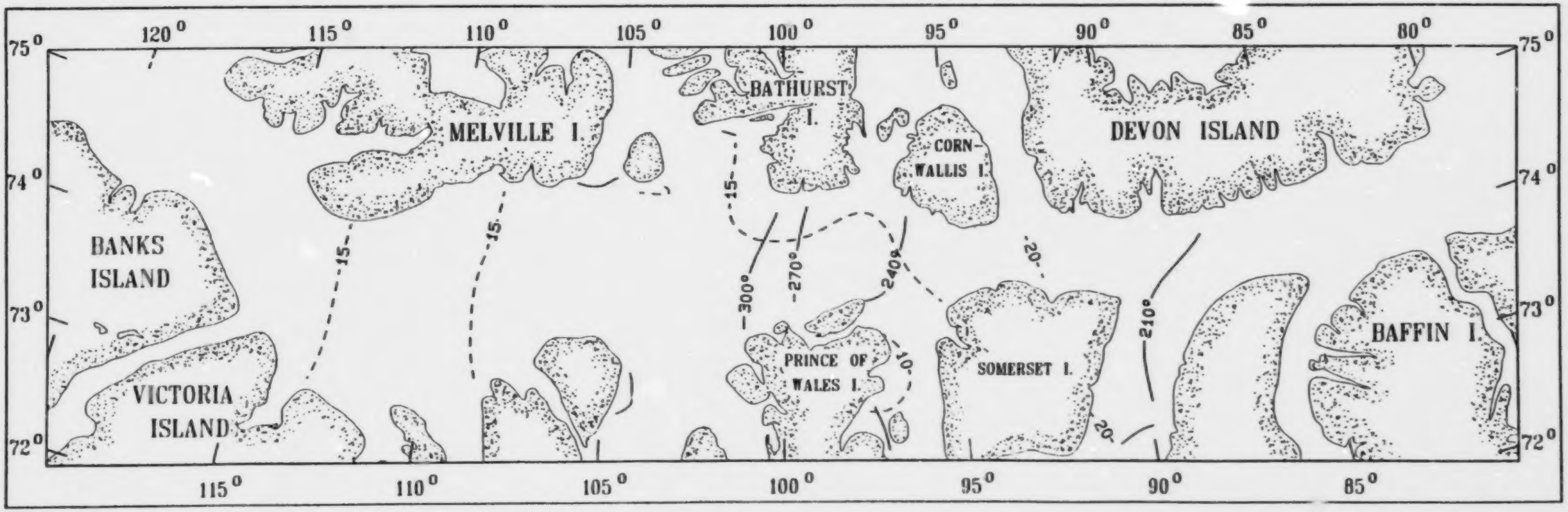
120°
115°
110°
105°
100°
95°
90°
85°
80°
75°
74°
73°
72°
BANKS ISLAND
VICTORIA ISLAND
MELVILLE I.
BATHURST I.
CORN-WALLIS I.
DEVON ISLAND
PRINCE OF WALES I.
SOMERSET I.
BAFFIN I.
15
15
15
300°
270°
240°
10
20
210°
20

Figure 4.1.3 Parry Channel S_2 co-phase and co-range diagram.

K1 TIDAL DATA

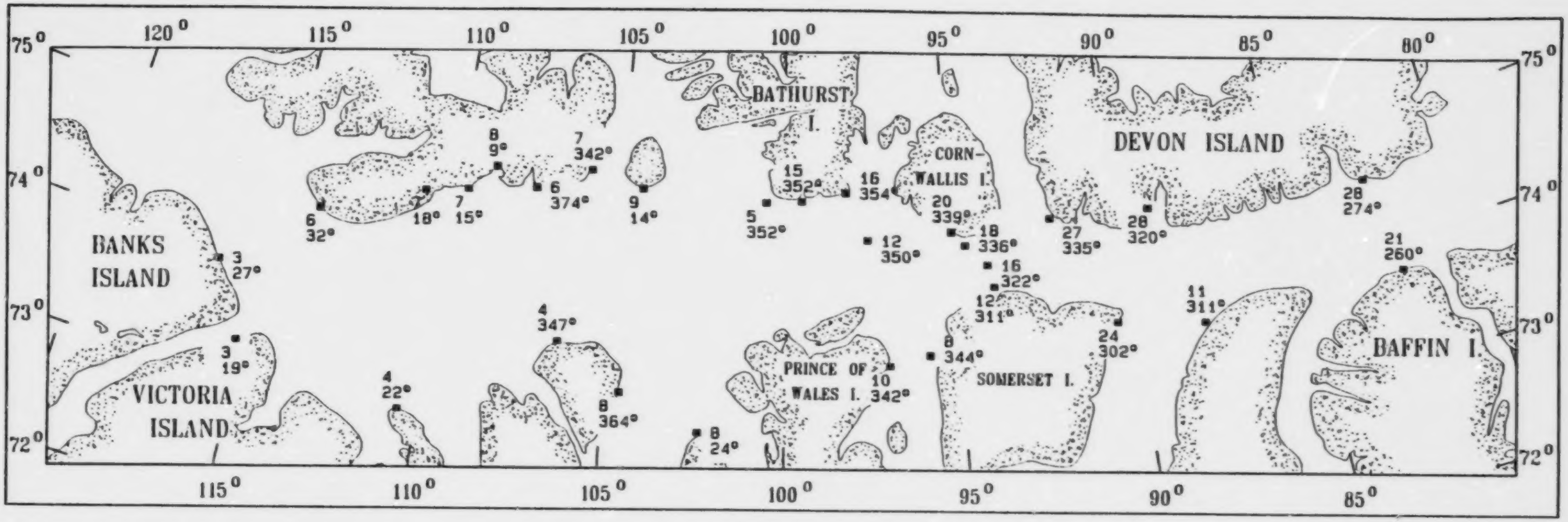
BANKS ISLAND
VICTORIA ISLAND
BATHURST I.
CORN-WALLIS I.
DEVON ISLAND
PRINCE OF WALES I.
SOMERSET I.
BAFFIN I.
3 27°
3 19°
6 32°
7 18°
7 15°
8 9°
6 374°
7 342°
9 14°
4 22°
4 347°
8 364°
8 24°
5 352°
15 352°
16 354°
12 350°
20 339°
18 336°
16 322°
12 311°
8 344°
10 342°
27 335°
28 320°
24 302°
11 311°
28 274°
21 260°
75°
74°
73°
72°
120°
115°
110°
105°
100°
95°
90°
85°
80°

K1 CO-AMPLITUDE AND CO-PHASE CONTOURS

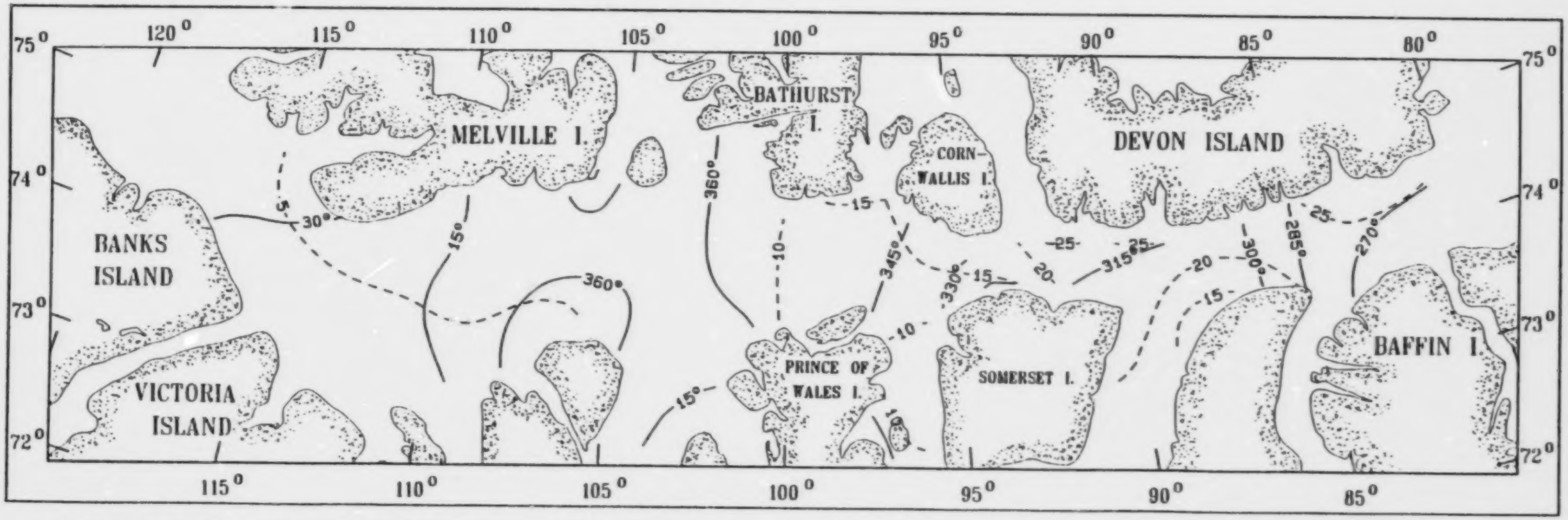
BANKS ISLAND
VICTORIA ISLAND
MELVILLE I.
BATHURST I.
CORN-WALLIS I.
DEVON ISLAND
PRINCE OF WALES I.
SOMERSET I.
BAFFIN I.
5
30°
15°
360°
360°
10
15
15°
345°
10
330°
15
10
20
25
315°
25
20
15
300°
285°
25
270°
75°
74°
73°
72°
120°
115°
110°
105°
100°
95°
90°
85°
80°

Figure 4.1.4 Parry Channel K_1 co-phase and co-range diagram.

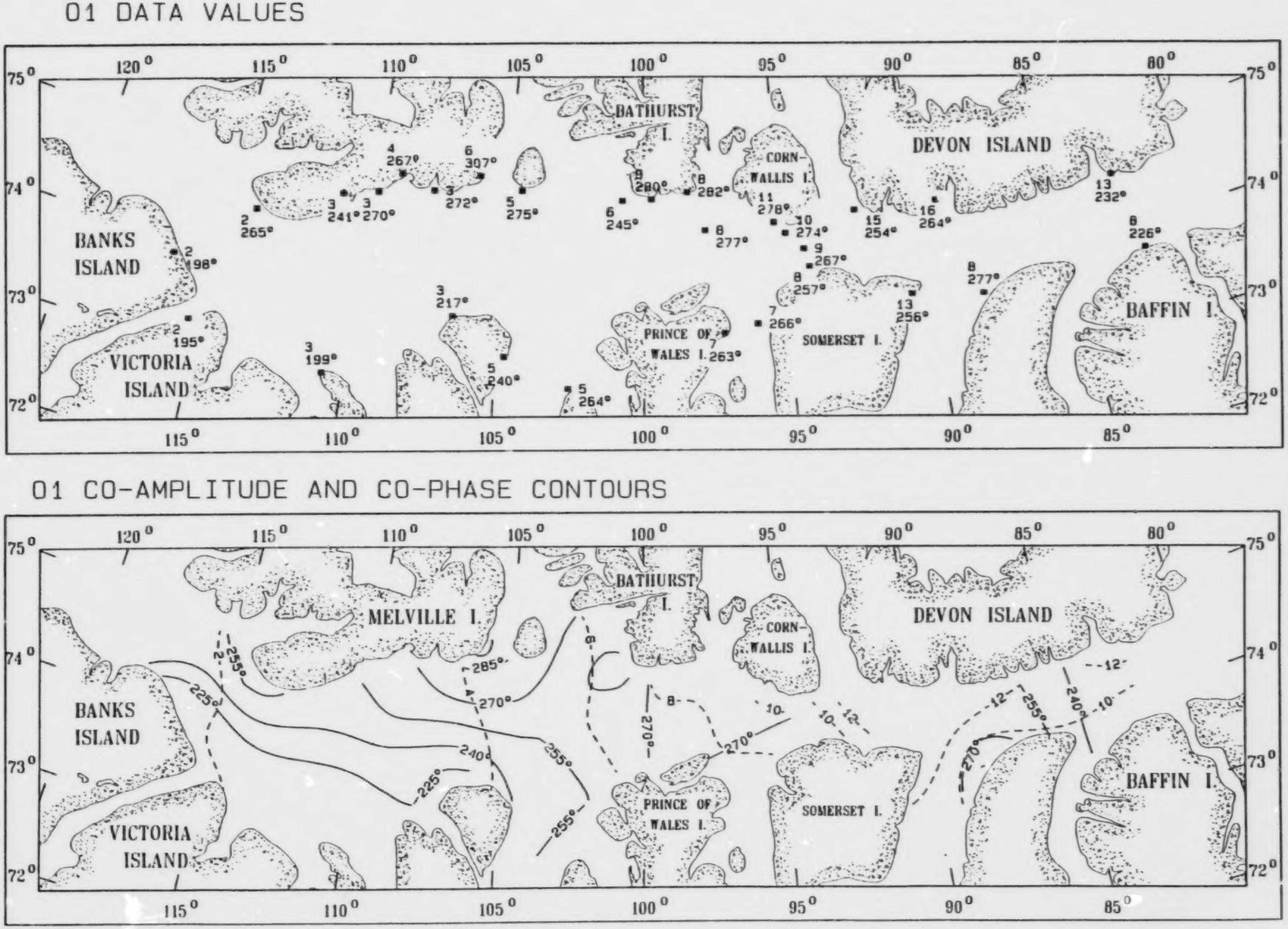

O1 DATA VALUES

O1 CO-AMPLITUDE AND CO-PHASE CONTOURS

BANKS ISLAND
VICTORIA ISLAND
MELVILLE I.
BATHURST I.
CORN-WALLIS I.
DEVON ISLAND
PRINCE OF WALES I.
SOMERSET I.
BAFFIN I.
120°
115°
110°
105°
100°
95°
90°
85°
80°
75°
74°
73°
72°
2 198°
2 195°
2 265°
3 241°
3 270°
4 267°
3 272°
6 307°
5 275°
3 217°
3 199°
5 240°
5 264°
6 245°
8 280°
8 282°
8 277°
11 278°
10 274°
9 267°
8 257°
7 266°
7 263°
15 254°
16 264°
13 256°
8 277°
13 232°
8 226°
225°
255°
2
240°
270°
285°
4
6
8
10
12

Figure 4.1.5 Parry Channel O_1 co-phase and co-range diagram.

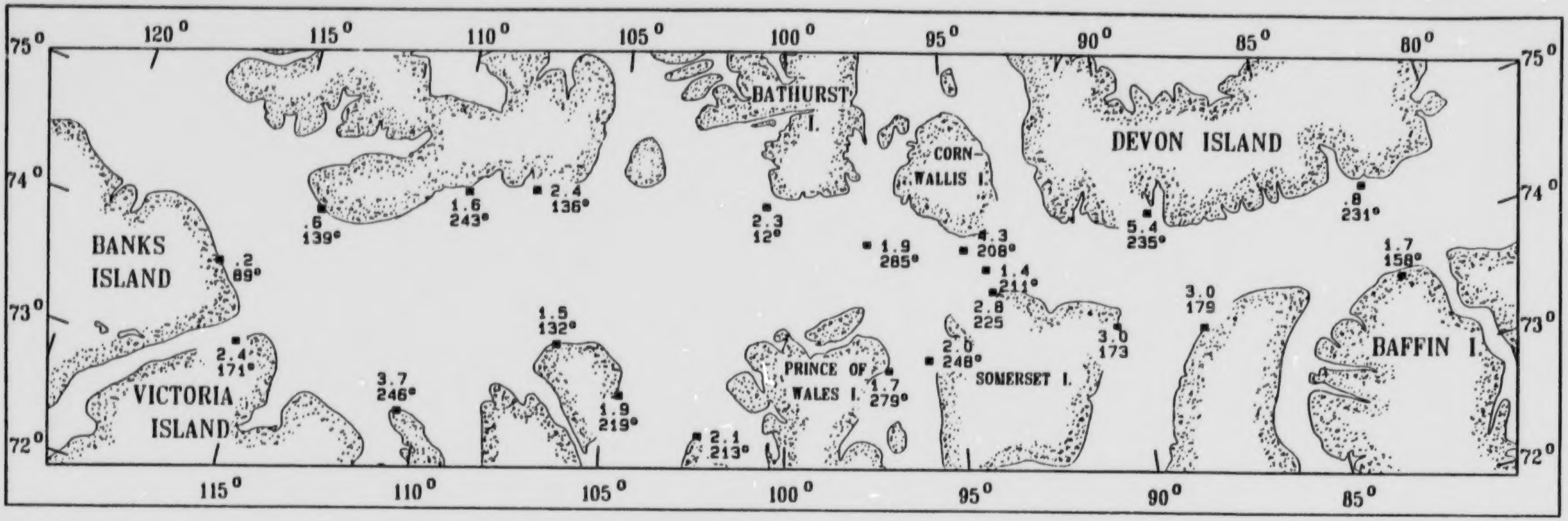

MSf DATA VALUES

75°
74°
73°
72°
120°
115°
110°
105°
100°
95°
90°
85°
80°
BANKS ISLAND
VICTORIA ISLAND
BATHURST I.
CORN-WALLIS I.
DEVON ISLAND
PRINCE OF WALES I.
SOMERSET I.
BAFFIN I.
.2 89°
2.4 171°
.6 139°
1.6 243°
2.4 136°
3.7 246°
1.5 132°
1.9 219°
2.1 213°
2.3 12°
1.9 285°
1.7 279°
2.0 248°
4.3 208°
1.4 211°
2.8 225
3.0 173
5.4 235°
3.0 179
.8 231°
1.7 158°

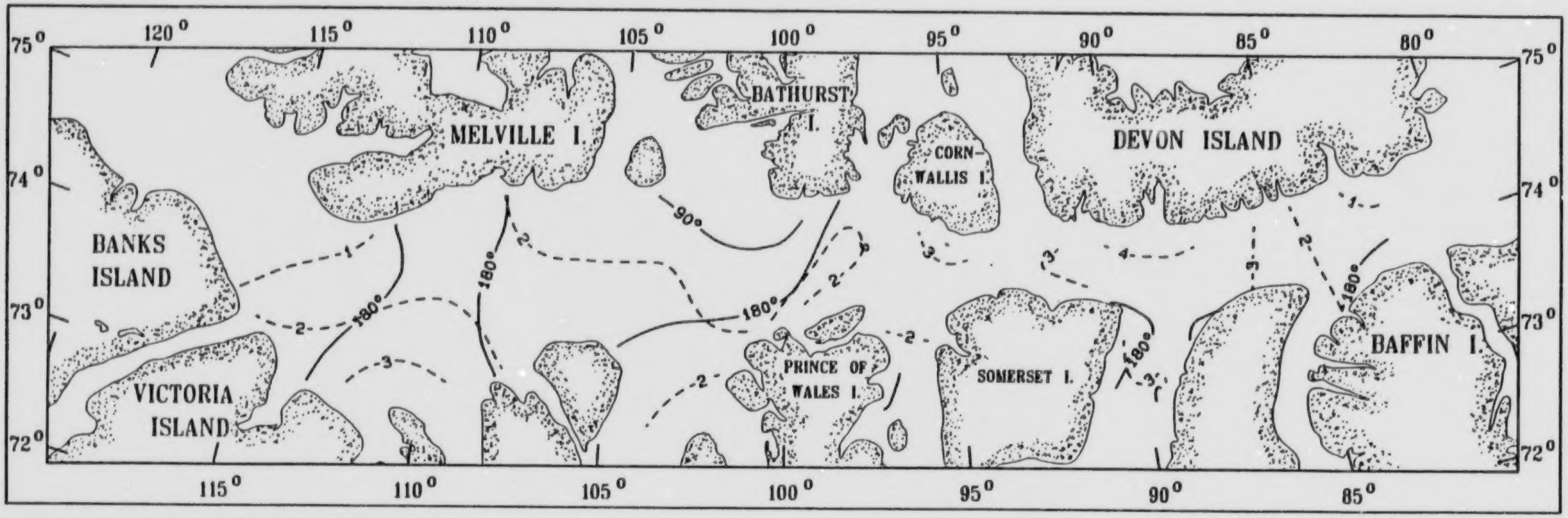

MSf CO-AMPLITUDE AND CO-PHASE CONTOURS

75°
74°
73°
72°
120°
115°
110°
105°
100°
95°
90°
85°
80°
BANKS ISLAND
VICTORIA ISLAND
MELVILLE I.
BATHURST I.
CORN-WALLIS I.
DEVON ISLAND
PRINCE OF WALES I.
SOMERSET I.
BAFFIN I.
1
2
180°
3
180°
2
90°
180°
2
2
3
3
4
2
180°
3
3
2
1
2
180°

Figure 4.1.6 Parry Channel MSf co-phase and co-range diagram.

MK3 DATA VALUES

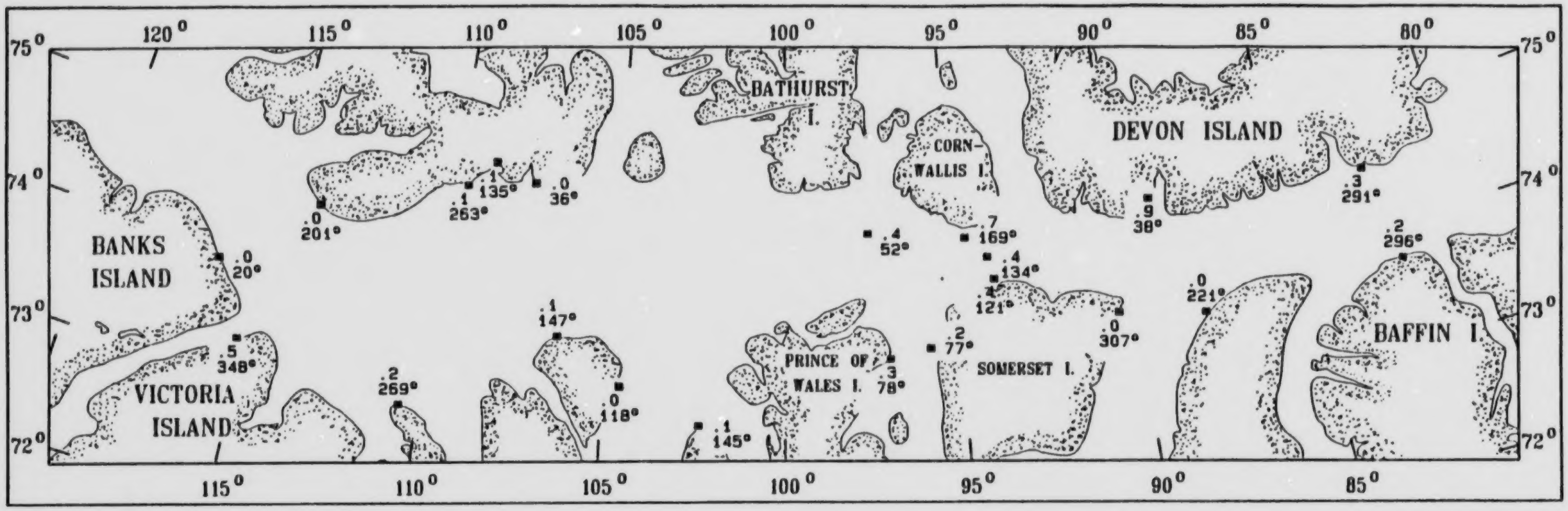
75°
74°
73°
72°
120°
115°
110°
105°
100°
95°
90°
85°
80°
BANKS ISLAND
VICTORIA ISLAND
BATHURST I.
CORN-WALLIS I.
DEVON ISLAND
PRINCE OF WALES I.
SOMERSET I.
BAFFIN I.
.0 20°
.5 348°
.0 201°
.1 263°
.1 135°
.0 36°
.2 269°
.1 147°
.0 118°
.1 145°
.4 52°
.3 78°
.7 169°
.4 134°
.4 121°
.2 77°
.9 38°
.0 307°
.0 221°
.3 291°
.2 296°

MK3 CO-AMPLITUDE AND CO-PHASE CONTOURS

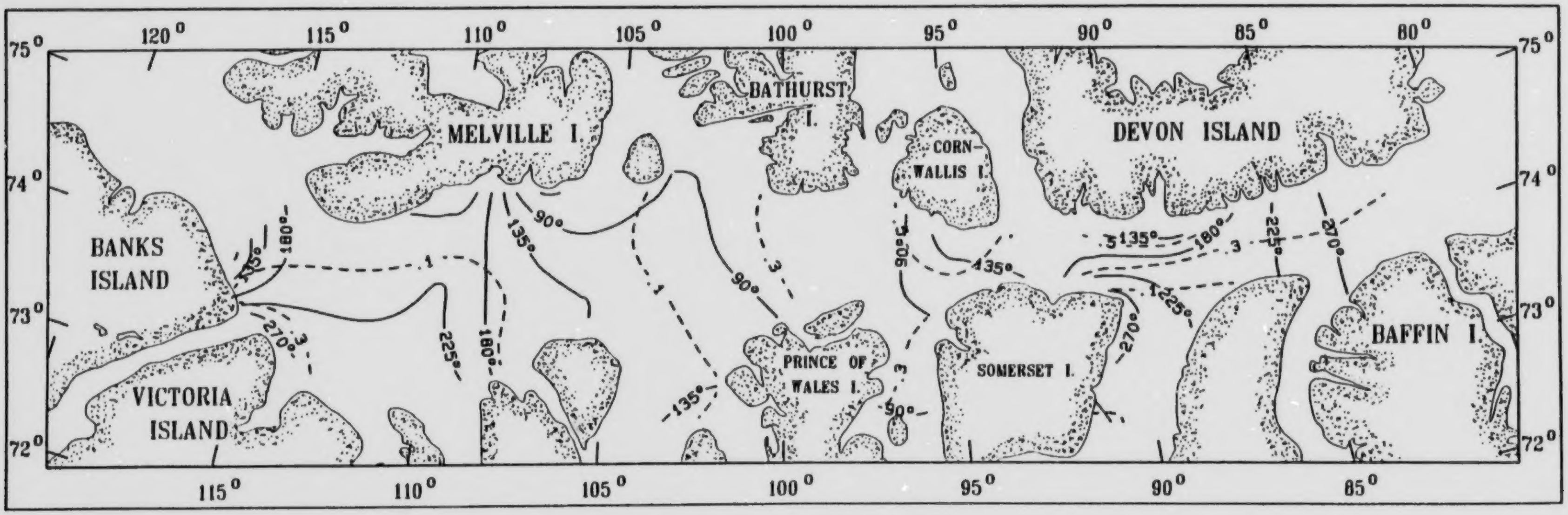
75°
74°
73°
72°
120°
115°
110°
105°
100°
95°
90°
85°
80°
BANKS ISLAND
VICTORIA ISLAND
MELVILLE I.
BATHURST I.
CORN-WALLIS I.
DEVON ISLAND
PRINCE OF WALES I.
SOMERSET I.
BAFFIN I.
135°
180°
.1
270°
.3
225°
180°
135°
90°
.1
90°
.3
135°
.3
90°
90°
135°
135°
.3
180°
.3
225°
270°
225°
270°

Figure 4.1.7 Parry Channel MK_3 co-phase and co-range diagram.

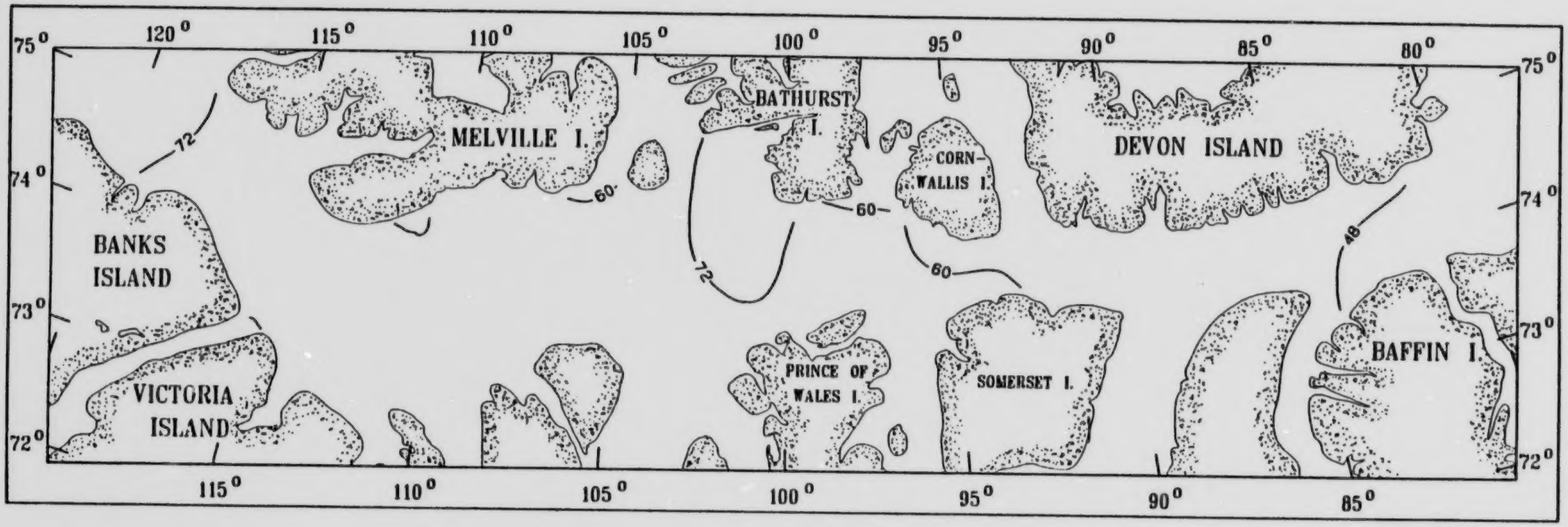

PHASE AGE (hrs)

75°
120°
115°
110°
105°
100°
95°
90°
85°
80°
75°
74°
73°
72°
BANKS ISLAND
VICTORIA ISLAND
MELVILLE I.
BATHURST I.
CORN-WALLIS I.
DEVON ISLAND
PRINCE OF WALES I.
SOMERSET I.
BAFFIN I.
72
72
60
60
60
48
115°
110°
105°
100°
95°
90°
85°

Figure 4.1.8 Parry Channel phase age.

(K1 + O1) / (M2 + S2)

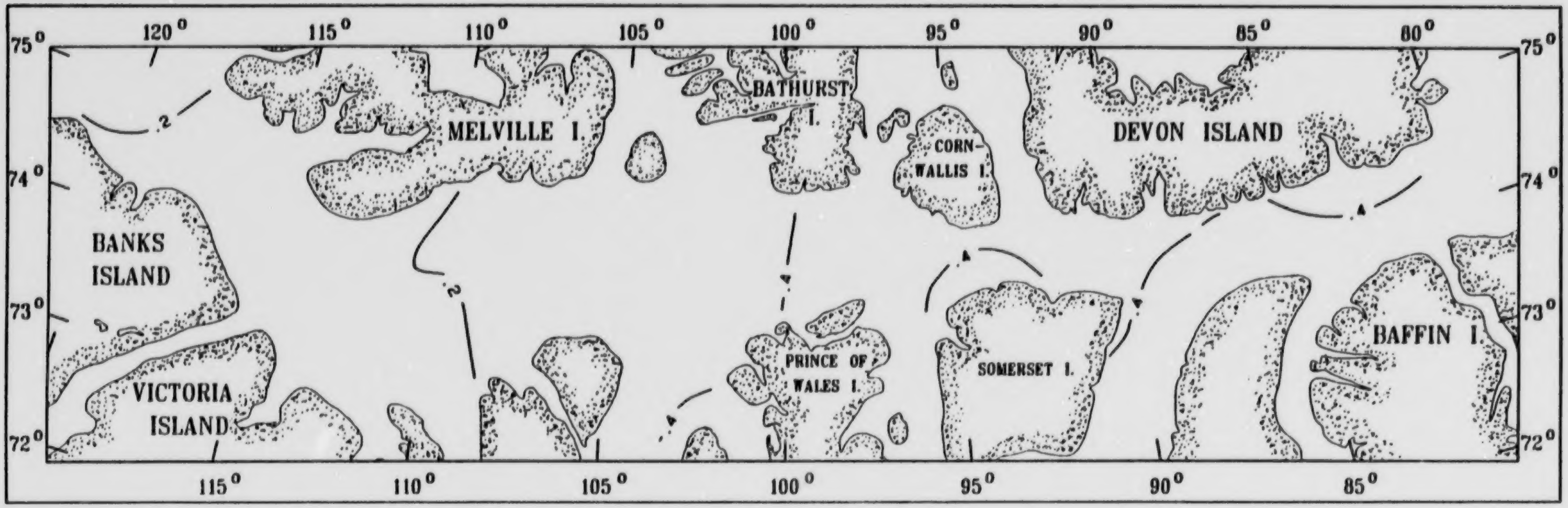
75°
74°
73°
72°
120°
115°
110°
105°
100°
95°
90°
85°
80°
BANKS ISLAND
VICTORIA ISLAND
MELVILLE I.
BATHURST I.
CORN-WALLIS I.
PRINCE OF WALES I.
SOMERSET I.
DEVON ISLAND
BAFFIN I.
.2
.2
.4
.4
.4
.4
.4
.4

Figure 4.1.9 Parry Channel tidal character.

M2 CO-AMPLITUDE AND CO-PHASE CONTOURS

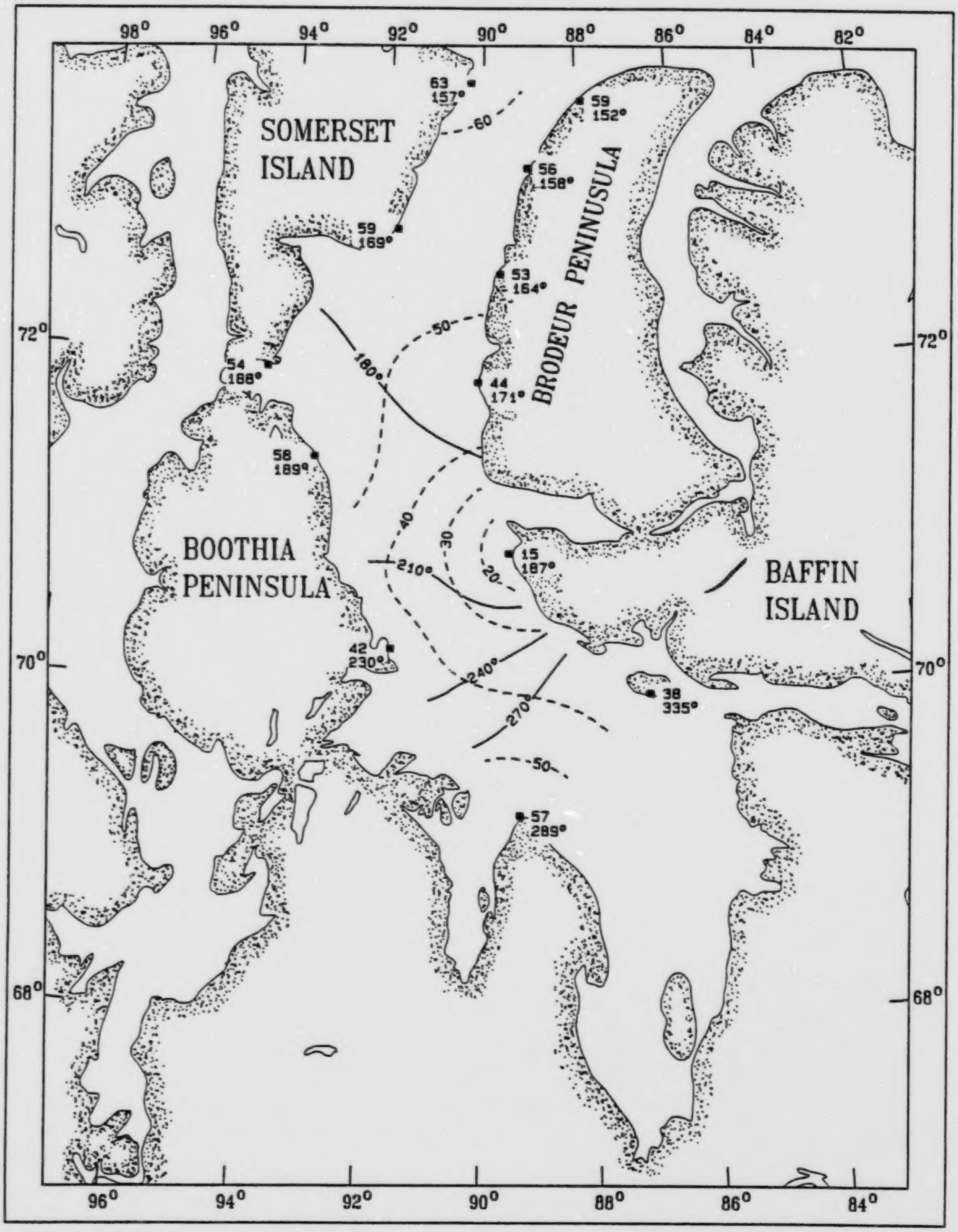
98°
96°
94°
92°
90°
88°
86°
84°
82°
SOMERSET ISLAND
BRODEUR PENINSULA
BOOTHIA PENINSULA
BAFFIN ISLAND
72°
70°
68°
63 157°
59 152°
60
56 158°
59 169°
53 164°
50
54 188°
180°
44 171°
58 189°
40
30
20
15 187°
210°
42 230°
240°
270°
38 335°
50
57 289°
96°
94°
92°
90°
88°
86°
84°

Figure 4.1.10 Prince Regent Inlet / Gulf of Boothia M_2 co-phase and co-range diagram.

N2 CO-AMPLITUDE AND CO-PHASE CONTOURS

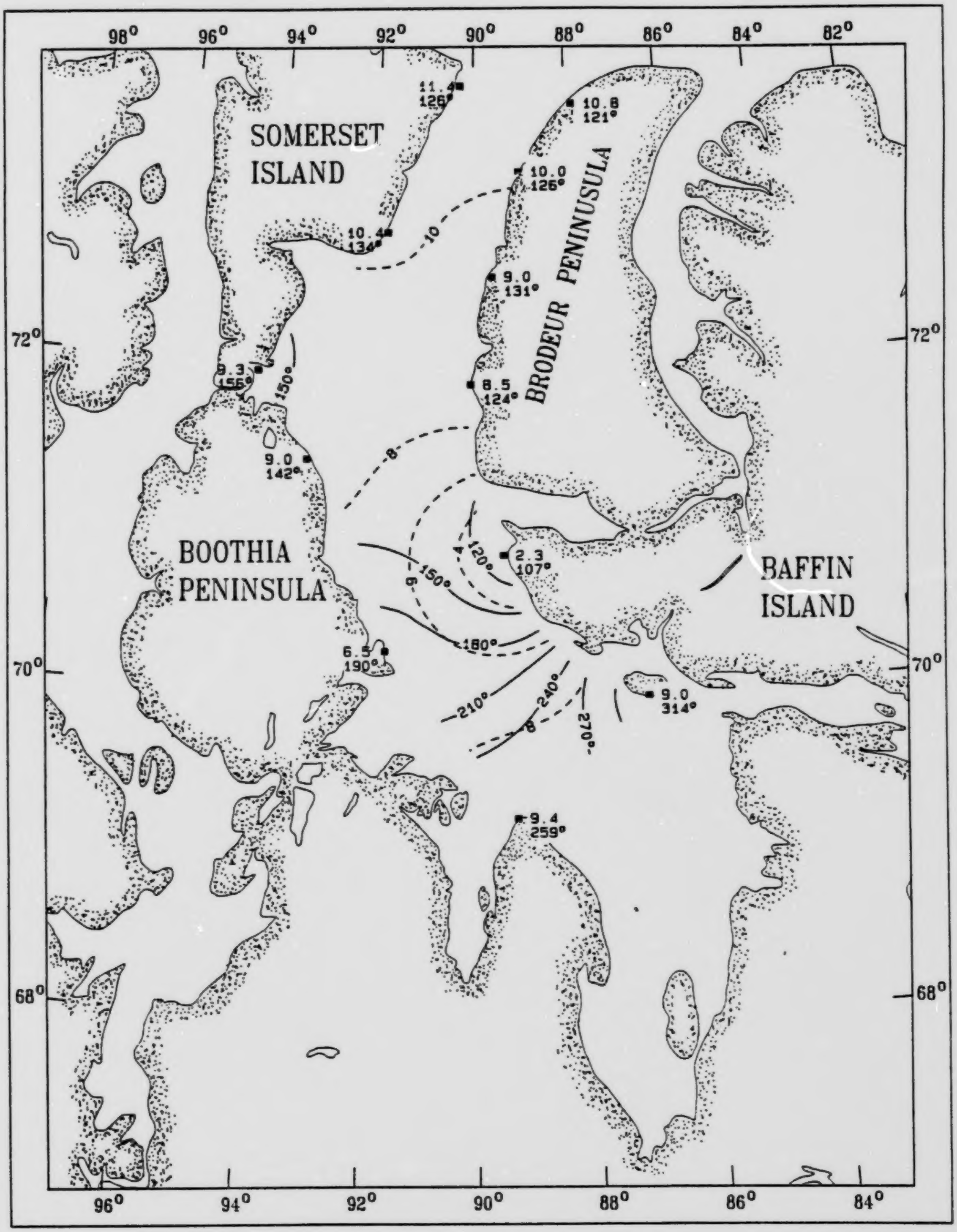
98°
96°
94°
92°
90°
88°
86°
84°
82°
72°
70°
68°
SOMERSET ISLAND
BRODEUR PENINSULA
BOOTHIA PENINSULA
BAFFIN ISLAND
11.4
126°
10.8
121°
10.0
126°
10.4
134°
10
9.0
131°
9.3
156°
150°
8.5
124°
9.0
142°
8
2.3
107°
4
120°
6
150°
180°
6.5
190°
210°
240°
8
270°
9.0
314°
9.4
259°
96°
94°
92°
90°
88°
86°
84°

Figure 4.1.11 Prince Regent Inlet / Gulf of Boothia N_2 co-phase and co-range diagram.

K1 CO-AMPLITUDE AND CO-PHASE CONTOURS

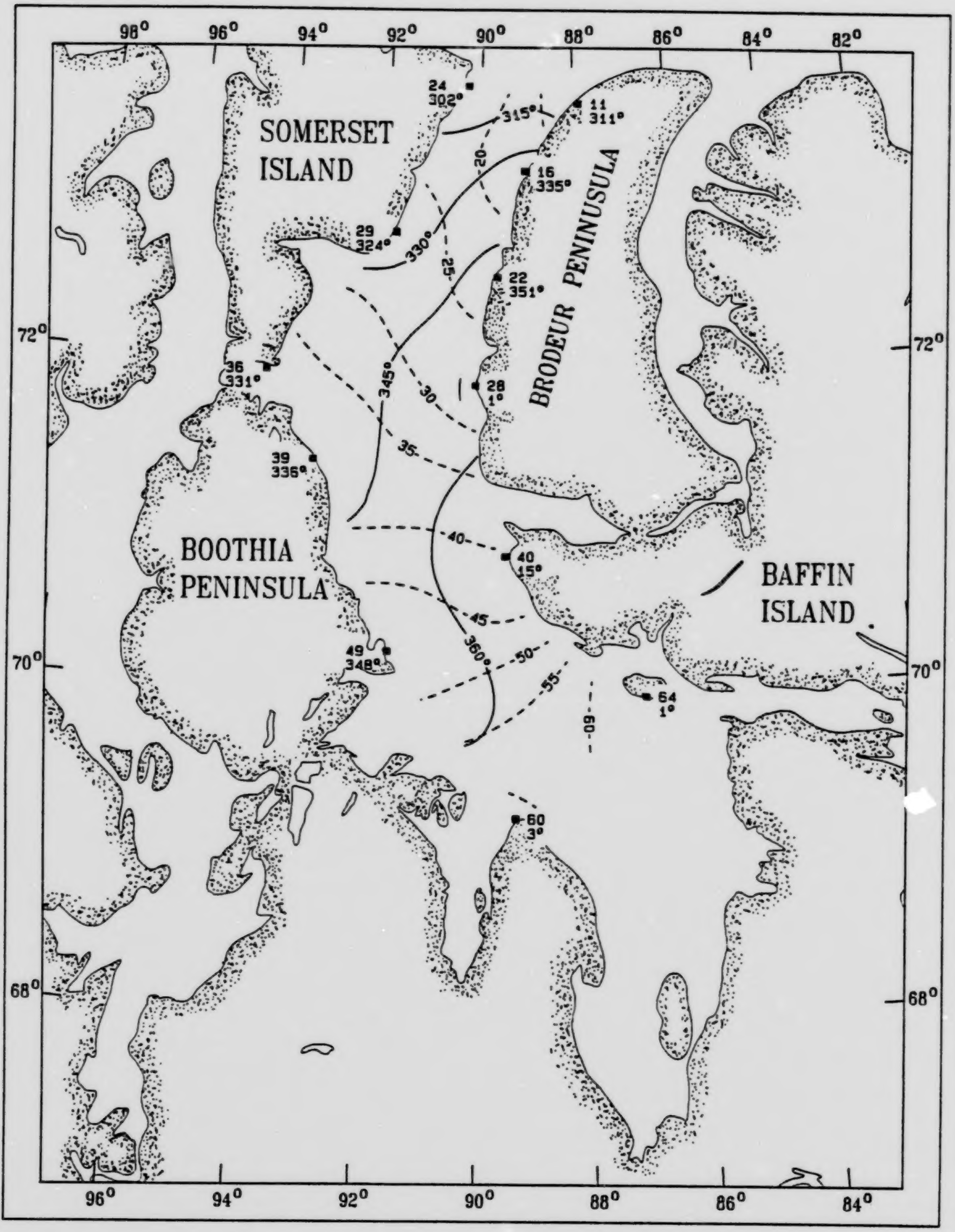
98°
96°
94°
92°
90°
88°
86°
84°
82°
72°
70°
68°
SOMERSET ISLAND
BRODEUR PENINSULA
BOOTHIA PENINSULA
BAFFIN ISLAND
24
302°
11
311°
315°
20
16
335°
29
324°
330°
25
22
351°
36
331°
345°
30
28
1°
39
336°
35
40
40
15°
45
49
348°
50
360°
55
60
64
1°
60
3°

Figure 4.1.12 Prince Regent Inlet / Gulf of Boothia K_1 co-phase and co-range diagram.

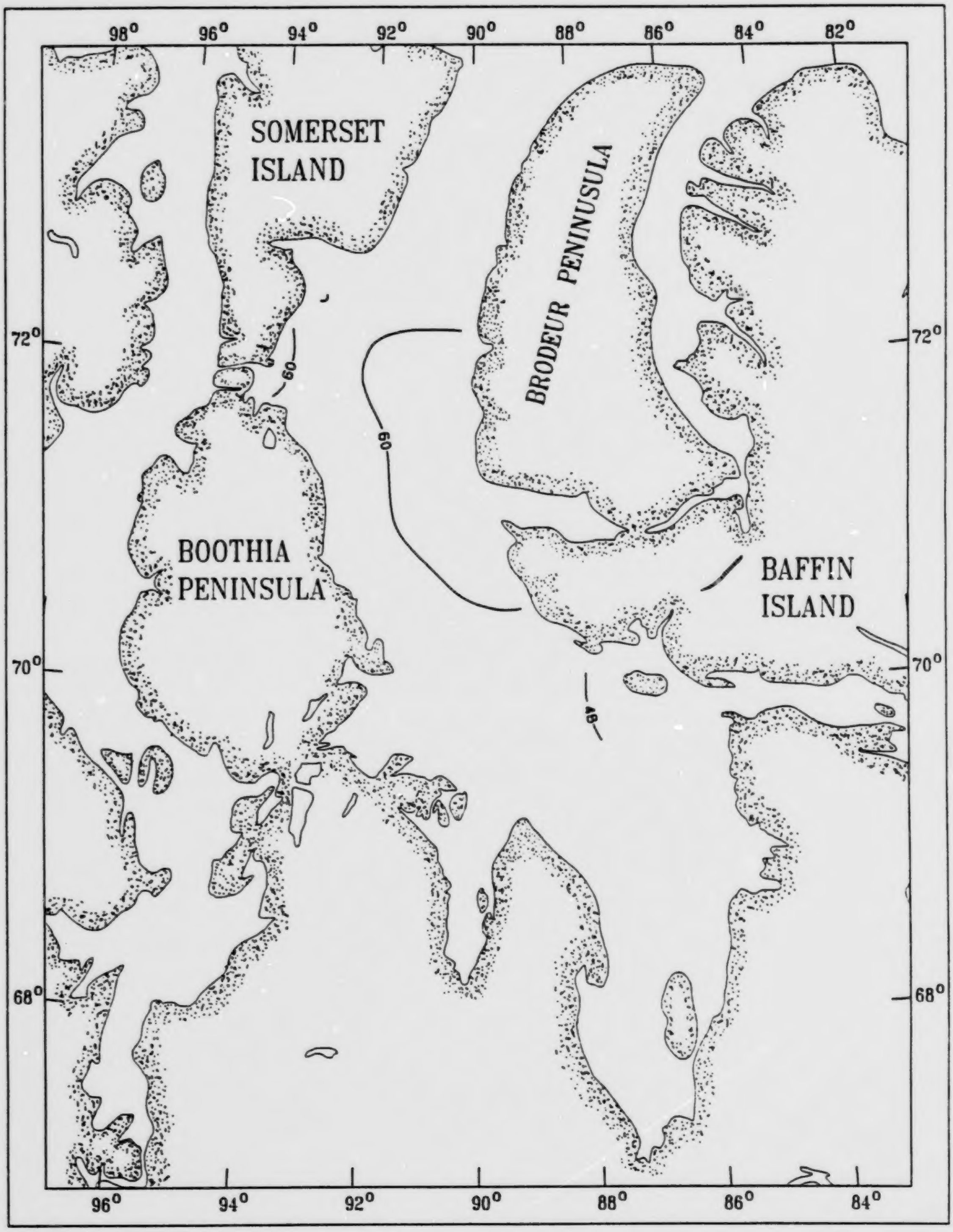
PHASE AGE (hrs)

98°
96°
94°
92°
90°
88°
86°
84°
82°
72°
70°
68°
SOMERSET ISLAND
BRODEUR PENINSULA
BOOTHIA PENINSULA
BAFFIN ISLAND
60
60
48
96°
94°
92°
90°
88°
86°
84°

Figure 4.1.13 Prince Regent Inlet / Gulf of Boothia phase age.

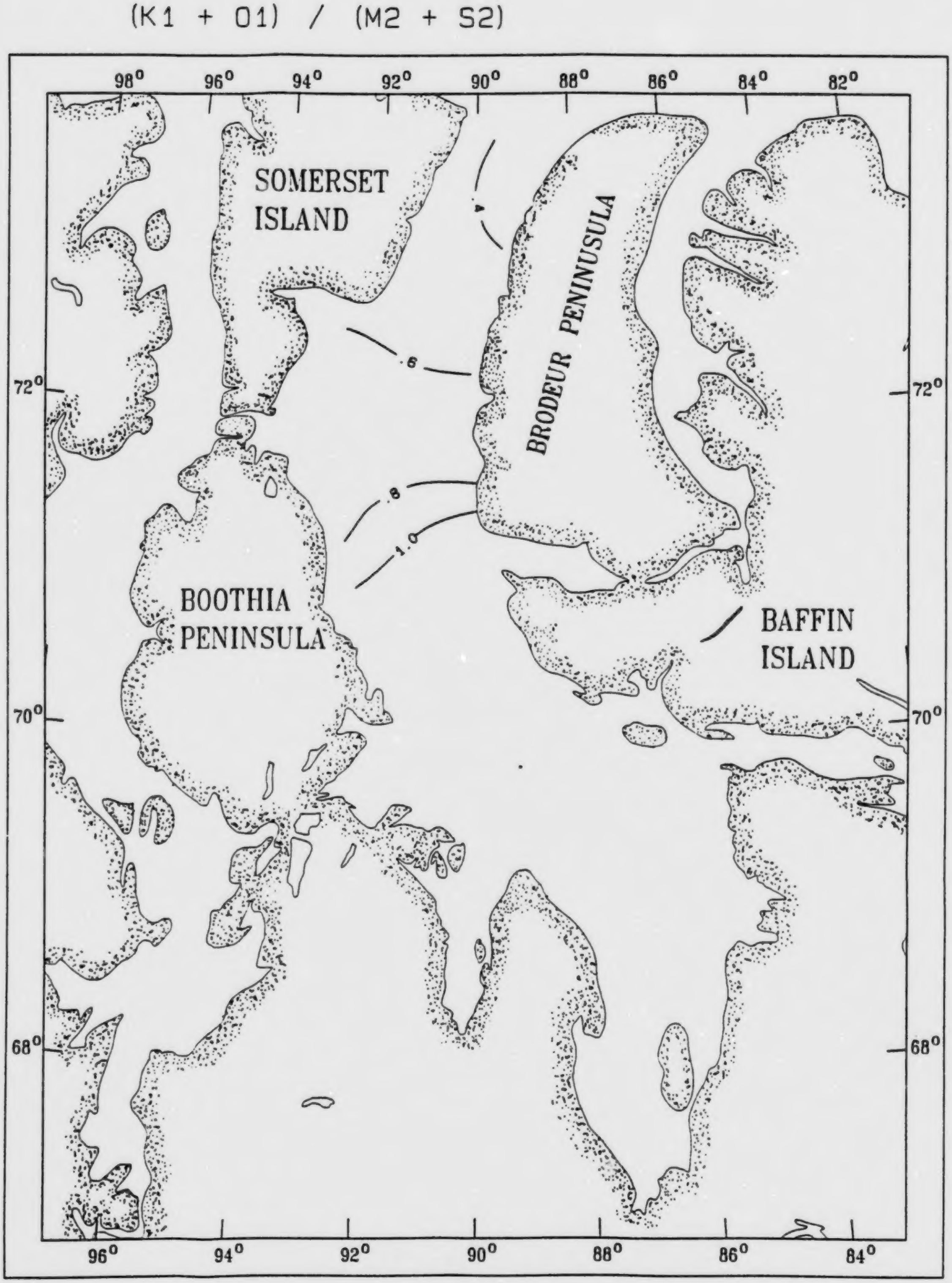
(K1 + O1) / (M2 + S2)
98°
96°
94°
92°
90°
88°
86°
84°
82°
72°
70°
68°
SOMERSET ISLAND
BRODEUR PENINSULA
BOOTHIA PENINSULA
BAFFIN ISLAND
.4
.6
.8
1.0
96°
94°
92°
90°
88°
86°
84°

Figure 4.1.14 Prince Regent Inlet / Gulf of Boothia tidal character.

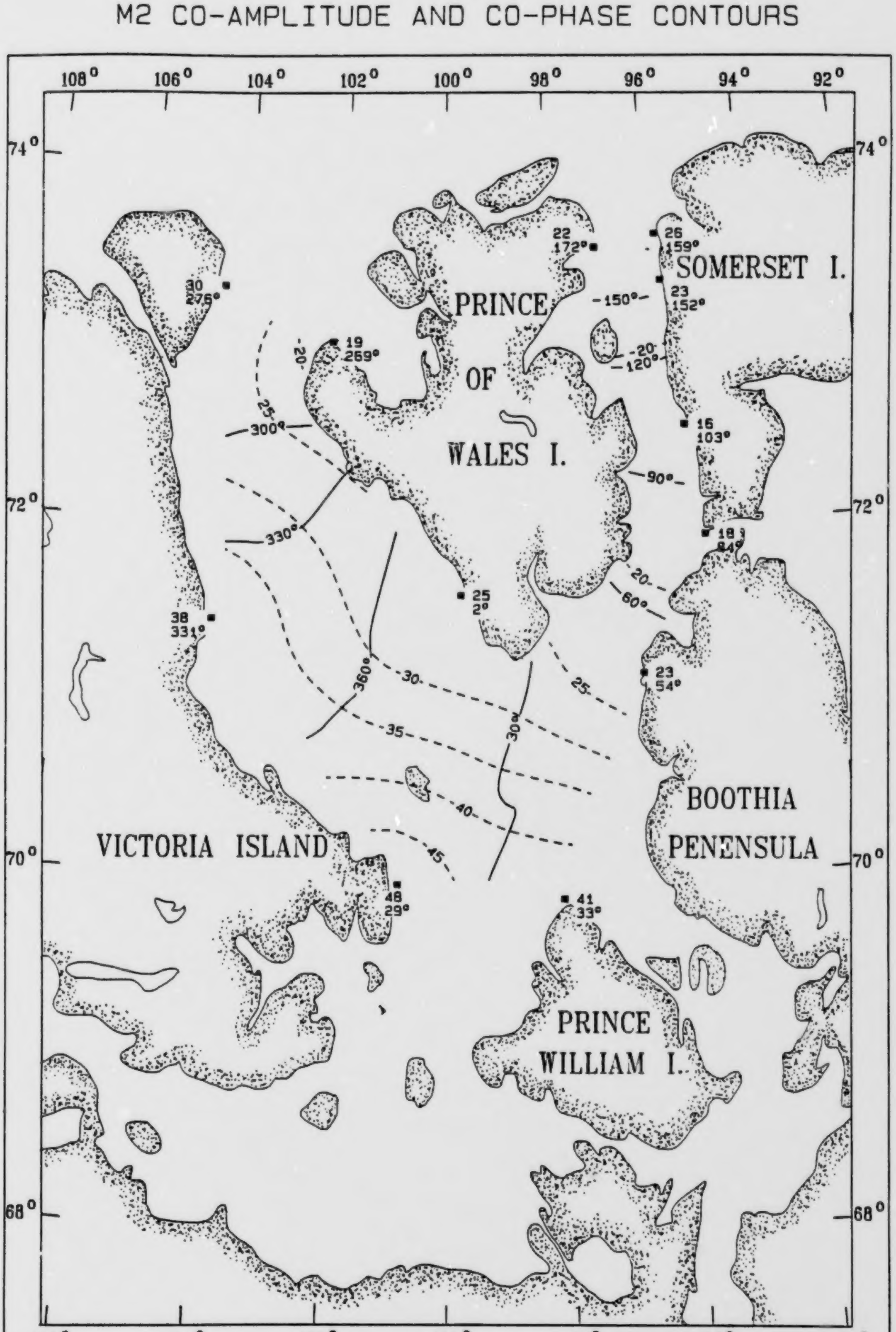
M2 CO-AMPLITUDE AND CO-PHASE CONTOURS
108°
106°
104°
102°
100°
98°
96°
94°
92°
74°
72°
70°
68°
106°
104°
102°
100°
98°
96°
94°
22
172°
26
159°
SOMERSET I.
23
152°
-150°-
30
276°
PRINCE
19
269°
-20-
-20-
-120°-
OF
25
-300°
16
103°
WALES I.
-90°-
330°
18
84°
20
60°
25
2°
38
331°
23
54°
360°
30
25
35
30°
BOOTHIA
PENENSULA
40
VICTORIA ISLAND
45
48
29°
41
33°
PRINCE
WILLIAM I.

Figure 4.1.15 M'Clintock Channel M_2 co-phase and co-range diagram.

K1 CO-AMPLITUDE AND CO-PHASE CONTOURS

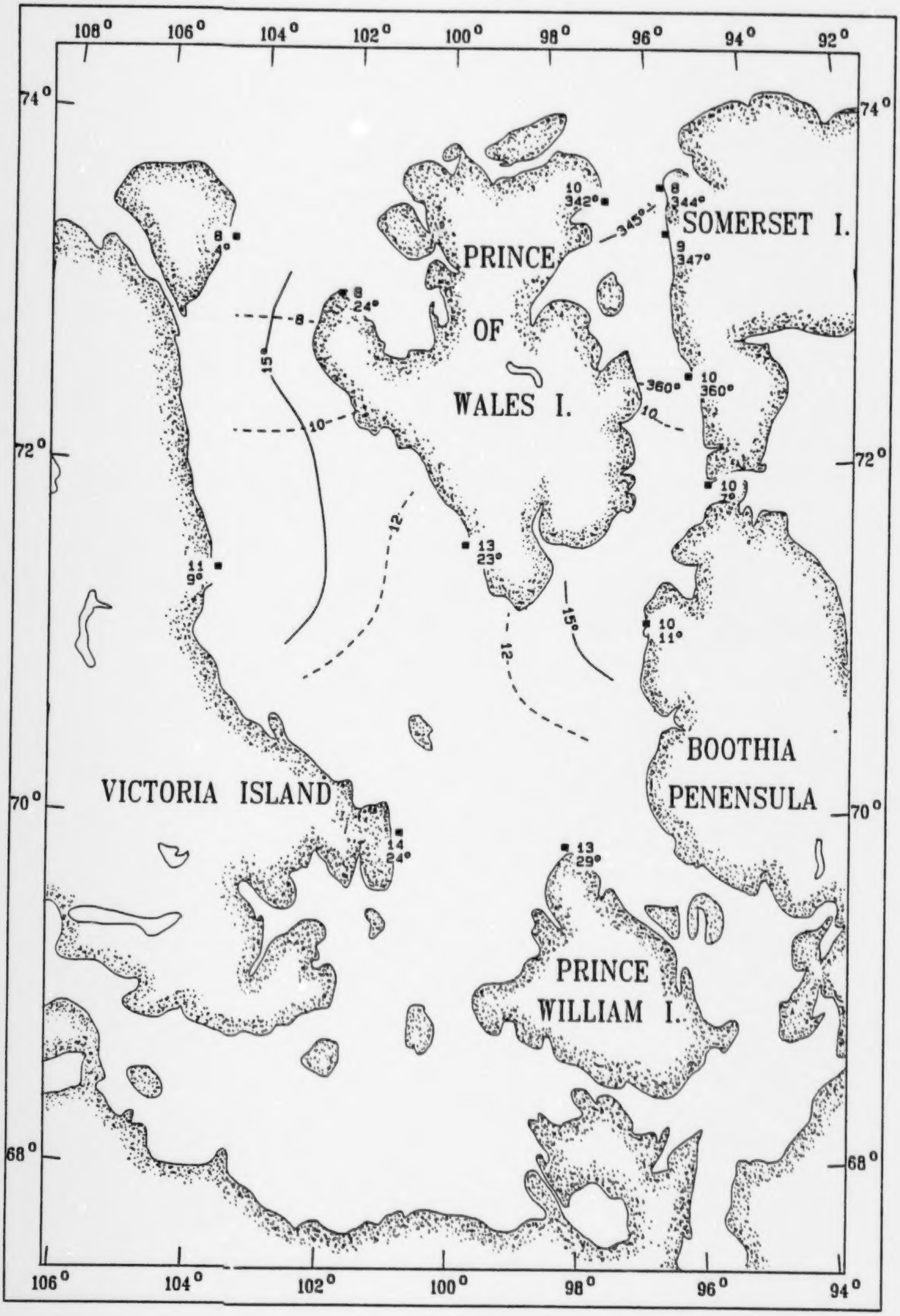
108°
106°
104°
102°
100°
98°
96°
94°
92°
74°
72°
70°
68°
PRINCE
OF
WALES I.
SOMERSET I.
VICTORIA ISLAND
BOOTHIA
PENENSULA
PRINCE
WILLIAM I.
8
4°
8
24°
10
342°
345°
8
344°
9
347°
360°
10
360°
10
10
7°
11
9°
13
23°
10
11°
14
24°
13
29°
8
10
12
15°
12
15°
106°
104°
102°
100°
98°
96°
94°

Figure 4.1.16 M'Clintock Channel K_1 co-phase and co-range diagram.

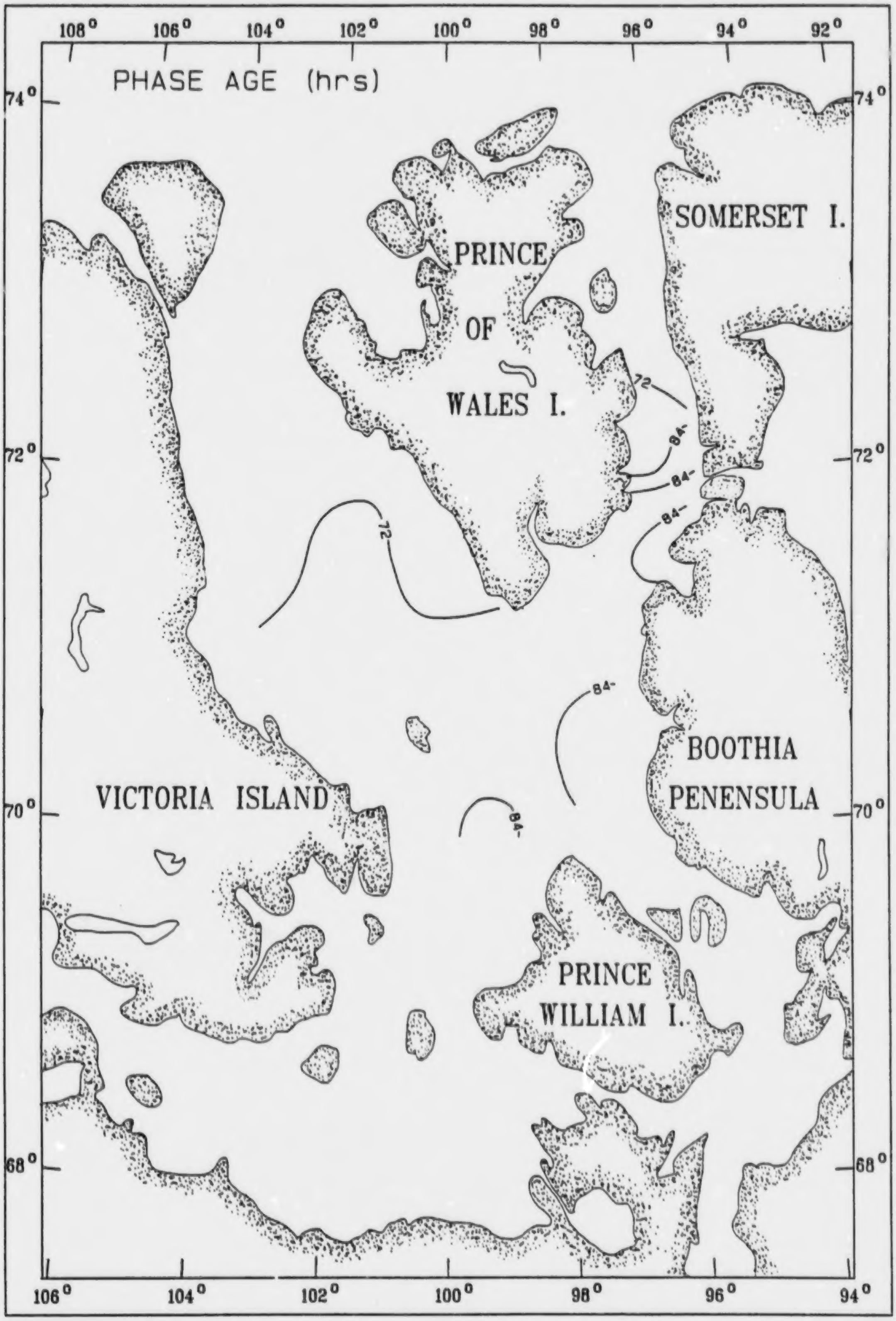
PHASE AGE (hrs)
108°
106°
104°
102°
100°
98°
96°
94°
92°
74°
72°
70°
68°
PRINCE OF WALES I.
SOMERSET I.
VICTORIA ISLAND
BOOTHIA PENENSULA
PRINCE WILLIAM I.
72
84
84
84
72
84
84
106°
104°
102°
100°
98°
96°
94°

Figure 4.1.17 M'Clintock Channel phase age.

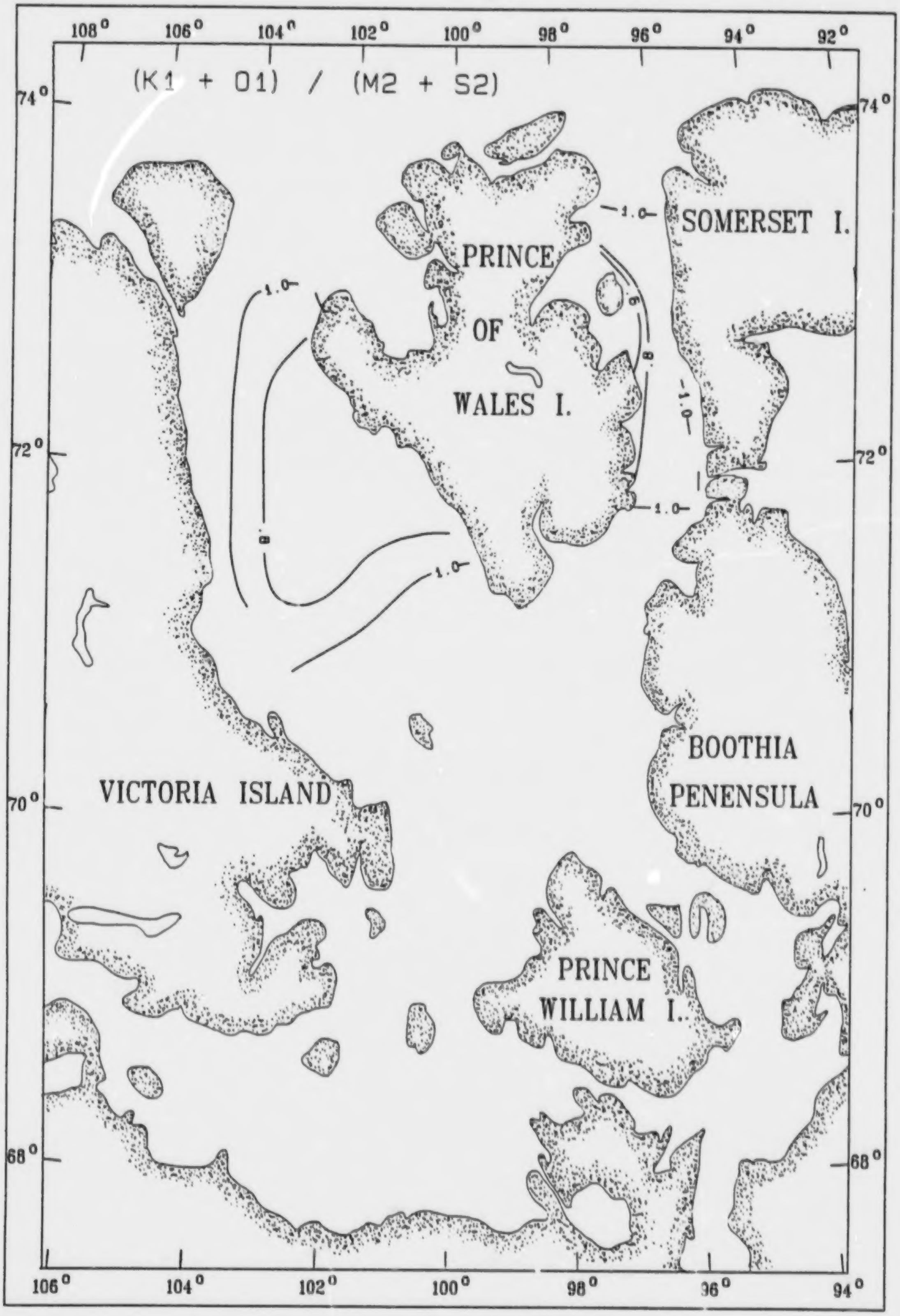
(K1 + O1) / (M2 + S2)
108°
106°
104°
102°
100°
98°
96°
94°
92°
74°
72°
70°
68°
106°
104°
102°
100°
98°
96°
94°
PRINCE
OF
WALES I.
SOMERSET I.
VICTORIA ISLAND
BOOTHIA
PENENSULA
PRINCE
WILLIAM I.
1.0
1.0
1.0
1.0
1.0
.8
.8
.9

Figure 4.1.18 M'Clintock Channel tidal character.

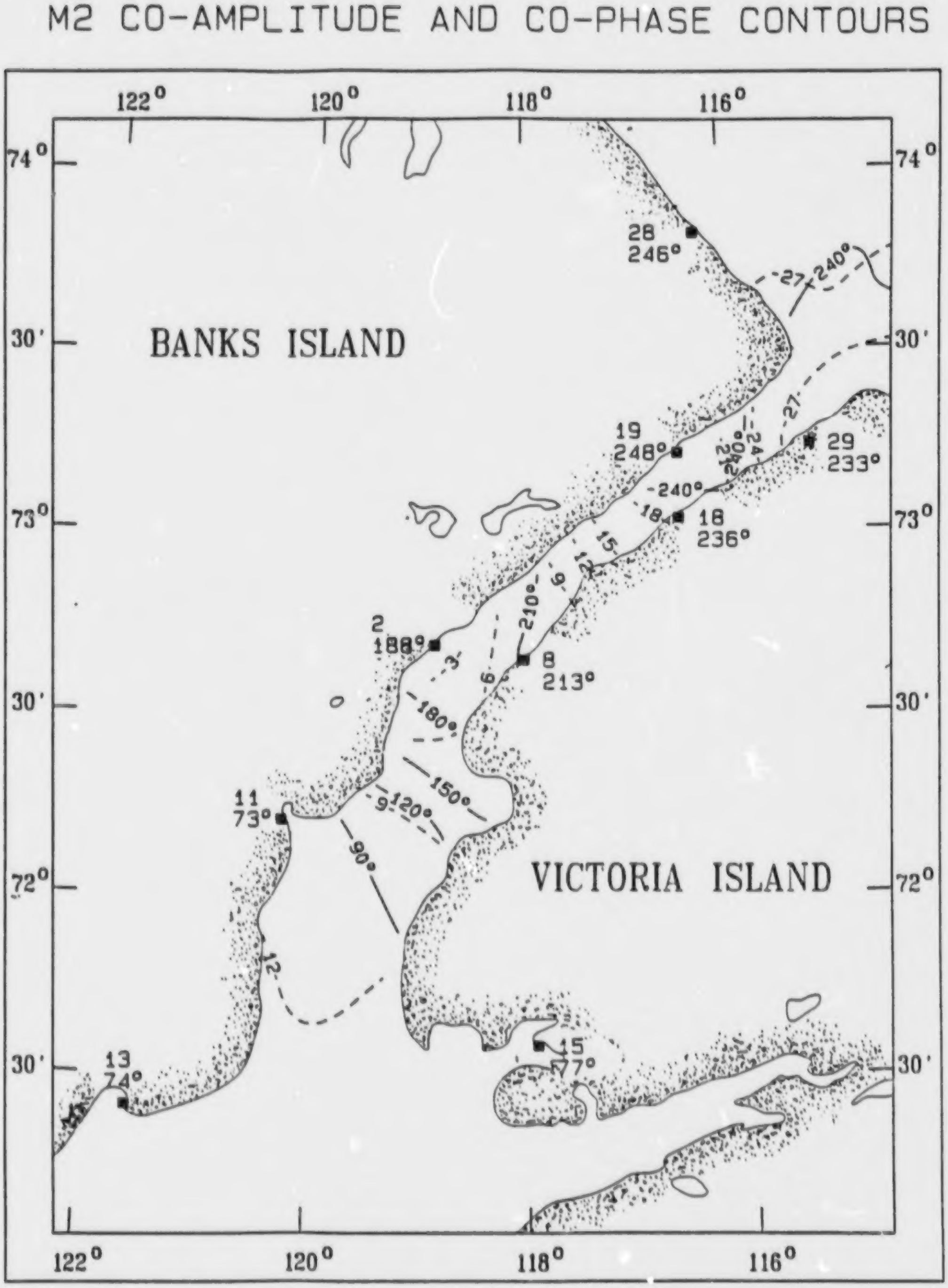
M2 CO-AMPLITUDE AND CO-PHASE CONTOURS
122°
120°
118°
116°
74°
30'
73°
72°
BANKS ISLAND
VICTORIA ISLAND
28
246°
27
240°
19
248°
24
240°
29
233°
18
236°
15
12
9
210°
2
188°
3
6
8
213°
180°
150°
120°
90°
11
73°
12
13
74°
15
177°

Figure 4.1.19 Prince of Wales Strait M_2 co-phase and co-range diagram.

K1 CO-AMPLITUDE AND CO-PHASE CONTOURS

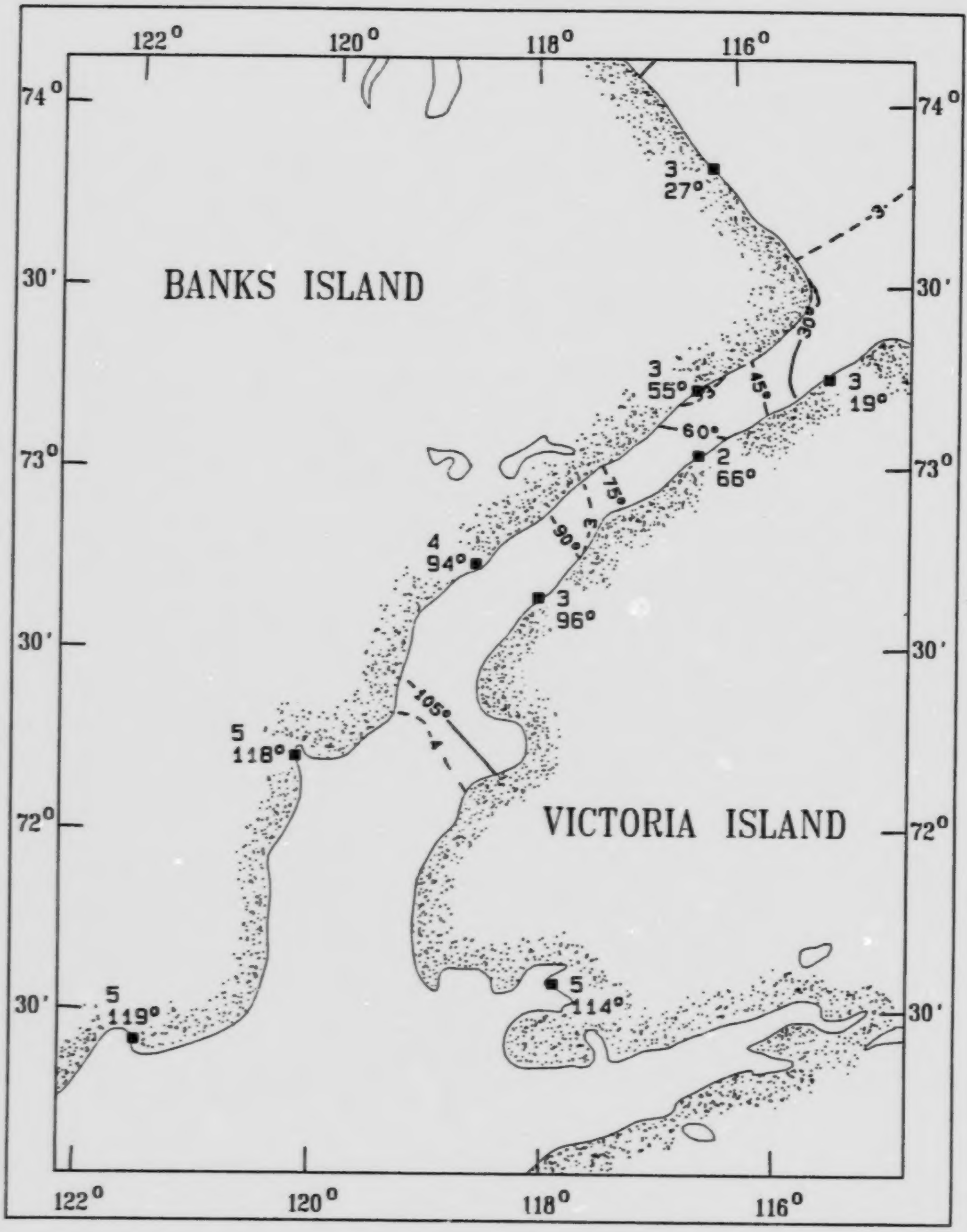
122°
120°
118°
116°
74°
30'
73°
30'
72°
30'
BANKS ISLAND
VICTORIA ISLAND
3
27°
3
30°
3
55°
45°
3
19°
60°
2
66°
75°
3
90°
4
94°
3
96°
105°
5
118°
4
5
119°
5
114°
122°
120°
118°
116°

Figure 4.1.20 Prince of Wales Strait K_1 co-phase and co-range diagram.

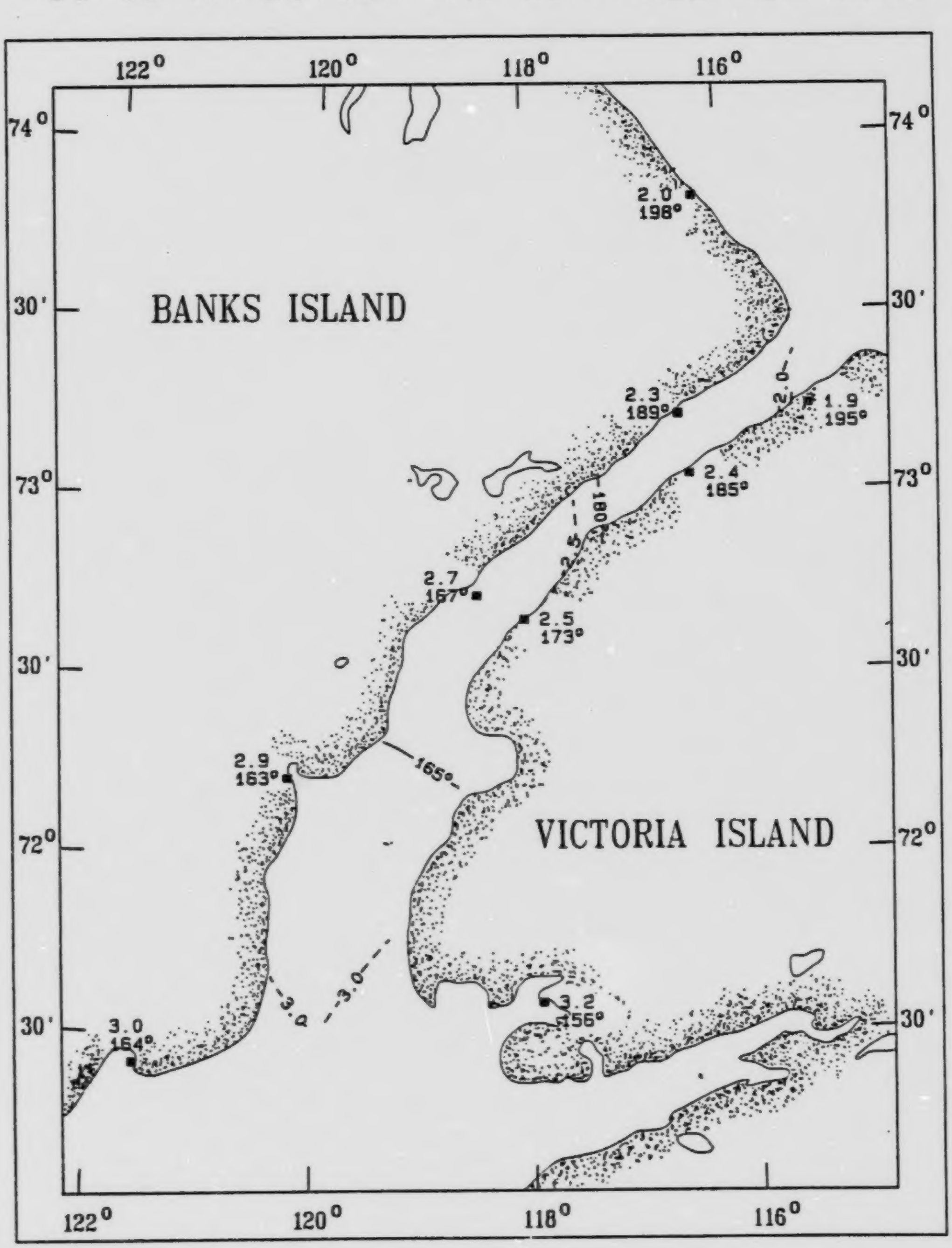
O1 CO-AMPLITUDE AND CO-PHASE CONTOURS

122°
120°
118°
116°
74°
30'
73°
30'
72°
30'
BANKS ISLAND
VICTORIA ISLAND
2.0
198°
2.3
189°
1.9
195°
2.0
2.4
185°
180°
2.5
2.7
167°
2.5
173°
2.9
163°
165°
3.0
3.0
3.0
164°
3.2
156°

Figure 4.1.21 Prince of Wales Strait O_1 co-phase and co-range diagram.

PHASE AGE (hrs)

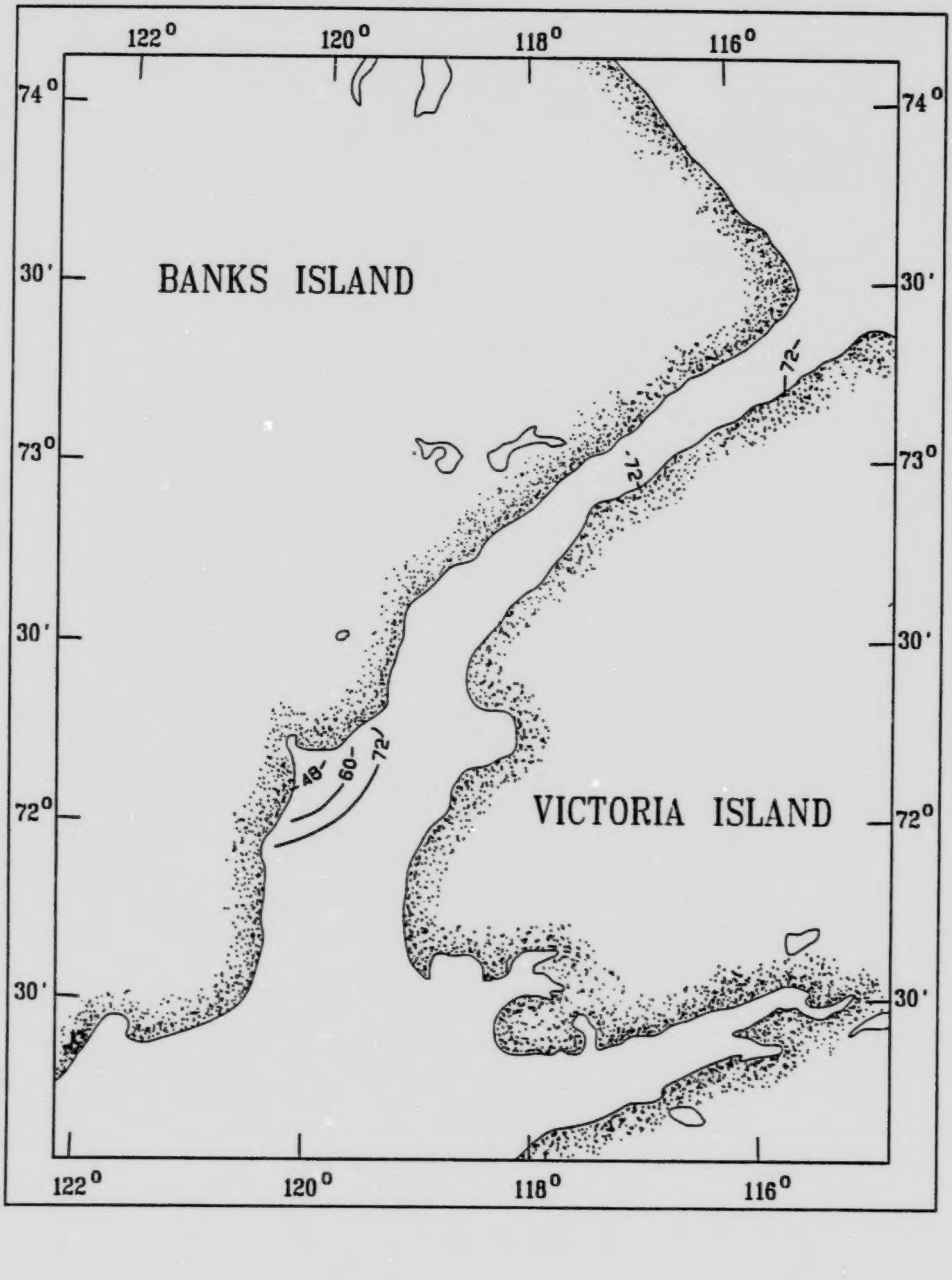
122°
120°
118°
116°
74°
30'
73°
30'
72°
30'
BANKS ISLAND
VICTORIA ISLAND
72
72
48
60
72

Figure 4.1.22 Prince of Wales Strait phase age.

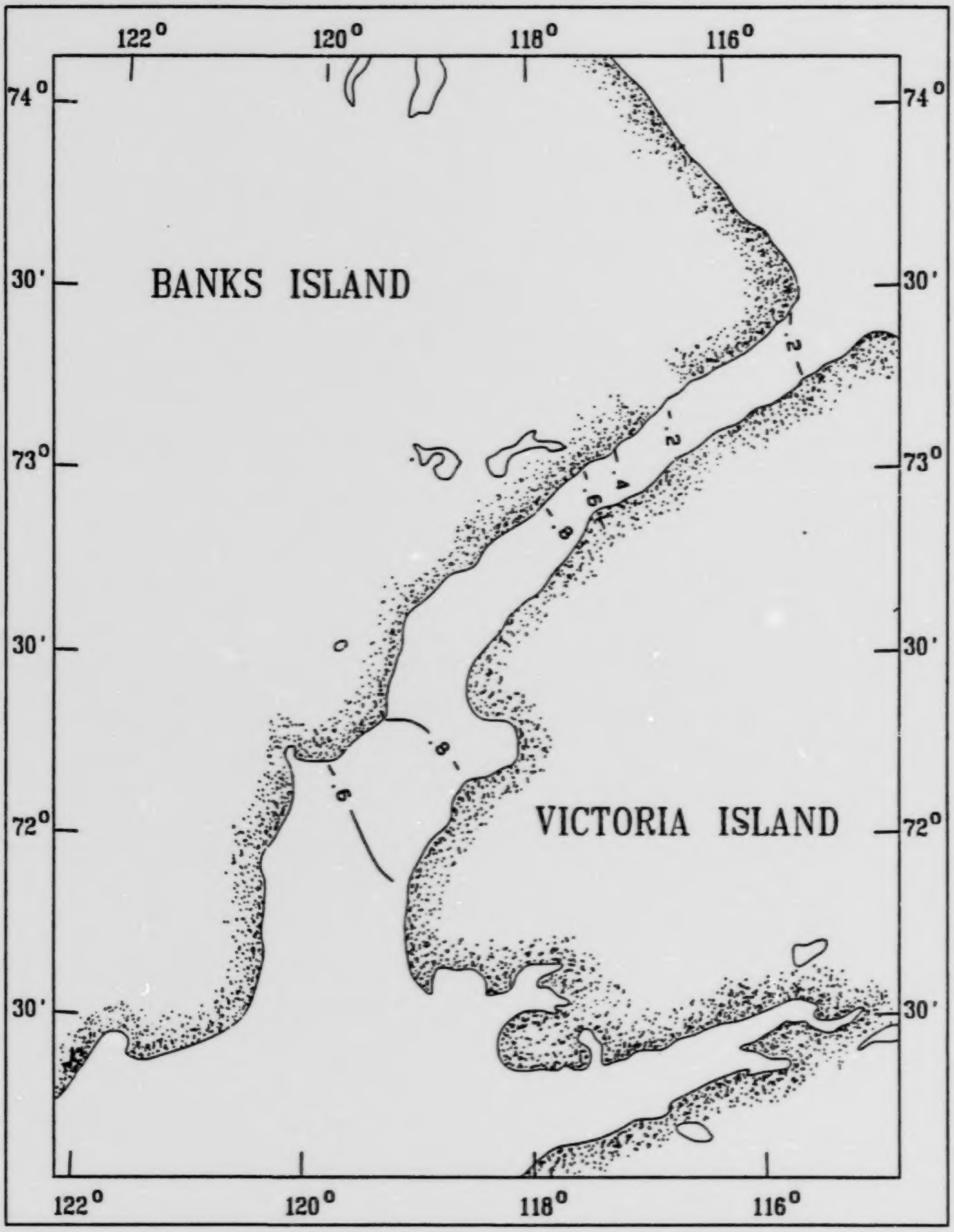

(K1 + O1) / (M2 + S2)

122°
120°
118°
116°
74°
30'
73°
30'
72°
30'
BANKS ISLAND
VICTORIA ISLAND
.2
.2
.4
.6
.8
0
.8
.6

Figure 4.1.23 Prince of Wales Strait tidal character.

M2 CO-AMPLITUDE AND CO-PHASE CONTOURS

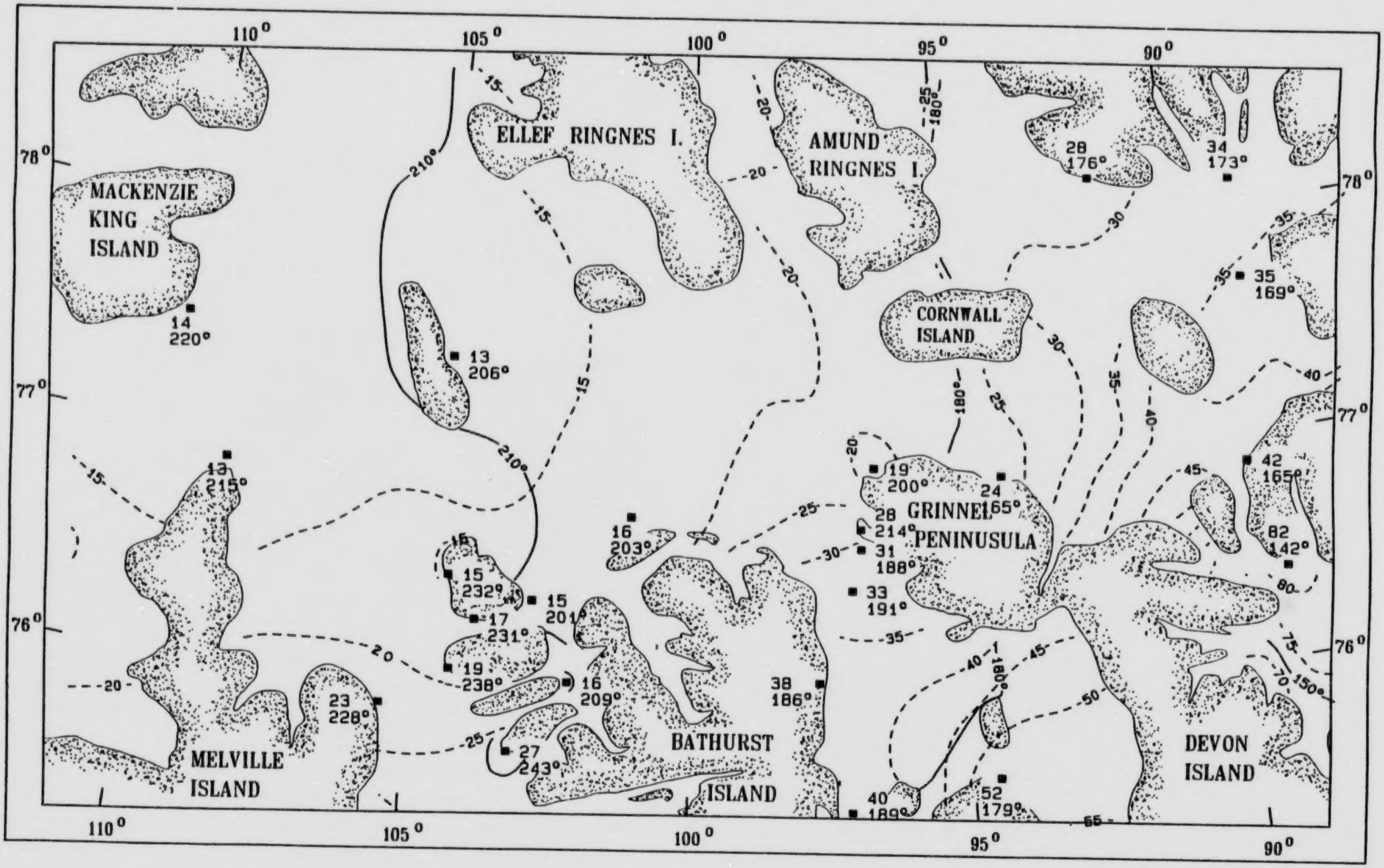
110°
105°
100°
95°
90°
78°
77°
76°
MACKENZIE KING ISLAND
ELLEF RINGNES I.
AMUND RINGNES I.
CORNWALL ISLAND
GRINNEL PENINUSULA
BATHURST ISLAND
MELVILLE ISLAND
DEVON ISLAND
14 220°
13 206°
13 215°
28 176°
34 173°
35 169°
42 165°
82 142°
19 200°
24 165°
28 214°
31 188°
33 191°
16 203°
15 232°
15 201°
17 231°
19 238°
16 209°
27 243°
23 228°
38 186°
40 189°
52 179°
210°
180°
150°
15
20
25
30
35
40
45
50
55
70
75
80

Figure 4.1.24 Queen Elizabeth Island Region M_2 co-phase and co-range diagram.

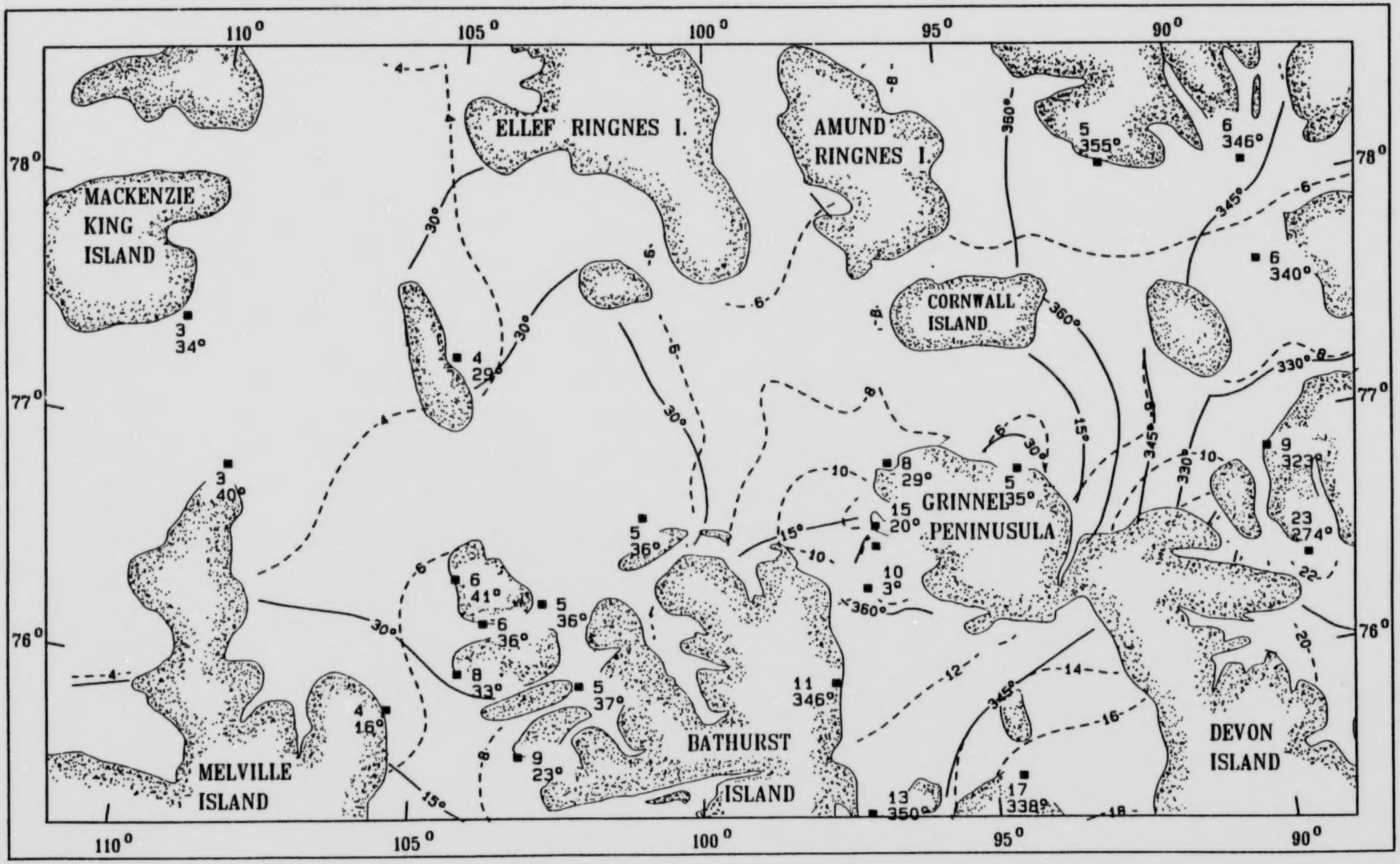

K1 CO-AMPLITUDE AND CO-PHASE CONTOURS

110°
105°
100°
95°
90°
78°
77°
76°
MACKENZIE KING ISLAND
ELLEF RINGNES I.
AMUND RINGNES I.
CORNWALL ISLAND
GRINNEL PENINUSULA
BATHURST ISLAND
MELVILLE ISLAND
DEVON ISLAND
3 34°
4 29°
3 40°
5 355°
6 346°
6 340°
9 323°
23 274°
8 29°
5 35°
15 20°
10 3°
5 36°
6 41°
5 36°
6 36°
8 33°
5 37°
9 23°
4 16°
11 346°
13 350°
17 338°
4
6
8
10
12
14
16
18
20
22
15°
30°
330°
345°
360°

Figure 4.1.25 Queen Elizabeth Island Region K_1 co-phase and co-range diagram.

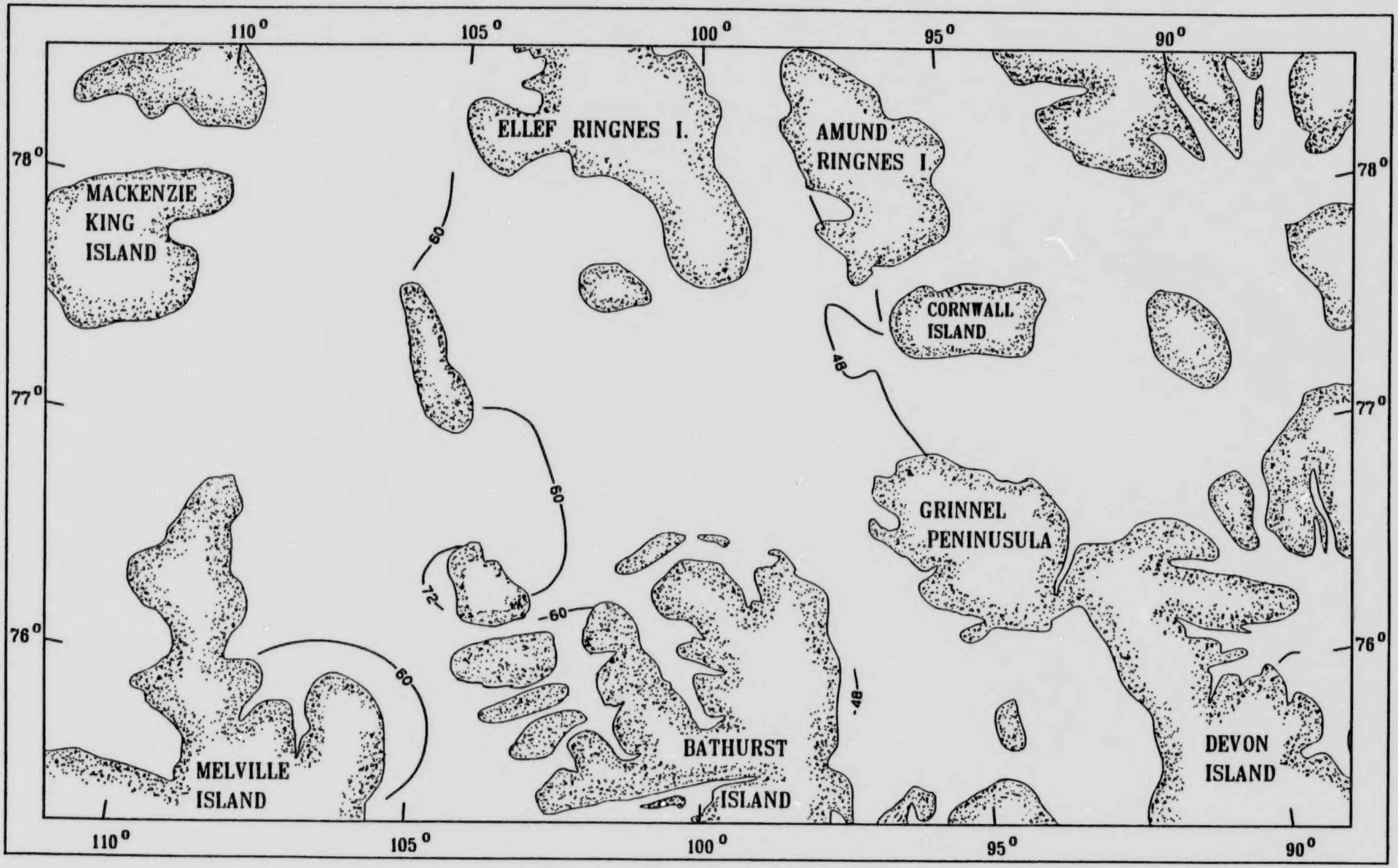

PHASE AGE (hrs)

110°
105°
100°
95°
90°
78°
77°
76°
ELLEF RINGNES I.
AMUND RINGNES I.
MACKENZIE KING ISLAND
CORNWALL ISLAND
GRINNEL PENINUSULA
MELVILLE ISLAND
BATHURST ISLAND
DEVON ISLAND
60
60
60
60
72
48
48

Figure 4.1.26 Queen Elizabeth Island Region phase age.

(K1 + O1) / (M2 + S2)

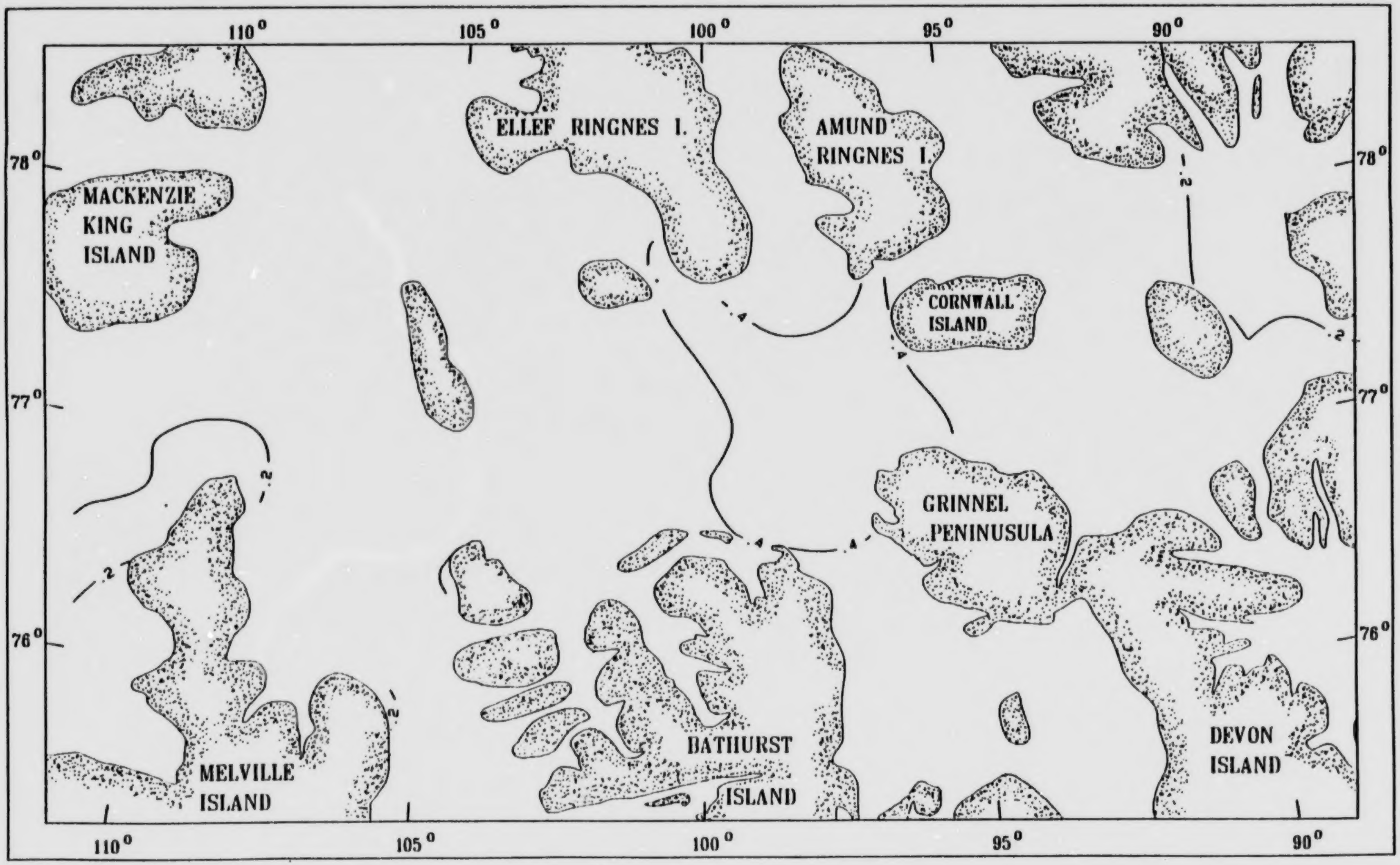
110°
105°
100°
95°
90°
78°
77°
76°
ELLEF RINGNES I.
AMUND RINGNES I.
MACKENZIE KING ISLAND
CORNWALL ISLAND
GRINNEL PENINUSULA
MELVILLE ISLAND
BATHURST ISLAND
DEVON ISLAND
.2
.4

Figure 4.1.27 Queen Elizabeth Island Region tidal character.

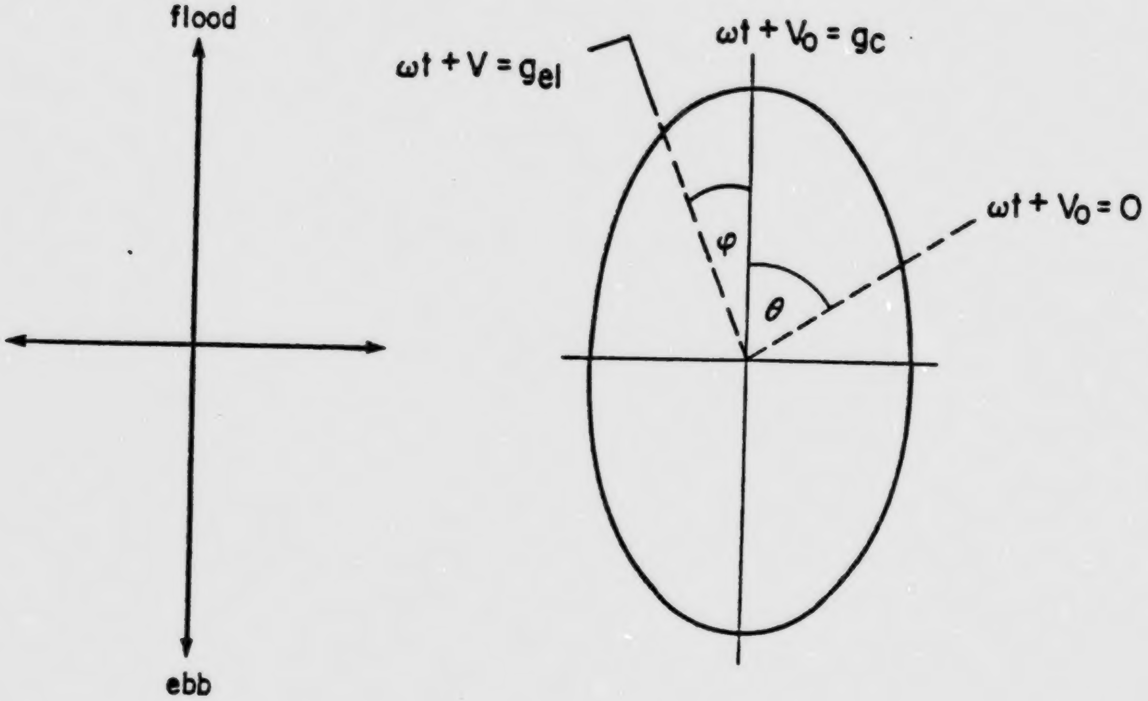
flood
ebb
$\omega t + V = g_{el}$
$\omega t + V_0 = g_c$
$\omega t + V_0 = 0$
φ
θ

θ = g current

ϕ = g elevation − g current = phase between maximum current and high water local

g_{el} = phase of local high water

The phase argument for currents is $\omega t + V_o - g_c$: maximum currents occur when $\omega t + V_o - g_c = 0°$, which defines the flood direction. The current vector in the above diagram rotates counter-clockwise, as indicated by the direction of the hook on the vector labelled $\omega t + V_o - g_c$.

Figure 4.2.1 Definition of ellipse parameters.

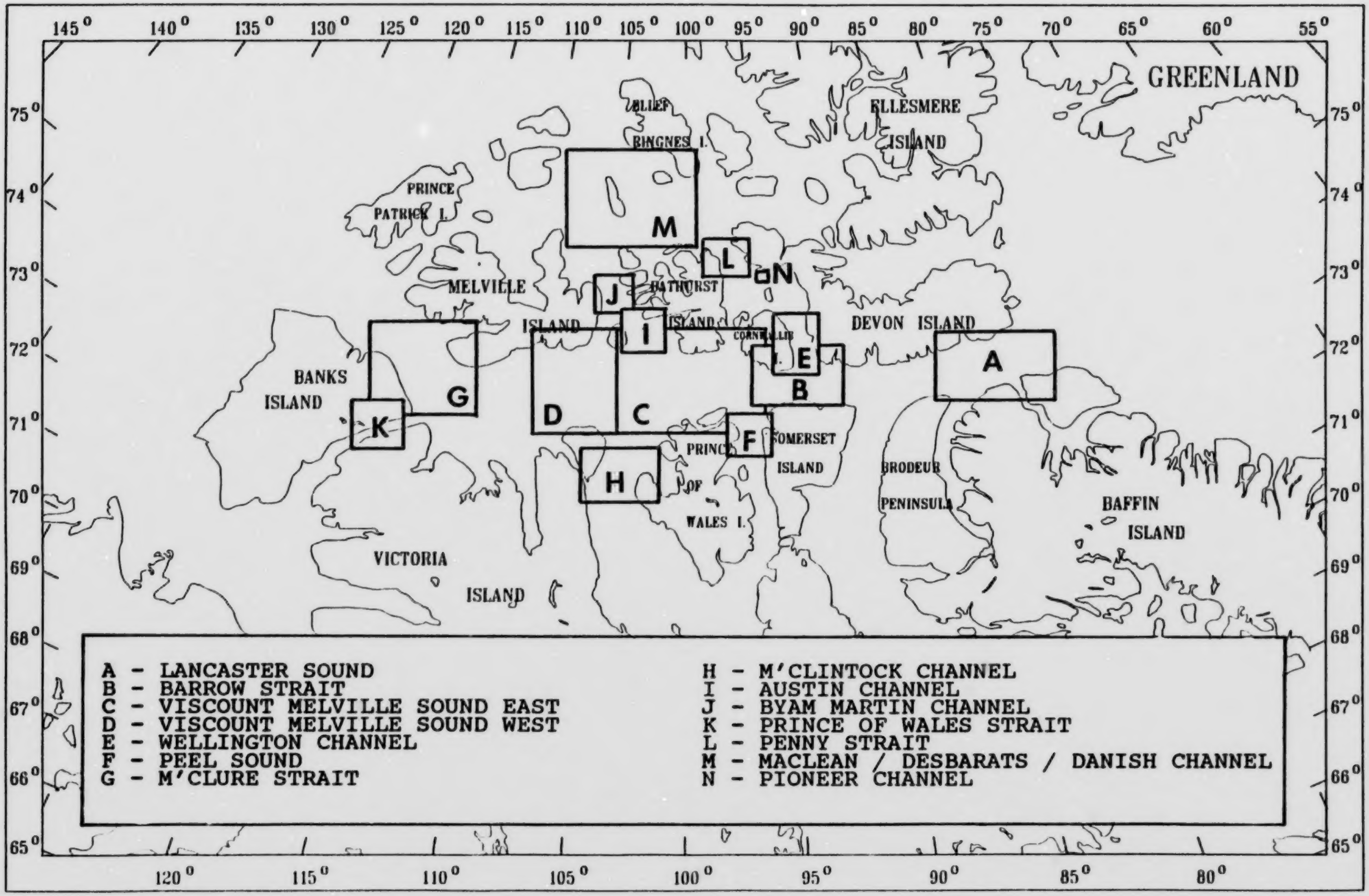
145°
140°
135°
130°
125°
120°
115°
110°
105°
100°
95°
90°
85°
80°
75°
70°
65°
60°
55°
75°
74°
73°
72°
71°
70°
69°
68°
67°
66°
65°
GREENLAND
ELLESMERE ISLAND
ELLEF RINGNES I.
PRINCE PATRICK I.
MELVILLE ISLAND
BATHURST ISLAND
CORNWALLIS I.
DEVON ISLAND
BANKS ISLAND
SOMERSET ISLAND
PRINCE OF WALES I.
BRODEUR PENINSULA
BAFFIN ISLAND
VICTORIA ISLAND
A
B
C
D
E
F
G
H
I
J
K
L
M
N
A - LANCASTER SOUND
B - BARROW STRAIT
C - VISCOUNT MELVILLE SOUND EAST
D - VISCOUNT MELVILLE SOUND WEST
E - WELLINGTON CHANNEL
F - PEEL SOUND
G - M'CLURE STRAIT
H - M'CLINTOCK CHANNEL
I - AUSTIN CHANNEL
J - BYAM MARTIN CHANNEL
K - PRINCE OF WALES STRAIT
L - PENNY STRAIT
M - MACLEAN / DESBARATS / DANISH CHANNEL
N - PIONEER CHANNEL
120°
115°
110°
105°
100°
95°
90°
85°
80°

Figure 4.2.2 Chart of the Arctic showing subregions used in the description of the horizontal distribution of tidal currents.

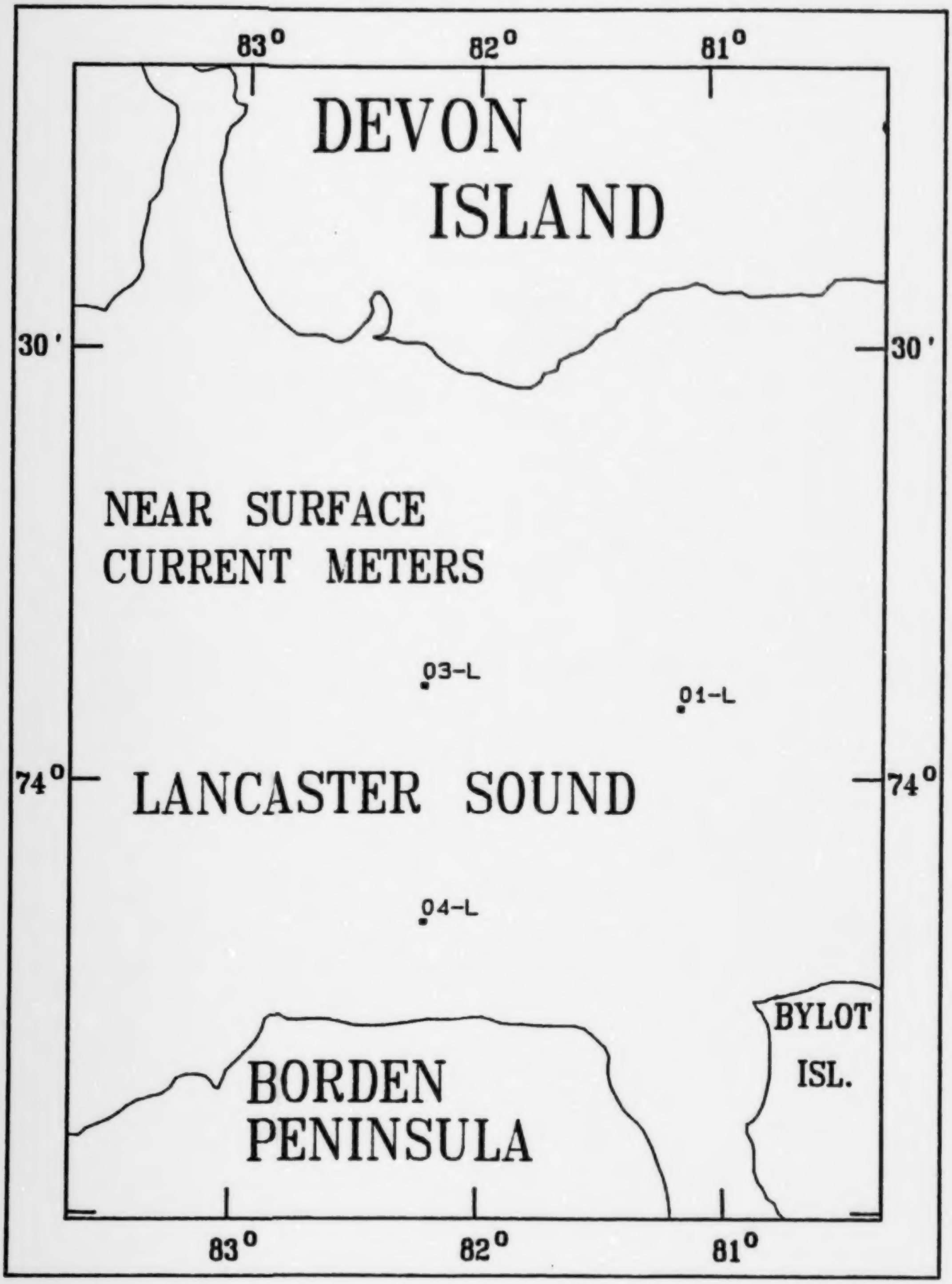
83°
82°
81°
DEVON ISLAND
30'
30'
NEAR SURFACE CURRENT METERS
03-L
01-L
74°
LANCASTER SOUND
74°
04-L
BYLOT ISL.
BORDEN PENINSULA
83°
82°
81°

Figure 4.2.3. Lancaster Sound current meter stations.

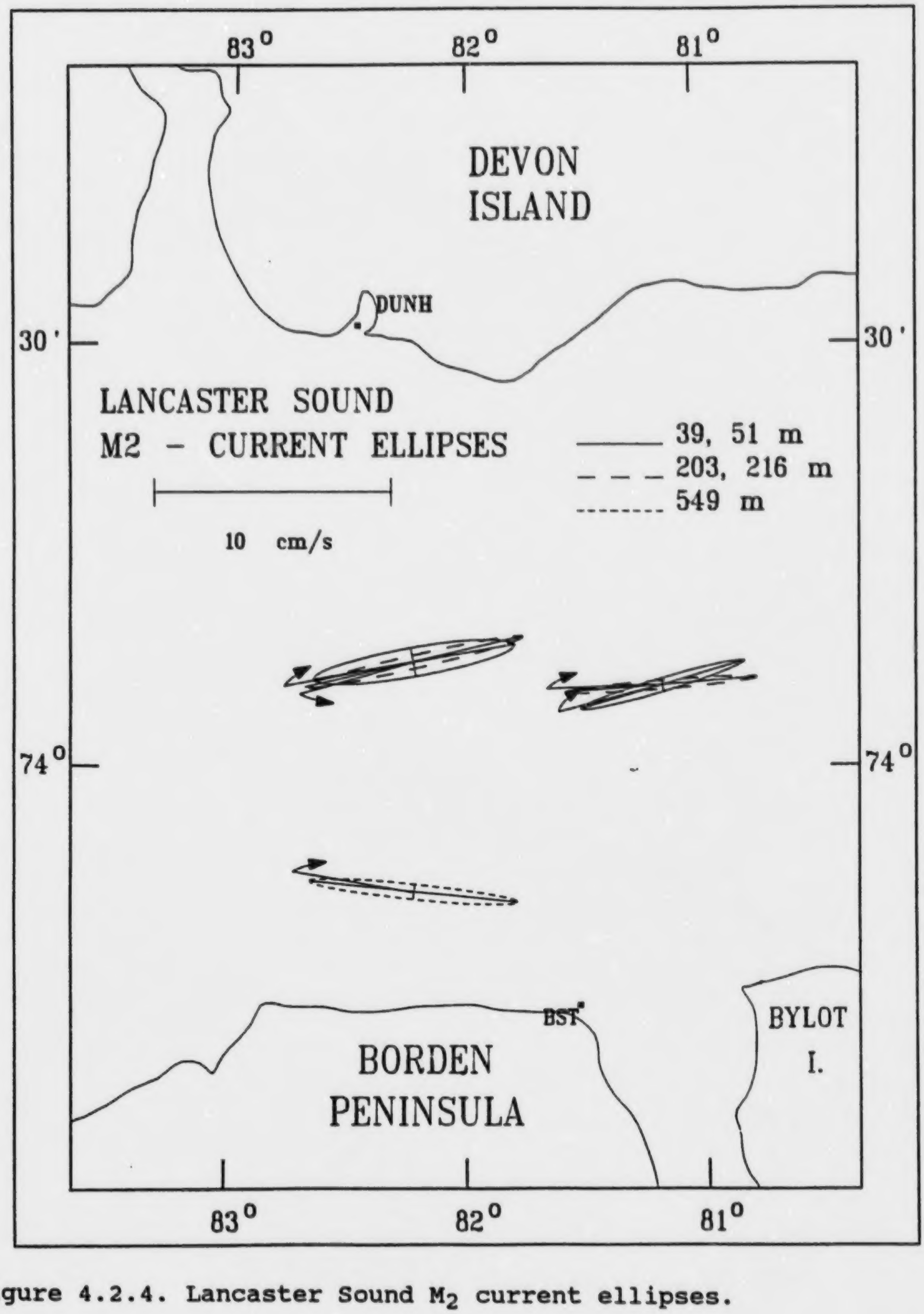
83°
82°
81°
DEVON
ISLAND
DUNH
30'
30'
LANCASTER SOUND
M2 - CURRENT ELLIPSES
10 cm/s
39, 51 m
203, 216 m
549 m
74°
74°
BST
BYLOT
I.
BORDEN
PENINSULA
83°
82°
81°

Figure 4.2.4. Lancaster Sound M_2 current ellipses.

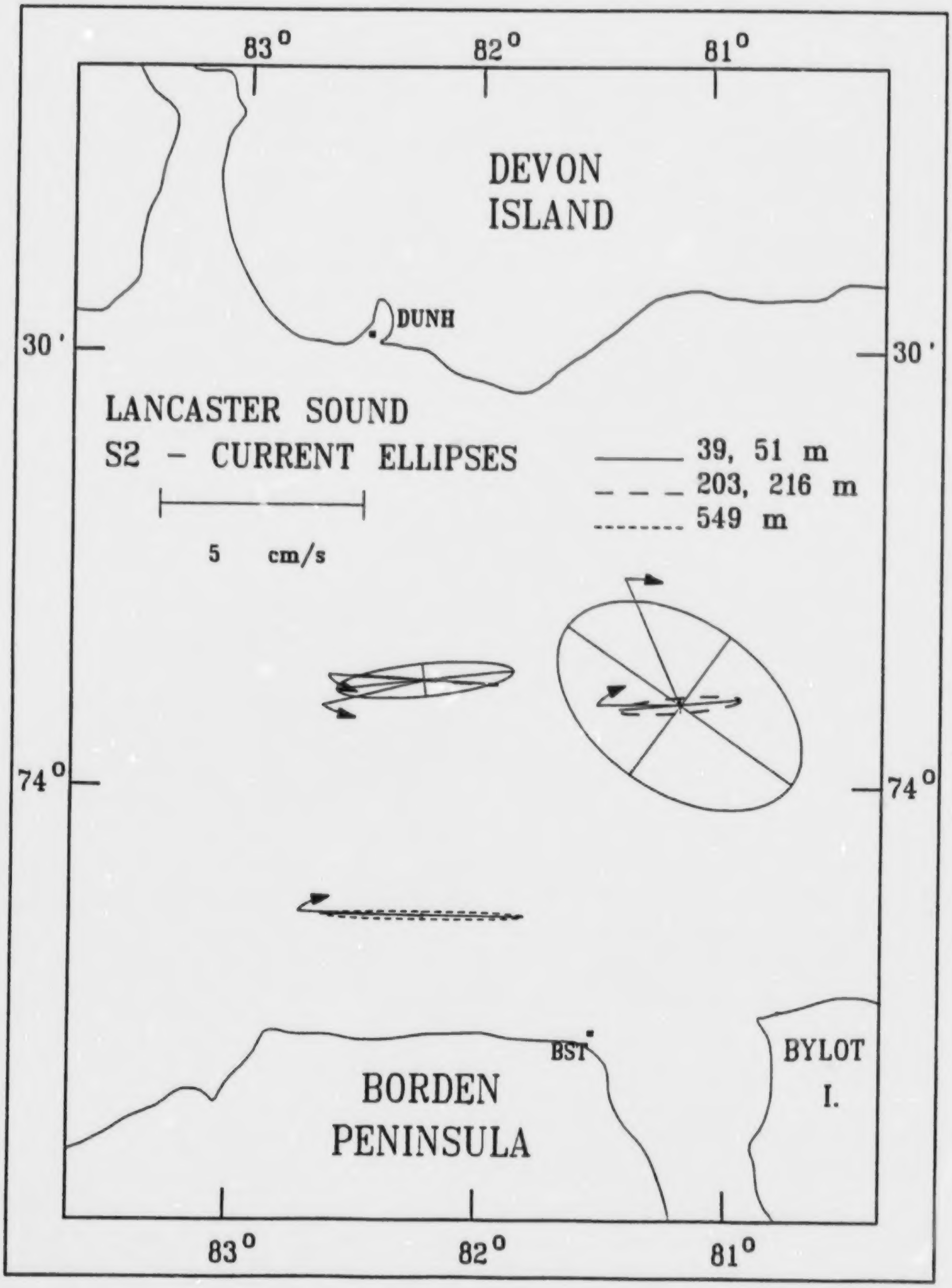
83°
82°
81°
DEVON ISLAND
DUNH
30'
LANCASTER SOUND
S2 - CURRENT ELLIPSES
5 cm/s
39, 51 m
203, 216 m
549 m
74°
BST
BORDEN PENINSULA
BYLOT I.

Figure 4.2.5. Lancaster Sound S_2 current ellipses.

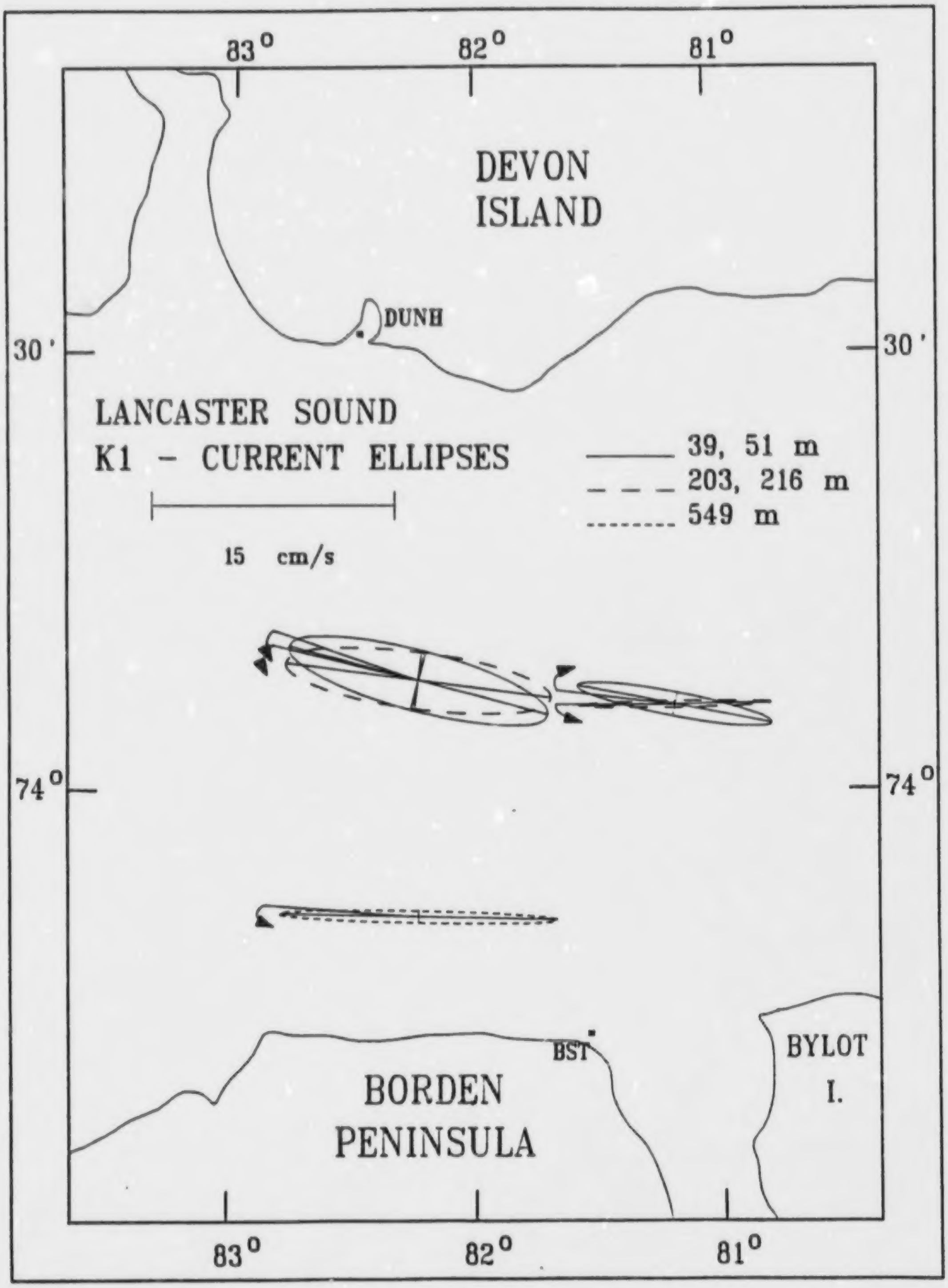
83°
82°
81°
DEVON
ISLAND
DUNH
30'
30'
LANCASTER SOUND
K1 - CURRENT ELLIPSES
39, 51 m
203, 216 m
549 m
15 cm/s
74°
74°
BST
BYLOT
I.
BORDEN
PENINSULA
83°
82°
81°

Figure 4.2.6. Lancaster Sound K_1 current ellipses.

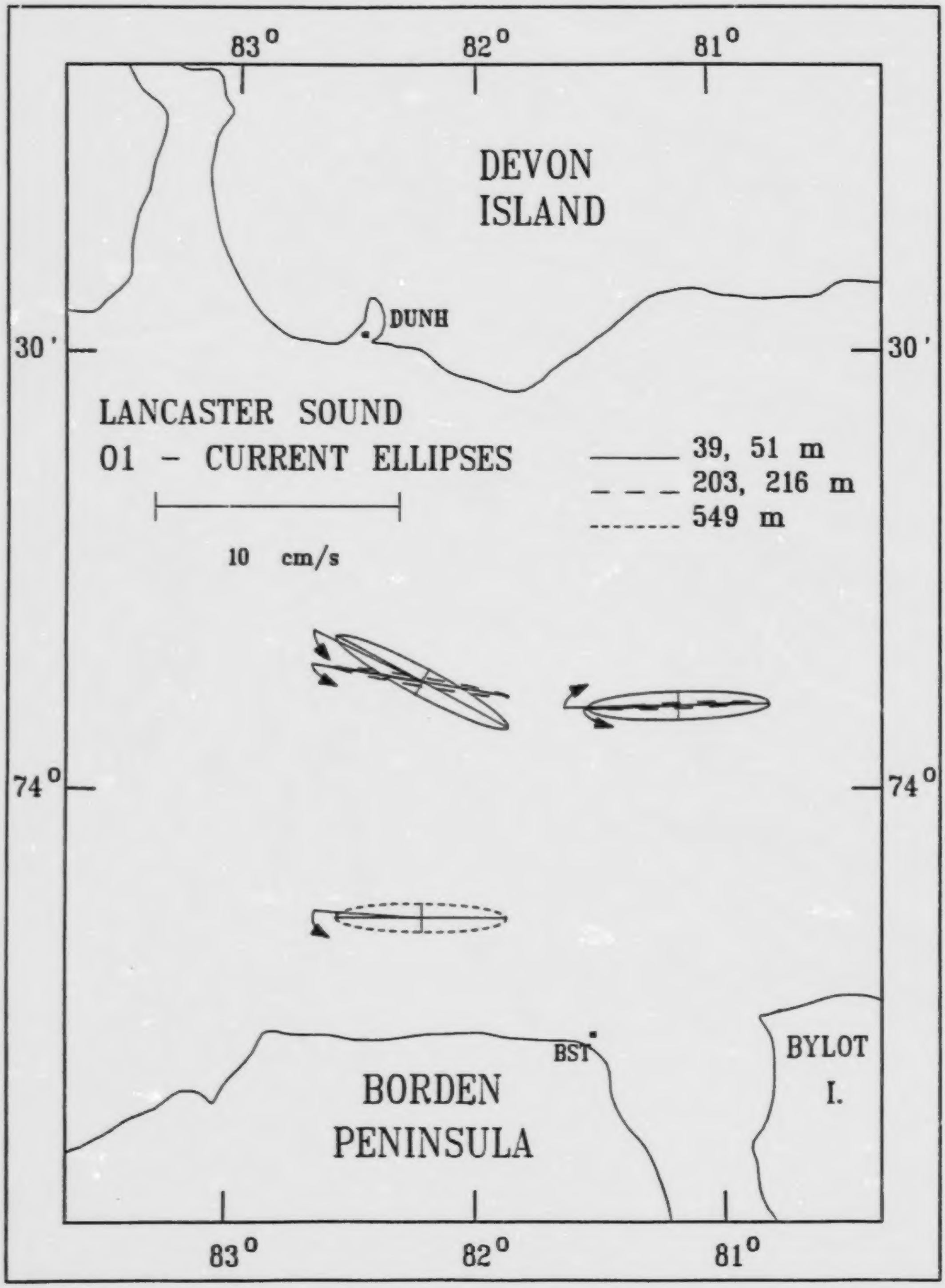
83°
82°
81°
DEVON ISLAND
DUNH
30'
LANCASTER SOUND
O1 - CURRENT ELLIPSES
39, 51 m
203, 216 m
549 m
10 cm/s
74°
BST
BORDEN PENINSULA
BYLOT I.

Figure 4.2.7. Lancaster Sound O_1 current ellipses.

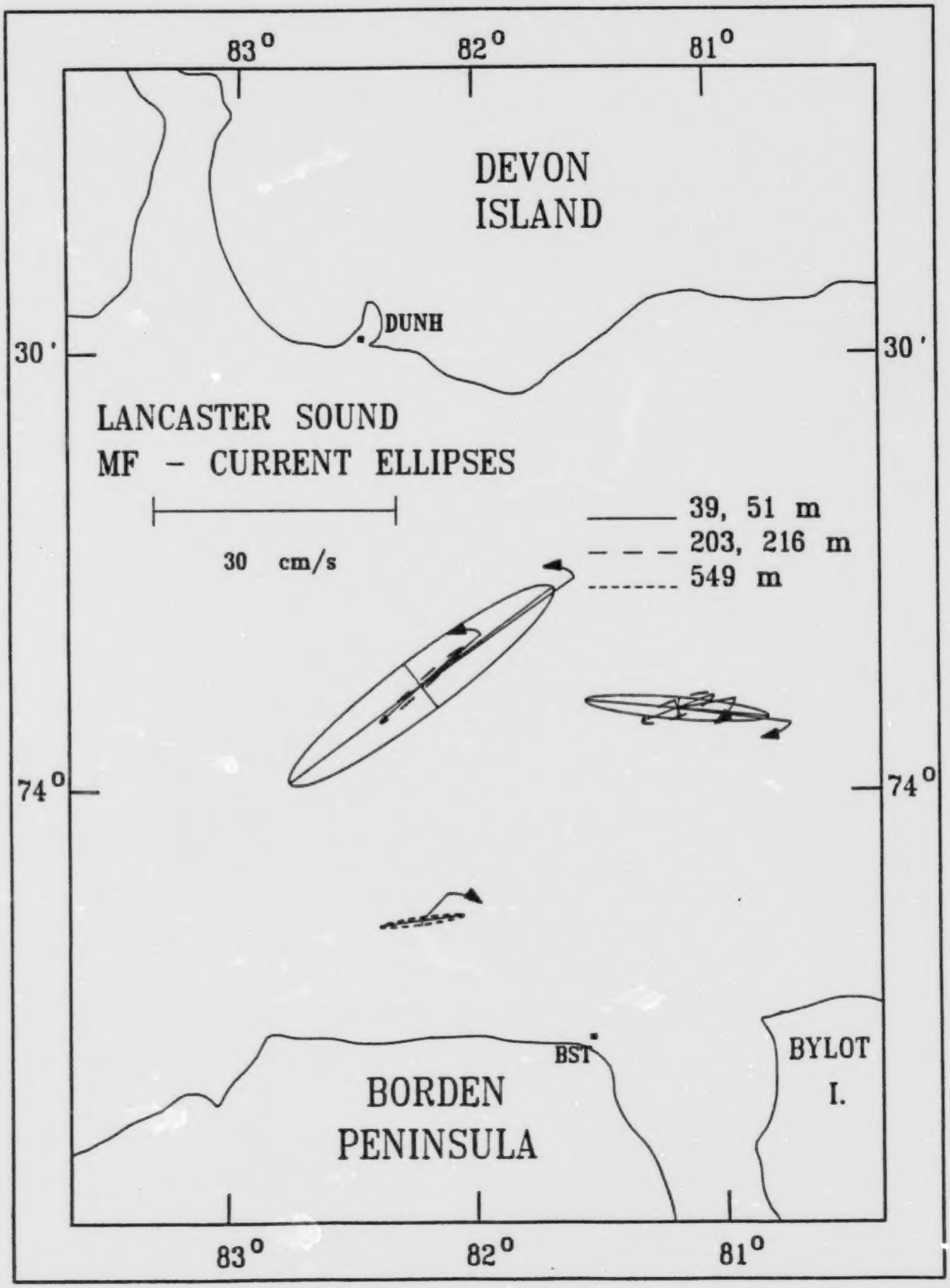
83°
82°
81°
DEVON
ISLAND
DUNH
30'
30'
LANCASTER SOUND
MF - CURRENT ELLIPSES
30 cm/s
39, 51 m
203, 216 m
549 m
74°
74°
BST
BYLOT
I.
BORDEN
PENINSULA
83°
82°
81°

Figure 4.2.8. Lancaster Sound Mf current ellipses.

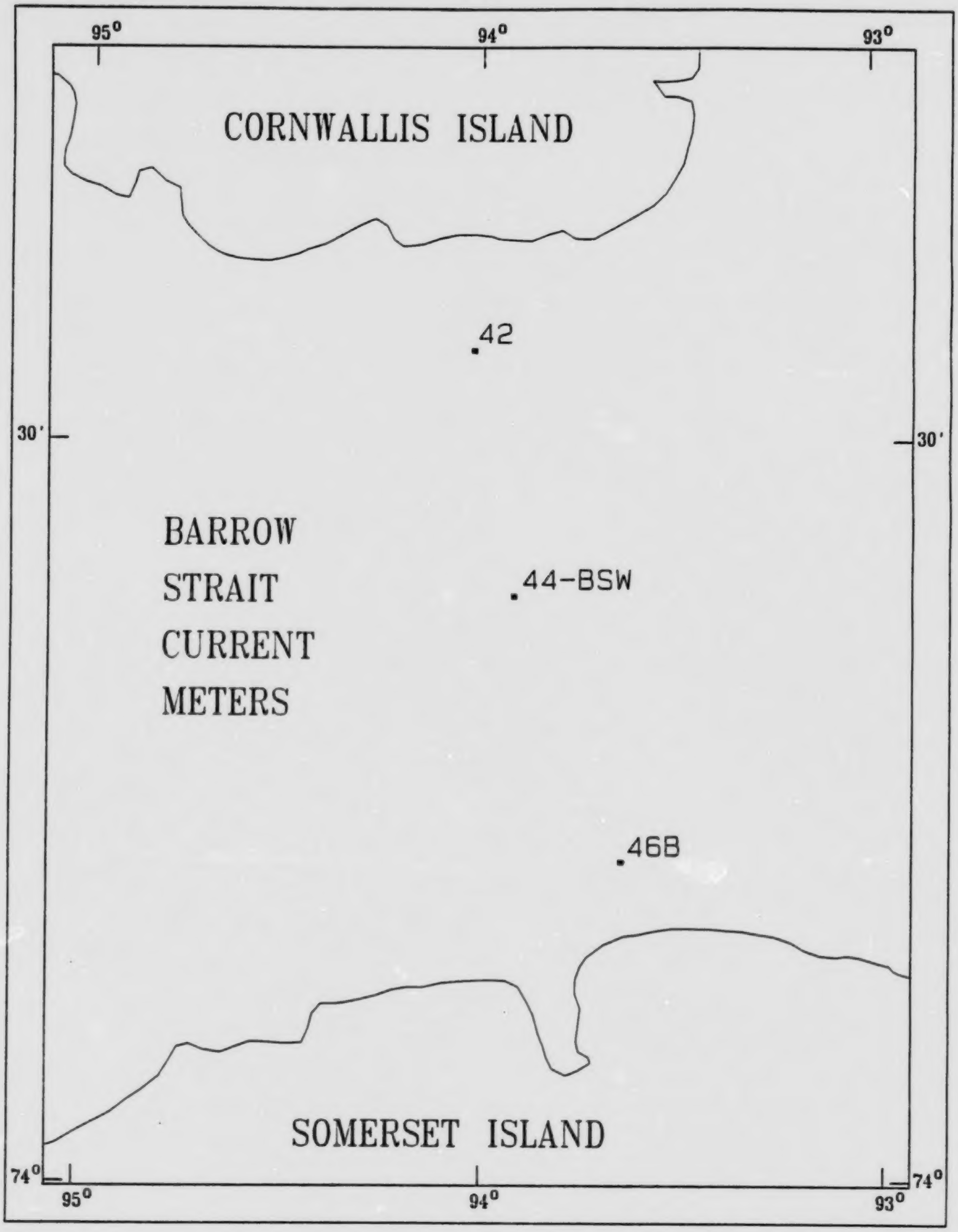
95°
94°
93°
CORNWALLIS ISLAND
42
30'
30'
BARROW
STRAIT
CURRENT
METERS
44-BSW
46B
SOMERSET ISLAND
74°
74°
95°
94°
93°

Figure 4.2.9. Barrow Strait current meter stations.

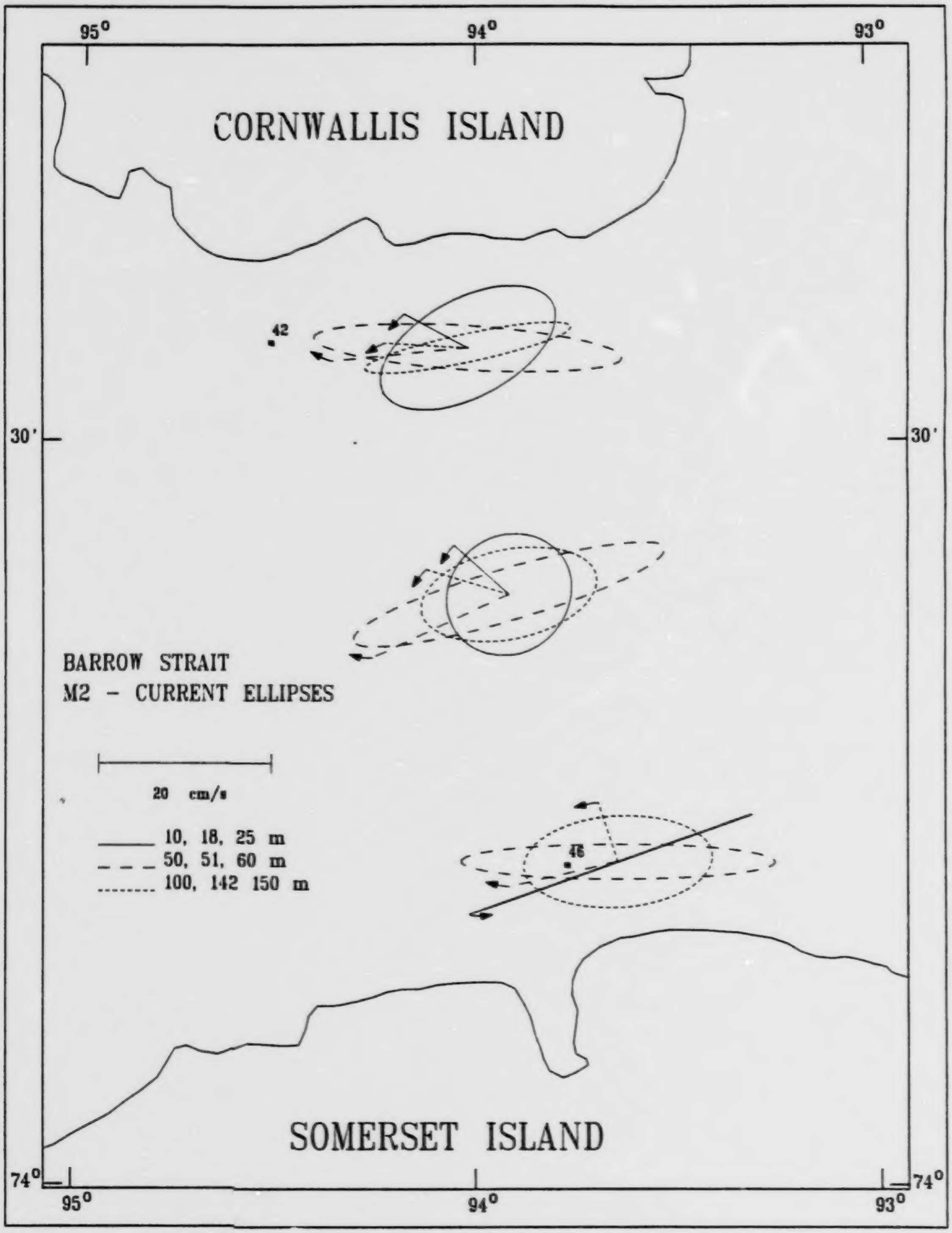
95°
94°
93°
CORNWALLIS ISLAND
42
30'
30'
BARROW STRAIT
M2 - CURRENT ELLIPSES
20 cm/s
10, 18, 25 m
50, 51, 60 m
100, 142 150 m
46
SOMERSET ISLAND
74°
74°
95°
94°
93°

Figure 4.2.10. Barrow Strait M_2 current ellipses.

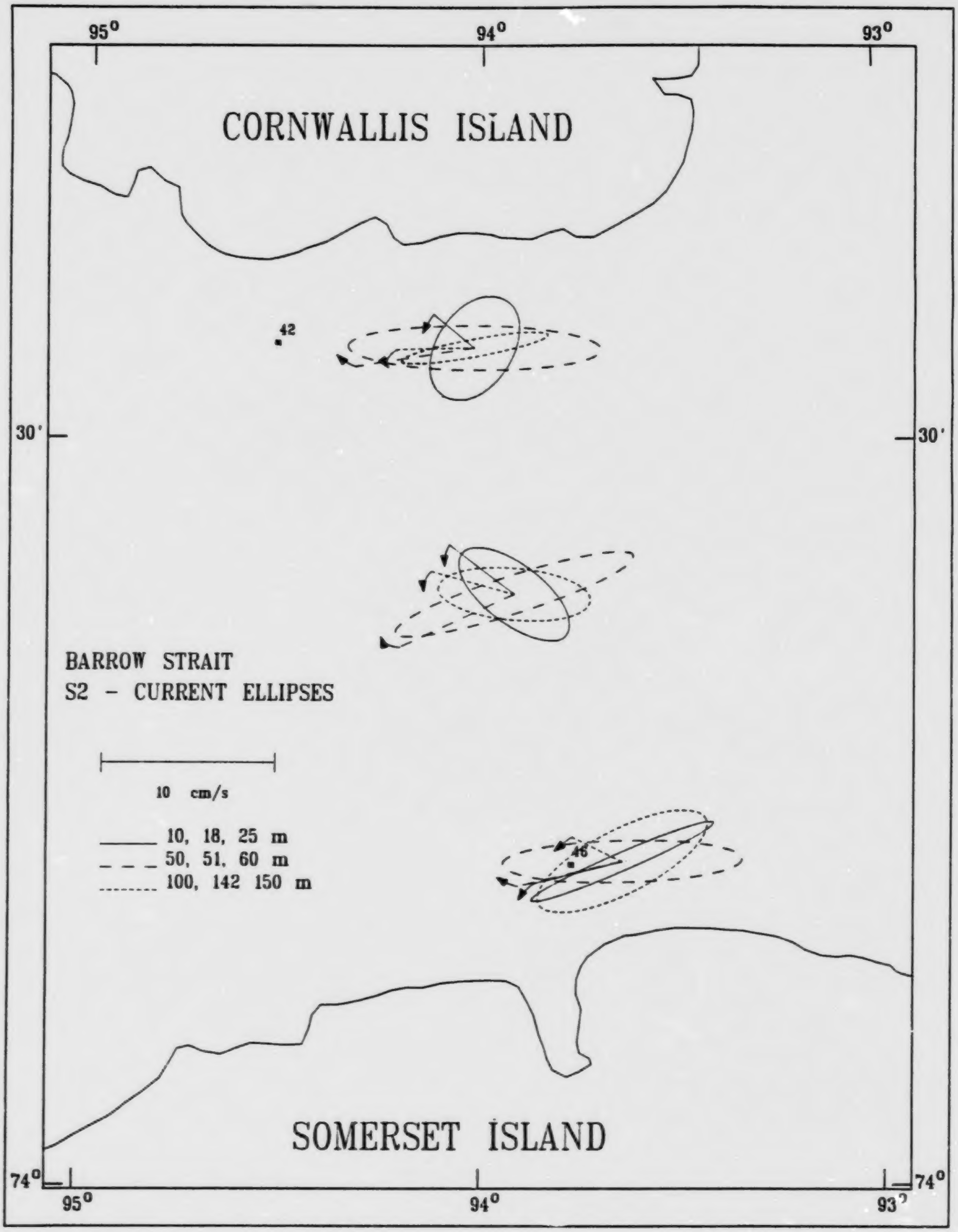
95°
94°
93°
CORNWALLIS ISLAND
42
30'
30'
BARROW STRAIT
S2 - CURRENT ELLIPSES
10 cm/s
10, 18, 25 m
50, 51, 60 m
100, 142 150 m
46
SOMERSET ISLAND
74°
74°
95°
94°
93°

Figure 4.2.11. Barrow Strait S_2 current ellipses.

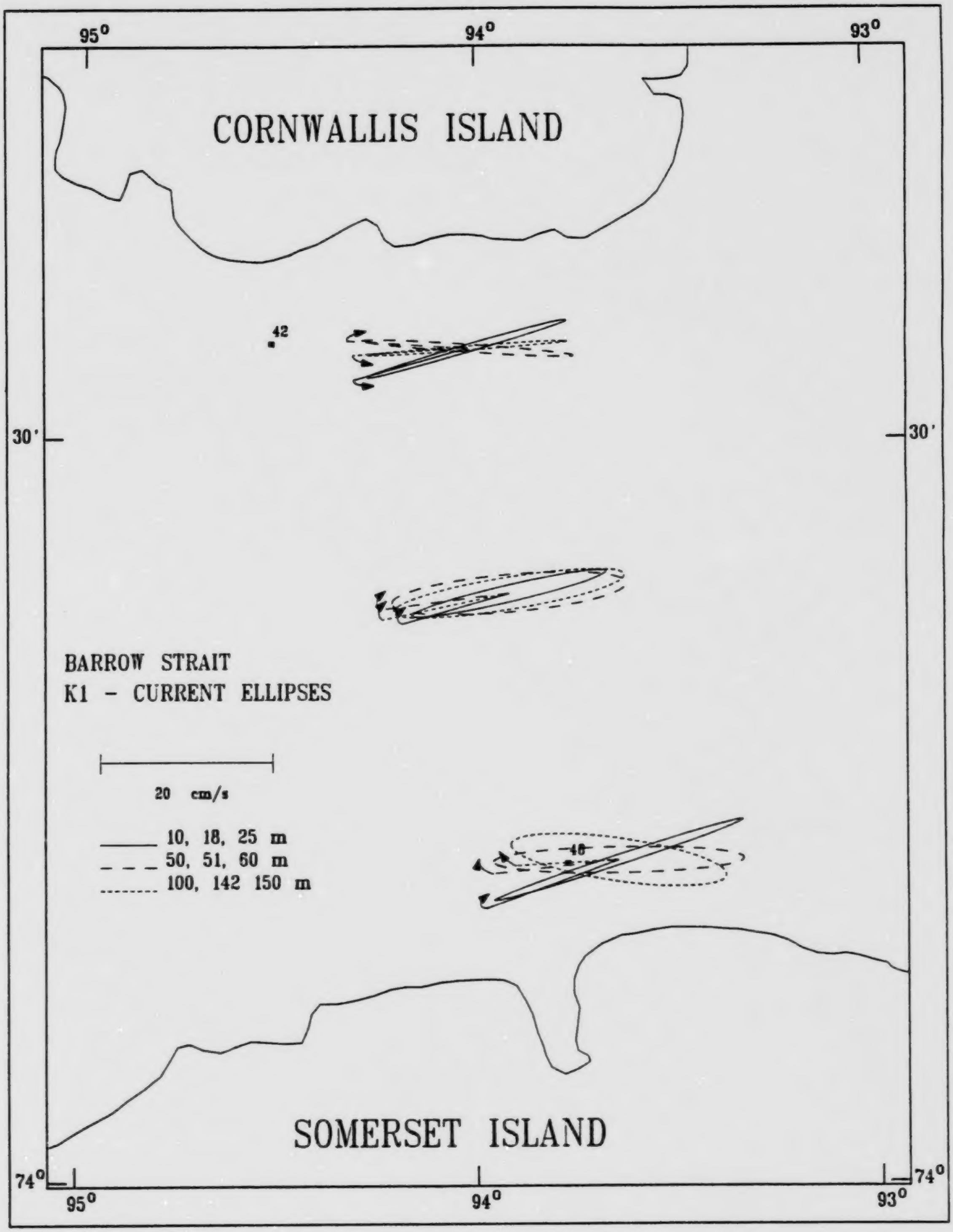
95°
94°
93°
CORNWALLIS ISLAND
42
30'
30'
BARROW STRAIT
K1 - CURRENT ELLIPSES
20 cm/s
10, 18, 25 m
50, 51, 60 m
100, 142 150 m
46
SOMERSET ISLAND
74°
74°
95°
94°
93°

Figure 4.2.12. Barrow Strait K_1 current ellipses.

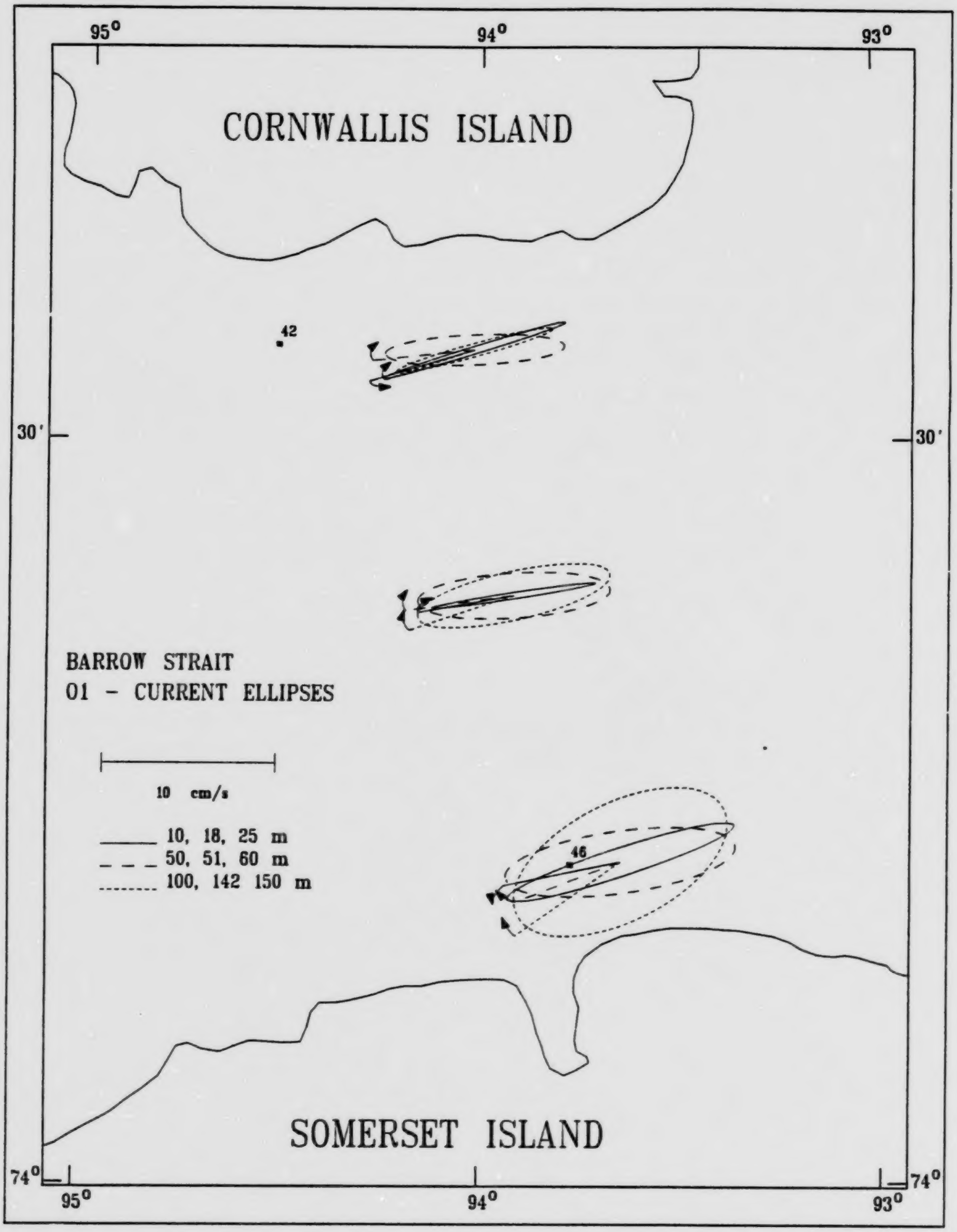
95°
94°
93°
CORNWALLIS ISLAND
42
30'
30'
BARROW STRAIT
O1 - CURRENT ELLIPSES
10 cm/s
10, 18, 25 m
50, 51, 60 m
100, 142 150 m
46
SOMERSET ISLAND
74°
95°
94°
93°
74°

Figure 4.2.13. Barrow Strait O_1 current ellipses.

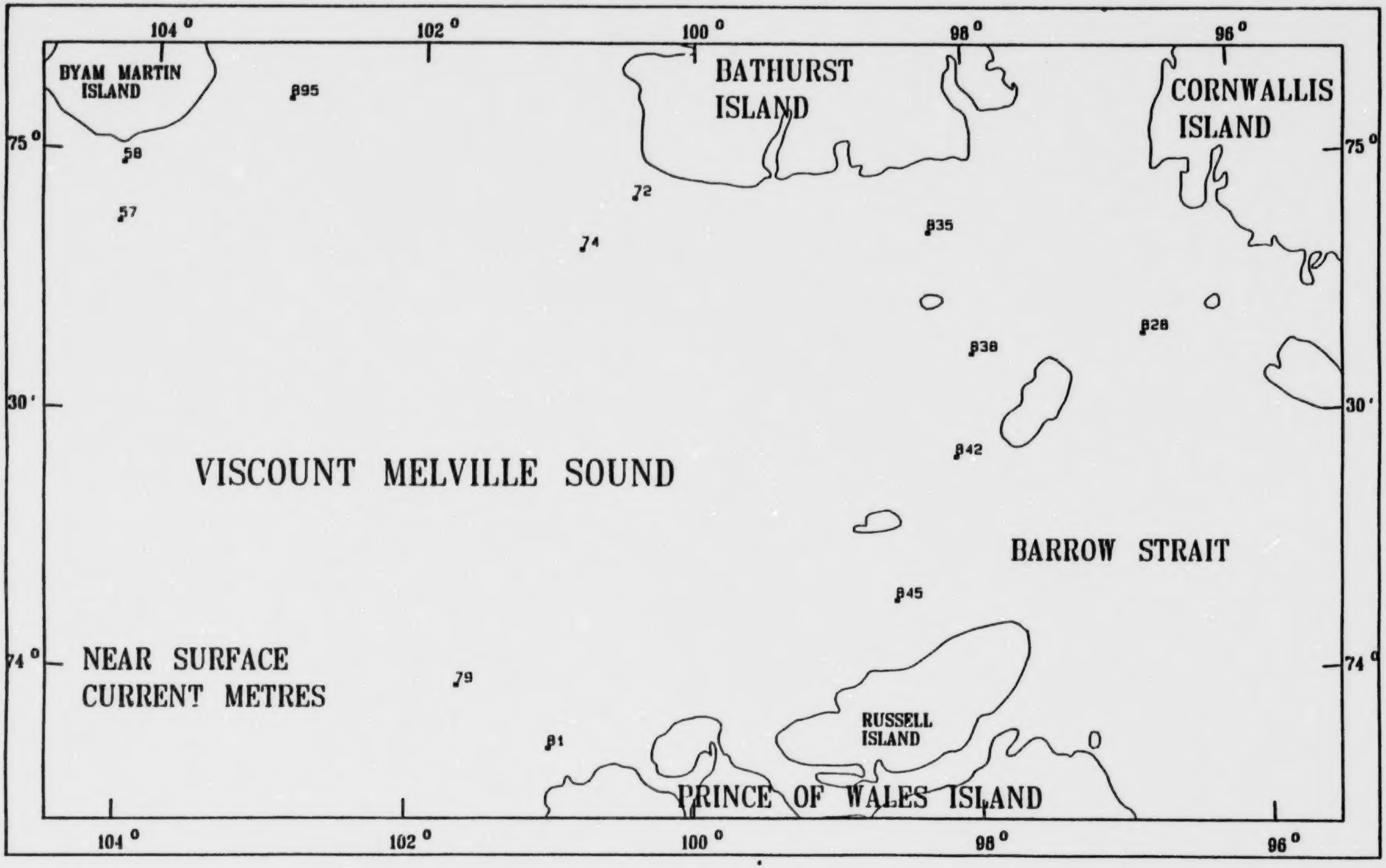
104°
102°
100°
98°
96°
75°
30'
74°
BYAM MARTIN ISLAND
BATHURST ISLAND
CORNWALLIS ISLAND
β95
58
57
72
74
β35
β28
β38
β42
β45
79
β1
VISCOUNT MELVILLE SOUND
BARROW STRAIT
NEAR SURFACE CURRENT METRES
RUSSELL ISLAND
PRINCE OF WALES ISLAND

Figure 4.2.14. Eastern Viscount Melville Sound current meter stations.

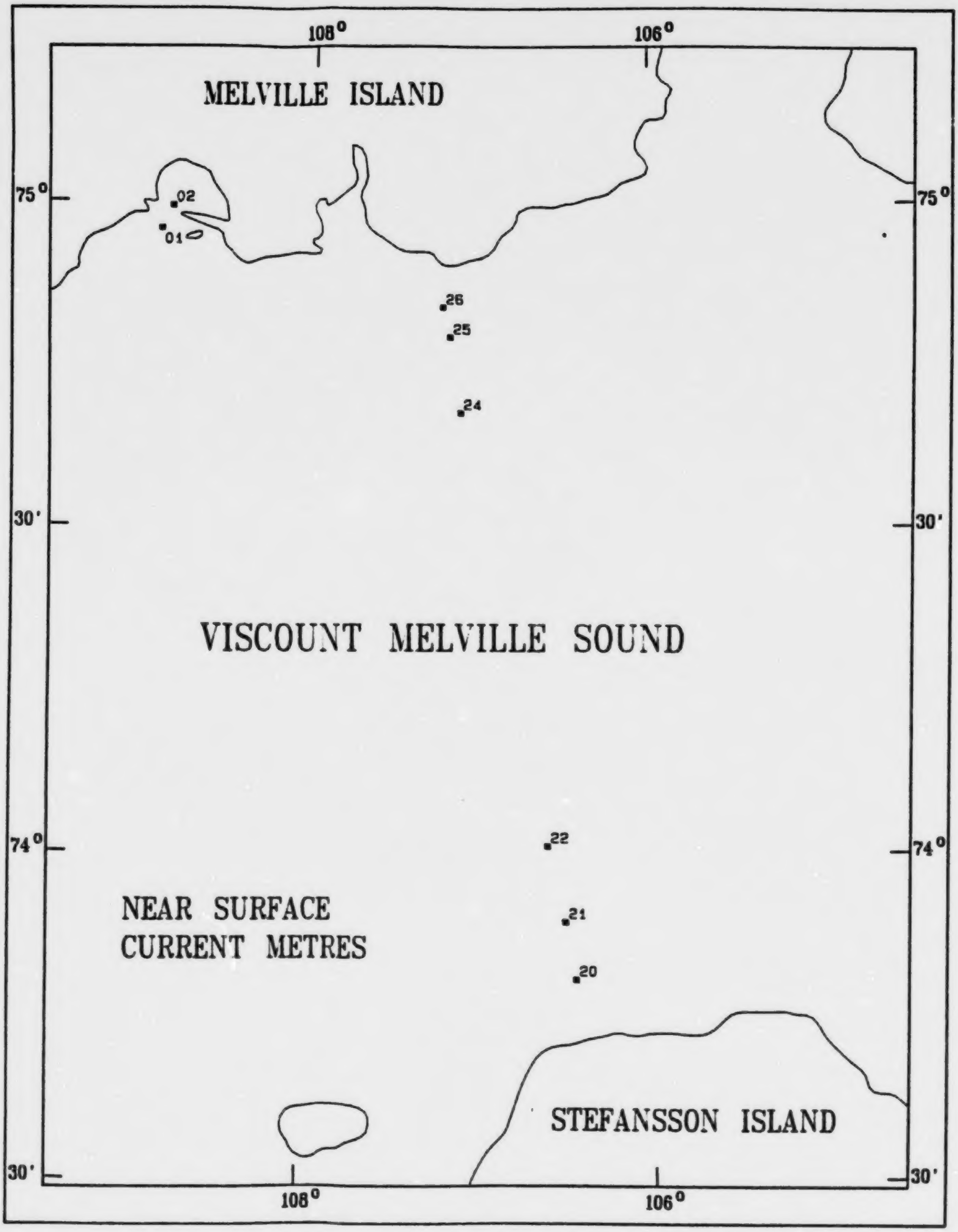
108°
106°
MELVILLE ISLAND
75°
02
01
26
25
24
30'
VISCOUNT MELVILLE SOUND
74°
22
21
20
NEAR SURFACE
CURRENT METRES
STEFANSSON ISLAND
30'
108°
106°

Figure 4.2.15. Western Viscount Melville Sound current meter stations.

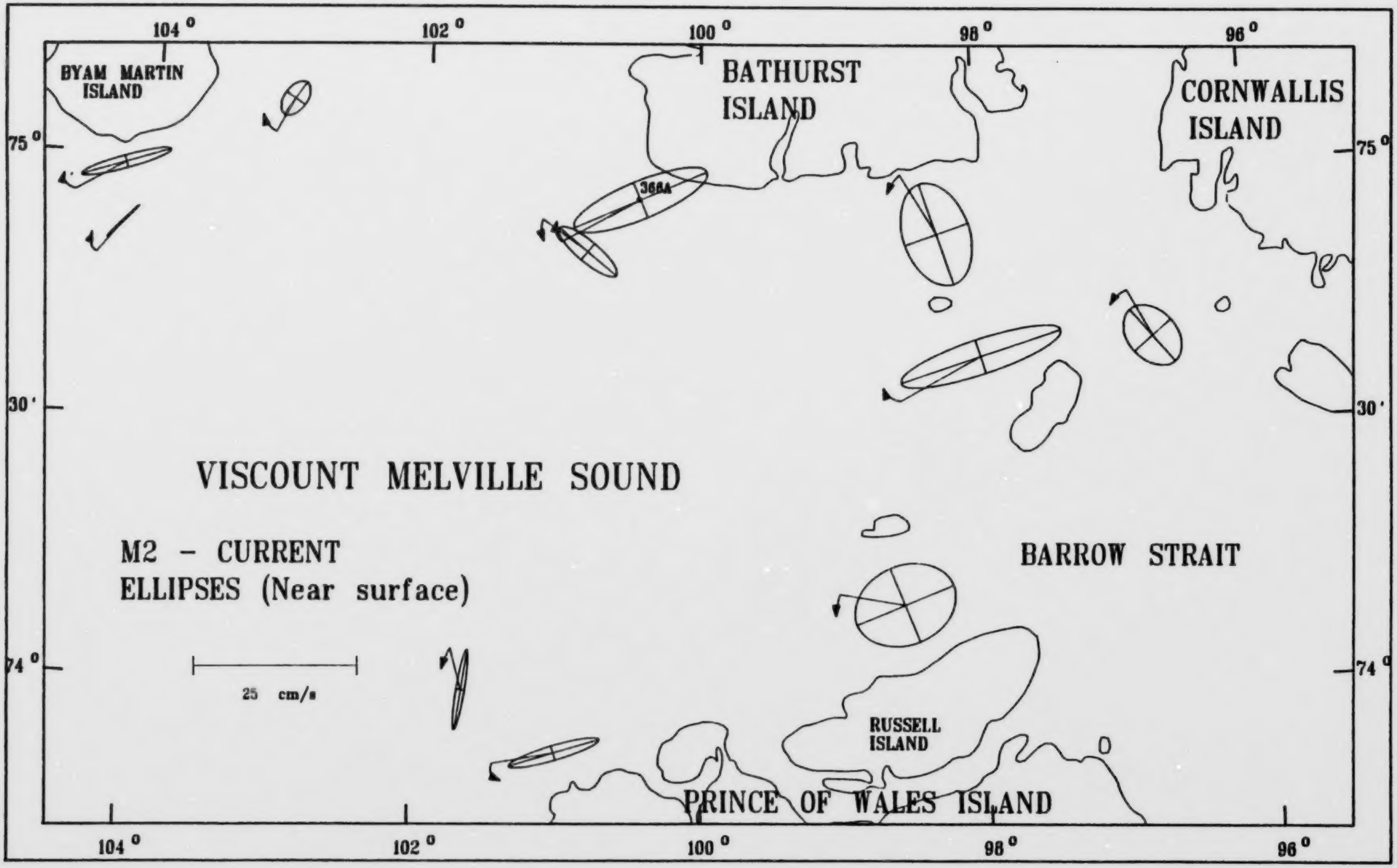
104 °
102 °
100 °
98 °
96 °
75 °
30 '
74 °
BYAM MARTIN ISLAND
BATHURST ISLAND
CORNWALLIS ISLAND
366A
VISCOUNT MELVILLE SOUND
M2 - CURRENT
ELLIPSES (Near surface)
25 cm/s
BARROW STRAIT
RUSSELL ISLAND
PRINCE OF WALES ISLAND

Figure 4.2.16. Eastern Viscount Melville Sound M_2 current ellipses.

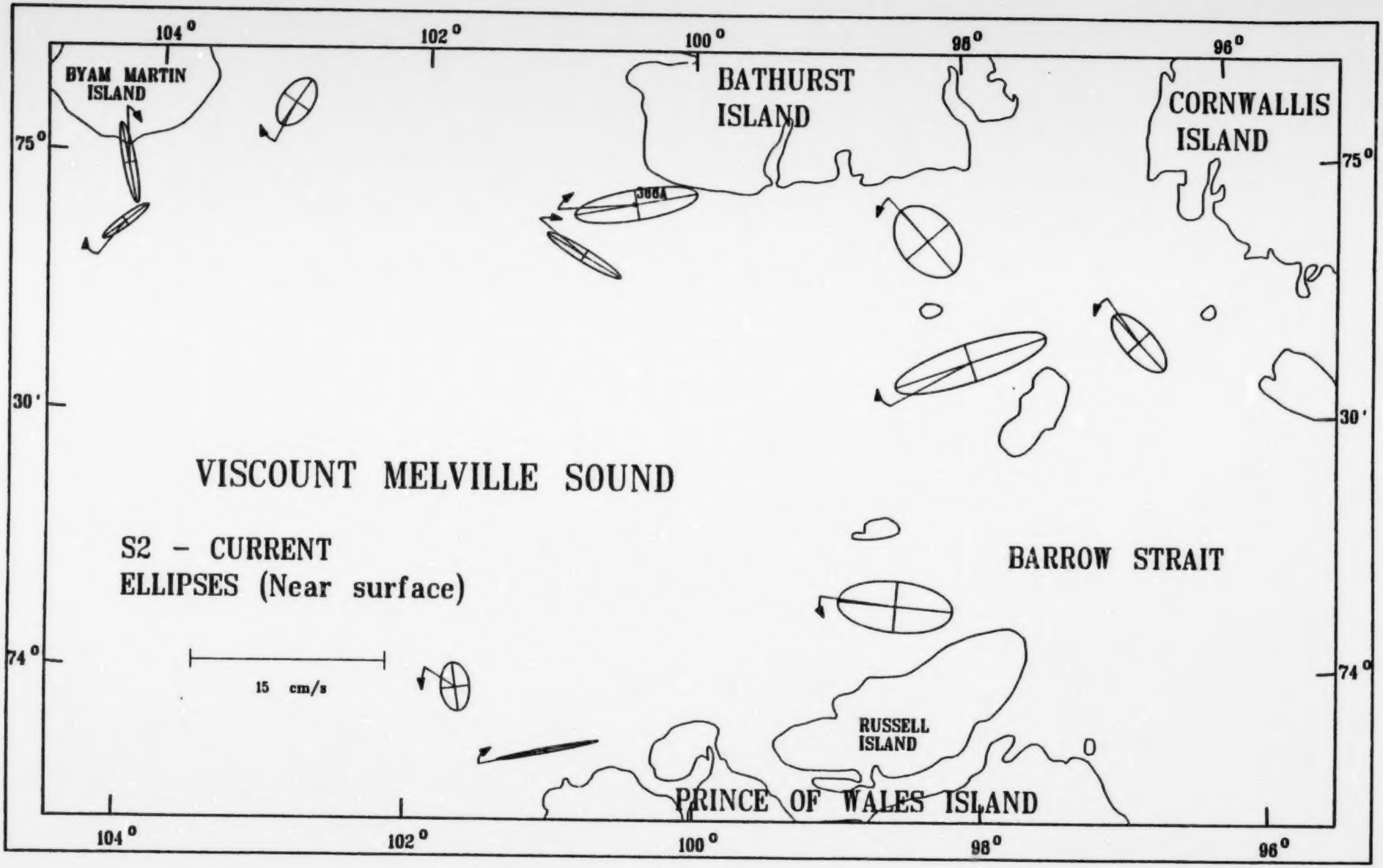
104°
102°
100°
98°
96°
75°
30'
74°
BYAM MARTIN ISLAND
BATHURST ISLAND
CORNWALLIS ISLAND
VISCOUNT MELVILLE SOUND
S2 - CURRENT
ELLIPSES (Near surface)
15 cm/s
BARROW STRAIT
RUSSELL ISLAND
PRINCE OF WALES ISLAND

Figure 4.2.17. Eastern Viscount Melville Sound S_2 current ellipses.

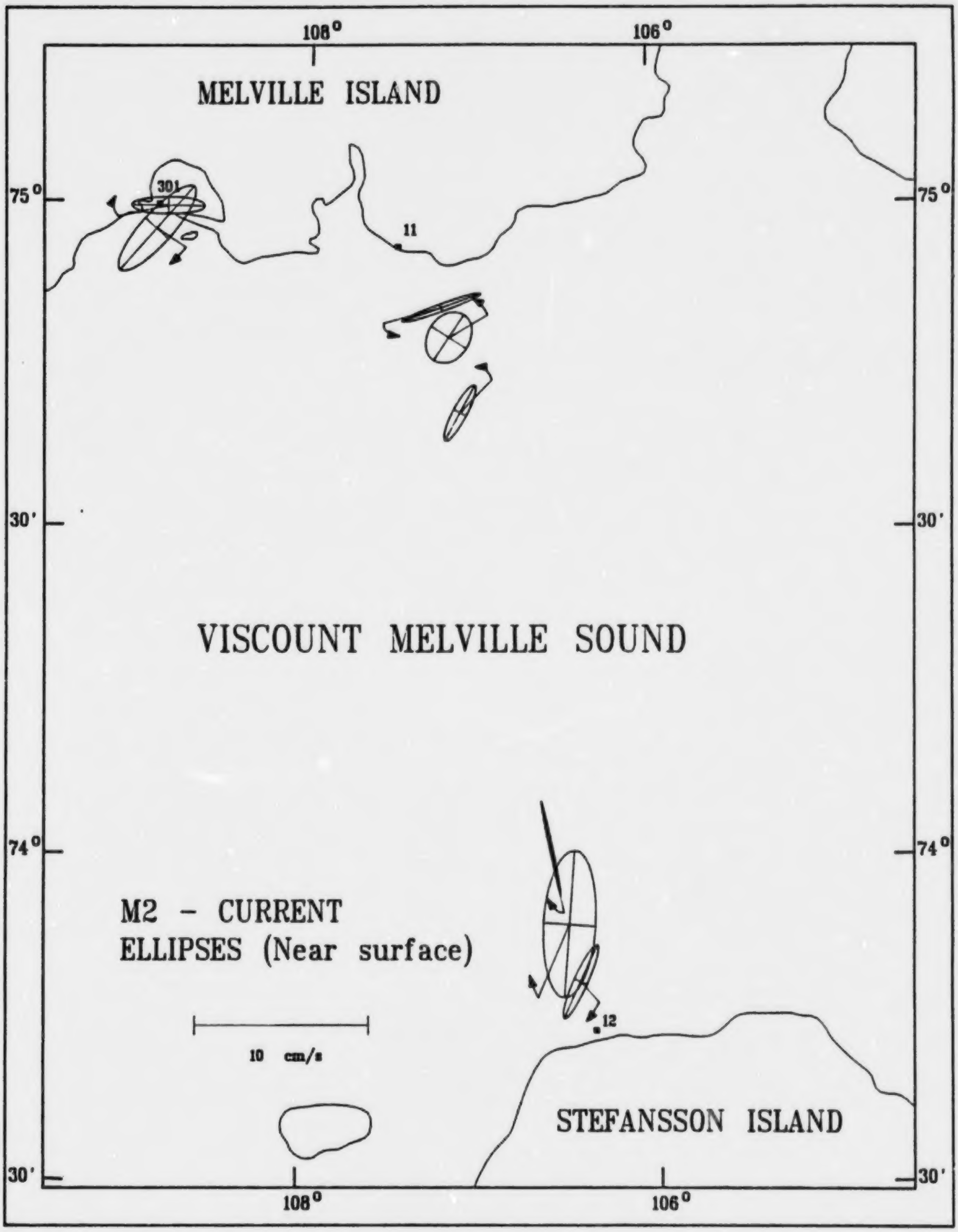
108°
106°
MELVILLE ISLAND
75°
301
11
30'
VISCOUNT MELVILLE SOUND
74°
M2 - CURRENT
ELLIPSES (Near surface)
10 cm/s
12
STEFANSSON ISLAND
30'
108°
106°

Figure 4.2.18. Western Viscount Melville Sound M_2 current ellipses.

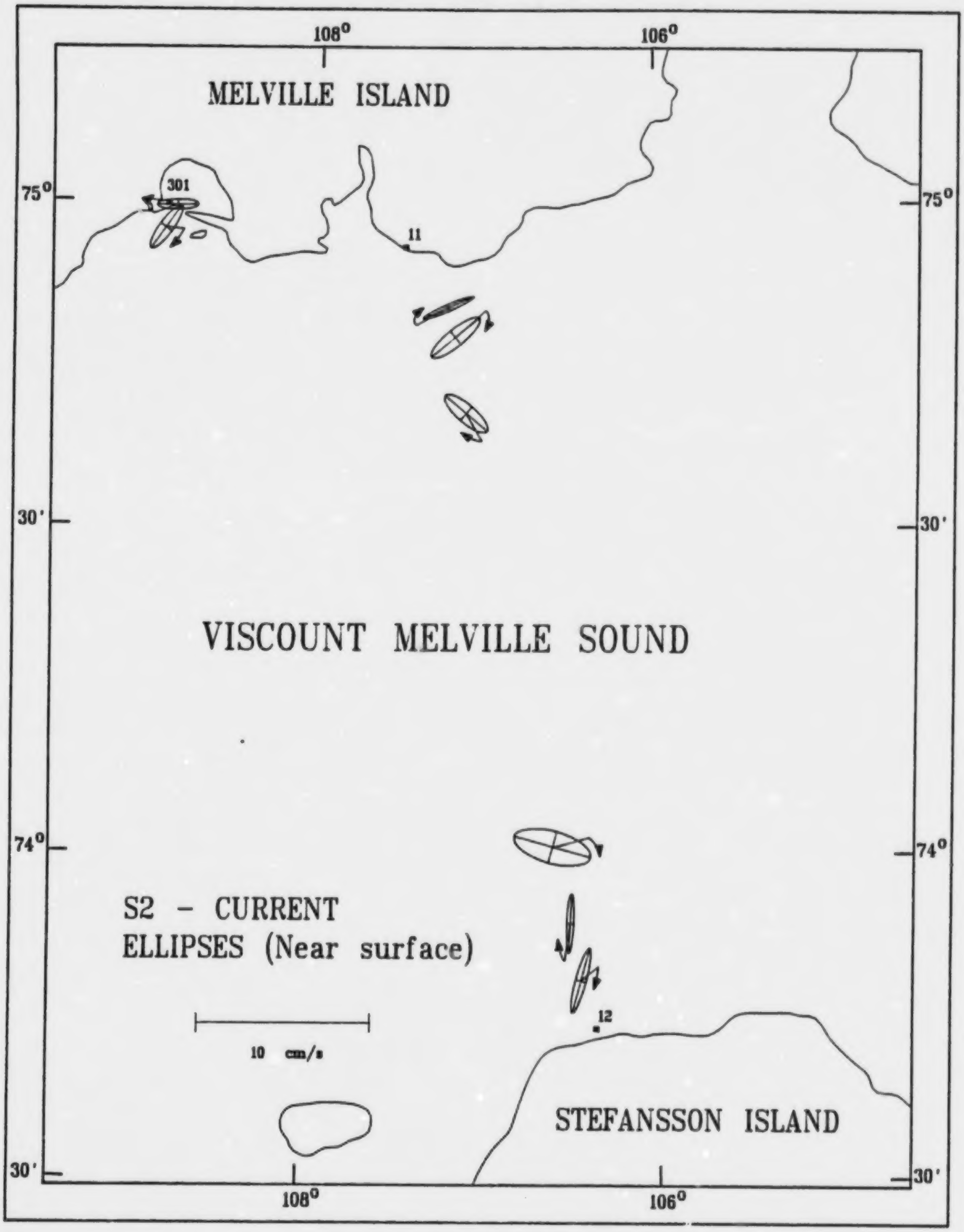
108°
106°
MELVILLE ISLAND
301
11
75°
30'
VISCOUNT MELVILLE SOUND
74°
S2 - CURRENT
ELLIPSES (Near surface)
10 cm/s
12
STEFANSSON ISLAND
30'
108°
106°

Figure 4.2.19. Western Viscount Melville Sound S_2 current ellipses.

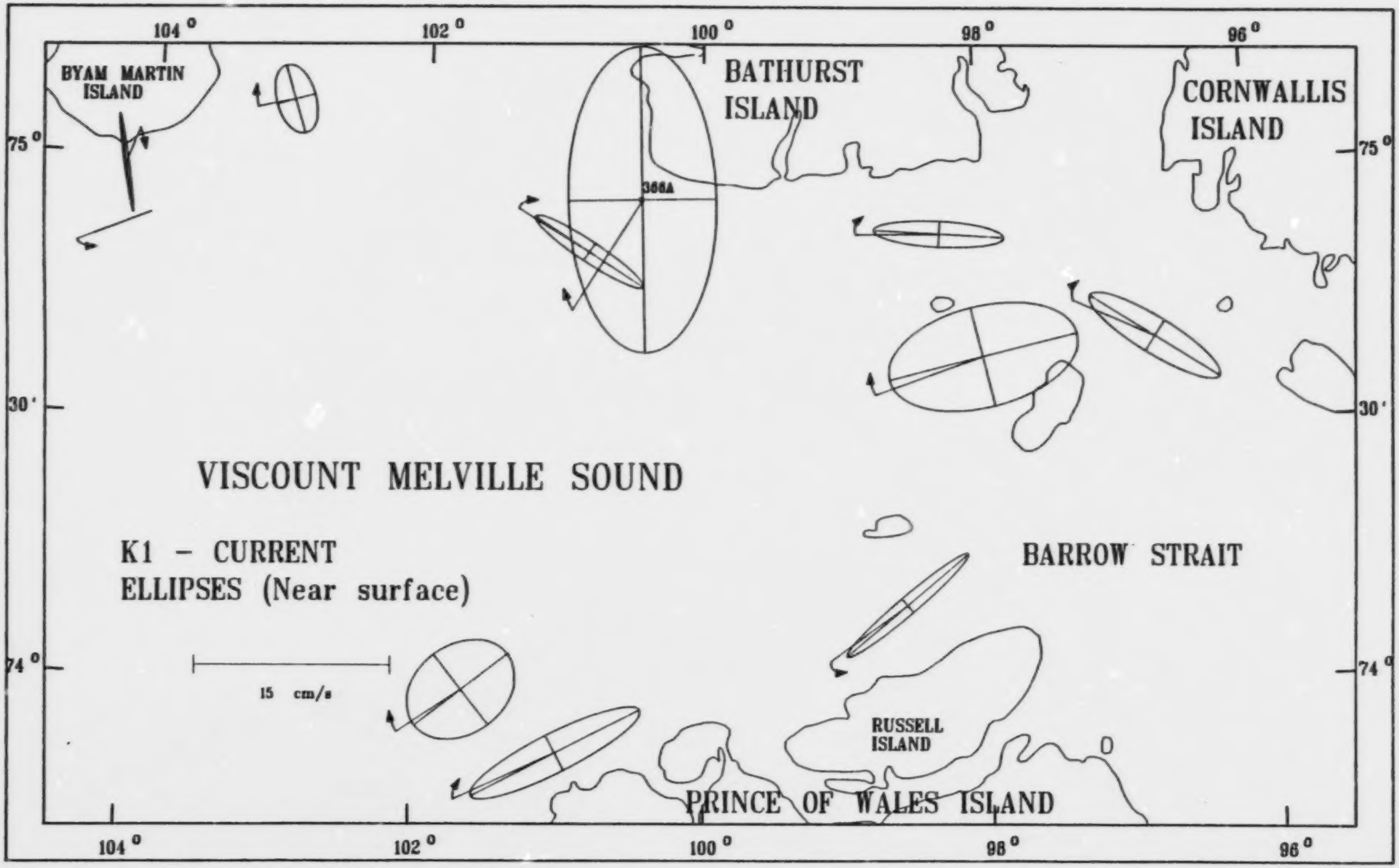
104 °
102 °
100 °
98 °
96 °
BYAM MARTIN ISLAND
BATHURST ISLAND
CORNWALLIS ISLAND
75 °
30 '
74 °
366A
VISCOUNT MELVILLE SOUND
K1 - CURRENT
ELLIPSES (Near surface)
15 cm/s
BARROW STRAIT
RUSSELL ISLAND
PRINCE OF WALES ISLAND

Figure 4.2.20. Eastern Viscount Melville Sound K_1 current ellipses.

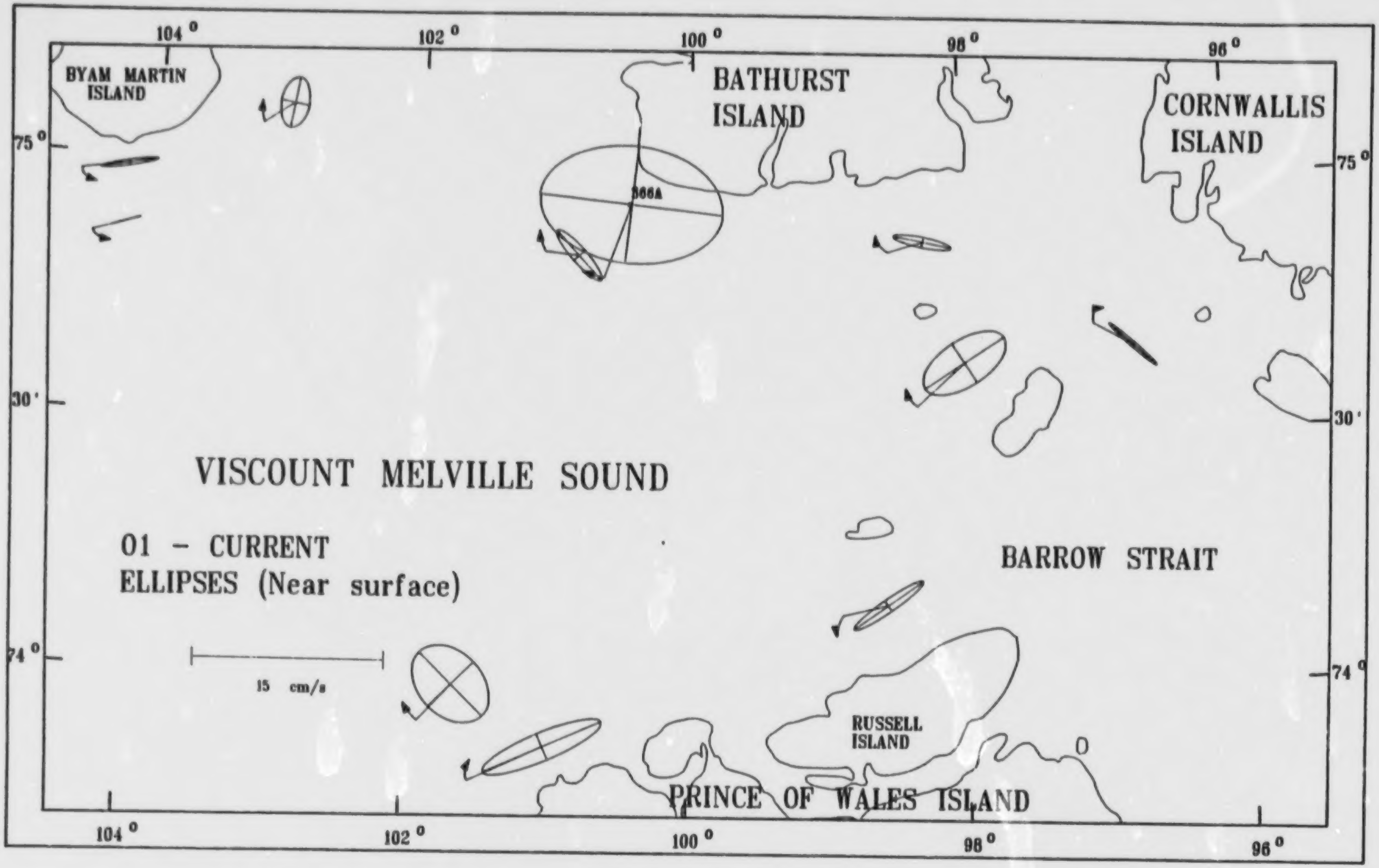
104 °
102 °
100 °
98 °
96 °
75 °
30 '
74 °
BYAM MARTIN ISLAND
BATHURST ISLAND
CORNWALLIS ISLAND
366A
VISCOUNT MELVILLE SOUND
BARROW STRAIT
01 - CURRENT
ELLIPSES (Near surface)
15 cm/s
RUSSELL ISLAND
PRINCE OF WALES ISLAND

Figure 4.2.21. Eastern Viscount Melville Sound O_1 current ellipses.

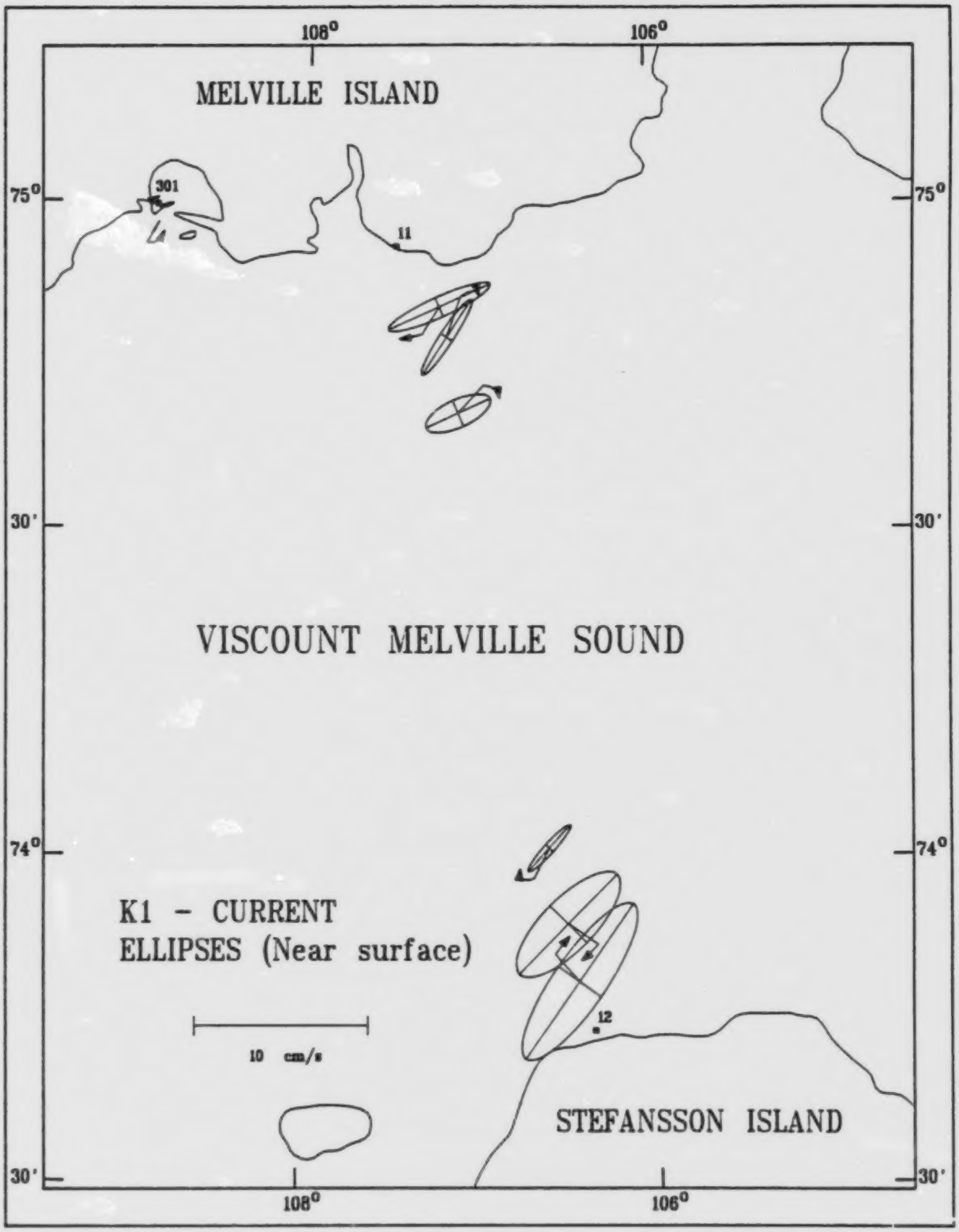
108°
106°
MELVILLE ISLAND
301
11
75°
75°
30'
30'
VISCOUNT MELVILLE SOUND
74°
74°
K1 - CURRENT
ELLIPSES (Near surface)
10 cm/s
12
STEFANSSON ISLAND
30'
30'
108°
106°

Figure 4.2.22. Western Viscount Melville Sound K_1 current ellipses.

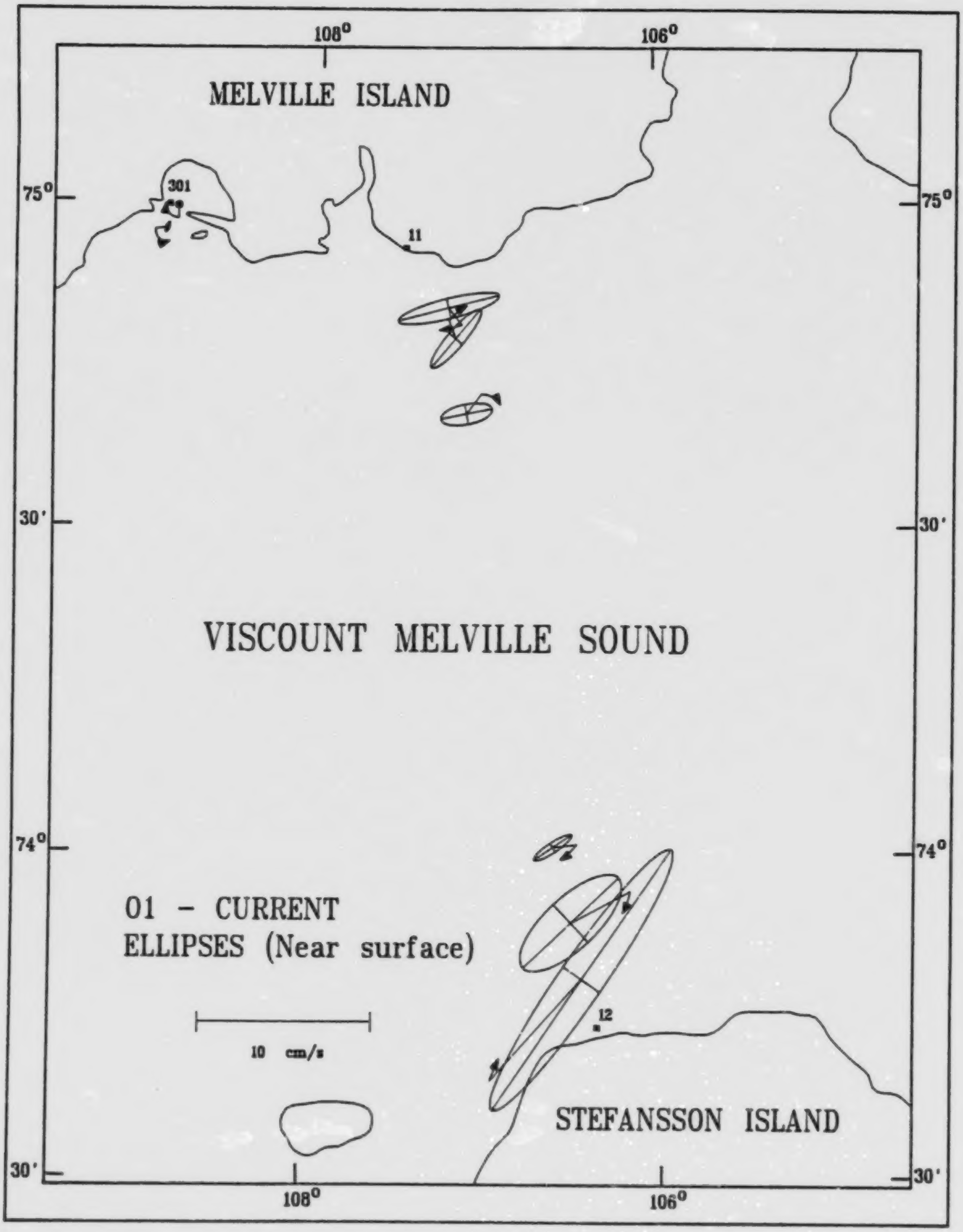
108°
106°
MELVILLE ISLAND
75°
301
11
30'
VISCOUNT MELVILLE SOUND
74°
01 - CURRENT
ELLIPSES (Near surface)
10 cm/s
12
STEFANSSON ISLAND
30'
108°
106°

Figure 4.2.23. Western Viscount Melville Sound O_1 current ellipses.

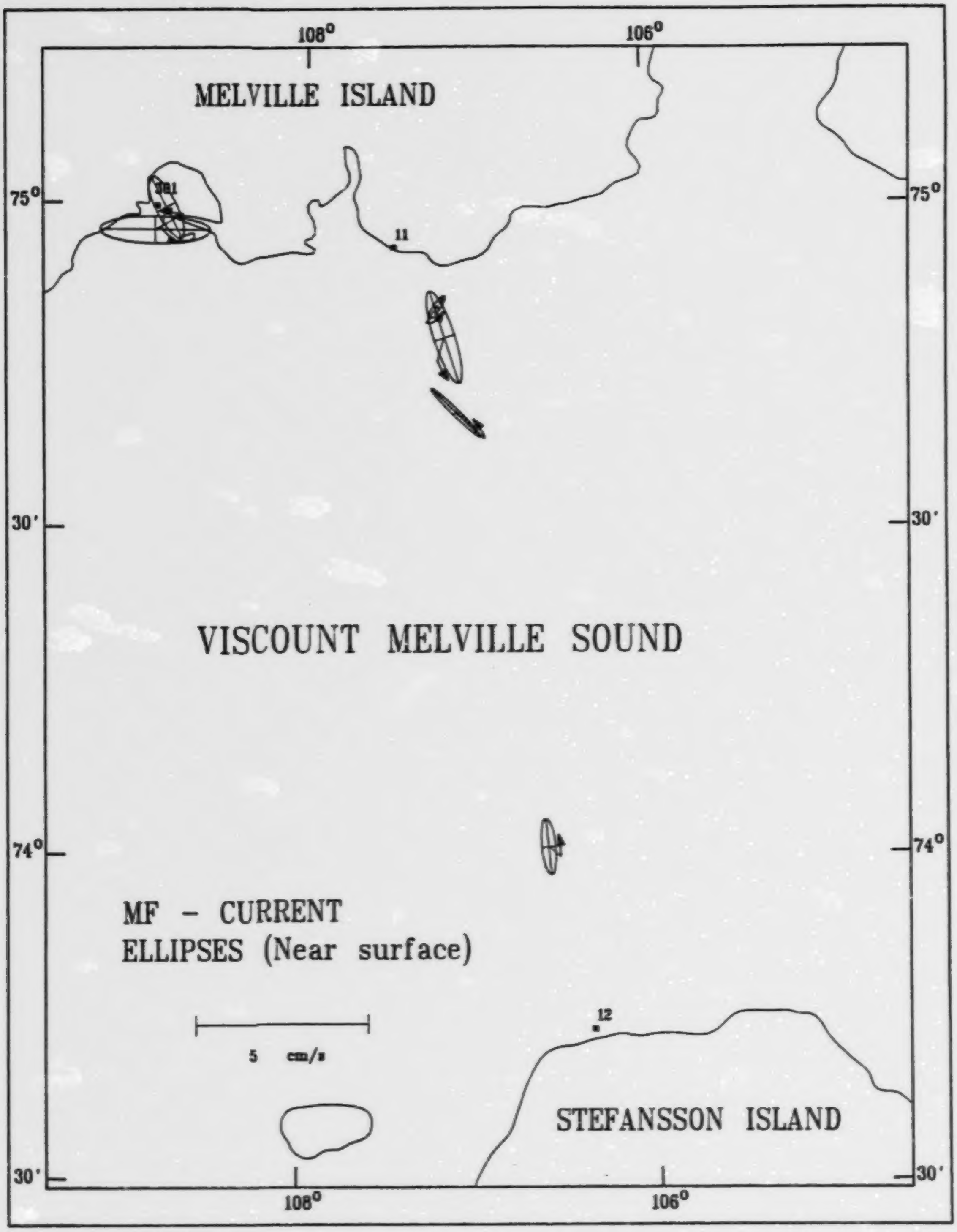
108°
106°
MELVILLE ISLAND
75°
301
11
30'
VISCOUNT MELVILLE SOUND
74°
MF - CURRENT
ELLIPSES (Near surface)
5 cm/s
12
STEFANSSON ISLAND
30'
108°
106°

Figure 4.2.24. Western Viscount Melville Sound Mf current ellipses.

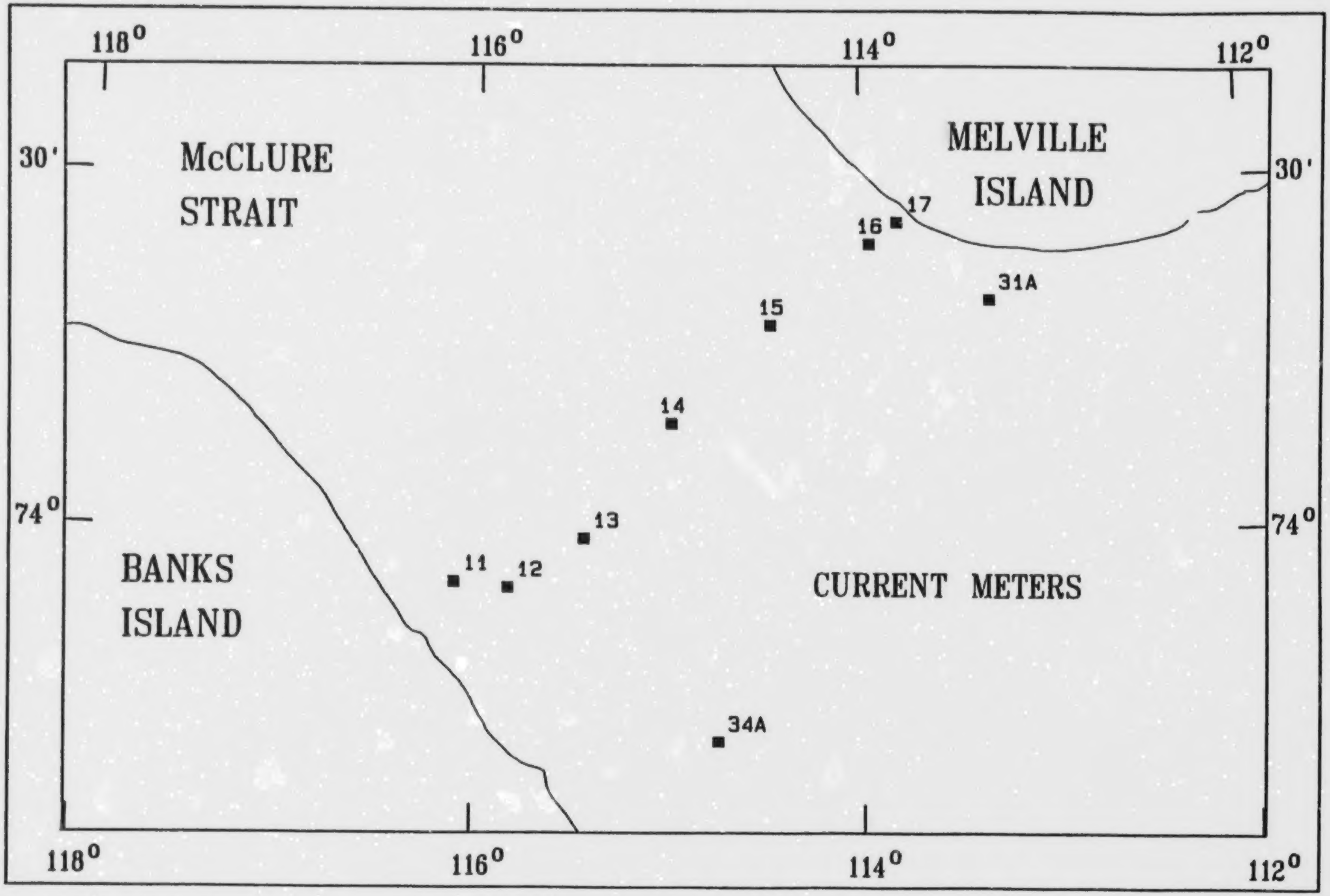
118°
116°
114°
112°
30'
74°
MELVILLE
ISLAND
McCLURE
STRAIT
BANKS
ISLAND
CURRENT METERS
17
16
31A
15
14
13
11
12
34A

Figure 4.2.25. M'Clure Strait current meter stations.

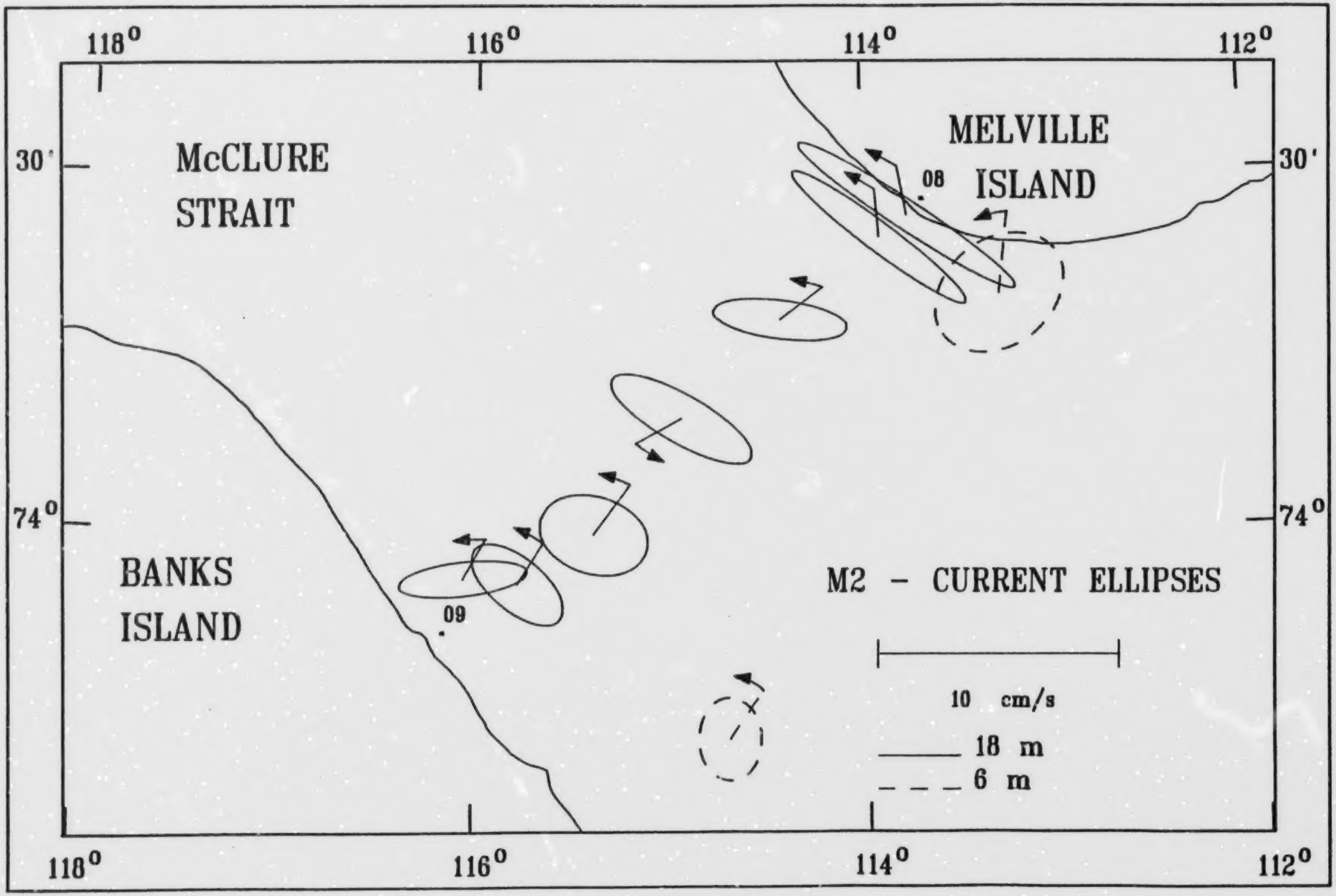
118°
116°
114°
112°
30'
74°
McCLURE
STRAIT
MELVILLE
ISLAND
BANKS
ISLAND
08
09
M2 - CURRENT ELLIPSES
10 cm/s
18 m
6 m

Figure 4.2.26. M'Clure Strait M_2 current ellipses.

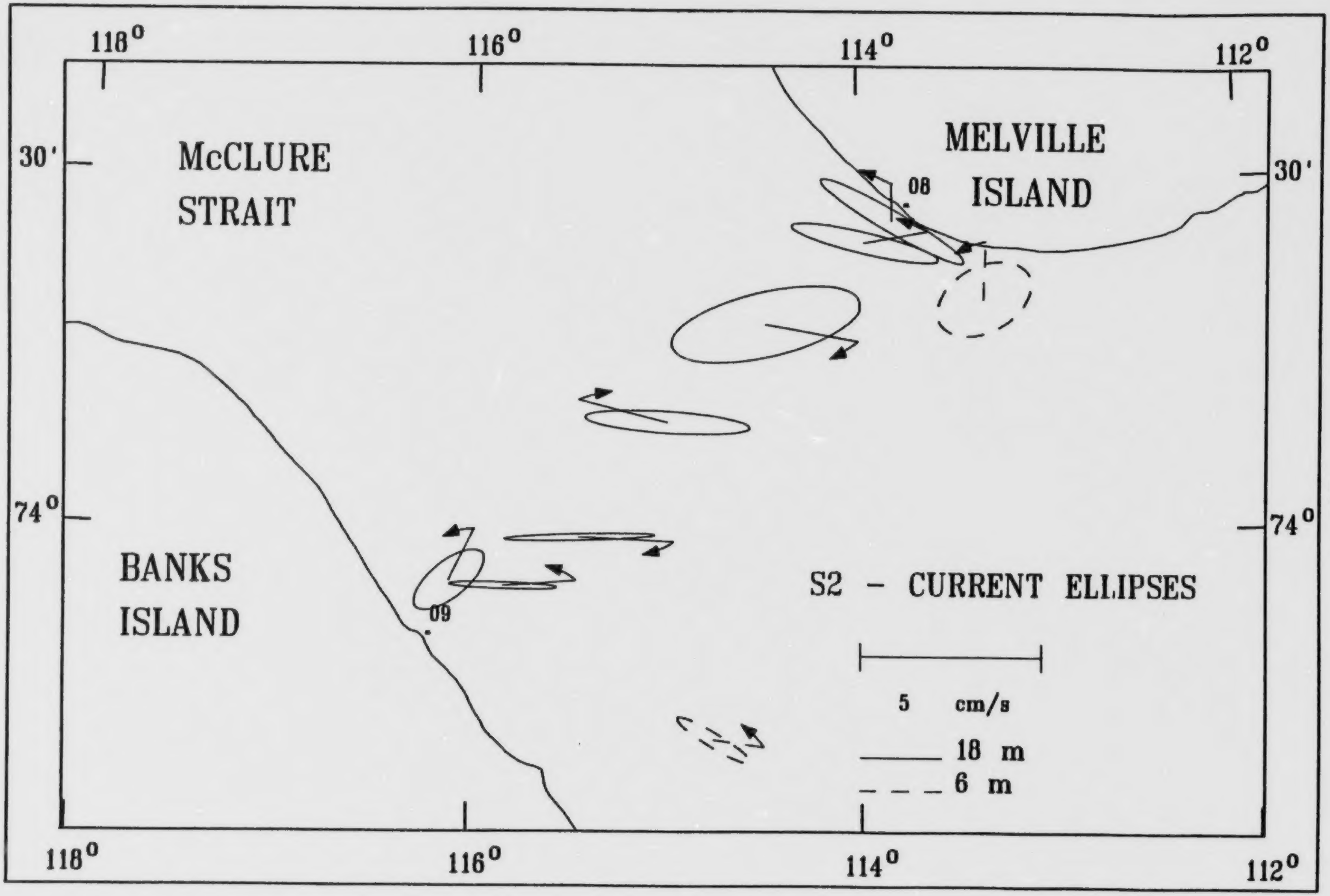
118°
116°
114°
112°
30'
74°
McCLURE STRAIT
MELVILLE ISLAND
BANKS ISLAND
08
09
S2 - CURRENT ELLIPSES
5 cm/s
18 m
6 m

Figure 4.2.27. M'Clure Strait S_2 current ellipses.

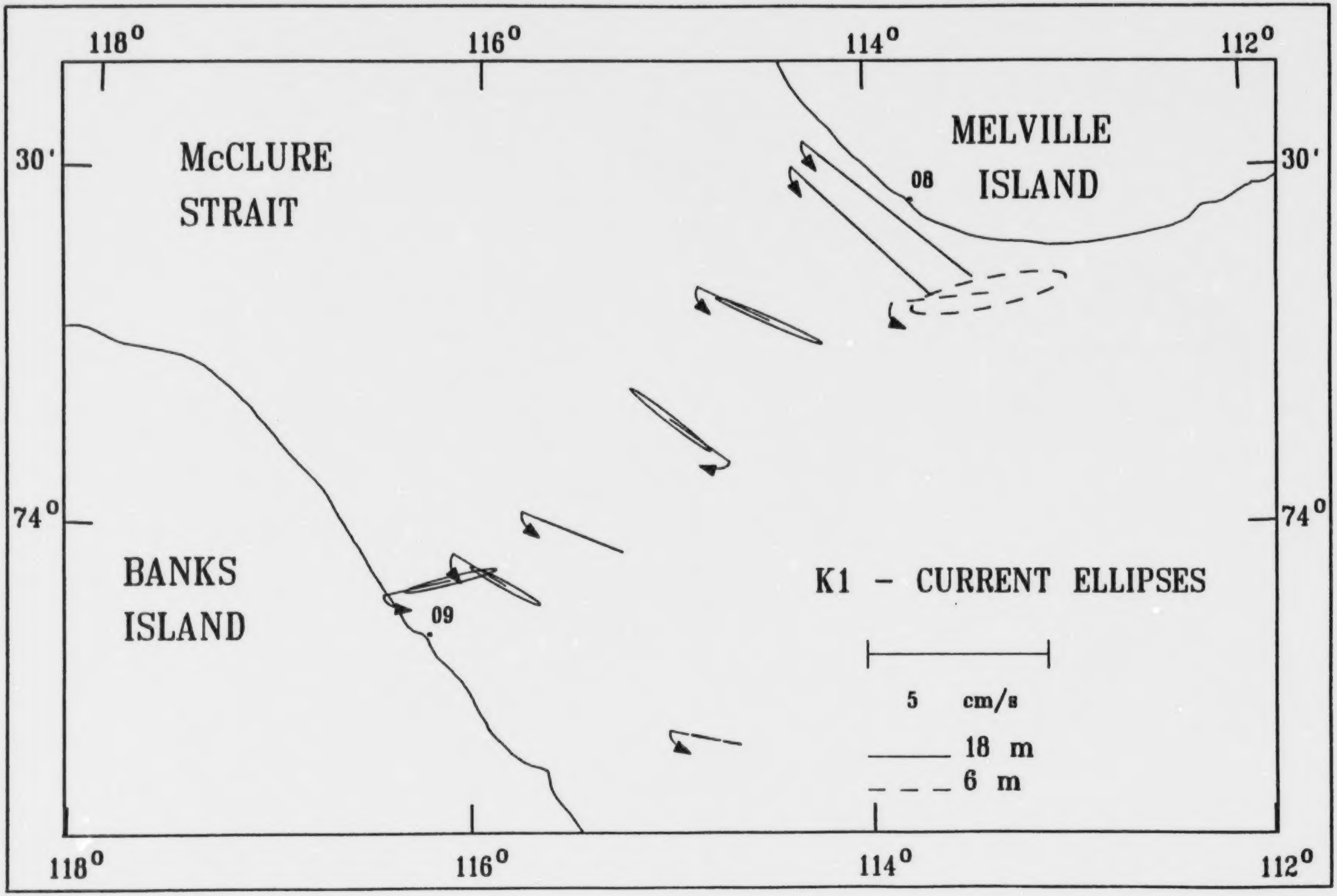
118°
116°
114°
112°
30'
30'
74°
74°
McCLURE STRAIT
MELVILLE ISLAND
BANKS ISLAND
08
09
K1 - CURRENT ELLIPSES
5 cm/s
18 m
6 m
118°
116°
114°
112°

Figure 4.2.28. M'Clure Strait K_1 current ellipses.

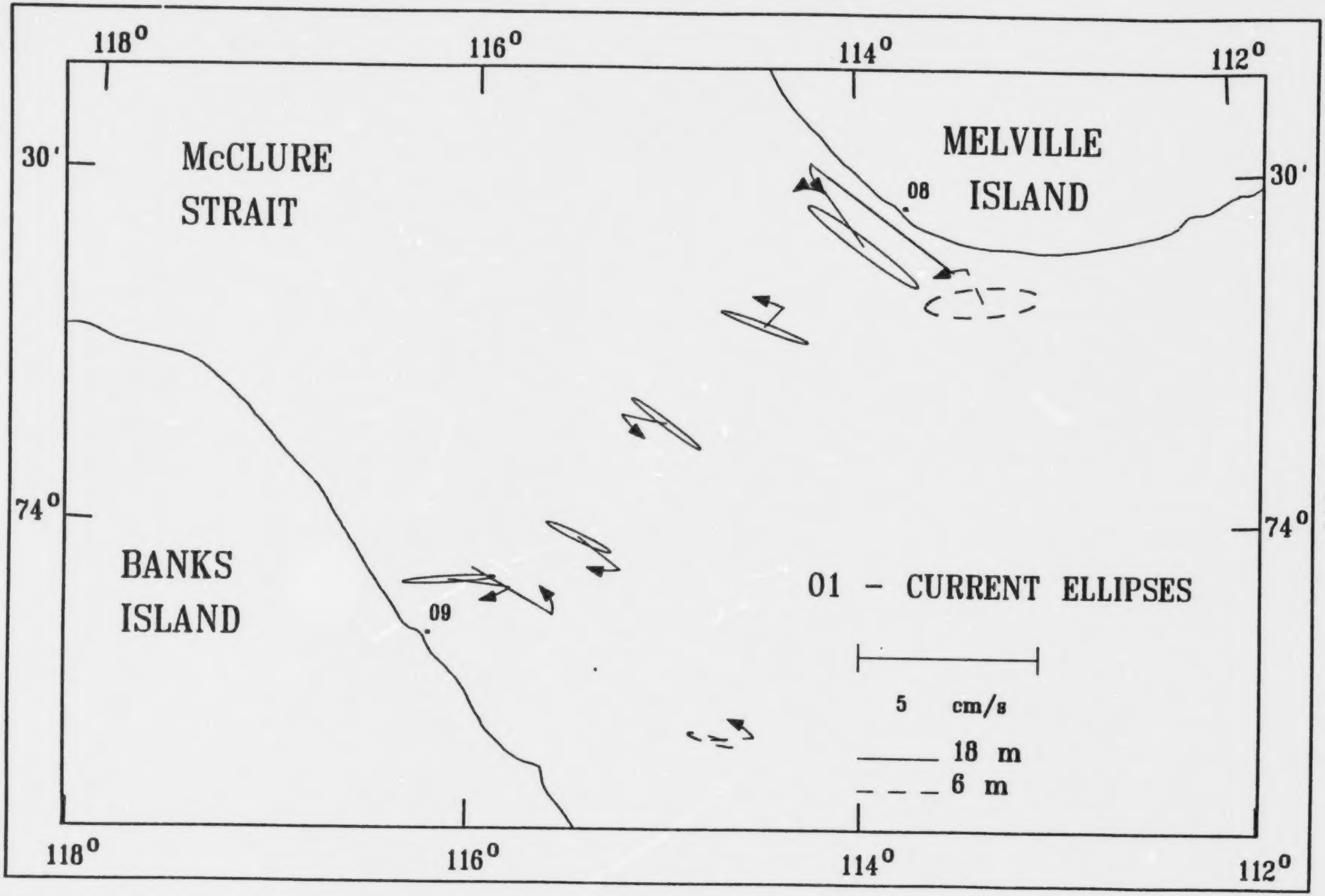
118°
116°
114°
112°
30'
74°
McCLURE
STRAIT
MELVILLE
ISLAND
BANKS
ISLAND
08
09
01 - CURRENT ELLIPSES
5 cm/s
18 m
6 m

Figure 4.2.29. M'Clure Strait O_1 current ellipses.

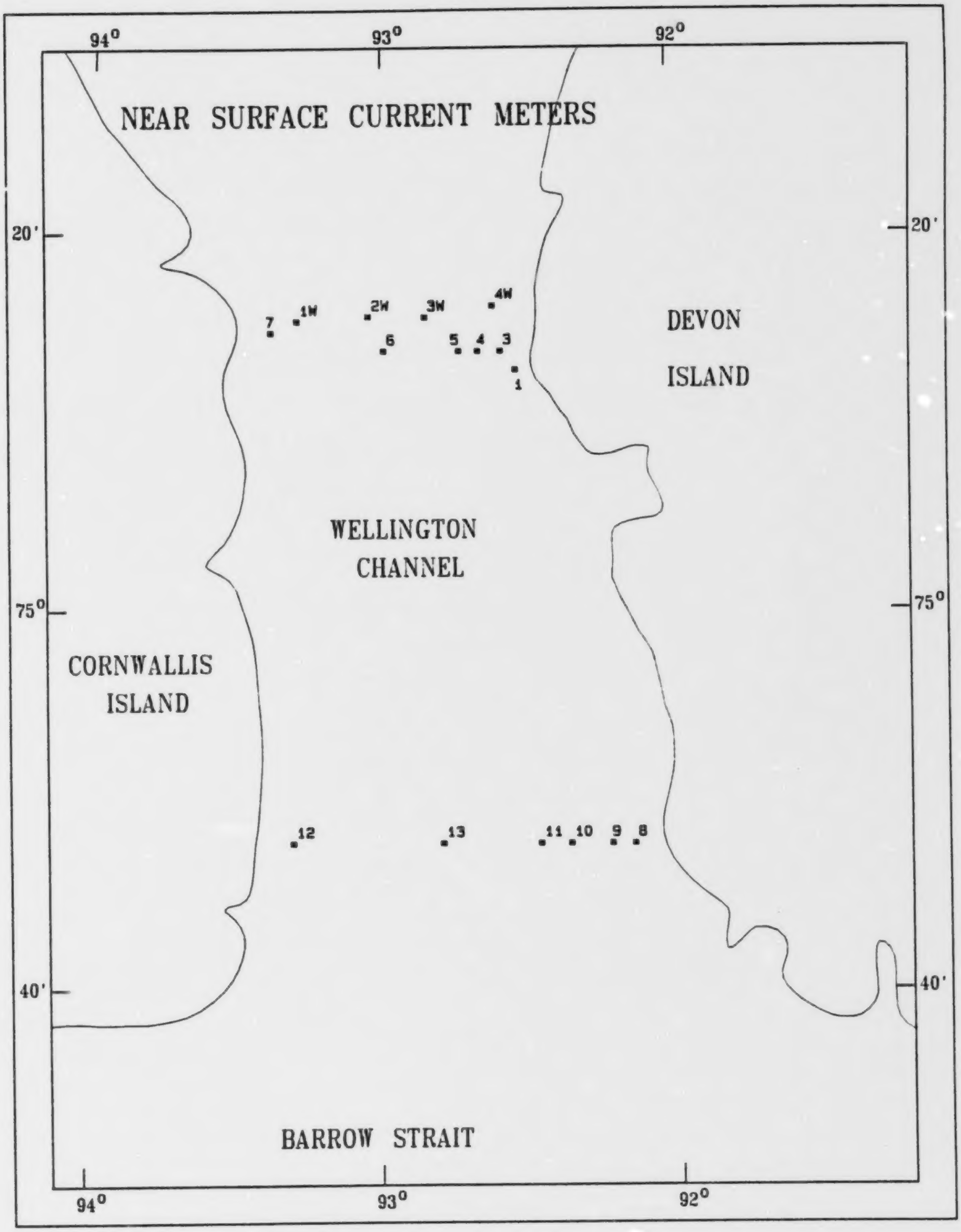
NEAR SURFACE CURRENT METERS
94°
93°
92°
20'
75°
40'
DEVON ISLAND
WELLINGTON CHANNEL
CORNWALLIS ISLAND
BARROW STRAIT
7
1W
2W
3W
4W
6
5
4
3
1
12
13
11
10
9
8

Figure 4.2.30. Wellington Channel current meter stations.

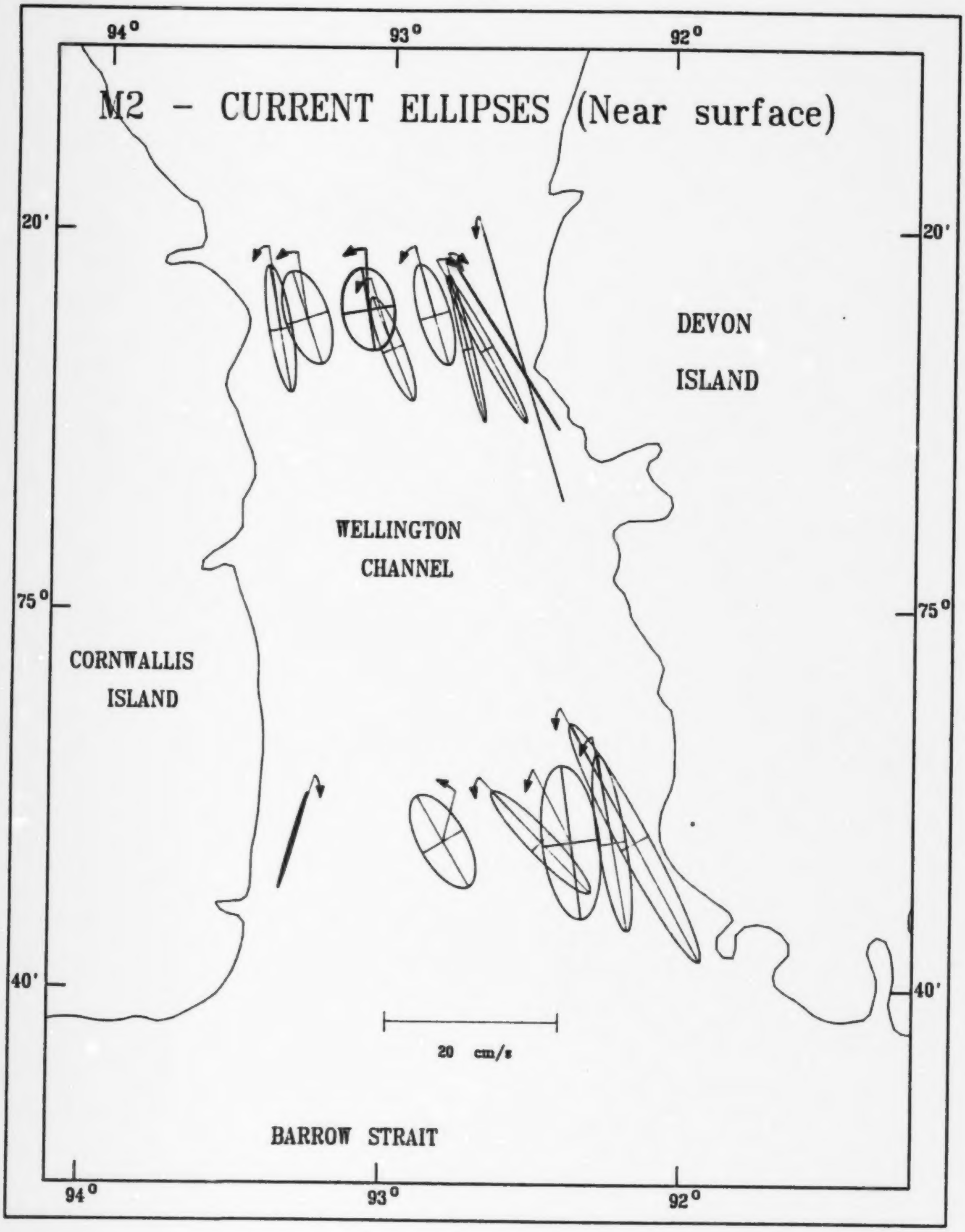
M2 - CURRENT ELLIPSES (Near surface)
94°
93°
92°
20'
75°
40'
DEVON ISLAND
WELLINGTON CHANNEL
CORNWALLIS ISLAND
BARROW STRAIT
20 cm/s

Figure 4.2.31. Wellington Channel M_2 current ellipses.

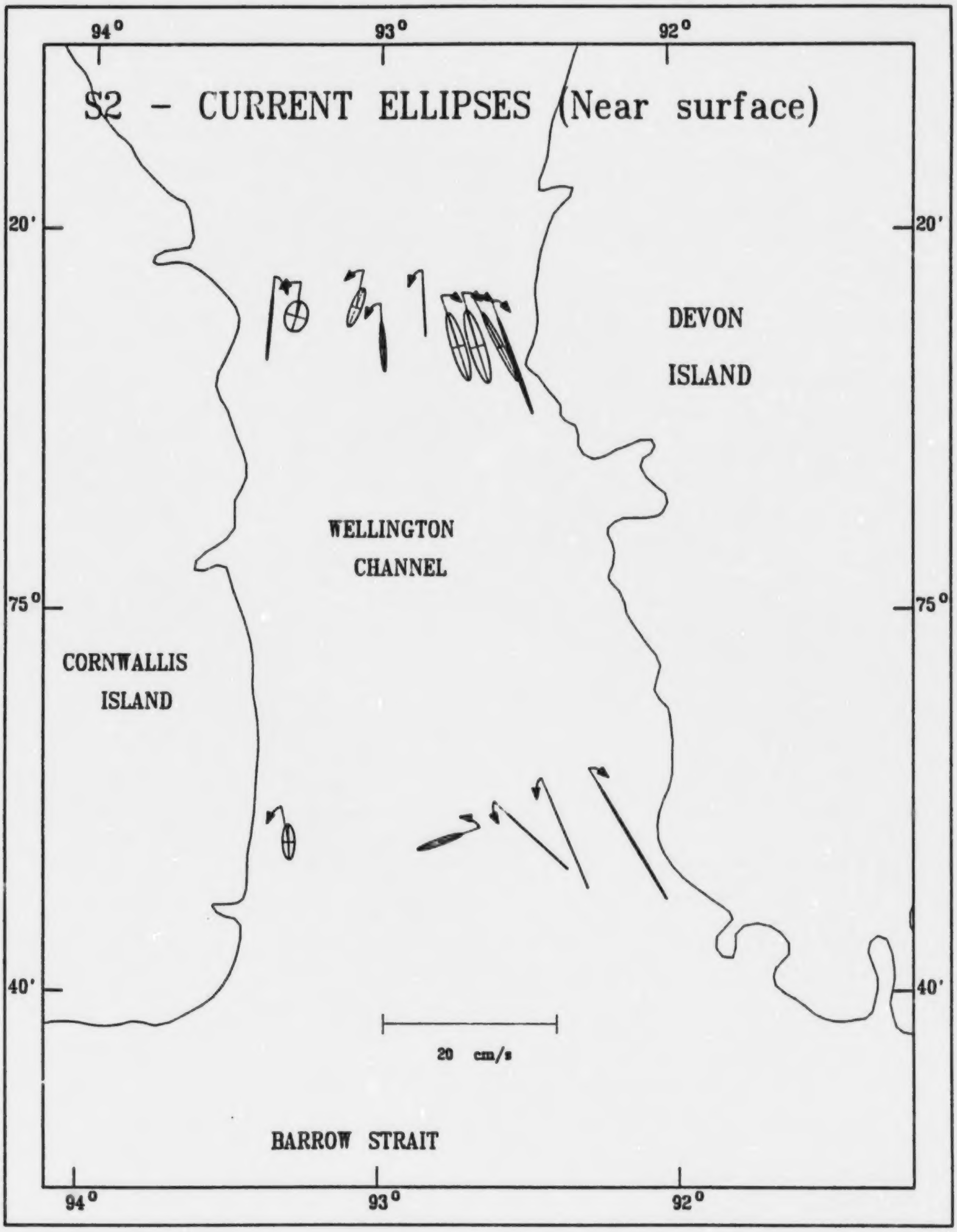
S2 - CURRENT ELLIPSES (Near surface)
94°
93°
92°
20'
75°
40'
DEVON
ISLAND
WELLINGTON
CHANNEL
CORNWALLIS
ISLAND
20 cm/s
BARROW STRAIT

Figure 4.2.32. Wellington Channel S_2 current ellipses.

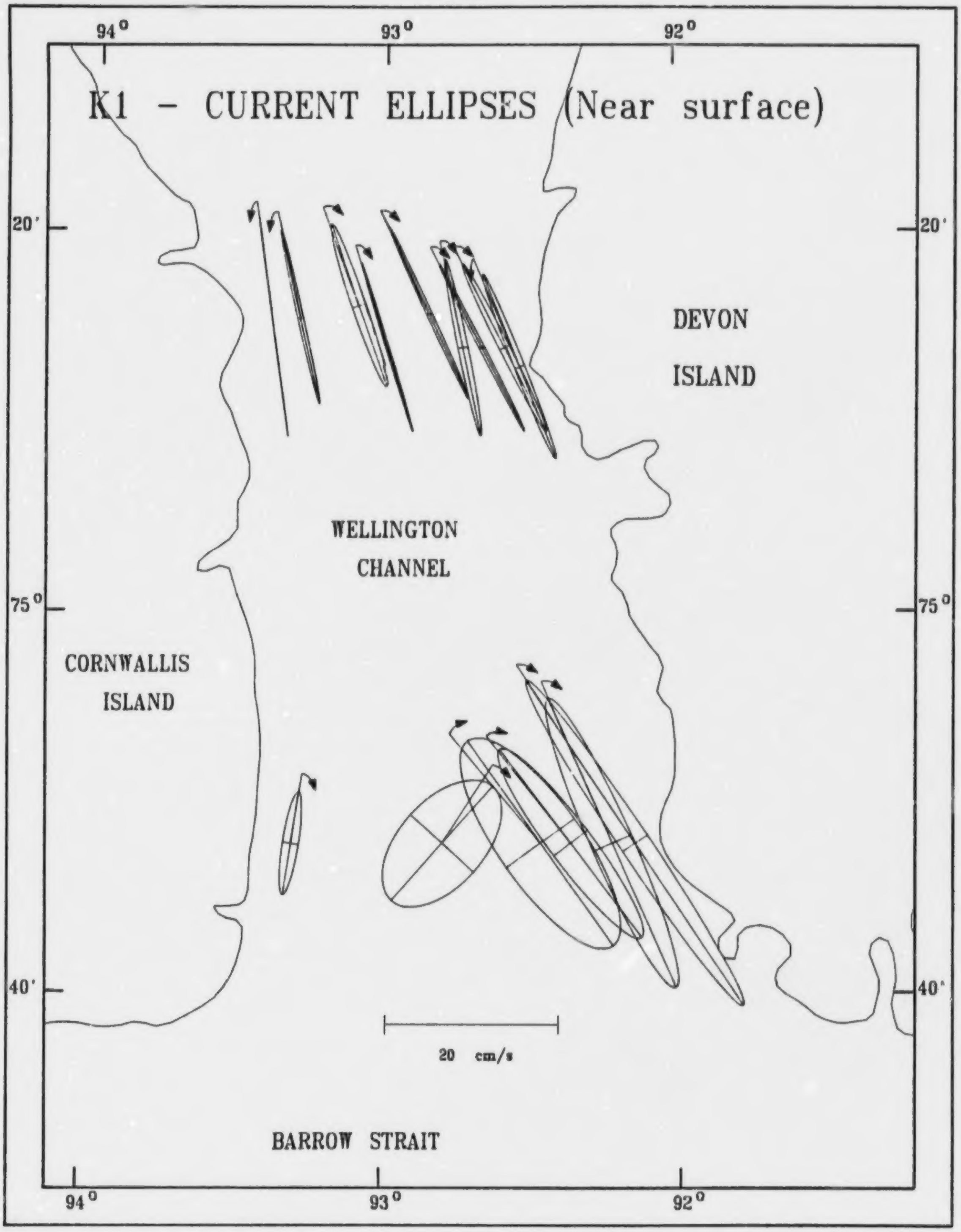
K1 - CURRENT ELLIPSES (Near surface)
94°
93°
92°
20'
75°
40'
DEVON
ISLAND
WELLINGTON
CHANNEL
CORNWALLIS
ISLAND
20 cm/s
BARROW STRAIT

Figure 4.2.33. Wellington Channel K_1 current ellipses.

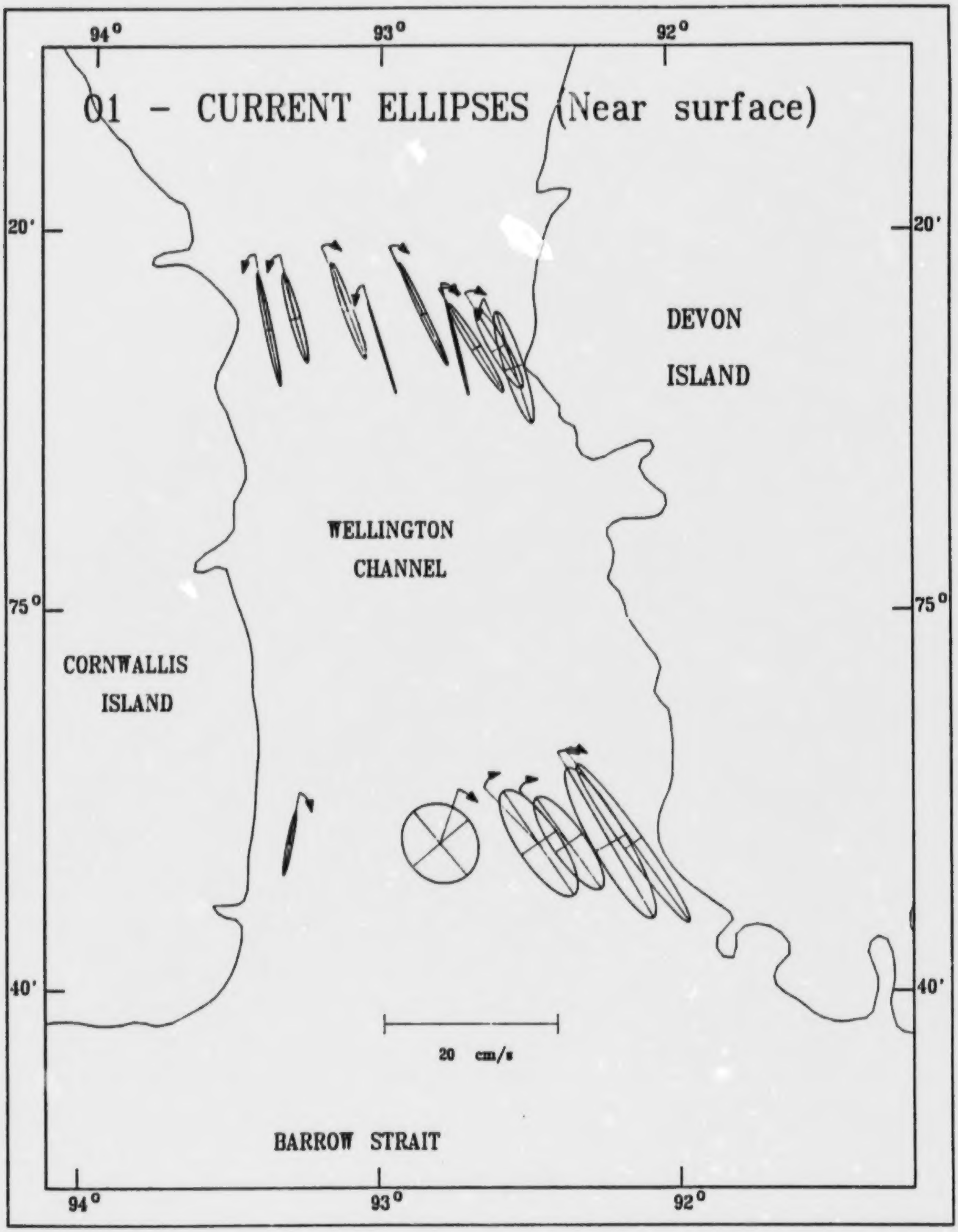
O1 - CURRENT ELLIPSES (Near surface)
94°
93°
92°
20'
75°
40'
DEVON
ISLAND
WELLINGTON
CHANNEL
CORNWALLIS
ISLAND
20 cm/s
BARROW STRAIT

Figure 4.2.34. Wellington Channel O_1 current ellipses.

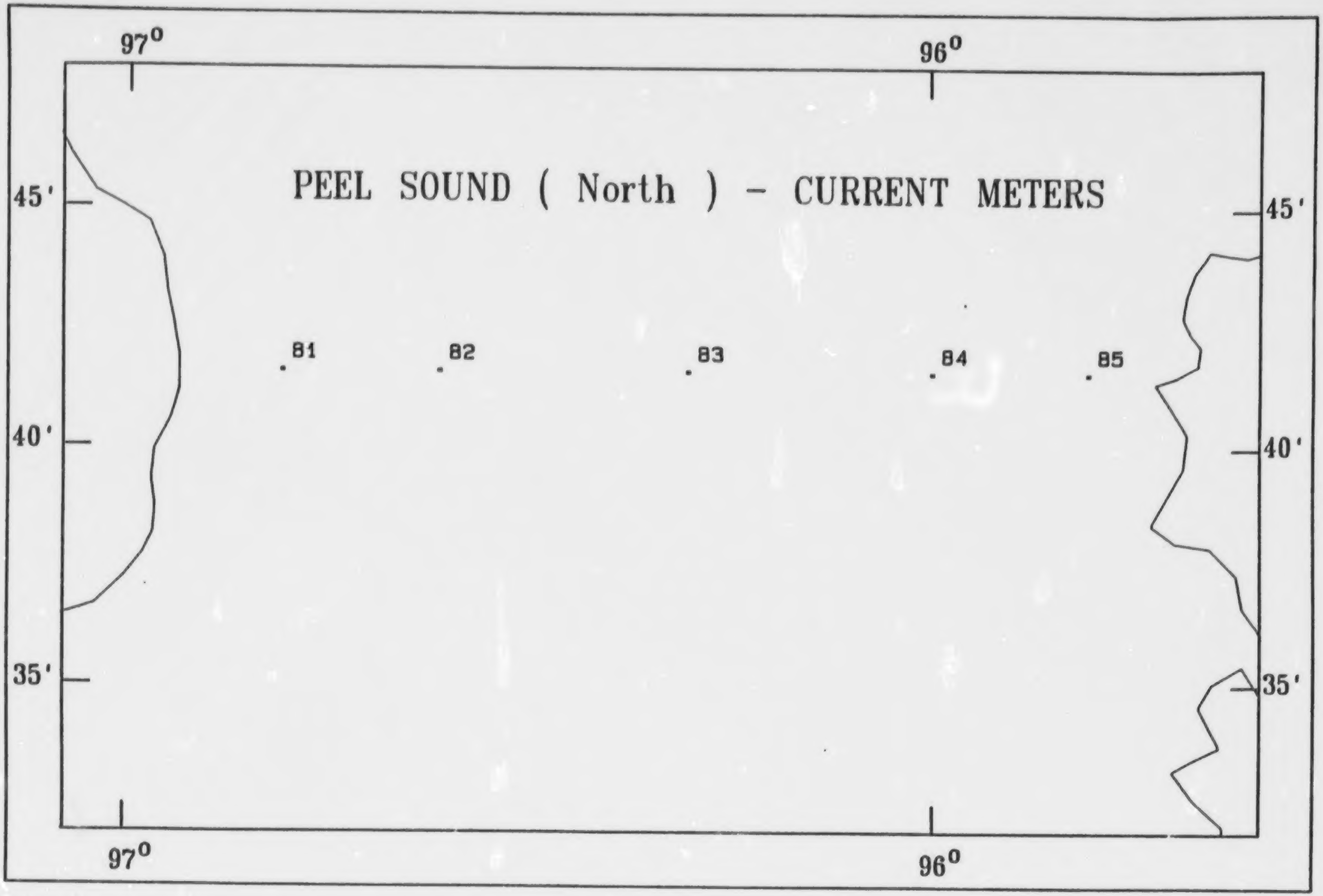
PEEL SOUND (North) - CURRENT METERS
97⁰
96⁰
45'
40'
35'
81
82
83
84
85

Figure 4.2.36. Peel Sound current meter stations.

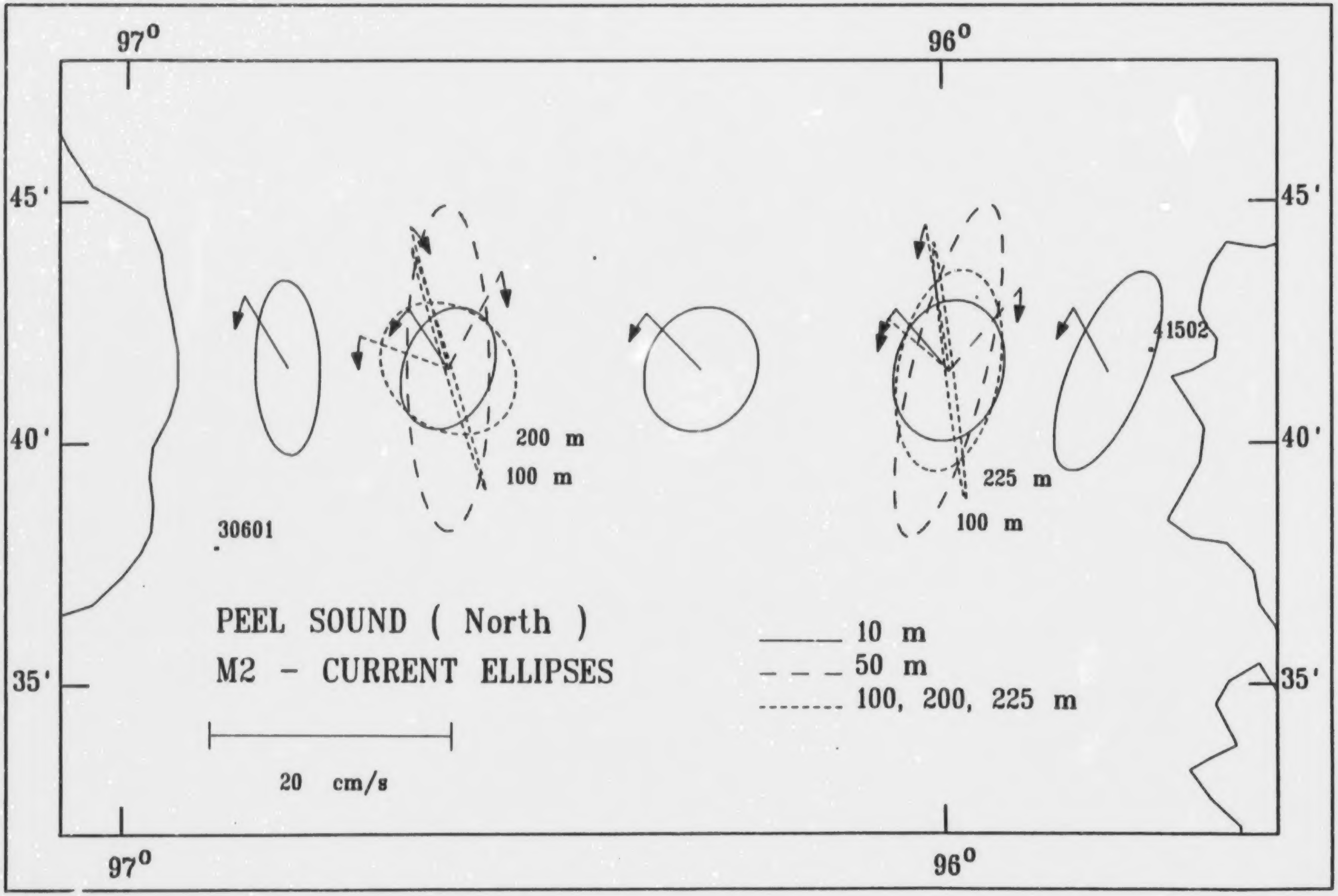
97⁰
96⁰
45'
40'
35'
45'
40'
35'
200 m
100 m
225 m
100 m
41502
30601
PEEL SOUND (North)
M2 - CURRENT ELLIPSES
10 m
50 m
100, 200, 225 m
20 cm/s
97⁰
96⁰

Figure 4.2.37. Peel Sound M_2 current ellipses.

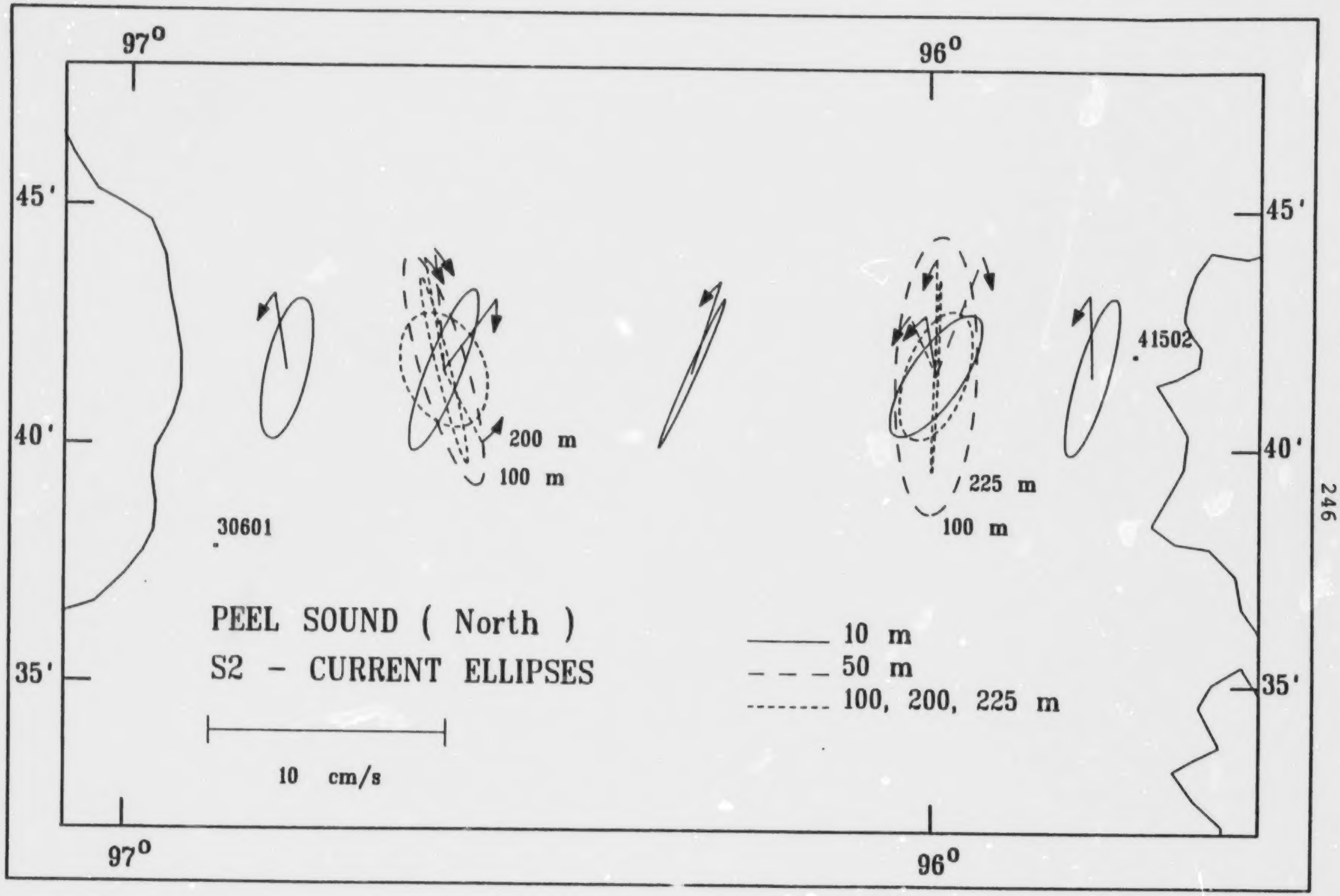
97°
96°
45'
40'
35'
45'
40'
35'
97°
96°
200 m
100 m
225 m
100 m
30601
41502
PEEL SOUND (North)
S2 - CURRENT ELLIPSES
10 cm/s
10 m
50 m
100, 200, 225 m

Figure 4.2.38. Peel Sound S_2 current ellipses.

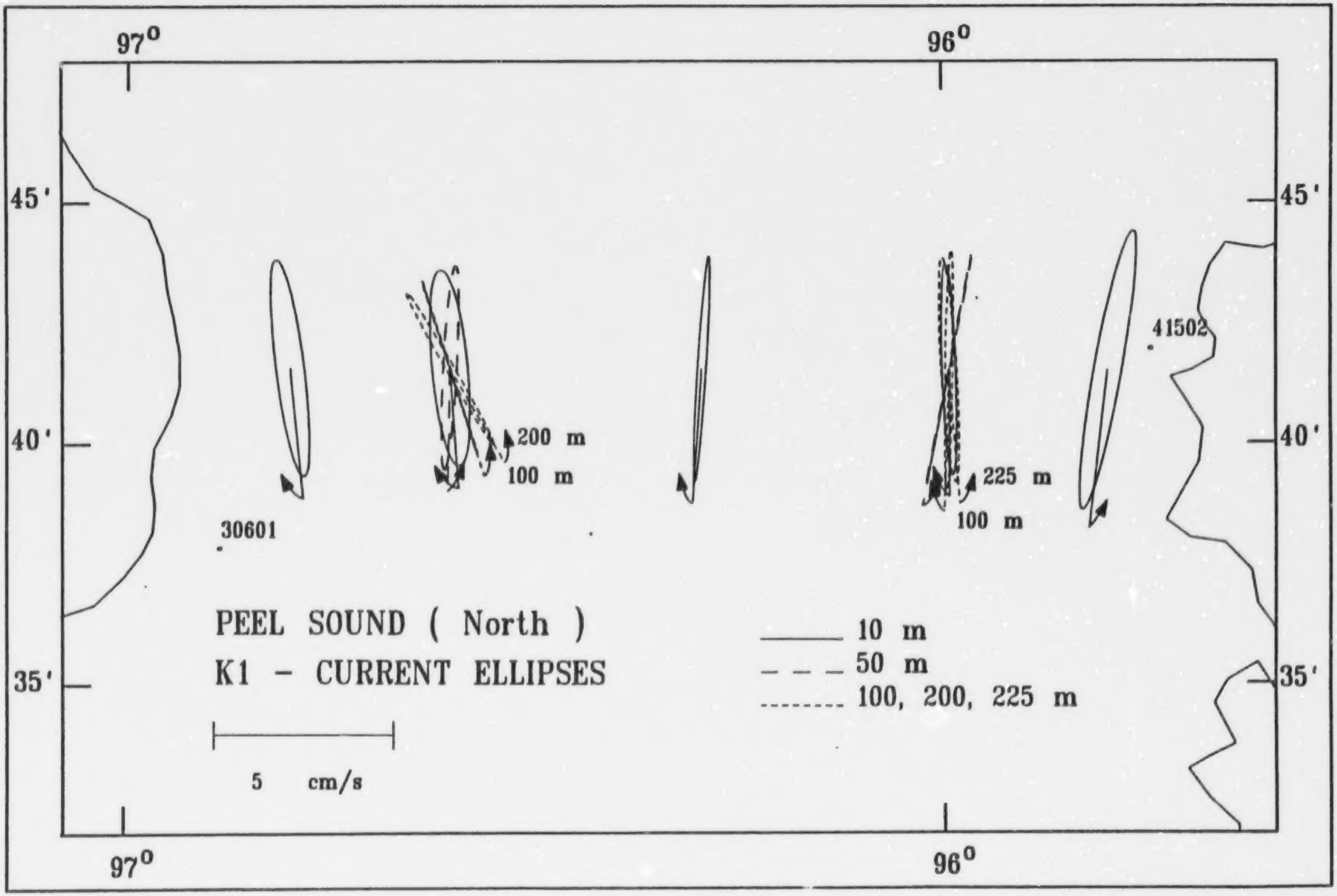
97°
96°
45'
40'
35'
45'
40'
35'
41502
200 m
100 m
225 m
100 m
30601
PEEL SOUND (North)
K1 - CURRENT ELLIPSES
10 m
50 m
100, 200, 225 m
5 cm/s
97°
96°

Figure 4.2.39. Peel Sound K_1 current ellipses.

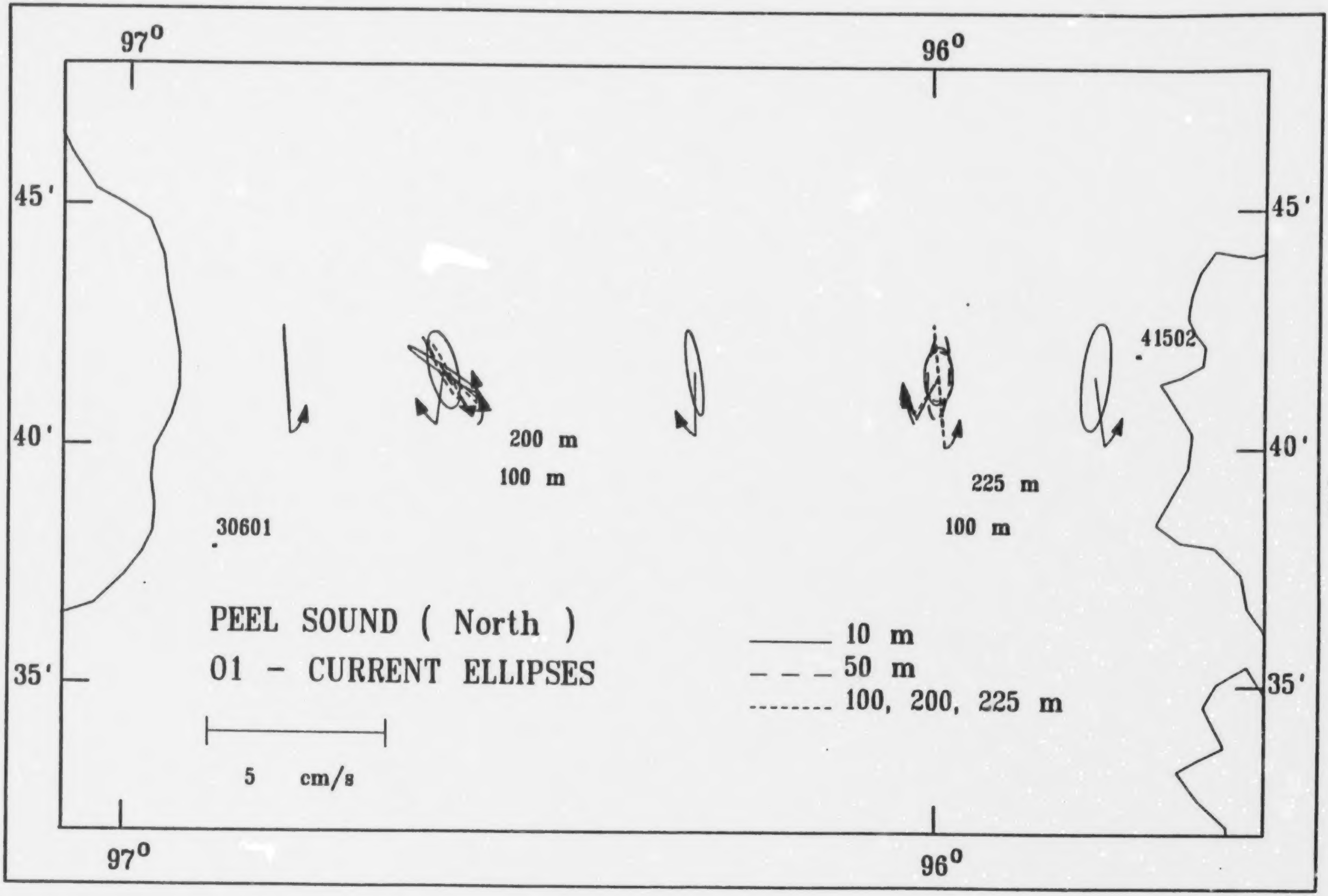
97⁰
96⁰
45'
40'
35'
41502
30601
200 m
100 m
225 m
100 m
PEEL SOUND (North)
01 - CURRENT ELLIPSES
10 m
50 m
100, 200, 225 m
5 cm/s

Figure 4.2.40. Peel Sound O_1 current ellipses.

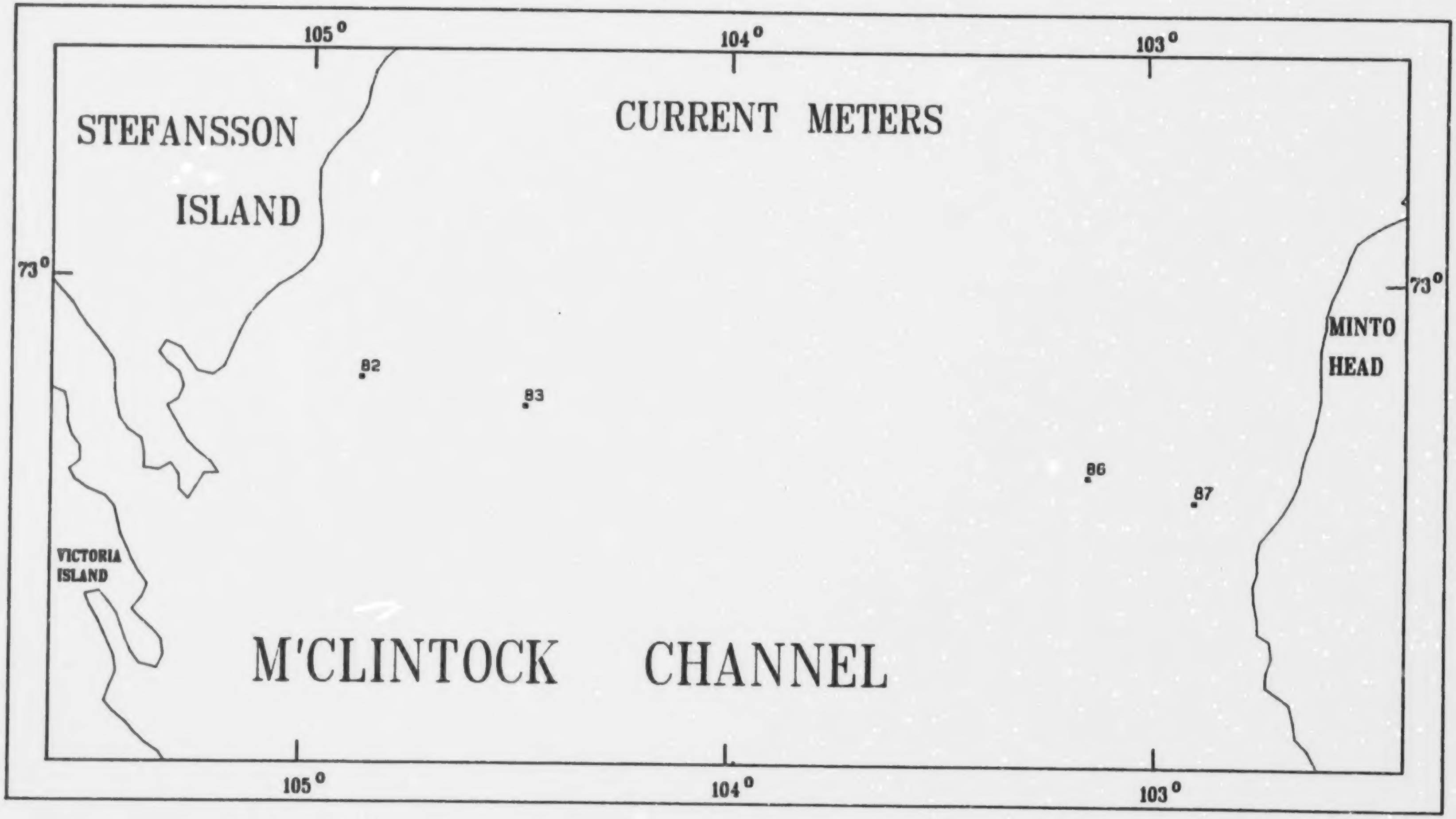
105°
104°
103°
STEFANSSON
ISLAND
CURRENT METERS
73°
MINTO
HEAD
73°
82
83
86
87
VICTORIA
ISLAND
M'CLINTOCK CHANNEL
105°
104°
103°

Figure 4.2.41. M'Clintock Channel current meter stations.

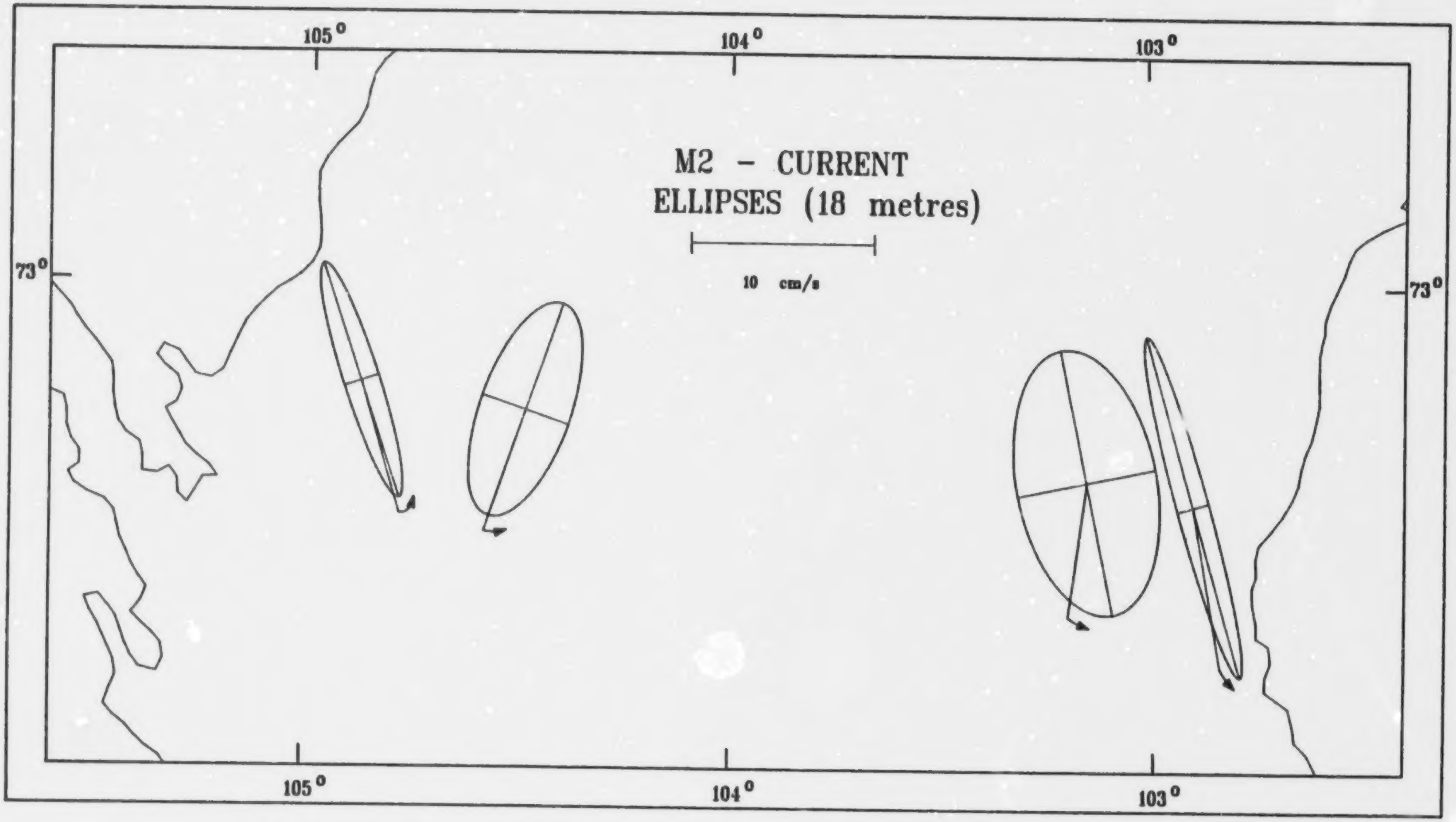
M2 - CURRENT
ELLIPSES (18 metres)
10 cm/s
105°
104°
103°
73°
73°
105°
104°
103°

Figure 4.2.42. M'Clintock Channel M_2 current ellipses.

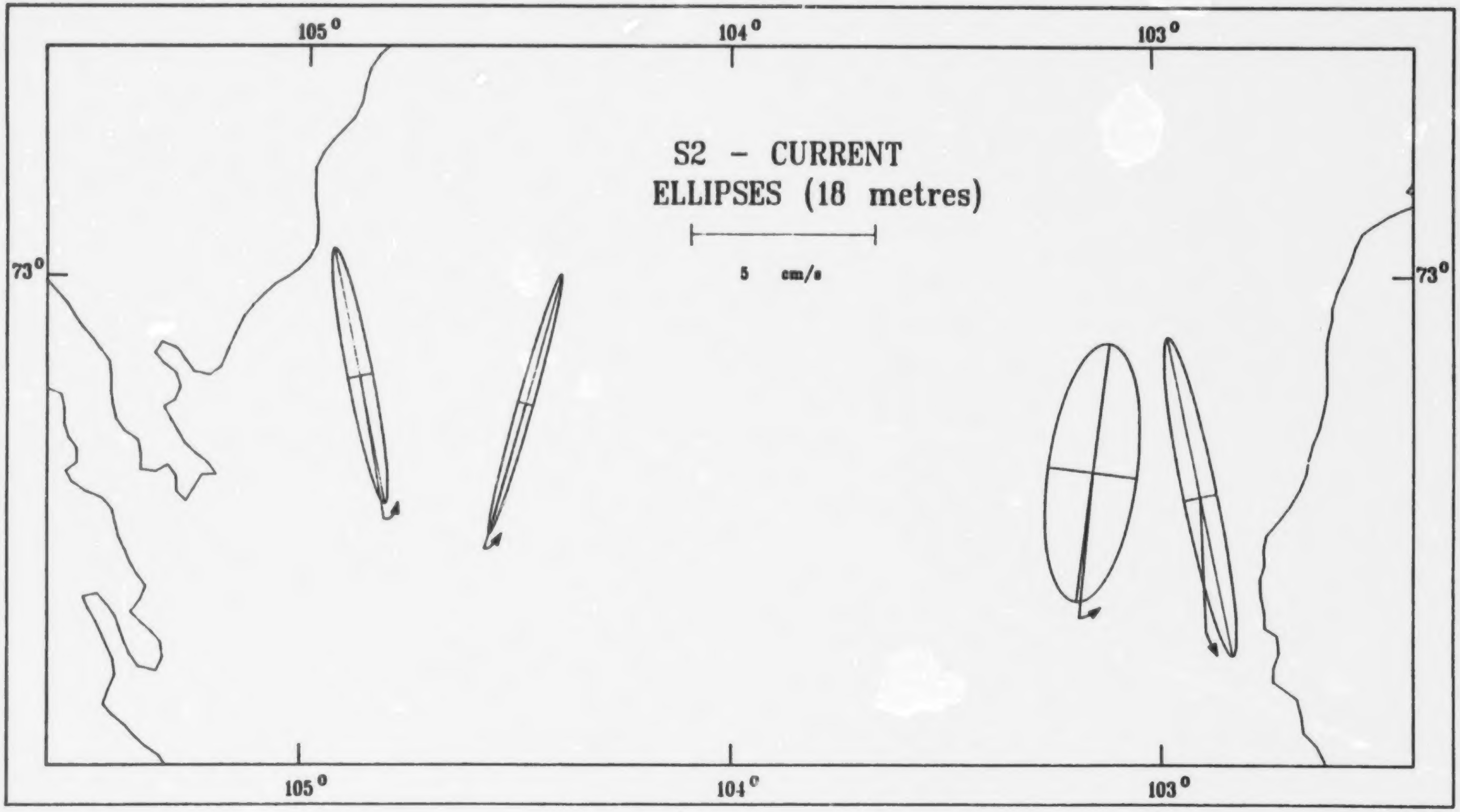
105°
104°
103°
S2 - CURRENT
ELLIPSES (18 metres)
5 cm/s
73°
73°
105°
104°
103°

Figure 4.2.43. M'Clintock Channel S_2 current ellipses.

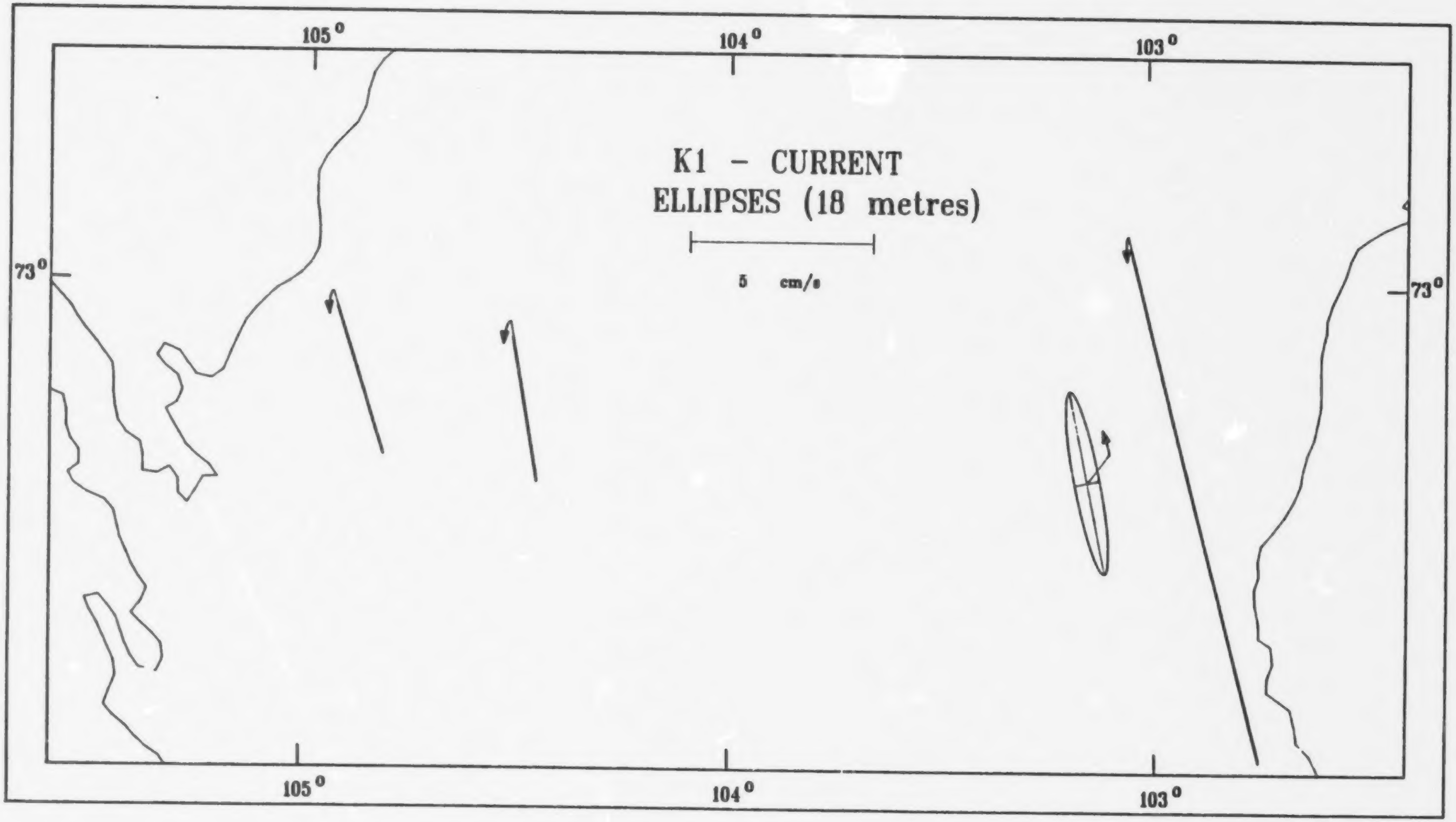
K1 - CURRENT
ELLIPSES (18 metres)
5 cm/s
105°
104°
103°
73°
73°
105°
104°
103°

Figure 4.2.44. M'Clintock Channel K_1 current ellipses.

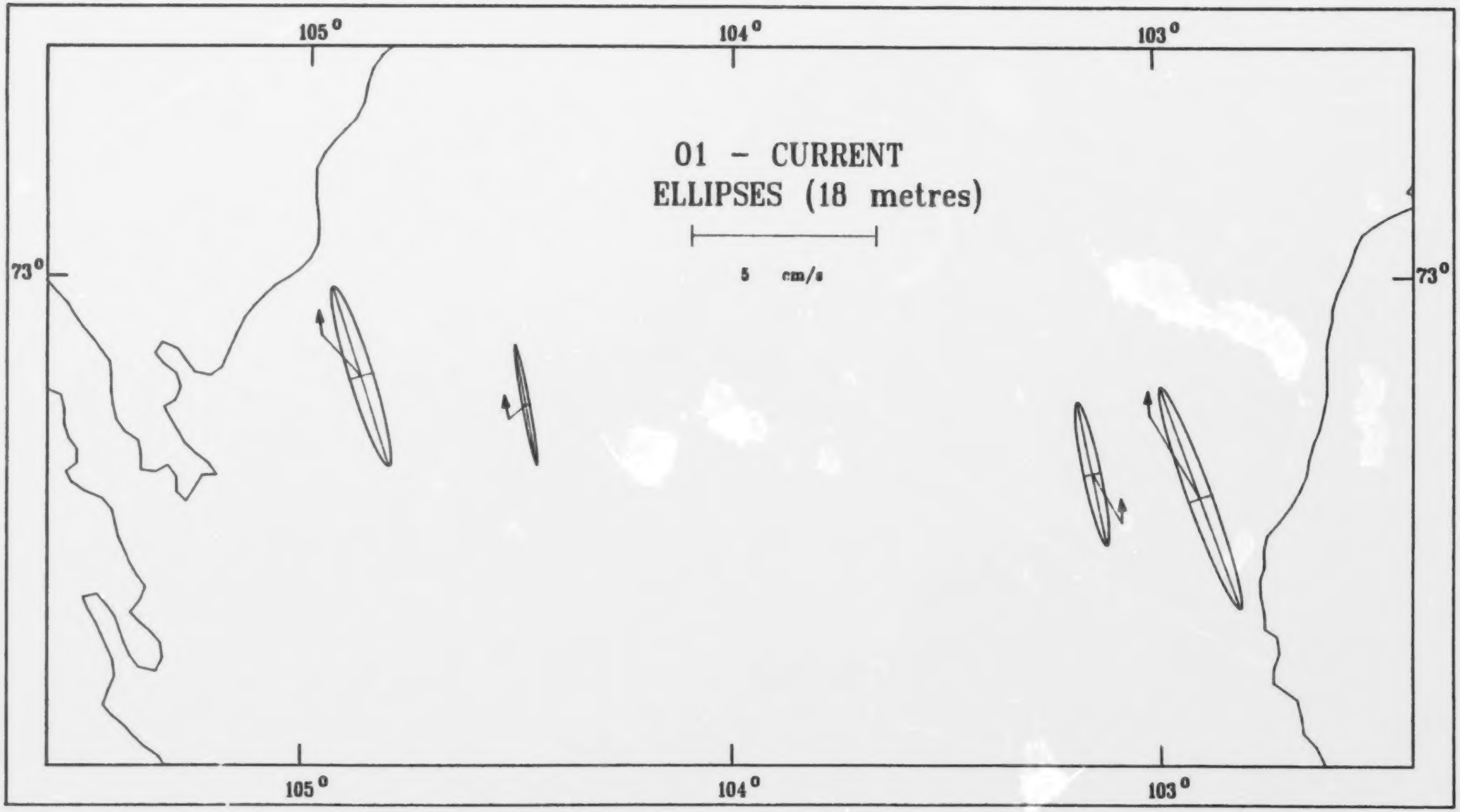
O1 - CURRENT
ELLIPSES (18 metres)
5 cm/s
105°
104°
103°
73°
73°
105°
104°
103°

Figure 4.2.45. M'Clintock Channel O_1 current ellipses.

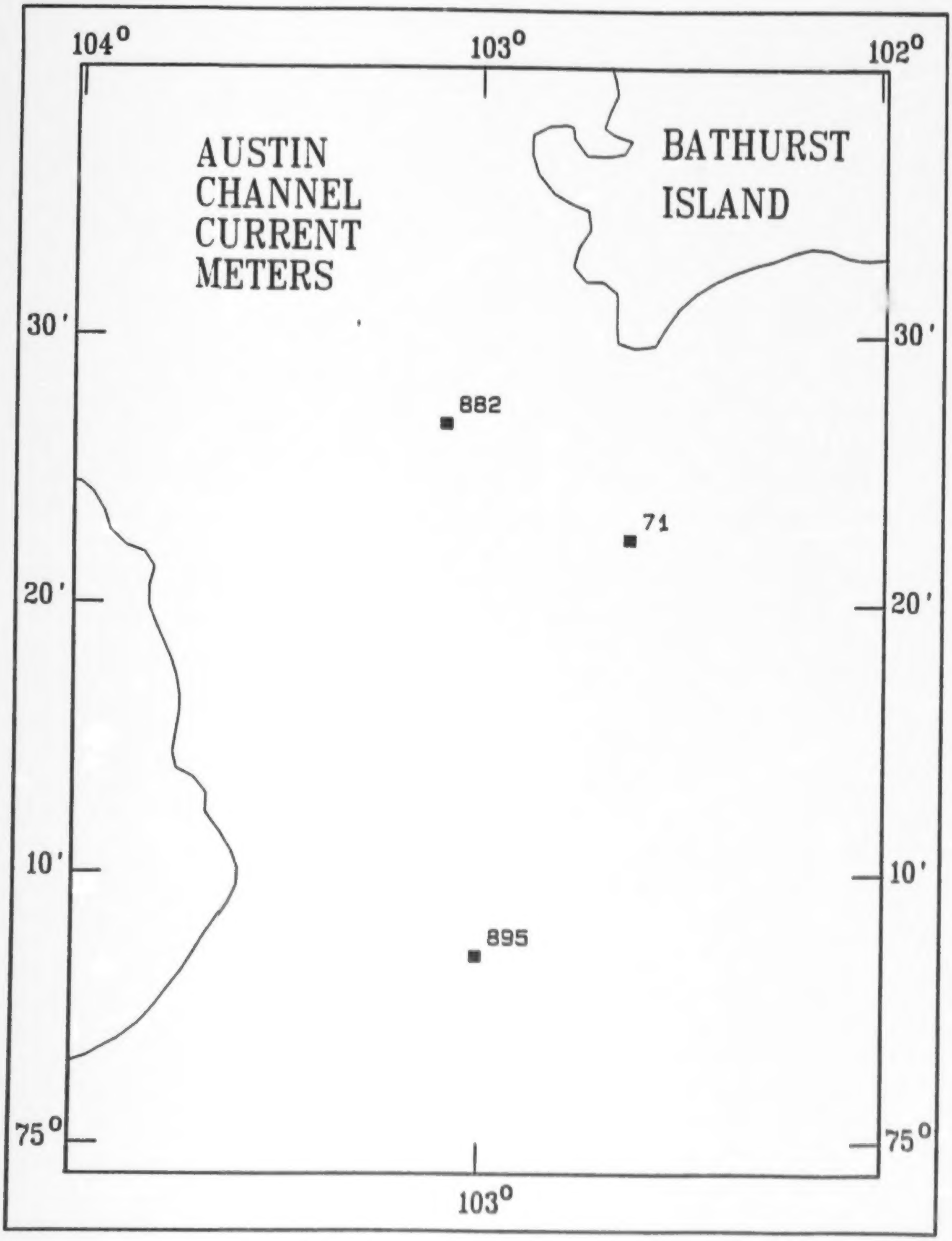
104°
103°
102°
AUSTIN CHANNEL CURRENT METERS
BATHURST ISLAND
30'
30'
882
71
20'
20'
10'
10'
895
75°
75°
103°

Figure 4.2.46. Austin Channel current meter stations.

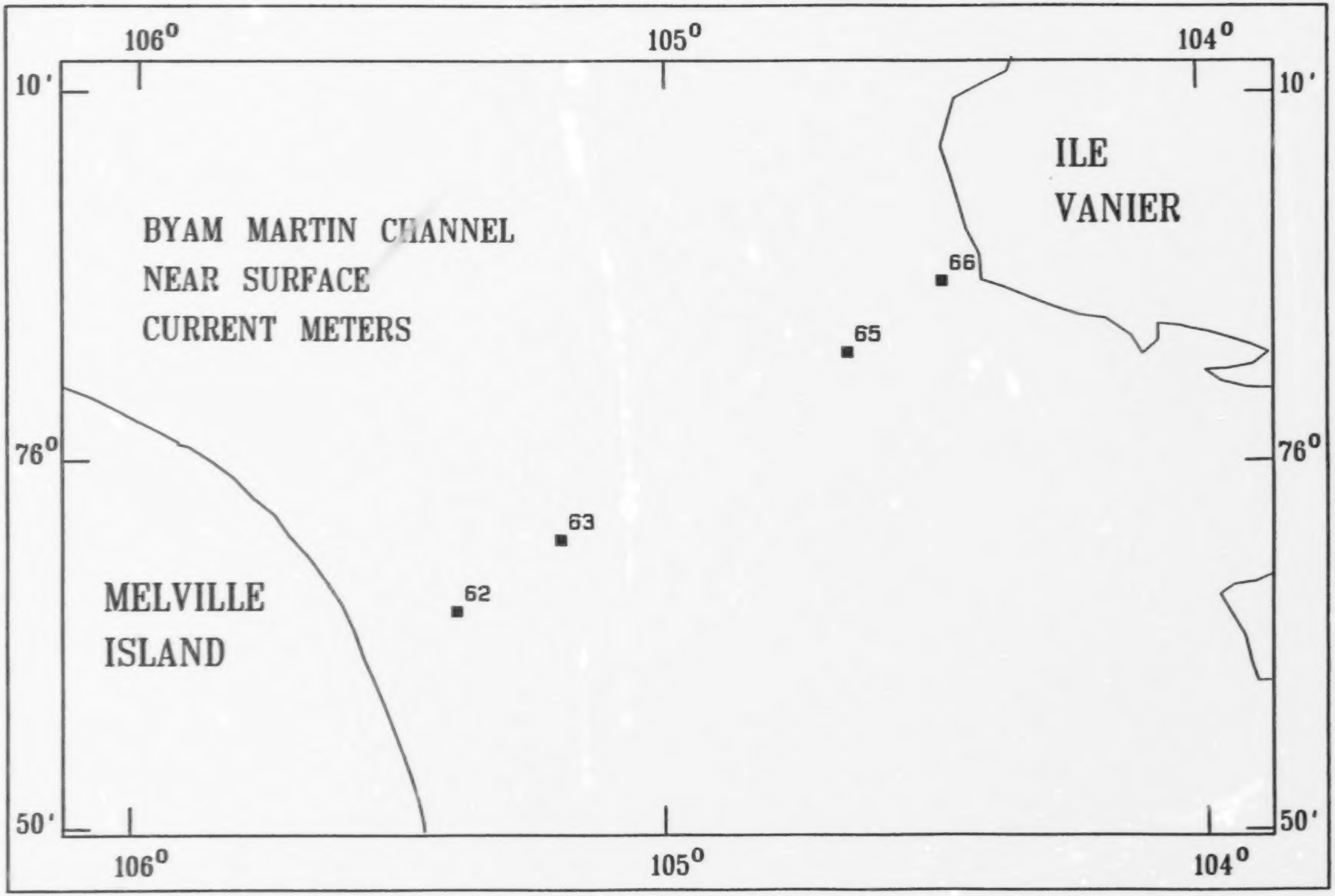
106°
105°
104°
10'
76°
50'
BYAM MARTIN CHANNEL
NEAR SURFACE
CURRENT METERS
ILE
VANIER
MELVILLE
ISLAND
66
65
63
62

Figure 4.2.47. Byam Martin Channel current meter stations.

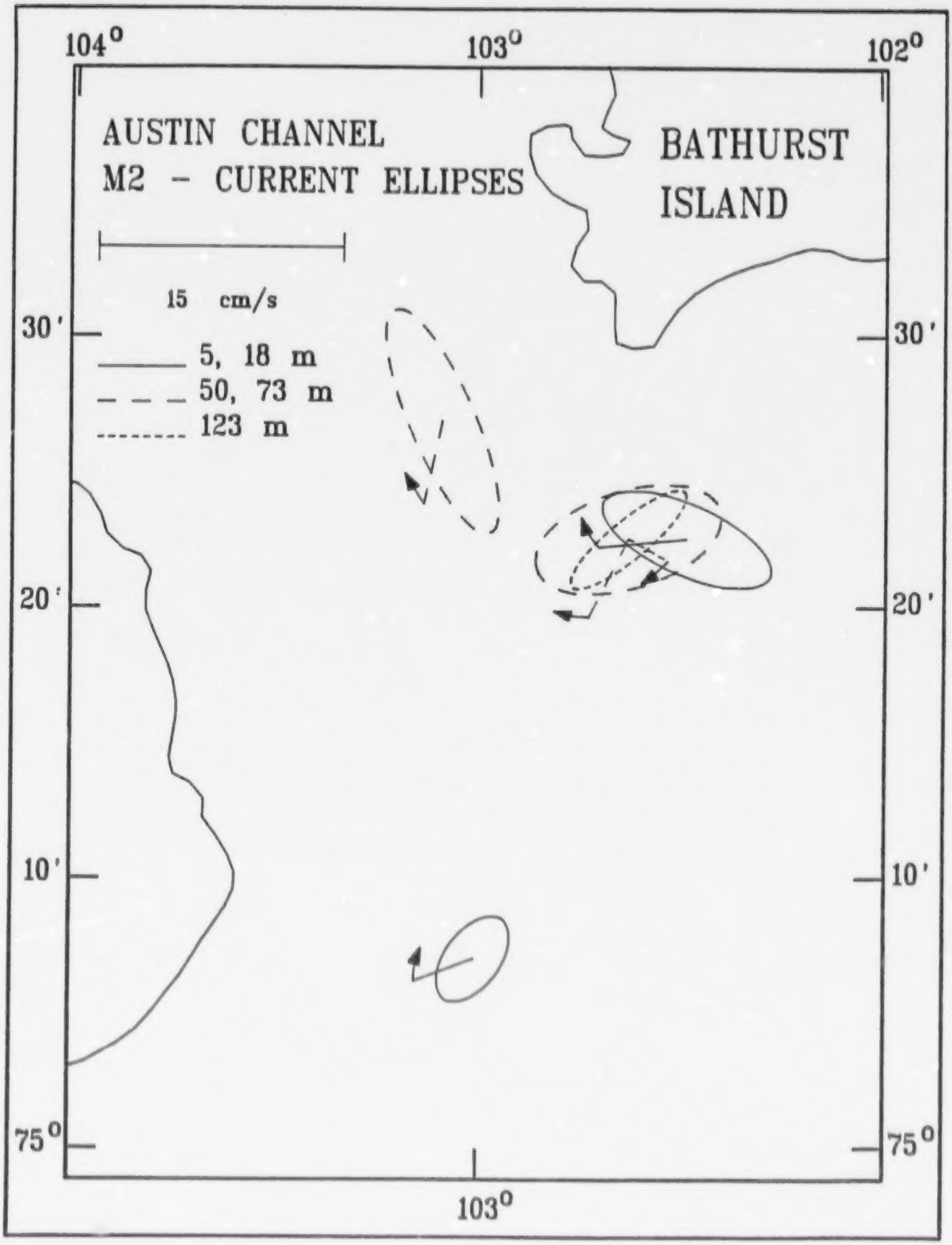
104°
103°
102°
AUSTIN CHANNEL
M2 - CURRENT ELLIPSES
BATHURST
ISLAND
15 cm/s
5, 18 m
50, 73 m
123 m
30'
20'
10'
75°
30'
20'
10'
75°
103°

Figure 4.2.48. Austin Channel M_2 current ellipses.

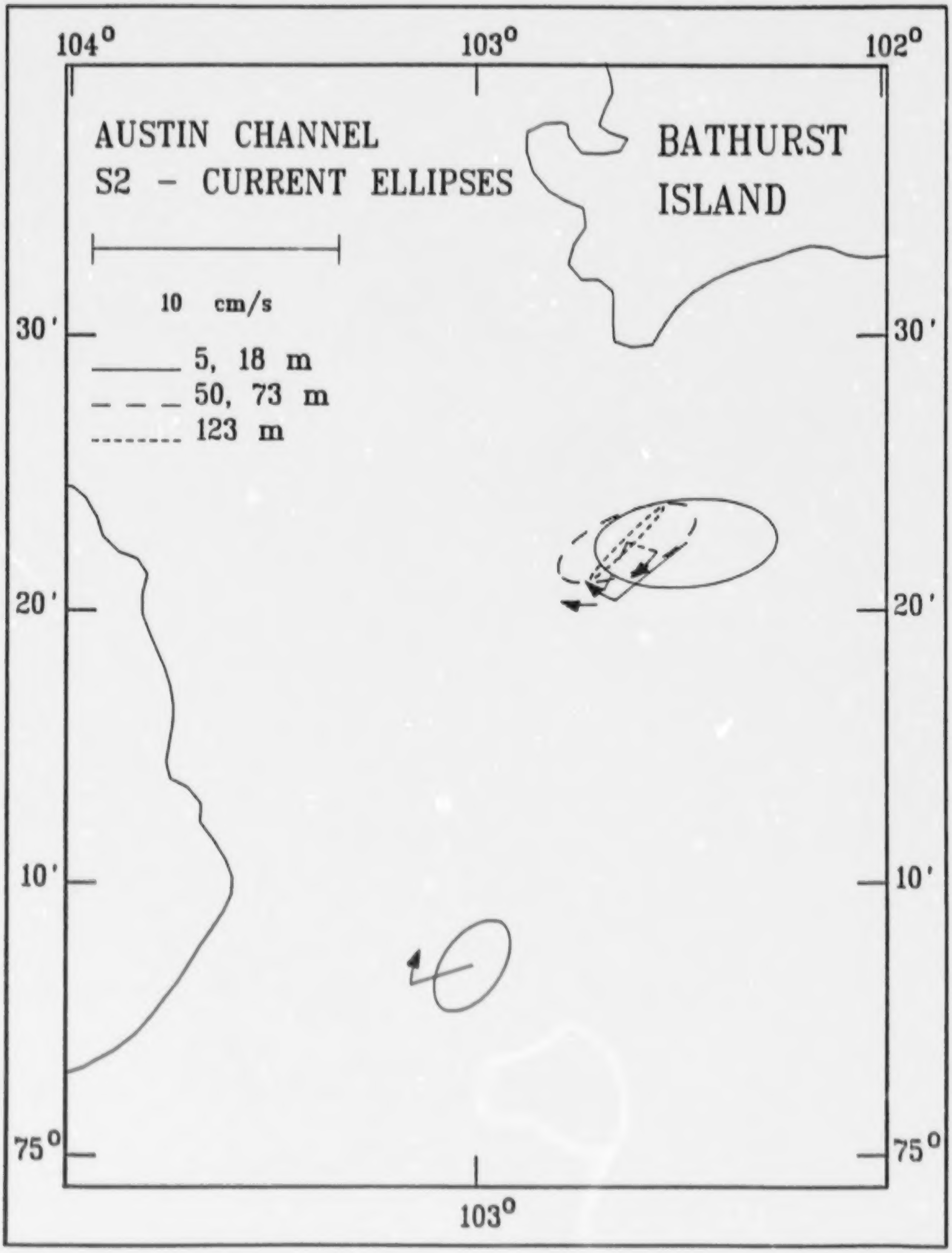
104°
103°
102°
AUSTIN CHANNEL
S2 - CURRENT ELLIPSES
BATHURST
ISLAND
10 cm/s
5, 18 m
50, 73 m
123 m
30'
20'
10'
75°
103°

Figure 4.2.49. Austin Channel S_2 current ellipses.

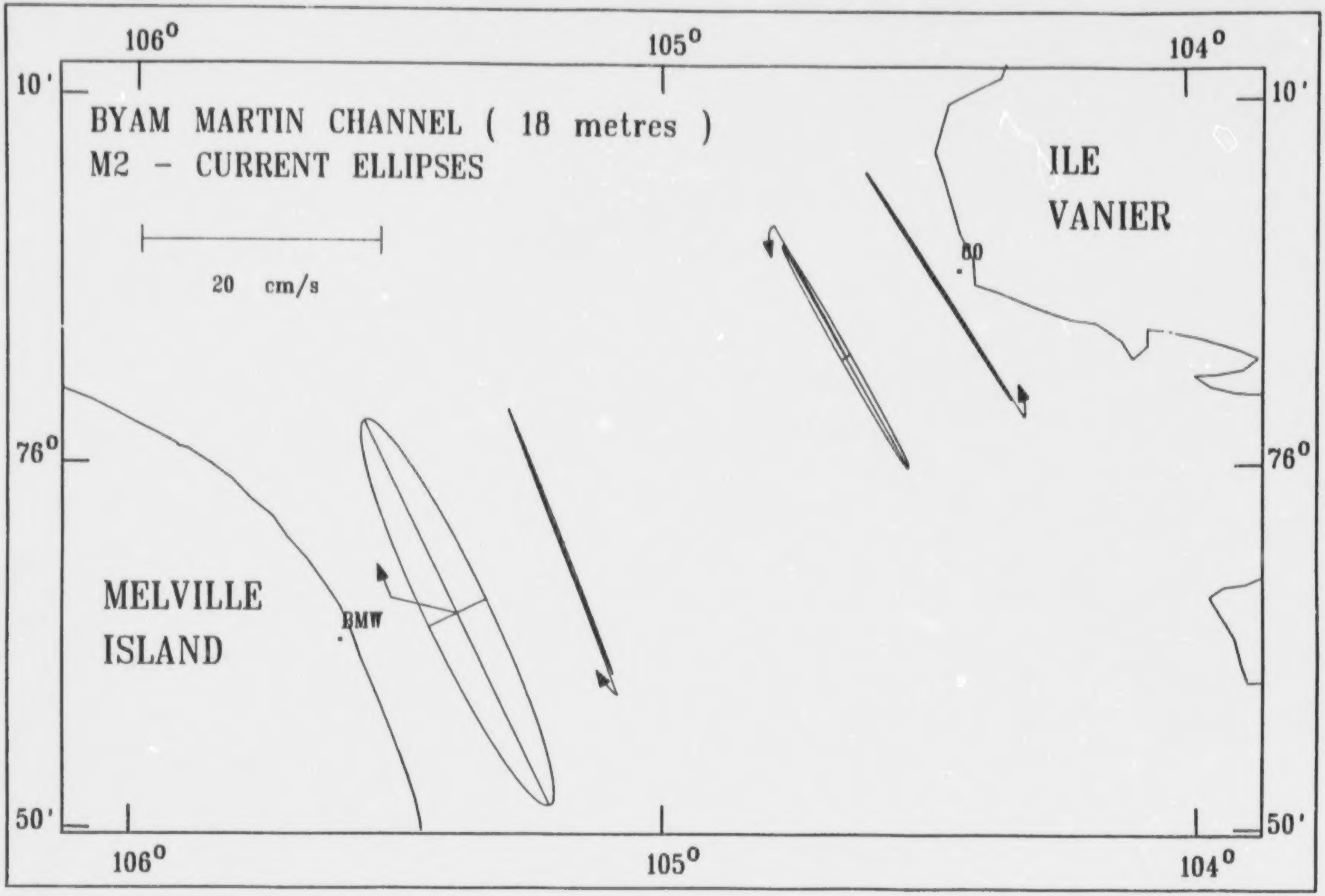
BYAM MARTIN CHANNEL (18 metres)
M2 - CURRENT ELLIPSES
20 cm/s
ILE VANIER
MELVILLE ISLAND
B0
BMW
106°
105°
104°
10'
76°
50'

Figure 4.2.50. Byam Martin Channel M_2 current ellipses.

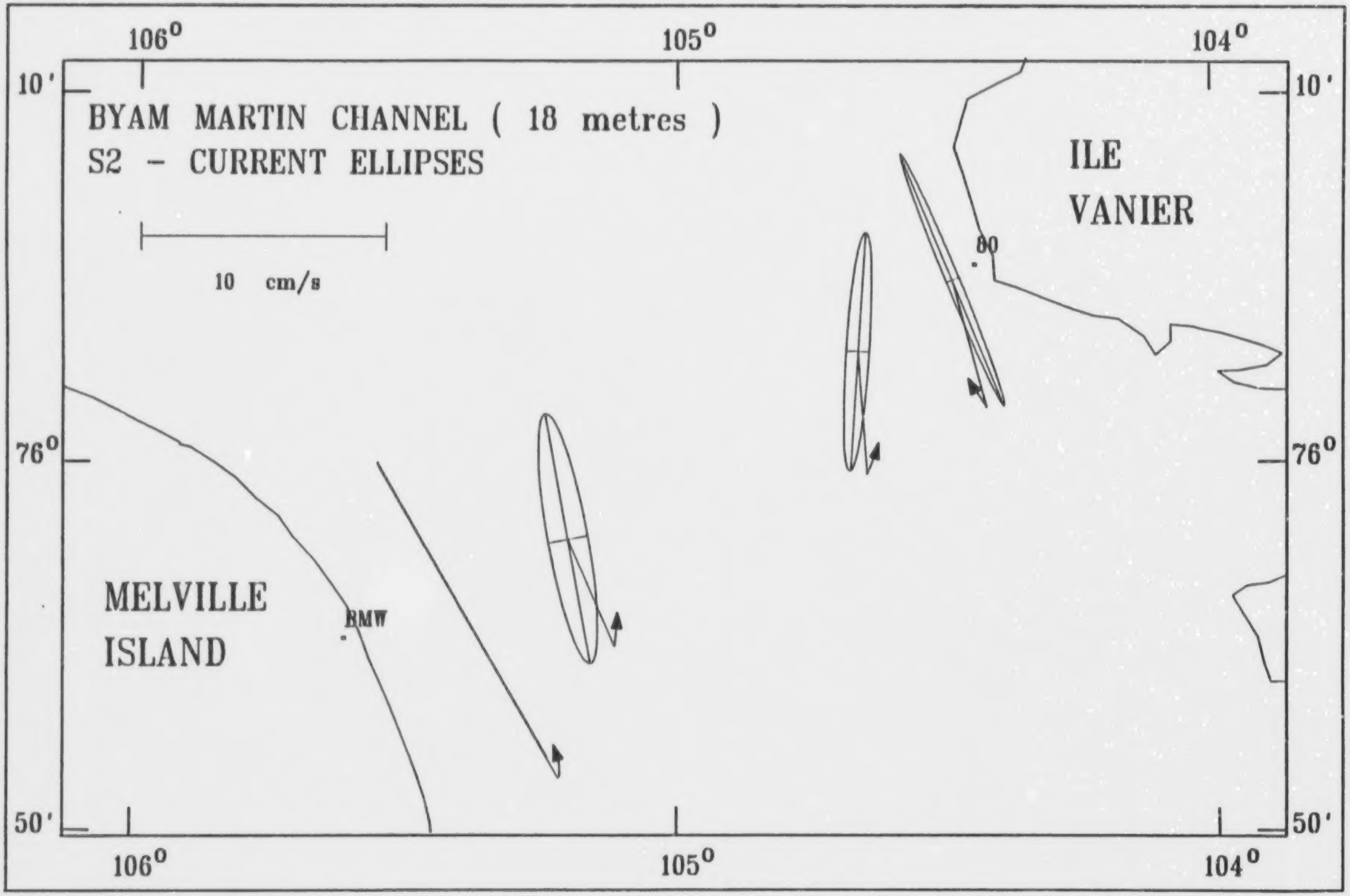
BYAM MARTIN CHANNEL (18 metres)
S2 - CURRENT ELLIPSES
10 cm/s
ILE
VANIER
MELVILLE
ISLAND
BO
BMW
106°
105°
104°
10'
76°
50'

Figure 4.2.51. Byam Martin Channel S_2 current ellipses.

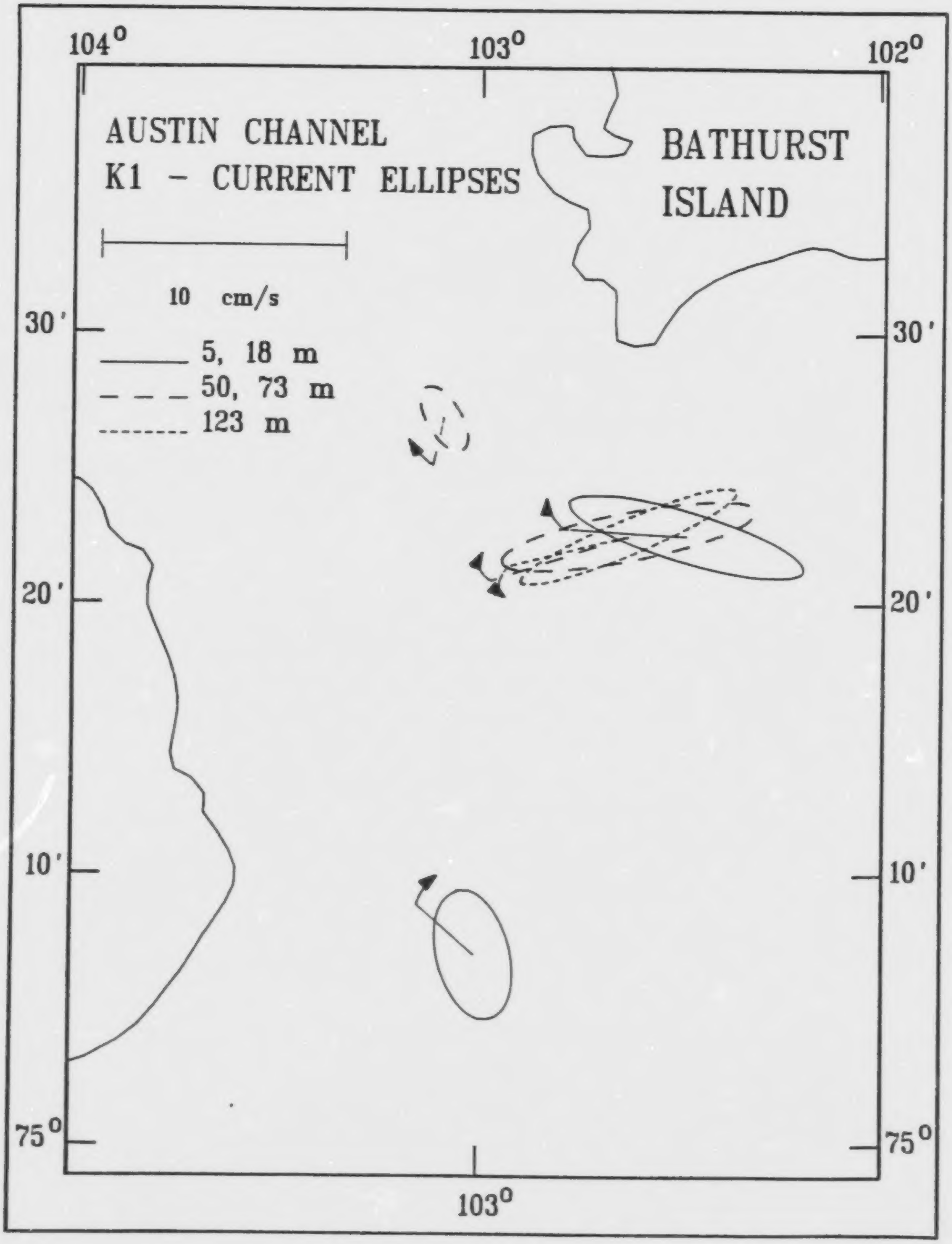
104°
103°
102°
AUSTIN CHANNEL
K1 - CURRENT ELLIPSES
BATHURST
ISLAND
10 cm/s
5, 18 m
50, 73 m
123 m
30'
20'
10'
75°
30'
20'
10'
75°
103°

Figure 4.2.52. Austin Channel K_1 current ellipses.

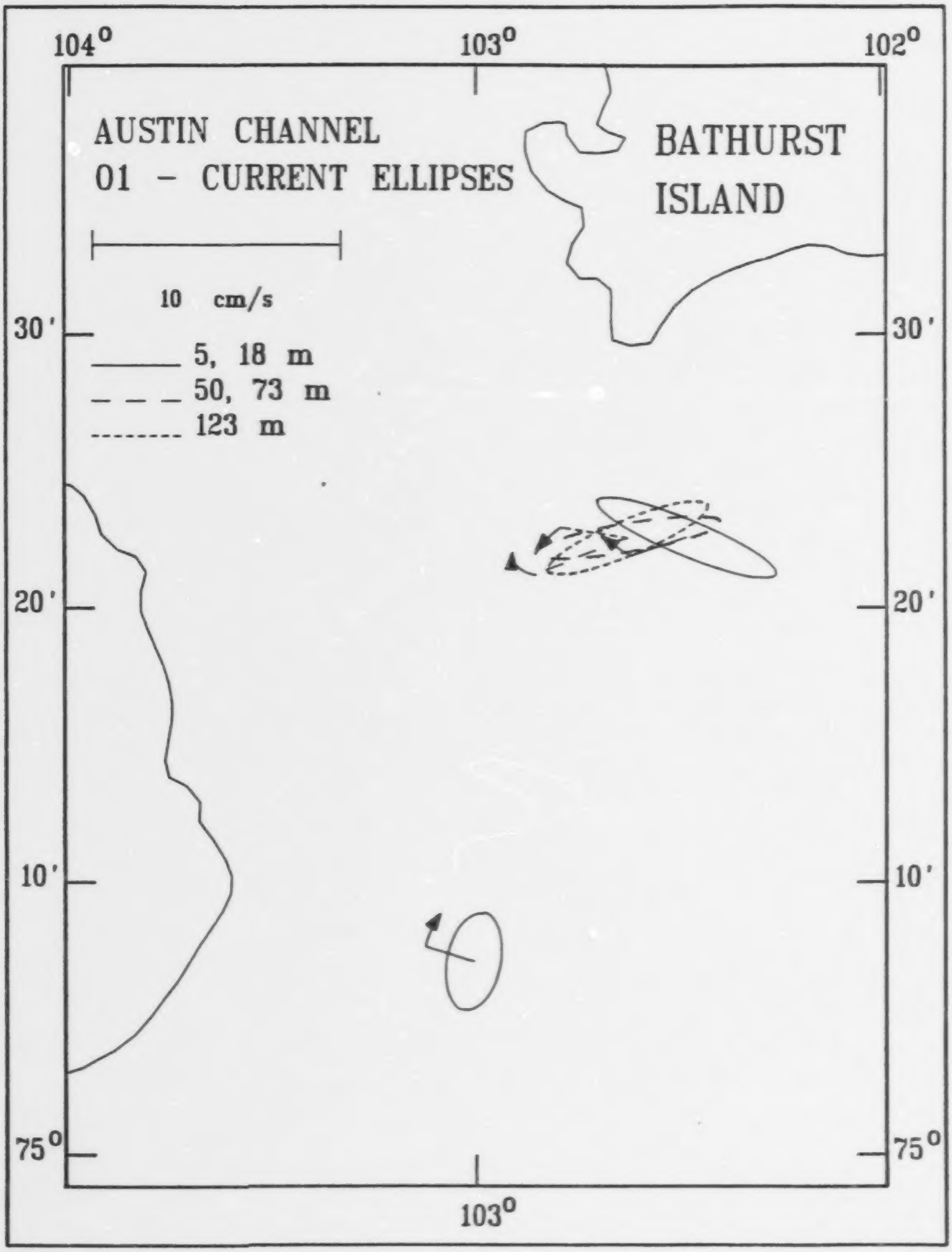
104°
103°
102°
AUSTIN CHANNEL
01 - CURRENT ELLIPSES
BATHURST
ISLAND
10 cm/s
5, 18 m
50, 73 m
123 m
30'
20'
10'
75°
103°

Figure 4.2.53. Austin Channel O_1 current ellipses.

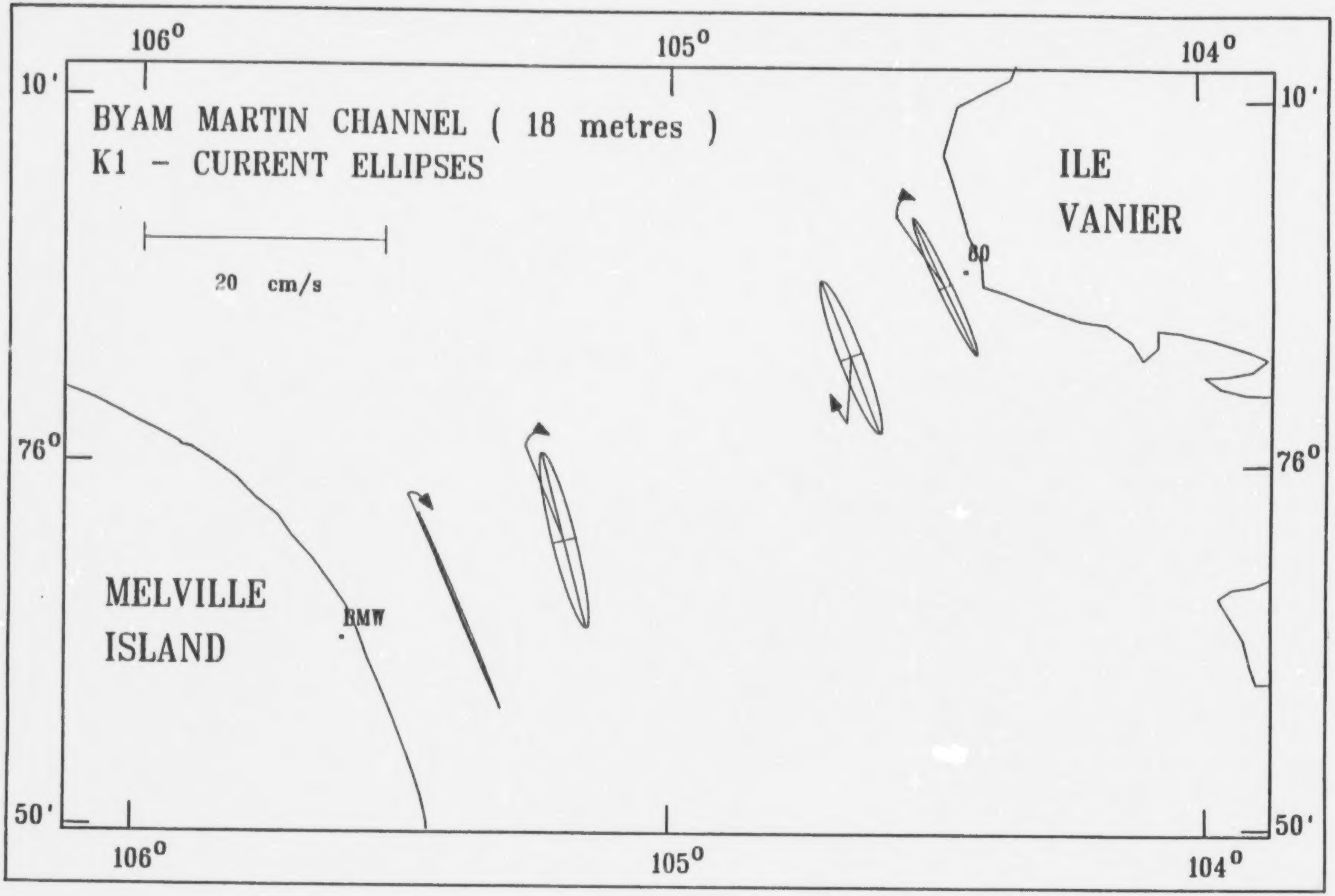
BYAM MARTIN CHANNEL (18 metres)
K1 - CURRENT ELLIPSES
20 cm/s
ILE
VANIER
MELVILLE
ISLAND
BMW
80
106°
105°
104°
10'
76°
50'

Figure 4.2.54. Byam Martin Channel K_1 current ellipses.

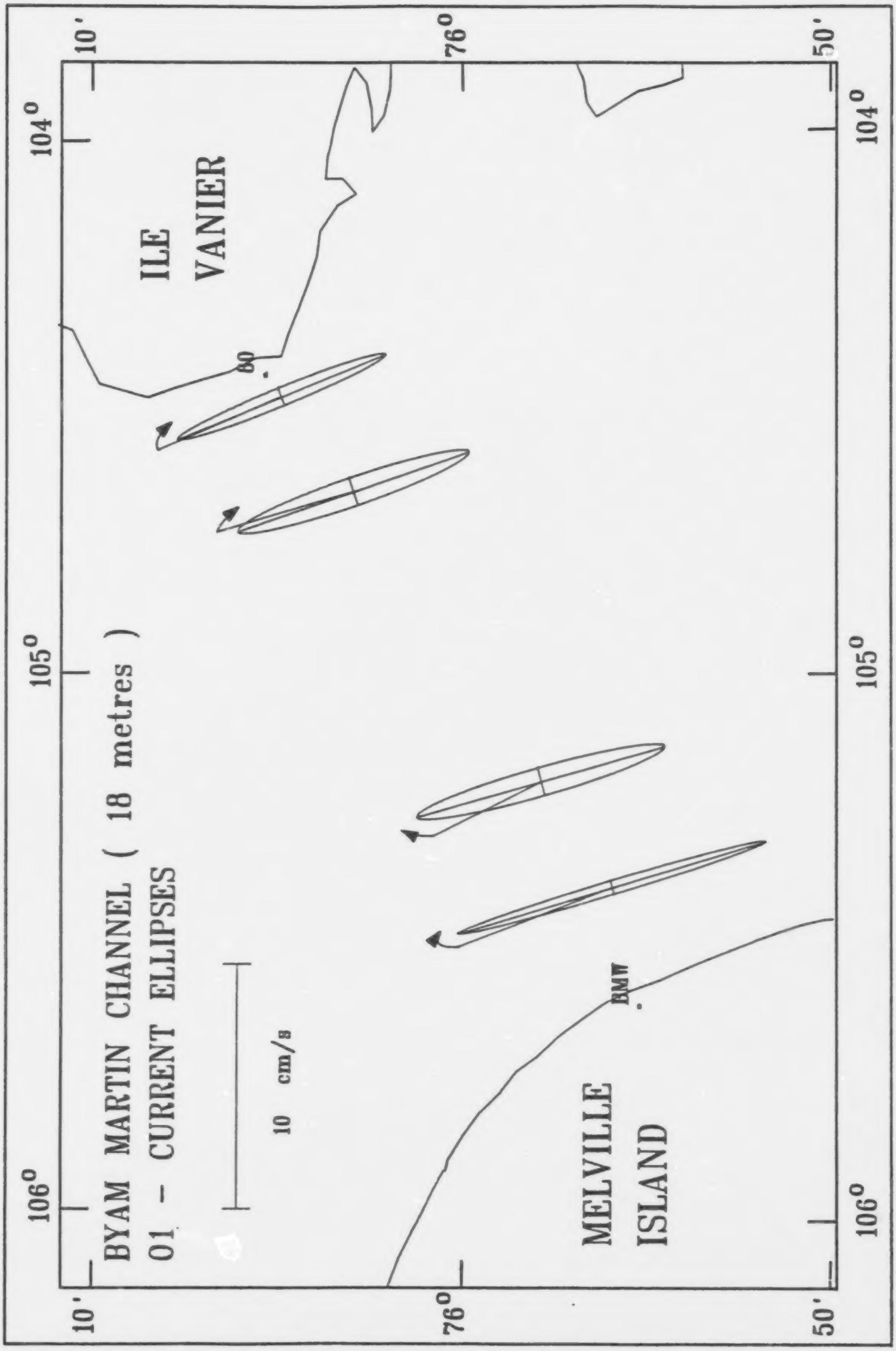
BYAM MARTIN CHANNEL (18 metres)
O1 - CURRENT ELLIPSES
10 cm/s
ILE
VANIER
MELVILLE
ISLAND
80
BMW
10'
76°
50'
104°
105°
106°

Figure 4.2.55. Byam Martin Channel O_1 current ellipses.

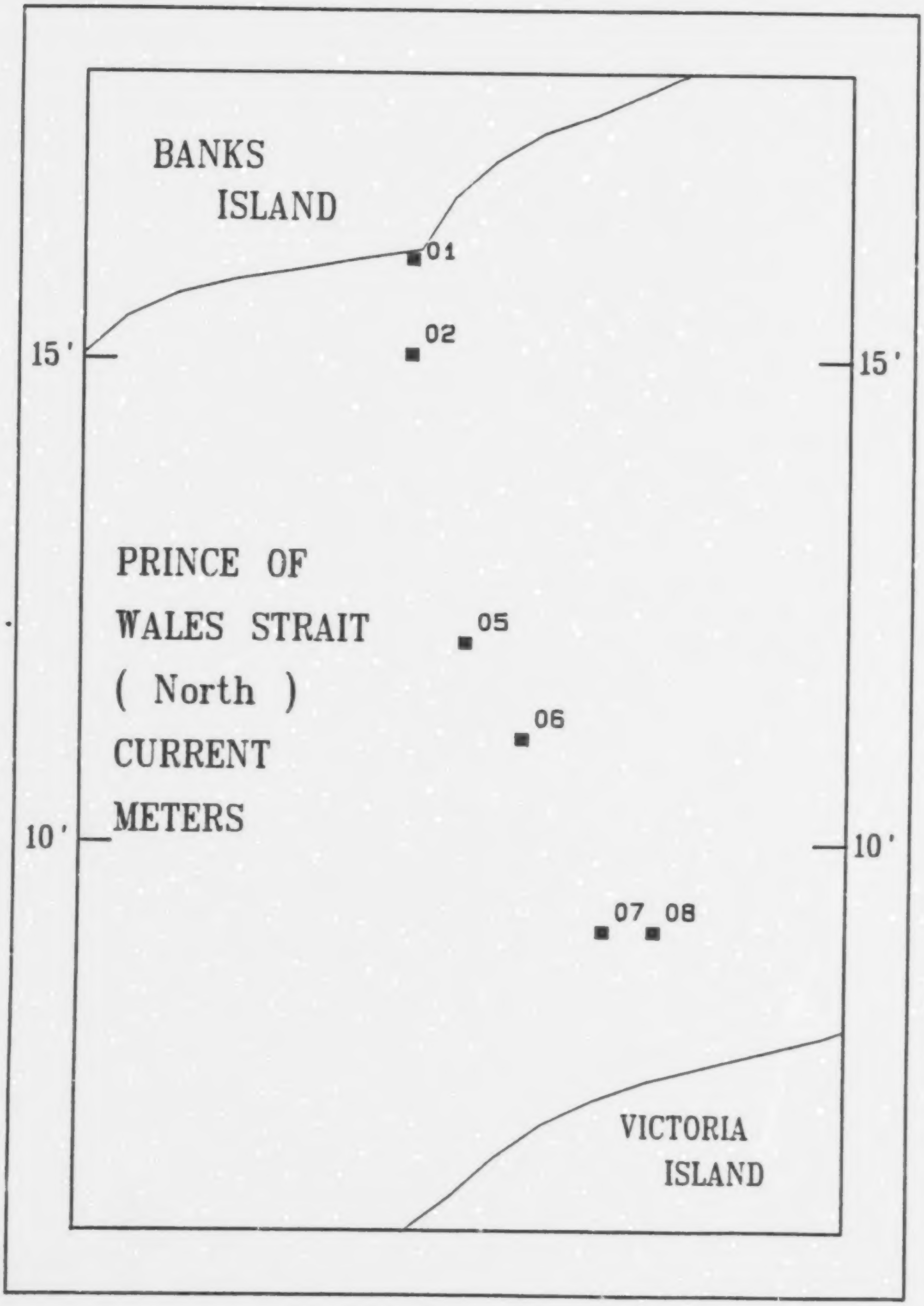
BANKS ISLAND
01
02
15'
15'
PRINCE OF WALES STRAIT (North) CURRENT METERS
05
06
10'
10'
07
08
VICTORIA ISLAND

Figure 4.2.56. Prince of Wales Strait current meter stations.

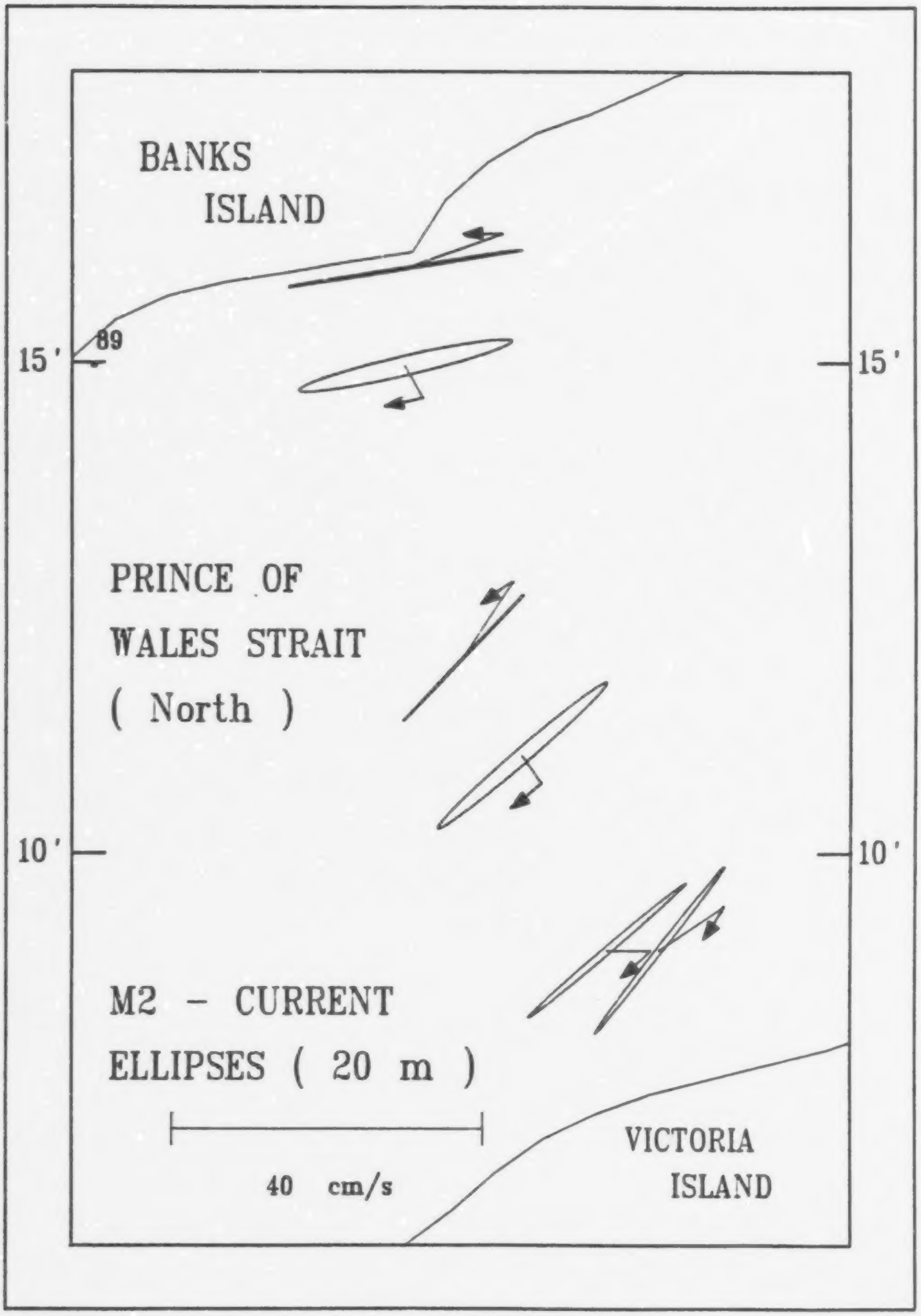
BANKS
ISLAND
89
15'
15'
PRINCE OF
WALES STRAIT
(North)
10'
10'
M2 - CURRENT
ELLIPSES (20 m)
40 cm/s
VICTORIA
ISLAND

Figure 4.2.57. Prince of Wales Strait M_2 current ellipses.

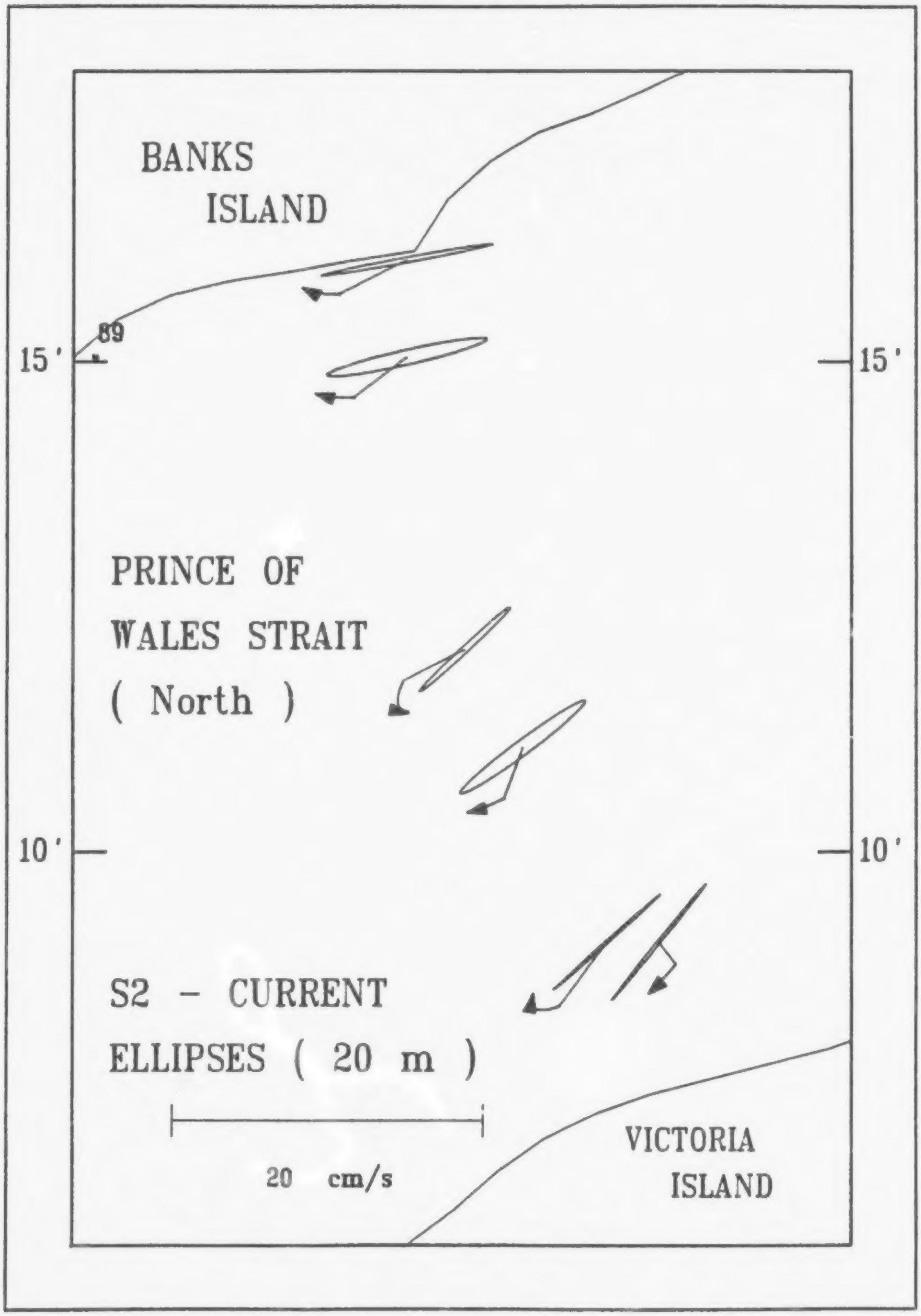
BANKS
ISLAND
89
15'
15'
PRINCE OF
WALES STRAIT
(North)
10'
10'
S2 - CURRENT
ELLIPSES (20 m)
20 cm/s
VICTORIA
ISLAND

Figure 4.2.58. Prince of Wales Strait S_2 current ellipses.

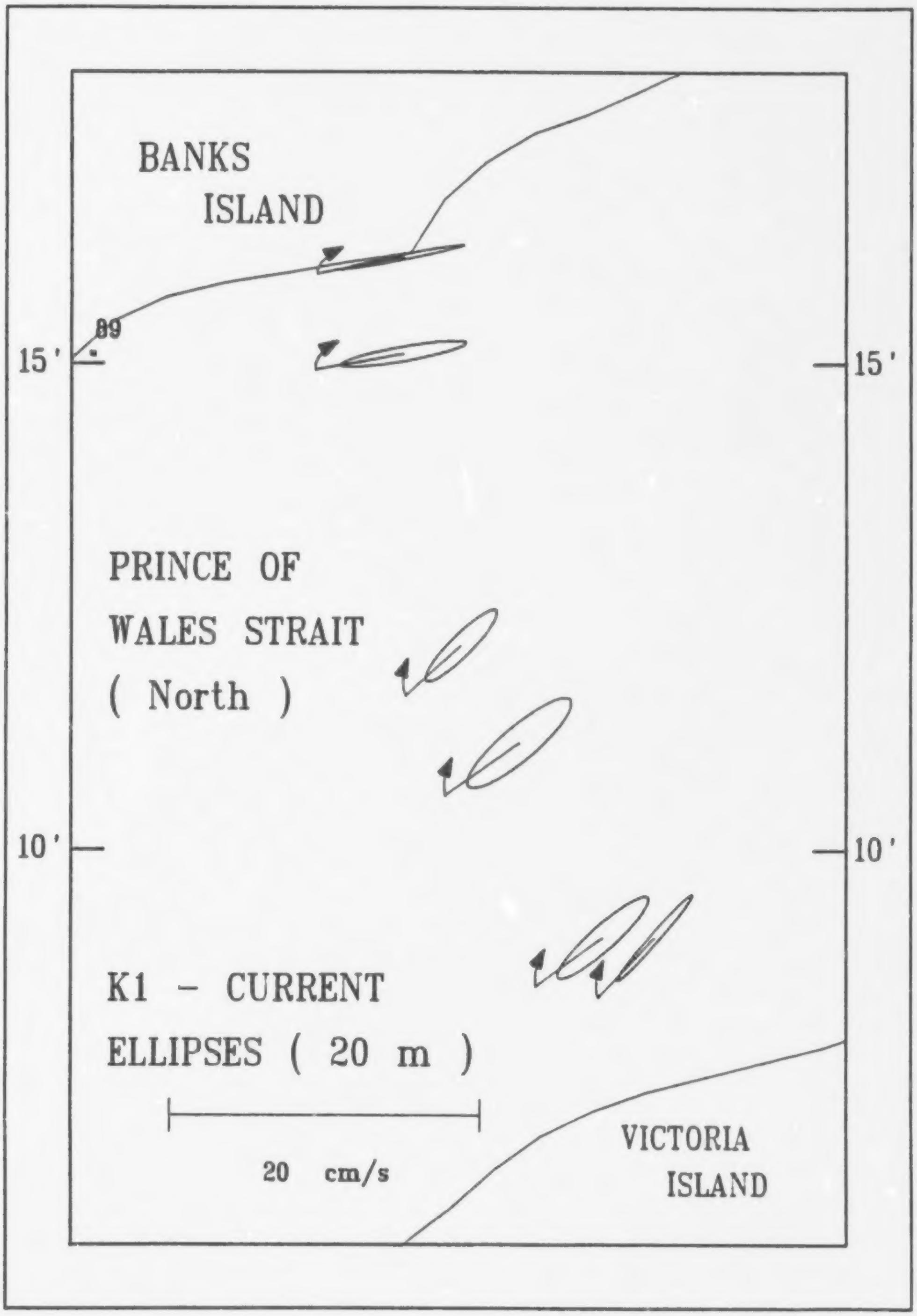
BANKS
ISLAND
89
15'
15'
PRINCE OF
WALES STRAIT
(North)
10'
10'
K1 - CURRENT
ELLIPSES (20 m)
20 cm/s
VICTORIA
ISLAND

Figure 4.2.59. Prince of Wales Strait K_1 current ellipses.

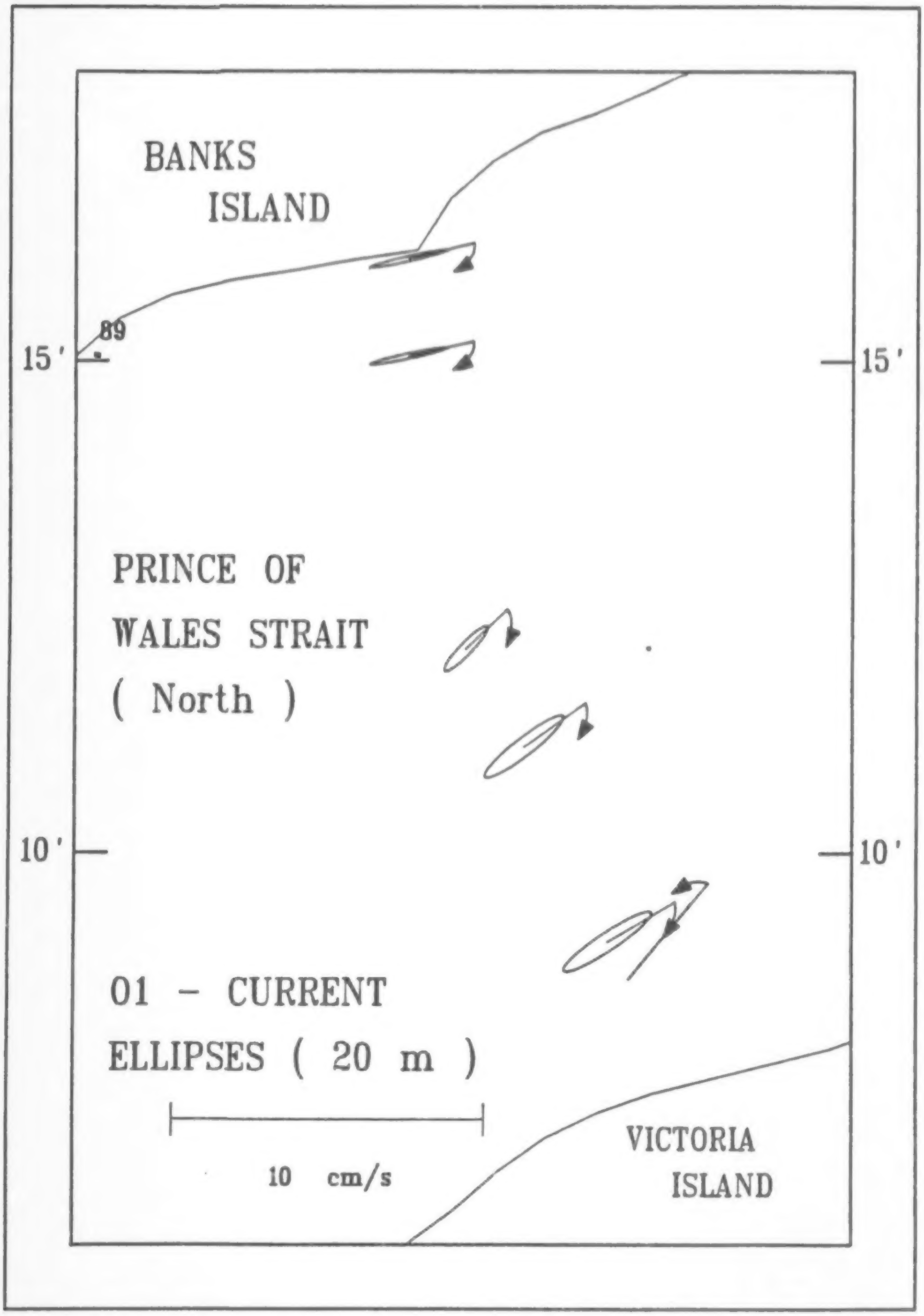
BANKS
ISLAND
89
15'
15'
PRINCE OF
WALES STRAIT
(North)
10'
10'
01 - CURRENT
ELLIPSES (20 m)
10 cm/s
VICTORIA
ISLAND

Figure 4.2.60. Prince of Wales Strait O_1 current ellipses.

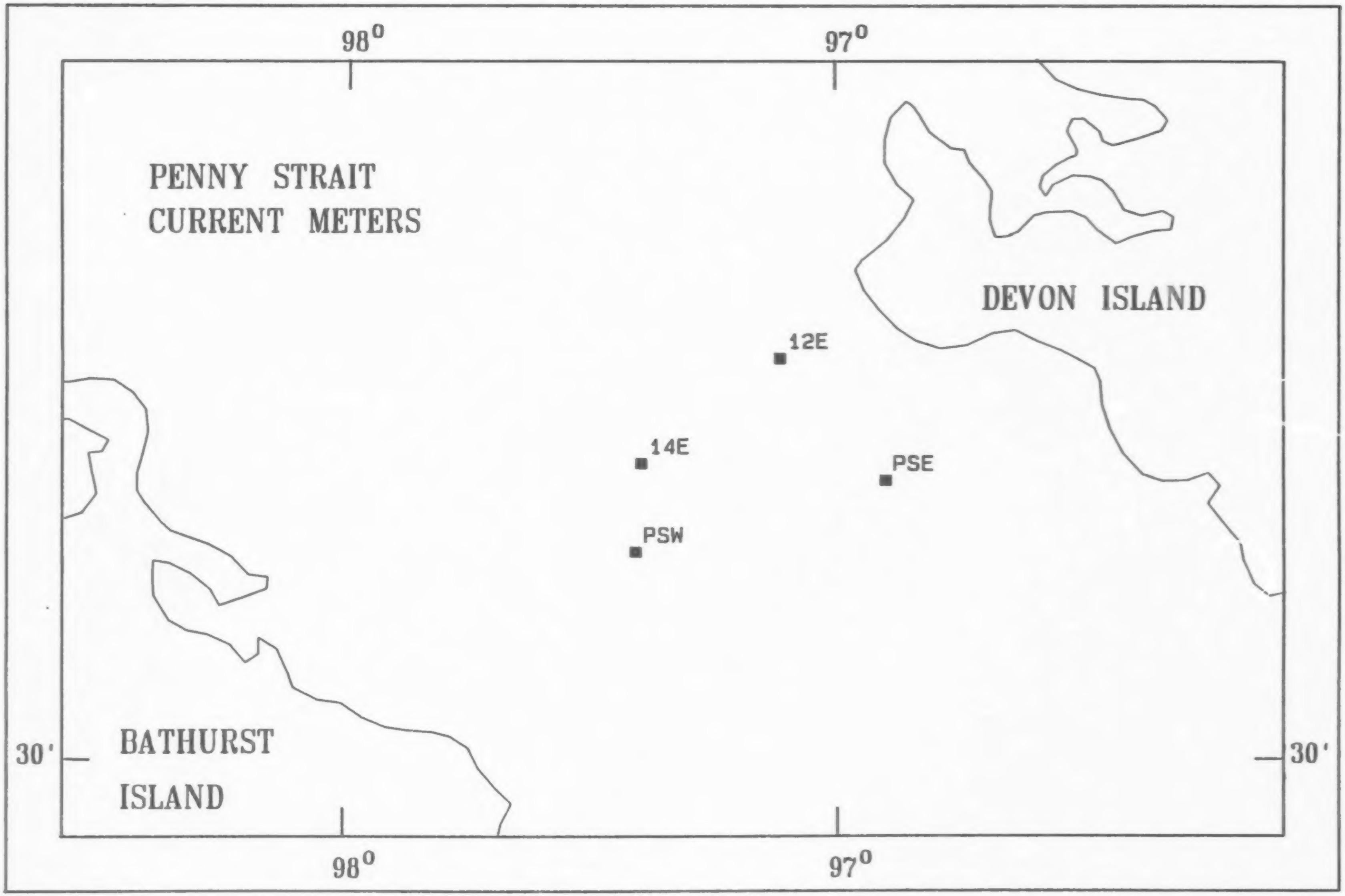
98⁰
97⁰
PENNY STRAIT
CURRENT METERS
DEVON ISLAND
12E
14E
PSE
PSW
30'
BATHURST
ISLAND
30'
98⁰
97⁰

Figure 4.2.61. Penny Strait current meter stations.

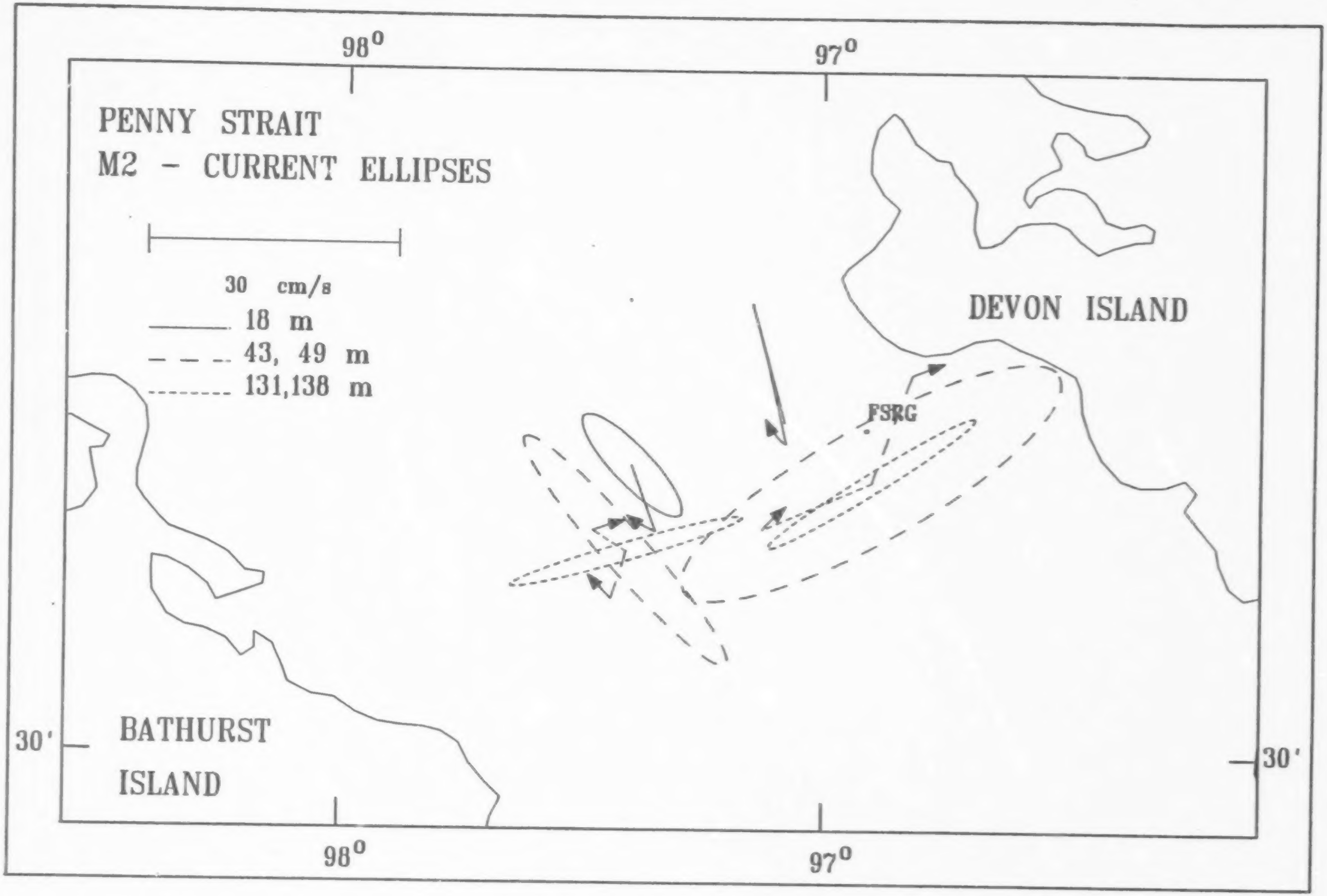
98°
97°
PENNY STRAIT
M2 - CURRENT ELLIPSES
30 cm/s
18 m
43, 49 m
131,138 m
DEVON ISLAND
FSRG
BATHURST
ISLAND
30'
30'
98°
97°

Figure 4.2.62. Penny Strait M_2 current ellipses.

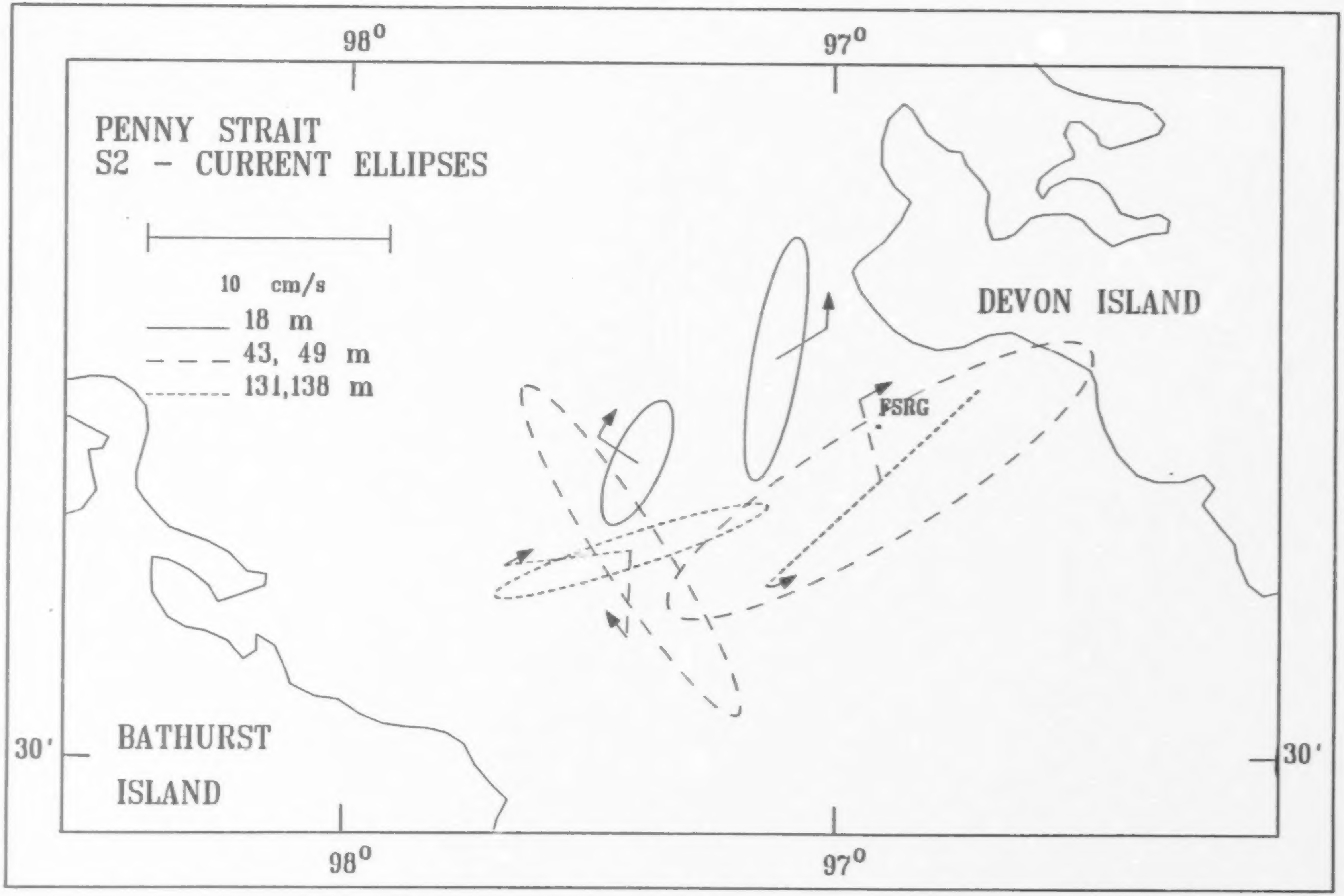
98⁰
97⁰
PENNY STRAIT
S2 - CURRENT ELLIPSES
10 cm/s
—— 18 m
– – – 43, 49 m
------- 131,138 m
DEVON ISLAND
FSRG
BATHURST
ISLAND
30'
30'
98⁰
97⁰

Figure 4.2.63. Penny Strait S_2 current ellipses.

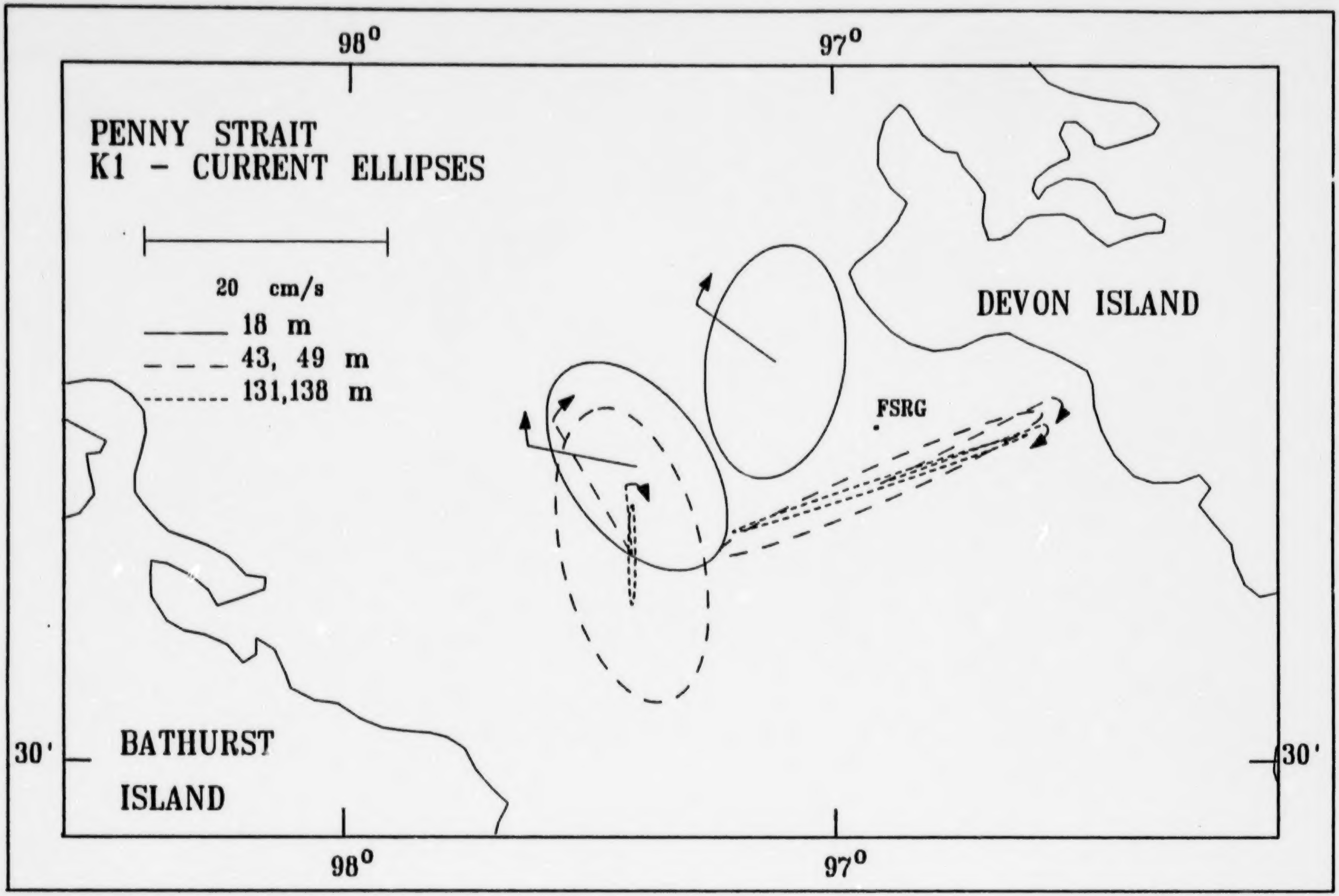
PENNY STRAIT
K1 - CURRENT ELLIPSES
20 cm/s
18 m
43, 49 m
131,138 m
DEVON ISLAND
BATHURST
ISLAND
FSRG
98⁰
97⁰
30'
30'
98⁰
97⁰

Figure 4.2.64. Penny Strait K_1 current ellipses.

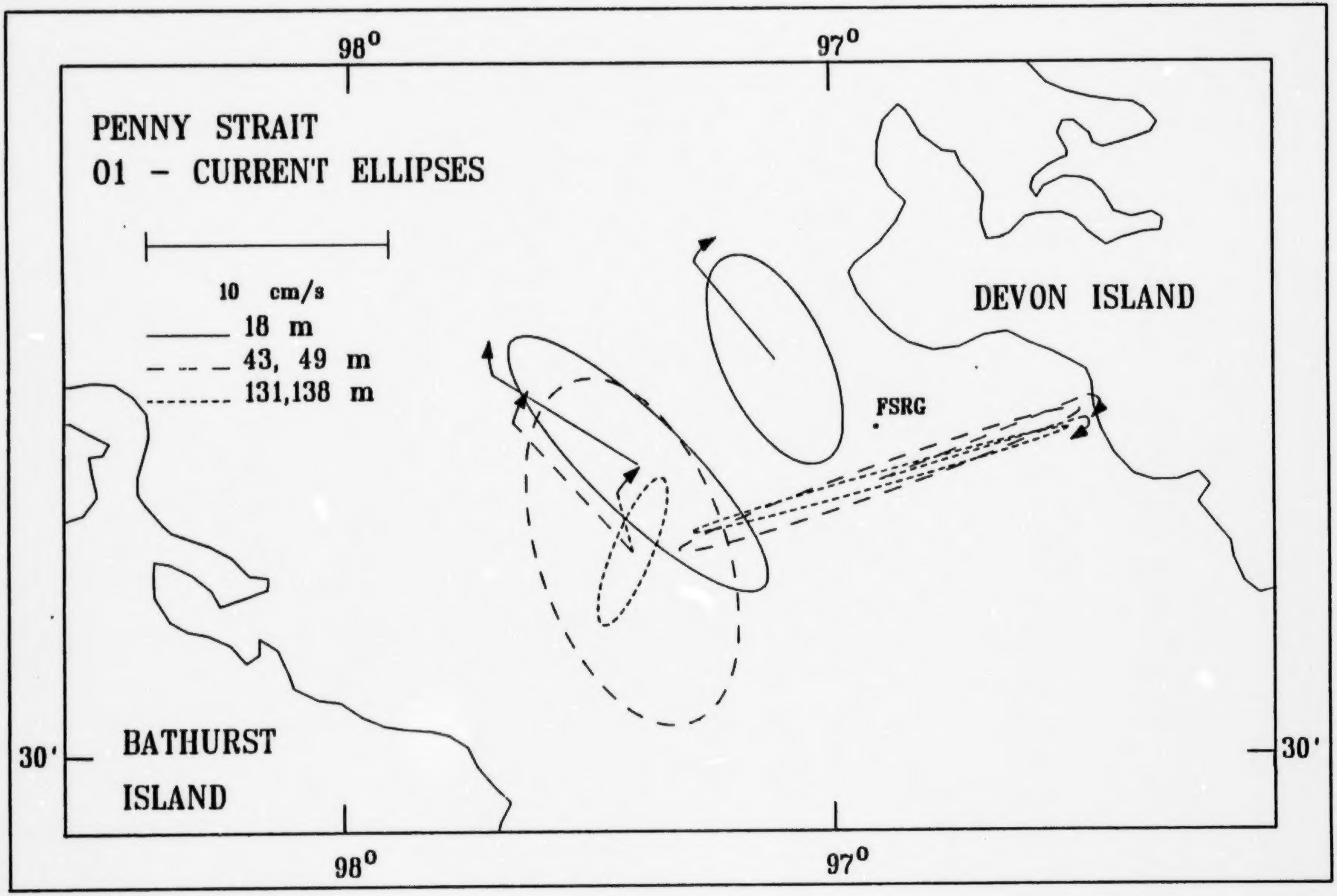
PENNY STRAIT
O1 - CURRENT ELLIPSES
10 cm/s
18 m
43, 49 m
131,138 m
DEVON ISLAND
FSRG
BATHURST
ISLAND
98°
97°
98°
97°
30'
30'

Figure 4.2.65. Penny Strait O_1 current ellipses.

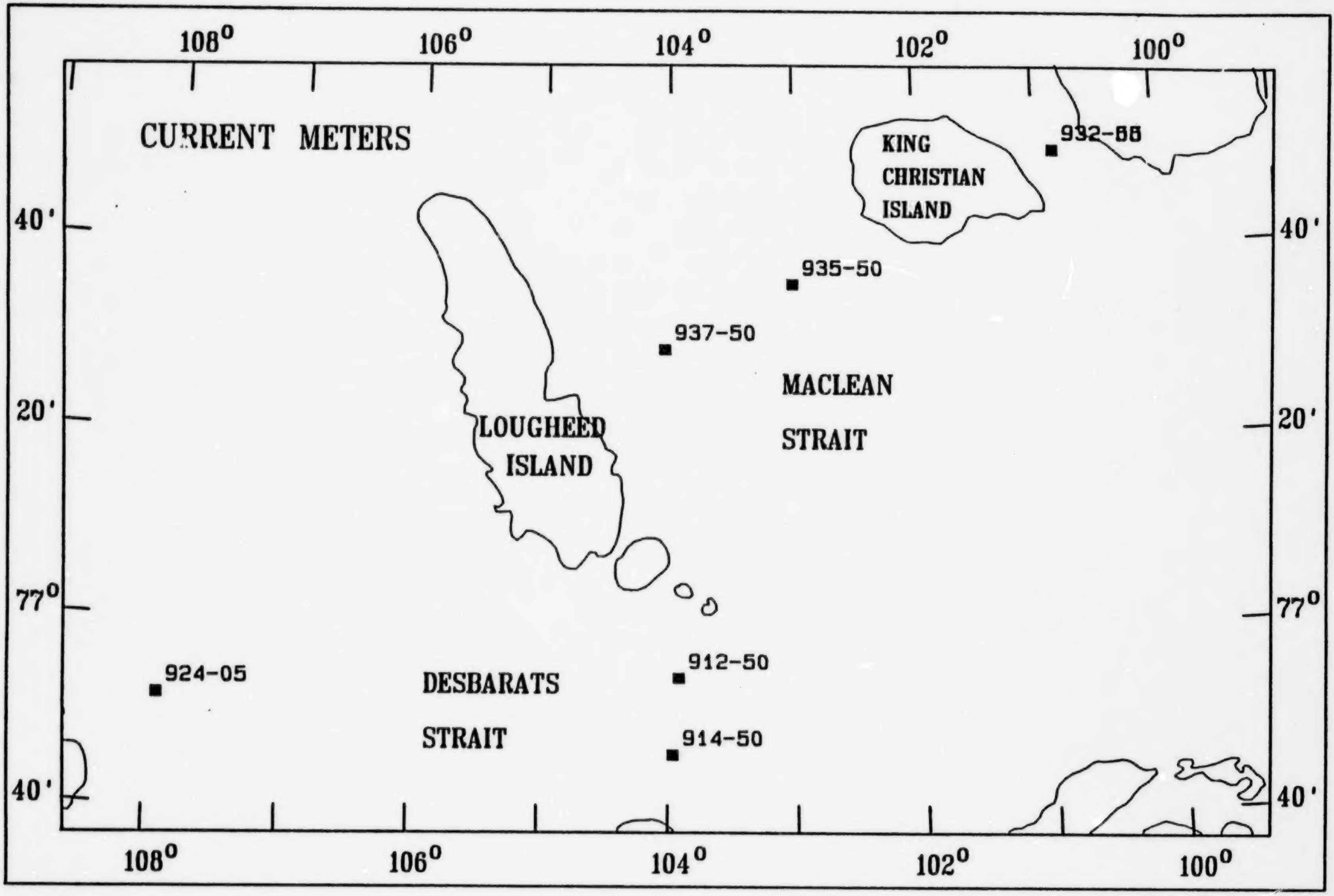
108⁰
106⁰
104⁰
102⁰
100⁰
40'
20'
77⁰
40'
CURRENT METERS
KING CHRISTIAN ISLAND
932-66
935-50
937-50
MACLEAN STRAIT
LOUGHEED ISLAND
924-05
DESBARATS STRAIT
912-50
914-50

Figure 4.2.66. Maclean / Desbarats / Danish Channel current meter stations.

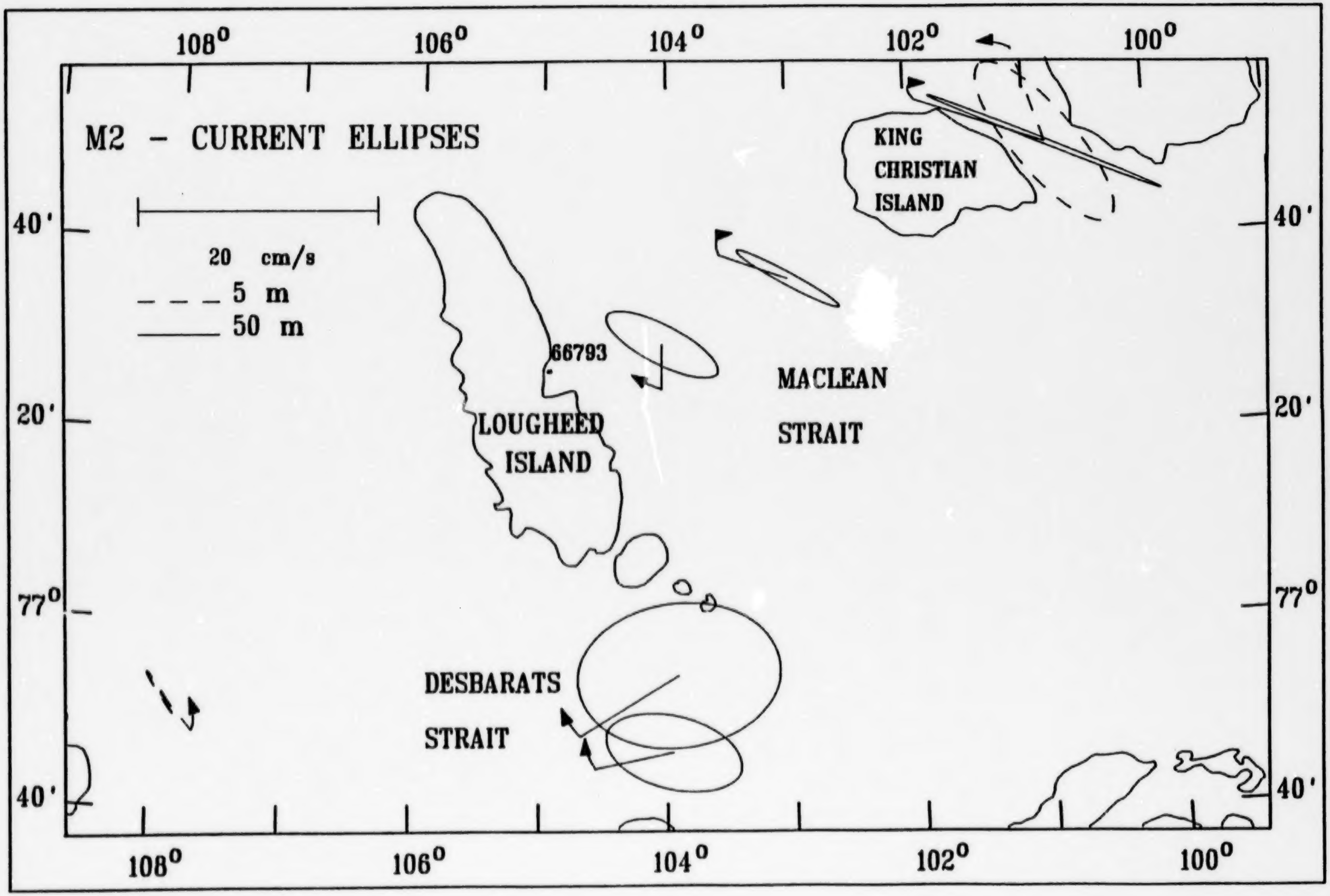
M2 - CURRENT ELLIPSES
20 cm/s
5 m
50 m
KING CHRISTIAN ISLAND
LOUGHEED ISLAND
66793
MACLEAN STRAIT
DESBARATS STRAIT
108°
106°
104°
102°
100°
40'
20'
77°
40'

Figure 4.2.67. Maclean / Desbarats / Danish Channel M_2 current ellipses.

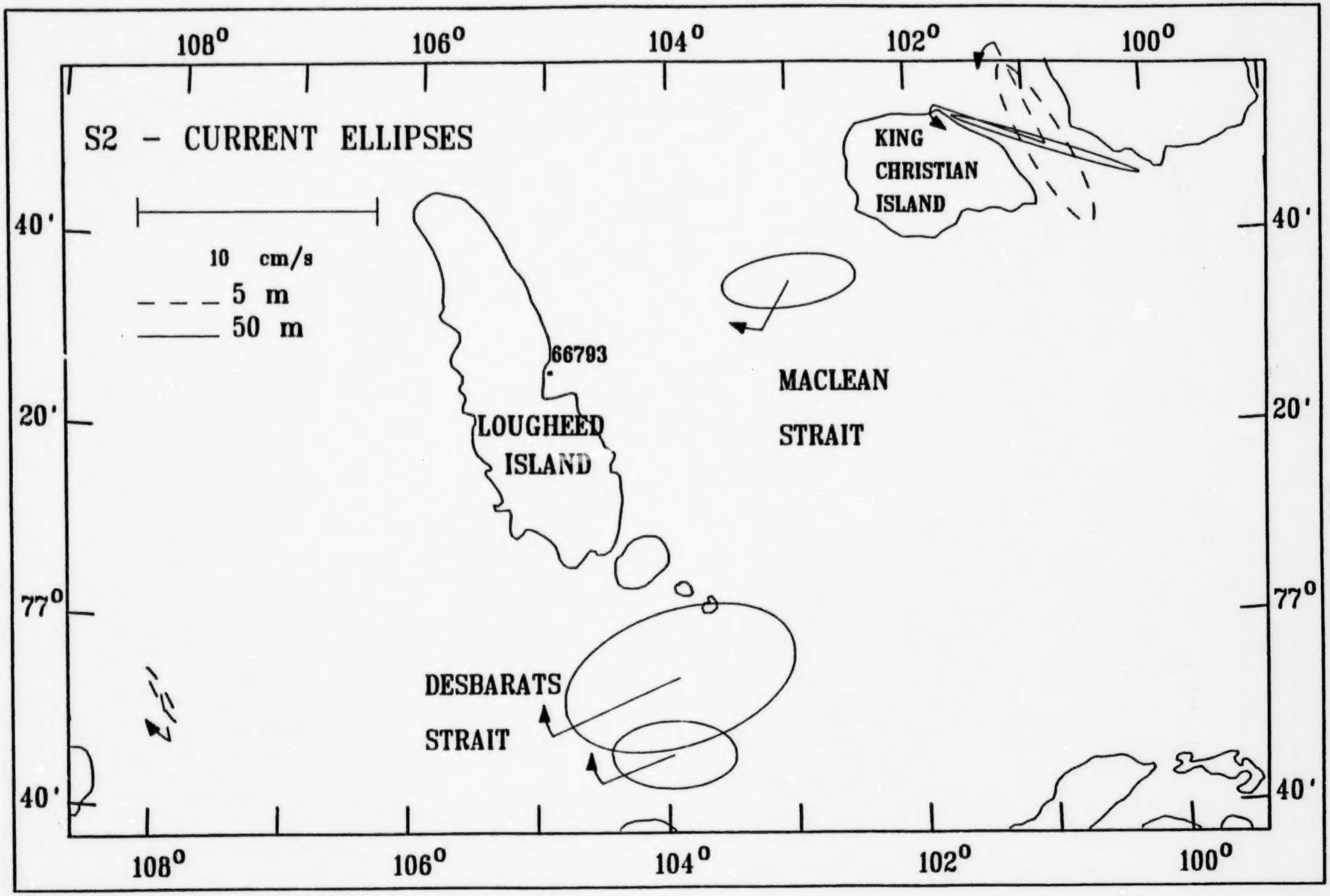
108°
106°
104°
102°
100°
S2 - CURRENT ELLIPSES
10 cm/s
5 m
50 m
KING
CHRISTIAN
ISLAND
40'
20'
77°
40'
66793
LOUGHEED
ISLAND
MACLEAN
STRAIT
DESBARATS
STRAIT

Figure 4.2.68. Maclean / Desbarats / Danish Channel S_2 current ellipses.

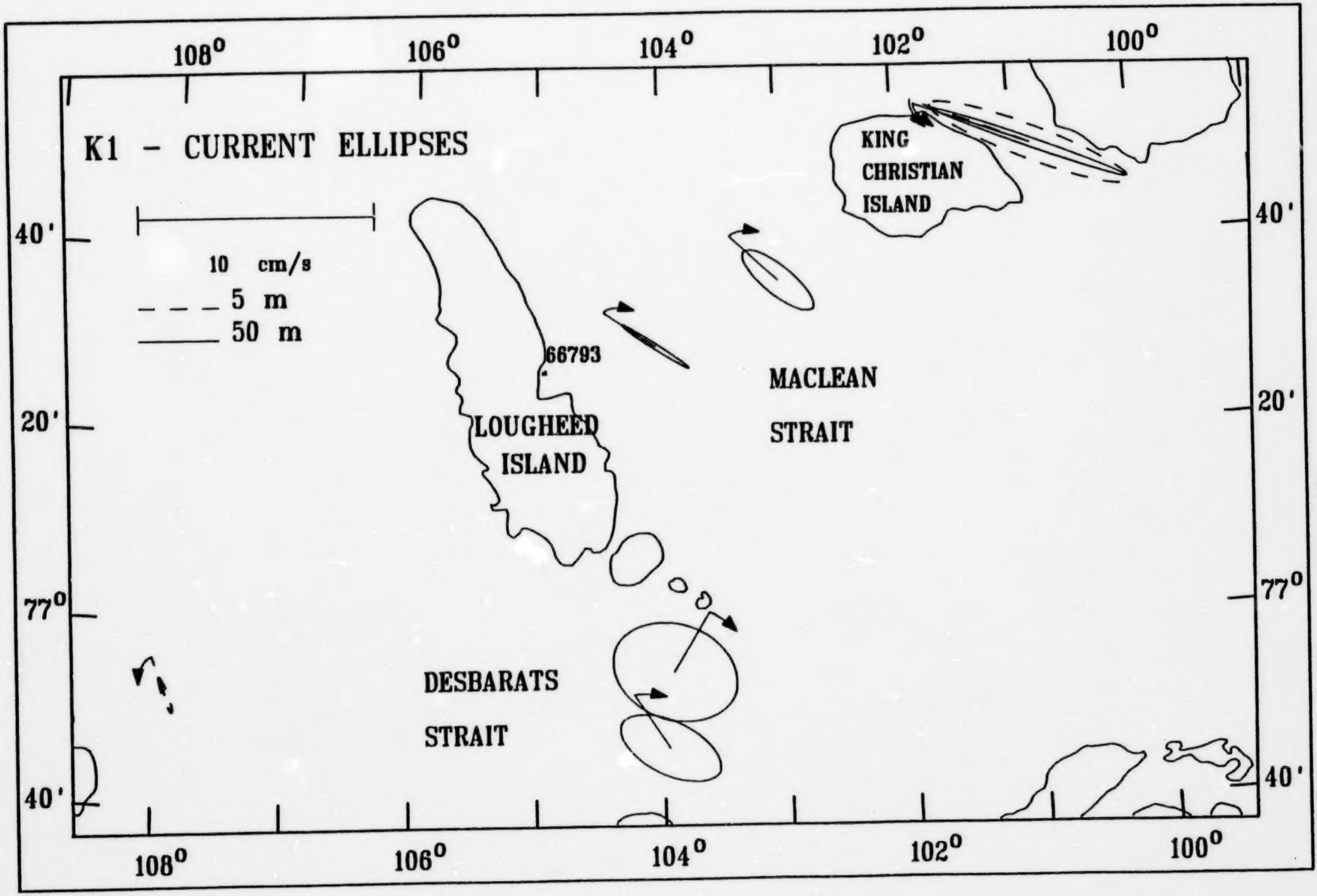
K1 - CURRENT ELLIPSES
10 cm/s
5 m
50 m
KING
CHRISTIAN
ISLAND
66793
LOUGHEED
ISLAND
MACLEAN
STRAIT
DESBARATS
STRAIT
108°
106°
104°
102°
100°
40'
20'
77°
40'

Figure 4.2.69. Maclean / Desbarats / Danish Channel K_1 current ellipses.

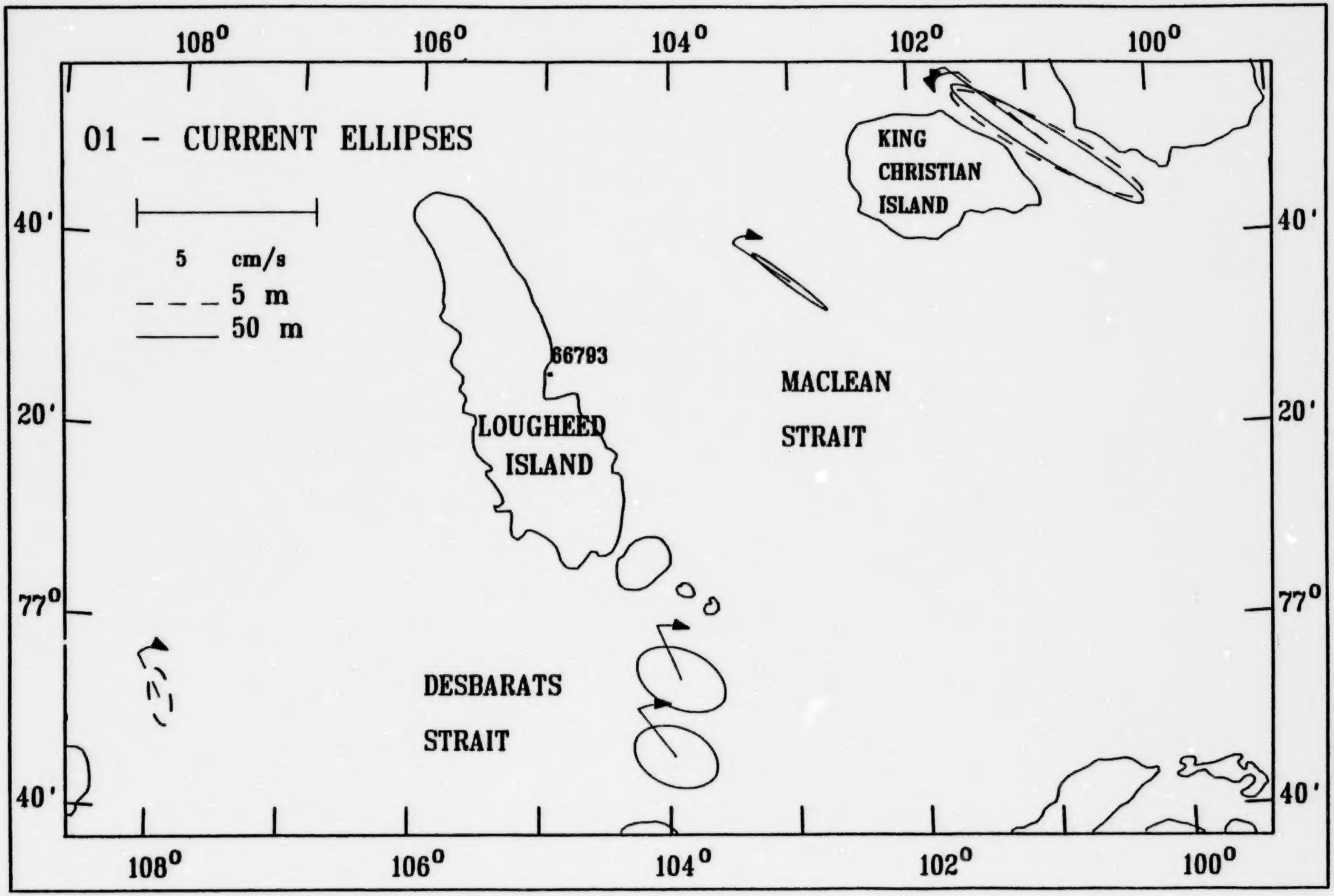
108⁰
106⁰
104⁰
102⁰
100⁰
01 - CURRENT ELLIPSES
5 cm/s
5 m
50 m
KING
CHRISTIAN
ISLAND
40'
20'
77⁰
40'
66793
LOUGHEED
ISLAND
MACLEAN
STRAIT
DESBARATS
STRAIT

Figure 4.2.70. Maclean / Desbarats / Danish Channel O_1 current ellipses.

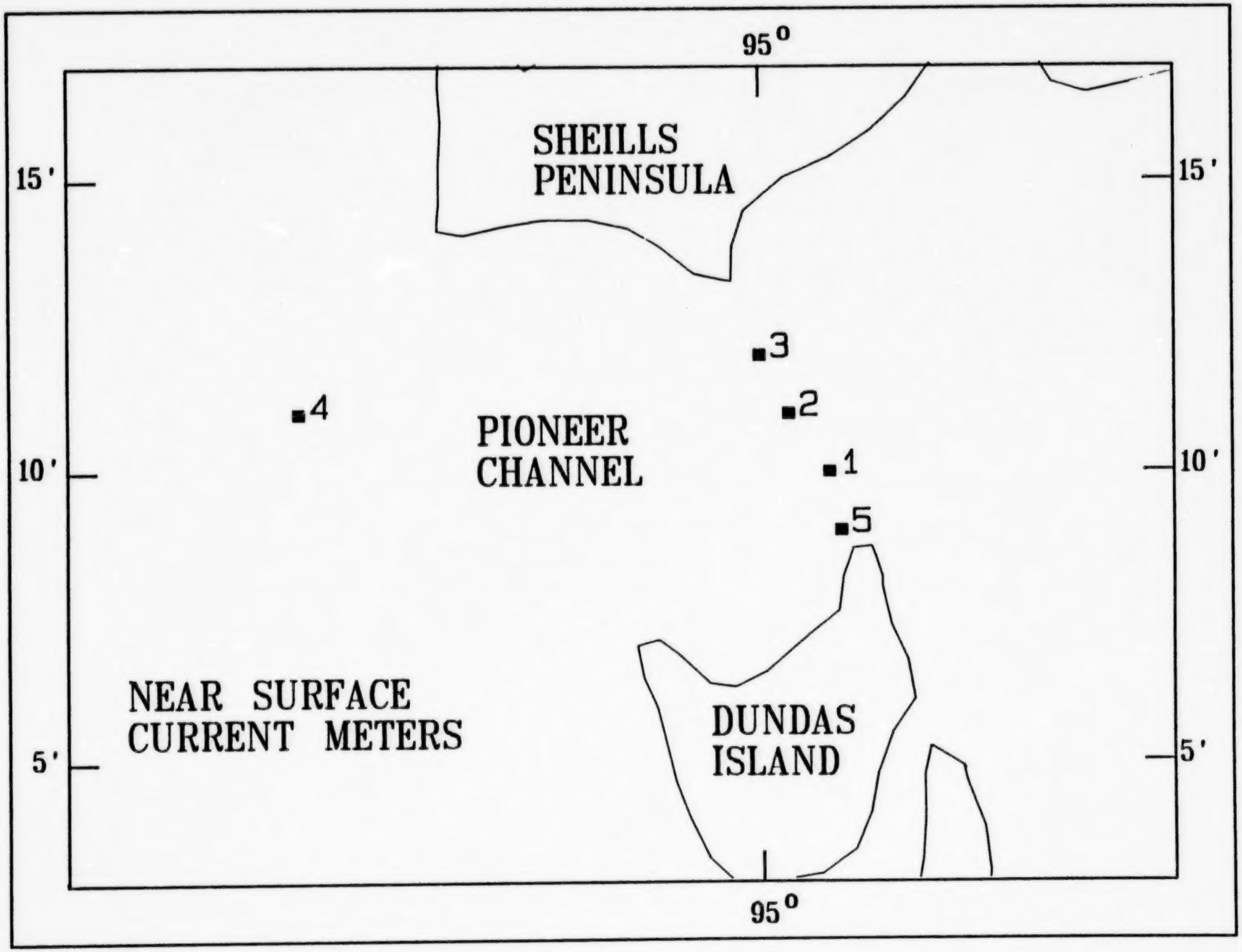
95°
SHEILLS
PENINSULA
15'
15'
3
2
4
PIONEER
CHANNEL
10'
1
10'
5
NEAR SURFACE
CURRENT METERS
DUNDAS
ISLAND
5'
5'
95°

Figure 4.2.71. Pioneer Channel current meter stations.

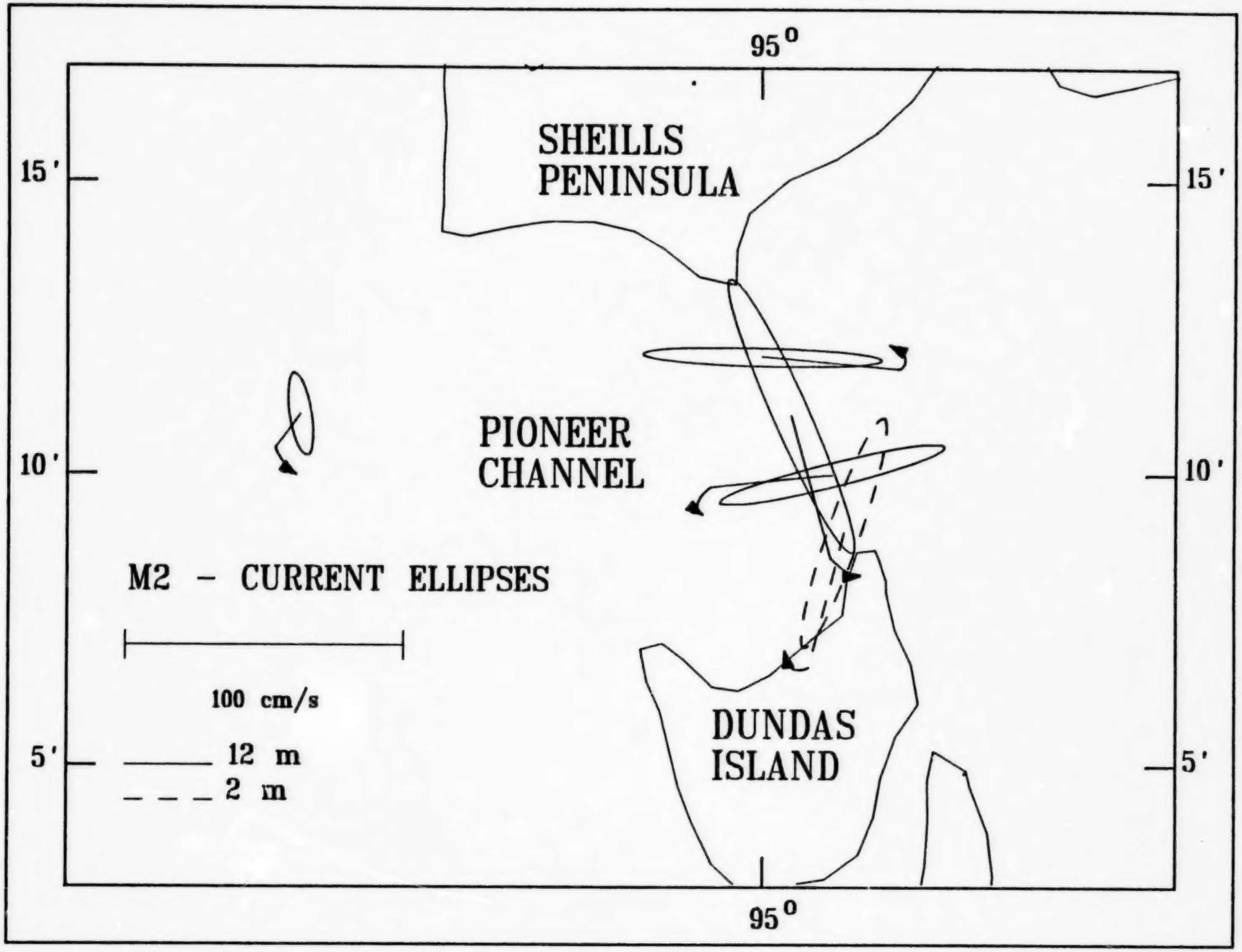
95°
95°
15'
10'
5'
15'
10'
5'
SHEILLS PENINSULA
PIONEER CHANNEL
DUNDAS ISLAND
M2 - CURRENT ELLIPSES
100 cm/s
12 m
2 m

Figure 4.2.72. Pioneer Channel M_2 current ellipses.

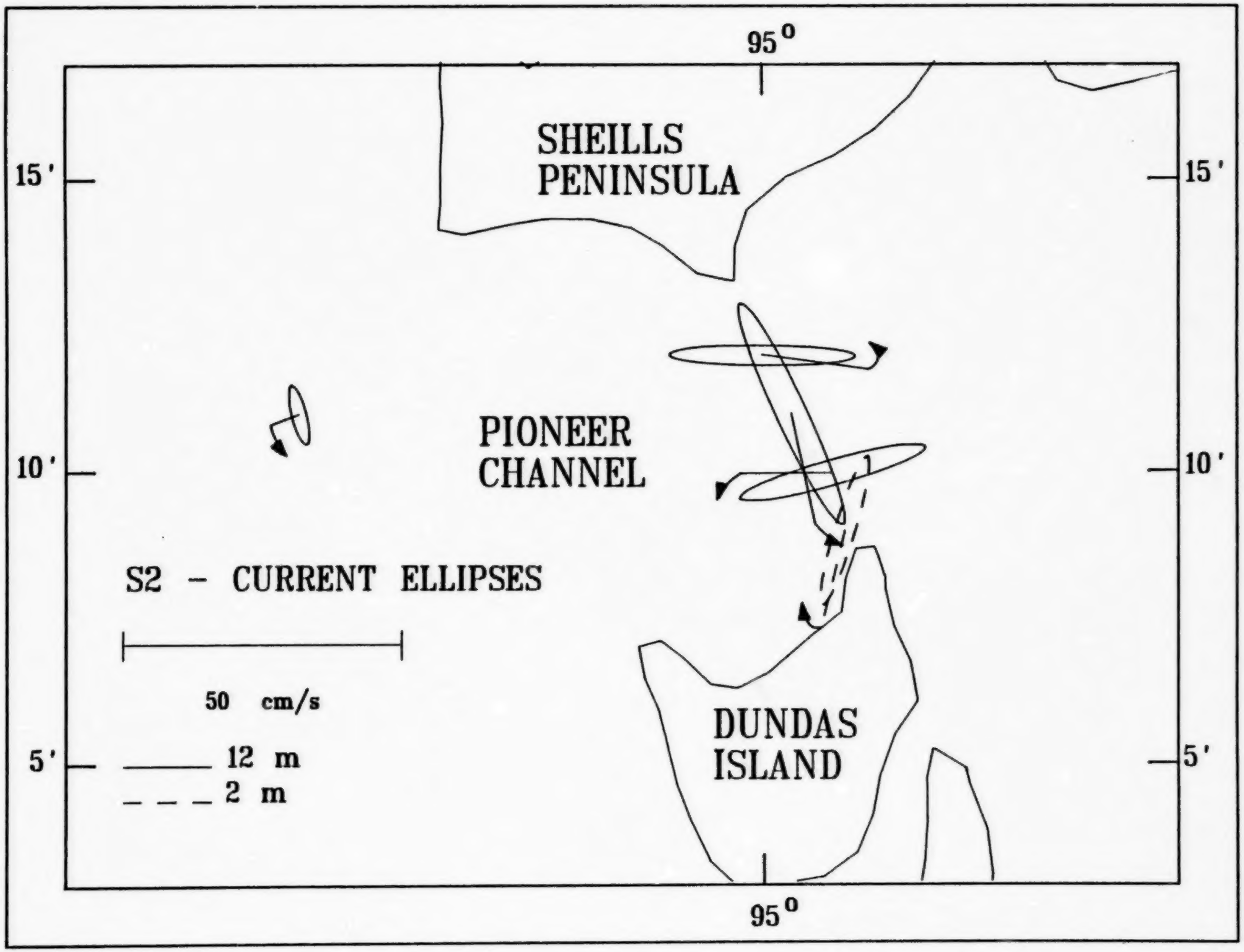
95⁰
SHEILLS PENINSULA
15'
15'
PIONEER CHANNEL
10'
10'
S2 - CURRENT ELLIPSES
50 cm/s
12 m
2 m
DUNDAS ISLAND
5'
5'
95⁰

Figure 4.2.73. Pioneer Channel S_2 current ellipses.

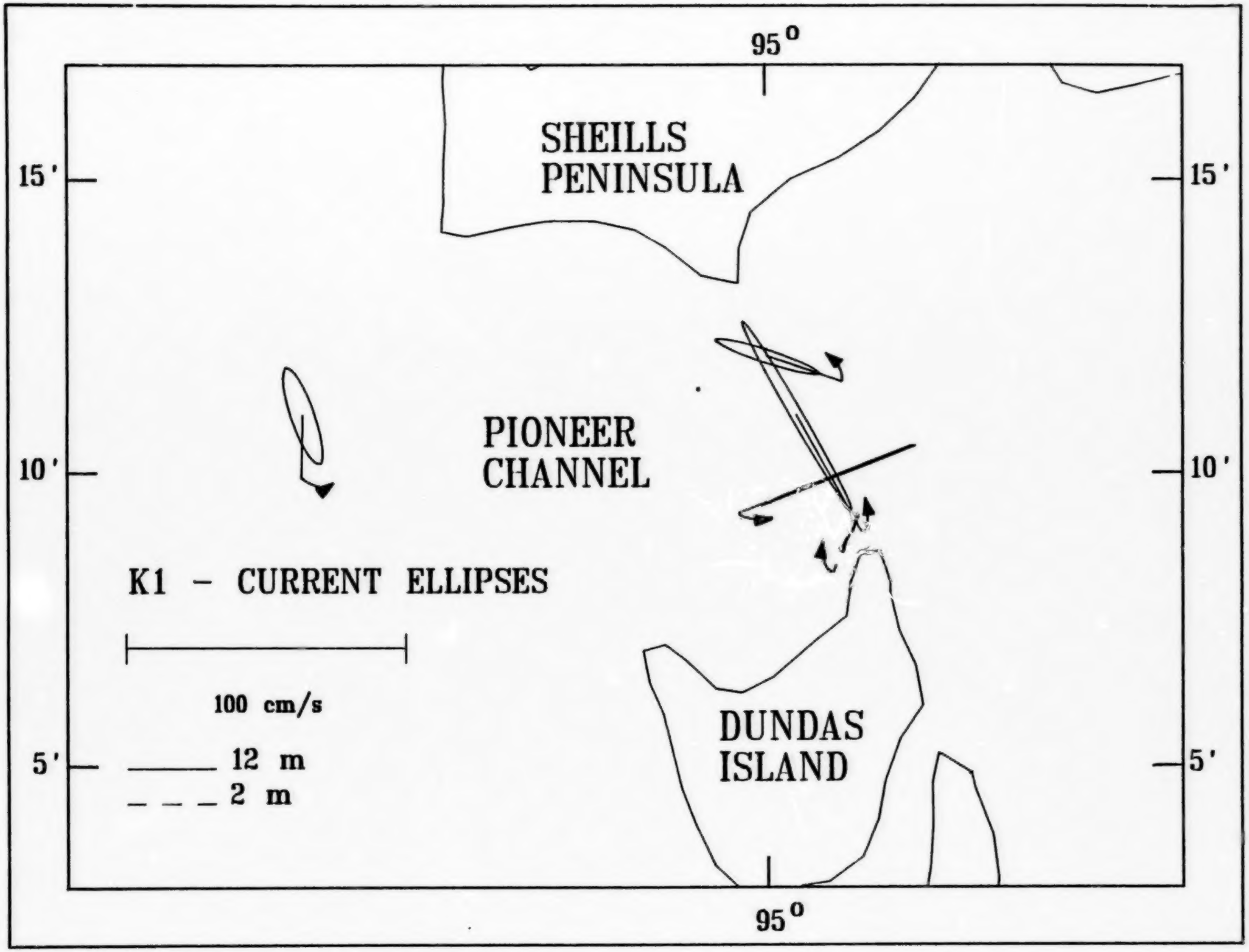
95°
SHEILLS
PENINSULA
15'
15'
PIONEER
CHANNEL
10'
10'
K1 - CURRENT ELLIPSES
100 cm/s
12 m
2 m
DUNDAS
ISLAND
5'
5'
95°

Figure 4.2.74. Pioneer Channel K_1 current ellipses.

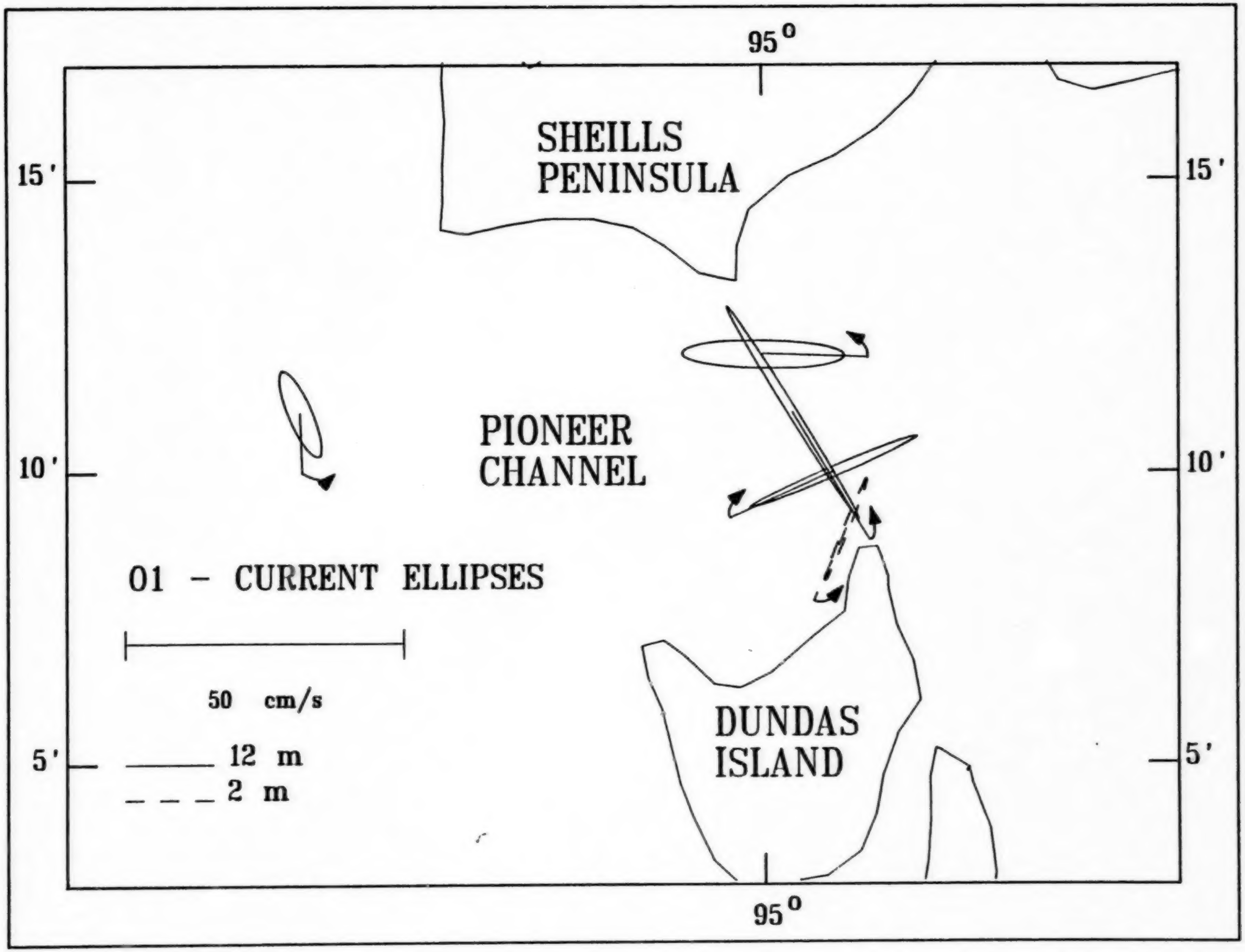
95⁰
SHEILLS PENINSULA
15'
15'
PIONEER CHANNEL
10'
10'
01 - CURRENT ELLIPSES
50 cm/s
12 m
2 m
DUNDAS ISLAND
5'
5'
95⁰

Figure 4.2.75. Pioneer Channel O_1 current ellipses.

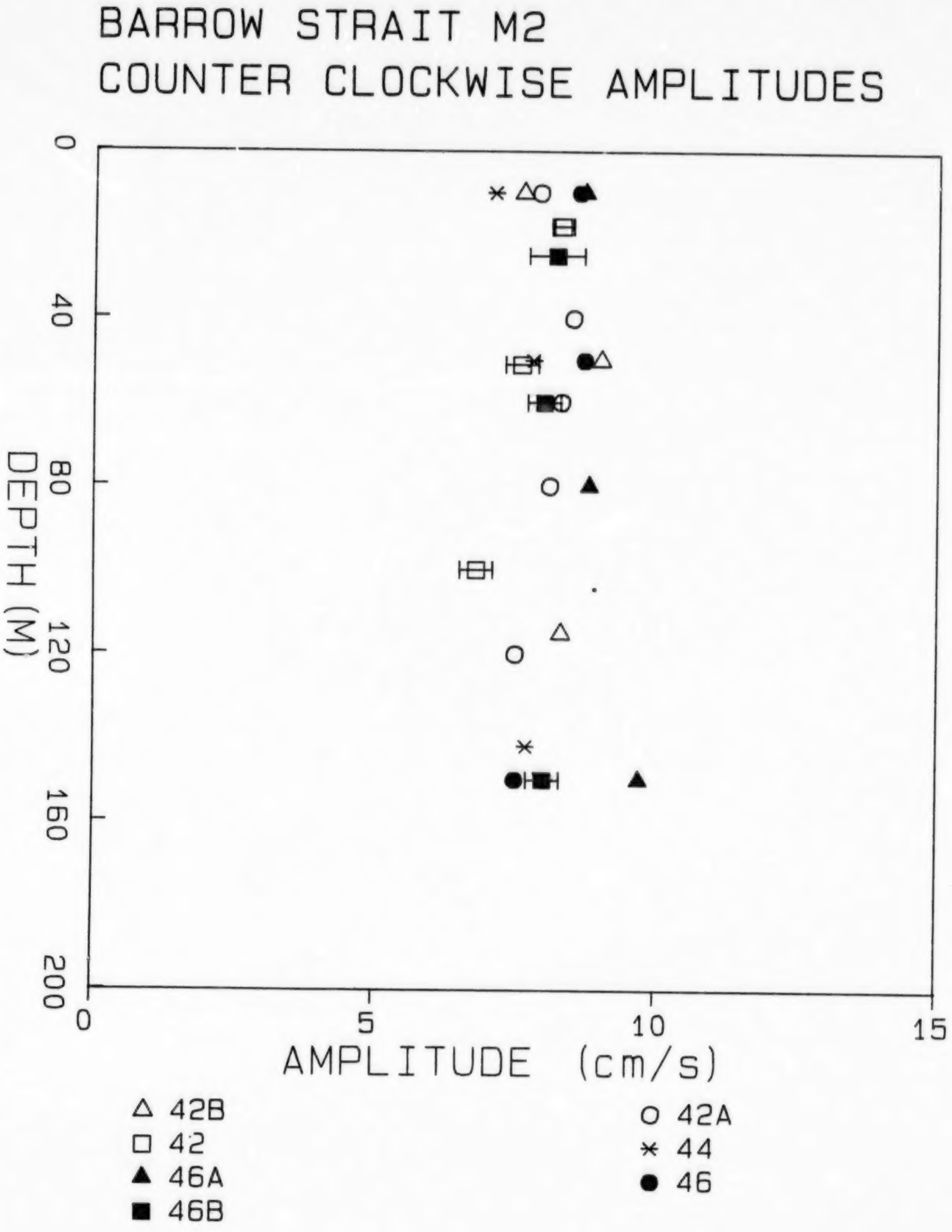

Figure 5.4.1 Vertical profile of the Amplitude of the M2 Counterclockwise component in Barrow Strait.

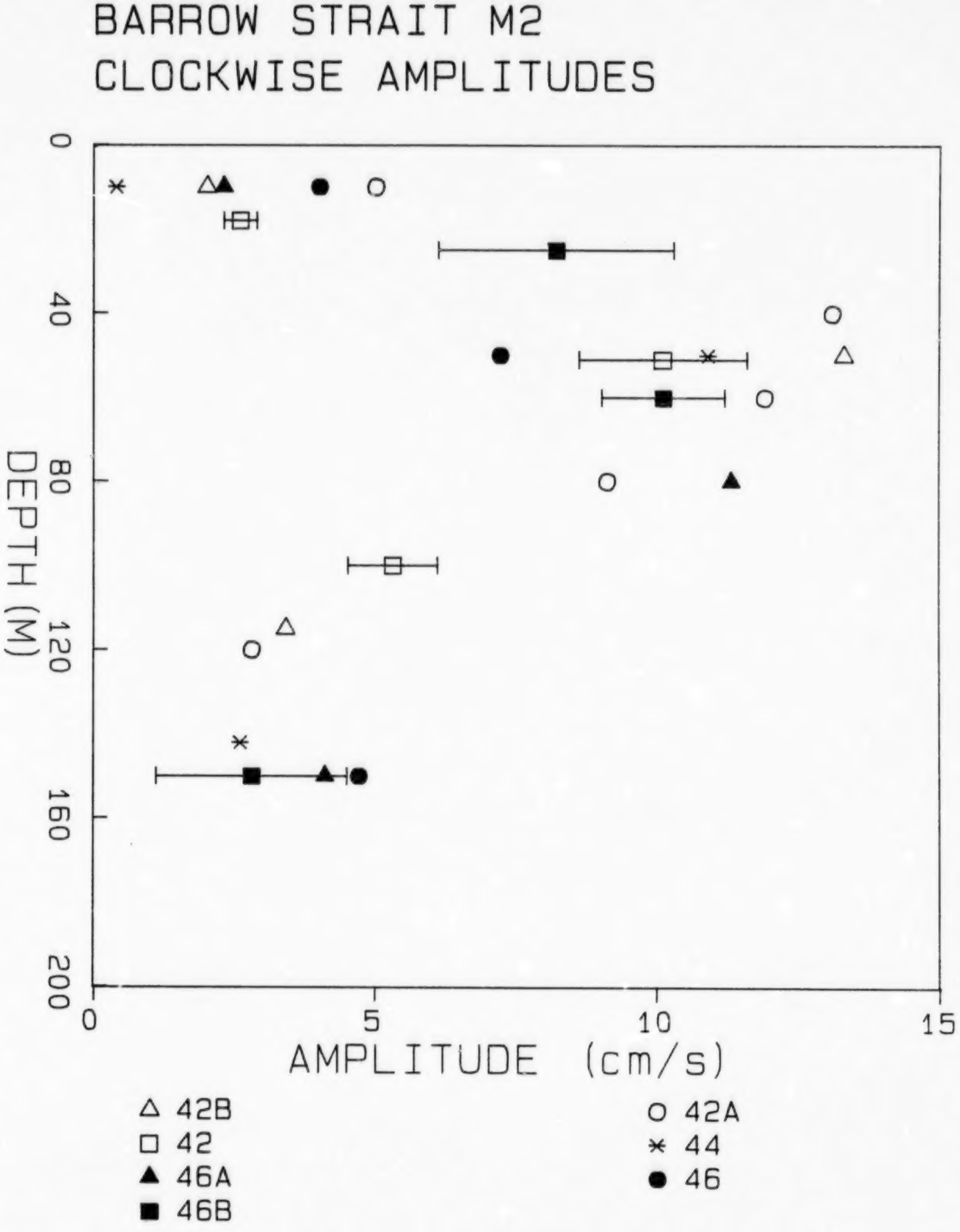

Figure 5.4.2 Vertical profile of the Amplitude of the M2 Clockwise component in Barrow Strait.

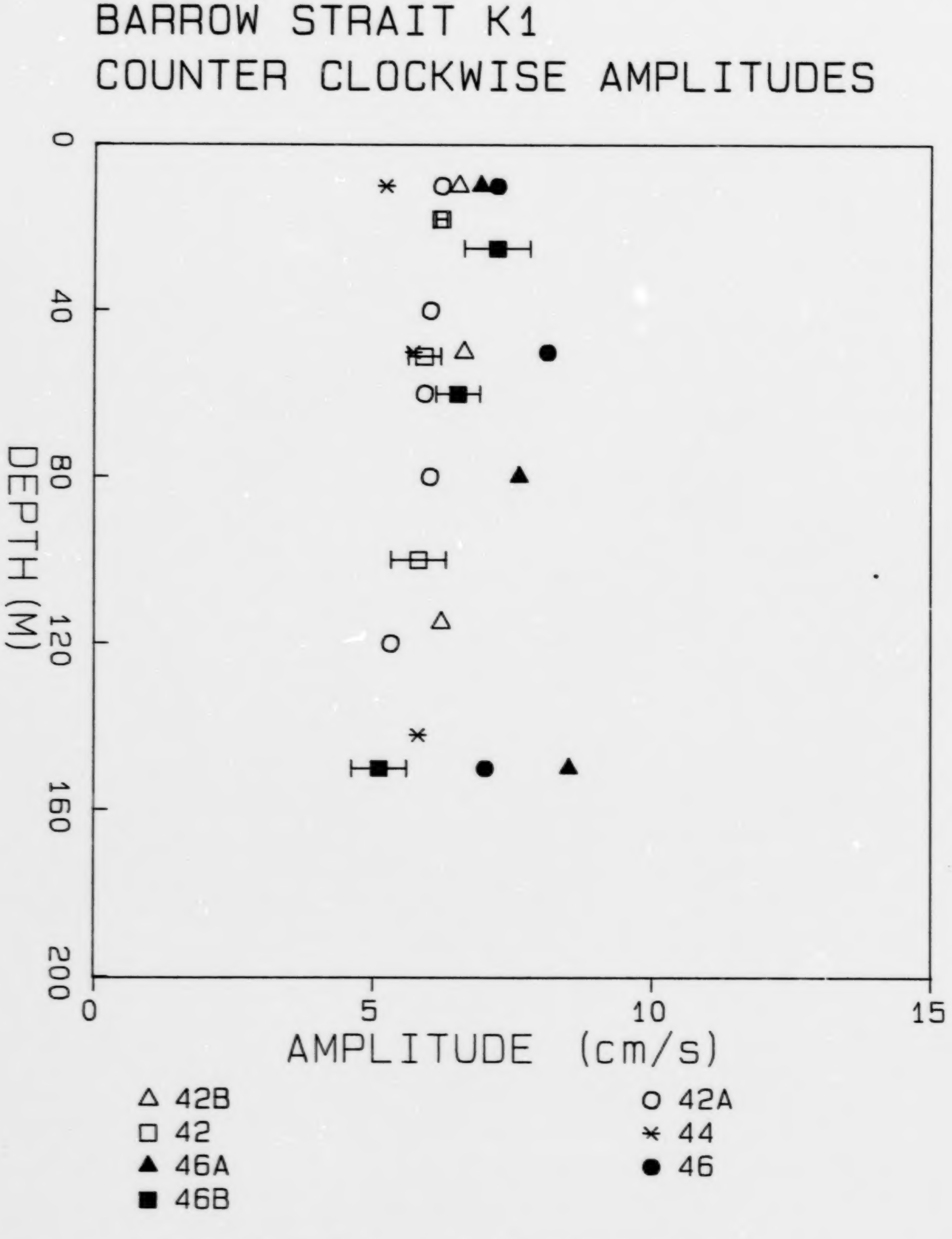

Figure 5.4.3 Vertical profile of the Amplitude of the K1 Counterclockwise component in Barrow Strait.

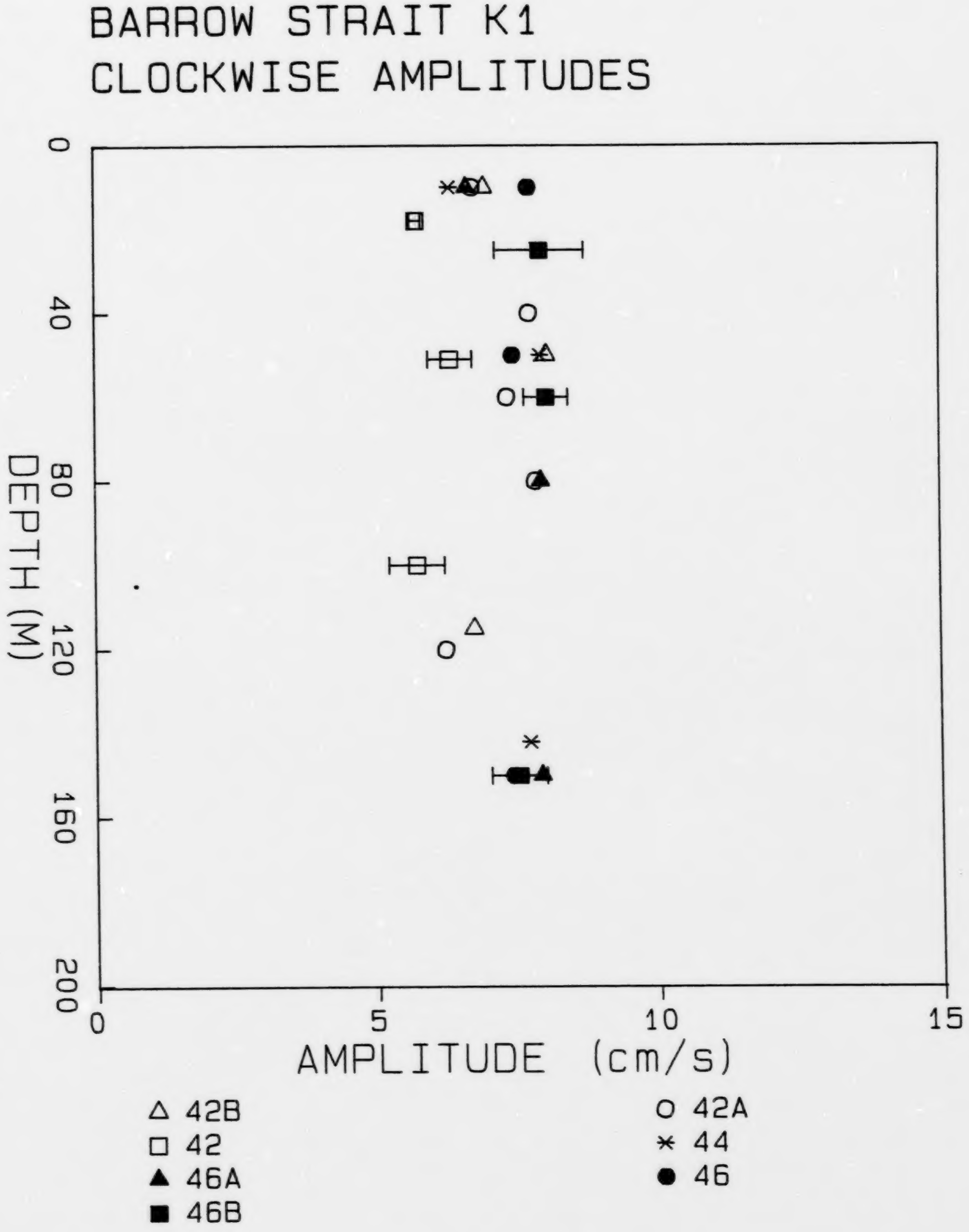

Figure 5.4.4 Vertical profile of the Amplitude of the K1 Clockwise component in Barrow Strait.

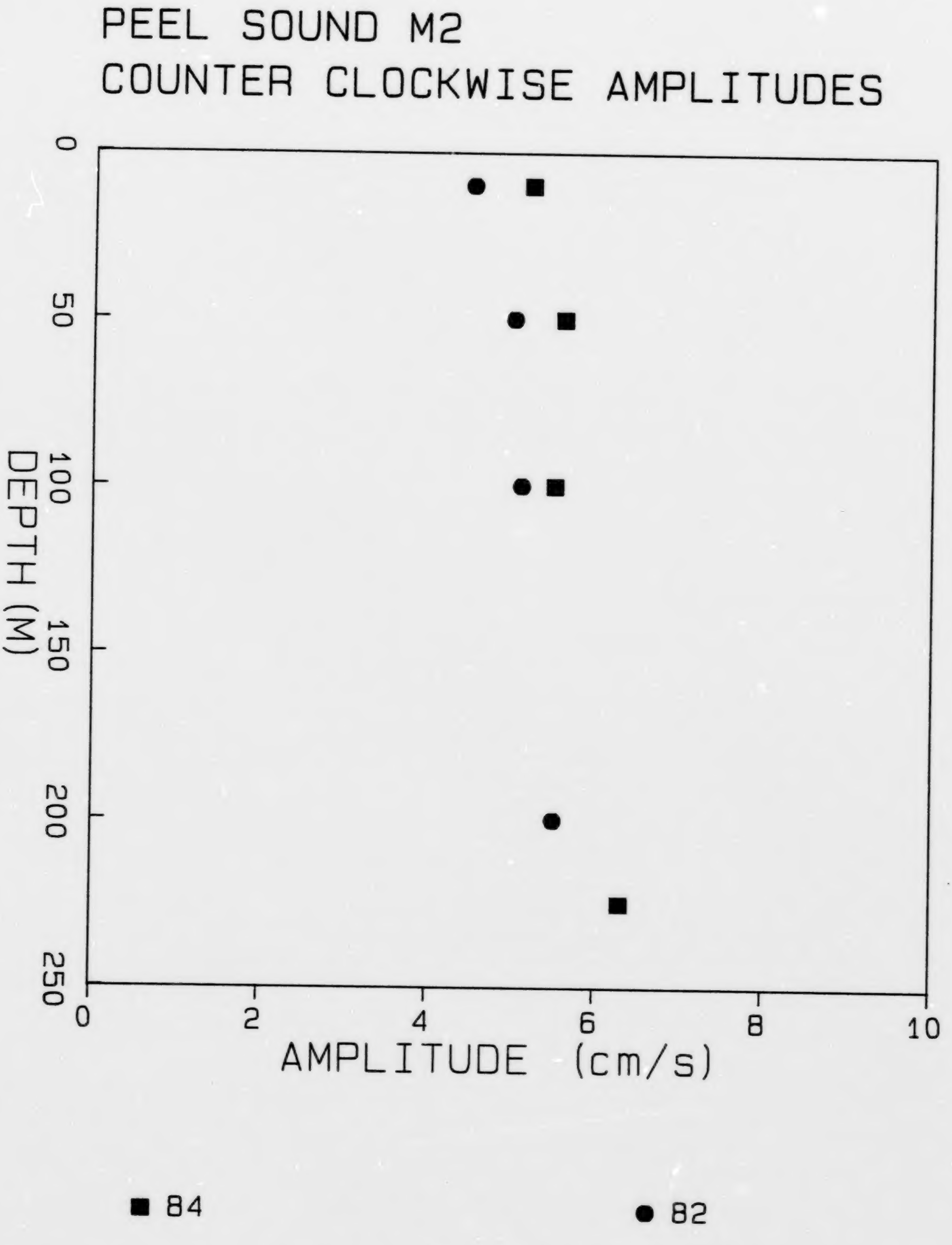

Figure 5.5.1 Vertical profile of the Amplitude of the M2 Counterclockwise component in Peel Sound.

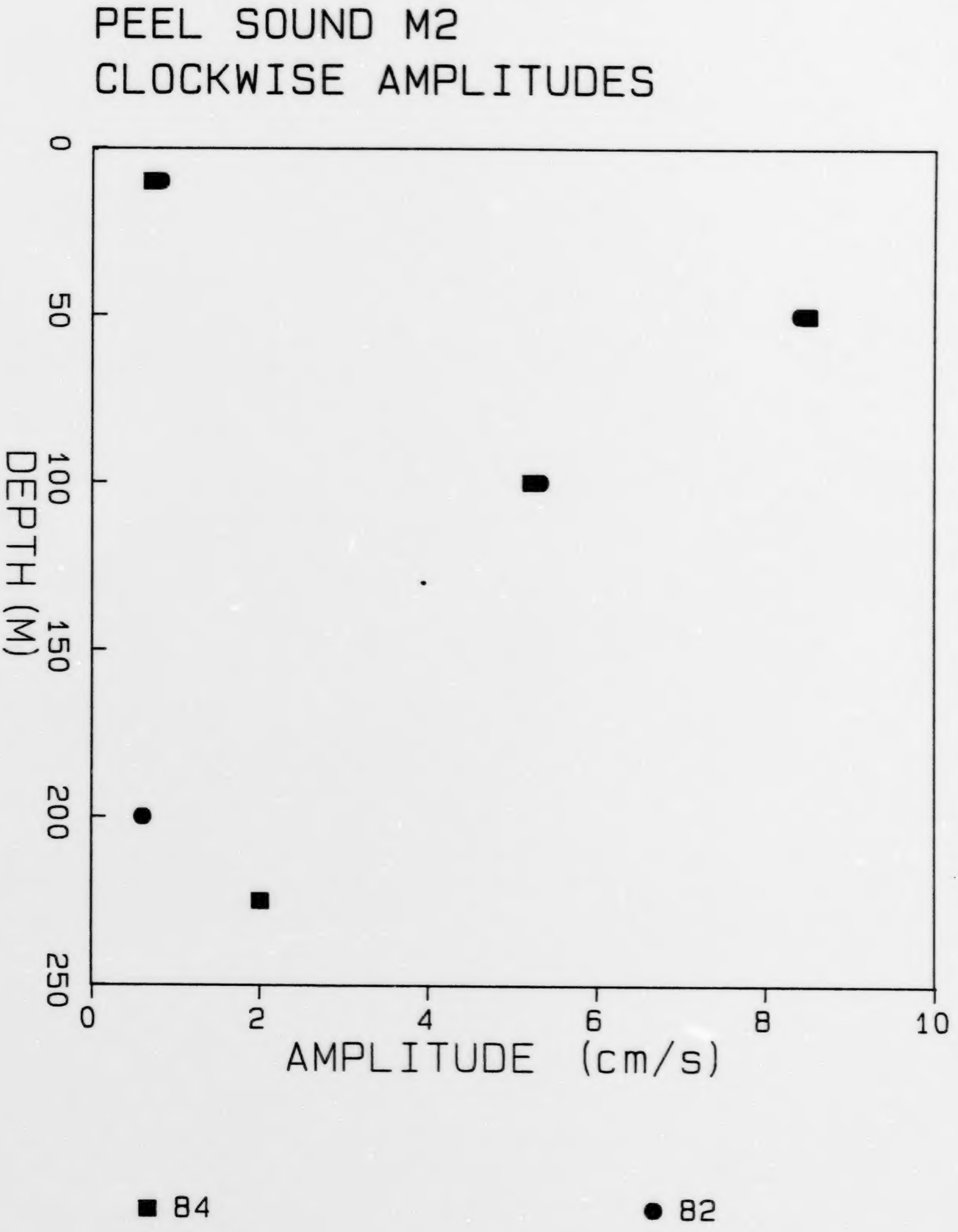

Figure 5.5.2 Vertical profile of the Amplitude of the M2 Clockwise component in Peel Sound.

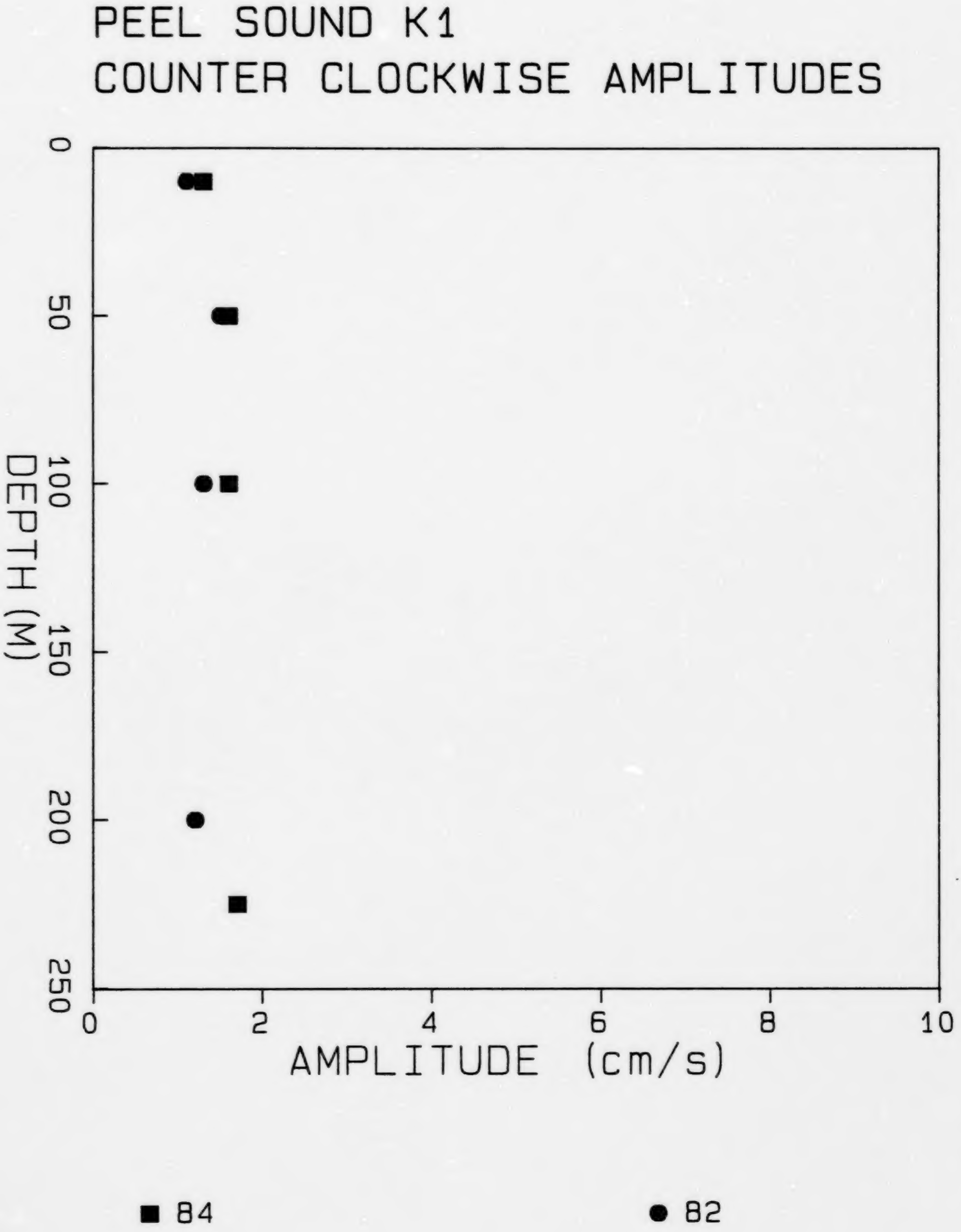

Figure 5.5.3 Vertical profile of the Amplitude of the K1 Counterclockwise component in Peel Sound.

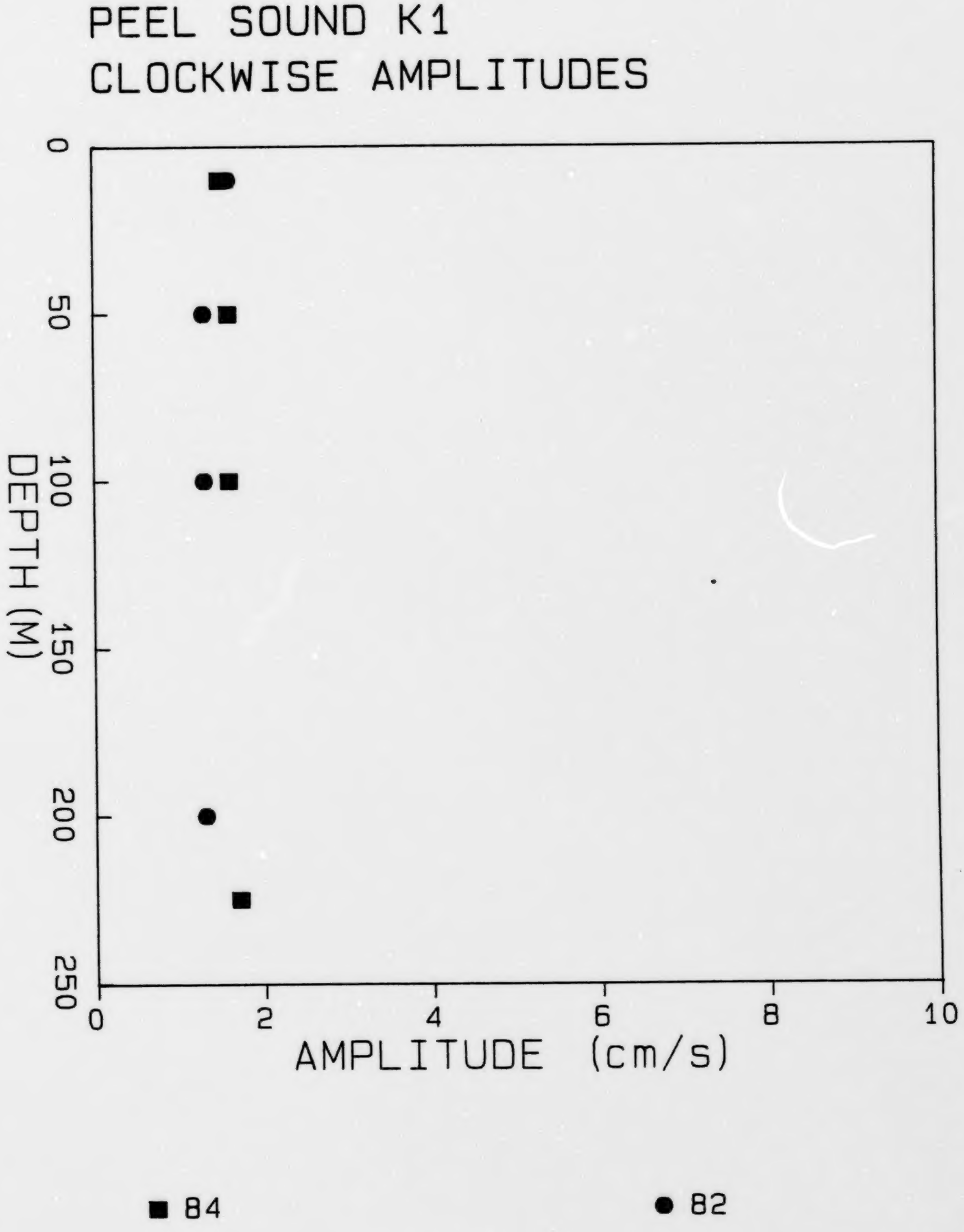

Figure 5.5.4 Vertical profile of the Amplitude of the K1 Clockwise component in Peel Sound.

M2

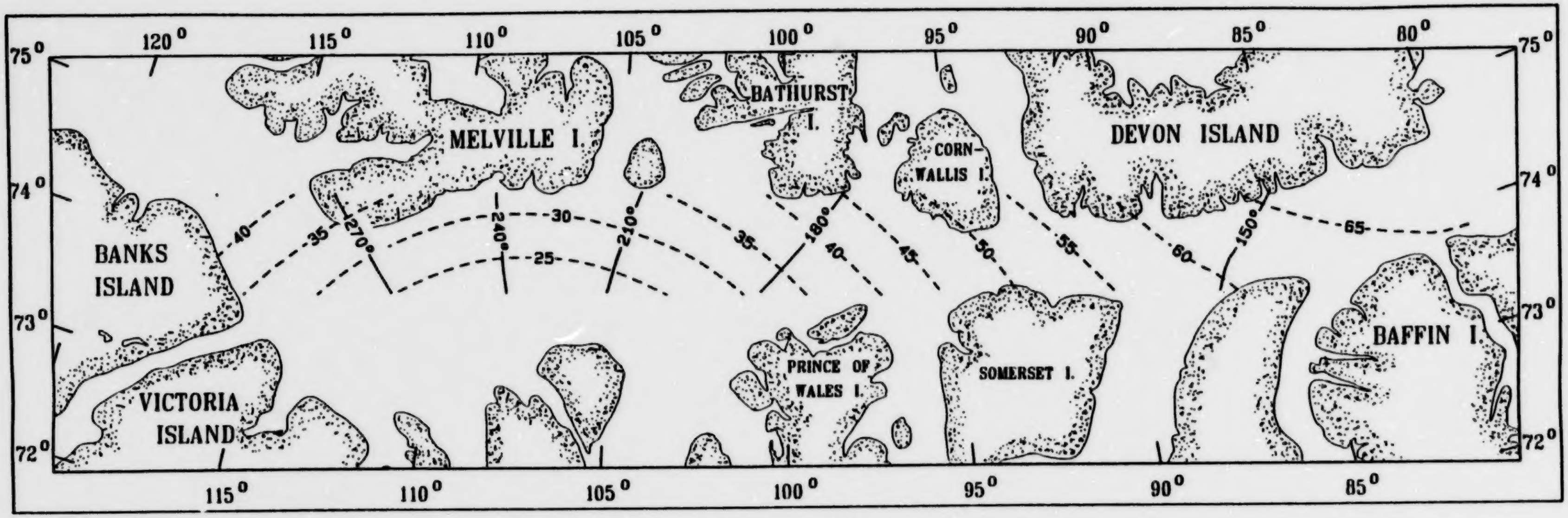
120°
115°
110°
105°
100°
95°
90°
85°
80°
75°
74°
73°
72°
MELVILLE I.
BATHURST I.
CORN-WALLIS I.
DEVON ISLAND
BANKS ISLAND
VICTORIA ISLAND
PRINCE OF WALES I.
SOMERSET I.
BAFFIN I.
40
35
270°
240°
30
25
210°
35
180°
40
45
50
55
60
150°
65

Figure 6.1.1 The Kelvin wave model for the M2 tide in Parry Channel.

K1

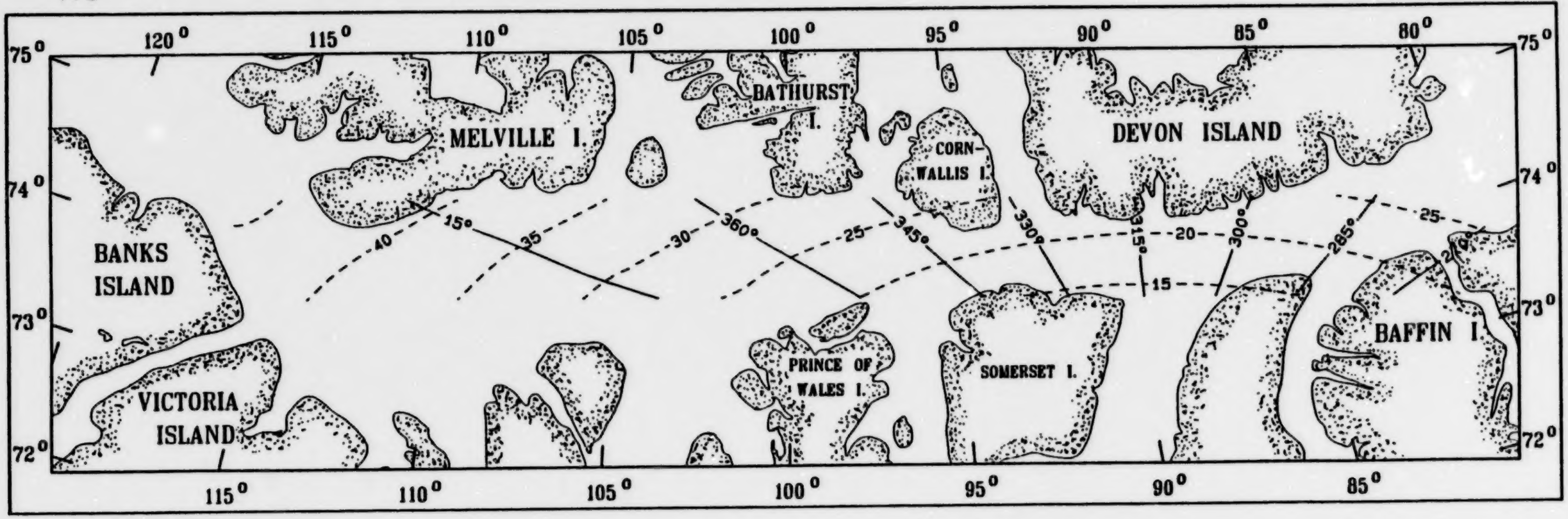
120°
115°
110°
105°
100°
95°
90°
85°
80°
75°
74°
73°
72°
MELVILLE I.
BATHURST I.
CORN-WALLIS I.
DEVON ISLAND
BANKS ISLAND
VICTORIA ISLAND
PRINCE OF WALES I.
SOMERSET I.
BAFFIN I.
40
15°
35
30
360°
25
345°
330°
315°
20
15
300°
285°
25
270°

Figure 6.1.2 The Kelvin wave model for the K1 tide in Parry Channel.

M2

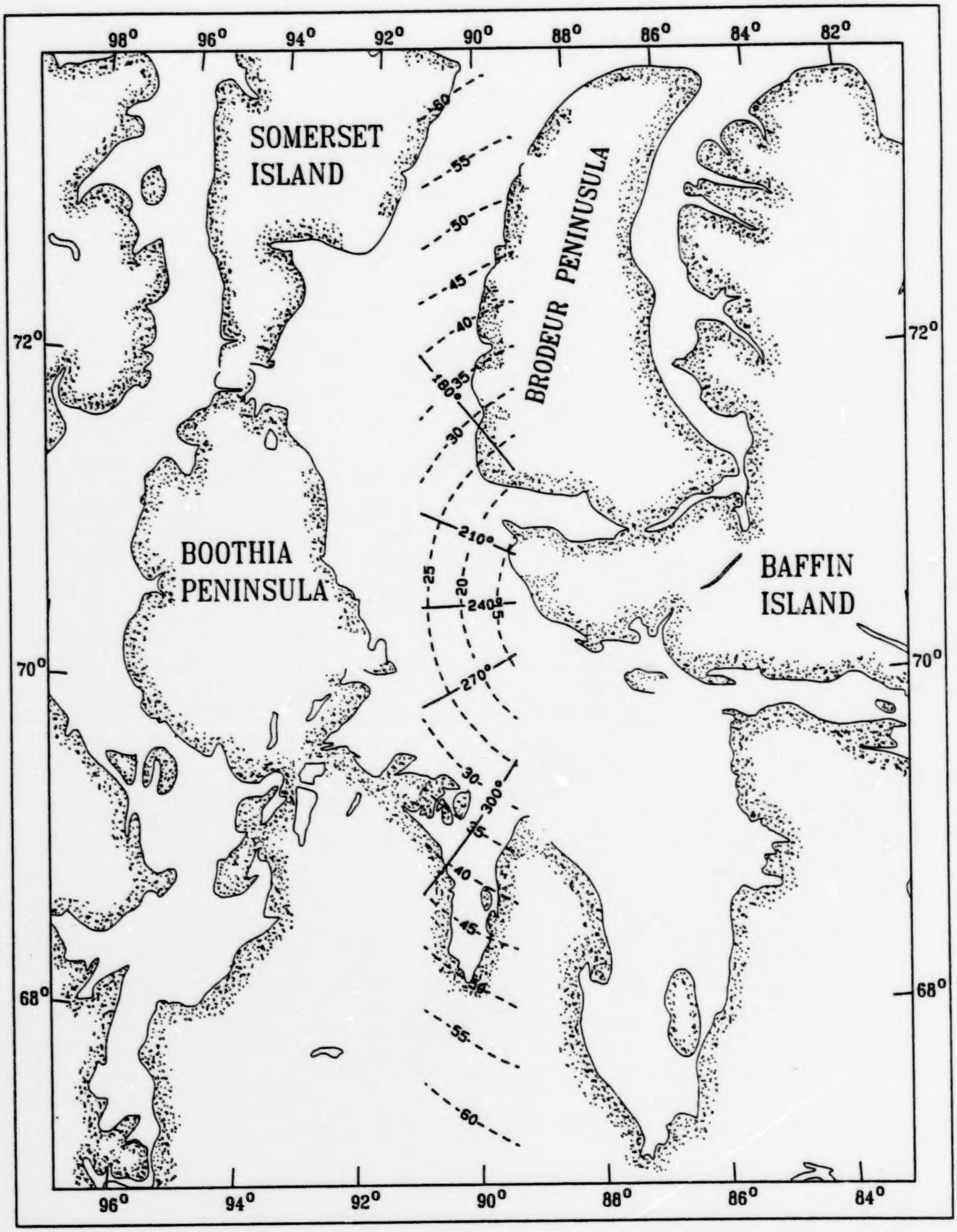
98°
96°
94°
92°
90°
88°
86°
84°
82°
72°
70°
68°
SOMERSET ISLAND
BRODEUR PENINSULA
BOOTHIA PENINSULA
BAFFIN ISLAND
60
55
50
45
40
35
30
180°
210°
240°
270°
300°
25
20
15
30
35
40
45
50
55
60

Figure 6.1.3. The Kelvin wave model for the M2 tide in the Gulf of Boothia system.

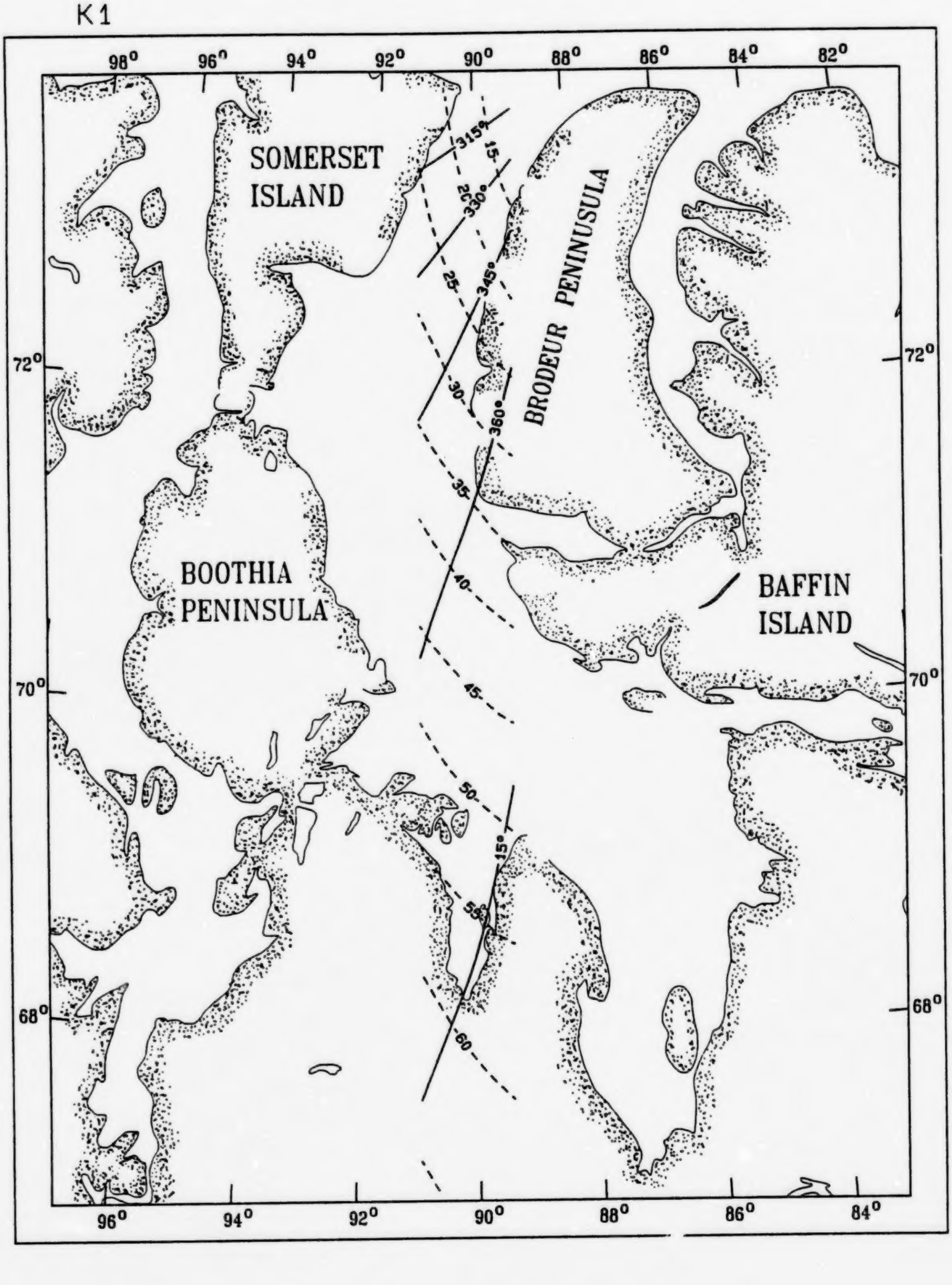
K1
98°
96°
94°
92°
90°
88°
86°
84°
82°
SOMERSET ISLAND
315°
15
20
330°
25
345°
30
360°
35
40
45
50
15°
55
60
BRODEUR PENINSULA
BOOTHIA PENINSULA
BAFFIN ISLAND
72°
70°
68°
96°
94°
92°
90°
88°
86°
84°

Figure 6.1.4. The Kelvin wave model for the K1 tide in the Gulf of Boothia system.

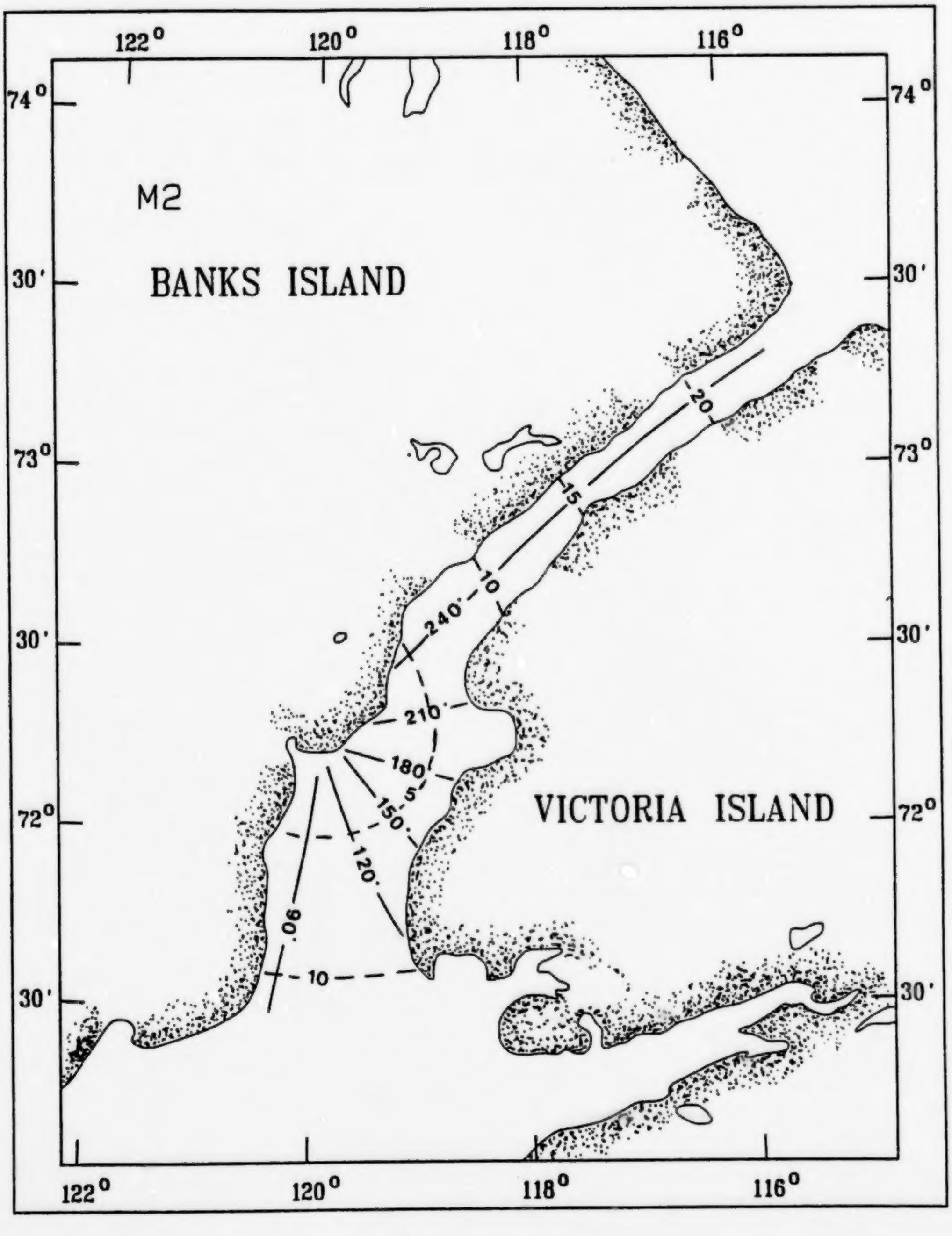
M2
BANKS ISLAND
VICTORIA ISLAND
122°
120°
118°
116°
74°
30'
73°
30'
72°
30'
20
15
10
240
210
180
5
150
120
90
10

Figure 6.1.5. The Kelvin wave model for the M2 tide in Prince of Wales Strait.

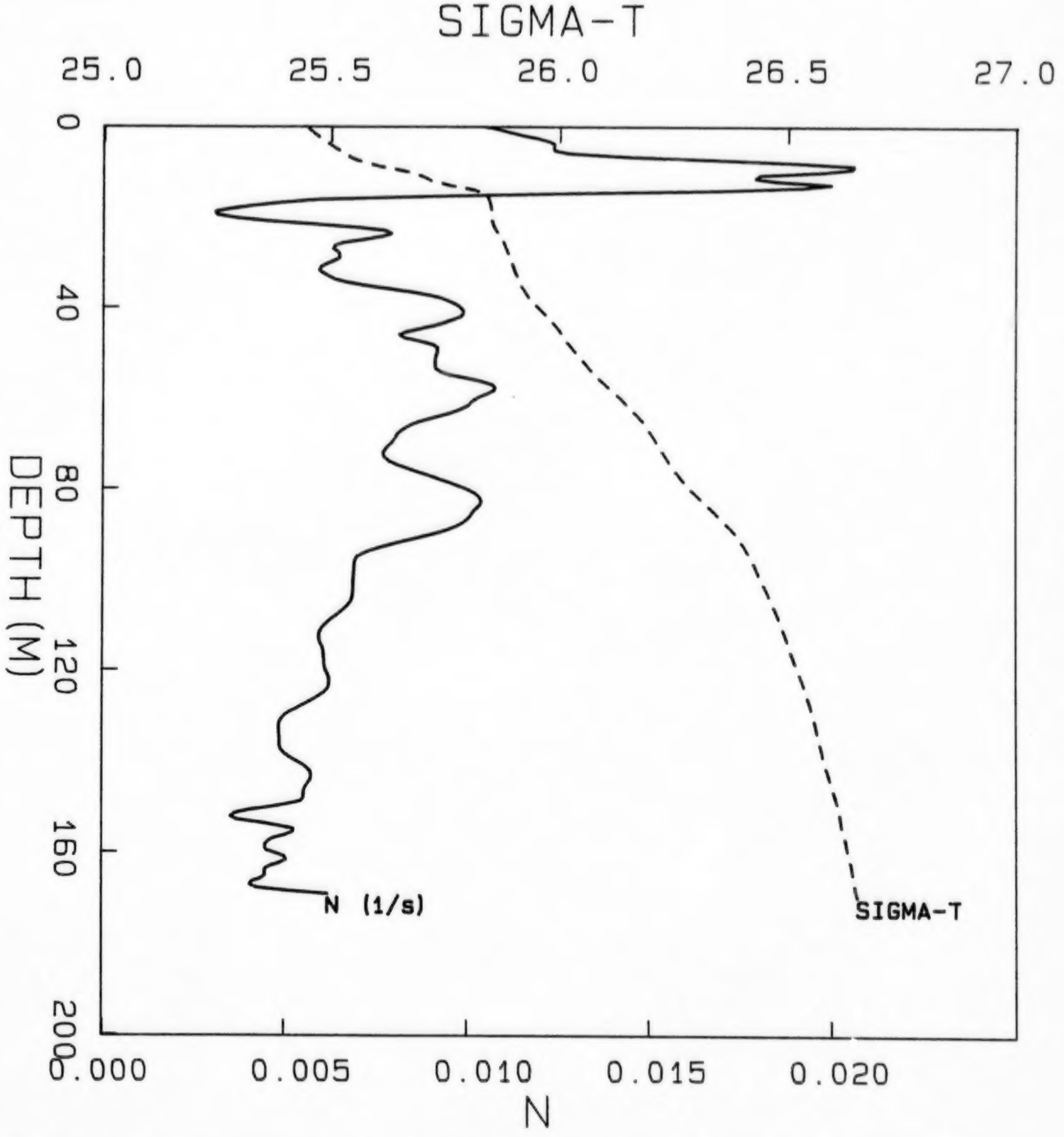

Figure 6.2.1. The vertical profile of density and Brunt-Väisälä frequency at a station in Barrow Strait.

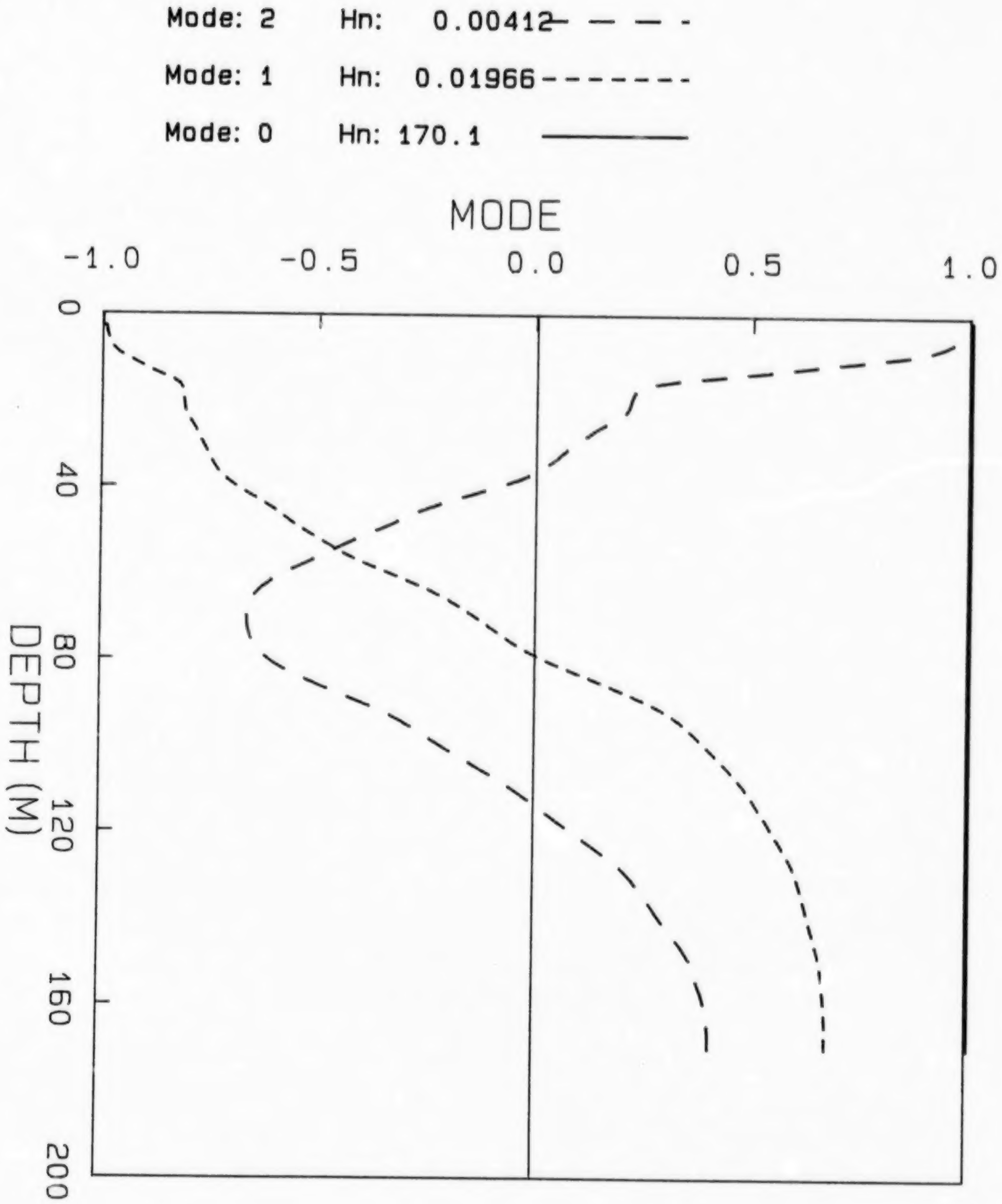

Figure 6.2.2. The barotropic and first two baroclinic modes corresponding to the density profile of Figure 6.2.1.

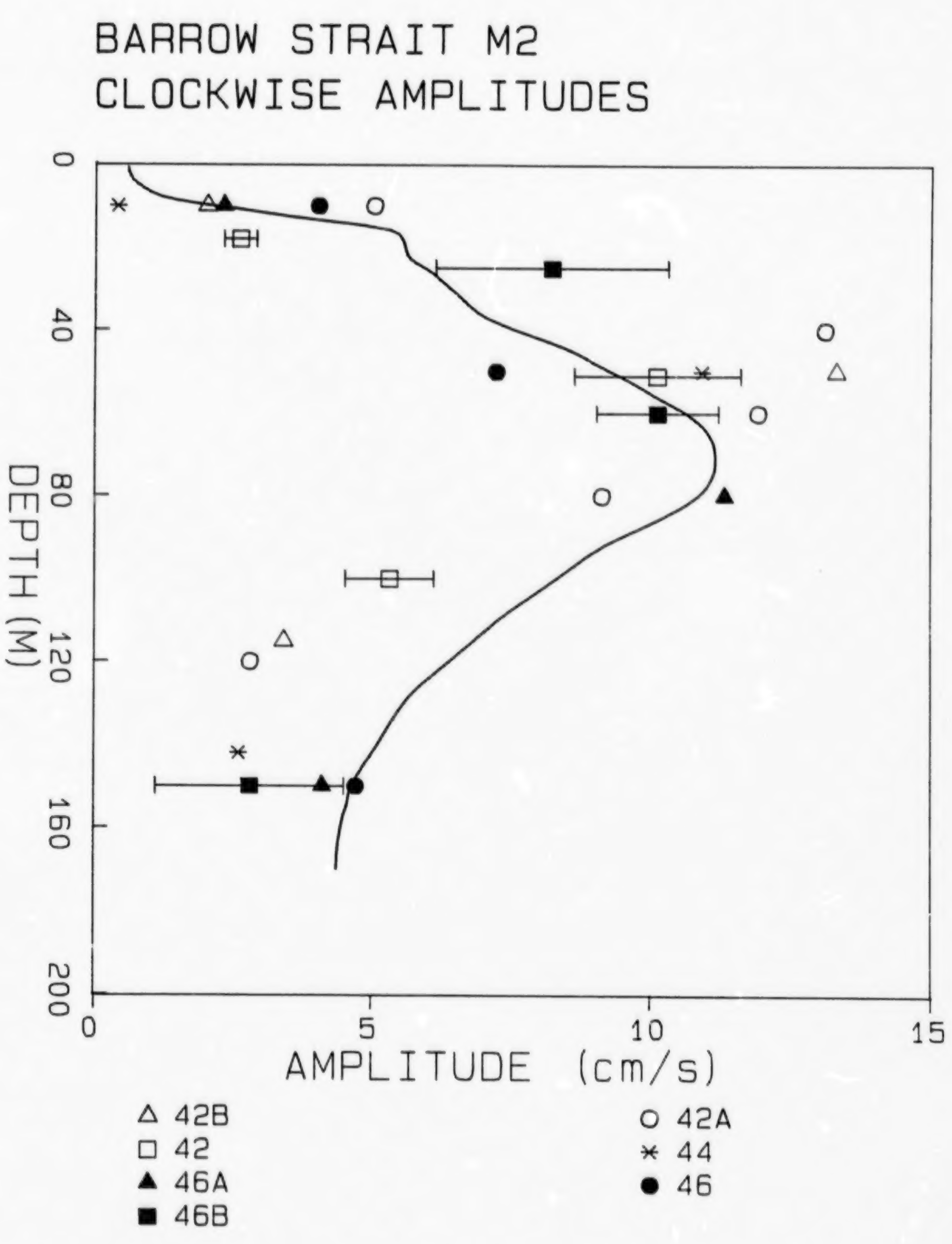

Figure 6.2.3. The fitted profile of clockwise amplitudes of the M2 currents at station 46B, and the observed data for Barrow Strait. Barotropic and second baroclinic modes were used.

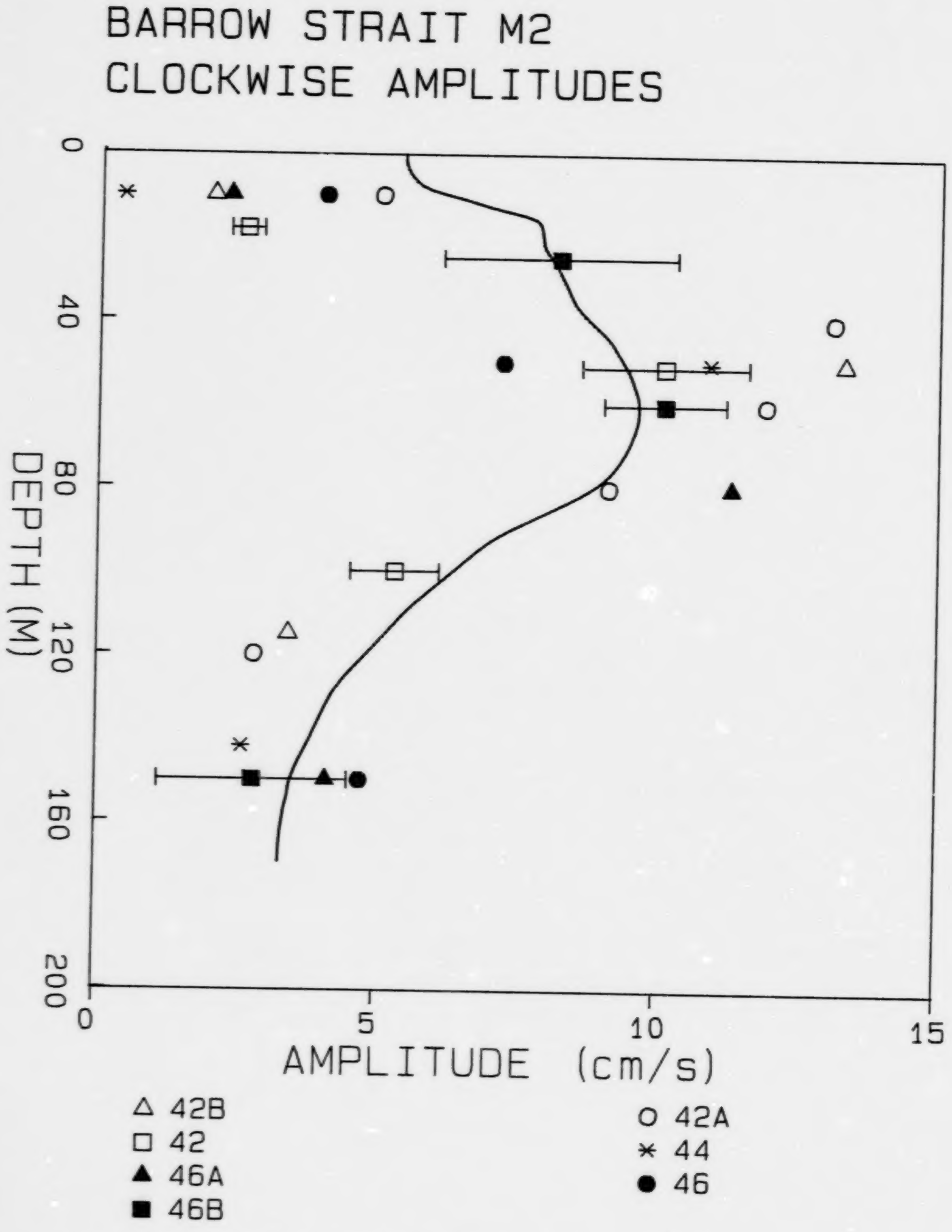

Figure 6.2.4. The fitted profile of clockwise amplitudes of the M2 currents at station 46B, and the observed data for Barrow Strait. Barotropic and first and second baroclinic modes were used.

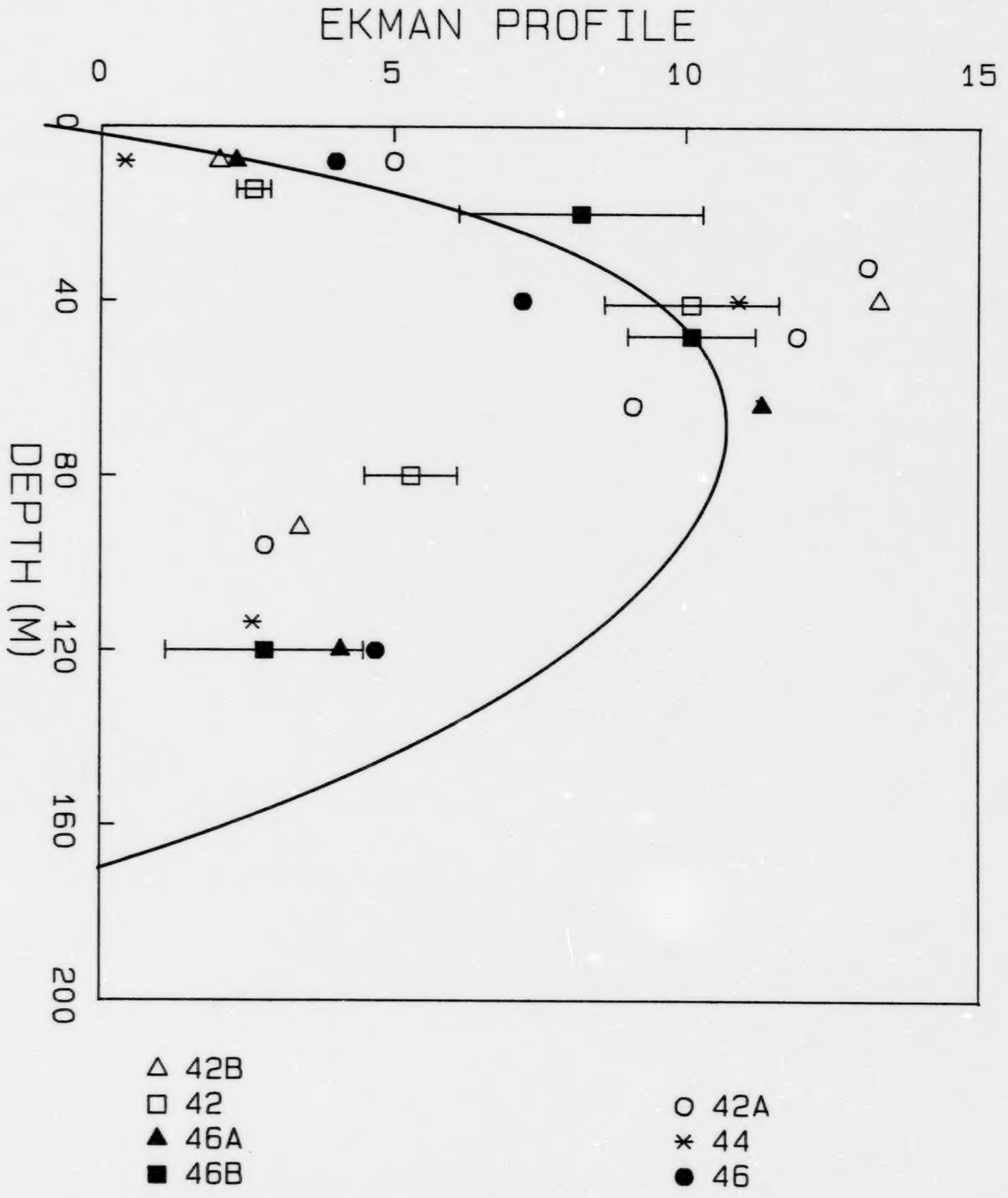

Figure 6.2.5. The fitted profile of clockwise amplitudes of the M2 currents at station 46B, and the observed data for Barrow Strait. An Ekman boundary layer model was used, eddy viscosity of 10 cm^2/s in the top layer, 50 cm^2/s in the bottom.

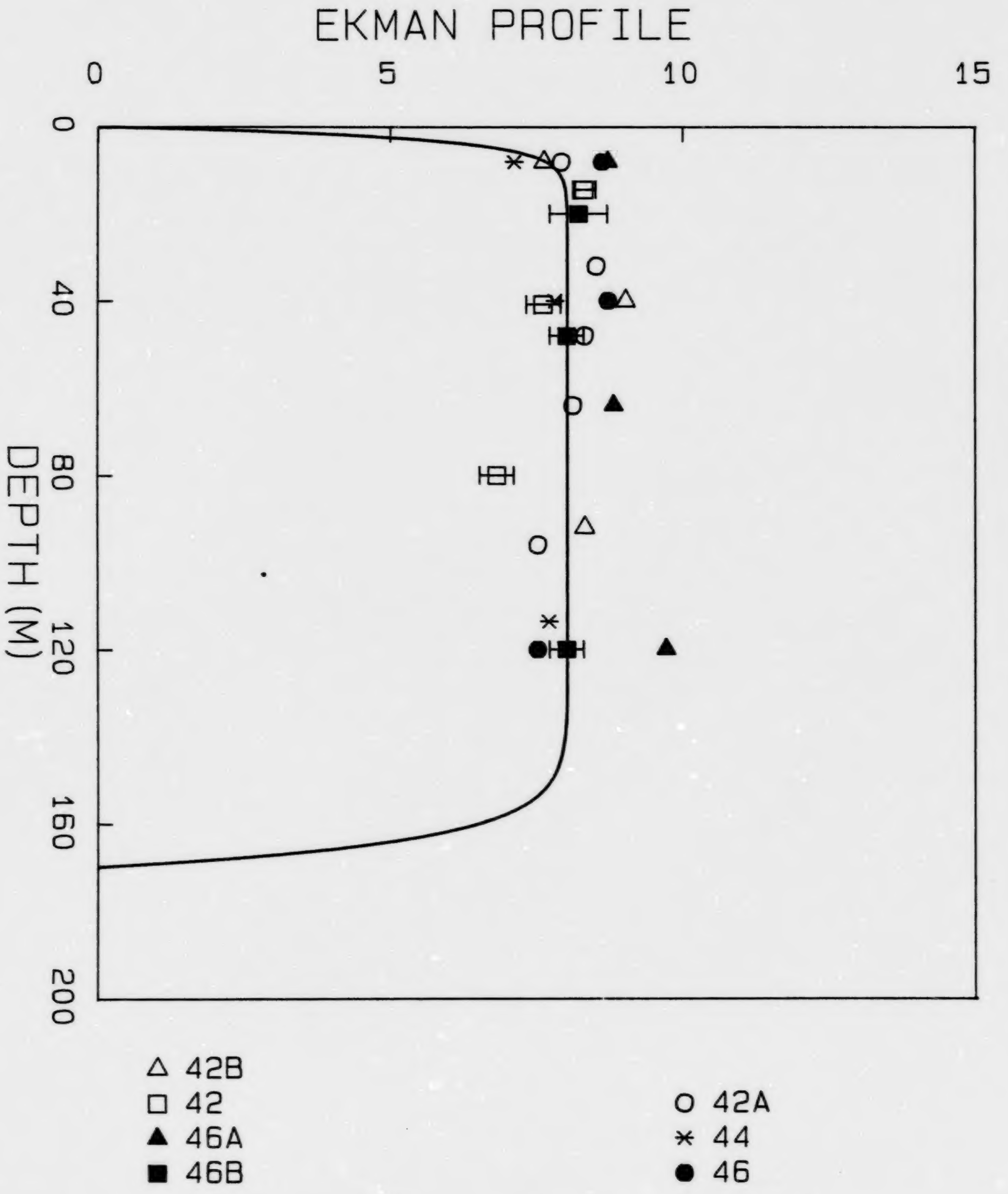

Figure 6.2.6. The fitted profile of counterclockwise amplitudes of the M2 currents at station 46B, and the observed data for Barrow Strait. An Ekman boundary layer model was used, eddy viscosity of 10 cm^2/s in the top layer, 50 cm^2/s in the bottom.

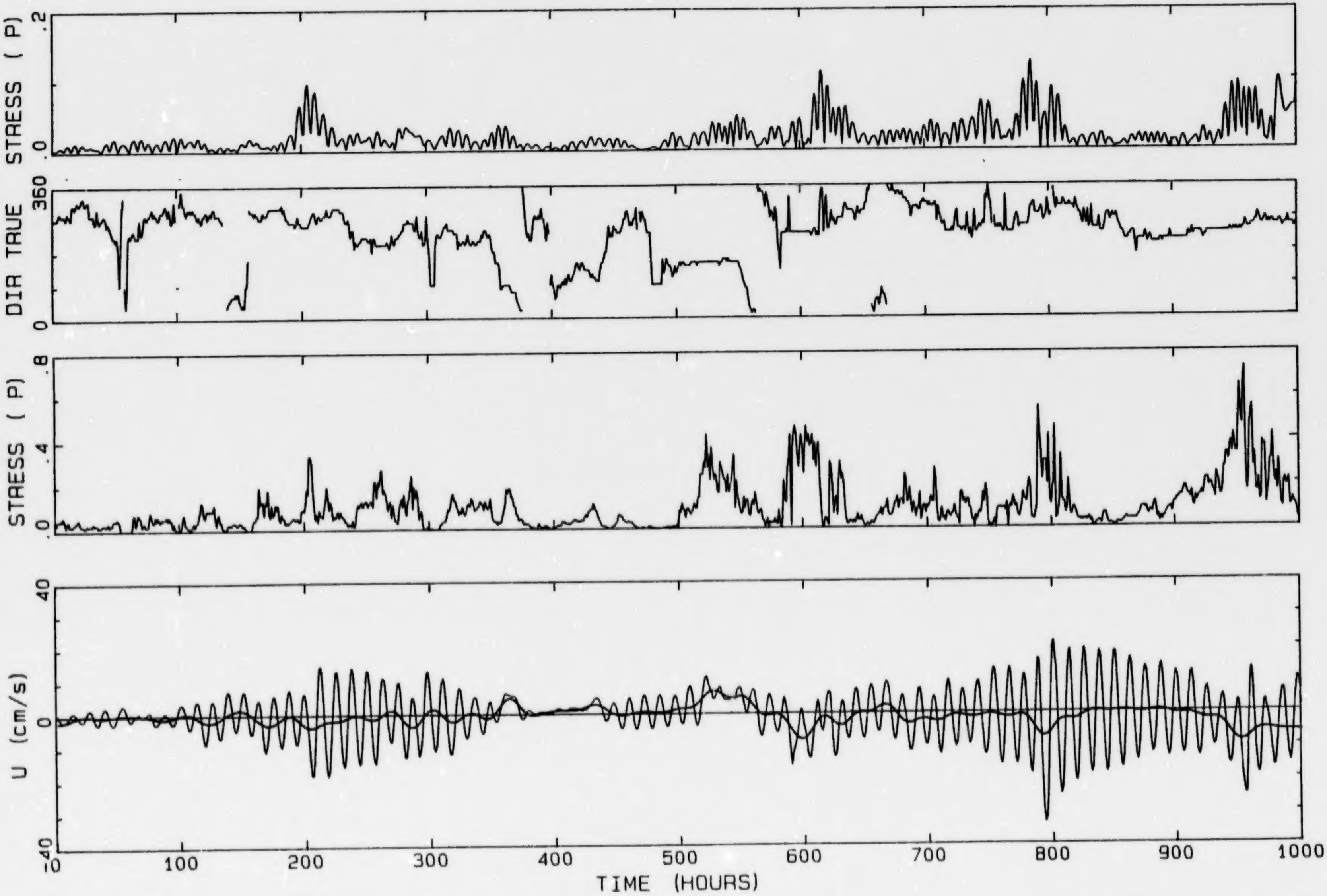

Figure 7.1. Inertial current model response to forcing by Resolute Bay winds for the 1000 hour period beginning 20 Sept 1984. The mixed layer depth is 20 m and the frictional decay time is 5 days. The lowest panel shows the east-west velocity component; the heavy line denotes the low-passed signal. The uppermost panel depicts the windstress magnitude in the inertial band (positive and negative frequencies).

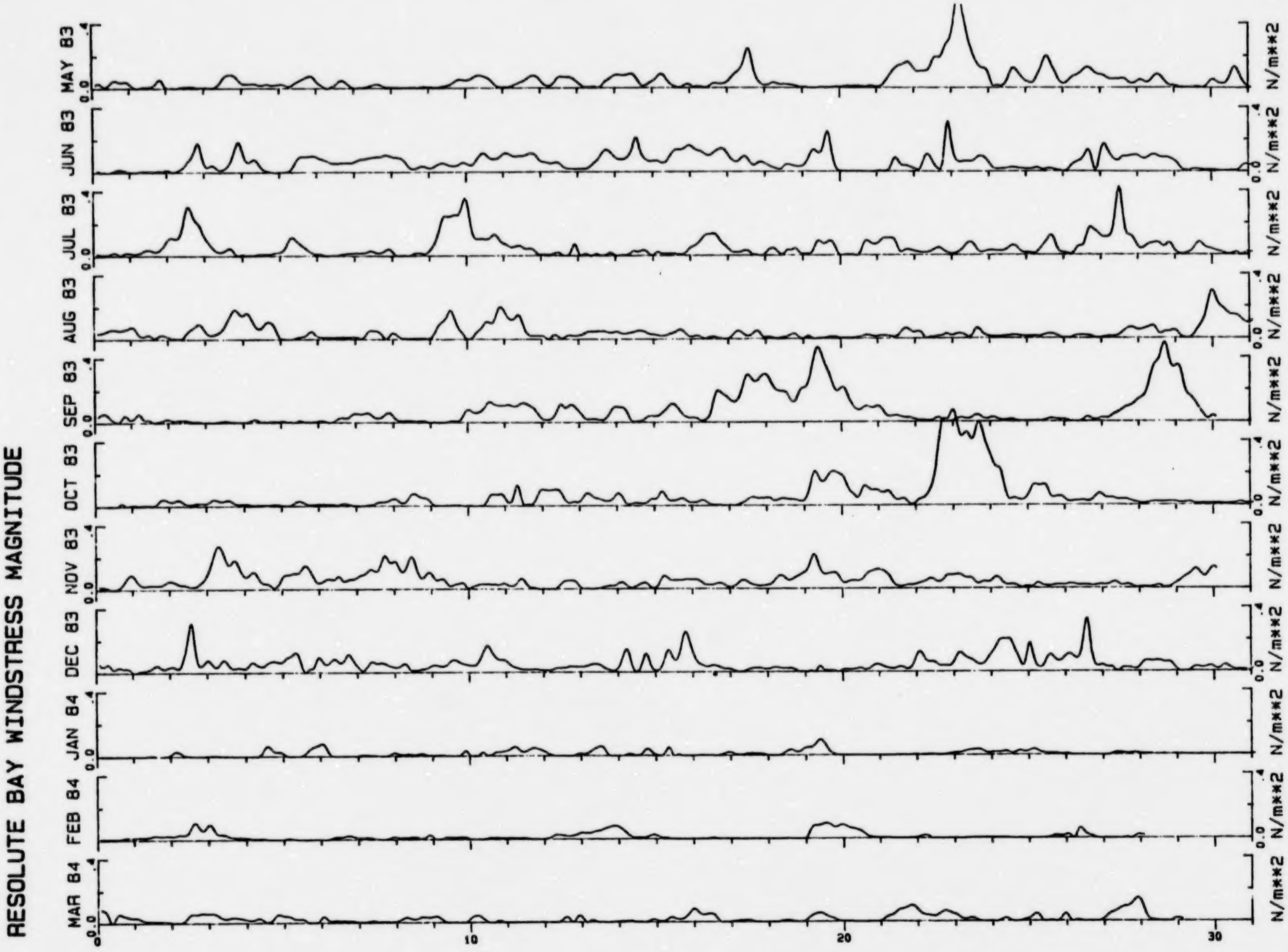

Figure 7.2 Resolute Bay windstress magnitude (in Pascals) during 1983-84.

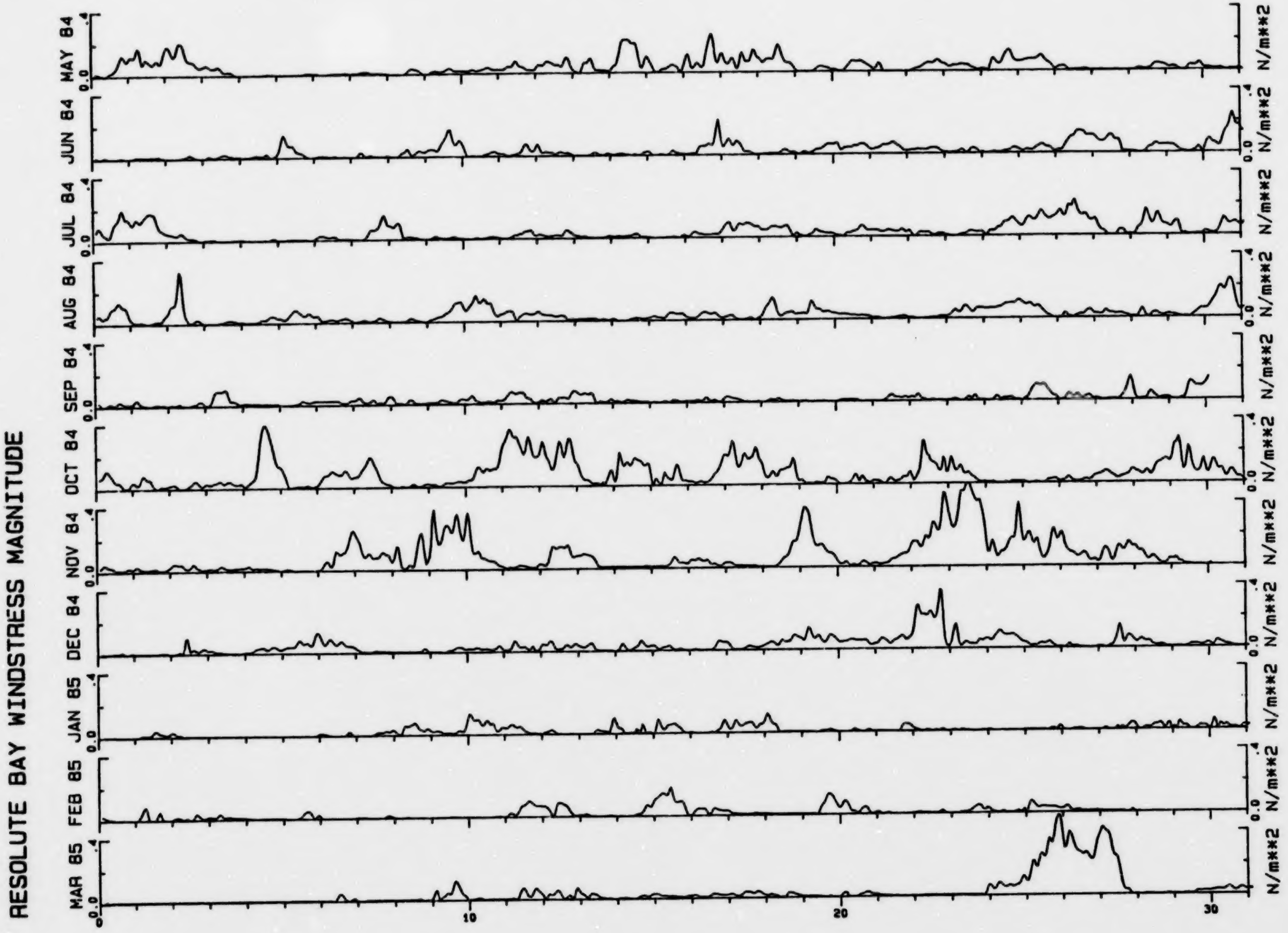

Figure 7.3 Resolute Bay windstress magnitude (in Pascals) during 1984-85.

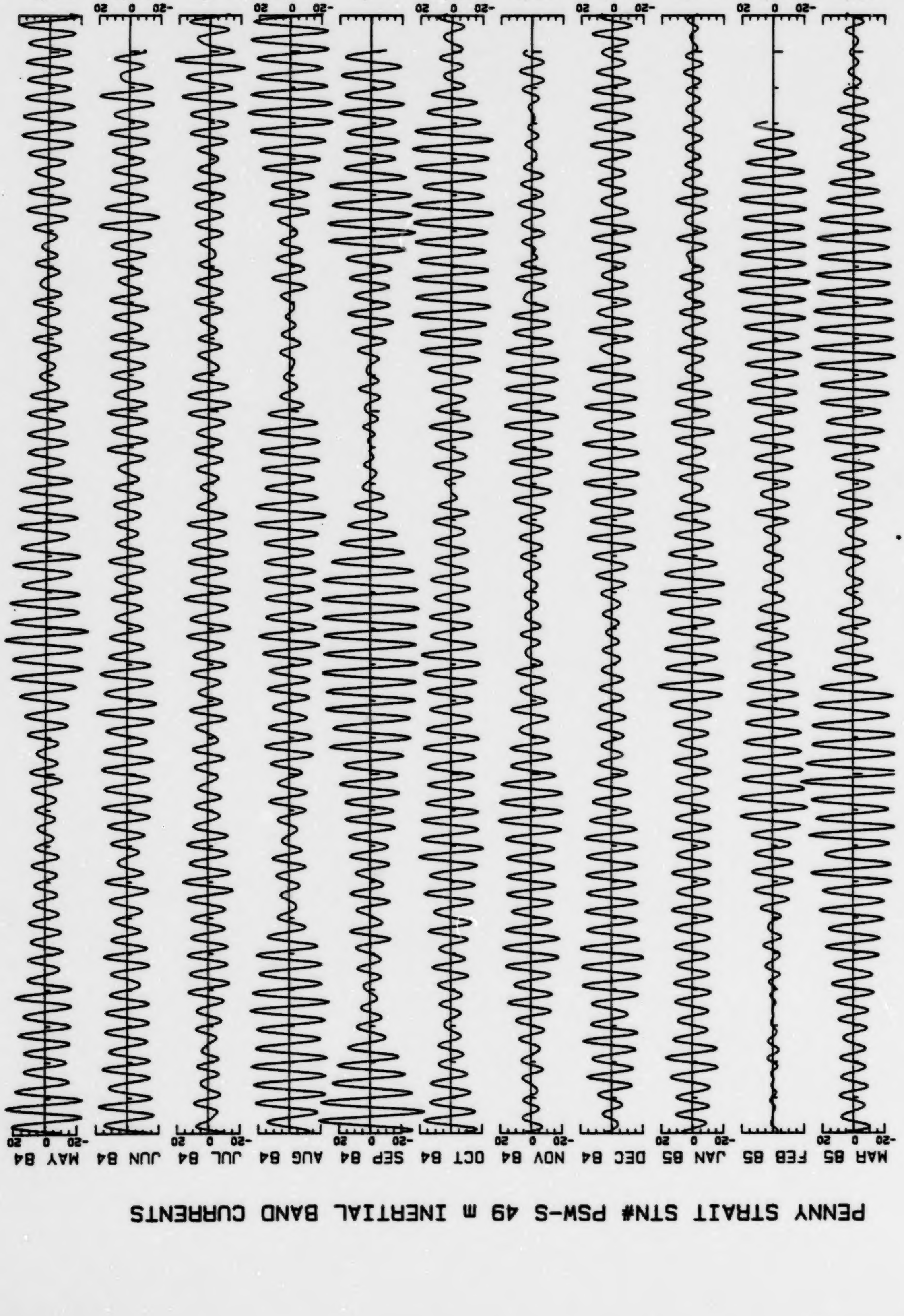

Figure 7.4 East-west component of the observed clockwise inertial band currents at PSW-S.

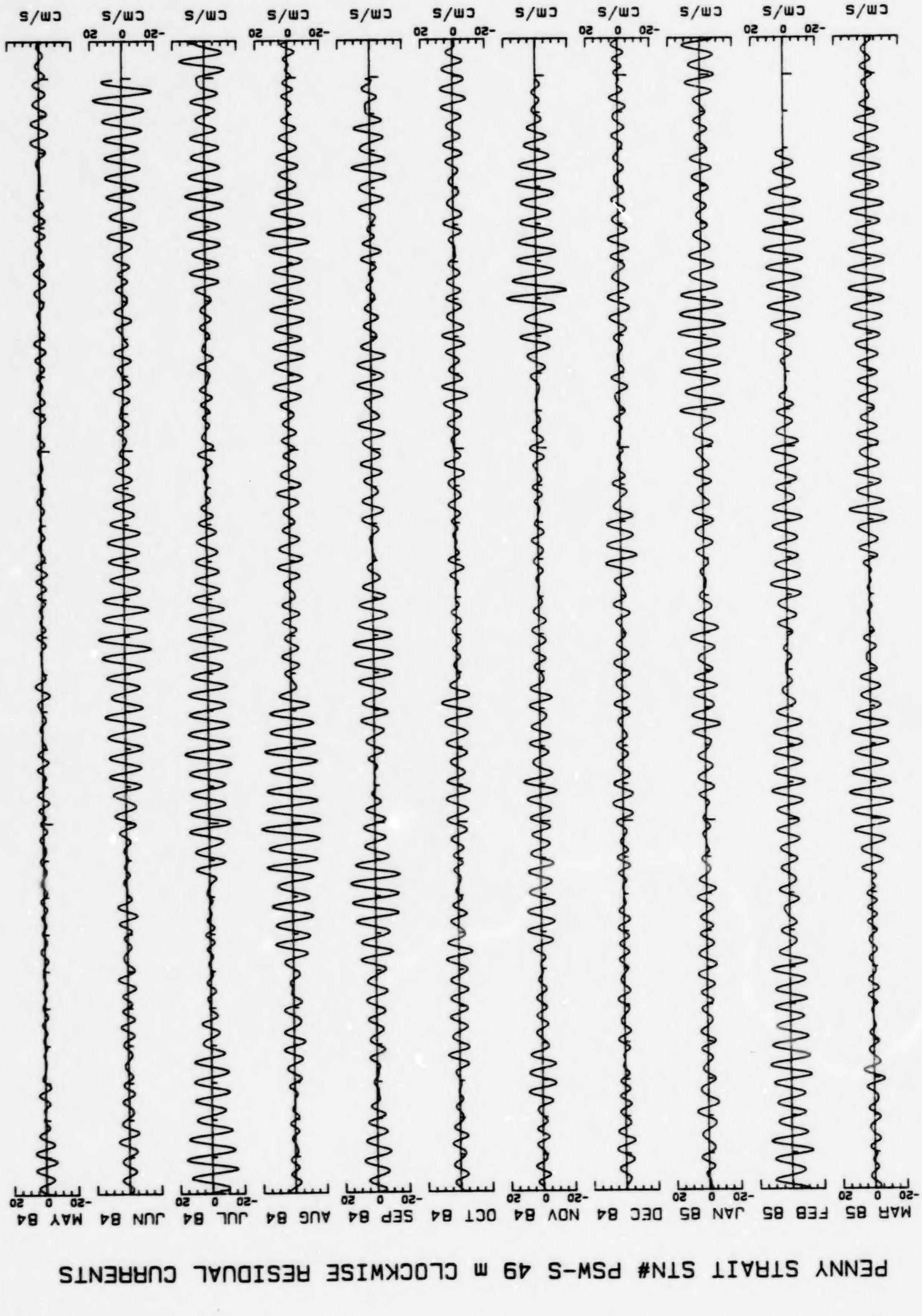

Figure 7.5 East-west component of the clockwise residual inertial band currents at PSW-S.

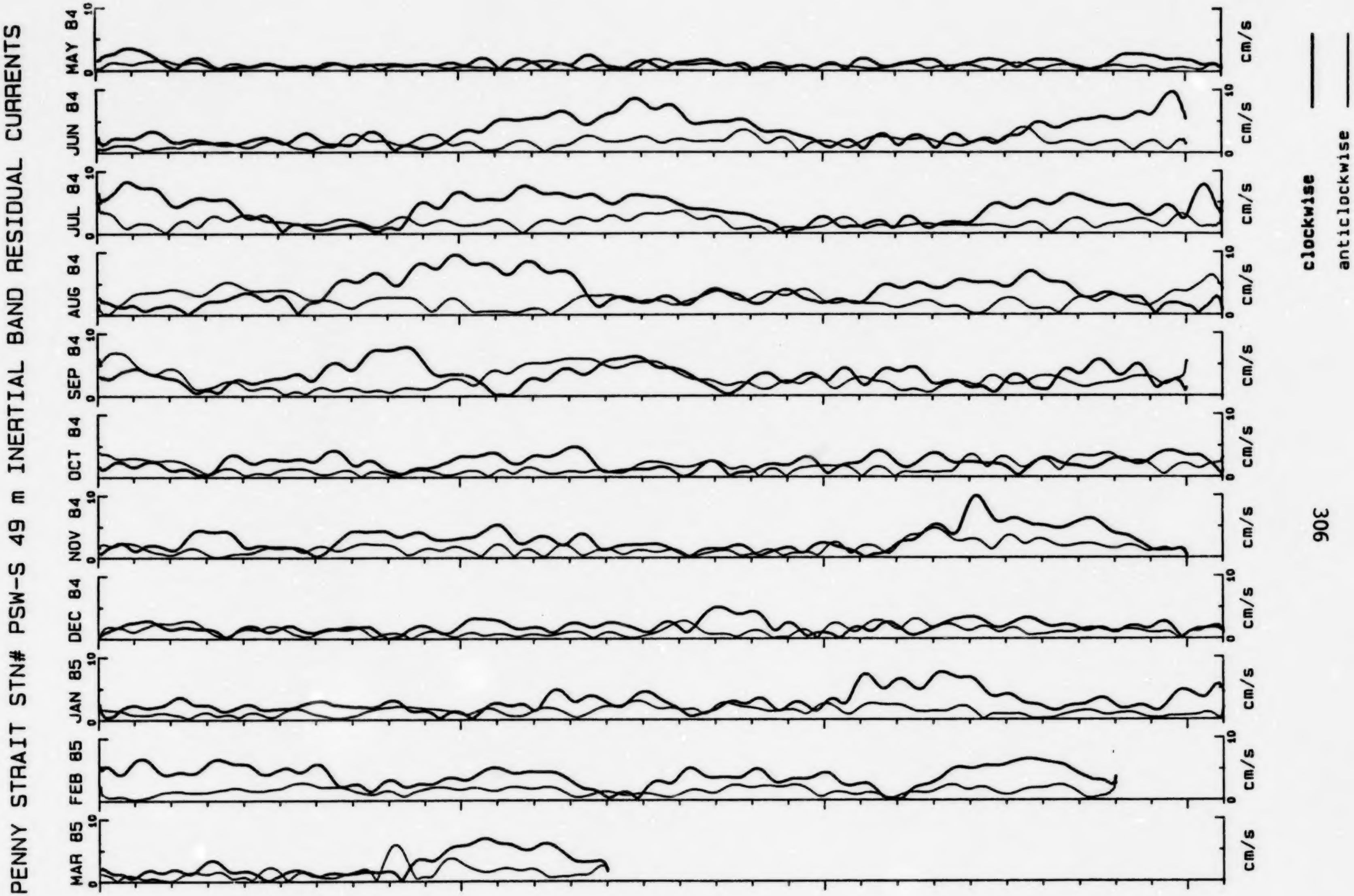

Figure 7.6 Clockwise and anticlockwise residual inertial band current magnitudes at PSW-S.

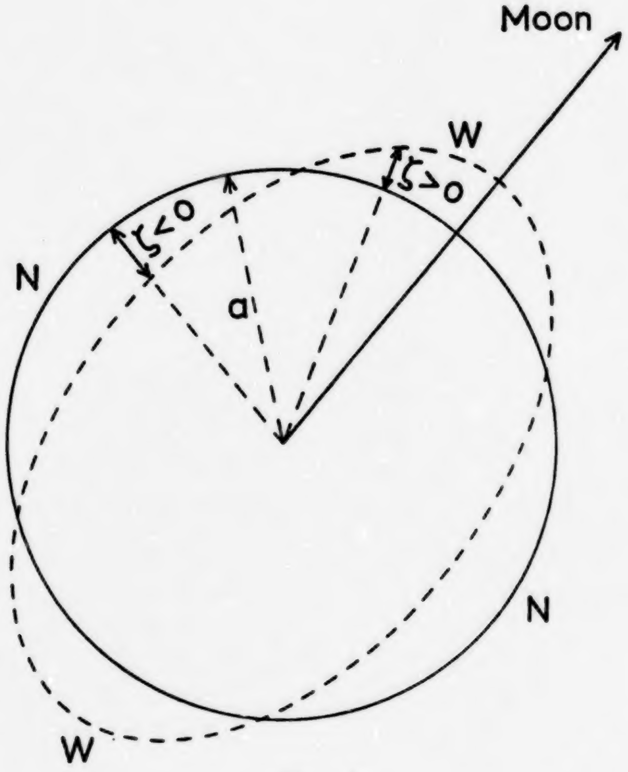
Moon
W
ζ>o
ζ<o
N
a
N
W

Fig. 5

Figure A.1. The lunar part of the astronomical tidal potential.

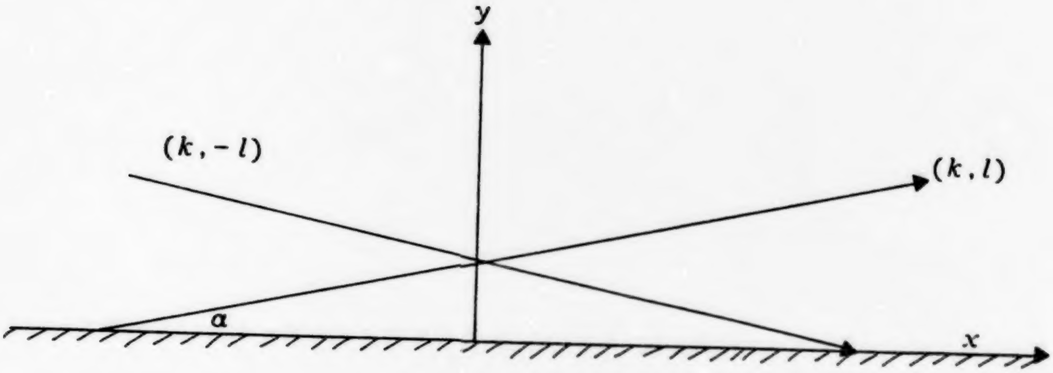

Figure A.2. The wave numbers for an incident and reflected Poincaré wave.

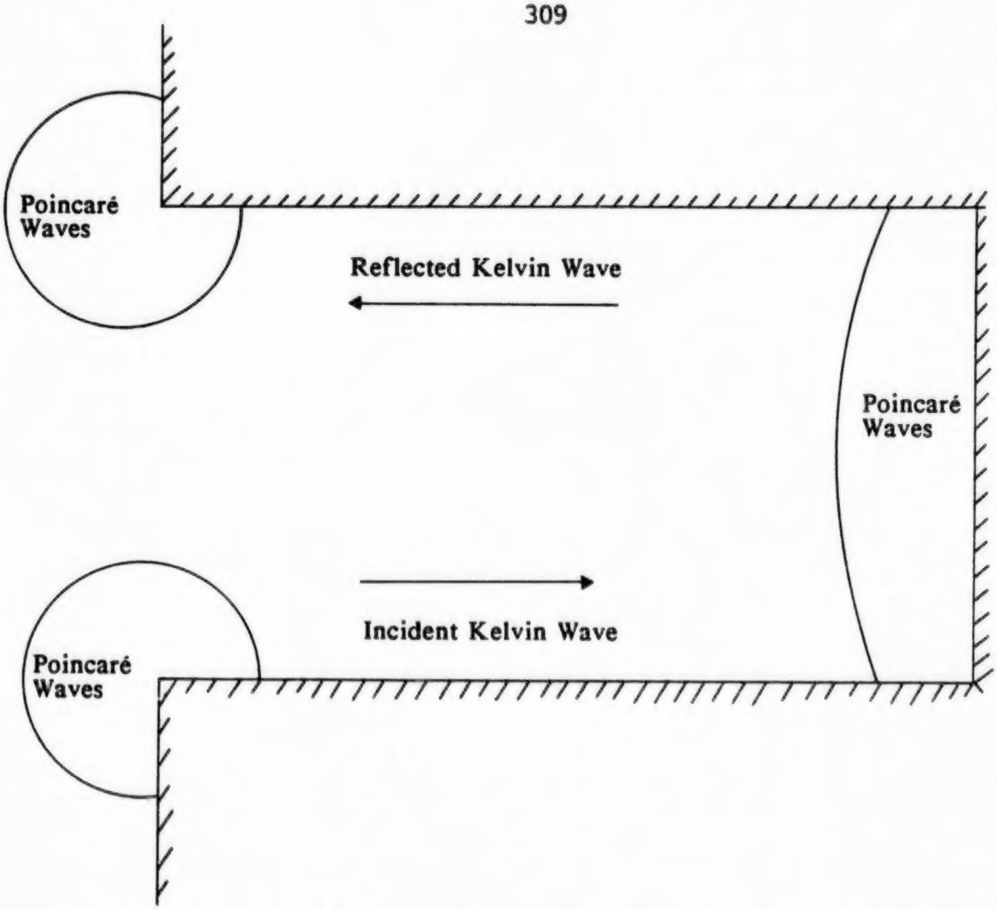
Poincaré Waves
Reflected Kelvin Wave
Poincaré Waves
Incident Kelvin Wave
Poincaré Waves

Figure A.3. A schematic diagram of tidal waves in a channel open at one end.

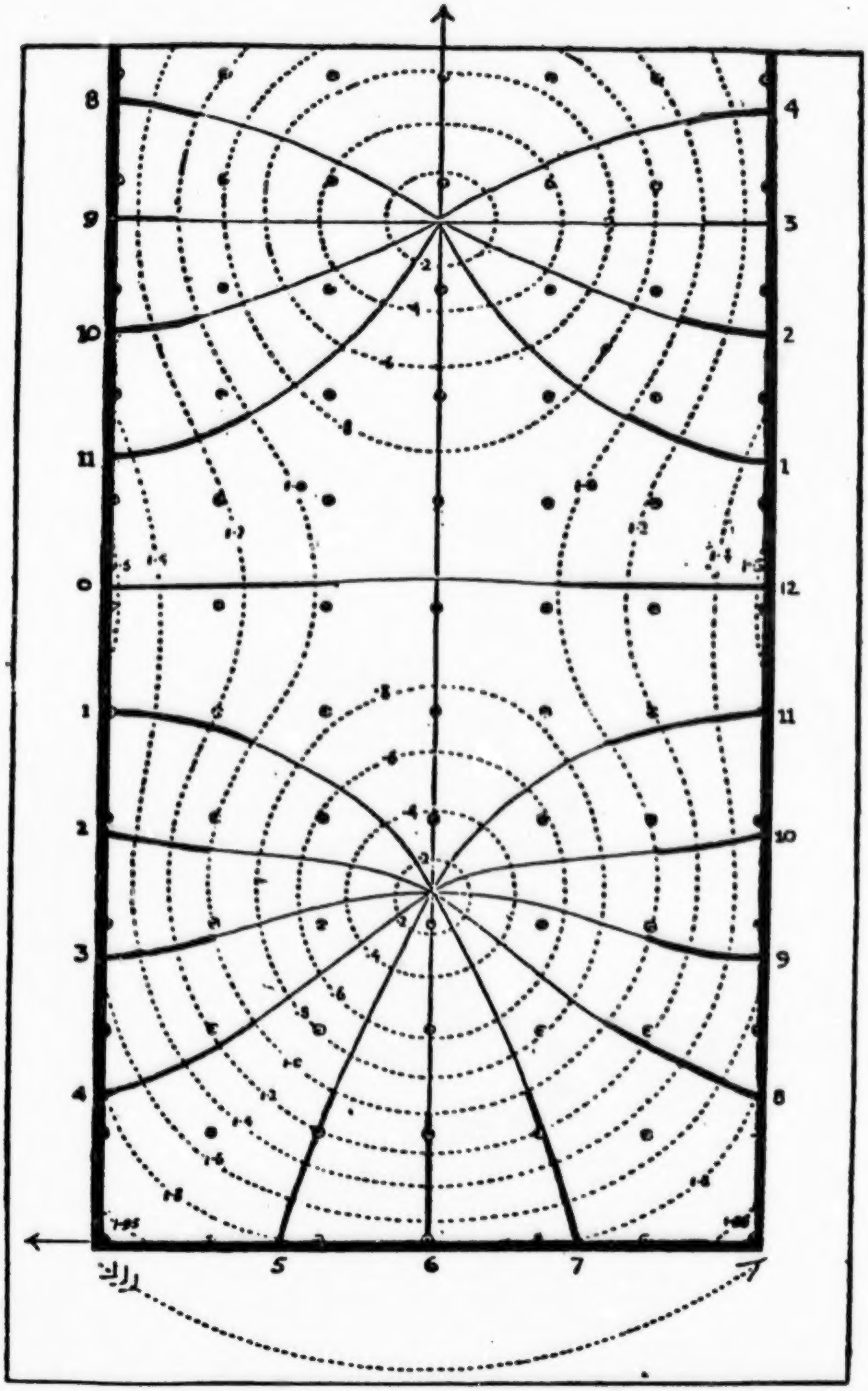
8
9
10
11
0
1
2
3
4
4
3
2
1
12
11
10
9
8
5
6
7

Figure A.4. The envelope of tidal amplitudes for a model of the Irish Sea (From Taylor, 1920).

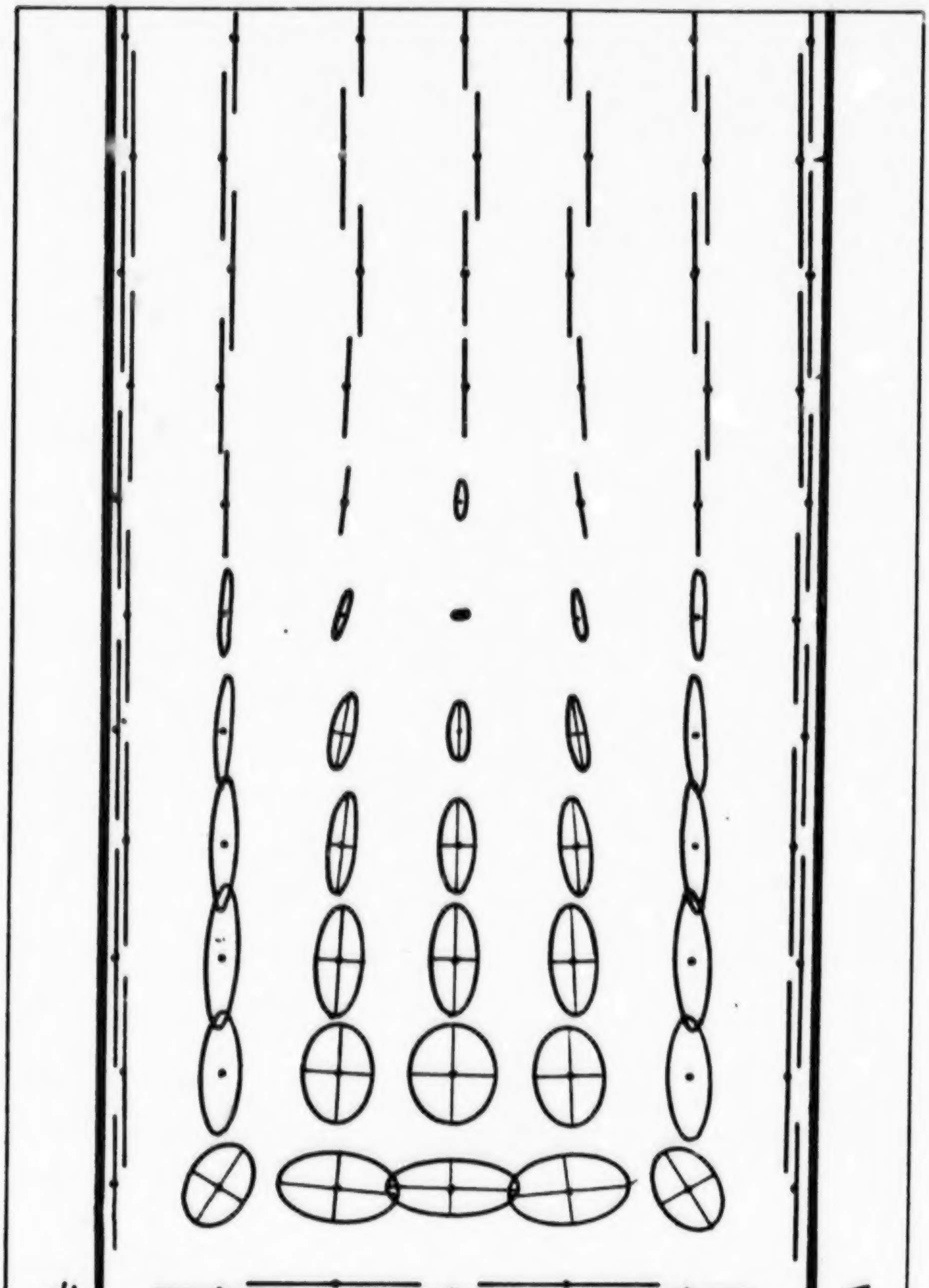

Figure A.5. Tidal current ellipse patterns for a model of the Irish Sea (From Taylor, 1920).

KELVIN PLUS POINCARE

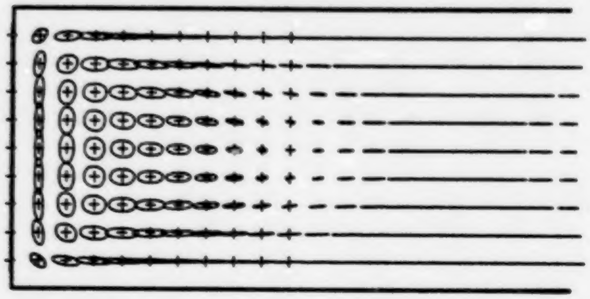

POINCARE ALONE

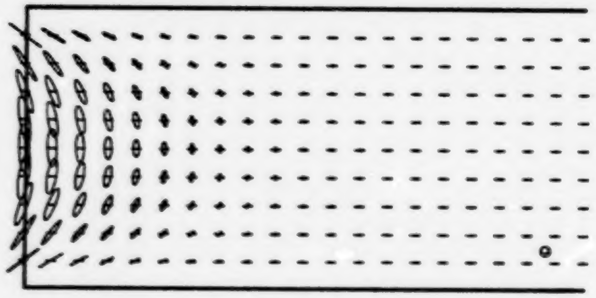

KELVIN ALONE

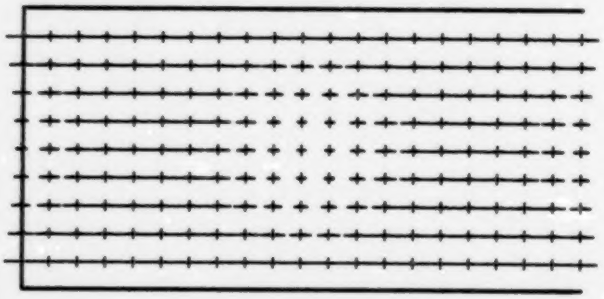

Figure A.6. Taylor's ellipse diagram for the Irish Sea, decomposed into separate Kelvin and Poincaré wave parts.

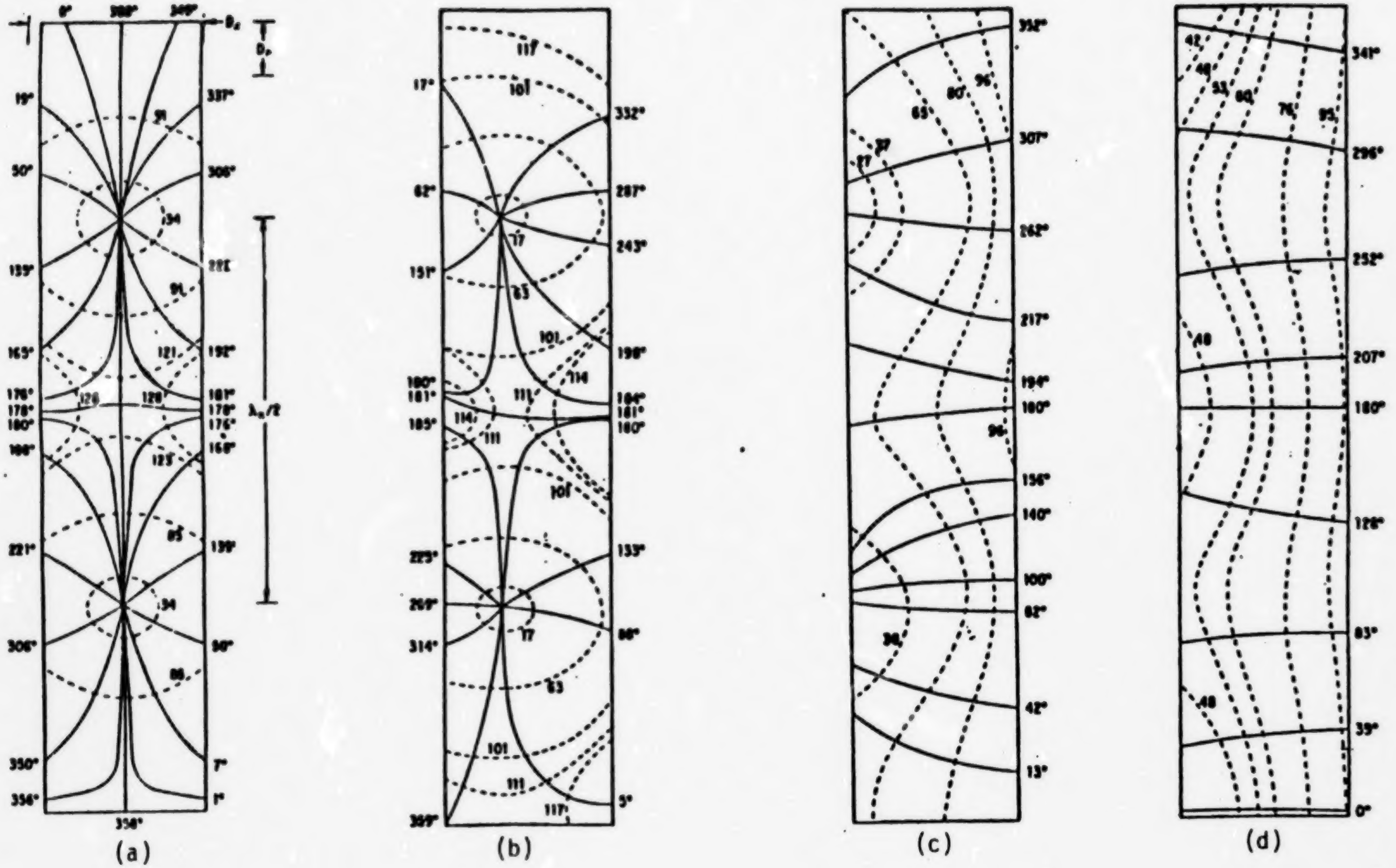
(a)
(b)
(c)
(d)
$\lambda_o/2$
0°
180°
352°
341°
296°
232°
207°
128°
83°
39°
0°

Figure A.7. The change in the amphidromic pattern as the reflected wave is successively reduced in amplitude (From Hendershott and Speranza, 1971).

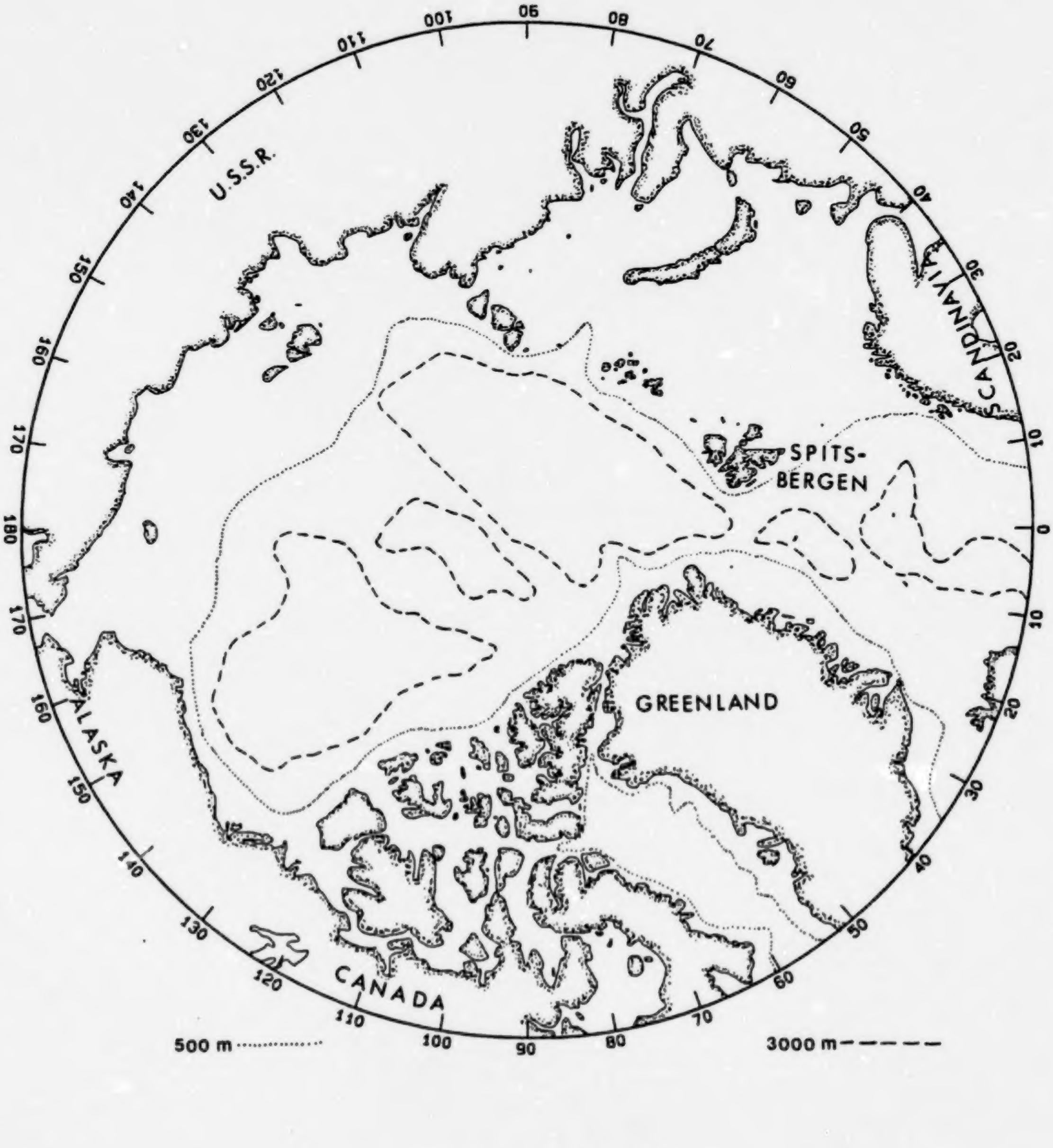
U.S.S.R.
SCANDINAVIA
SPITS-
BERGEN
GREENLAND
ALASKA
CANADA
500 m
3000 m
180
170
160
150
140
130
120
110
100
90
80
70
60
50
40
30
20
10
0

Figure B.1. Base map of the Arctic Ocean.

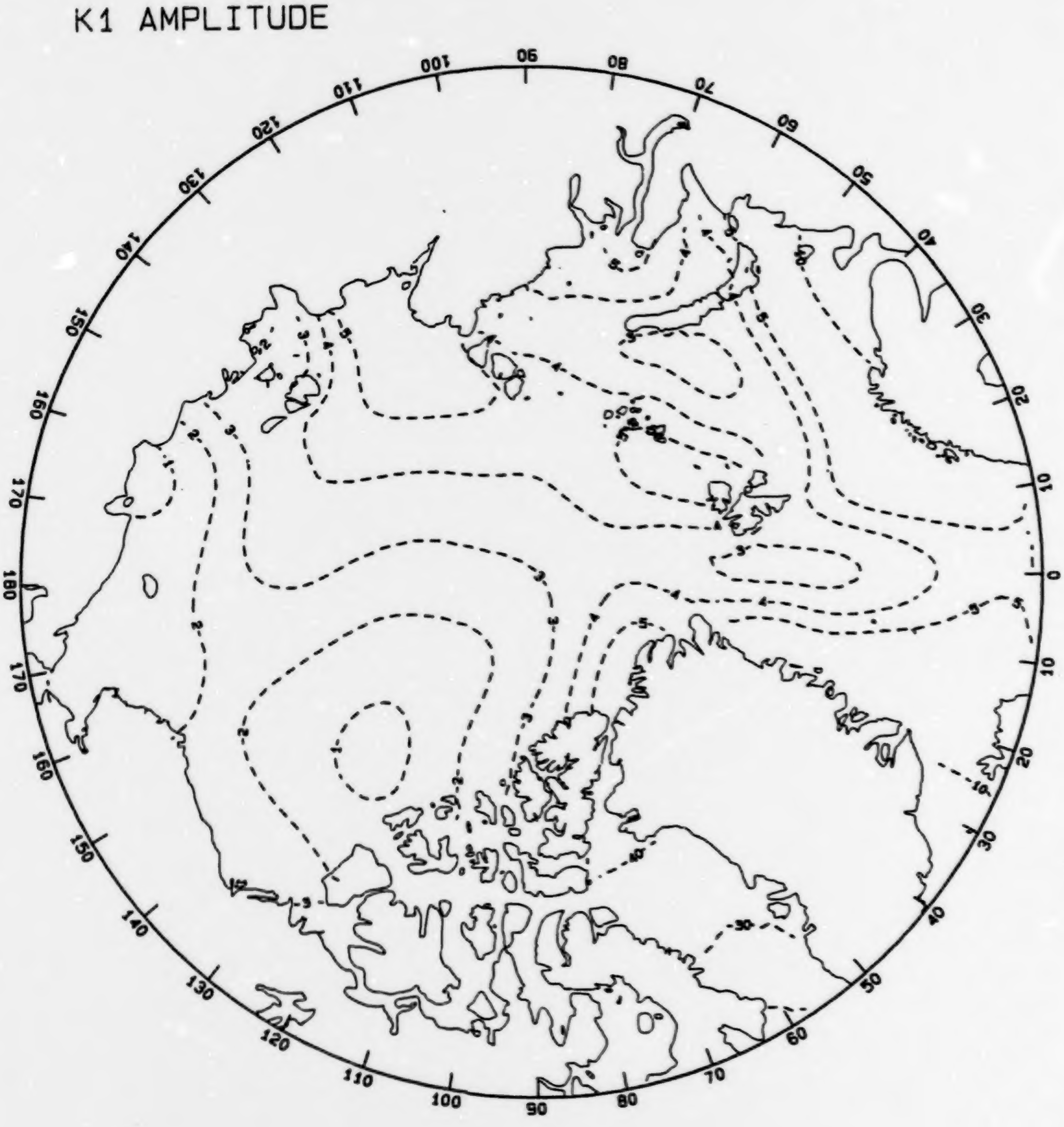
K1 AMPLITUDE
90
80
70
60
50
40
30
20
10
0
10
20
30
40
50
60
70
80
90
100
110
120
130
140
150
160
170
180
170
160
150
140
130
120
110
100

Figure B.2. Amplitude contours of the K1 tide in the Arctic Ocean, as calculated by Schwiderski.

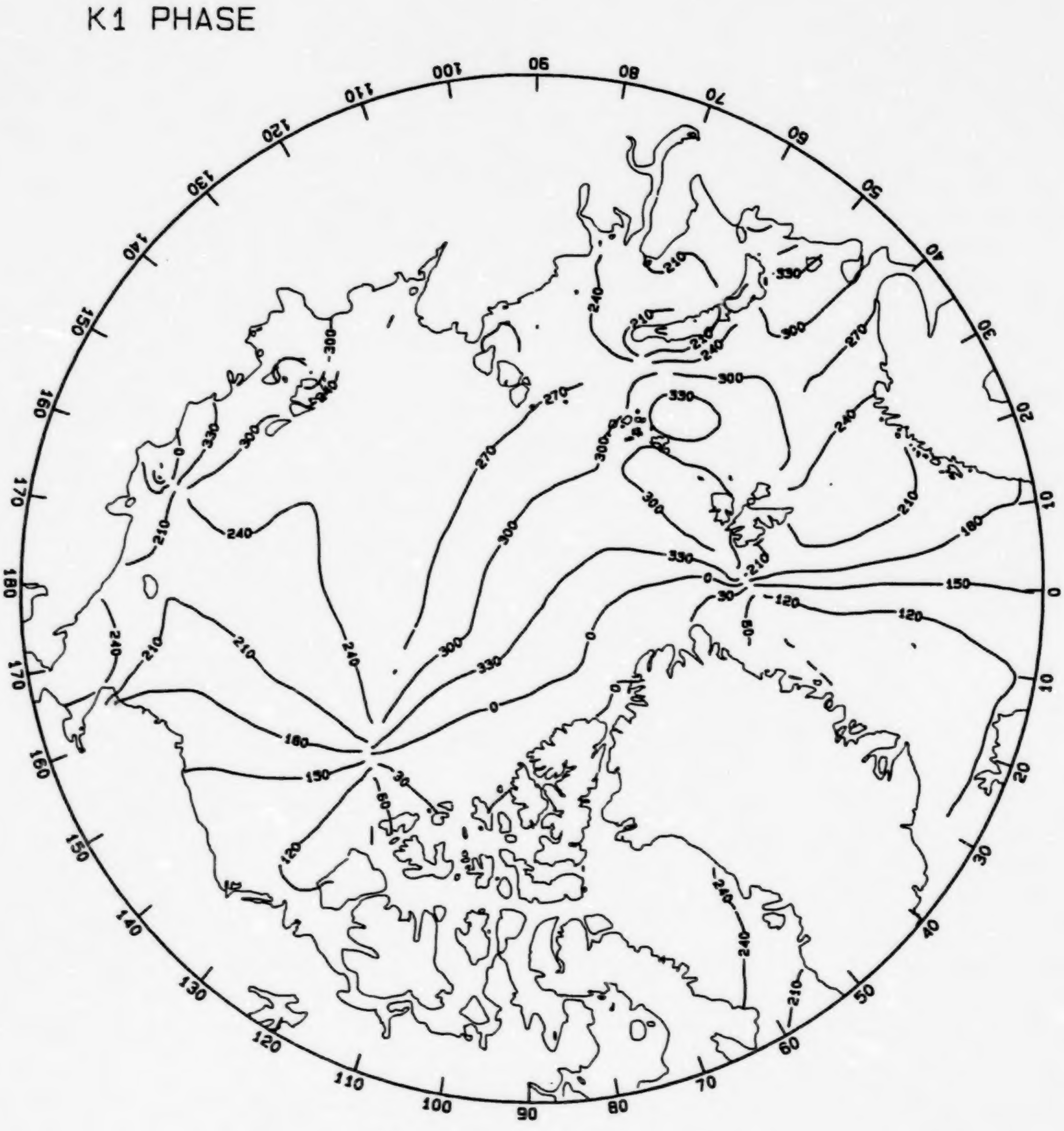
K1 PHASE
90
100
110
120
130
140
150
160
170
180
80
70
60
50
40
30
20
10
0
150
120
180
240
210
270
300
330
0
30
60

Figure B.3. Phase contours of the K1 tide in the Arctic Ocean, as calculated by Schwiderski.

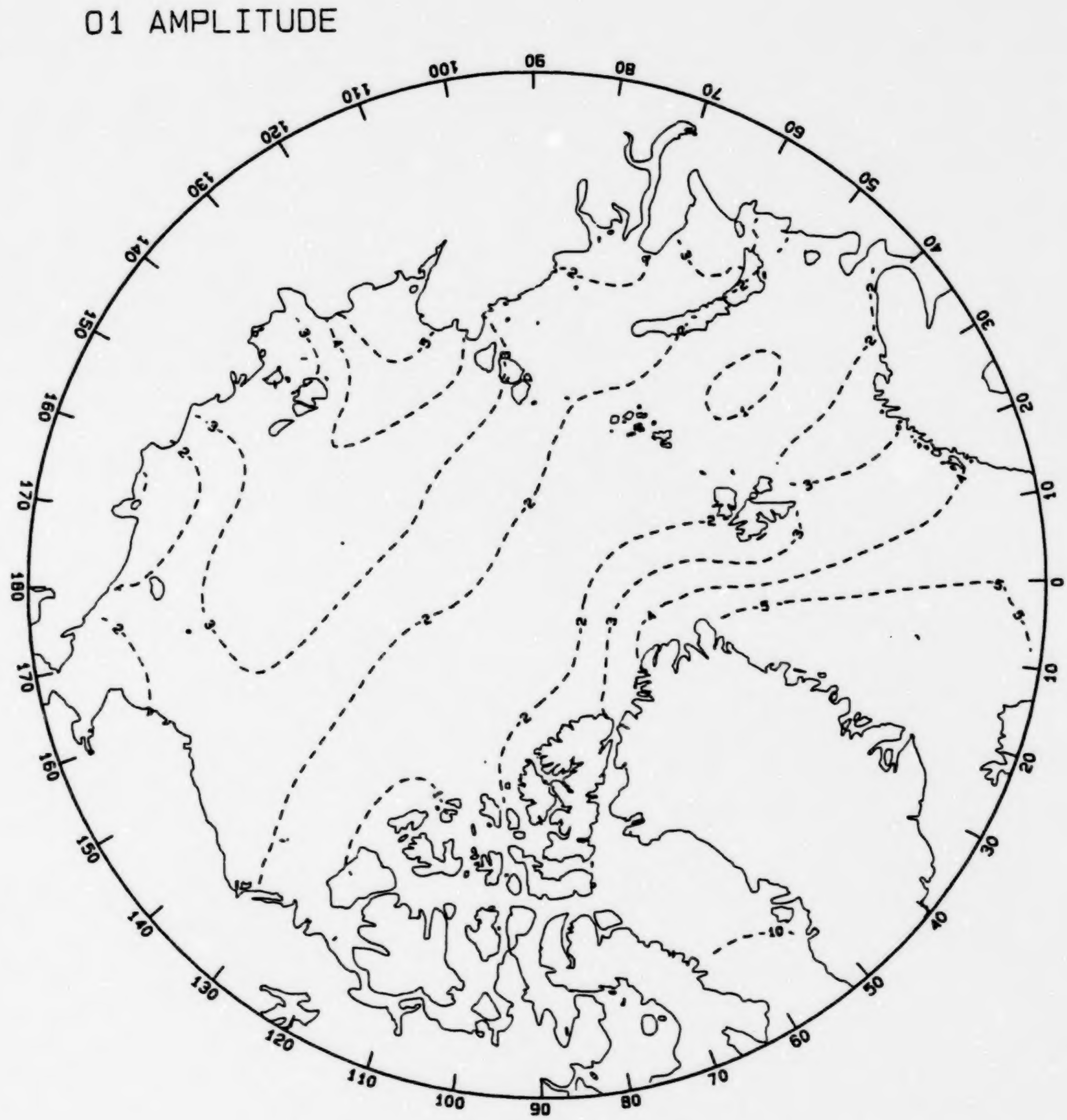
O1 AMPLITUDE
90
80
70
60
50
40
30
20
10
0
10
20
30
40
50
60
70
80
90
100
110
120
130
140
150
160
170
180
170
160
150
140
130
120
110
100
1
2
3
4
5
10

Figure B.4. Amplitude contours of the O1 tide in the Arctic Ocean, as calculated by Schwiderski.

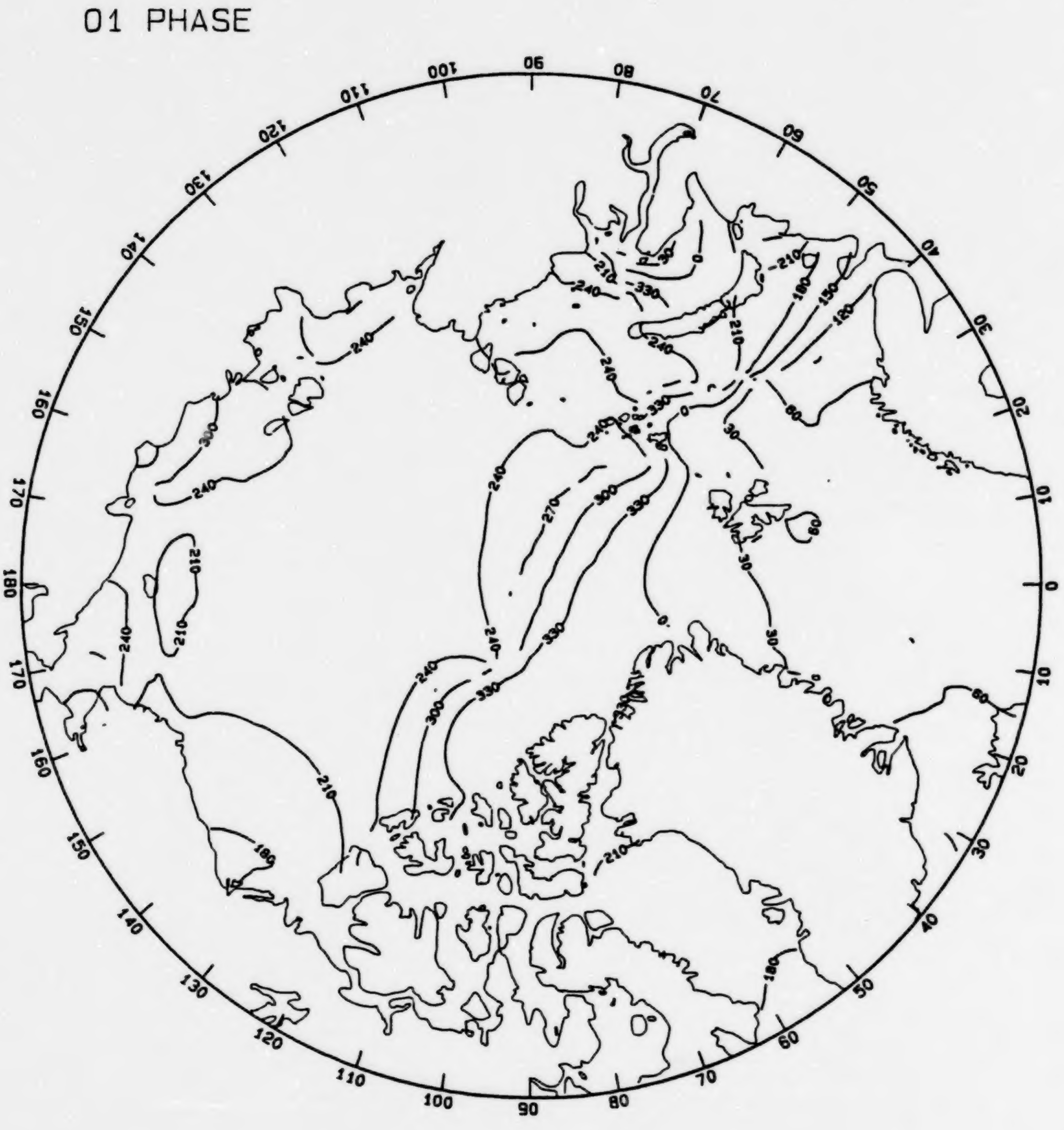
O1 PHASE
90
80
70
60
50
40
30
20
10
0
10
20
30
40
50
60
70
80
90
100
110
120
130
140
150
160
170
180
170
160
150
140
130
120
110
100
240
300
240
210
210
240
240
270
300
330
330
240
300
330
210
180
210
180
0
30
30
60
60
30
60
90
120
150
180
210
210
240
330
0
210
240
330
210

Figure B.5. Phase contours of the O1 tide in the Arctic Ocean, as calculated by Schwiderski.

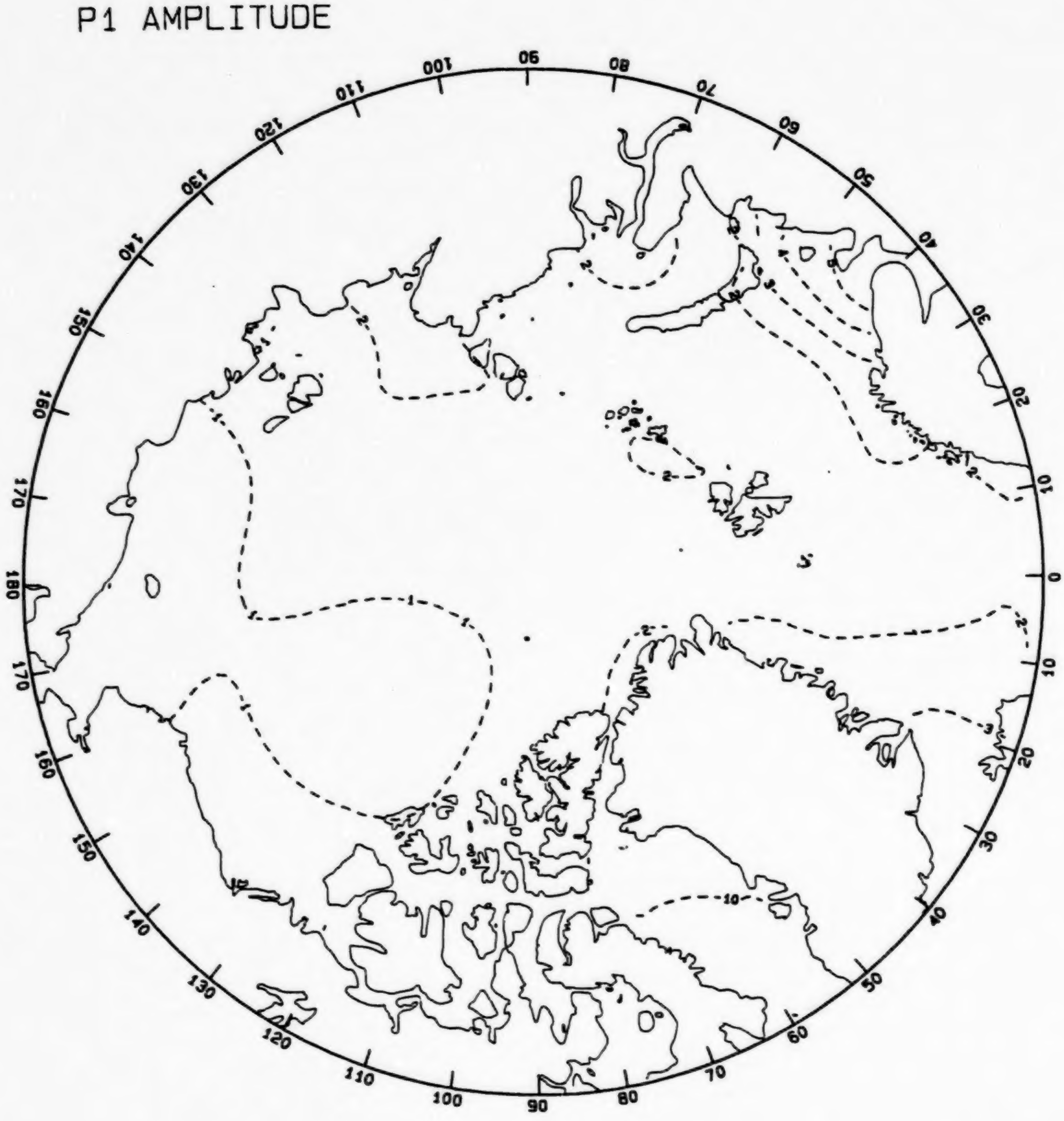
P1 AMPLITUDE
90
80
70
60
50
40
30
20
10
0
10
20
30
40
50
60
70
80
90
100
110
120
130
140
150
160
170
180
170
160
150
140
130
120
110
100
2
3
1
10

Figure B.6. Amplitude contours of the P1 tide in the Arctic Ocean, as calculated by Schwiderski.

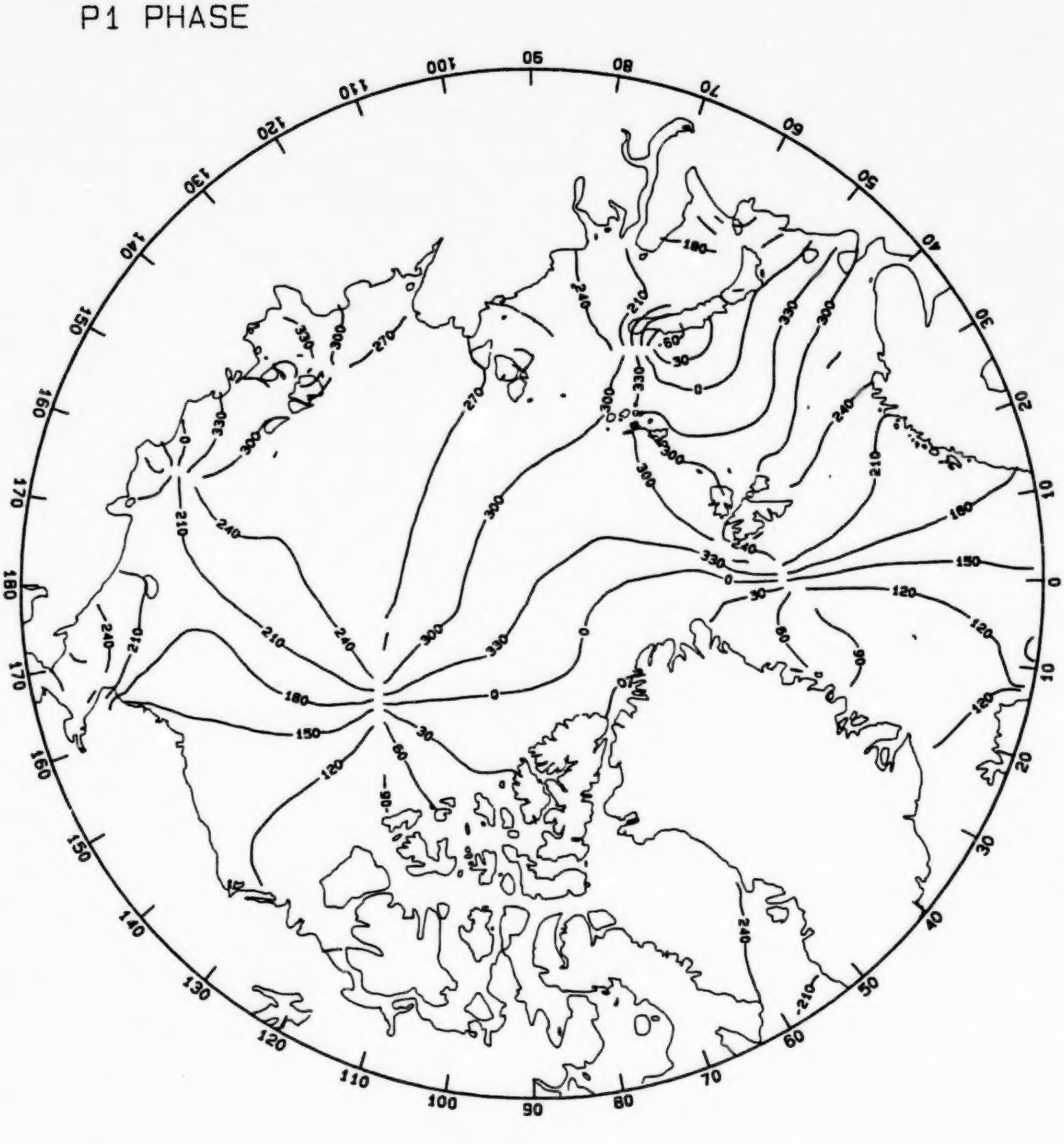
P1 PHASE
0
30
60
90
120
150
180
210
240
270
300
330
10
20
30
40
50
60
70
80
90
100
110
120
130
140
150
160
170
180

Figure B.7. Phase contours of the P1 tide in the Arctic Ocean, as calculated by Schwiderski.

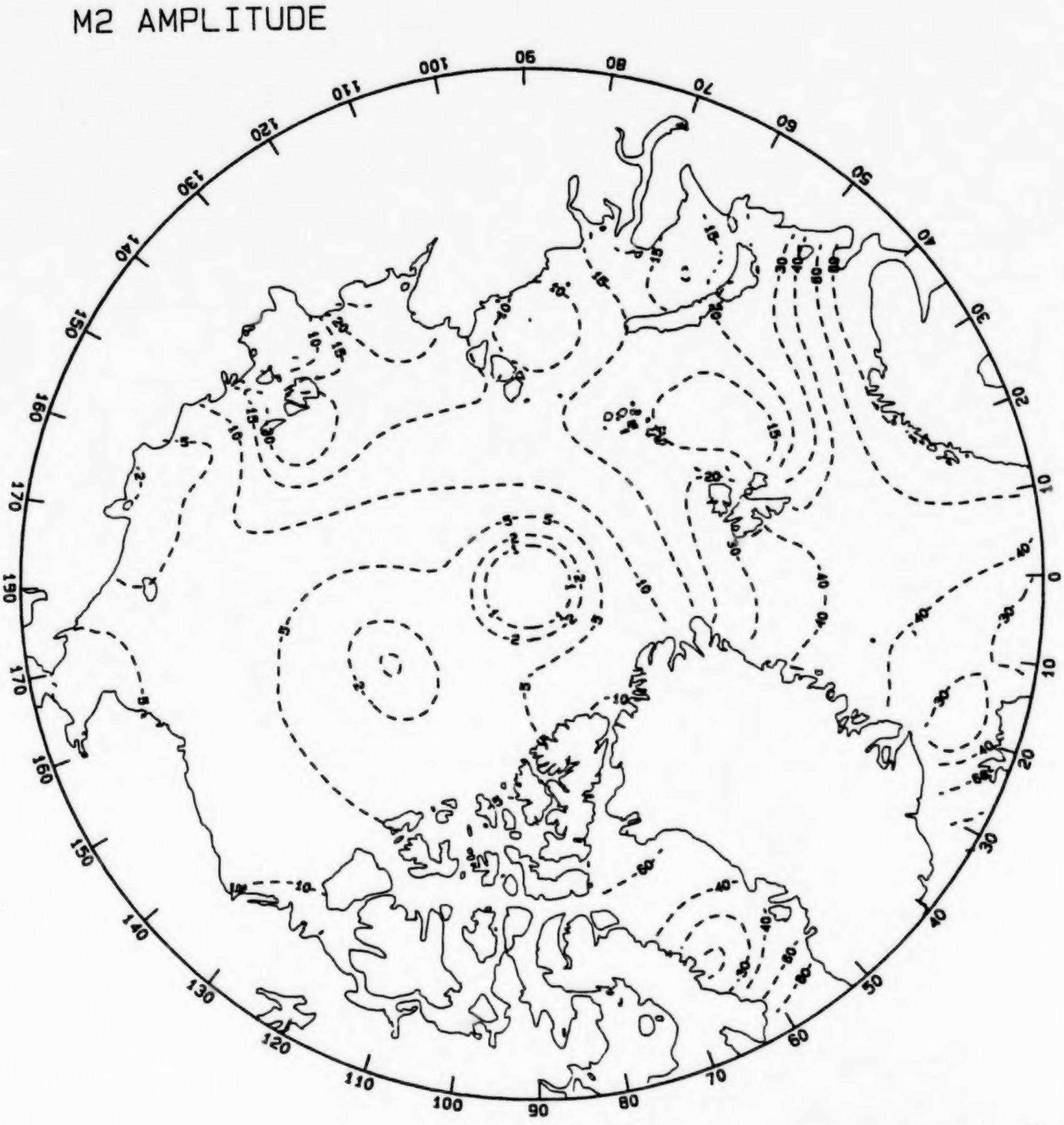
M2 AMPLITUDE
100
90
80
70
60
50
40
30
20
10
0
10
20
30
40
50
60
70
80
90
100
110
120
130
140
150
160
170
180
170
160
150
140
130
120
110

Figure B.8. Amplitude contours of the M2 tide in the Arctic Ocean, as calculated by Schwiderski.

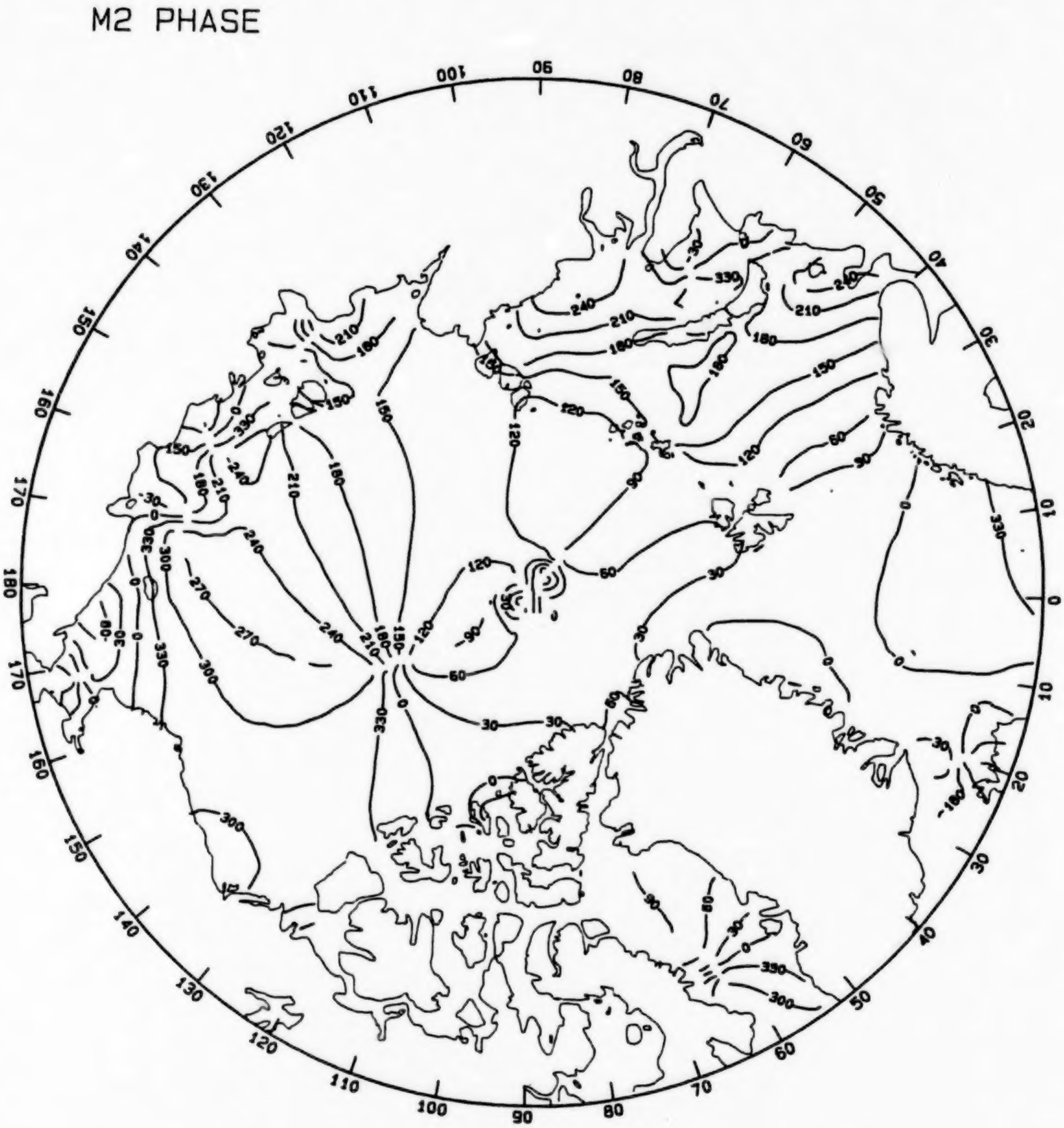
M2 PHASE
90
80
70
60
50
40
30
20
10
0
10
20
30
40
50
60
70
80
90
100
110
120
130
140
150
160
170
180
170
160
150
140
130
120
110
100
240
210
180
150
120
90
60
30
0
330
300
270
240
210
180
150
120
90
60
30
0
330
300

Figure B.9. Phase contours of the M2 tide in the Arctic Ocean, as calculated by Schwiderski.

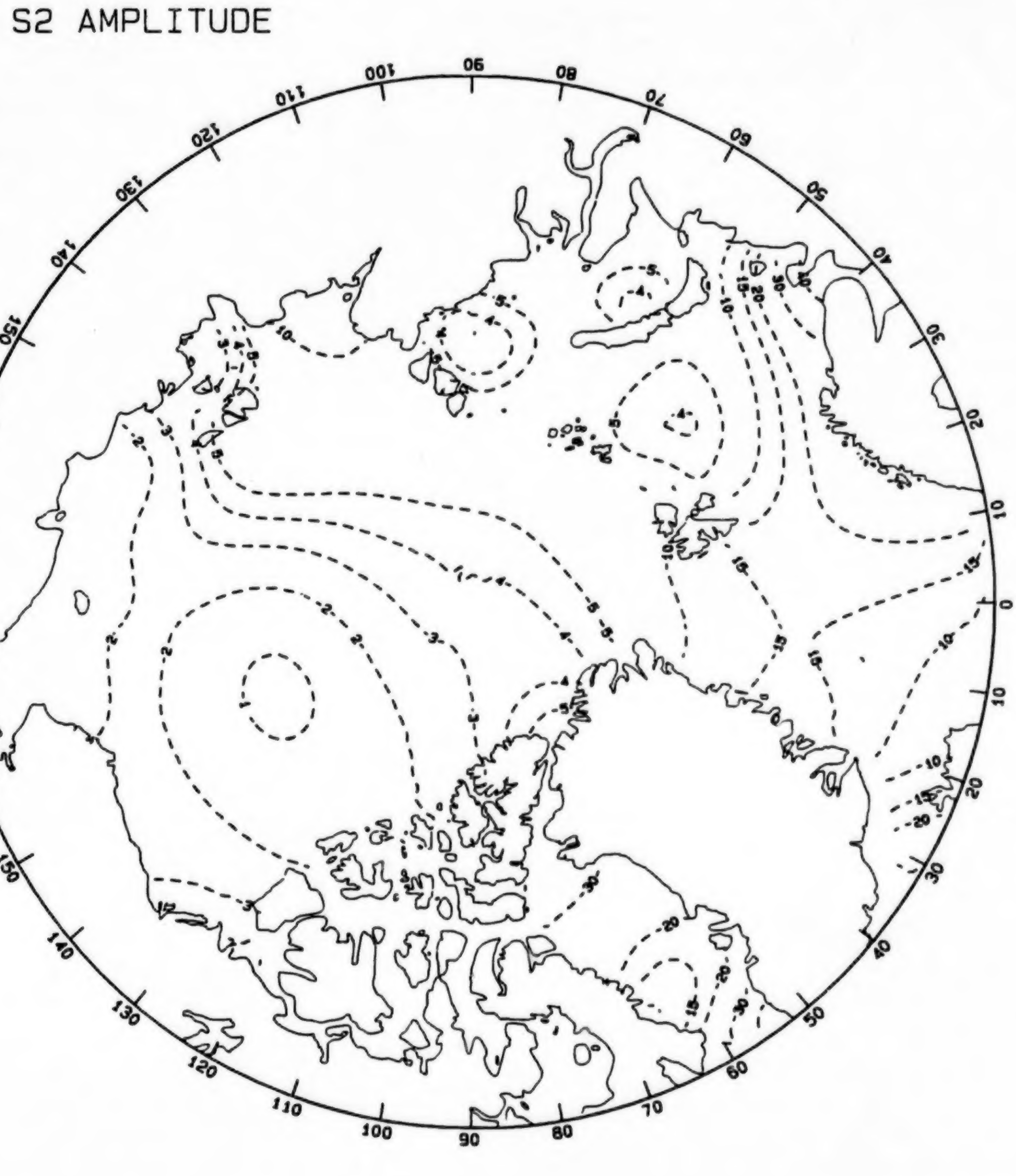
S2 AMPLITUDE
120
110
100
90
80
70
60
50
40
30
20
10
0
10
20
30
40
50
60
70
80
90
100
110
120
130
140
150
160
170
180
170
160
150
140
130

Figure B.10. Amplitude contours of the S2 tide in the Arctic Ocean, as calculated by Schwiderski.

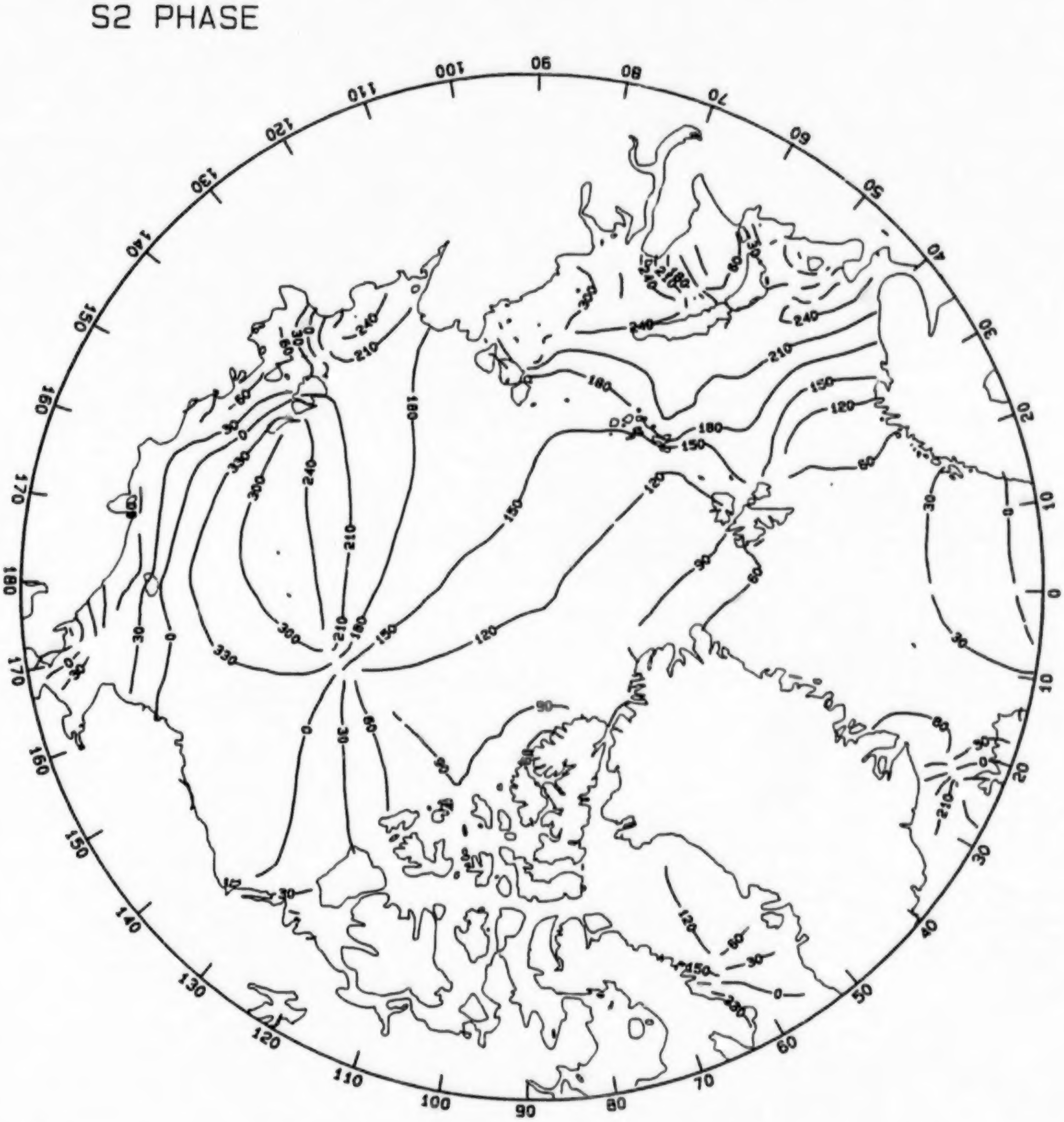
S2 PHASE
100
90
80
70
60
50
40
30
20
10
0
110
120
130
140
150
160
170
180
300
330
240
210
180
150
120
90
60
30
0

Figure B.11. Phase contours of the S2 tide in the Arctic Ocean, as calculated by Schwiderski.

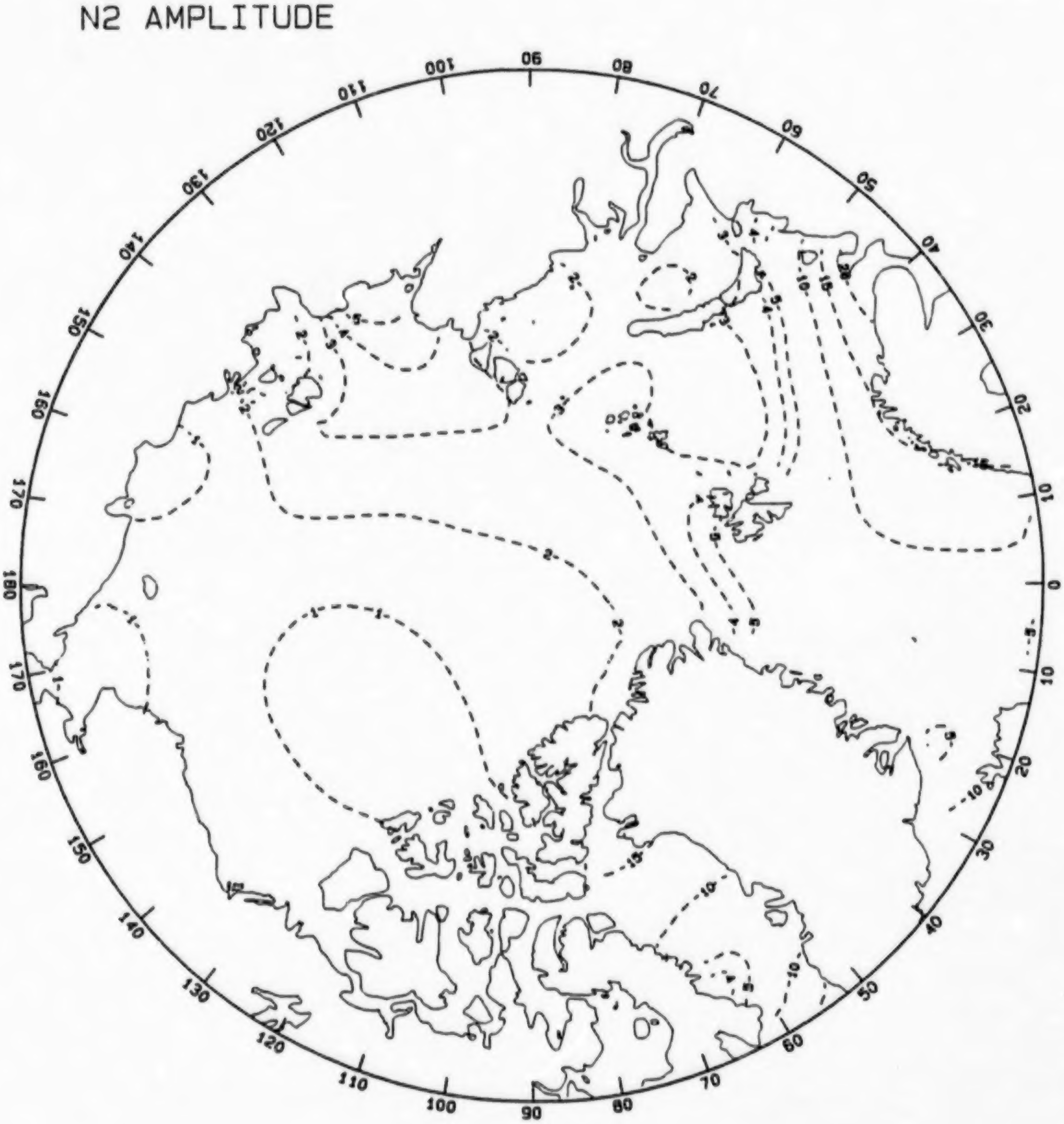
N2 AMPLITUDE
100
90
80
70
60
50
40
30
20
10
0
10
20
30
40
50
60
70
80
90
100
110
120
130
140
150
160
170
180
170
160
150
140
130
120
110

Figure B.12. Amplitude contours of the N2 tide in the Arctic Ocean, as calculated by Schwiderski.

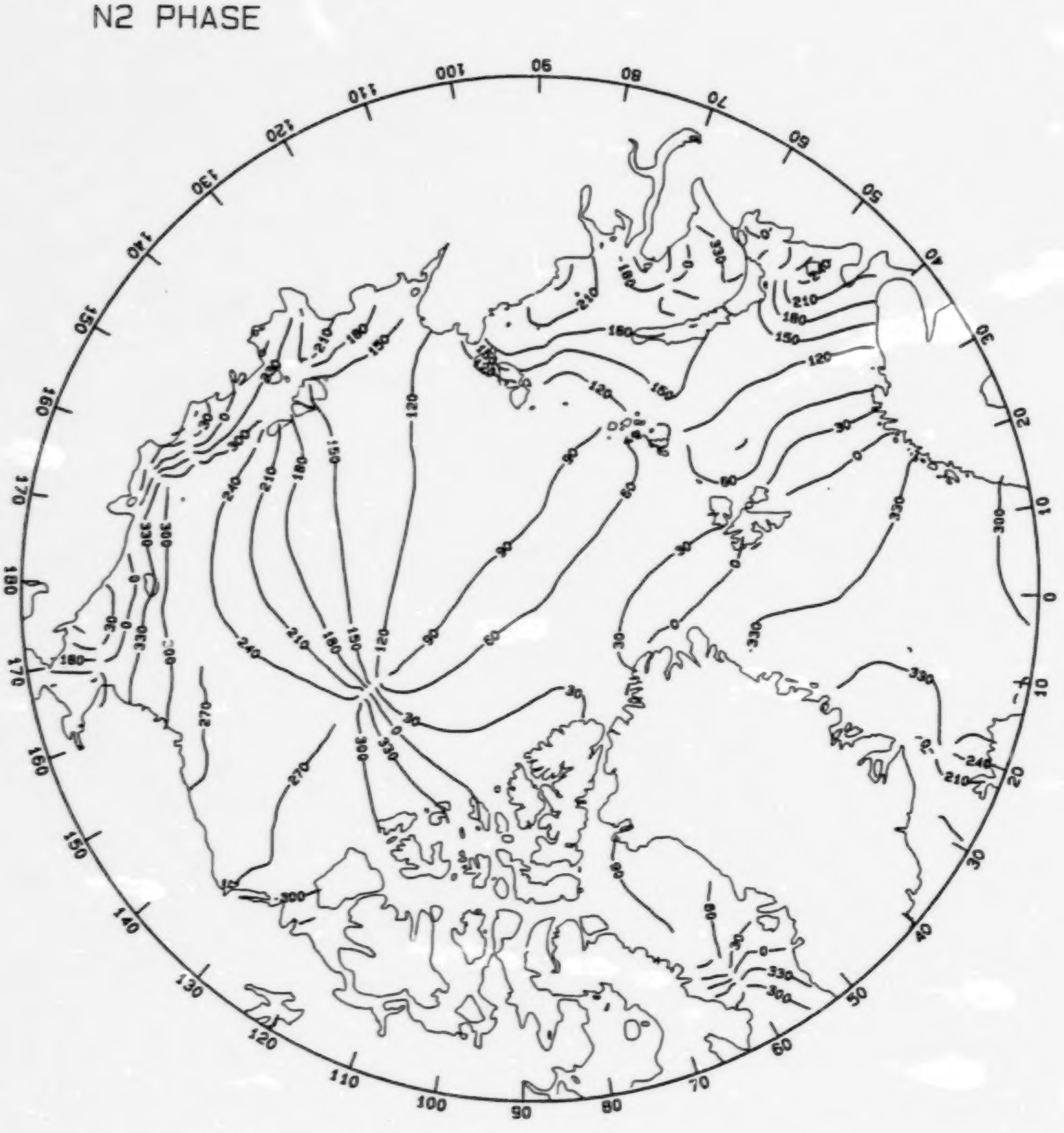
N2 PHASE
100
90
80
70
60
50
40
30
20
10
0
10
20
30
40
50
60
70
80
90
100
110
120
130
140
150
160
170
180
170
160
150
140
130
120
110
210
180
150
120
90
60
30
0
330
300
270
240

Figure B.13. Phase contours of the N2 tide in the Arctic Ocean, as calculated by Schwiderski.

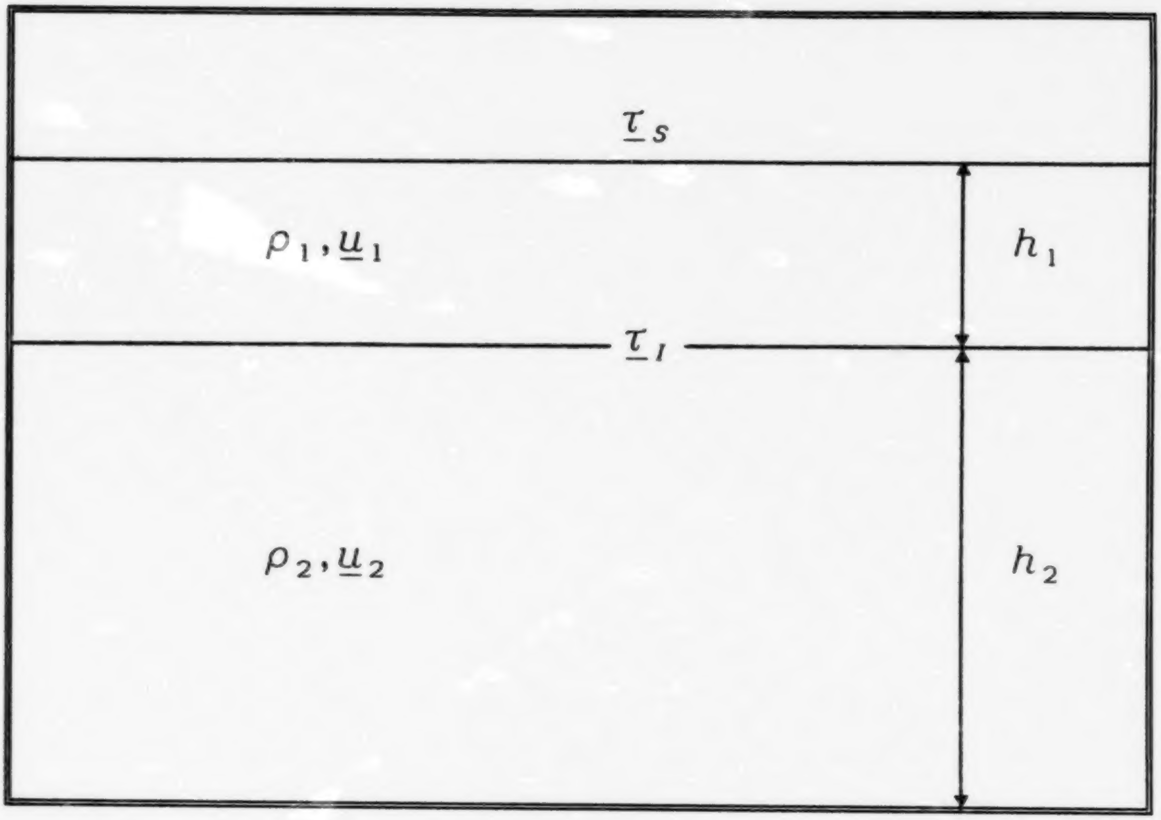
$\underline{\tau}_s$
$\rho_1, \underline{u}_1$
h_1
$\underline{\tau}_I$
$\rho_2, \underline{u}_2$
h_2

Figure D.1. Schematic illustration of the modified Pollard-Millard model.

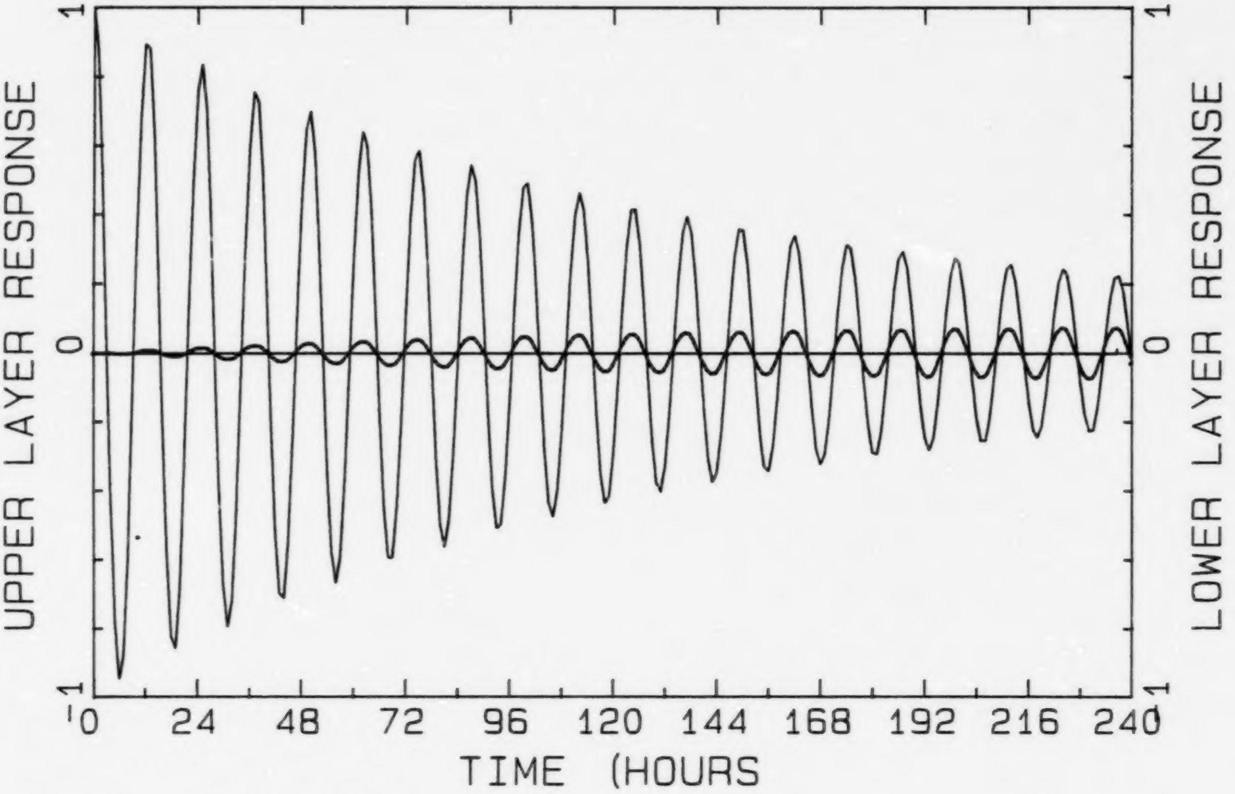

Figure D.2 Real part of (1) the upper layer impulse response function (light curve) and (2) the lower layer impulse response function (heavy line), both normalised by $\sigma_1 h_1$.

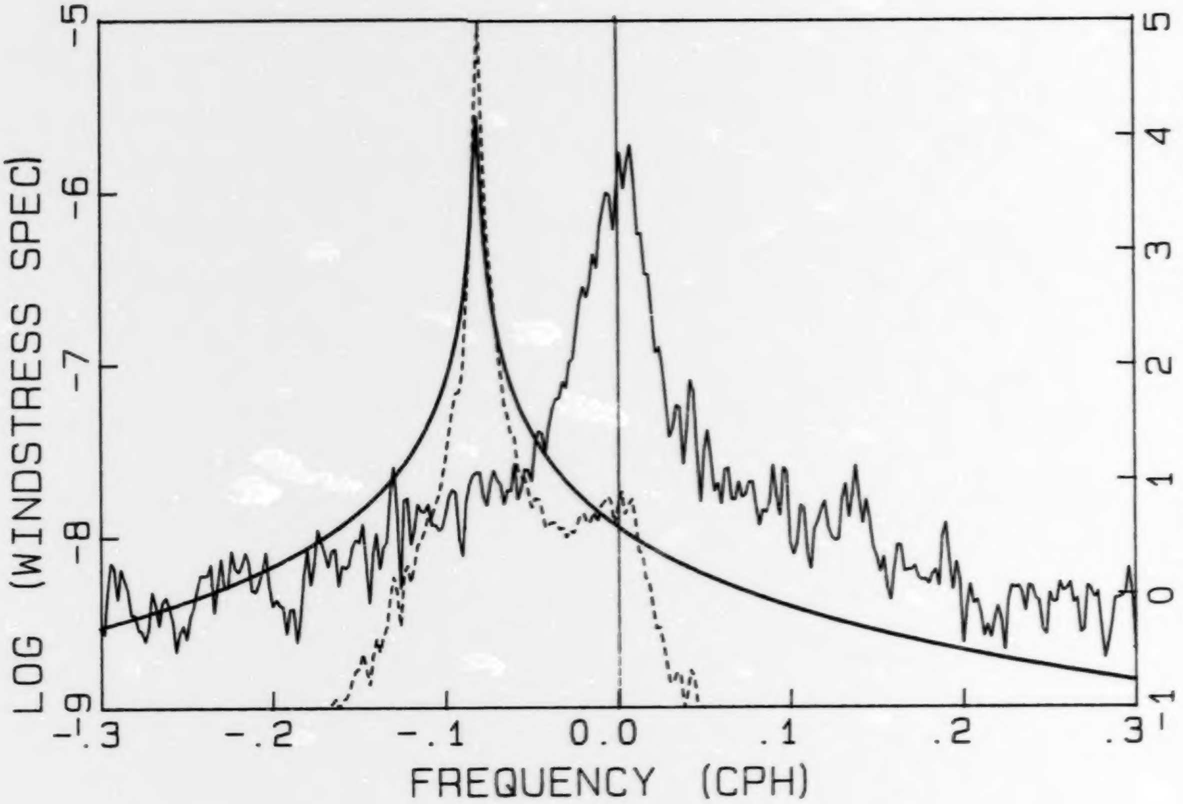

Figure D.3 The 1984 windstress spectrum for Resolute Bay, the baroclinic gain (heavy line), and the predicted upper layer current spectrum (dotted line) normalised to one.